Isothermal Transport of Carbon Dioxide and Hydrogen Sulphide in Porous Media: Blockage by Adsorbed Films

by

Sarah Butler

A thesis submitted for the degree of
Doctor of Philosophy
in the University of London
and the Diploma of Membership of the Imperial College

Chemistry Department
Imperial College
London SW7

January 1987

Abstract

A study has been made of the flow of H_2S, CO_2, N_2 and He and binary mixtures thereof through porous membranes made from compacted powders . The membrane materials utilized were Zeolite NaX, a carbon molecular sieve, Carbolac carbon powder and Graphon, a graphitised carbon powder. "Conventional" boundary conditions (as used in the majority of work originating from the Barrer school) were employed, with gas pressures less than one atmosphere. Both steady state and transient state flow have been characterised and analysis aided by the documentation of adsorption isotherms for each system. Where a Poiseuille flow component was present, results have been analysed using the Carman-Arnell equation (Carman and Arnell 1948) and also by means of a "Universal plot" for each membrane. The Graphon and Carbolac membranes were found to give an "extra flux" for sorbable gases, which was associated with the adsorbed layers and analysis has involved the calculation of the "extra" permeability for each system. Diffusion coefficients were also calculated and from them activation energies for diffusion were calculated. Binary mixtures comprising one strongly adsorbed gas and one non sorbed or weakly-adsorbed gas were flowed through the Graphon and Carbolac membranes and the results analysed in terms of blockage of the gas phase flow by adsorbed layers. Where possible steady state and transient state separation factors have been evaluated for binary mixtures. The suitability of the membrane materials studied, for industrial gas separation using either a continuous or non-continuous process has been discussed.

ACKNOWLEDGEMENTS

I would like to thank my supervisor Mr. R. Ash for his continued enthusiasm and good humour throughout this project, also my industrial supervisor Dr. A. A. Rizvi for his advice and moral support.

I am also indebted to the members of Project 209 (BP Research Centre Sunbury) for the use of their McBain balance, and to the members of the technical staff at Imperial College without help from whom this project could not have been completed.

My special thanks must go to Dr. I. S. Kerr, for help with computing, Mr. H. J. Rudd for extra maths lessons, Dr. L. Pratt for advice on inorganic chemistry, and last but by no means least, Dr. T. G. Fowler for his help, support, and encouragement.

Contents

List of Tables 8

List of Figures 10

List of symbols used 18

Chapter 1: Introduction 21

Chapter 2: Theoretical Background 23

2.1 Introduction 24

2.2 Flow in a single capillary 24

2.3 Flow in a porous medium 30

2.4 "Conventional" flow conditions: steady state flow 32

2.5 Transient state flow 34

2.5.1 Breakthrough time procedure 36

2.5.2 Time lag equation 41

2.6 Flow of sorbed gases 48

2.7 Relevant adsorption background 51

Chapter 3: Experimental 57

3.1 Membranes 59

Materials used 59

3.1.1 Zeolite NaX 59

3.1.2 Carbon molecular sieve 62

3.1.3 Carbolac 63

3.1.4 Graphon 64

3.1.5 Membrane construction 66

3.1.6 Outgassing procedure 69

3.2 The Gases 69

3.2.1 Gas suppliers and purity 69

3.2.2 Gas bottling apparatus 70

3.2.3 Precautions taken with H_2S usage 70

3.3 General features of high vacuum apparatus 73

3.3.1 Pumping system 74

3.3.2 Temperature control 74

3.3.3 Temperature measurement 76

3.3.4 McLeod gauges 76

3.4 Adsorption isotherm determination 79

3.4.1 (McBain balance) Description of apparatus 79

3.4.2 Experimental technique 81

3.4.3 Volumetric apparatus 82

3.5 Isothermal Flow Apparatus 84

The Flow of Single Gases 84

3.5.1 (Molecular sieve membranes) description of apparatus 84

3.5.2 Experimental technique 88

The Flow of Binary Mixtures 89

3.5.3 Description of apparatus 89

3.5.4 The Circulating Pump 92

3.5.5 Experimental technique 93

Chapter 4: Results 96

4.1 Adsorption Isotherms 97

4.4.1 Introduction 97

4.1.2 NaX Isotherms 97

4.1.3 CMS characterisation 100

4.1.4 CMS isotherms 103

4.1.5 Carbolac isotherms 105

4.1.6 Graphon isotherms 108

4.2 Single Gas Flow 116

4.2.1 Introduction 116

4.2.2 NaX Membrane 1 116

4.2.3 NaX Membrane 2 125

4.2.4 CMS Membrane 131

4.2.5 Carbolac Membrane 139

4.2.6 Graphon Membrane 152

4.3 Binary Mixture Flow 166

4.3.1 Introduction 166

4.3.2 Carbolac Membrane 168

4.3.3 Graphon Membrane 171

4.3.4 Error Analysis 178

Chapter 5: Discussion 181

5.1 Discussion of adsorption isotherms 183

5.1.1 Isotherms on molecular sieve materials 183

5.1.2 Carbolac isotherms 192

5.1.3 Graphon isotherms 199

5.1.4 Isosteric heats of adsorption 212

5.2 Discussion of flow results on molecular sieve membranes (NaX1, NaX2, and CMS) 219

5.2.1 Introduction 219

5.2.2 Low pressure behaviour of the integral permeability 220

5.2.3 Knudsen and Poiseuille permeabilities 223

5.2.4 $\tilde{K}\sqrt{M/T}$ versus $1/\bar{\lambda}$ plots 227

5.2.5 Break-through time procedure 236

5.2.6 Theoretical determination of time lags 240

5.3 Discussion of single gas flow results on Graphon and Carbolac membranes 246

5.3.1 Introduction 246

5.3.2 Helium flow 247

5.3.3 Flow of sorbable gases: $\tilde{K}$ and J_∞ 253

5.3.4 Flow of sorbable gases: $\tilde{K}_s/\tilde{K}_g$ and $\tilde{K}_s/A$ 259

5.3.5 Diffusion coefficients 268

5.4 Binary mixture flow 284

5.4.2 Relationship between ν, $\tilde{K}$ and $\tilde{K}_{R(He)}$ 285

5.4.3 The shape of the blockage curve 297

5.4.4 Blockage behaviour of different sorbable gases 303

5.4.5 Blockage of gases other than He 308

5.5 Application of results to gas separation 313

5.5.1 Introduction 313

5.5.2 Continuous flow separation of gas mixtures 314

5.5.3 Transient state separations 323

5.5.4 Separation of H_2S from gas mixtures 341

Chapter 6: Summary of Results and Recommendations for Further Work 345

Appendix A: Adsorption Isotherms 349

Appendix B: Flow Data 371

References 401

List of Tables

3.1 Membrane Material Characteristics i) Molecular sieves

3.2 Membrane Material Characteristics ii) Carbons

3.3 Characteristics of molecular sieve membranes

3.4 Characteristics of carbon membranes

3.5 Intial outgassing conditions

3.6 Impurities present in gases used

3.7 Measurement McLeod gauge characteristics

3.8 Quartz spring properties

3.9 Characteristics of adsorption apparatus

3.10 Outgoing volume of single gas flow apparatus

3.11 Outgoing volume of Graphon and Carbolac apparatus

3.12 Partial pressures of He, N_2 and Ar in mixture experiments

4.1.1 Weight loss on outgassing

4.2.1 Systems for which single gas flow was investigated

4.2.2 $K \sqrt{M/T}$ values for He flow through this Carbolac membrane

4.2.3 $K \sqrt{M/T}$ values for He flow through this Graphon membrane

4.3.1 Binary mixtures studied

4.3.2 Estimated maximum errors

5.1.1 Comparison of b and ν_m values from Langmuir plots

5.1.2 a) Equivalent surface area of NaX calculated from isotherms at 195K BET ν_m values

5.1.2 b) Equivalent surface areas of CMS calculated from BET plot of CO_2 at 195k and O_2 at 77K

5.1.2 c) Void volumes (VV)

5.1.3 Surface area of Carbolac obtained from BET plots

5.1.4 Carbolac surface areas, (this study)

5.1.5 Graphon, BET surface area from low temperature N_2 isotherms

5.1.6 Correlation between the pressure at the minimum of the BET plot and that at the point of inflection of the isotherm

5.1.7 a) CO_2 Molecular areas and associated monolayer capacities for Graphon.

5.1.7 b) H_2S molecular areas and associated monolayer capacities for Graphon

5.2.2 a) Low pressure behaviour of $\tilde{K}$ versus p,

5.2.3 a) Poiseuille Permeability constants $\tilde{K}_1'$

5.2.3 b) Knudsen Permeability constants $\tilde{K}_K$ and $\tilde{K}_K'$

5.2.4 Table of viscosities and λ_1 values

5.2.5 Breakthough time procedure

a) CO_2/NaX 1

b) CO_2/NaX 2

c) N_2/NaX 2

d) H_2S/NaX 2

e) CO_2/CMS

5.3.1 $\tilde{K}\sqrt{M/T}$ for He flow

5.3.2 $\tilde{Dg}$, $\tilde{Dg}^{cyl}$, $\tilde{\kappa g}$ for He flow

5.3.3 $\tilde{K}_s/\tilde{K}_g$ and $\tilde{K}_s/A$

5.5.1 Summary of adsorption and detection time results

List of figures

2.1 Schematic representation of Webers (1954) three flow components

2.2a Detection time (t_1) and time-lag (L)

2.2b A "true break-through time" (as Barrer 1954)

2.3 Gas concentrations in membrane for boundary conditions in equation (30)

2.4 Adsorption isotherm types BET classification

3.1 A sodalite cage. /The structure of NaX.

3.2 The membrane assembly (Graphon and Carbolac)

3.3 Gas bottling apparatus

3.4 A pumping system

3.5 Leaky dewar system

3.6 A McLeod gauge

3.7 McBain spring balance

3.8 Volumetric adsorption apparatus

3.9 Diagram of apparatus for measurement of single gas flow

3.10 Diagram of apparatus for measurement of binary mixture flow (Graphon and Carbolac)

4.1.1 Adsorption isotherms CO_2 and NaX

4.1.2 Adsorption isotherms H_2S on NaX

4.1.3 Adsorption isotherms N_2 on CMS pellets

4.1.4 Adsorption isotherm O_2 on CMS (77 K)

4.1.5 Adsorption isotherms CO_2 on CMS pellets

4.1.6 Adsorption isotherms N_2 on Carbolac

4.1.7 Adsorption isotherms H_2S on Carbolac

4.1.8 Adsorption isotherms N_2 on Graphon pellets

4.1.9 Adsorption isotherms CO_2 on Graphon pellets (volumetric determination)

4.1.10 Adsorption isotherms CO_2 on Graphon 195 K

4.1.11 Adsorption isotherms H_2S on Graphon pellets

4.1.12 Adsorption isotherm SF_6 on Graphon pellets 195K

4.2.1 Sample outgoing pressure versus time graphs
He flow through Zeolite membrane 1

4.2.2 Sample outgoing pressure versus time graphs
CO_2 flow through Zeolite membrane 1

4.2.3 Sample outgoing pressure versus time graphs
CO_2 flow through Zeolite membrane 1

4.2.4 Integral permeability and steady state flux versus ingoing pressure: He flow through Zeolite membrane 1

4.2.5 Integral permeability and steady state flux versus ingoing pressure: CO_2 flow through Zeolite membrane 1

4.2.6 Timelag and break-through time versus ingoing pressure:
CO_2 flow through Zeolite membrane 1

4.2.7 Integral permeability and steady state flux versus ingoing pressure: He flow through Zeolite membrane 2

4.2.8 Integral permeability and steady state flux versus ingoing pressure: N_2 flow through Zeolite membrane 2

4.2.9 Integral permeability and steady state flux versus ingoing pressure: H_2S flow through Zeolite membrane 2.

4.2.9a Integral permeability and steady state flux versus ingoing pressure: CO_2 flow through Zeolite membrane 2

4.2.9b Time-lags versus ingoing pressure: CO_2 flow through Zeolite membrane 2

4.2.10 Time-lag versus ingoing pressure: N_2 and H_2S flow through Zeolite membrane 2

4.2.11 Sample outgoing pressure versus time graphs
CO_2 flow through CMS membrane

4.2.12 Integral permeability and steady state flux versus ingoing pressure: He flow through CMS membrane

4.2.13 Integral permeability and steady state flux versus ingoing pressure: He flow through CMS membrane

4.2.14 Integral permeability and steady state flux versus ingoing pressure: N_2 flow through CMS membrane

4.2.15 Integral permeability and steady state flux versus ingoing pressure: H_2S flow through CMS membrane

4.2.16 Integral permeability and steady state flux versus ingoing pressure: CO_2 flow through CMS membrane.

4.2.17 Time-lag amd break through time versus ingoing pressure: CO_2 flow through CMS

4.2.18 Integral permeability and steady state flux versus ingoing pressure: He flow through Carbolac membrane

4.2.19 Variation of He permeability at 195K with run number Carbolac membrane

4.2.20 Sample outgoing pressure versus time graphs: N_2 on Carbolac membrane

4.2.21 Integral permeability and steady state flux versus ingoing pressure: N_2 flow through Carbolac membrane

4.2.22 Variation of N_2 permeability with run number at 195K Carbolac membrane

4.2.23 Sample outgoing pressure versus time graphs, CO_2 through Carbolac membrane

4.2.24 Integral permeability and steady state flux versus ingoing pressure: CO_2 flow through Carbolac membrane

4.2.25 Time lag and detection time versus ingoing pressure CO_2 flow through Carbolac membrane

4.2.26 Integral permeability and steady state flux versus ingoing pressure: H_2S flow through Carbolac membrane

4.2.27 Time lag and detection time versus ingoing pressure H_2S flow through Carbolac membrane

4.2.28 Integral permeability and steady state flux versus ingoing pressure: He flow through Graphon membrane

4.2.29 Integral permeability and steady state flux versus ingoing pressure: N_2 flow through Graphon membrane

4.2.30 Sample outgoing pressure versus time graph CO_2 through Graphon membrane

4.2.31 Integral permeability versus ingoing pressure CO_2 flow, Graphon membrane

4.2.32 Steady state flux versus ingoing pressure CO_2 flow, Graphon membrane

4.2.33 Integral permeability versus ingoing pressure H_2S flow, Graphon membrane

4.2.34 Steady state flux versus ingoing pressure H_2S flow, Graphon membrane

4.2.35 Integral permeability versus ingoing pressure C_3H_8 flow through Graphon membrane

4.2.36 Steady state flux versus ingoing pressure C_3H_8 flow through Graphon membrane

4.2.37 Integral permeability and steady state flux versus ingoing pressure: SF_6 flow through Graphon membrane at 195K

4.2.38 Integral permeability and steady state flux versus ingoing pressure: Ar flow through Graphon membrane at 184K

4.3.1 $\underset{\sim}{K}_R$ versus p_1/p_o, CO_2/He and CO_2/N_2, Carbolac

4.3.2 $\underset{\sim}{K}_R$ versus p_1/p_o, H_2S/He and H_2S/N_2, Carbolac

4.3.3 $\underset{\sim}{K}_R$ versus p_1/p_o, CO_2/He Graphon

4.3.4 $\underset{\sim}{K}_R$ versus p_1/p_o, Ar/CO_2 Graphon

4.3.5 $\underset{\sim}{K}_R$ versus p_1/p_o, H_2S/He Graphon

4.3.6 $\underset{\sim}{K}_R$ versus p_1/p_o, H_2S/N_2 Graphon

4.3.7 $\underset{\sim}{K}_R$ versus p_1/p_o, C_3H_8/He Graphon

4.3.8 K_R versus p_1/p_o, SF_6/He Graphon 184K

5.1.1 Langmuir plots CO_2/NaX

5.1.2 Langmuir plots H_2S/NaX

5.1.3 Langmuir plot O_2/CMS 77K

5.1.4 Langmuir plot CO_2/CMS

5.1.6 Adsorption isotherms (P. Sharma) CO_2/Carbolac powder

5.1.7 BET plot P. Sharma's results CO_2/Carbolac/195K

5.1.8 BET plot, H_2S/Carbolac

5.1.9 BET plot, CO_2/Graphon

5.1.10 Plot of $p/p_{o(min)}$ from BET plot versus T

5.1.11 BET plots and correlation of $p/p_{o(min)}$ with T
H_2S/Graphon

5.1.12 $\ell n\{\theta p_o/(1 - \theta)p\}$ versus θ for CO_2/Graphon
a) 184K, b) 190K

5.1.13 $\ell n\{\theta p_o/(1 - \theta)p\}$ versus θ for CO_2/Graphon
c) 195K, d) 200K

5.1.14 $\ell n\{\theta p_o/(1 - \theta)p\}$ versus θ for H_2S Graphon
a) 195K, b) 213.2K

5.1.15 $\ell n\{\theta p_o/(1 - \theta)p\}$ versus θ for H_2S/Graphon
c) 243.2K, d) 273.2K

5.1.16 Isosteric heat of adsorption CO_2/NaX

5.1.17 Isosteric heat of adsorption H_2S/NaX

5.1.18 Isosteric heat of adsorption CO_2/CMS

5.1.19 Isosteric heat of adsorption H_2S/Carbolac

5.1.20 Isosteric heat of adsorption H_2S/Graphon

5.1.21 Isosteric heat of adsorption CO_2/Graphon

5.1.22 $\ell n(p)$ versus 1/T plots: CO_2/Graphon

5.2.1 $K \sqrt{M/T}$ versus $1/\bar{\lambda}$ NaX membrane 1

5.2.2 $K \sqrt{M/T}$ versus $1/\bar{\lambda}$ NaX membrane 1
results of Mr. R. Ash compared with those of the author

5.2.3a $K \sqrt{M/T}$ versus $1/\bar{\lambda}$ NaX membrane 2

5.2.3b $K \sqrt{M/T}$ versus $1/\bar{\lambda}$ NaX membrane 2

5.2.4a $K \sqrt{M/T}$ versus $1/\bar{\lambda}$ CMS membrane

5.2.4b $K \sqrt{M/T}$ versus $1/\bar{\lambda}$ CMS membrane

5.2.5 Theoretical and experimental time lags
CO_2 flow through Zeolite membrane 1

5.2.6 Theoretical and experimental time lags through Zeolite membrane 2 a) H_2S flow b) CO_2 flow

5.2.7 Theoretical and experimental time lags CO_2 flow through CMS

5.3.1 Carbolac: flux calculated from permeability a) He, b) N_2

5.3.2 $\underset{\sim}{K}\sqrt{M/T}$ versus $1/\bar{\lambda}$ He flow: Carbolac

5.3.3 Schematic diagram of $\underset{\sim}{K}$ versus p_1 behaviour

5.3.4 Schematic diagram of $\underset{\sim}{K}$ versus p_1 behaviour

5.3.5 $\underset{\sim}{K}$ calculated from J_∞: SF_6/Graphon

5.3.6 SF_6/Graphon (R. W. Baker)

5.3.7 $\underset{\sim}{K}_s/\underset{\sim}{K}_g$: N_2 flow Carbolac

5.3.8 $\underset{\sim}{K}_s/\underset{\sim}{K}_g$: H_2S flow Carbolac

5.3.9 $\underset{\sim}{K}s/A$: H_2S flow Carbolac

5.3.10 $\underset{\sim}{K}s/\underset{\sim}{K}_g$ and $\underset{\sim}{K}_S/A$: a) N_2/Graphon b) SF_6/Graphon

5.3.11 $\underset{\sim}{K}s/\underset{\sim}{K}_g$: CO_2/Graphon

5.3.12 $\underset{\sim}{K}s/A$: CO_2/Graphon

5.3.13 $\underset{\sim}{K}_s/A$ versus p_1: H_2S Graphon

5.3.14 $\underset{\sim}{K}_s/\underset{\sim}{K}_g$ versus T a) CO_2/Graphon, b) H_2S Graphon

5.3.15 Diffusion coefficients: N_2/Carbolac

5.3.16 Diffusion coefficients: CO_2/Carbolac

5.3.17 Diffusion coefficients: H_2S/Carbolac

5.3.18 $\underset{\sim}{D}$ and D: CO_2/Graphon 184K

5.3.19 $\underset{\sim}{D}$ versus ν: CO_2/Graphon

5.3.20 $\underset{\sim}{D}$ versus ν: CO_2/Graphon

5.3.21 $\underset{\sim}{D}$ and D: H_2S/Graphon

5.3.21a J_∞ versus c_1: H_2S/Graphon

5.3.22 $\underset{\sim}{D}$ and D: SF_6/Graphon

5.3.23 $\tilde{D}$ and D : N_2/Graphon

5.3.24 Concentration dependence of E : CO_2/Graphon
$\tilde{D} = \tilde{D}_o \exp(-E/RT)$

5.3.25 Concentration dependence of E : CO_2/Graphon
$D = D_o \exp(-E/RT)$

5.3.26 Concentration dependence of E : H_2S Graphon
$\tilde{D} = \tilde{D}_o \exp(-E/RT)$

5.3.27 Concentration dependence of E : H_2S Graphon
$D = D_o \exp(-E/RT)$

5.3.28 &nD versus 1/T : CO_2/Graphon

5.4.1 Triple plot CO_2/Carbolac 195K

5.4.2 Triple plot CO_2/Carbolac 273.2K

5.4.3 Triple plot H_2S/Carbolac 195K

5.4.4 Triple plot H_2S/Carbolac 273.2K

5.4.5 Triple plot CO_2/Graphon 184K

5.4.6 Triple plot CO_2/Graphon 213.2K

5.4.7 Triple plot H_2S/Graphon 195K

5.4.8 Triple plot H_2S/Graphon 273.2K

5.4.9 Triple plot SF_6/Graphon 195K

5.4.10 Variation of $\tilde{K}_R$ for He/hydrocarbon mixtures

5.4.10a Variation of $\tilde{K}_R$ with p_1/p_o for He/CO_2 mixtures

5.4.10b Variation of $\tilde{K}_R$ with p_1/p_o for H_2S/He mixtures

5.4.11 Variation of $\tilde{K}_R$ with p_1/p_o for two Carbolac membranes

5.4.12 CO_2/N_2/Carbolac: blockage curve

5.4.13 H_2S/N_2/Carbolac: blockage curve

5.4.14 Blockage of He by CO_2 or hydrocarbons: Graphon

5.4.15 Blockage of He/Graphon membrane

5.4.16 CO_2/Ar/Graphon: blockage curve

5.4.17 H_2S/N_2/Graphon: blockage curve

5.4.18 CO_2/N_2/Graphon: blockage curve (C F Bott)

5.5.1 CO_2/He and CO_2/N_2 separation factors: Carbolac

5.5.2 H_2S/He and H_2S/N_2 separation factors : Carbolac

5.5.3 CO_2/He, CO_2/Ar and CO_2/N_2 separation factors: Graphon

5.5.4 H_2S/He and H_2S/N_2 separation factors: Graphon

5.5.5 SF_6/He separation factors: Graphon 195K

5.5.6 Apparatus used to investigate the use of Zeolites as selective adsorbents for H_2S

5.5.7a Diagram of four column PSA system developed by Bergbau-Forschung GmbH

5.5.7b Sequence of process steps in a PSA four column system

5.5.8 Transient state separation factors CO_2/He/Carbolac 195K

5.5.8a Transient state separation factors for He from the He/CO_2/ Carbolac system at 195K

5.5.9 Transient state separation factors CO_2/He/Carbolac 273.2K

5.5.10 Transient state separation factors CO_2/N_2/Carbolac 195K

5.5.11 Transient state separation factors CO_2/N_2/Carbolac 273.2K

5.5.12 Transient state separation factors H_2S/He/Carbolac 195K

5.5.13 Transient state separation factors H_2S/He/Carbolac 273.2K

5.5.14 Transient state separation factors H_2S/N_2/Carbolac 195K

5.5.15 Transient state separation factors H_2S/N_2/Carbolac 273.2K

List of symbols used

A	Internal surface area of membrane/$m^2 m^{-3}$
Ac	Membrane cross sectional area /m^2
A_p	Cross sectional area of pore or capillary/m^2
α	$\tilde{K}_p/\tilde{K}_K'$ (Time lag equation)/$N^{-1}m^2$
α	Separation factor
b	Constant (Langmuir equation)/$cmHg^{-1}$
BTT	Breakthrough time/s
c	Constant (BET equation)/
$c, c^o c^\ell$	Total gas concentration/mol(m^3 of membrane)$^{-1}$ at any point within, at the ingoing and outgoing faces of the membrane respectively
c_g	Gas phase concentration/mol(m^3 of membrane)$^{-1}$
$c_g', c_g^{o'}$	Gas phase concentration/mol(m^3 of gas phase)$^{-1}$ at any point within, and at the ingoing face of the membrane,
c_s	Gibbs surface excess concentration/mol(m^3 of membrane)$^{-1}$
c_s'	Gibbs surface excess concentration/mol(m^2 of surface)$^{-1}$
c_m'	Gibbs surface excess concentration at monolayer capacity /mol(m^2 of surface)$^{-1}$
d	Capillary diameter/m
δ	Coefficient (Carman-Arnell equation)
D	Diffusion coefficient/$m^2 s^{-1}$
$\tilde{D}$	Integral diffusion coefficient/$m^2 s^{-1}$
D_{s2}	Diffusion coefficient for surface flow/$m^2 s^{-1}$
D_1'	Diffusion coefficient (Break through time procedure)/$m^2 s^{-1}$

D_p	Diffusion coefficient for Poiseuille flow/ $mol^{-1}\,m^5 s^{-1}$
E	Activation energy for diffusion/$Jmol^{-1}$
ϵ	Porosity m^3 (m^3 porous medium)$^{-1}$
f	Proportion of molecules randomly reflected from pore walls
$\eta_{A:B}$	Separation factor
η	Viscosity/ $kg\,m^{-1}s^{-1}$
θ	Coverage ($\frac{\nu}{\nu_m}$)
θ	$\tilde{K}_p' p/\tilde{K}_K'$ (Time lag equation)
J_∞	Steady state molar flux/$mols^{-1}$
J_g	Gas phase flux/$mols^{-1}$
J_s	Extra flux/$mols^{-1}$
J_A	Flux per unit area/mol $s^{-1}m^{-2}$
K_1	Adsorbate adsorbent equilibrium constant
$\tilde{K}$	Integral permeability/m^2s^{-1}
$\tilde{K}_K, \tilde{K}_K'$	Integral permeability for Knudsen flow/m^2s^{-1}
$\tilde{K}_p, \tilde{K}_p'$	Integral permeabilities for Poiseuille flow/ $m^3 s\,kg^{-1}$
$\tilde{K}_s$	Integral extra flow permeability/m^2s^{-1}
$\tilde{K}_g$	Integral gas phase flow permeability/m^2s^{-1}
k	Kozeny constant
k_1	Shape factor for Knudsen flow
k_o	Shape factor for Poiseuille flow
k_2	Tortuosity factor
ℓ	Length of capillary or membrane/m
L	Time lag/s
$\bar{\lambda}$	Mean free path of gas molecules/m
M	Molar mass/ $kg\,mol^{-1}$

p	Pressure/cmHg or Nm^{-2}
$\bar{p}$	Mean pressure/cmHg or Nm^{-2}
p_1, p_2	Ingoing and outgoing pressure respectively
p_o	Saturation vapour pressure/cmHg
q_{ST}	Isosteric heat of adsorption/$Jmol^{-1}$
r	Radius of capillary/m
r_h	Hydraulic radius/m
R	Gas constant/$Jmol^{-1}K^{-1}$
t	Time/s
t_1	Detection time/s
T	Temperature of experiment/K
T_R	Room Temperature/K
V	Outgoing volume/m^3
ν	Amount adsorbed/cm^3STPg^{-1}
ν_m	Monolayer capacity/cm^3STPg^{-1}
x	Distance/m
x_A	Mol fraction of component A
ζ	Value of x at which C = 0 (Break through time procedure)
y	bp_1 (Time lag equation)
Z	$\zeta/\sqrt{Dt}.2$ (Break through time procedure)

CHAPTER 1

INTRODUCTION

The efficient and economical separation of the components of gas mixtures is a subject of great interest in many fields of industry, particularly those concerned with the production of chemicals or of energy.

Traditionally gas mixtures have been separated either by chemical reactions (e.g. the removal of CO_2 and H_2S by slaked lime), or by cryogenic methods. However in recent years the use of both porous and non porous membranes for continuous flow separations and beds of adsorbent for non continuous separations has increased. Examples of these types of process are described in Section 5.5.2 and 5.5.3. The field of membrane technology is an expanding one as indicated by the high attendance at the 4th BOC Priestley Conference (1986) entitled "Membranes in gas separation and enrichment". This was the first large conference on the subject to be held in Britain and the utilisation of membranes for the separation of a wide variety of gas mixtures was discussed. These included

i) the sweetening of natural gas by removal of CO_2 and H_2S

ii) O_2/N_2 separation

iii) H_2 separation from process gas e.g. NH_3 from NH_3 synthesis or coke oven gas

iv) He separation from diving gas.

The removal of H_2S is particularly important both for economical and environmental reasons. Stringent standards have been adopted worldwide in order to control atmospheric pollution and hence the waste products from the numerous industrial operations of which H_2S is a by-product (e.g. the Claus process for production of sulphur) must be strictly monitored. H_2S must also be removed from systems which utilise catalytic processes (as it causes sulphur poisoning of catalysts), and from both "substitute natural gas" following 'hydro desulphurization' and from natural gas.

This study has been concerned with the flow of H_2S, CO_2, N_2 and He through four porous membranes formed by compaction of fine powders. Previous investigations into this type of membrane (Ash Barrer and Pope 1963b, Ash Barrer and Lowson 1973, for example) have proved that high gas separation factors may be obtained in this manner. Continuous separation by porous media may occur as a result of the following phenomena:

a) Knudsen flow (Section 5.5.2)

b) Extra flow (when layers of an adsorbable gas can block the pores to the gas phase flow of a less sorbable component (Section 5.5.2)

c) Activated diffusion (when the pore entrance is of molecular dimensions (Koresh and Soffer 1983)

d) Thermo osmosis (Rizvi 1982)

Activated diffusion may also be one of the causes of selective adsorption upon which many transient separation processes are based. (Section 5.5.3)

Chapter 2 Theoretical Background

2.1 Introduction

2.2 Flow in a single capillary

2.3 Flow in a porous medium

2.4 "Conventional flow" conditions : steady state flow

2.5 Transient state flow

2.5.1 Breakthrough time procedure

2.5.2 Time lag equation

2.6 Flow of sorbed gases

2.7 Relevant adsorption background

CHAPTER 2

THEORETICAL BACKGROUND

2.1 Introduction

Much of the theory of gas flow through porous media is based upon flow through a single capillary, which exhibits many of the same phenomena. In this chapter the equations of flow for single capillaries and their application to porous media will be discussed, with attention being given to a) transient state flow, and the prediction of time lags and breakthrough times and b) 'extra' flow and the resulting blockage effects.

2.2 Flow in a single capillary

Gas flow through a capillary may occur through different mechanisms:

1) Knudsen flow (molecular streaming)
2) Poiseuille flow (streamline flow with slip)
3) Turbulent flow
4) Orifice flow

of which turbulent flow and orifice flow are not within the range of the phenomena to be discussed. Equations relating to Knudsen and Poiseuille flow are summarised by Barrer (1954).

At low pressures (in the cmHg range), the mean free path

of the gas molecules ($\bar{\lambda}$) may exceed the capillary diameter (d). In this case the effect of molecule-molecule collisions is assumed to be negligible and pure molecular streaming occurs which obeys Ficks Law (Fick 1855).

$$\frac{\partial c}{\partial t} = D \frac{\partial^2 c}{\partial x^2} \qquad (1)$$

where D is the diffusion coefficient, c is gas concentration, x is distance and t is time. Flow of this kind is called Knudsen flow as it was first investigated by Knudsen (1909) who obtained the following expression for the diffusion coefficient.

$$D = \frac{4}{3} r \sqrt{\frac{2RT}{\pi M}} \quad \frac{(2 - f)}{f} \qquad (2)$$

Where r is the capillary radius, T, the temperature of the experiment, M, the molar mass of the gas, R, the gas constant and f, the proportion of molecules striking the walls which are reflected at random. (f is usually equated to 1). If Fick's definition of flux (J) (1855)

$$\frac{J_\infty}{A_p} = - D \frac{dc}{dx} \qquad \text{where } A_p \text{ is the capillary cross-sectional area} \qquad (3)$$

is applied to equation (2) an expression for the molar flux ($J_\infty/mols^{-1}$) results

$$J_\infty = \frac{4}{3} r \sqrt{\frac{2RT}{\pi M}} \quad \frac{(2 - f)}{f} \quad A_p \frac{\Delta c}{\ell} \qquad (4)$$

where Δc is the concentration difference between the ends of the capillary and, ℓ, the length of the capillary.

The integral permeability ($\tilde{K}$) is then defined in terms of the flux

$$\tilde{K} = \frac{J\ell}{A_p \Delta c} \tag{5}$$

and hence the permeability in the Knudsen flow regime ($\tilde{K}_K$) is equal to the diffusion coefficient.

Since molecule-wall collisions are dominant at these pressures, it is expected that the components of a mixture of gases would flow through the capillary independently of each other. The following relationship follows from equations (4) and (5).

$$\tilde{K}_1 \left(\frac{M_1}{T_1}\right)^{\frac{1}{2}} = \tilde{K}_2 \left(\frac{M_2}{T_2}\right)^{\frac{1}{2}} \tag{6}$$

where subscripts 1 and 2 represent different gases and their associated properties.

Pollard and Present (1948) have derived equation (2) by a method which gives a different value of the numerical constant

$$D = \frac{\pi r}{2} \sqrt{\frac{2RT}{\pi M}} \left(\frac{2 - f}{f}\right) \tag{7}$$

They were also able to offer an explanation for the initial decrease followed by a minimum observed in some $\tilde{K}$ versus pressure graphs (for example Knudsen (1909), Carman (1950) from Gaede's data for the flow of H_2 between parallel plates (1913)) in terms of the increase in molecule-molecule collisions, in the direction of flow with increasing pressure. This would only apply to capillary

tubes or long straight pores and not to porous media in which the pores are kinked so that no straight part can be much longer than the pore diameter. Hence no initial decrease in $\tilde{K}$ with increasing pressure was predicted for porous media.

If the mean free path of the molecule is much less than the radius of the capillary, then molecule-molecule collisions become important and the flow becomes streamlined (Poiseuille flow) and depends upon the viscosity of the gas. The following equation for the permeability of a gas through a capillary tube results

$$\tilde{K} = \frac{r^2 \bar{p}}{8 \eta} + \frac{\pi r}{4} \sqrt{\frac{2RT}{\pi M}} \left(\frac{2 - f}{f} \right) \tag{8}$$

Where η = the viscosity of the gas and $\bar{p}$ the mean pressure. The last term represents the contribution of slip-flow to the transport (Millikan 1923). The equation may be written

$$\tilde{K} = \frac{r^2 \bar{p}}{8\eta} + \frac{4r}{3} \delta \sqrt{\frac{2RT}{\pi M}} \tag{9}$$

(assuming f = 1)

where δ is a coefficient which changes with the ratio $d/\bar{\lambda}$. This correlates with equation (2) and it can be seen that $\tilde{K}$ reduces to $\tilde{K}_K$ at low pressures. This equation has been generalised by Carman and Arnell (1948) by the introduction of shape factors k_1 and k_o and the hydraulic radius (r_h) (defined in equation (14) Section 2.3) for application to capillaries of any cross sectional shape.

$$\tilde{K} = \frac{r_h^2 \bar{p}}{k_o \eta} + \frac{8 r_h}{3} \frac{\delta}{k_1} \left(\frac{2RT}{\pi M}\right)^{\frac{1}{2}} \qquad (10)$$

Another analysis of gas flow in this region has been made by Weber (1954) and reviewed by Barrer (1963).

In this analysis three flow components are identified:

i) Poiseuille flow

ii) Conduction flow (resulting from slippage at the walls)

iii) Diffusive flow (resulting from diffusion in a pressure gradient)

The resultant permeability is related to the Knudsen permeability

$$\tilde{K} = \tilde{K}_K \left\{ \frac{3\pi}{64} \frac{r}{\bar{\lambda}} + \frac{\pi}{4} \left[\frac{(2r/\bar{\lambda})}{1 + (2r/\bar{\lambda})} \right] + \left[\frac{1}{1 + (2r/\bar{\lambda})} \right] \right\} \qquad (11)$$

and it may be seen that

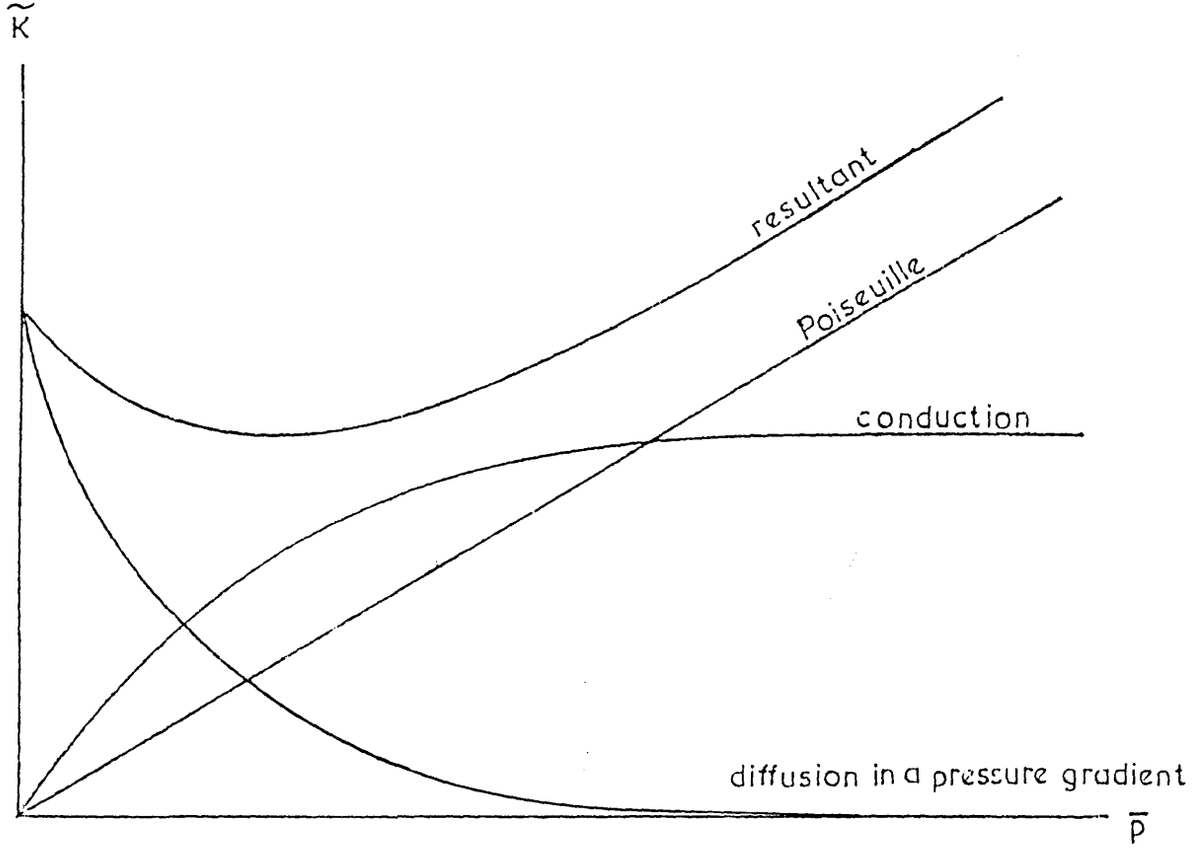
when $r/\bar{\lambda} \rightarrow \infty$ (high pressures)

then $\tilde{K} \rightarrow \tilde{K}_K \left(\frac{3\pi}{64} \frac{r}{\bar{\lambda}}\right)$ (Poiseuille flow) (12)

and when $r/\bar{\lambda} \rightarrow 0$ (low pressures)

then $\tilde{K} \rightarrow \tilde{K}_K$ (Knudsen flow) (13)

A schematic representation of the three components and resultant permeability is given in fig. 2.1. This analysis only applies when the pressure difference between ends of the capillary is small compared to the mean pressure, and other equations exist for different conditions (Ash Barrer and Nicholson 1963).



(fig 2·1) Schematic representation of Webers (1954) three flow components

2.3 Flow in a porous medium

Porous media differ from the uniform capillary tubes referred to in Section 2.2 in that passages through them may be tortuous, and non-uniform and a network of interconnected "blind" and "open" pores results. Those used in this study have been made by the compression of fine powders. The flow of gases through membranes fabricated in this manner may be described in terms of diffusion coefficients or permeability coefficients, which may then be interpreted in relation to the molecular properties of the diffusing gases and to the pore geometry of the medium. This involves the problem of relating the properties of a heterogeneous medium to those of its component phases. Many different models have been used to represent porous media, they include

i) a lattice of empty cubic cells joined into a network by narrower rectangular necks (Flood et al 1952)

ii) the 'dusty gas' model (Derjaguin and Bakanov 1957)

iii) capillary network models (Nicholson and Petropoulos 1971, 1973, 1975, 1984)

iv) Statistical Mechanical Models (Lee and O'Connell 1986)

The most frequently used model is that of a bundle of parallel cylindrical capillaries. While this is one of the simplest and least realistic models, it may however provide valuable information when utilized on a semi-empirical basis.

The "hydraulic radius" of the membrane r_h is defined as

$$r_h = \frac{\text{cross-sectional area of pores normal to direction of flow}}{\text{circumference of pores presented to gas}} \qquad (14)$$

for a cylindrical capillary this gives

$$r_h = \frac{\pi r^2}{2\pi r} = \frac{r}{2} \qquad (15)$$

for a porous membrane

$$r_h = \frac{\varepsilon}{A} \qquad (16)$$

where ε and A are the porosity ($m^3(m^3$ of membrane$)^{-1}$) and the surface area ($m^2(m^3$ of membrane$)^{-1}$) respectively. A tortuosity factor k_2 may also be defined as

$$k_2 = \frac{\text{length of kinked capillaries}}{\text{length of membrane}} \qquad (17)$$

Hence $\varepsilon = A_p k_2$ (18)

where A_p is now the cross-sectional area of all the pores traversing unit cross section of the bed.

Also $k_2^2 k_o = k$ (Kozeny constant $\simeq 5$) and $k_2^2 k_1 = k'$

Equation (10) then becomes

$$\tilde{K} = \frac{\varepsilon^3 \bar{p}}{A^2 \eta k} + \frac{8\delta}{3k'} \frac{\varepsilon^2}{A} \left(\frac{2RT}{\pi M}\right)^{\frac{1}{2}} \qquad (19)$$

(Carman and Arnell 1948)

Equation 19 may be written in the form

$$\tilde{K} = \tilde{K}_p \bar{p} + \tilde{K}_K \qquad (19a)$$

where $\tilde{K}_p$ is termed the Poiseuille Permeability and $\tilde{K}_K$ is the Knudsen permeability as defined in Section 2.2. If the ingoing pressure of gas is constant and the outgoing pressure close to zero (as in the "Conventional flow" conditions Section 2.4) then p_1 (the ingoing pressure) is approximately twice $\bar{p}$. The equation may then be written

$$\tilde{K} = \tilde{K}_p' \, p_1 + \tilde{K}_K' \qquad (19b)$$

where $\tilde{K}_p'$ is $\tilde{K}_p/2$ and $\tilde{K}_K'$ is the intercept at $p_1 = 0$ obtained by extrapolating the linear portion of the graph of $\tilde{K}$ versus p_1.

2.4 "Conventional flow" conditions: Steady state flow

This technique employs an ingoing pressure which is approximately constant (p_1) and an outgoing pressure (p_2) which is negligible in comparison with p_1. These conditions have been used in the majority of work originating from this laboratory. The boundary conditions are as follows

$$\begin{aligned} c(0,t) &= c^0 \text{ (constant)} \quad t > 0 \\ c(\ell,t) &= c^\ell(t) \ll c^0 \text{ for all } t > 0 \\ c(x,0) &= 0 \quad 0 < x < \ell \end{aligned} \qquad (20)$$

where the membrane is bounded by planes at $x = 0$ and $x = \ell$

c^0 is the ingoing concentration and c^ℓ the outgoing concentration.

The concentrations within the membrane may be divided into two components c_s, the Gibbs surface excess and c_g, the gas phase concentration (both in mol$(m^3$ porous media$)^{-1}$)

$$c = c_s + c_g \tag{21}$$

These may be related to more convenient quantities $c_s'/(\text{mol}(\text{m}^2 \text{ surface area})^{-1})$ and $c_g'/(\text{mol}(\text{m}^3 \text{ pore volume})^{-1})$ by the equations

$$c_g = \varepsilon c_g' \tag{22}$$

and $$c_s = A c_s' \tag{23}$$

c_g' may be calculated from the pressure (p/Nm^{-2}) of the gas, assuming ideality

$$c_g' = \frac{p}{RT} \tag{24}$$

Where R is the gas constant $(\text{JK}^{-1} \text{ mol}^{-1})$ and T, the temperature (K), and c_s' is related to c_g' via the adsorption isotherm. Hence the steady state flux $(J_\infty/\text{mols}^{-1})$ may be experimentally determined using the relationship

$$J_\infty = \frac{V}{RT_R} \cdot \frac{dp_2}{dt} \tag{25}$$

where $\frac{dp_2}{dt}$ $(\text{Nm}^{-2} \text{ s}^{-1})$ is the rate of increase of outgoing pressure, in the outgoing volume $V(\text{m}^3)$ when steady state flow has been achieved and T_R is the room temperature. The corresponding integral permeability $\tilde{K}/\text{m}^2 \text{ s}^{-1}$ is calculated using the equation

$$\tilde{K} = \frac{V}{T_R} \cdot \frac{\ell}{Ac} \cdot \frac{T}{p_1} \left[\frac{dp_2}{dt}\right] \tag{26}$$

Where T is the membrane temperature and Ac the cross-sectional area of the membrane.

2.5 Transient State Flow

The equations (25) and (26) relate to steady state flow, however after gas is admitted to the membrane at t = 0 for a while little or no gas appears at the outgoing face of the membrane. Then the rate of efflux builds up to a constant (steady state) value. Fig. 2.2a shows the form of the outgoing pressure versus time plot obtained. Extrapolation of the linear portion to cut the t axis gives an intercept (L) the "time-lag" of Barrer (1948) which is given by

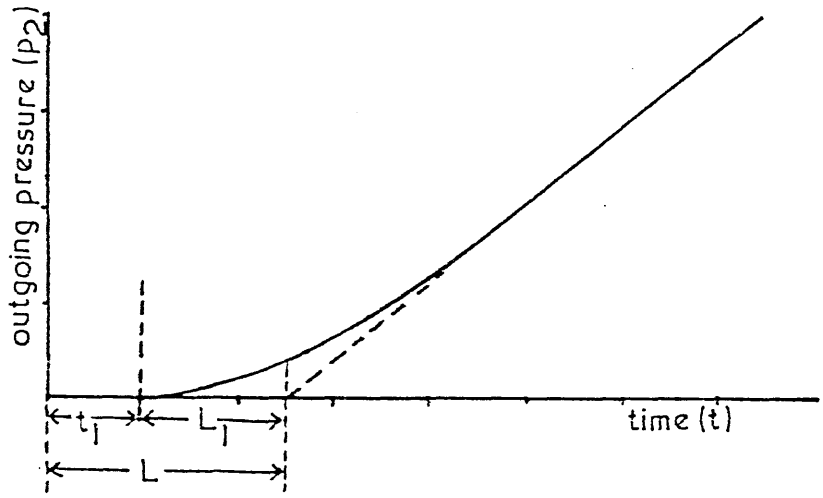
$$L = k_2^2 \ell^2/6D \qquad (27)$$

for the flow of a non sorbed gas, or for Henry Law adsorption. where D is the diffusion coefficient of the gas in the membrane.

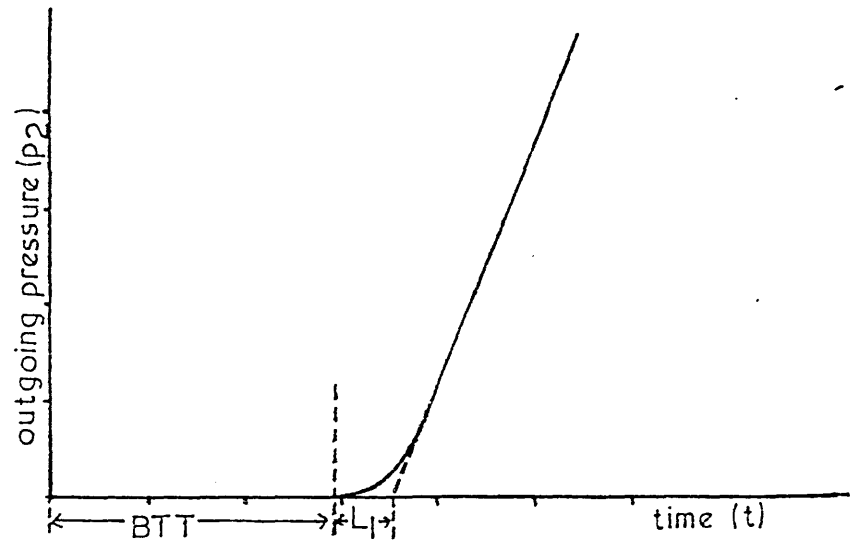
For the purposes of this study the time at which gas is detectable at the outgoing side of the membrane has been termed the "detection time" (t_1). In cases where $\frac{dp_2}{dt}$ increases quickly (Fig. 2.2b) after the detection time and the steady state value is soon obtained, the gas may be said to have "broken-through" the membrane and the term "breakthrough-time" (BTT) as used by Barrer (1954) may be applied to the detection time. Hence the total time lag (L) is given by

$$L = t_1 + L_1 \qquad (28)$$

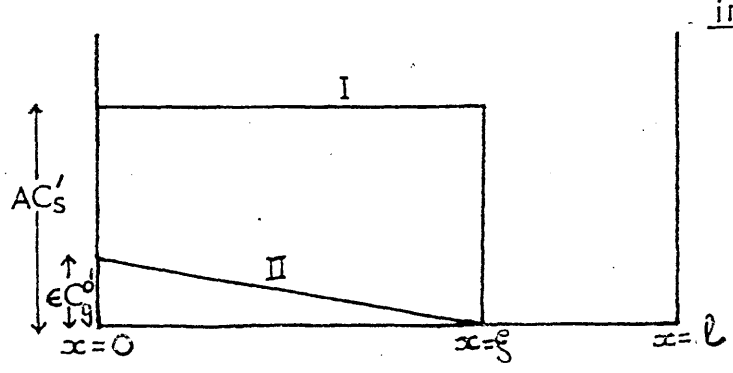
(fig 2·2 a) Detection time (t_l) and time lag (L)



(fig 2·2 b) A "true break-through time" (as Barrer 1954)



(fig 2·3) Gas concentrations in membrane for boundary conditions in equation (30)



At point ξ as a function of t, Curve I shows amount adsorbed per cm^3 of medium and Curve II, the amount in gas phase per cm^3 of medium

$$\text{or} \quad L = BTT + L_1 \tag{29}$$

where L_1 is the residual time lag, also shown in fig. 2.2.

2.5.1 Break-through time procedure

Barrer (1954) has developed an equation relating the product of the break-through time and the steady state flux to the surface concentration of adsorbed molecules $c_s'/\text{mol}(\text{m}^2 \text{ surface area})^{-1}$ for gas flow with adsorption where an immobile saturated monolayer of gas is laid down at all points reached by the diffusing gas. This condition is represented graphically in fig. 2.3.

For the boundary conditions

$$\begin{aligned} Ac_s' &= \text{const for } 0 < x < \xi \\ c_g'(0,t) &= c^0 \text{ (constant)} \quad t \geq 0 \\ c_g'(x,0) &= 0 \text{ for } 0 < x < \ell \\ c_g'(\xi,t) &= 0 \text{ for } 0 < \xi < \ell \end{aligned} \tag{30}$$

the equation of flow

$$D\, \partial^2 c_g'/\partial x^2 = \partial c_g'/\partial t \tag{31}$$

is satisfied by

$$c_g' = c_g^{o\prime} \left[1 - A \operatorname{erf}\left(\frac{x}{2\sqrt{Dt}}\right)\right] \tag{32}$$

where A is a constant. This satisfies the conditions at $x = \xi$ (i.e. $c_g' = 0$), if $A \operatorname{erf} Z = 1$ (where $Z = \frac{\xi}{2\sqrt{Dt}}$). Hence Z must be

constant and

$$c_g' = c_g^{o'} \left[1 - \frac{\text{erf}(x/(2\sqrt{Dt}))}{\text{erf } Z} \right] \tag{33}$$

The flux per unit area (J_A) at $x = \xi$ can be found from equation (33) by differentiation using the "function of a function" rule

$$J_A = -D\left(\frac{\partial c_g}{\partial x}\right)_{\xi} = -\varepsilon D\left(\frac{\partial c_g'}{\partial x}\right)_{\xi} \tag{3}$$

$$\Longrightarrow \frac{\partial c_g'}{\partial x} = -\frac{\varepsilon c_g^{o'}}{\text{erf } Z} \cdot \frac{1}{\sqrt{\pi}} \left[\exp\left(\frac{-x^2}{4Dt}\right) \right] \cdot \frac{1}{\sqrt{Dt}} \tag{34}$$

$$J_A = \frac{\varepsilon c_g^{o'} D}{\sqrt{\pi D}\,\text{erf } Z \exp Z^2} \cdot \frac{1}{\sqrt{t}} \equiv \frac{\alpha}{\sqrt{t}} \tag{35}$$

Conservation of mass at $x = \xi$ gives

$$J_A = \frac{\alpha}{\sqrt{t}} = Ac_s' \frac{d\xi}{dt} \tag{36}$$

$$\alpha \int_o^t \frac{dt}{\sqrt{t}} = Ac_s' \int_o^t \frac{d\xi}{dt}\, dt = Ac_s' \int_o^{\xi} d\xi$$

$$\text{i.e. } 2\alpha t = Ac_s'\xi \quad \text{or} \quad \xi = \frac{2\alpha\sqrt{t}}{Ac_s'} \tag{36a}$$

By substitution of equation (36a) into equation (35) and using $Z = \xi/2\sqrt{Dt}$ the relation

$$Z\,\text{erf}Z \exp Z^2 = \varepsilon c_g^{o'}/A c_s' \sqrt{\pi} \tag{37}$$

is obtained.

At breakthrough time t = BTT, and $\xi = \ell$

$$Z^2 = \frac{\ell^2}{4D(BTT)}$$

For systems in which a true break-through, similar to that of Barrer (1954) has occurred as assumed above (fig. 2.2b). Then $\varepsilon c_g^{o'}$ is much less than Ac_s' and L approximates to BTT. The steady state distribution in the gas phase is then nearly maintained so that equation (33) can be replaced by

$$c_g' = c_g^{o'} \left(1 - \frac{x}{\xi}\right) \tag{33a}$$

in this case $J_A = -D\left(\frac{\partial c}{\partial x}\right)_\xi = +\frac{\varepsilon c_g^{o'} D}{\xi}$ (35a)

and $Ac_s' \left(\frac{d\xi}{dt}\right) = +\frac{\varepsilon c_g^{o'} D}{\xi}$

$$\text{giving } \frac{D}{\xi} = \frac{A c_s'}{\varepsilon c_g^{o'}} \left(\frac{d\xi}{dt}\right) \tag{36b}$$

at t = BTT, $\xi = \ell$ and $J_A = J_{A\infty}$, hence integration of (36b) gives

$$BTT = \frac{A c_s' \ell^2}{2\varepsilon c_g^{o'} D} \tag{40}$$

and

$$J_{A\infty} \cdot BTT = Ac_s' \ell/2$$

A system in which surface diffusion occurs may be approached by

considering the adsorbed film to comprise an immobile saturated monolayer and a weakly-adsorbed mobile second layer of concentration c_{s2}' which is proportional to the gas phase concentration ($c_{s2}' = k_{s2}\, c_g'$).

The diffusion coefficient in this layer is then D_{s2}. In this case the diffusion equation may be written as

$$\frac{\partial(c_g' + c_g' k_{s2}\, A/\varepsilon)}{\partial t} = \frac{D\,\partial^2 c_g'}{\partial x^2} + D_{s2}\, k_{s2}\, A/\varepsilon \left(\frac{\partial^2 c_g'}{\partial x^2}\right) \qquad (42)$$

$$\text{or} \quad (1 + Ak_{s2}/\varepsilon)\frac{\partial c_g'}{\partial t} = D\left(1 + \frac{Ak_{s2}}{\varepsilon}\,\frac{D_{s2}}{D}\right)\frac{\partial^2 c_g'}{\partial x^2} \qquad (43)$$

By defining

$$D_1' \equiv D\,\frac{(1 + D_{s2}\, k_{s2}\, A/D\varepsilon)}{(1 + k_{s2}\, A/\varepsilon)} \qquad (44)$$

equation (42) may be reduced to

$$\frac{\partial c_g'}{\partial t} = D_1'\,\frac{\partial^2 c_g'}{\partial x^2} \qquad (45)$$

Using the simplified procedure and equation(33)(above) the flux may be obtained as before

$$J_A = -\varepsilon\left(1 + \frac{Ak_{s2}}{\varepsilon}\right) D_1' \left(\frac{\partial c_g'}{\partial x}\right)_\xi \qquad (35b)$$

$$= \frac{\varepsilon c_g^{o'} (1 + Ak_{s2}/\varepsilon) D_1'}{\xi}$$

$$= A c_s' \frac{\partial \xi}{\partial t}$$

giving $$D_1' = \frac{A c_s'}{\varepsilon c_g^{o'} (1 + Ak_{s2}/\varepsilon)} \frac{\partial \xi}{\partial t} \qquad (36b)$$

at $\xi = \ell$ and $t = BTT$ this gives

$$BTT = \frac{A c_s' \ell^2}{2\varepsilon c_g^{o'} (1 + Ak_{s2}/\varepsilon)} \cdot \frac{1}{D_1'} \qquad (40a)$$

and hence $$J_{A^\infty} . BTT = A c_s' \ell/2 \qquad (41)$$

which is the result obtained when surface diffusion is not taken into account.

Finally the same equation (41) may be obtained for a system which possesses combined Knudsen and Poiseuille flow in the gas phase as well as a mobile weakly adsorbed second layer.

In this case it it is assumed that, $\varepsilon c^{o'} (1 + Ak_{s2}/\varepsilon)$ is much less than Ac_s' and so the steady state is nearly maintained in the gas phase and the mobile second layer. The diffusion coefficient for Poiseuille flow D_p is defined

$$D_p \frac{\partial^2 c_g^2}{\partial x^2} = \frac{\partial c_g}{\partial t} \qquad (45)$$

and the same procedure followed resulting again in equation (41)

$$J_{A\infty}.B.TT = \ell A c_s'/2$$

This equation has been applied to the results obtained in this study for gas flow through NaX and CMS membranes Section 5.2.5.

2.5.2 Time-lag Equation

An expression for the time-lag (L) (as defined in Section 2.5 (fig. 2.2)) of an adsorbable gas flowing through a membrane has been developed by Mr. R. Ash (1986) for systems obeying the Langmuir equation. (Langmuir 1916, 1918) and for the absence of "extra" flow.

$$\frac{\nu}{\nu_m} = \frac{bp}{1 + bp} \qquad (46)$$

Where ν = the volume of gas adsorbed, ν_m = monolayer capacity, p = the equilibrium pressure and b = a constant. The time lag is expressed in terms of b, ν_m, which may be obtained from the adsorption isotherm, ingoing pressure p_1, the Knudsen permeability $\tilde{K}_K'$ and the Poiseuille permeability $\tilde{K}_p'$ which may be obtained from steady state flow experiments using the Carman-Arnell equation, in the form (19b) by plotting $\tilde{K}$ versus p_1.

$$\tilde{K} = \tilde{K}_p' p_1 + \tilde{K}_K' \qquad (19b)$$

The full derivation of this expression for L is rather lengthy, and will therefore not be included. However, since this work has not been published elsewhere, an outline of the method used will be given in the following pages.

The mass balance equation $\frac{\partial c}{\partial t} = (-)\frac{\partial J}{\partial x}(x,t)$ (A1)

the relationship between flux per unit cross-section and the differential permeability

$$J(xt) = (-)\ K \frac{\partial c_g'}{\partial x} \tag{A2}$$

and ideality of the gases used:

$$c_g' = p/RT \tag{A3}$$

are initially assumed. Combination of equations (A1) to (A3) then gives:

$$\frac{\partial c}{\partial t} = \frac{\partial}{\partial x}\left\{\frac{K}{RT}\ \frac{\partial p}{\partial x}\right\} \tag{A4}$$

Integration of equation (A4) from x to ℓ following the method of Frisch (1957) gives

$$\int_x^{\ell} \frac{\partial c}{\partial t}\, dx = \frac{1}{RT}\left[\int_x^{\ell} K(p)\frac{\partial p}{\partial x}\right] \tag{A5}$$

$$= -J(\ell,t) - \frac{K(p)}{RT}\frac{\partial p}{\partial x} \tag{A5}$$

A second integration between 0 and ℓ gives

$$\int_0^{\ell}\int_x^{\ell} \frac{\partial c}{\partial t}\, dx dx = -\ell.J(\ell.t) - \int_0^{\ell} \frac{K(p)}{RT}\frac{\partial p}{\partial x}\, dx \tag{A6}$$

$$= -\ell.J(\ell,t) + \int_0^{p_0} \frac{K(p)}{RT}\, dp \tag{A7}$$

(where p_0 = ingoing pressure)

Hence

$$J(\ell,t) = \frac{1}{\ell RT} \int_0^{p_o} K(p)\, dp - \frac{1}{\ell} \int_0^{\ell} \int_x^{\ell} \frac{\partial c}{\partial t}\, dx\, dx \qquad (A8)$$

and using $J_\infty = -\frac{K(p)}{RT} \frac{dp(x)}{dx} = \frac{1}{\ell RT} \int_0^{p_o} K(p)\, dp$ (A9)

equation (A8) becomes

$$J(\ell,t) = J_\infty - \frac{1}{\ell} \int_0^{\ell} \int_x^{\ell} \frac{\partial c}{\partial t}\, dx\, dx \qquad (A10)$$

The quantity of gas exiting the membrane $Q(\ell,t)$ is then given by the expression

$$Q(\ell,t) = \int_0^t J(\ell,t)\, dt = J_\infty t - \frac{1}{\ell} \int_0^t \int_0^{\ell} \int_x^{\ell} \frac{\partial c}{\partial t}\, dx\, dx\, dt \qquad (A11)$$

$$= J_\infty t - \frac{1}{\ell} \int_0^{\ell} \int_x^{\ell} c(x,t)\, dx\, dx \qquad (A12)$$

For large t, $Q(\ell,t) \rightarrow Q_\infty(\ell,t) = J_\infty(t - L)$ (A13)

where L is the time lag

Hence from equation (A12) and (A13)

$$J_\infty . L = \frac{1}{\ell} \int_0^\ell \int_x^\ell c(x)\, dx\, dx \tag{A14}$$

$$\text{hence } L = \int_0^\ell \int_x^\ell c(x)\, dx\, dx / (\ell\, J_\infty) \tag{A15}$$

and using equation (A9)

$$L = \frac{RT \int_0^\ell \int_x^\ell c(x)\, dx\, dx}{\int_0^{p_o} K(p)\, dp} \tag{A16}$$

Integration by parts of the numerator, then gives

$$L = RT \int_0^\ell x\, c(x)\, dx \Big/ \int_0^{p_o} K(p)\, dp \tag{A17}$$

c(x) may be written in terms of the gas phase and surface phase concentrations

$$\begin{aligned} c(x) &= c_g(x) + c_s(x) \\ &= \varepsilon\, c_g'(x) + A\, c_s'(x) \\ &= \varepsilon \frac{p(x)}{RT} + A \frac{c_m' \, b\, p(x)}{1 + b\, p(x)} \end{aligned} \tag{A18}$$

$$\text{hence } \int_0^\ell x\, c(x)\, dx = \int_0^\ell x \left\{ \frac{\varepsilon}{RT}\, p(x) + A\, c_m' \frac{b\, p(x)}{1 + b\, p(x)} \right\} dx \tag{A19}$$

$$= \frac{\varepsilon}{RT} \int_0^{\ell} x\, p(x)\, dx + A\, b\, c_m' \int_0^{\ell} x \frac{p(x)}{1 + b p(x)}\, dx$$

(A20)

Equation (A20) may then be transformed to

$$\int_0^{\ell} x\, c(x)\, dx = \frac{\frac{\varepsilon}{RT} \int_0^{\ell} \ell p(x) \int_{p(x)}^{p_o} K(u)\, du\, dx}{\int_0^{p_o} K(u)\, du} + \frac{Ab\, c_m' \int_0^{\ell} \ell \frac{p(x)}{1+bp(x)} \int_{p(x)}^{p_o} K(u)\, du\, dx}{\int_0^{p_o} K(u)\, du}$$

(A21)

$$= \frac{\varepsilon}{RT}\, \ell^2 \frac{\int_0^{p_o} wK(w) \int_w^{p_o} K(u)\, du\, dw}{\left(\int_0^{p_o} K(u)\, du\right)^2} + Abc_m'\, \ell^2 \frac{\int_0^{p_o} \frac{wK(w)}{1+bw} \int_w^{p_o} K(u)\, du\, dw}{\left(\int_0^{p_o} K(u)\, du\right)^2}$$

(A22)

using the relationships

$$\frac{x}{\ell} \int_0^{p_o} K(u)\, du = \int_{p(x)}^{p_o} K(u)\, du$$

and $$\frac{-\ell . K(p)}{\int_0^{p_o} K(u)\, du} \cdot \frac{dp}{dx} = 1$$

Substitution of equation (A22) into equation (A17) then gives

$$L = \varepsilon l^2 \frac{\int_o^{p_o} wK(w) \int_w^{p_o} K(u)\, du\, dw}{\left(\int_o^{p_o} K(u)\, du\right)^3} + \text{ART. } bc_m' \ell^2 \frac{\int_o^{p_o} \frac{wK(w)}{1+bw} \int_w^{p_o} K(u)\, du\, dw}{\left(\int_o^{p_o} K(u)\, du\right)^3} \qquad \text{(A23)}$$

The Carman-Arnell equation is written

$$K(u) = \tilde{K}_K' (1 + \alpha u) \quad \text{where} \quad \alpha = \tilde{K}_p / \tilde{K}_{K'} \qquad \text{(A24)}$$

so that

$$\int_w^{p_o} K(u)\, du = \tilde{K}_K' p_o\left(1 + \frac{\alpha}{2} p_o\right) - \tilde{K}_K' w \left(1 + \frac{\alpha}{2} w\right) \qquad \text{(A25)}$$

The integrals from equation (A23) are of standard form and are readily evaluated (Dwight 1947).

The resulting expression

$$L = \frac{\varepsilon \ell^2 \{1/6 + 5\theta/12 + 4\theta^2/15\}}{\tilde{K}_K' (1+\theta)^3}$$

$$+ \frac{\ell^2 b c_m' ART}{\tilde{K}_K' y^5 (1+\theta)^3} \left\{ \left[(y^3(y+2)/2) - y^2(1+y)\, \ell n(1+y) \right] \right.$$

$$+ \theta \left[(y^2(2y+3)(y-2)/2) + y(y+1)(3-y)\, \ell n(1+y) \right]$$

$$\left. + \theta^2 \left[y\left(\frac{y^3}{2} - \frac{4y^2}{3} - y + 2\right) + 2(y^2-1)\, \ell n(1+y) \right] \right\}$$

where $y = bp_1$ and $\theta = \tilde{K}_p' . p_1 / \tilde{K}_K'$

Equation 26 should predict the time lag, regardless of the rectangularity of the adsorption isotherm, provided the system exhibits adsorption of a Langmuir type and conforms to the Carman-Arnell equation for combined Knudsen and Poiseuille flow.

2.6 Flow of Sorbed Gases

In some systems flow greater than that expected for pure gas phase transport occurs. This has been discussed in reviews by Carman (1956), Barrer (1979) and Kammermeyer (1975). In such cases the extra flux is associated with transport of molecules in the adsorbed phase and hence the total flux may be divided into J_g, the component due to Knudsen flow and J_s, the component due to extra flow (or "surface flow").

$$J_\infty = J_g + J_s \tag{46}$$

The integral steady state permeabilities relating to these flux componenets may then be defined

$$\tilde{K} = \frac{J}{A_c} \cdot \frac{l}{\Delta c_g'} \qquad \text{(total permeability)}$$

$$\tilde{K}_g = \frac{J_g}{A_c} \cdot \frac{l}{\Delta c_g'} \qquad \text{(gas phase permeability)} \qquad (47)$$

$$\tilde{K}_s = \frac{J_s}{A_c} \cdot \frac{l}{\Delta c_g'} \qquad \text{(extra permeability)}$$

and hence

$$\tilde{K} = \tilde{K}_g + \tilde{K}_s \qquad (48)$$

It has been proved (Ash Barrer and Lowson 1973) that in the temperature range 78K to 573K He may be considered a non sorbed gas, and it may therefore be used for the evaluation of $\tilde{K}_g$ using the equation

$$\tilde{K}_g = \tilde{K}_{He} \left(\frac{M^{He}}{M}\right)^{\frac{1}{2}} \qquad (49)$$

where M^{He}, M are molar masses and $\tilde{K}_{He}$ is the experimental He permeability at the temperature of the $\tilde{K}$ determination. This technique may be used to evaluate the purely gas phase flow of a sorbable gas and hence the extra flow component. Helium can also be used in binary mixture experiments, as a non-sorbed indicator to evaluate the degree of blockage of the gas phase by an adsorbed film of the sorbable component. (Ash Barrer and Pope, 1963b, Ash Barrer and Lowson 1973, Ash Barrer and Sharma 1976, Hamilton 1980).

Employing Ficks equation (3)

$$\frac{J_\infty}{A_c} \equiv - D \frac{dc}{dx} \tag{3}$$

the overall differential diffusion coefficient D may be defined. An integral diffusion coefficient $\tilde{D}$ may also be defined by

$$\frac{J_\infty}{A_c} \equiv \tilde{D} \frac{\Delta c}{\ell} = \tilde{D} \frac{c^o}{\ell} \tag{50}$$

$$\text{where } \tilde{D}(c^o) = \frac{1}{c^o} \int_o^{c^o} D(c)\, dc \tag{51}$$

$$\text{and hence } D(c^o) = \tilde{D}(c^o) + c^o \left(\frac{\partial \tilde{D}}{\partial c^o}\right) \tag{52}$$

Upon integration of equation (3) under the boundary conditions employed in steady state flow (equation 20)

$$\frac{J_\infty}{A_c} = \frac{1}{\ell} \int_o^{c^o} D\, dc \tag{53}$$

is obtained which yields upon differentiation

$$D(c^o) = \frac{\ell}{A_c} \left(\frac{\partial J_\infty}{\partial c^o}\right) , \tag{54}$$

the form of the equation which has been used in this study to obtain values of D.

Diffusion coefficients for gasphase flow and extra flow may

be defined in the same manner as those for the total flow.

The differential diffusion coefficient for gas phase flow D_g is defined by

$$\frac{J_g}{A_c} \equiv - D_g \frac{dc_g}{dx}$$

Integrating over the range x = 0 to x = ℓ this becomes

$$\frac{J_g}{A_c} = \frac{1}{\ell} \int_0^{c_g^{o'}} D_g \, dc_g' \qquad (58)$$

where $c_g^{o'}$ = gas phase concentration at x = 0.

This may be expressed in terms of $\tilde{K}_g$ using equation (47)

$$\tilde{K}_g = \frac{1}{c_g^{o'}} \int_0^{c_g^{o'}} \varepsilon D_g \, dc_g' \qquad (59)$$

$\tilde{K}_g$ has been shown by use of He to be independent of concentration for the Graphon and Carbolac membranes, therefore D_g must also be independent and the equation (59) may be written in the form

$$\tilde{K}_g = \varepsilon D_g \qquad (60$$

2.7 Relevant Adsorption Background

Adsorption studies were made in order to facilitate interpretation of the flow results and were not therefore the main purpose of the

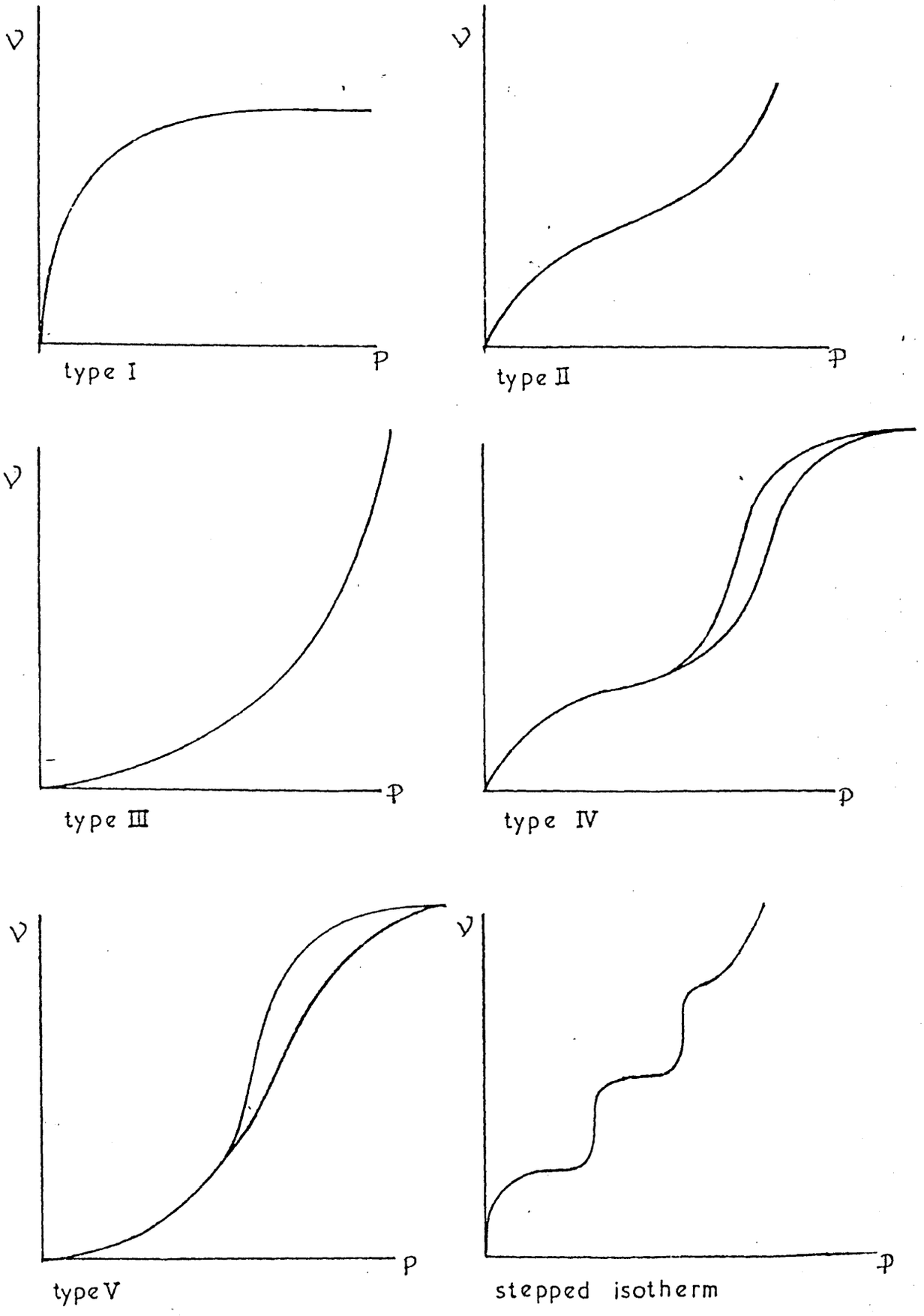
experimental work. For this reason only a brief summary of relevant theory will be given.

Adsorption is a consequence of the surface forces (physical or chemical) of a solid, attracting molecules of a gas or vapour. This results in physical adsorption as observed in this study, or chemisorption. As stated in Section 2.6 some systems exhibit a considerable extra flux due to adsorbed molecules, and (as shown in Section 2.5.2 and Section 2.5.3) the transient state of flow is also dependent upon the degree of adsorption. Therefore, knowledge of the adsorption isotherm and derived quantities are instrumental in the interpretation of flow data.

The adsorption isotherm is a plot of the amount adsorbed $\nu/(cm^3\ STP\ g^{-1})$ as a function of the equilibrium gas phase concentration $c_g'(mol\ m^{-3})$ or more normally the equilibrium pressure (p/cm Hg) for an ideal gas). The isotherm shape may vary but the majority can be grouped into five classes (Brunauer, Emmett and Teller 1938) shown in fig. 2.4.

Isotherms of type I are usually analysed in terms of the Langmuir model which assumes that the gas molecules are adsorbed onto definite sites on the surface of the adsorbent, that each site can accommodate only one adsorbed molecule, and that no molecular interactions occur between adsorbed molecules. This model was initially developed for an open surface; however many microporous adsorbents also yield this type of isotherm due to the filling of pores with gas molecules, hence yielding

(fig 2·4) Adsorption isotherm types BET classification (type)



an occlusion volume, rather than a monolayer capacity.

The Langmuir equation

$$\frac{\nu}{\nu_m} = \frac{bp}{1+bp} \tag{61}$$

was originally derived kinetically (Langmuir 1918), however a statistical derivation has been given by Fowler.

The BET model which is commonly used in the analysis of type II/type IV isotherms is based on the Langmuir model, however it allows for multilayer adsorption, whereas the Langmuir equation allows only for monolayer coverage.

The model, first developed by Brunauer Emmett and Teller (1938) assumes that

a) in all layers except the first the heat of adsorption is equal to the molar heat of condensation q_L.

b) that in all layers except the first evaporation-condensation conditions are identical

c) that when the saturated vapour pressure is reached the sorbate condenses to a bulk liquid on the surface of the solid.

The resulting equation is

$$\frac{p}{\nu(p^o - p)} = \frac{1}{\nu_m c} + \frac{c - 1}{\nu_m c}\,\frac{p}{p^o} \tag{62}$$

where p^o = the saturated vapour pressure and c = a constant.

Values of the monolayer capacity v_m may be obtained from either equation (61) or (62) from which, knowing the area of an adsorbed molecule, the surface area of the adsorbent may be calculated.

Type III/type V isotherms may not be analysed by any such simple procedure. Gregg and Sing (1982) conclude that the BET procedure for the evaluation of monolayer capacity is not applicable to type III or type V isotherms. The method of analysis adopted in this study is that of Beebe et al 1964. It utilizes an equation for localised monomolecular adsorption which allows approximately for adsorbate-adsorbate interaction.

$$\frac{p}{p_o} = \frac{\theta}{K_1(1 - \theta)} e^{-K_m\theta} \qquad (63)$$

where θ= coverage = v/v_m, K_1 = the adsorbate-adsorbent equilibrium constant and K_m = w/kT where w is the interaction energy between a pair of neighbouring adsorbate molecules.

The equation was derived using statistical mechanics by Fowler (1936) and is used in the form

$$\ell n\left(\frac{\theta}{1-\theta}\right) - \ell n\left(\frac{p}{p_o}\right) = \ell n\ K_1 + K_m\theta \qquad (64)$$

$\ell n\left(\frac{\theta}{1-\theta}\right) - \ell n\left(\frac{p}{p_o}\right)$ is plotted against θ for various values

of the monolayer capacity (ν_m) (and hence the area occupied by an adsorbed molecule (a_m)) and the value giving the best straight line is assumed to be the correct one. In this way the monolayer capacity for systems exhibiting type III isotherms may be determined if the surface area is already known.

For all types of adsorption isotherm the isosteric heat of adsorption, $q_{ST}(J\ mol^{-1})$ can be calculated from isotherms measured over a range of temperatures. A Clausius-Clapeyron type relationship to the isotherm at constant coverage is used:

$$q_{ST} = - R \left[\frac{\partial\ \ell n\ p}{\partial\ 1/T} \right]_{\nu}$$

The heat of adsorption is generally expected to alter significantly in the vicinity of monolayer coverage, decreasing to a value approaching that of the heat vapourisation.

This variation is caused by the joint effects of, the energetic non-uniformity of the adsorbent surface and the interaction of adsorbate molecules in the adsorbed film itself.

Chapter 3 Experimental

3.1 The Membranes

Membrane materials 3.1.1 Zeolite NaX

3.1.2 Carbon molecular sieve

3.1.3 Carbolac

3.1.4 Graphon

3.1.5 Membrane construction

3.1.6 Outgassing procedure

3.2 The Gases

3.2.1 Gas suppliers and purity

3.2.2 Gas bottling apparatus

3.2.3 Precautions taken with H_2S usage

3.3 General Features of High Vacuum Apparatus

3.3.1 Pumping system

3.3.2 Temperature control

3.3.3 Temperature measurement

3.3.4 McLeod gauges

3.4 Adsorption Isotherm Determination

McBain balance 3.4.1 Description of apparatus

3.4.2 Experimental technique

3.4.3 Volumetric adsoprtion apparatus

3.5 Isothermal Flow Apparatus

Isothermal flow apparatus for single gases

(Molecular sieve membranes) 3.5.1 Description of apparatus

3.5.2 Experimental technique

Isothermal flow apparatus for binary mixtures

3.5.3 Description of apparatus

3.5.4 The circulating pump

3.5.5 Experimental technique

3.1 Membrane Materials

Four different membrane materials with widely varying physical characteristics were chosen for study. They were Zeolite NaX, a molecular sieve carbon, Carbolac carbon, a high surface area channel black and Graphon carbon, a graphitised form of channel black Spheron 6.

3.1.1 Zeolite NaX

NaX is a synthetic form of the naturally occurring mineral faùjasite; it is a crystalline compound with unit cell formula

$$(Na^{+})_{81}(H_3O^{+})_5(AlO_2^{-})_{86}(SiO_2)_{106}(H_2O)_{262}.$$

Alumino Silicates are composed of SiO_4^{4-} and AlO_4^{5-} tetrahedra which are linked through common oxygen atoms and may exhibit various structural characteristics. Depending upon the way in which the tetrahedra are joined, three different classes of zeolite may be identified:-

1. Fibrous Zeolites, e.g. natrolite in which linkages of the tetrahedra are more numerous in one crystallographic direction than in the plane at right angles to it.
2. Lamellar Zeolites e.g. stilbite montmorillonite in which structural linkages are more numerous in one plane than in the direction perpendicular to it.
3. Three dimensional network zeolites e.g. faùjasite, mordenite, chazabite, in which, binding is equally strong in all directions.

(Barrer 1978)

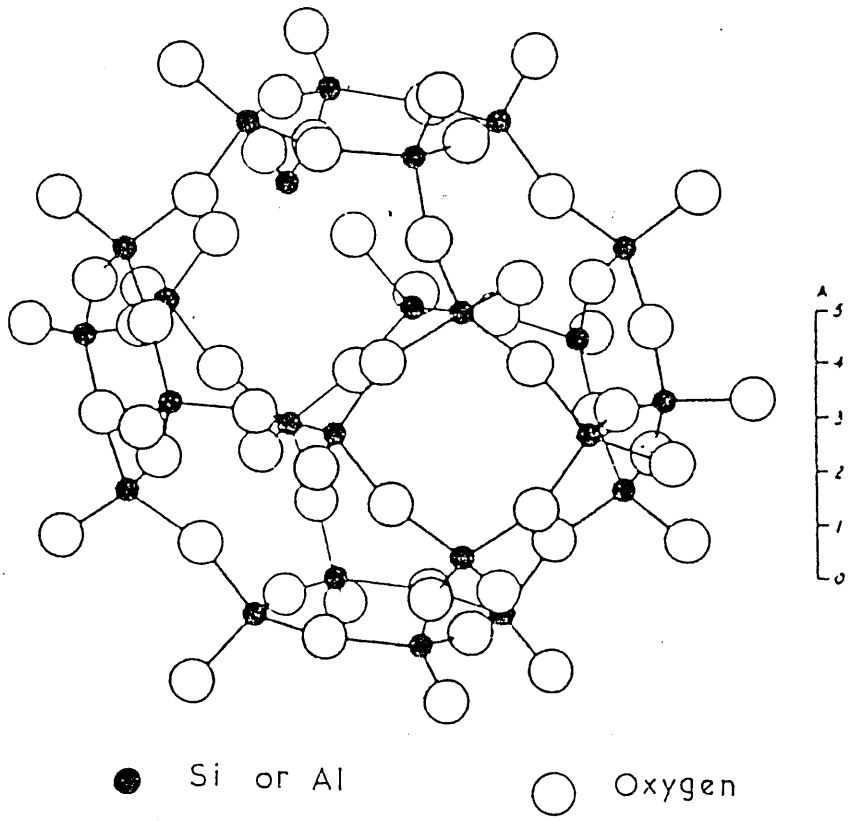
NaX and related zeolite NaY have topographically similar aluminosilicate framework structures but differ in the SiO_2:Al_2O_3 ratio. It has been shown (Freeman and Stamires 1961) that the SiO_2:Al_2O_3 ratio varies uniformly between 2.1 and 5.2. The X form has been designated a ratio between 2.1 and 3.0 and the Y form from 3.0 to 5.2.

The main structural characteristic of this type of zeolite is the arrangement of octahedral sub units, called Sodalite cages, in a tetrahedral array see fig. 3.1. The sodalite cages are linked together, by hexagonal prism, subunits comprising $12(Si,Al)O_4$ tetrahedra. Thus three types of cavity exist in the lattice (Dwyer and Dyer 1984).

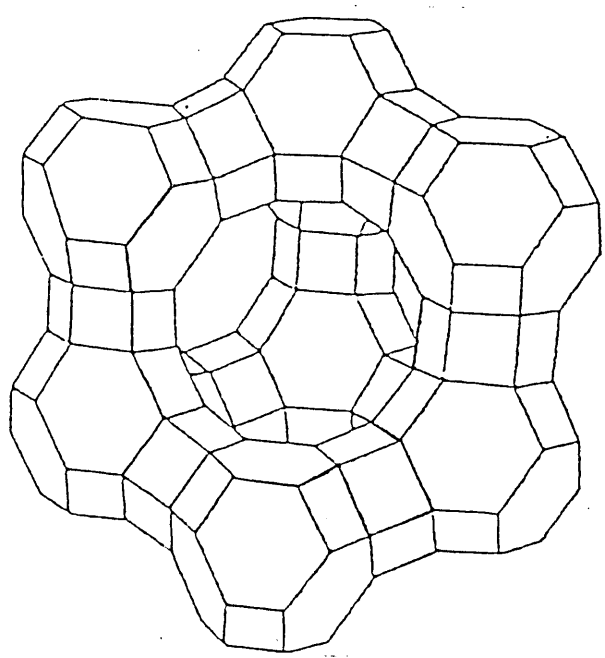
1. "super cages" between the octahedral subunit of diameter 12 - 13 Å, joined tetrahedrally through windows of diamter 7.5 Å.
2. Sodalite cages, octahedra of diameter 6.6 Å
3. Hexagonal prisms, connecting octahedral subunits diameter 2.2 Å.

Unless dehydrated, faujasite-type zeolites contain about 235 water molecules per unit cell, distributed throughout the super cages and the sodalite cages. The position of the sodium ions in NaX, vary with the degree of hydration and it has been suggested that there may be as many as six different types of cation site (Breck 1974) The sample of zeolite NaX used in this study was supplied by Linde Air Products Ltd.

(fig 3·1) A Sodalite Cage



The Structure of Zeolite X



Characteristics of this material may be found in table 3.1.

3.1.2 Carbon molecular sieve (CMS)

The carbon molecular sieve was produced by Bergbau-Forshung GmbH (Juntgen et al 1981) using a process claimed to produce a "uniform material" of narrow pore size distribution.

The original material used in the manufacturing process was bituminous coal, which was ground to grain size of less than 40 μm. The pulverised coal was then oxidised in air using a fluidized bed at temperatures below the ignition temperature, formed into pellets 2 to 3 mm long and carbonized in a rotary drum. This procedure produced a 'uniform starting material which could then be activated to give the desired characteristics'. The carbon molecular sieve used in this study had been treated under cracking conditions for hydrocarbons, thus depositing carbon at the mouths of the pores. It is currently used for the recovery of Nitrogen from air. The carbon may also be activated using steam and a product manufactured in this way may be used for He or H_2 recovery from coke gas.

Clear evidence of the molecular sieving property of carbons was first observed by Franklin (1945 who found that fluids were excluded from heat treated coals in order of molecular size. Dacey and Thomas (1954) later published a through study of the molecular sieve properties of polyvinylidene charcoal. Since then much investigation of carbon molecular sieves produced by the pyrolysis of polymers has taken place.

Koresh and Soffer (1980) have shown that it is possible to close pores by high temperature sintering or to widen them by oxidative burn off or by treatment with nitric acid (Barton and Koresh 1983). In a recent investigation (Koresh and Soffer 1983) it has been proved that the pore dimensions of a carbon membrane may be adjusted by simple thermochemical treatments in order to achieve optimal separation power.

3.1.3 Carbolac

Carbolac is a carbon black which has small highly divided particles and hence a very high surface area. It was primarily produced for pigmenting high quality black lacquers and is manufactured by the partial combustion of natural gas, followed by treatment with air at $538^{o}C$, to increase the amount of chemisorbed oxygen on the surface. The sample used in this study was supplied by Godfrey L. Cabot Inc.

Xray crystallographic examination of carbon blacks such as Carbolac has showed the existence of well defined layer planes similar to those in graphite but with more random orientation. (Briscoe and Warren 1942). These are piled in stacks (three to five layers deep) called crystallites,in which the layer planes are parallel to and equidistant from each other. The crystallites in turn are aggregated forming black spheroidal particals.Electron microscopic studies show individual particles to have a mean diameter of 100 $\overset{o}{A}$ (Smith 1961) and by comparing this data with the measured BET surface area of approximately 1000 $m^2 g^{-1}$ for Carbolac it may be deduced that internal surfaces account for a considerable

proportion of the total surface area. Dacey (1967) gives a value of 0.17 $cm^3 g^{-1}$ as the internal pore volume from which he calculates a value of 8.5 Å for the internal pore radius.

The nature of the surface of Carbolac has been investigated by thermal decomposition (Anderson and Emmett 1952). The gases evolved in this process included H_2, CO_2 and CO and the existence of a monomolecular layer of chemisorbed oxygen atoms on the carbon surface was suggested.

3.1.4 Graphon

Graphon is a graphitised carbon black, formed by heating channel black Spheron 6 to between 2700° C and 3000° C. Before graphitisation the crystallites in Spheron 6 are ordered according to the "concentric crystallite" model (Harling and Heckman 1966). This postulates an outer shell of larger more perfect crystallites with layer planes orientated parallel to the particle surface and a less well ordered centre portion.

During graphitisation changes in crystallite size and orientation occur (Hess et al 1968). The crystallites increase in size and become more uniform and when the layer diameter increases to above 10 nm the layers begin to position themselves as in Graphite. The outer shell of the particle becomes thicker and more complete leaving a void in the centre.

This graphitisation produces a carbon with particles of regular size and shape, with considerably less surface area than a

non graphitised material. The Graphon used in this study was supplied by Godfrey L Cabot Inc. Details are given in table 3.1.

Table 3.1 Membrane Material Characteristics

i) Molecular Sieves

	NaX	Carbon Molecular Size
Equivalent Surface Area/m^2 g^{-1}	-	510 (this study)
Void Volume/ cm^3 g^{-1}	0.296 (Breck 1974)	.169 (this study)
Porosity m^3/m^{-3}_o	0.500 (Breck 1974)	
Pore diameter/A	7.5 (Breck 1974)	2.8 - 3.0 (this study)
Density/g cm^{-3}	1.93 (Breck 1974)	1.44 (this study)

Table 3.2 Membrane Material Characteristics

ii) Carbons

	Carbolac	Graphon
Surface Area (N_2)/m^2 g^{-1}	950 (Lowson 1968)	89.7 (Hamilton 1980)
He Density/g cm^{-3}	2.12 (Lowson 1968)	1.97 (Hamilton 1980)
Particle size/mμ	3.5 (Lowson 1968)	36 (Cabot Inc.)
pH	3.0 (Lowson 1980)	10.6 (Cabot Inc.)
Av. Layer plane diameter/nm	1.86 (Briscoe and Warren 1942)	8.7 (Hess et al 1968)
Av. crystallite thickness/nm	1.31 (Briscoe and Warren 1942)	4.3 (Hess et al 1968)

3.1.5 Membrane Construction

The zeolite and carbon molecular sieve membranes were made by compaction of powder into a Veridiaglass tube, using a vice. Three such membranes were studied:- zeolite membrane 1, constructed by Mr. R. Ash (1955) and used by him to study Ne, Ar, N_2, He and O_2 flow (unpublished results); zeolite membrane 2, a smaller membrane constructed for this study; a membrane of similar dimensions to zeolite membrane 1, manufactured from powdered carbon molecular sieve material which had been passed through a 200 mesh sieve, to ensure small particle size, also constructed for this study. The method of construction used resulted in extremely open membranes of high permeability. The characteristics of these membranes are given in table 3.3.

Table 3.3 Characteristics of molecular sieve membranes

	Zeolite 1	Zeolite 2	Carbon Molec Sieve
length/m	0.0375	0.01628	0.03421
cross sectional Area/10^{-5} m^2	1·26	0·935	1·901
Pre outgassing weight/g	0.3341	0.1512	0.7193
outgassed weight/g	0.2506	0.1134	0.6833
Porosity (OG)	0.723	0.520	0.2703

The Carbolac and Graphon membranes were made by incremental compaction of the free powder in stainless steel cylindrical holders. Both membranes featured a side port at the ingoing face to enable circulation of the gas mixture on the ingoing side as shown in fig. 3.2.

The Graphon membrane was constructed by Dr. R. T. Lowson (1968) and used by him in an investigation of Helium flow (Ash, Barrer and Lowson 1970) and subsequently by Dr. A. D. Hamilton in an investigation of Helium blockage by hydrocarbons.

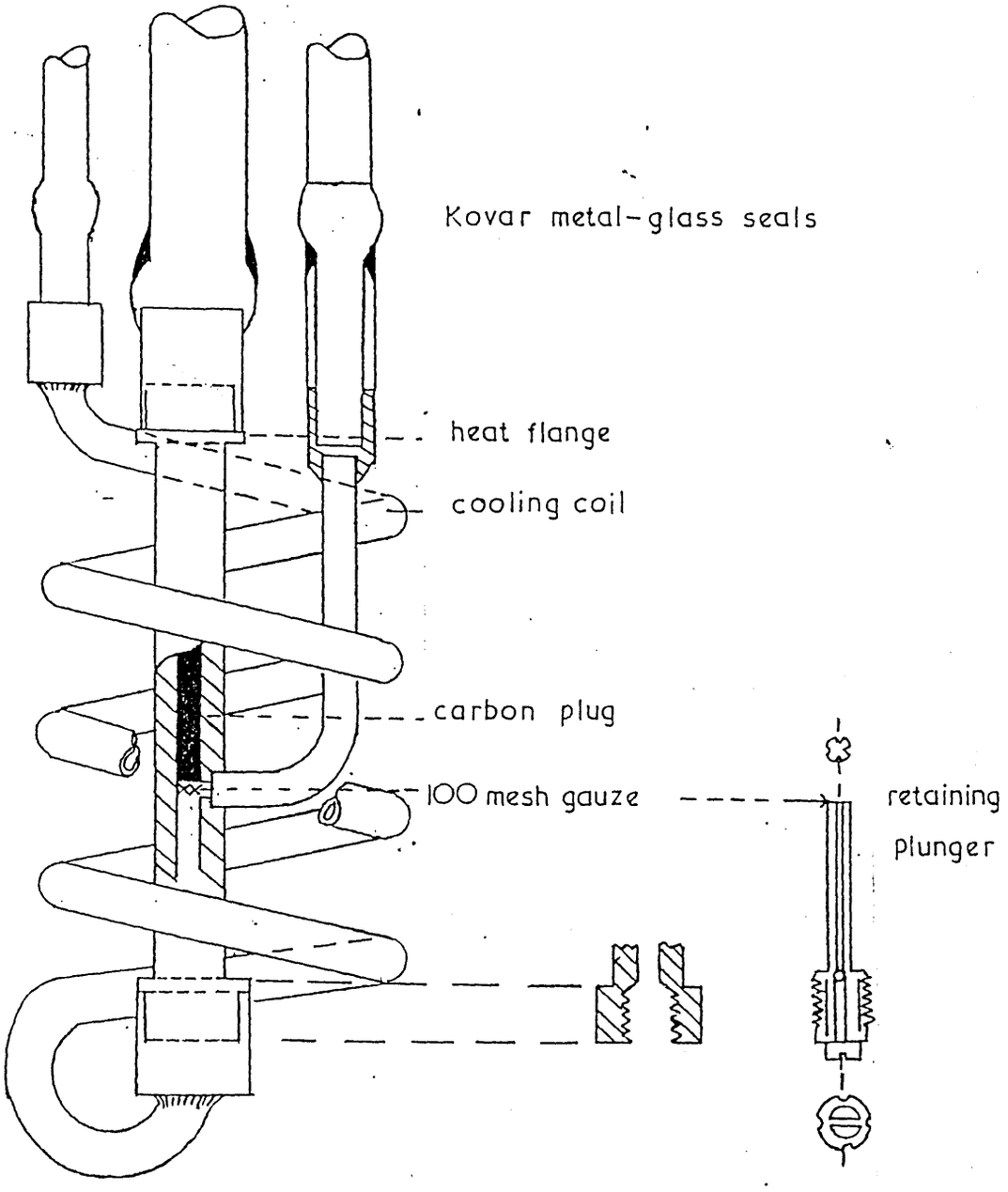
The Carbolac membrane was also constructed by Dr. R. T. Lowson (1968) and used in an investigation of Helium blockage by ammonia. Details of construction may be found in his Ph.D. thesis.

Data and the membrane characteristics are listed in table 3.4.

Table 3.4 Characteristics of carbon membranes

	Carbolac	Graphon
length/m	0.00976	0.00971
cross sectional area/10^{-6} m^2	7.119	7.146
Pre out gassing		
Weight of Adsorbent/g	0.0762	0.0692
outgassed weight/g	0.0694	0.0692
Porosity	0.528	0.494

(fig 3·2) The Membrane Assembly (Graphon & Carbolac)



3.1.6 Outgassing procedure

Before use, both membranes and adsorbent samples were outgassed at 10^{-6} cmHg under the temperature conditions detailed in table 3.5. This treatment removed any adsorbed material from the surface of the solid and was repeated between sets of steady state experiments and before Time-lags were measured.

Table 3.5 Initial Out gassing Conditions

Material	temp/^{o} C	time/hrs
Zeolite NaX	25	24
	then 360	16
Carbon Molec. Sieve	350	24
Carbolac	300	72
Graphon	200	24

3.2.1 Gases

The main gases used with all four membranes were He, N_2, H_2S and CO_2, but some SF_6, Ar and Propane flow was also investigated for the Graphon membrane. The He, N_2, Ar and CO_2 were BOC "research grade" of specified purity (> 99.99%) and were supplied either in one litre pyrex glass bulbs filled to atmospheric pressure or in small size 'c' cylinders containing 50 litres at atmospheric pressure.

H_2S and SF_6 were obtained from Argo International Ltd. in Lecture bottles (H_2S 99.5% and SF_6 99.9%), and a gas bottling

apparatus was constructed in order to dry these gases and transfer them to pyrex glass bulbs where necessary. Table 3.6 lists the impurities present in the gases used.

3.2.2 Gas bottling apparatus

The gas bottling apparatus included a drying tube containing troughs of P_2O_5 and a series of cold traps.

Gas from a lecture bottle entered the apparatus through a length of previously evacuated rubber pressure tubing, and passed immediately over the drying agent. The gas leaving the drying tube passed into the series of cold traps being frozen out and pumped upon in each one, at each stage a mercury bubbler indicated the approximate gas pressure and prevented over-pressurization. The pyrex glass bulbs could be blown on to the end of the apparatus and removed for use after filling.

3.2.3 Precautions taken with H_2S usage

H_2S is both highly poisonous and inflammable, it was therefore important that adequate precautions were taken while it was in use. Extractor fans were installed into the laboratory in case of leakage and all rotary pumps and bubblers were vented to the fume cupboard via an H_2S scrubbing system.

The H_2S scrubbing system comprised two Dreschel bottles linked together by the inlets, and a column of self indicating silica gel. One Dreschel bottle contained Sodium Hypochlorite solution (which reacts with H_2S forming H_2SO_4) and the other was

(fig 3·3) Gas Bottling Apparatus

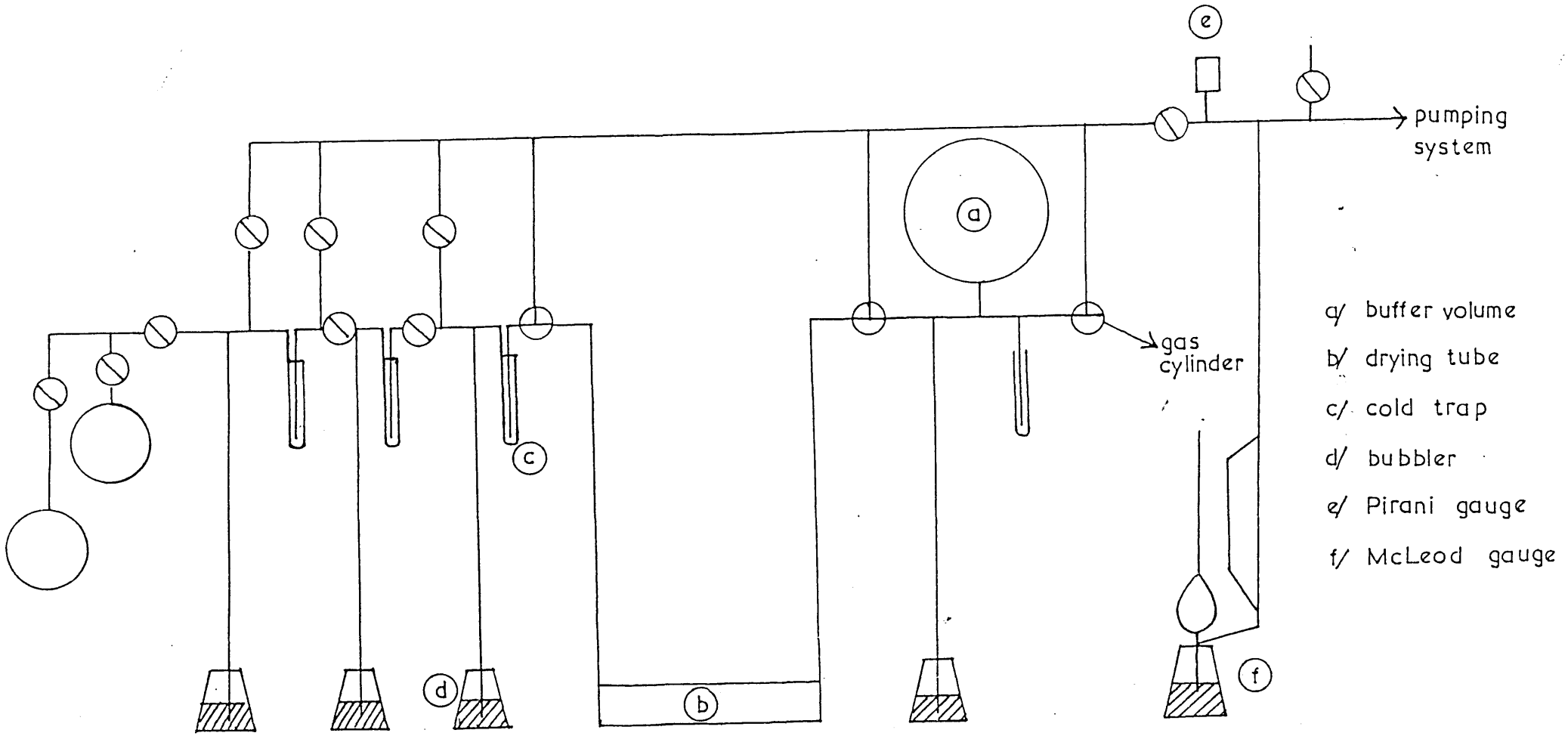


Table 3.6

Impurities present in the Gases used

CO_2 99.9996%	H_2S 99.5%
N_2 2 ppm	Propane 810 ppm
O_2 < 1 ppm	O_2 30 ppm
H_2 < 1 ppm	N_2 75 ppm
CO < 1 ppm	Propylene 2700 ppm
Hydrocarbons < 1 ppm	H_2O 31 ppm
moisture 1 ppm	$(CH_3)_2S$ 31 ppm
He 99.9997%	N_2 99.9992%
Ne < 1 ppm	Ar 5 ppm
N_2 < 1 ppm	H_2 < 7 ppm
O_2 < 1 ppm	O_2 < 1 ppm
H_2 0.5 ppm	He < 1 ppm
moisture < 1 ppm	Ne < 1 ppm
Hydrocarbons < 1 ppm	CO_2 0.5 ppm
	Hydrocarbons 0.5 ppm
	moisture 1 ppm

to prevent suck back of the solution along the outlet.tube and into the rotary pump. After pumping out large volumes of H_2S the Sodium Hypochlorite solution was renewed, the following reaction having occurred (Kolthoff and Belcher 1957).

$$H_2S(g) + 4NaOCl \rightarrow H_2SO_4 + 4NaCl$$

Some colloidal sulphur was also produced depending upon the temperature and acidity of the solutions so that frequent cleaning of the outlet-tubes was necessary. The silica gel columns removed the last traces of H_2S from the gas emerging from the Dreschel bottles by reaction with the indicator $Co\ Cl_2$.

$$H_2S + CoCl_2 \rightarrow 2HCl + CoS$$

Since CoS is black a colour change in the silica gel indicator showed when the column had been saturated and needed replacement.

3.3 General Features

The apparatus used was constructed from Pyrex glass tubing using an oxygen/natural gas blow torch. The McBain balance utilized greaseless PTFE high vacuum stopcocks (J. Young Ltd.), however in all other cases ground glass stopcocks (Springhams Ltd.) were used, lubricated with Apiezon N vacuum grease. Cone-and-socket joints were sealed using Apiezon N or Picein wax.

In all experiments mercury levels were measured using cathetometers (Precision Tool and Instrument Co) accurate to $\pm\ 10^{-5}$ m, and time measured using Rone stopwatches.

3.3.1 Pumping System (fig. 3.4)

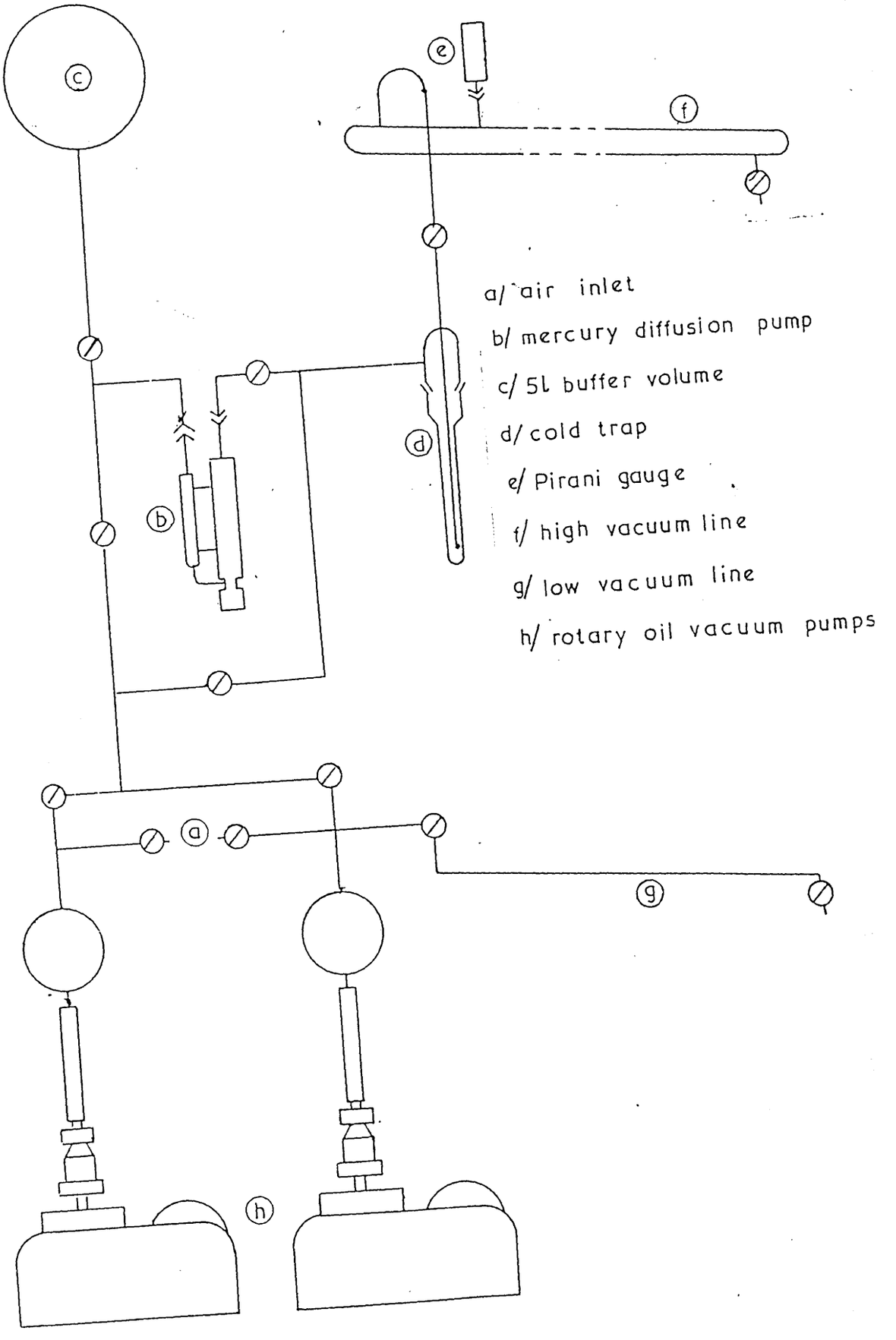
The pumping system for the high vacuum line consisted of a two stage rotary oil pump (Edwards High Vacuum Ltd.) capable of producing a vacuum of 10^{-4} cmHg in series with a mercury diffusion pump. With the aid of a liquid N_2 cold trap for condensable vapours a vacuum of $\sim 10^{-6} - 10^{-7}$ cmHg could be maintained. Since the evacuation of H_2S was required, vacuum pump oil containing anti corrosion additives (Edwards Grade 17 or Grade 18) was used in the rotary pumps. The 5ℓ buffer volume incorporated in the system allowed frequent oil changes and other routine maintenance to be carried out without shutting the diffusion pump down. Pressure in the high vacuum line was monitored using a Pirani Gauge (Edwards G5C-2) with control unit (model 8.2) range $1 - 10^{-5}$ cmHg and a Mcleod Gauge, range $10^{-2} - 10^{-7}$ cmHg. A second rotary pump was used for preliminary evacuation of the system and for adjustment of the mercury levels in McLeod gauges and manometers via the low vacuum line.

3.3.2 Temperature Control

a) Outgassing Temperatures

High temperatures required during outgassing were achieved using an electric furnace controlled by a Variac transformer. The furnace consisted of resistance wire, wound around a fused silica cylinder and insulated with Zetex temperature resistant rope. (Willcox Ltd.)

(fig 3·4) A Pumping System



b) Cryostats

Adsorption and flow experiments were performed between 184 K and 273 K. At 273 K an ice bath was used to maintain the correct temperature. The development of a leaky dewar system was necessary. In this system a partially evacuated flask, connected to the low vacuum line, was surrounded by refrigerant fluid, (liquid N_2) and filled with a thermostatting liquid (petroleum ether B Pt. 60° C - 80° C). The temperature was controlled to $\pm$ 1 K using a bimetallic spiral regulator and Sunvac relay system with a 25 watt heating lamp. Efficient stirring of the thermostatting fluid was also necessary, to minimize temperature gradients, and was achieved using a glass paddle stirrer driven by an electric motor.

3.3.3 Temperature Measurement

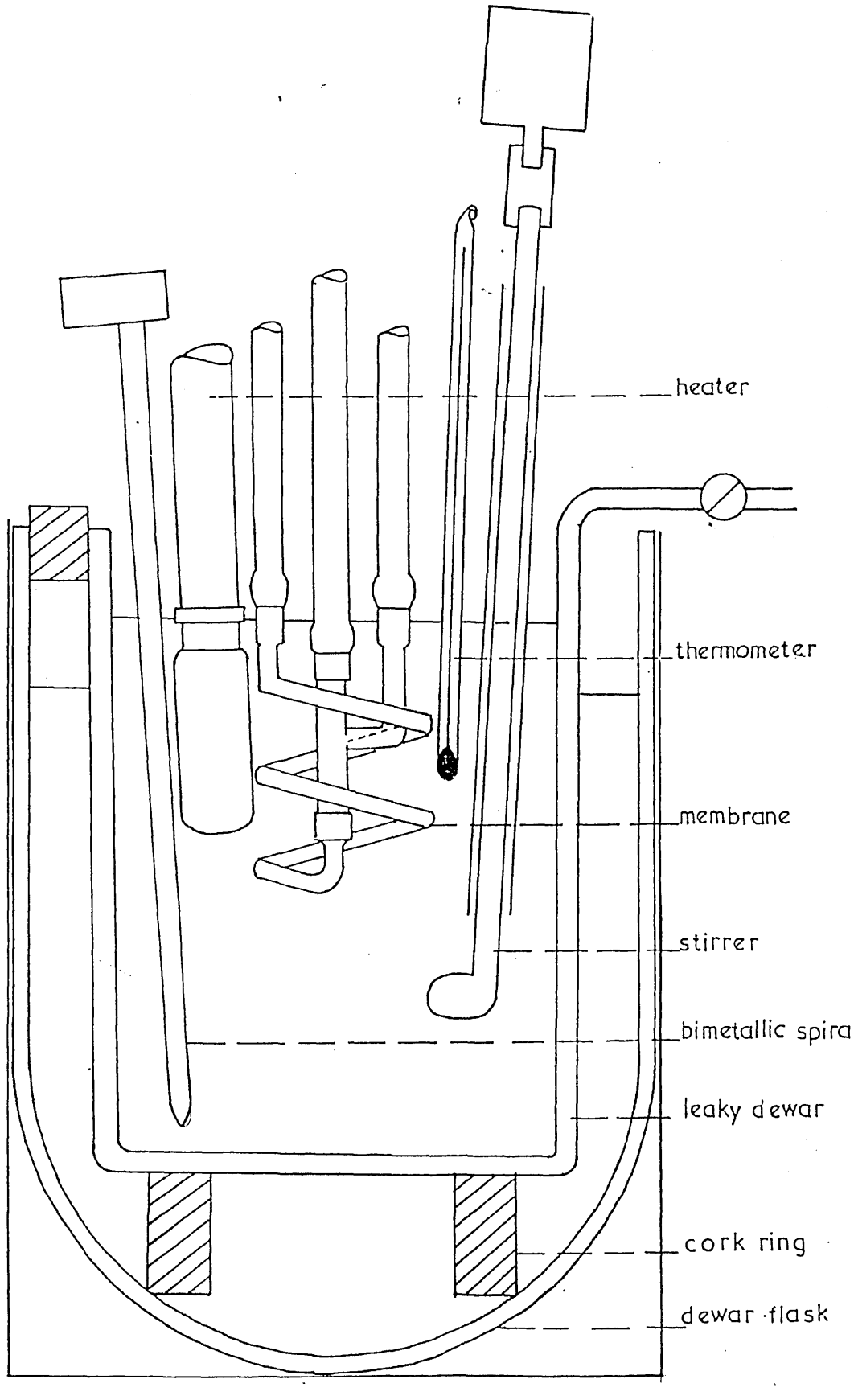
A series of mercury-in-glass thermometers (Sugden Powell Ltd.) were used to monitor temperatures above 0° C.

For low temperatures toluene thermometers (Zeal Ltd.) with a stated tolerance of $\pm$ 1° C between - 120° C and 30° C, were used and were cross calibrated against an ammonia vapour pressure thermometer.

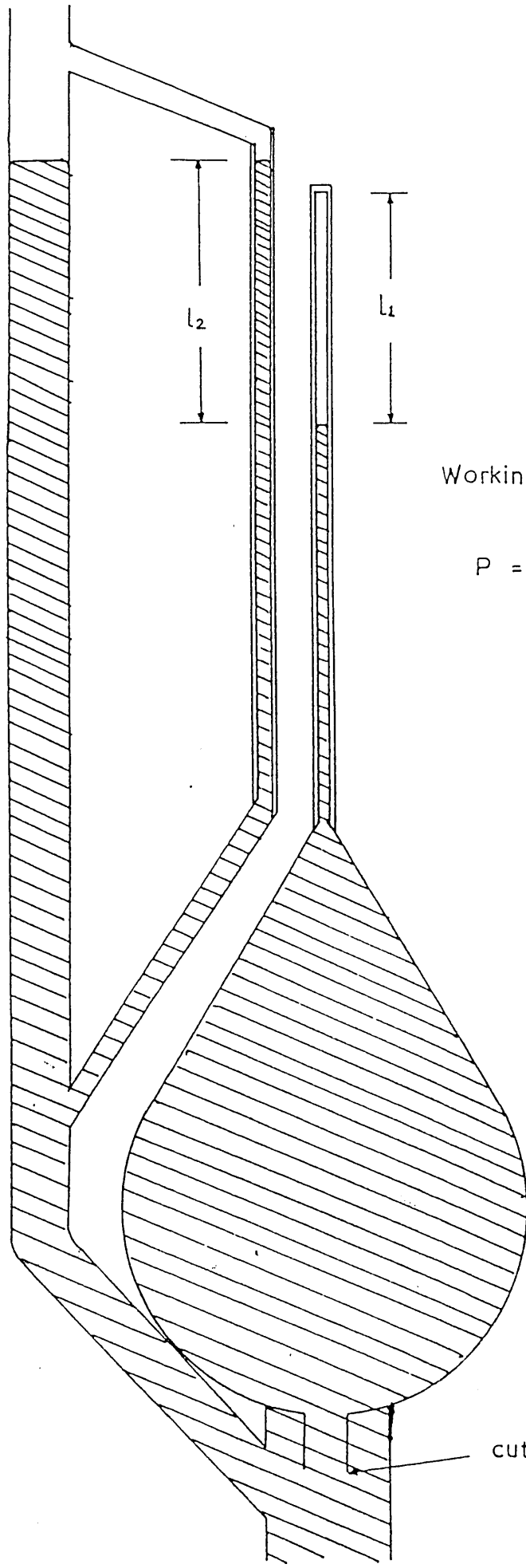
3.3.4 McLeod Gauges and Manometers

McLeod gauges were used for accurate pressure measurement on the outgoing side of the membrane and to monitor the vacuum in the system. To reduce 'sticking' clean filtered mercury was used in them and in the manometers, care being taken to minimize mercury sulphide formation by excluding impure H_2S from all mercury

(fig 3·5) Leaky Dewar System



(fig 3·6) A McLeod Gauge



Working Equation

$$P = \frac{l_1 l_2 a}{V - l_1 a}$$

P = pressure

V = volume

a = capillary cross section

surfaces. Pure H_2S was found not to react with mercury (Roberts 1931) and could be admitted safely to the McLeod Gauges and manometers. The characteristics of the McLeod gauges are given in table 3.7.

Table 3.7 Measurement McCleod Gauge Characteristics

Apparatus	Capillary cross sectional area/10^{-6} m^2	Bulb volume /10^{-3} dm^3
Graphon Apparatus	3.236	367.7
Carbolac Apparatus	3.142	301.1
Molecular Sieve Apparatus	3.215	378.01

3.4 Adsorption Isotherm Determination

McBain Balance

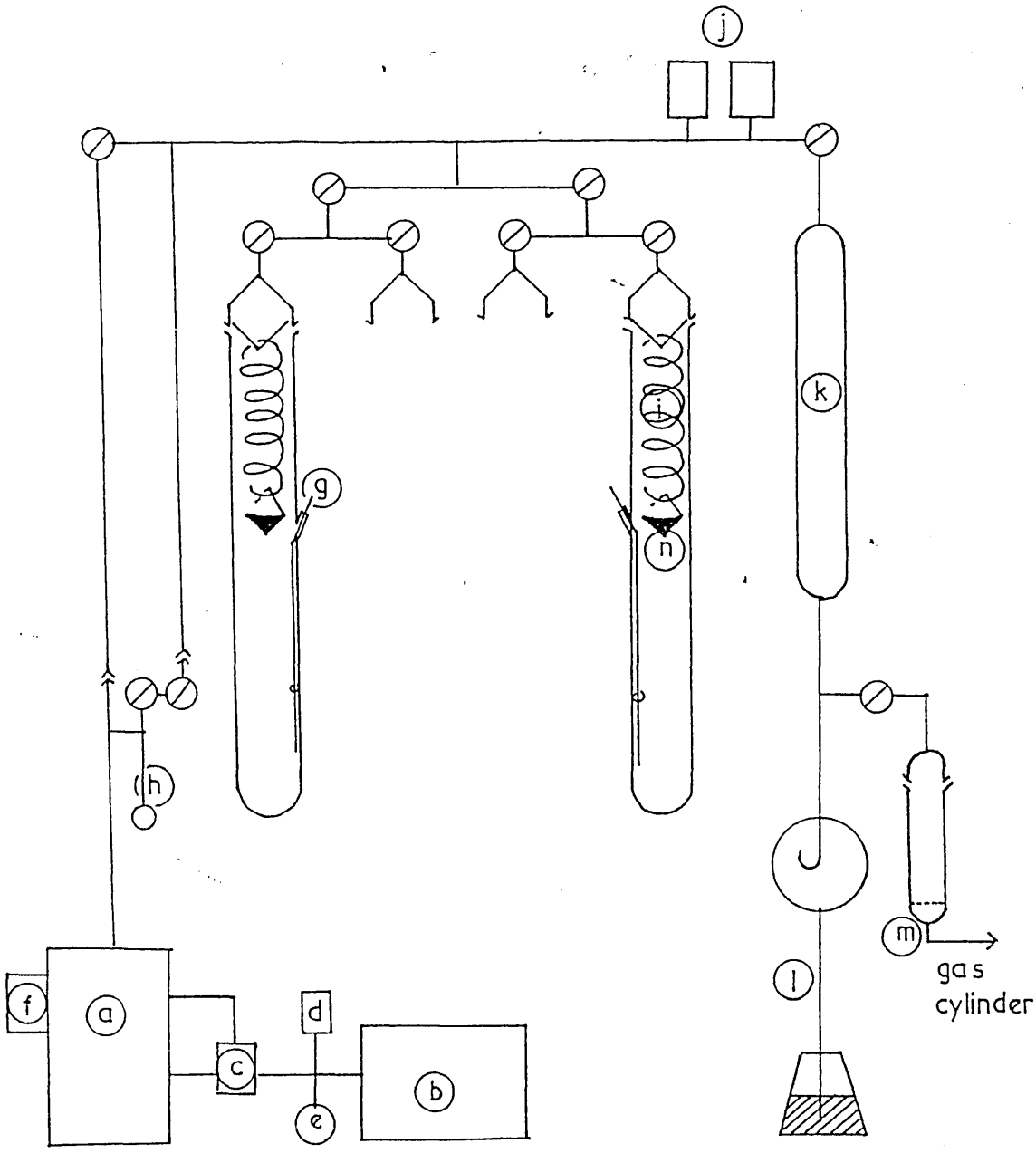
Adsorption isotherms for H_2S and CO_2 were measured using a McBain balance during two four week industrial training periods at British Petroleum Research Centre, Sunbury.

3.4.1 Description of Apparatus

The McBain balance was constructed from Pyrex glass tubing and greaseless PTFE taps (J. Young Ltd.). A combined pumping unit (Edwards High Vacuum Ltd.) was used to evacuate the system, this comprised a Diffstak, water cooled oil diffusion pump, a backing/roughing valve, a rotary vacuum pump and a Pirani gauge. A vacuum approaching 10^{-9} cmHg could be obtained at the top of the diffusion pump where it was measured by a Penning 8 Vacuum gauge.

The quartz balance spings (Thermal Syndicate Ltd.) were

(fig 3·7) Mc Bain Spring Balance



a/ Diffstak diffusion pump
b/ rotary pump
c/ roughing/backing valve
d/ Pirani gauge head
e/ air inlet
f/ Penning 8 vacuum gauge head
m/ drying column
g/ thermocouple
h/ cold trap
i/ silica spring
j/ pressure transducer
k/ ingoing buffer volume
l/ oil filled bubbler
n/ sample holder

enclosed in qlass sample tubes 90 cm long which were sealed onto the apparatus by use of rubber 'O' rings and spherical joint clips. The sample was placed in an aluminium sample holder and suspended by a thin glass hook at the correct height in the tube. The assembly could then be immersed in a cryostat and the temperature measured using an electronic thermometer (Comark Ltd.), thermocouples of which were sealed into a side arm of the sample tube with Araldite and constrained at the side of the tube by small glass rings. The characteristics of the springs are given in table 3.8.

Table 3.8 Quartz Spring properties

Maximum weight	1 g
Maximum extension	30 cm
Sensitivity	25 cm g^{-1}

3.4.2 Experimental Technique

Prior to measuring an adsorption isotherm the springs were calibrated using known .1 g weights and a calibration curve plotted. The samples were then inserted and outgassed under the conditions detailed in table 3.5. Equilibrium times varied between 20 minutes and 1½ hours at which point the final extension of the spring and the equilibrium pressure (measured on a pressure transducer (Schaevitz Ltd.)) were recorded. Both adsorption and desorption isotherms were determined and graphs of amount adsorbed (v/cm^3 STP g^{-1} against equilibrium pressure p /cm Hg were compiled.

3.4.3 Volumetric Adsorption Apparatus

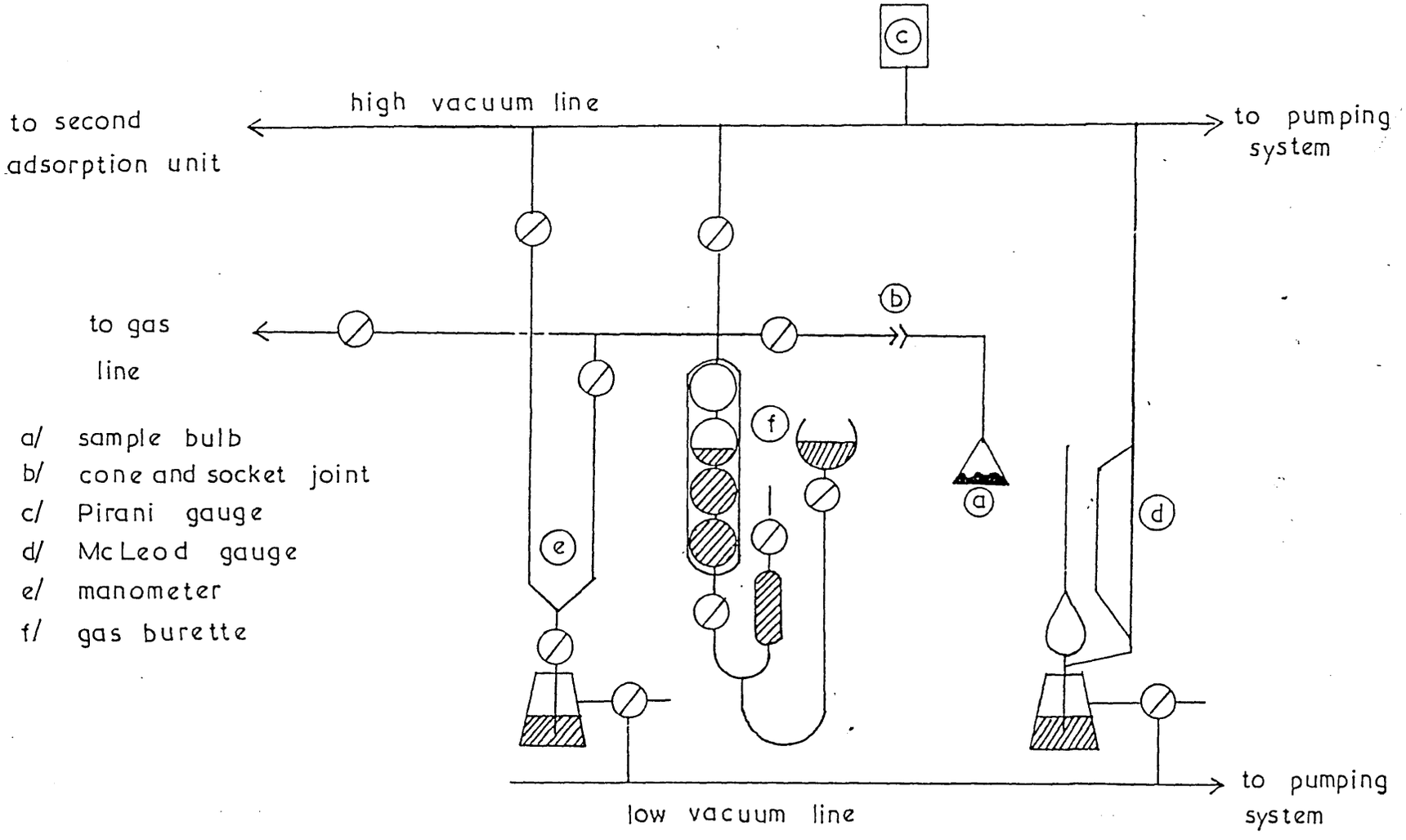
Adsorption isotherms for N_2 and CO_2 on Graphon were measured using a volumetric adsorption apparatus. Some isotherms for CO_2 on the carbon molecular sieve were also measured in this way in order to make a crosscheck between the volumetric and gravimetric methods and as a comparison between the powdered and pelletized form of the sample.

Description of the apparatus

A standard volumetric adsorption apparatus was employed, as shown in figure 3.8. It had been constructed originally by Dr. R. J. B. Craven (1976) for an adsorption kinetics study and was subsequently used by Dr. A. D. Hamilton for the measurement of adsorption isotherms. The pressure was measured using a manometer made from 10 mm precision bore Veridia glass tubing.

3 mm bore capillary tubing was used throughout to minimise dead volume. The sample was inserted into a glass bulb and connected to the apparatus via a tap and a cone and socket joint. Prior to measuring an adsorption isotherm the doser volume of the apparatus and the cold volume of the sample bulb at the appropriate temperature (ϕ_T) were determined by helium expansion, and the sample outgassed. The standard volumetric technique for isotherm determination is well documented and will not be discussed here. The isotherms were presented in the same manner as those determined by gravimetric means. The volumetric adsorption apparatus consisted of two units, enabling two isotherms to be determined simultaneously. Essential

(fig 3·8) Volumetric Adsorption Apparatus



characteristics are listed in table 3.9. The results were calculated using a computer programme written for a Commodore microcomputer.

Table 3.9 Characteristics of Adsorption Apparatus

	Unit 1	Unit 2
Doser Volume/cm^3	29.246	30.934
Manometer cross sectional area/cm^2	0.420	0.420
Gas burette volume 1	23.552	22.061
volume 2	29.194	31.089
volume 3	41.030	42.063
volume 4	52.266	49.652

3.5 Isothermal Flow Apparatus

3.5.1 Isothermal Flow Apparatus for Single Gases (Molecular Sieve Membranes)

In this study the flow of single gases was examined through the carbon molecular sieve and zeolite membranes. The apparatus built for this purpose (fig. 3.9 and plate 1) maintained at a constant pressure difference across the membrane.

This technique involves keeping the ingoing pressure constant and the outgoing pressure negligible by means of large buffer volumes. The majority of the previous work originating from these laboratories has also employed this type of system.

The apparatus consisted of a gas line, an ingoing side, a membrane and an outgoing side. The ingoing side comprised a manometer,

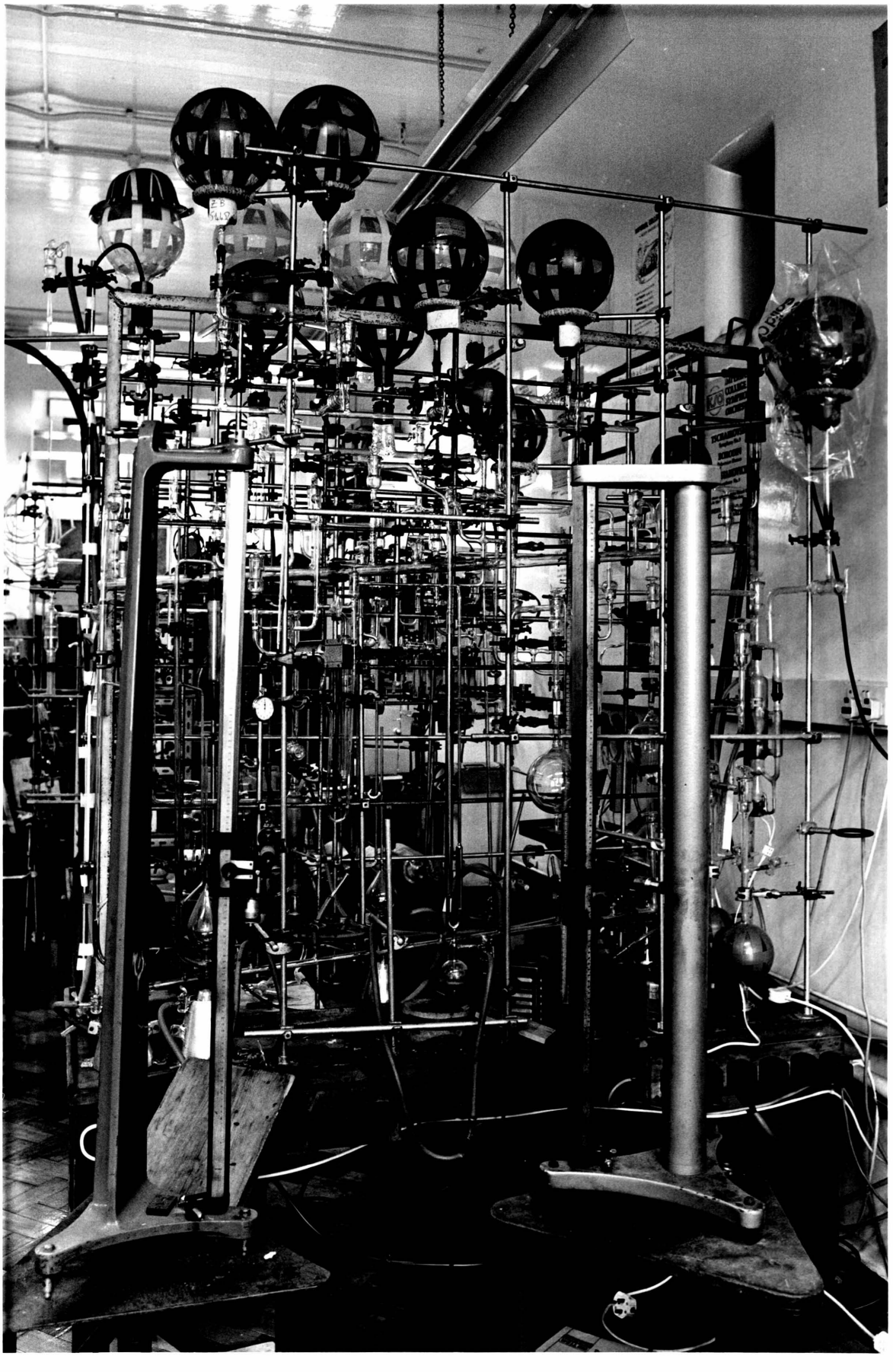
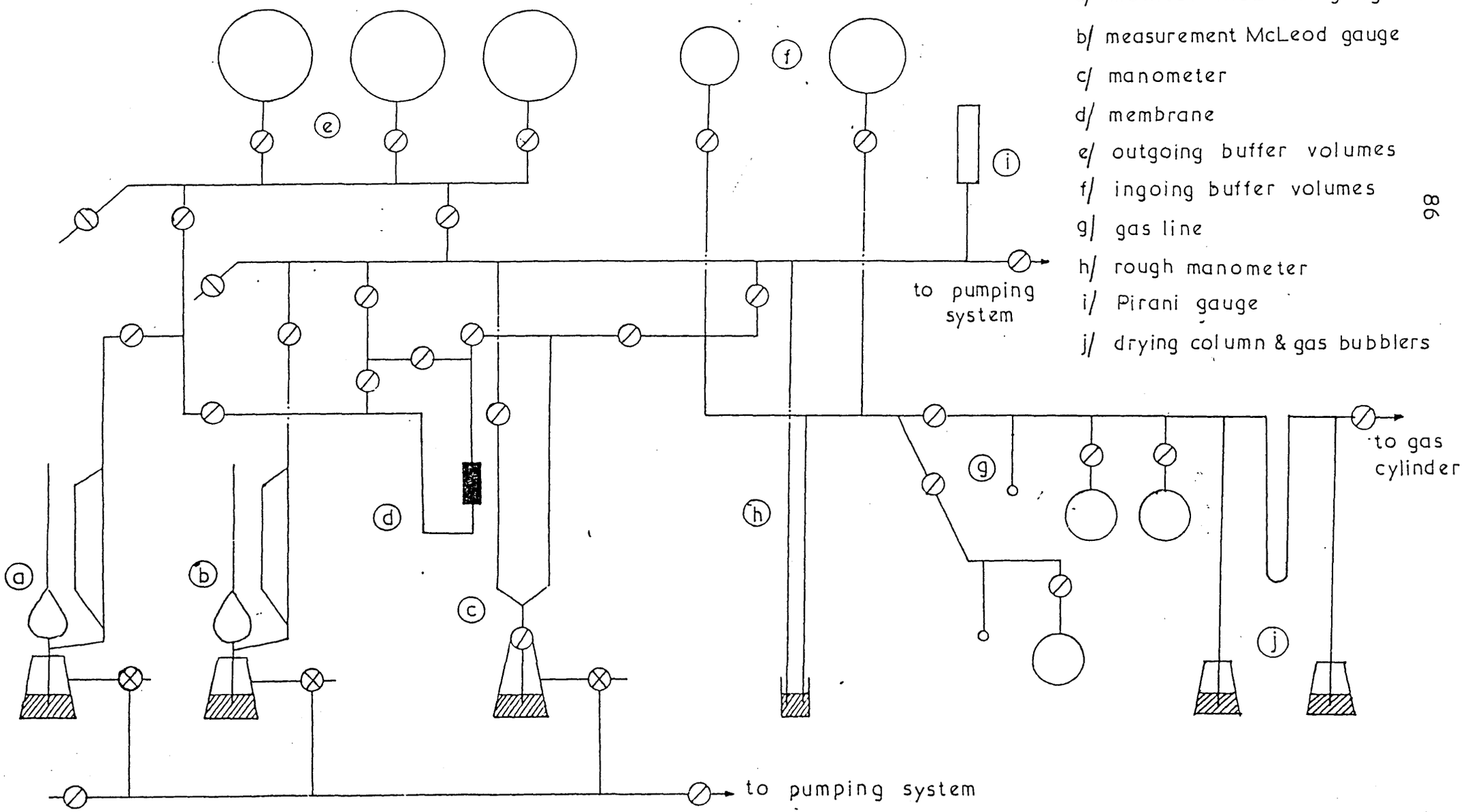


Plate 1. Single Gas flow apparatus (CMS and zeolite membranes)

(fig 3·9) Diagram of Apparatus for Measurement of Single Gas Flow



and buffer volume approaching 40 ℓ, which was necessary in order to maintain a constant ingoing pressure head, as the membranes studied were of an extremely open nature. The outgoing side consisted of a McLeod gauge and four buffer volumes which had been calibrated by the repeated addition of distilled water. The dead space volume was also calculated by helium expansion and is included in the resulting outgoing volumes which are listed in table 3.10.

Table 3.10 Outgoing volume of single gas flow apparatus

Component buffer volume	Volume/10^{-3} m^3	Σ outgoing volume/10^{-3} m^3
McLeod gauge and dead space	1.040	1.040
α	5.410	6.450
β	5.365	11.815
γ	5.396	17.211
δ	5.445	22.656

The apparatus for flow of single gases was initially constructed by Dr. D. E. G. Whiting for an investigation using a membrane composed of Sterling S. carbon. It was subsequently modified by Miss K. Hollinshead for work on zeolite membrane 1.

3.5.2

The membrane was outgassed under the required conditions (table 3.5) and surrounded by a cryostat of the correct temperature. Gas was admitted to the ingoing side and the pressure measured using the manometer. At the beginning of the experiment gas was admitted to the membrane and a stopwatch was started. The build up of gas in the outgoing volumes was then monitored at regular time intervals using the McLeod gauge until steady state flow had been achieved and measured. This necessitated plotting outgoing pressure (p_2) against time (t) until a straight line of at least ten points was obtained. The outgoing volume was varied in order to keep p_2 in the range of the McLeod gauge and at less than 0.1% of p_1. The steady state permeability and flux were then evaluated using the following equations

$$\tilde{K} = V \frac{\ell}{A_c} \frac{dp_2}{dt} \frac{1}{60} \frac{1}{p_1} \frac{T}{T_R}$$

where $\tilde{K}$ = integral permeability /m^2 s^{-1}

V = outgoing volume/m^3

A_c = cross-sectional area of membrane/m^2

ℓ = length of membrane/m

$\frac{dp_2}{dt}$ = gradient of the graph of p_2 against t/cmHg min^{-1}

p = ingoing pressure/cmHg

T = Membrane temperature/K

and

$$J_\infty = \frac{V}{RT_R} \frac{dp_2}{dt} \frac{1333.2}{60} \frac{1}{\rho}$$

where

J_∞ = the steady state flux/mol s^{-1}

R = the Molar gas constant (8.3143 JK^{-1} mol^{-1})

ρ = the ratio of the density of mercury at 273.2 K to the density of mercury at room temperature (densities taken from Weast 1970).

The numerical factor 1333.2 cmHg Pa^{-1} converted pressure from cmHg at 273.2 K to pascals.

3.5.3 Isothermal flow apparatus for single species and binary mixture flow (Graphon and Carbolac membranes)

The apparatus employed to investigate gas flow through the Graphon and Carbolac membranes (fig. 3.10) (plate 2) could be used to examine the flow of either single gases or binary gas mixtures.

The design of the apparatus differed from that upon which the molecular sieve membranes were mounted, in that the ingoing side included a Toepler pump for the composition of gas mixtures, a circulating pump for circulation of the mixture past the membrane face, and a cold trap for separation of the component gases after the experiment. A different membrane assembly was also needed as described in part 3.1.5. A series of cold traps was also incorporated into the outgoing side in order to separate the outgoing

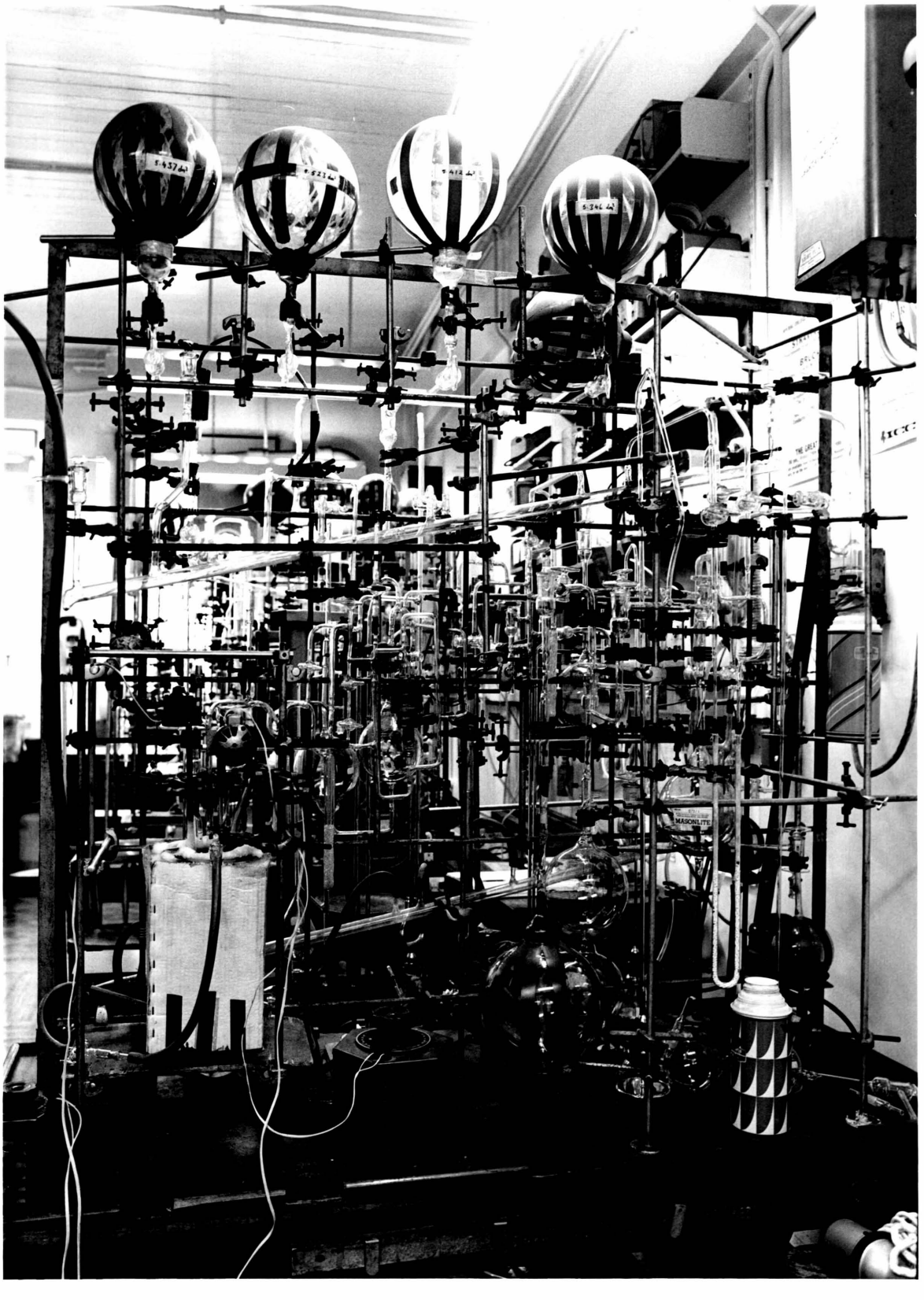
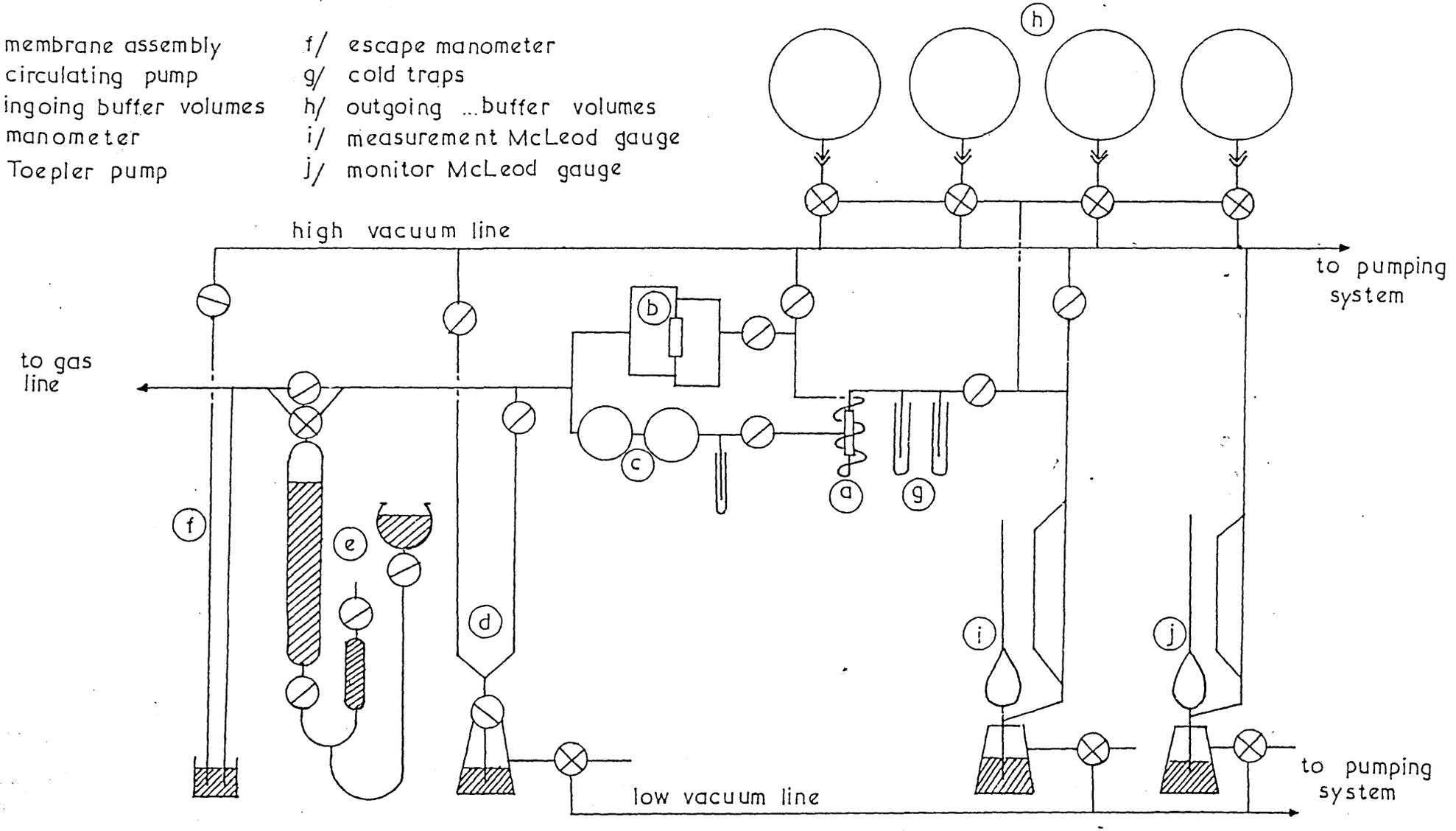


Plate 2. Isothermal flow apparatus for single species and binary mixtures (Graphon and Carbolac membranes)

(fig 3·10) Diagram of Apparatus for Measurement of Binary Gas Mixture Flow (Graphon & Carbolac)

a/ membrane assembly
b/ circulating pump
c/ ingoing buffer volumes
d/ manometer
e/ Toepler pump
f/ escape manometer
g/ cold traps
h/ outgoing ...buffer volumes
i/ measurement McLeod gauge
j/ monitor McLeod gauge



gas mixture. The outgoing volumes of the Graphon and Carbolac apparatus are given in table 3.11.

3.5.4 The Circulating Pump

The circulating pump was used in gas mixture experiments to ensure uniformity of composition at the ingoing face of the membrane. It was a reciprocating plunger pump similar in design to that used by Barrer and Robins (1953).

The piston was a 2 cm diameter glass tube filled with lengths of soft iron packed with asbestos wool and vacuum sealed. It was surrounded by a copper wire coil and reciprocated under the action of an intermittent current supplied by a control unit. The valves were ground into their settings to be gas tight and the whole assembly was constant volume in operation.

Table 3.11 Outgoing volume of Graphon and Carbolac Apparatus

component	GRAPHON		CARBOLAC	
buffer volume	Volume/$10^{-3}m^3$	Σ outgoing volume	Volume/$10^{-3}m^3$	Σ outgoing volume
McLeod gauge and dead space	.829	.829	.735	.735
α	5.437	6.277	3.266	4.001
β	5.523	11.810	5.464	9.466
γ	5.412	17.229	5.272	14.738
δ	5.346	22.593	5.552	20.314

3.5.5 Experimental technique for binary mixture transport

Steady state flow of the more adsorbable component was established as described in section 3.5.2 and the gas was frozen out in the cold traps on the outgoing side of the membrane. This technique was tested and found to be successful giving an outgoing pressure of gas which was too low to be detectable using the McLeod gauge. The ingoing pressure of the sorbable component was measured with the Toepler pump fully raised, the mercury level in the pump was then lowered to accept a dose of Helium, Nitrogen or Argon from the gas line.

This was expelled into the ingoing side via the two way tap at the top of the Toepler pump and the process repeated until the required partial pressure of gas had been reached. The approximate partial pressure of the non sorbable component used varied depending upon the gas and the membrane in use. For increased accuracy and ease of calculation of result, a partial pressure at which the permeability ceased to be pressure dependent was most desirable. The approximate pressures used are given in table 3.12.

Table 3.12 Partial Pressures of Helium, Nitrogen and Argon in mixture experiments

System	Pressure
Graphon/Helium/sorbable component	3 - 4 cmHg
Graphon/Nitrogen/sorbable component	3 - 4 cmHg
Graphon/Argon/sorbable component	3 - 4 cmHg
Carbolac/Helium/sorbable component	5 cmHg
Carbolac/Nitrogen/sorbable component	7 cmHg

When the correct composition had been achieved, the circulation pump was switched on and the outgoing pressure of the less sorbable component, or indicator gas (i.e. He, N_2 or Ar) was measured as a function of time. In theory the Toepler pump could be used to keep the ingoing pressure constant but in practice this was not necessary due to adequate buffering on the ingoing side. The permeability of the less sorbable component in the mixture was calculated using the Commodore microcomputer and compared with the permeability of that gas flowing under the same conditions as a single species.

The ratio of the two permeabilities K_R was calculated

e.g. for He $K_R = K_{He(mix)}/K_{He(pure)}$

where $K_{He(mix)}$ is the permeability of He in the mixture

and $K_{He(pure)}$ is the permeability of He as a single species at the same temperature and pressure.

When the experiment had been completed the adsorbable gas was recovered by freezing out in the cold trap on the ingoing side while impurities were pumped away.

Chapter 4 Results

4.1 Adsorption isotherms
- 4.1.1 Introduction
- 4.1.2 NaX isotherms
- 4.1.3 CMS characterisation
- 4.1.4 CMS isotherms
- 4.1.5 Carbolac isotherms
- 4.1.6 Graphon isotherms
- 4.1.7 Error analysis

4.2 Single gas flow
- 4.2.1 Introduction
- 4.2.2 NaX membrane 1
- 4.2.3 NaX membrane 2
- 4.2.4 CMS membrane
- 4.2.5 Carbolac membrane
- 4.2.6 Graphon membrane

4.3 Binary mixture flow
- 4.3.1 Introduction
- 4.3.2 Carbolac membrane
- 4.3.3 Graphon membrane
- 4.3.4 Error analysis

4.1 Adsorption Isotherms

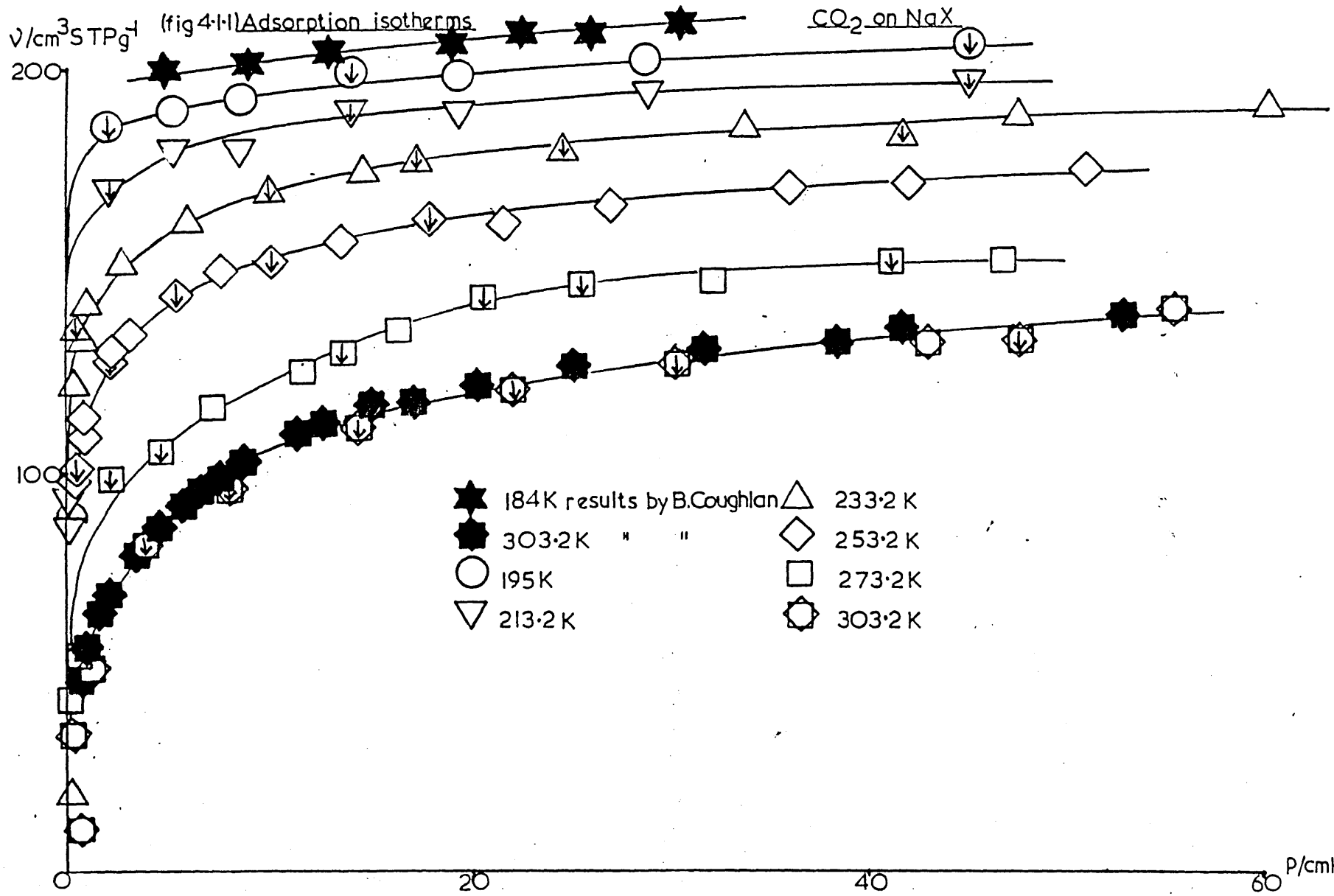
4.1.1 Introduction

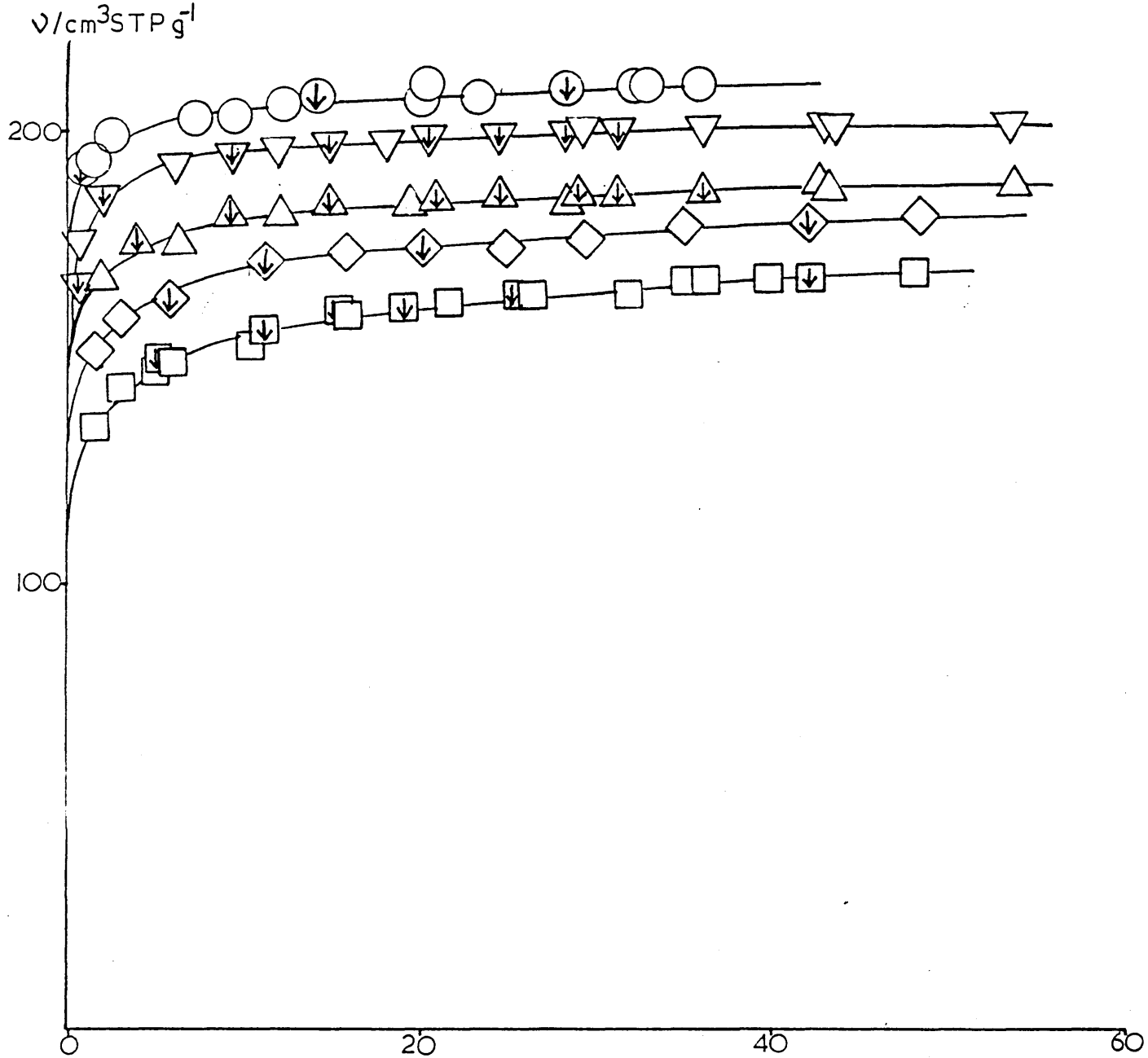
The determination of adsorption isotherms was primarily necessary in order to aid interpretation of the flow data; however in the case of the carbon molecular sieve, the properties of which have not been well documented, additional isotherms were measured. In general sets of isotherms for CO_2, H_2S and N_2 were determined on each of the four adsorbents at the temperatures used for the flow experiments. All isotherms were measured using the McBain balance unless otherwise stated and desorption points are marked.

4.1.2 Adsorption isotherms for NaX

NaX is a well characterised zeolite and hence the adsorption of CO_2 on NaX was measured initially in order to ensure repeatability and reproducibility of the isotherms determined using the newly constructed McBain balance. The isotherms obtained are shown in fig. 4.1.1 and the good agreement between the isotherm determined at 303.2 K and that measured by Dr. B. Coughlan (1964) at the same temperature using a volumetric apparatus is also illstrated. The observed weight-loss of 25.7% on outgassing NaX also agreed with that obtained by Dr. Coughlan (table 4.1.1 p115).

The other temperatures at which this system was studied were 195 K, 213.2 K, 233.2 K, 253.2 K and 273.2 K and all the isotherms were found to be reversable and reproducible. H_2S adsorption on


(fig 4·1·1) Adsorption isotherms
CO_2 on NaX
V/cm³ STP g⁻¹
200
100
0
20
40
60
P/cmHg
184K results by B.Coughlan
303·2K " "
195K
213·2K
233·2K
253·2K
273·2K
303·2K



(fig 4·1·2) Adsorption isotherms

H_2S on NaX

○ 195 K
▽ 213·2 K
△ 233·2 K
◇ 253·2 K
□ 273·2 K

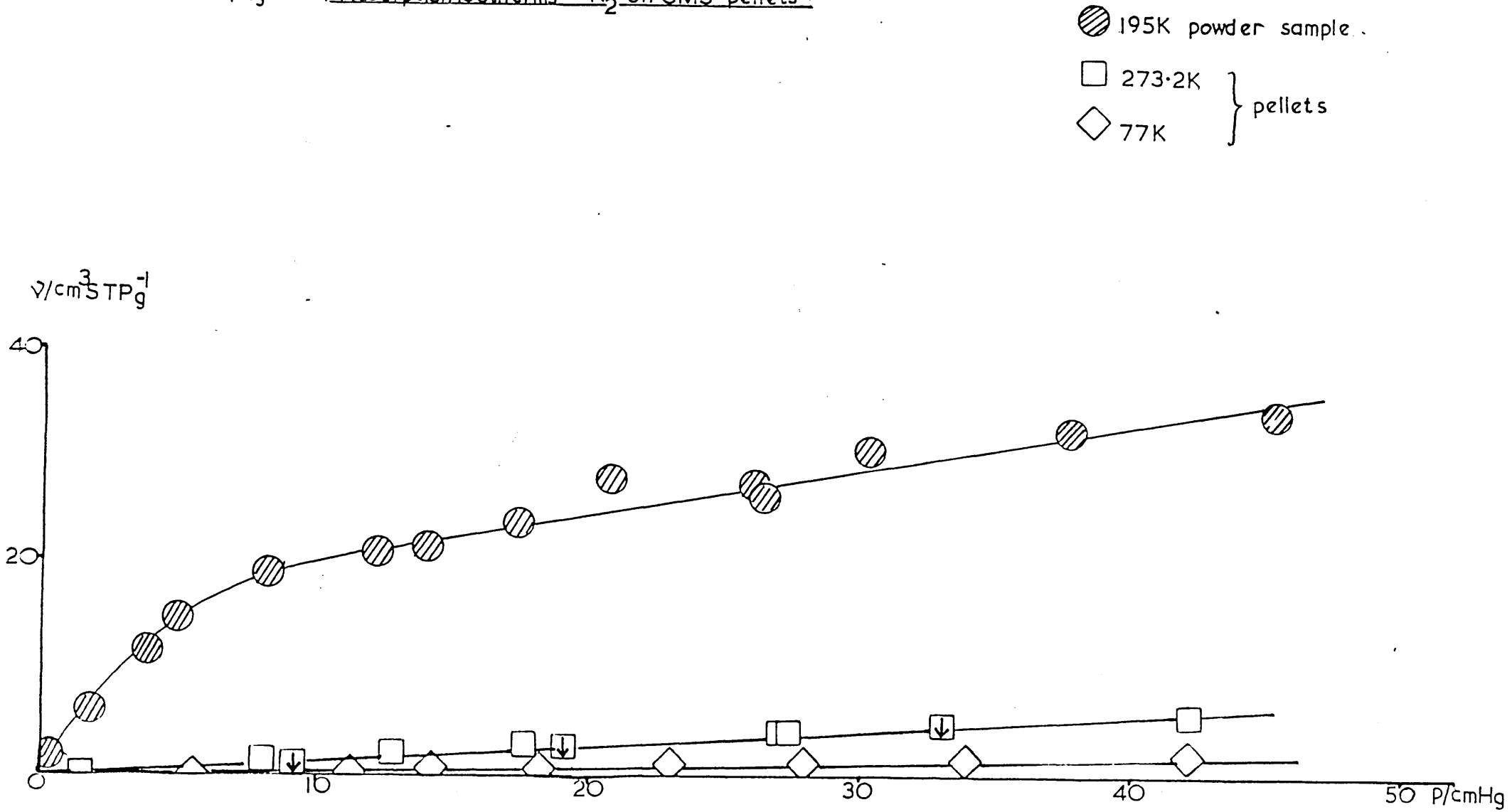
NaX was investigated at the same temperatures as CO_2 and the resulting isotherms are shown in fig. 4.1.2. In this system a yellow deposit was formed upon the surface of the sample at 303.2 K and therefore isotherm measurement was not possible at this temperature. The deposit was thought to be sulphur formed as a product of the catalytic decomposition of H_2S, as it sublimed on outgassing and the sample returned to its original weight.

The fouling of a zeolite X bed with sulphur during experiments with H_2S has also been reported by Fails and Harris (1960). Slight visible evidence of sulphur decomposition was observed at 273.2 K, however at this temperature the deposit was not sufficient to be detectable on the McBain balance and the adsorption isotherms obtained were reversable and reproducible. At all temperatures 5% to 10% more H_2S than CO_2 was found to be adsorbed at the same pressure. For both gases the isotherms obtained were of type 1 in the BET classification and were extremely rectangular in form. The adsorption of nitrogen by the same bulk sample of NaX has already been measured in this laboratory (Sutherland 1956) and was therefore not repeated in this study.

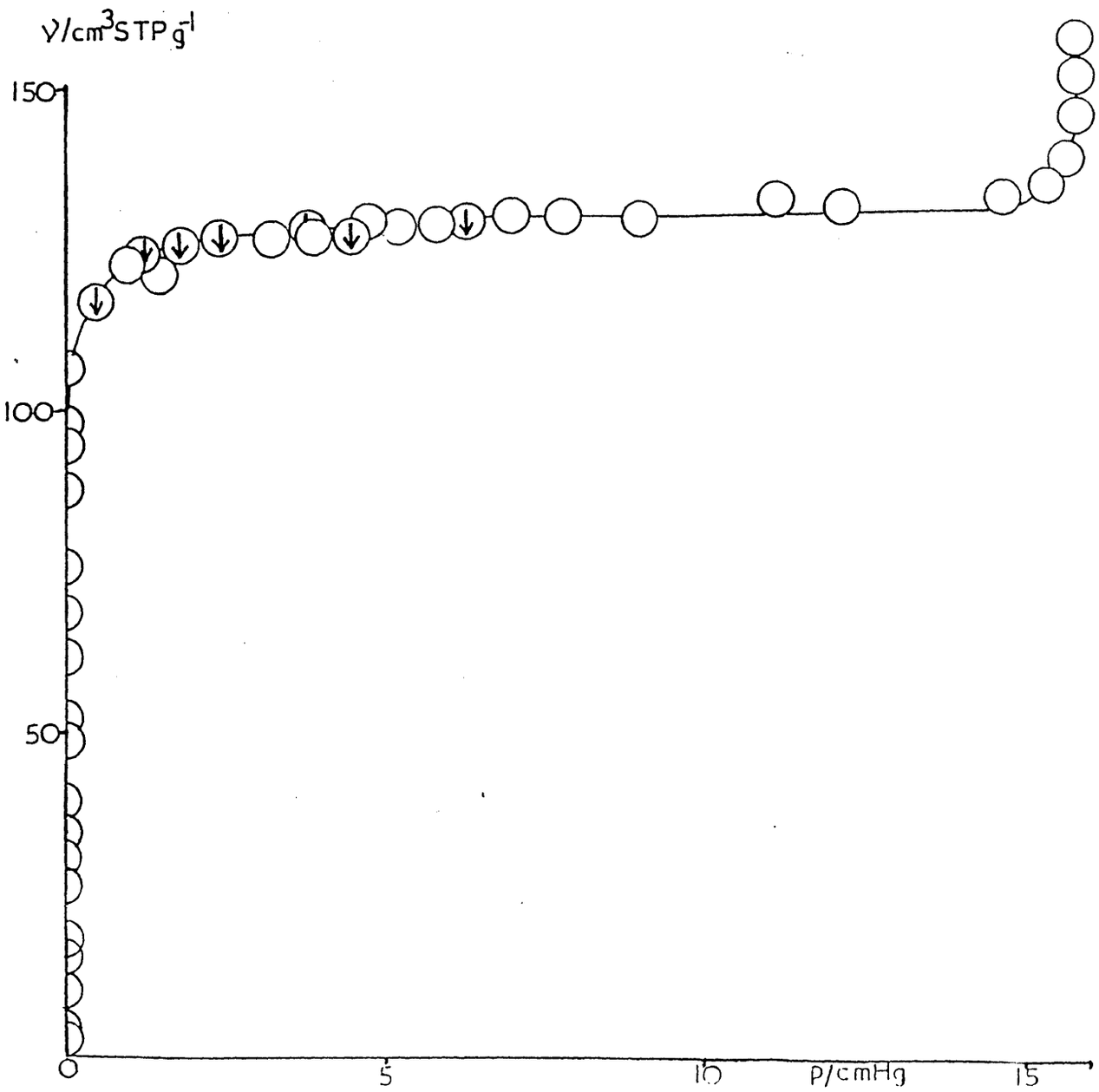
4.1.3 Characterization of Carbon Molecular Sieve

The density of the carbon molecular sieve was determined using helium expansion from a gas burette to measure the empty and full volumes of the sample bulb. A resulting value of 1.44 gcm^{-3} was obtained for both the powdered and pelletized samples. It is usual to measure the available surface area and void volume by N_2 adsorption

(fig 4·1·3) Adsorption isotherms N_2 on CMS pellets



(fig 4·1·4) Adsorption isotherm O_2 on CMS 77K



at liquid nitrogen temperature; however the pores of this material are too small to admit N_2 molecules. (Juntgen et al, 1981). As a result N_2 uptake was negligible on the pelletized sample and only slightly greater on the powdered sample, some of the pores of which had been opened when the pellets were pulverized.

The isotherms obtained are shown in fig. 4.1.3 but the internal surface area could not be calculated from them.

Fig. 4.1.4 shows the adsorption isotherm for oxygen on the carbon molecular sieve. O_2 molecules are smaller than N_2 and could therefore penetrate the pore system of the carbon and were assumed to use the full internal surface area. The value of 14.1 $Å^2$ was used as the area of an adsorbed O_2 molecule (Gregg and Sing, 1982) and a surface area of 510 $m^2\ g^{-1}$ resulted from the saturation value. The volume occupied by an adsorbed O_2 molecule was calculated from the density of liquid O_2 at 77K, using the formula

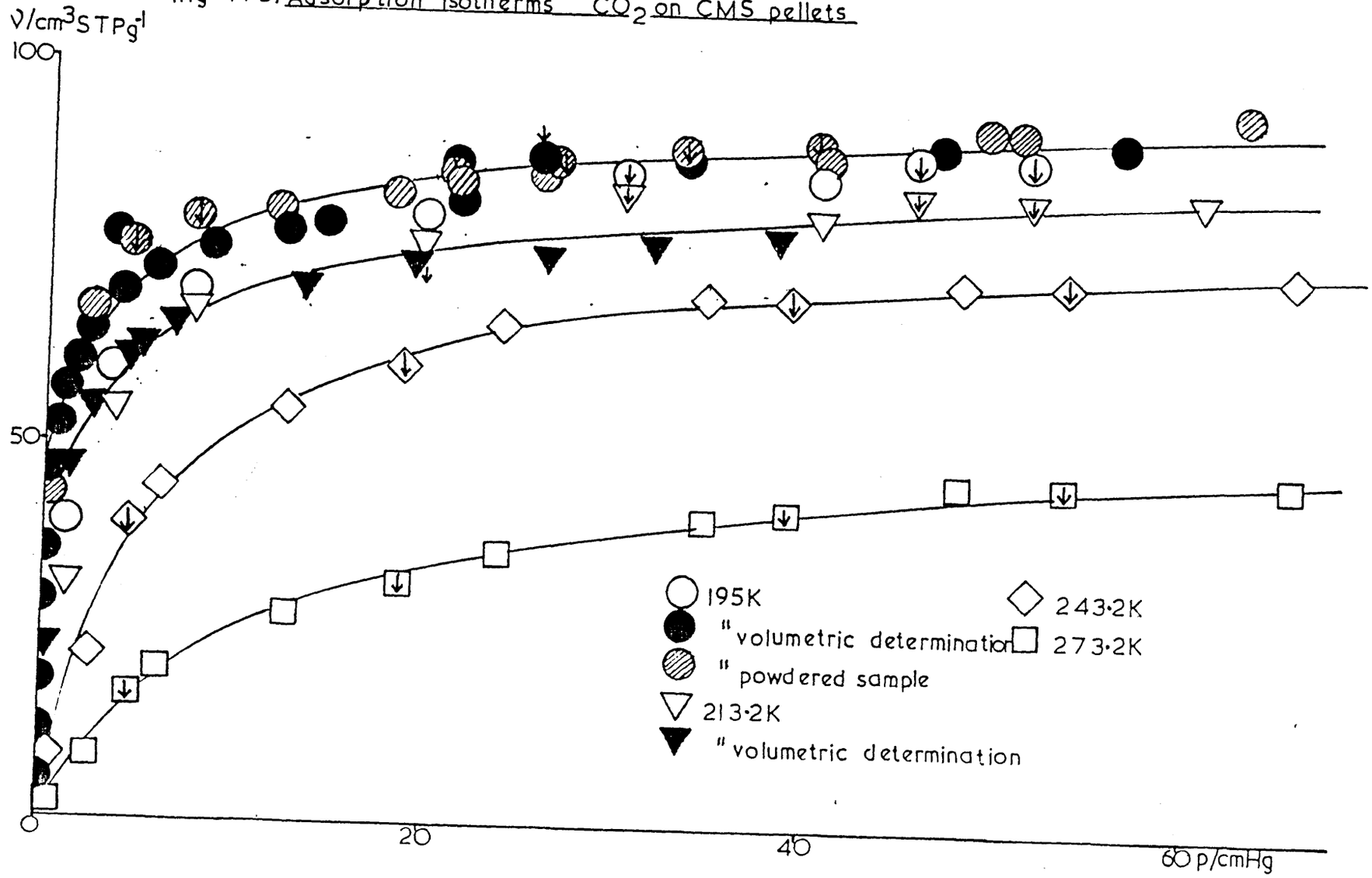
$$\text{Volume} = f\ (M/\rho_L\ L) \qquad \text{(Gregg and Sing 1982)}$$

Where M = molecular mass/kg mol^{-1}, ρ_L = liquid density/kgm^{-3}, L = Avogadro constant/mol^{-1} and f is a dimensionless factor which depends upon the packing of the molecules. In this case cubic close packing was assumed giving f = 1.091, which led to a void volume of 0.169 $cm^3\ g^{-1}$.

4.1.4 Adsorption of CO_2 and H_2S on Carbon Molecular Sieve

Adsorption isotherms of CO_2 on the carbon molecular sieve at 195K, 213.2K, 243.2K and 273.2K are shown in fig. 4.1.5, all

(fig 4·1·5) Adsorption isotherms CO_2 on CMS pellets



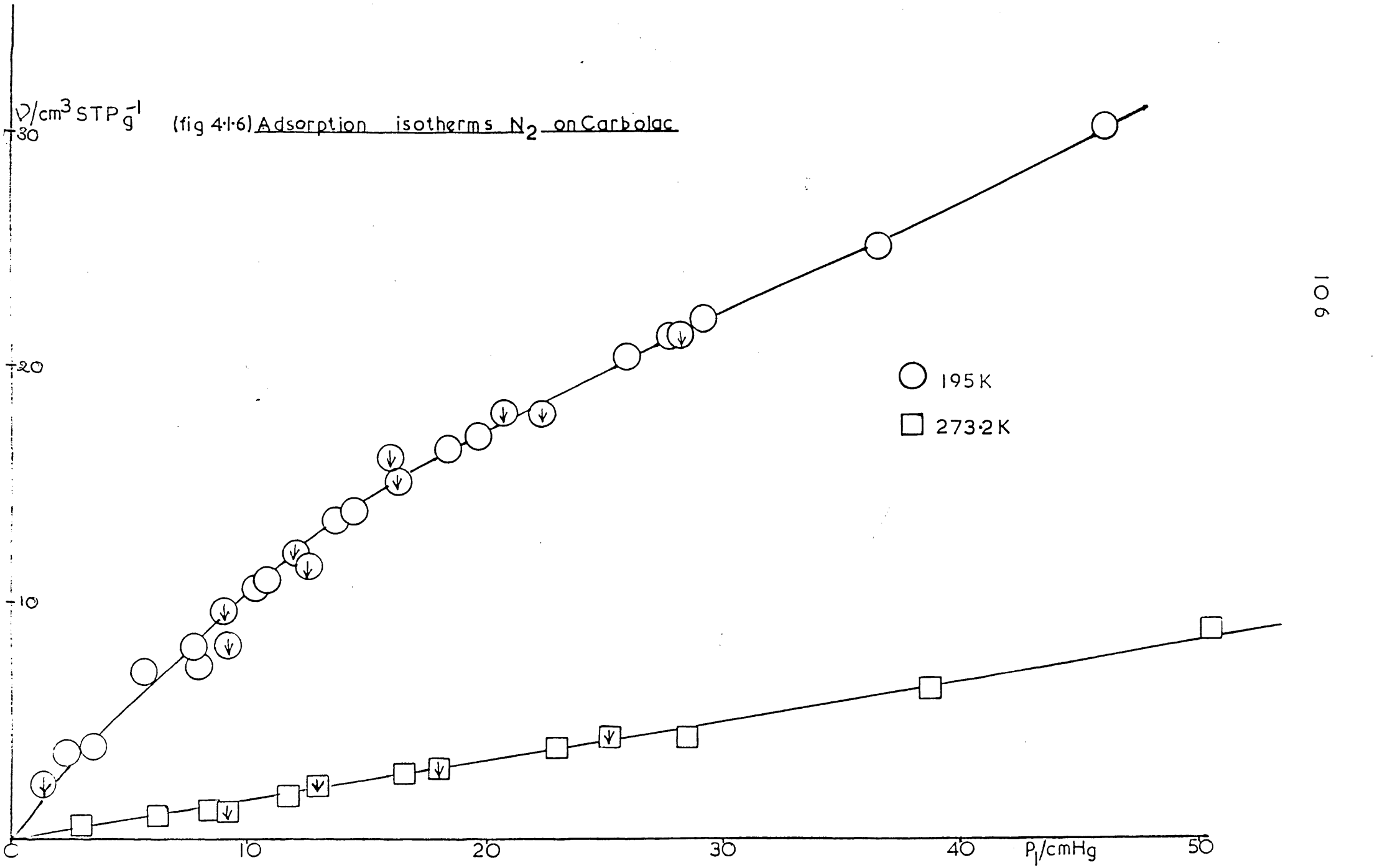
were reversable and reproducible and were of type 1 in the BET classification. Comparison with fig. 4.1.1 shows that the carbon molecular sieve uptake of CO_2 is approximately 40% of that of NaX, at the same temperature and pressure and the isotherms obtained are slightly less rectangular in form. The adsorption isotherms obtained using the volumetric apparatus are in reasonable agreement (less than 4% difference) with those obtained using the McBain balance, and those measured at 195K on the powdered sample agree well with measurements on the pellets at that temperature. The saturation value of CO_2 adsorbed at 195K (88 $cm^3 STP g^{-1}$) was used to calculate the surface area using values of 22.2 $Å^2$ and 20.6 $Å^2$ as the area taken by one adsorbed CO_2 molecule (Gregg and Sing).

The resulting surface areas obtained were 523 $m^2 g^{-1}$ and 485 $m^2 g^{-1}$ compared with 510 $m^2 g^{-1}$ calculated using the O_2 isotherm at 77K. H_2S at a pressure of 20 cmHg was admitted to sorption samples at 195K and 273.2K, but uptake was extremely slow and equilibrium adsorption had not been obtained after 6 hours.

It was concluded that H_2S adsorption must be dependent upon the rate of diffusion of molecules into the pore system of the carbon, thus it was impractical to measure adsorption isotherms of this system in the time available.

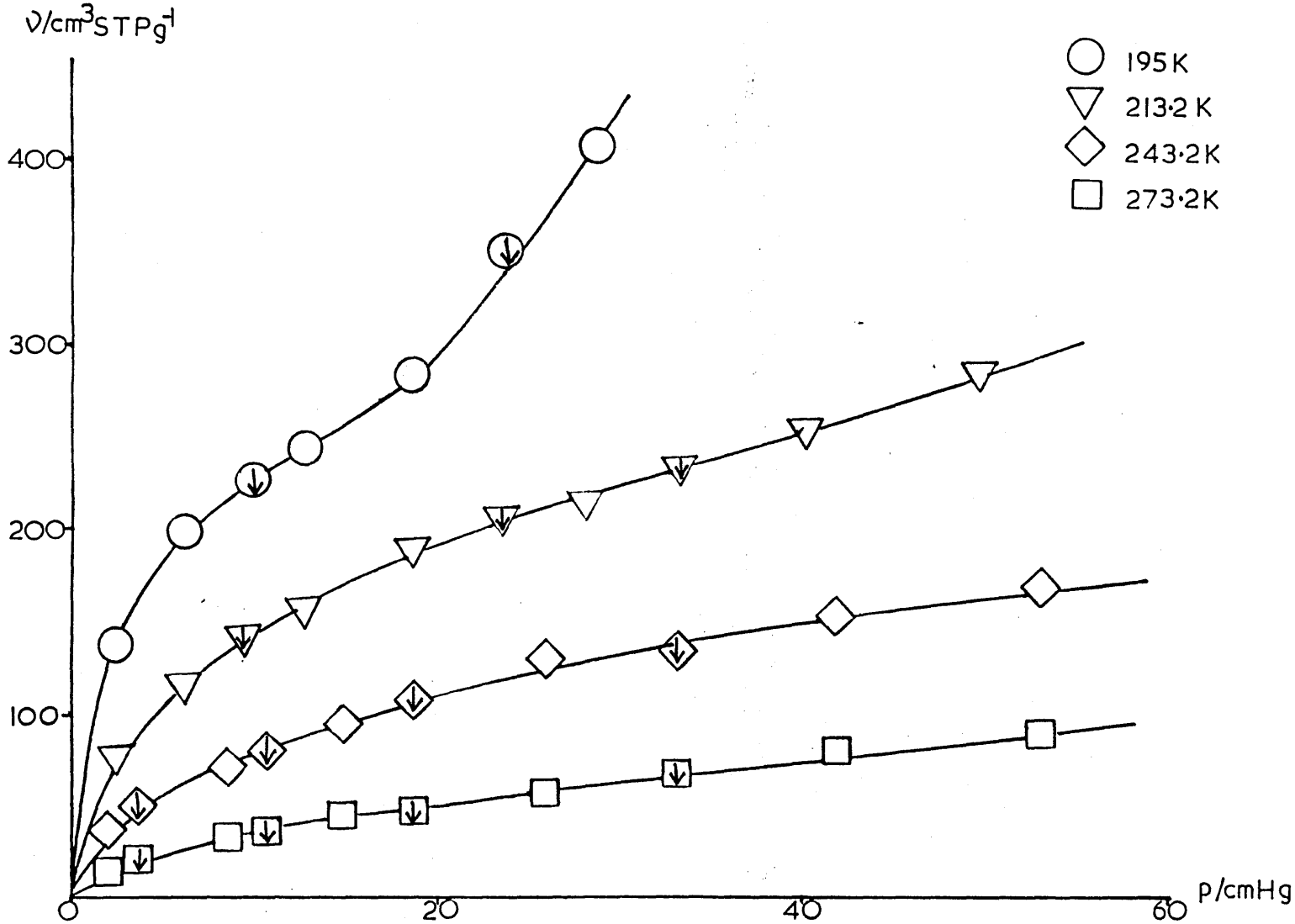
4.1.5 Adsorption Isotherms of N_2 and H_2S on Carbolac

Adsorption isotherms for CO_2 on Carbolac at 195K, 209K, 233.2K, 250.3K and 273.2K had been measured in this laboratory by



(fig 4·1·6) Adsorption isotherms N_2 on Carbolac

(fig 4·1·7) Adsorption isotherms H_2S on Carbolac



Dr. P. Sharma (1976) and were not determined in this study. No measurement of N_2 adsorption on Carbolac powder above 77K could be found in the literature. Isotherms at 195K and 273,2K were determined volumetrically by the author and they are shown in fig. 4.1.6. Very little N_2 was adsorbed at these temperatures and extreme care was necessary in order to minimise errors. A sample of Carbolac was outgassed on the McBain balance and a weight loss of 9.2% was observed as compared with Sharma's value of 9.2% (table 4.1.1). H_2S adsorption was then measured at 195K, 213.2K, 243.2K and 273.2K on this sample (fig. 4.1.7). The isotherms obtained were reversable and reproducible and of type II in the BET classification. Comparison with fig. 4.1.2 and with Sharma's CO_2 isotherms on Carbolac showed that the volume of H_2S adsorbed was more than twice that adsorbed by NaX and also twice the volume of CO_2 adsorbed by Carbolac at the same temperature.

4.1.6 Adsorption Isotherms of N_2, CO_2, H_2S and SF_6 on Graphon

Fig. 4.1.8 shows the adsorption of N_2 on Graphon at 195K and 273.2K. The isotherms were determined volumetrically and were found to be reversible and slightly curved convex to the pressure axis. At 273.2K less than 1 $cm^3 STP g^{-1}$ of N_2 was detectable on Graphon using the volumetric adsorption apparatus and extreme care was necessary for an accurate determination of the isotherm.

CO_2 adsorption on Graphon was also measured volumetrically and the isotherms obtained are shown in fig. 4.1.9. It was necessary to determine CO_2 isotherms over a wide range of temperatures (184K,

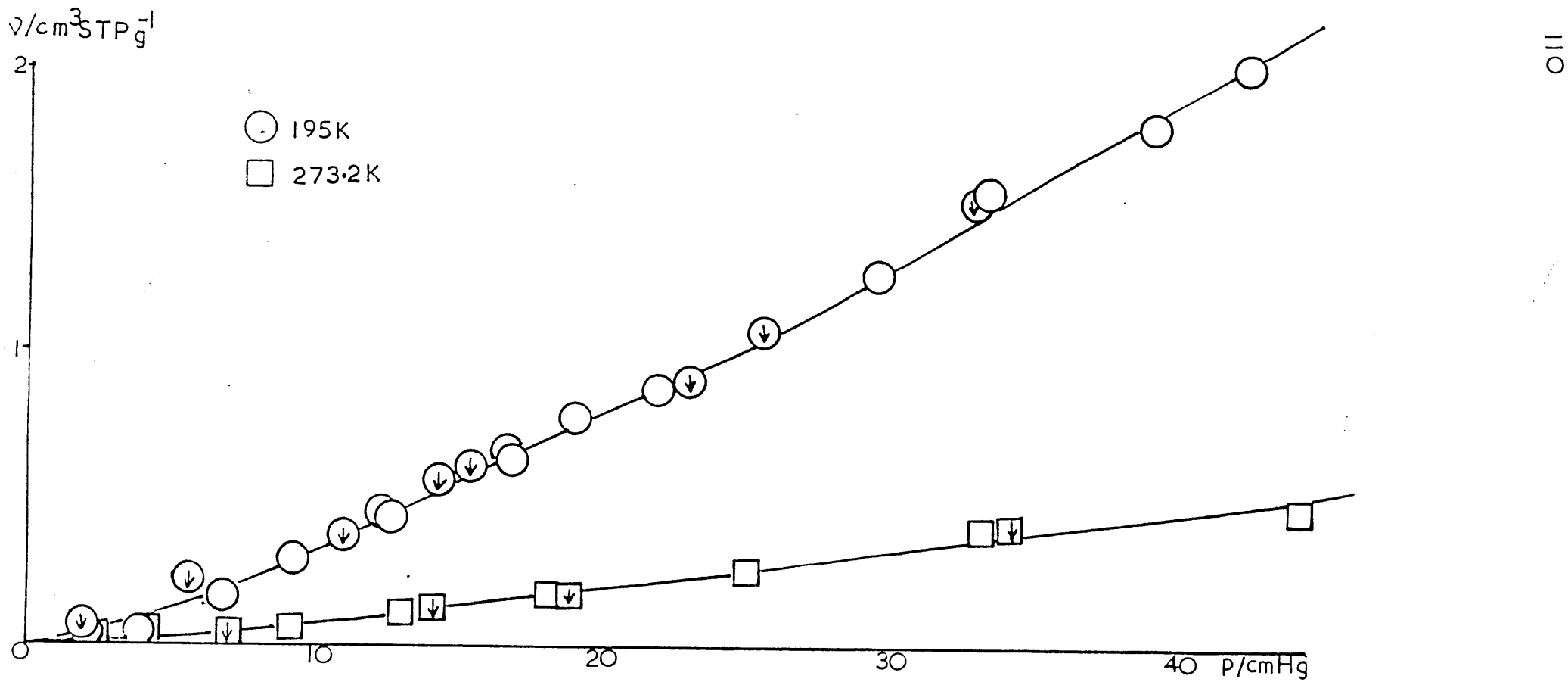
190.5K, 195K, 200K, 213.2K, 218.2K and 273.2K) in order to make full analysis of the results of A.P. Sharpe (1983) and P. Ferdani (1982). The isotherm obtained at 195K on Graphon pellets was compared with one determined by Dr. A. A. Rizvi (1981) on a different sample of Graphon, and with an isotherm determined by the author upon Graphon powder from which the membrane had been fabricated (fig. 4.1.10).

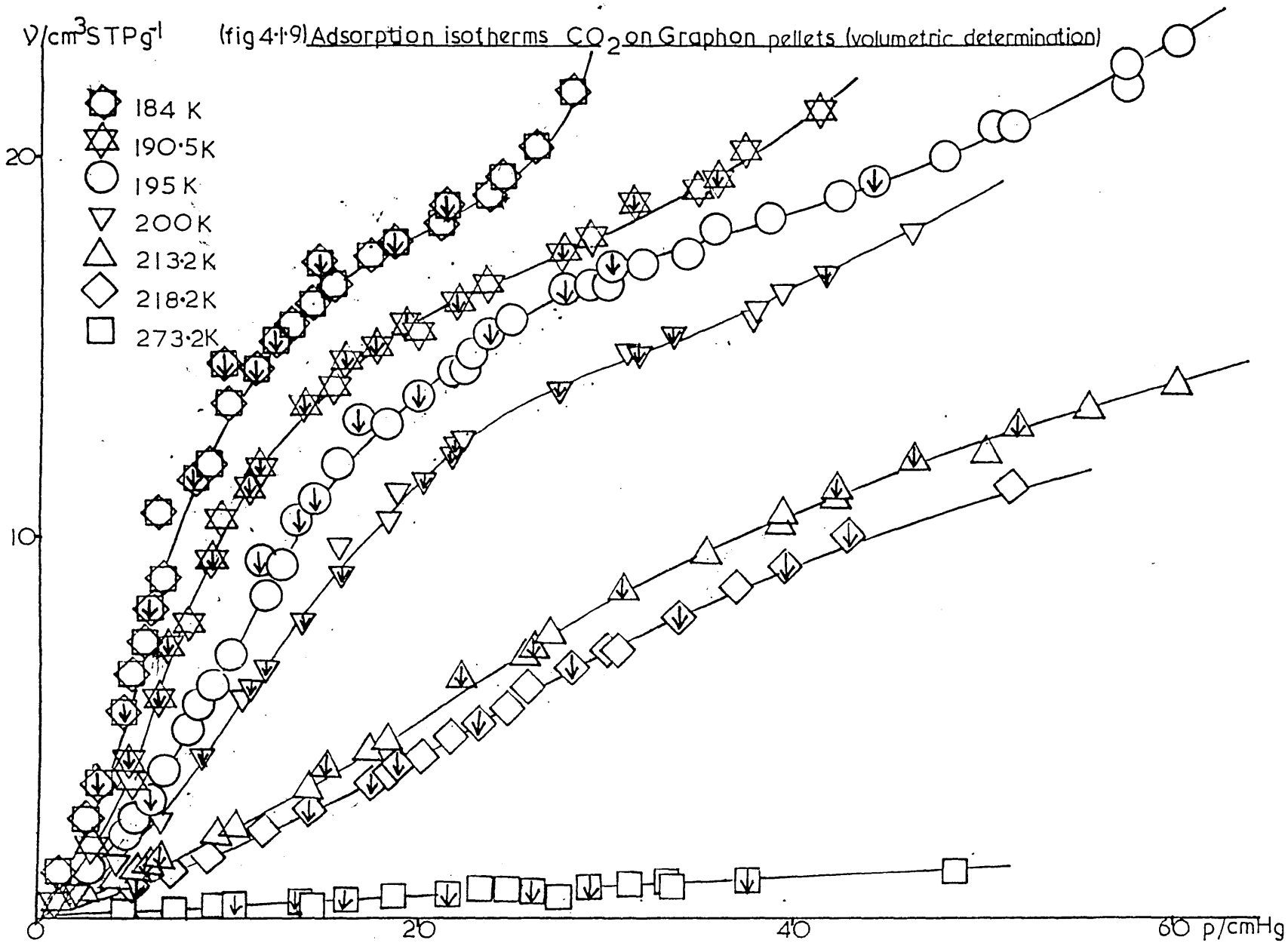
Agreement between the three isotherms was good at lower pressures; however above 20 cmHg, slight divergence was noticed (approx. 4%).

Fig. 4.1.11 shows the adsorption of H_2S by Graphon pellets at 195K, 213.2K, 243.2K and 273.2K. The isotherms obtained show similarity to the CO_2 isotherms fig. 4.1.9, being convex to the pressure axis at low pressures (type III/type V in the BET classification), but the volume of H_2S adsorbed was approximately twice that of CO_2 at the same temperature and pressure.

Fig. 4.1.12 shows the adsorption isotherm for SF_6 adsorption on Graphon pellets at 195K, obtained by Mr. R. Bhusate in this laboratory. All the isotherms obtained both on Graphon powder and pellets were found to be completely reversable and reproducible, and no weight loss from any of the Graphon samples was observed on outgassing.

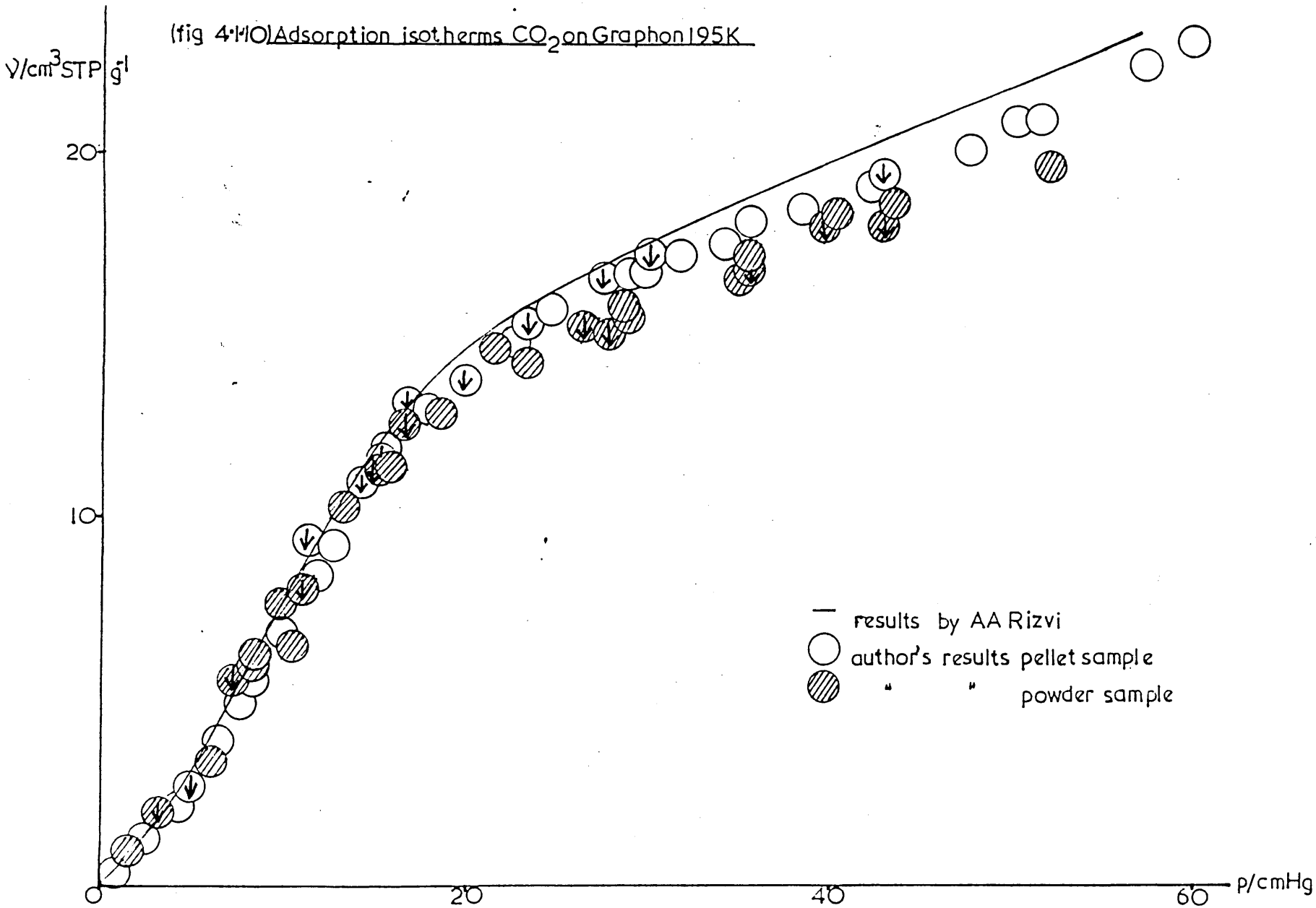
(fig 4·1·8) Adsorption isotherm N_2 on Graphon pellets



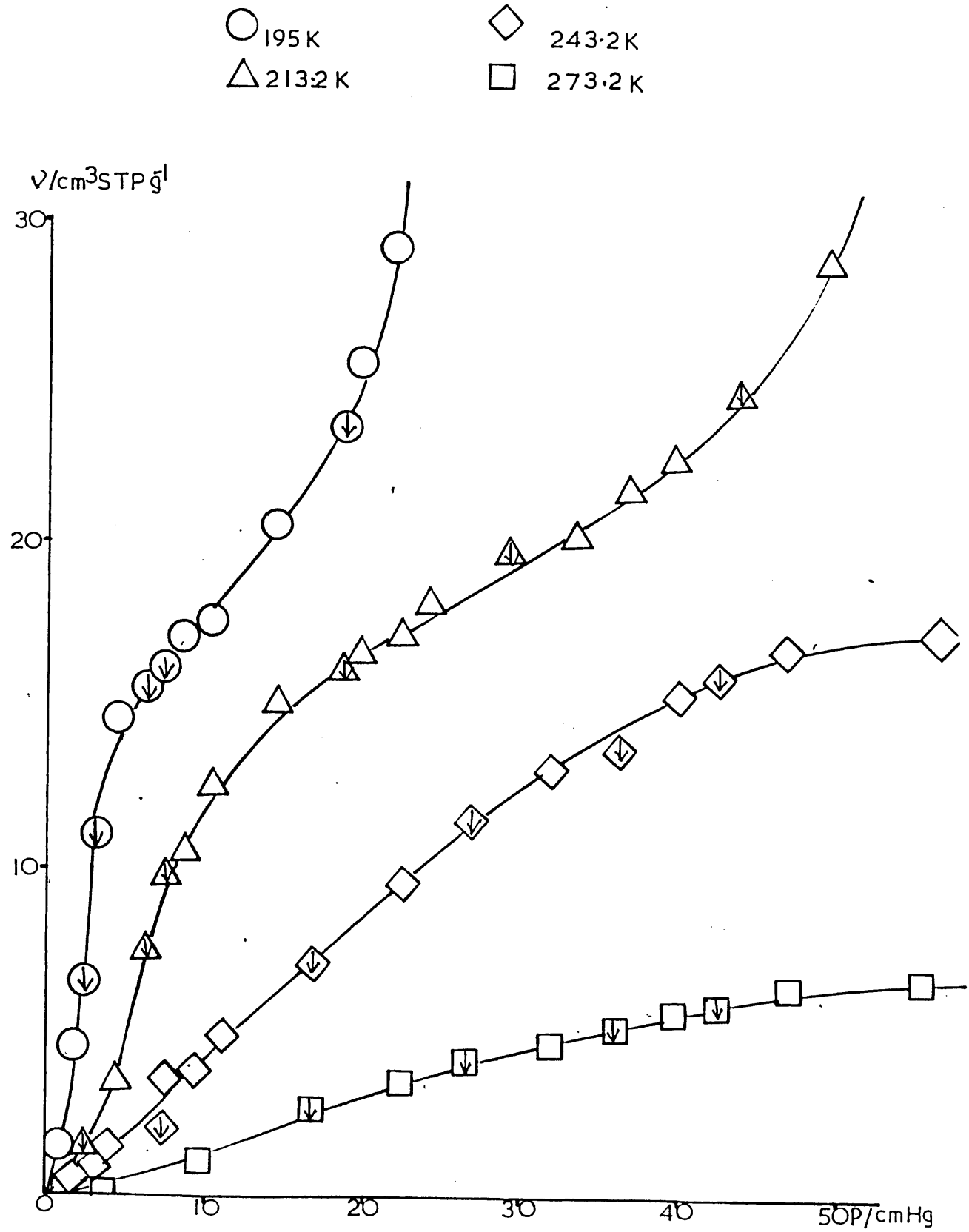


(fig 4·1·9) Adsorption isotherms CO_2 on Graphon pellets (volumetric determination)

(fig 4·1·10) Adsorption isotherms CO_2 on Graphon 195K



(fig 4·1·11) Adsorption isotherms H_2S on Graphon pellets



(fig 4·1·12) Adsorption isotherm

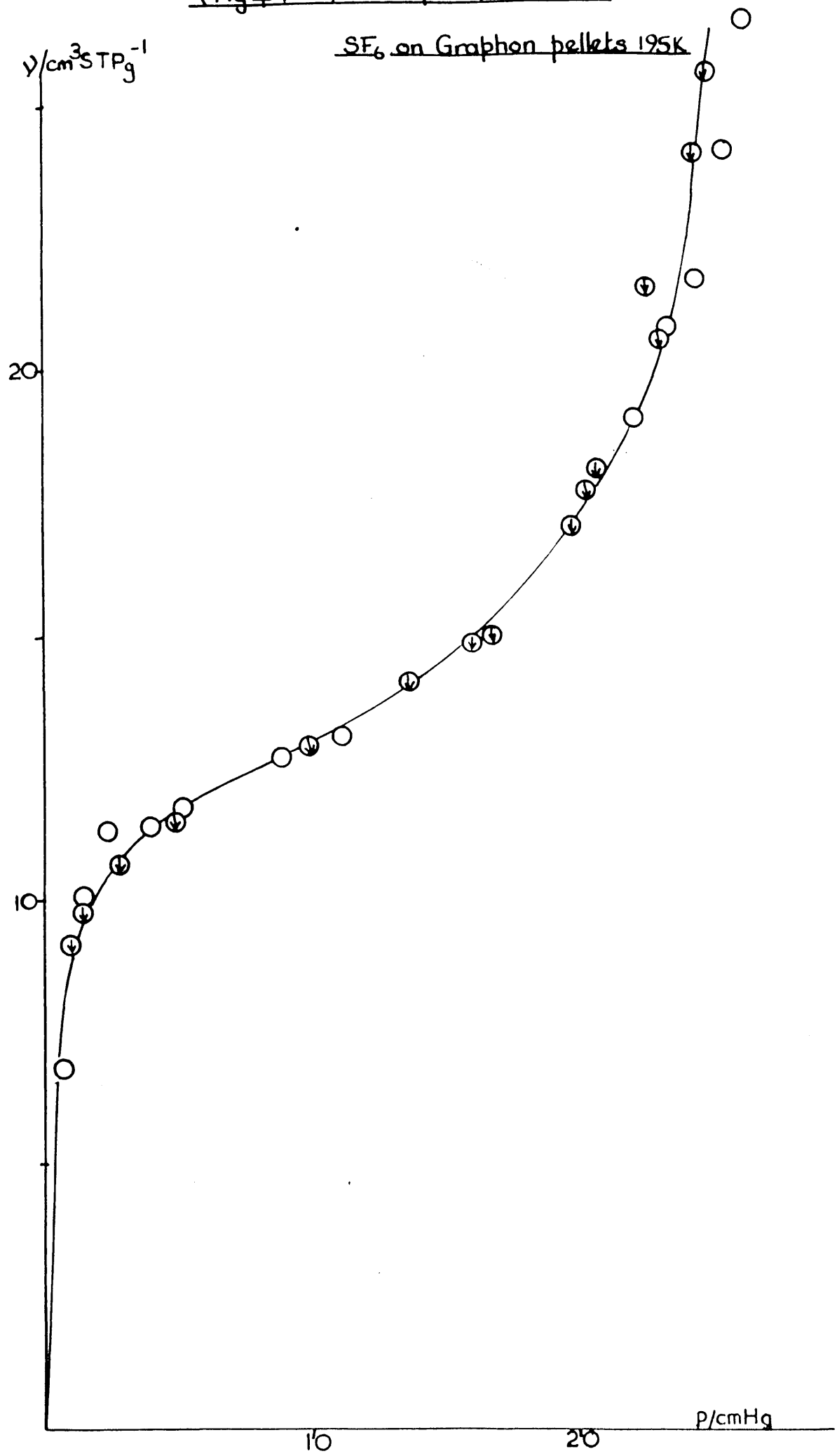


Table 4.1.1

Weight loss on outgassing

Sample	% weight loss (this study)	(other values)
NaX	25.7	25.7 (Coughlan)
CMS	5.75	-
Carbolac	9.2	9.5 (Sharma)
Graphon	0	0 (Hamilton)

4.1.7 Error Analysis

Random errors in the determination of adsorption isotherms may arise from temperature fluctuations, and from uncertainty in volume calibrations and in cathetometer readings. Temperature fluctuations were minimised by use of a leaky-dewar cryostat with efficient stirring; the temperature was closely monitored using pre-calibrated Toluene thermometers and fluctuations minimised to less than 1° C.

The main source of error in the gravimetric system was the use of the cathetometer to measure the small change in the length of the spring. This combined with uncertainty in the sample weight to give a maximum error of $\pm$ 4% at low pressures. In the volumetric system the main sources of error were the error in calibration of the doser volume and sample bulb volume and that in measuring the pressure. These combined to give error limits of $\pm$ 2% at low pressures. The greater scatter of points on adsorption isotherms

measured using the McBain balance may therefore be attributed to the small sample weights, which were made necessary by the characteristics of the spring used. (max. weight 1 g, max. extension 25 cm). For all the isotherms measured the maximum percentage error occurred at low pressures and the majority of points fall well within the quoted limits.

4.2 Single Gas Flow Results

4.2.1 Introduction

For all the membranes, isothermal measurements for single gases were made under a constant pressure difference and the effect of varying the temperature and the ingoing pressure examined.

The systems studied are given in table 4.2.1.

4.2.2 Single gas flow results for zeolite membrane 1

The passage of He and CO_2 was investigated through this membrane and the results for He were compared with those obtained by Mr. R. Ash for He flow in 1955. Since the flow of several gases through this membrane has been well documented, (Mr. R. Ash, 1955, Miss K. Hollinshead, 1985) H_2S was not passed through it, as the possibility of a catalytic reaction damaging the membrane could not be ignored. cf. section 4.1.2. The appearance of sulphur upon zeolite during the measurement of H_2S isotherms at 30° C indicated that fouling of the membrane was probable at the higher temperatures.

All the membranes used were "calibrated" using He, which was

Table 4.2.1 Systems for which single gas flow was investigated

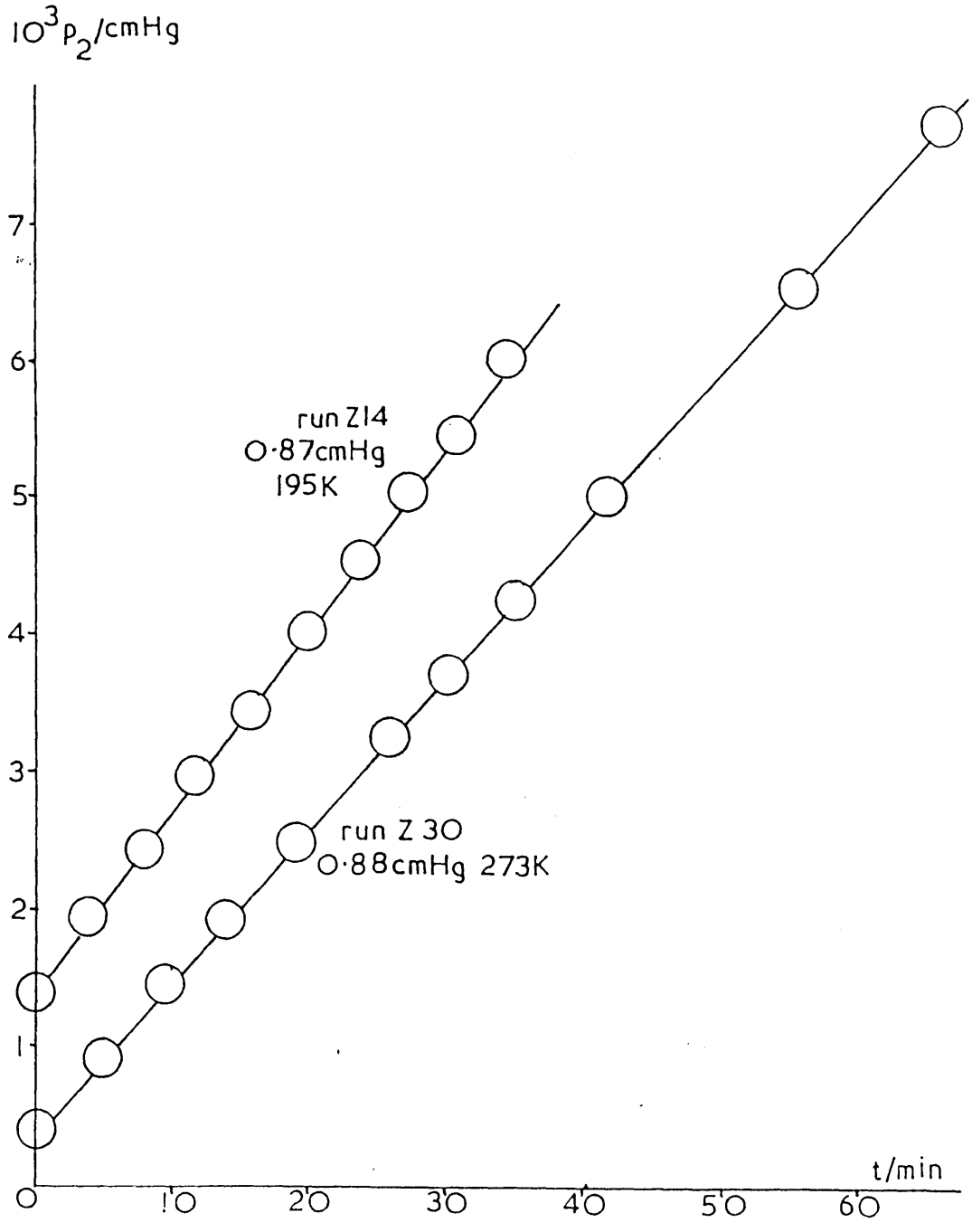
Membrane	Gas	Membrane	Gas
Zeolite 1	He	Graphon	He
	CO_2		N_2
Zeolite 2	He		Ar
	N_2		CO_2
	H_2S		H_2S
Carbon Molecular Sieve	He		C_3H_8
	N_2		SF_6
	CO_2		
	H_2S		
Carbolac	He		
	N_2		
	CO_2		
	H_2S		

Detailed tabulated results are given in Appendix B

not adsorbed by any of the materials investigated and could therefore be utilized to measure gas phase flow. Helium could be detected at the outgoing side of zeolite membrane 1 within 1 minute of its admission to the ingoing side and steady state flow was quickly established. Sample steady state outgoing pressure versus time graphs are shown in fig. 4.2.1 . Fig. 4.2.4 shows the variation of the integral permeability and steady state flux of He with ingoing pressure. The permeability is linearly dependent upon pressure and the flux curve is convex to the pressure axis indicating that Poiseuille flow is present. At 273.2K the permeabiity graph levels off at low pressures, however this effect is not observed at 195K. When CO_2 was admitted to the ingoing side of zeolite membrane 1 considerable time lapsed before gas was detected on the outgoing side as shown in fig. 4.2.2 and 4.2.3. This time has been designated the break-through time (BTT) (Barrer, 1954). When steady state flow was established, linear graphs of p_2 versus t could be plotted and extrapolated to $p_2 = 0$ to give the time lag (TL) as shown in fig. 4.2.3. For CO_2 flow at 195K the steady state was established soon after the breakthrough and the breakthrough time was often equal to the time lag as shown in fig. 4.2.2. However at 273.2K the p_2 vs. t graphs showed a curve before entering the linear portion. The time lags obtained at 195K exceeded those obtained at 273.2K, and at both temperatures they increased with decreasing pressure as shown in fig. 4.2.6. The integral permeability and steady state flux were also plotted against ingoing pressure (fig. 4.2.5) and were found to follow the same trends as those for He flow.

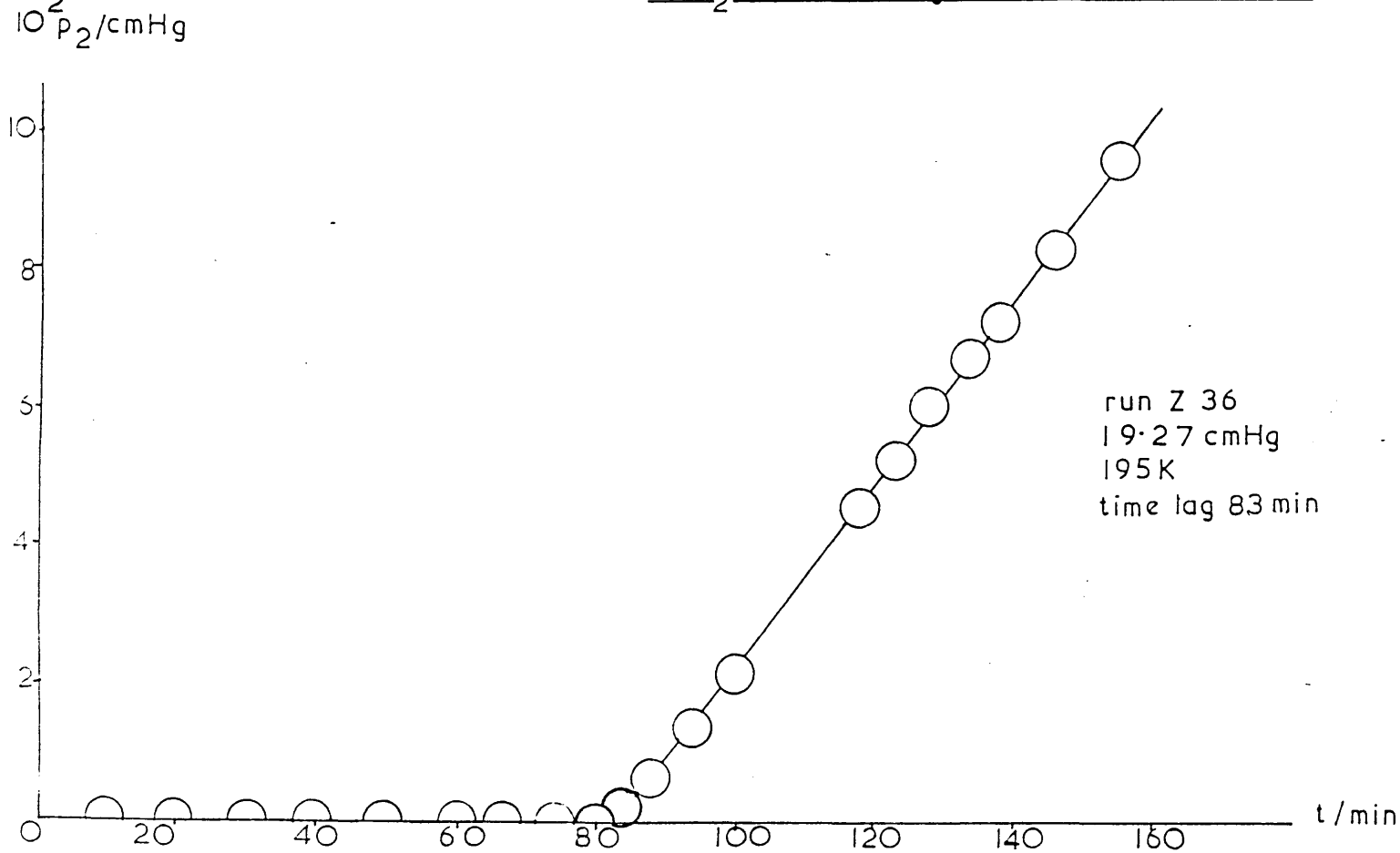
(fig 4·2·1) Sample outgoing pressure versus time graphs

He flow through Zeolite membrane I

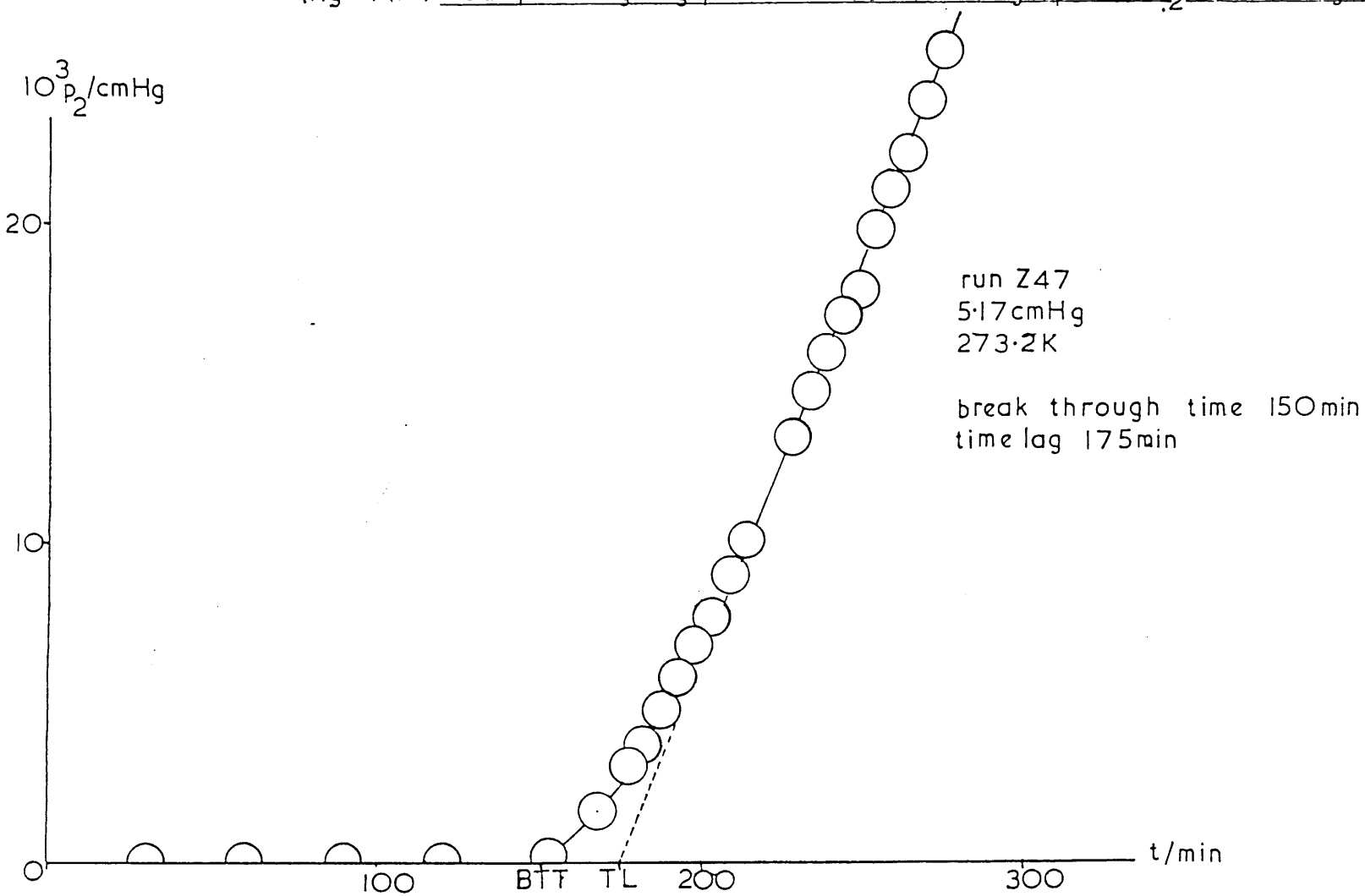


(fig 4·2·2) Sample outgoing pressure versus time graphs

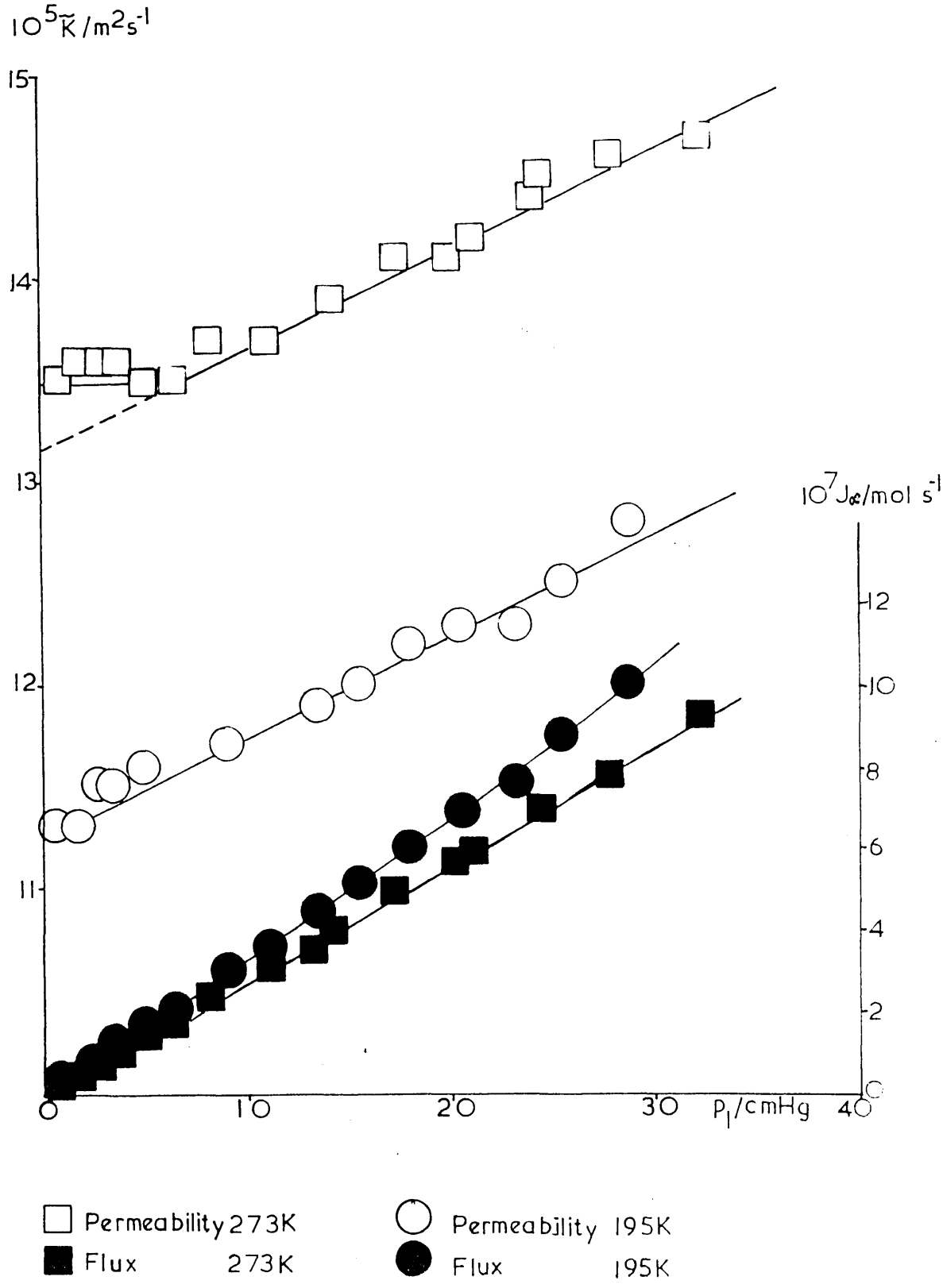
CO_2 flow through Zeolite membrane I



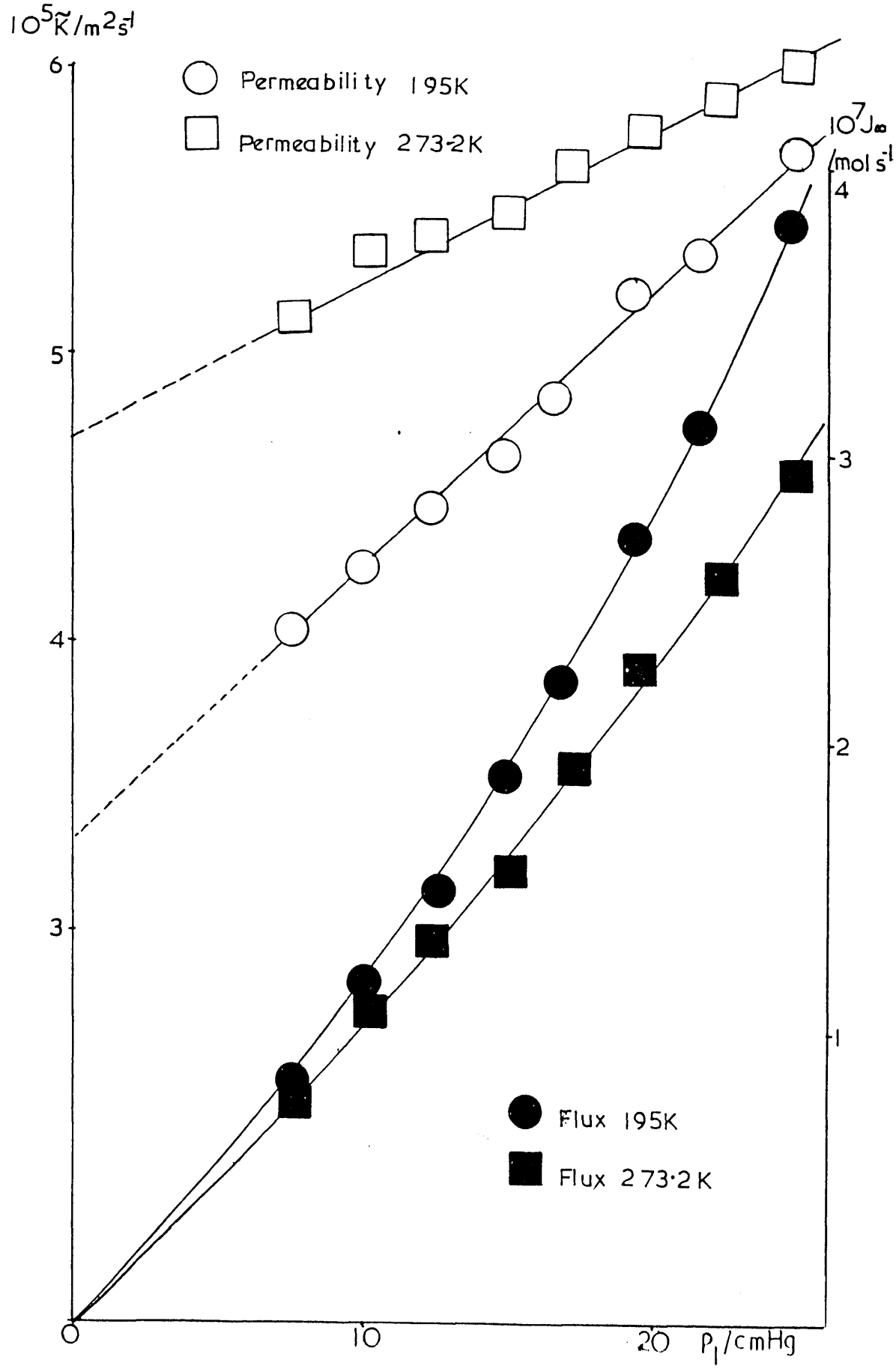
(fig 4·2·3) Sample outgoing pressure versus time graphs CO_2 flow through Zeolite membrane I



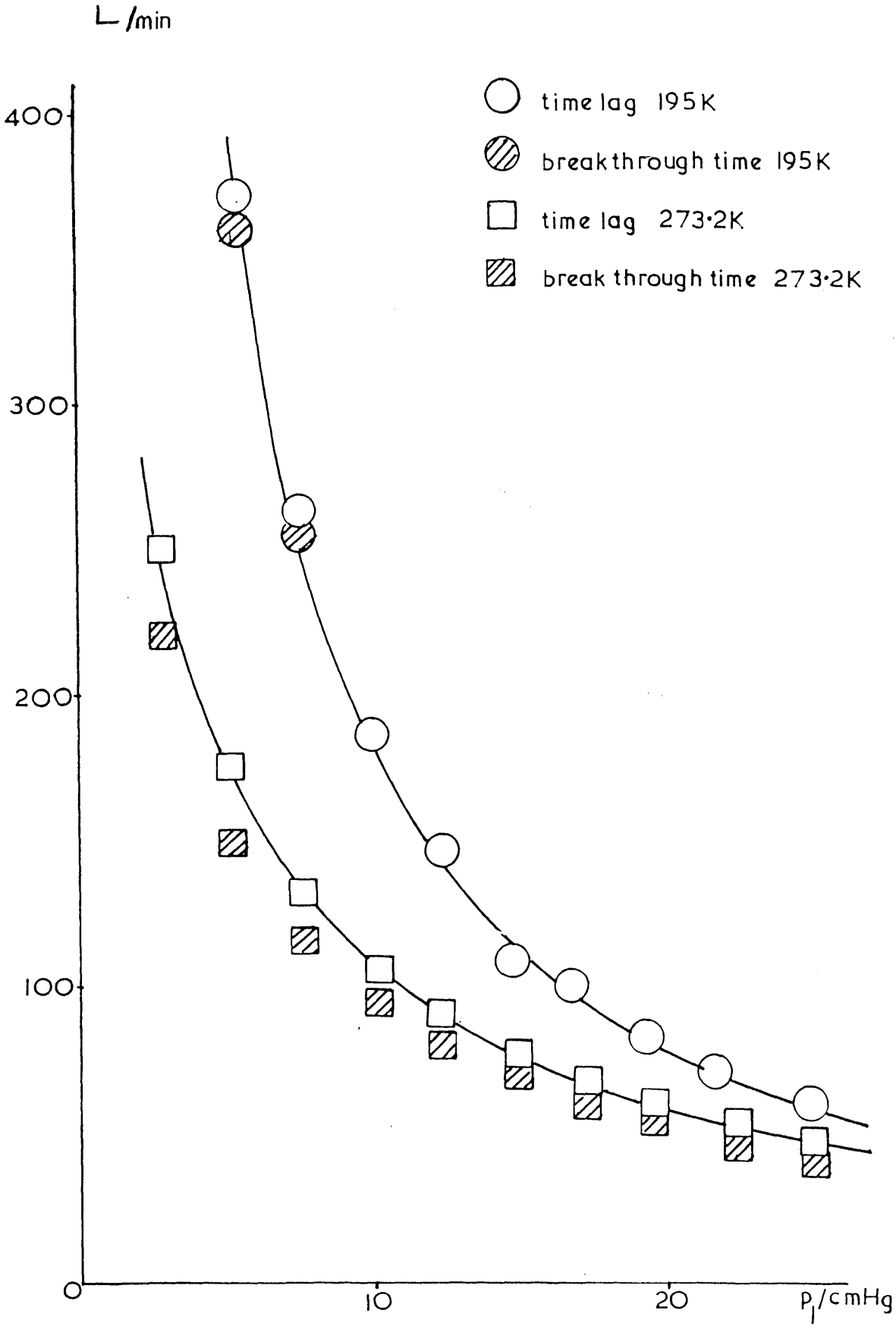
(fig 4·2·4) Integral permeability and steady state flux versus ingoing pressure; He flow through Zeolite membrane I



(fig 4·2·5) Integral permeability and steady state flux versus ingoing pressure: CO_2 flow through Zeolite membrane I



(fig 4·2·6) Time lag and break through time versus ingoing pressure: CO_2 flow through Zeolite membrane1



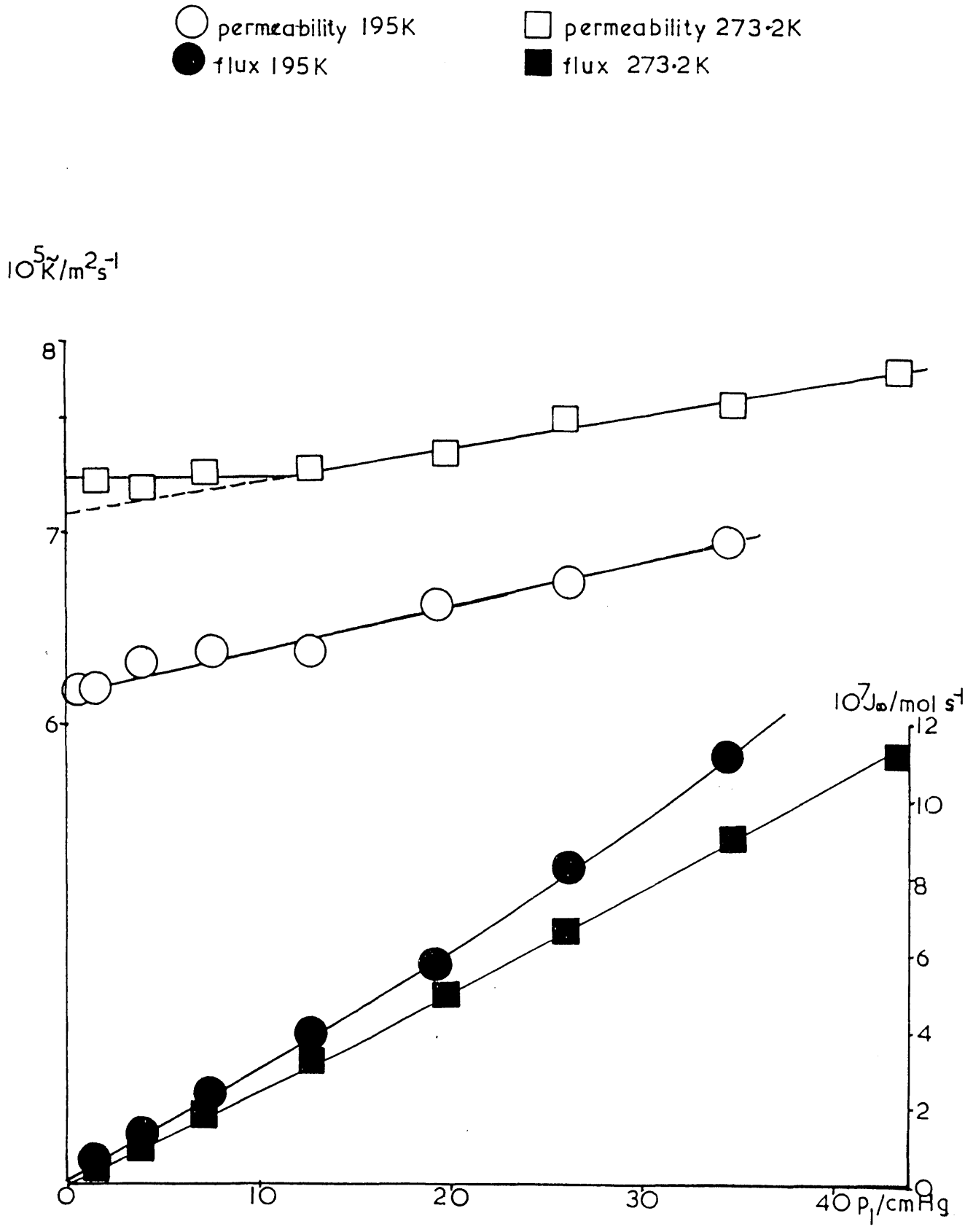
4.2.3 Single gas flow results for zeolite membrane 2

Zeolite membrane 2 was constructed in order to give moderate time lags and an easily measurable gas flow rate. (This was necessary as the length of the time lags achieved by zeolite membrane 1 precluded low pressure CO_2 experiments. The outgoing pressure versus time graphsobtained for He flow through zeolite membrane 2 were similar to those for membrane 1, and the graphs of He permeability and flux (fig. 4.2.7) also showed marked similarity to those obtained for membrane 1.

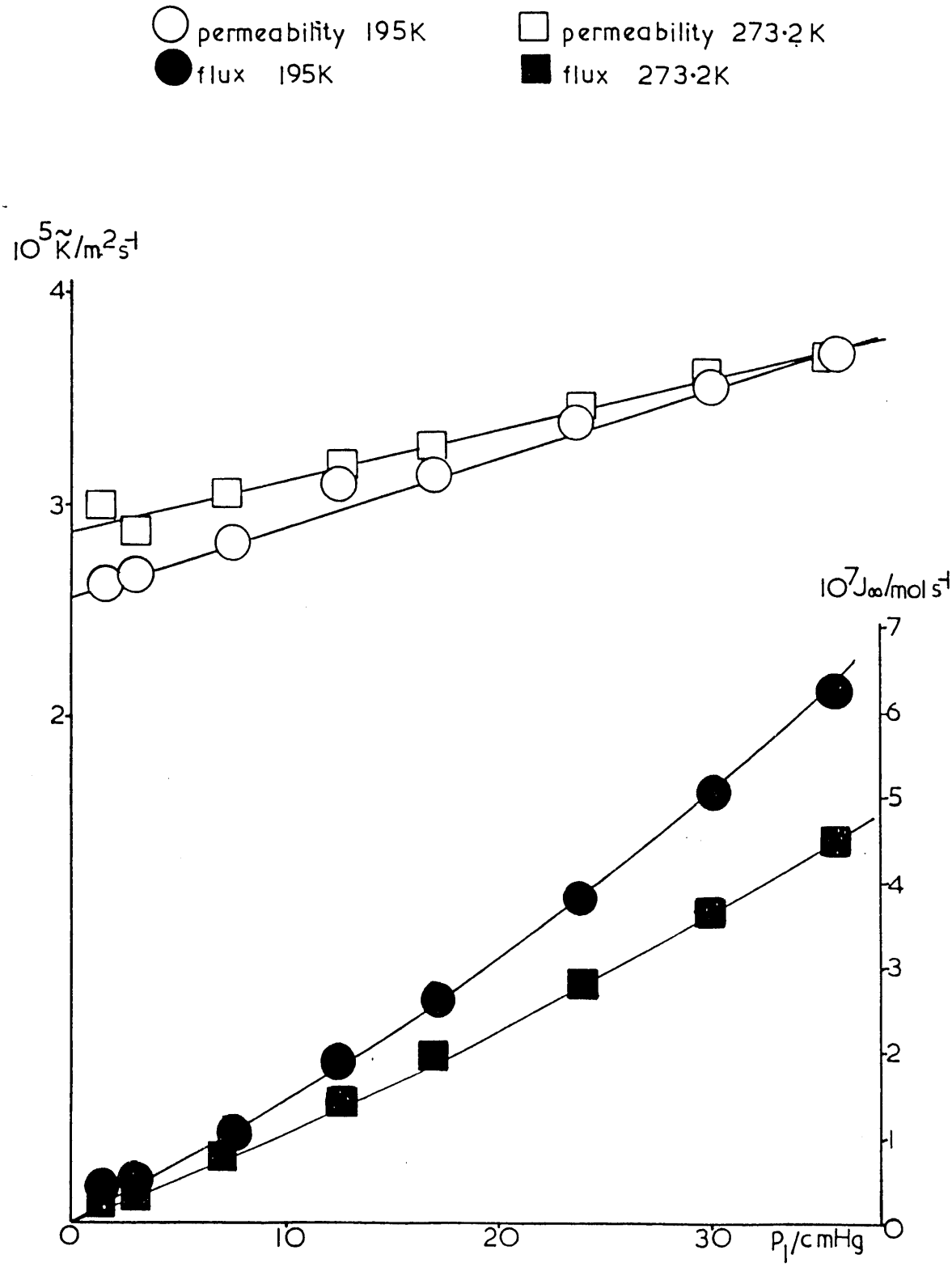
When N_2 was passed through membrane 2 short time lags were obtained at 195K as may be seen in fig. 4.2.10, however at 273.2K no measurable time lags were observed. Fig. 4.2.8 shows the pressure dependence of the permeability and flux of N_2. The permeability graph shows little deviation from linearity while the flux curve is convex to the pressure axis.

H_2S flow was investigated at 195K only,in order to avoid sulphur formation on the membrane. The time lags obtained were considerably greater than those for N_2 as may be seen in fig. 4.2.10.
Figure 4.2.9 shows the integral permeability and steady state flux of H_2S through zeolite membrane 2 which shows similarity to those obtained for N_2 (fig. 4.2.8). Figure 4.2.9 a and b show CO_2 flow through zeolite membrane 2 at 195K for comparison with CO_2 flow through membrane 1 (fig. 4.2.4).

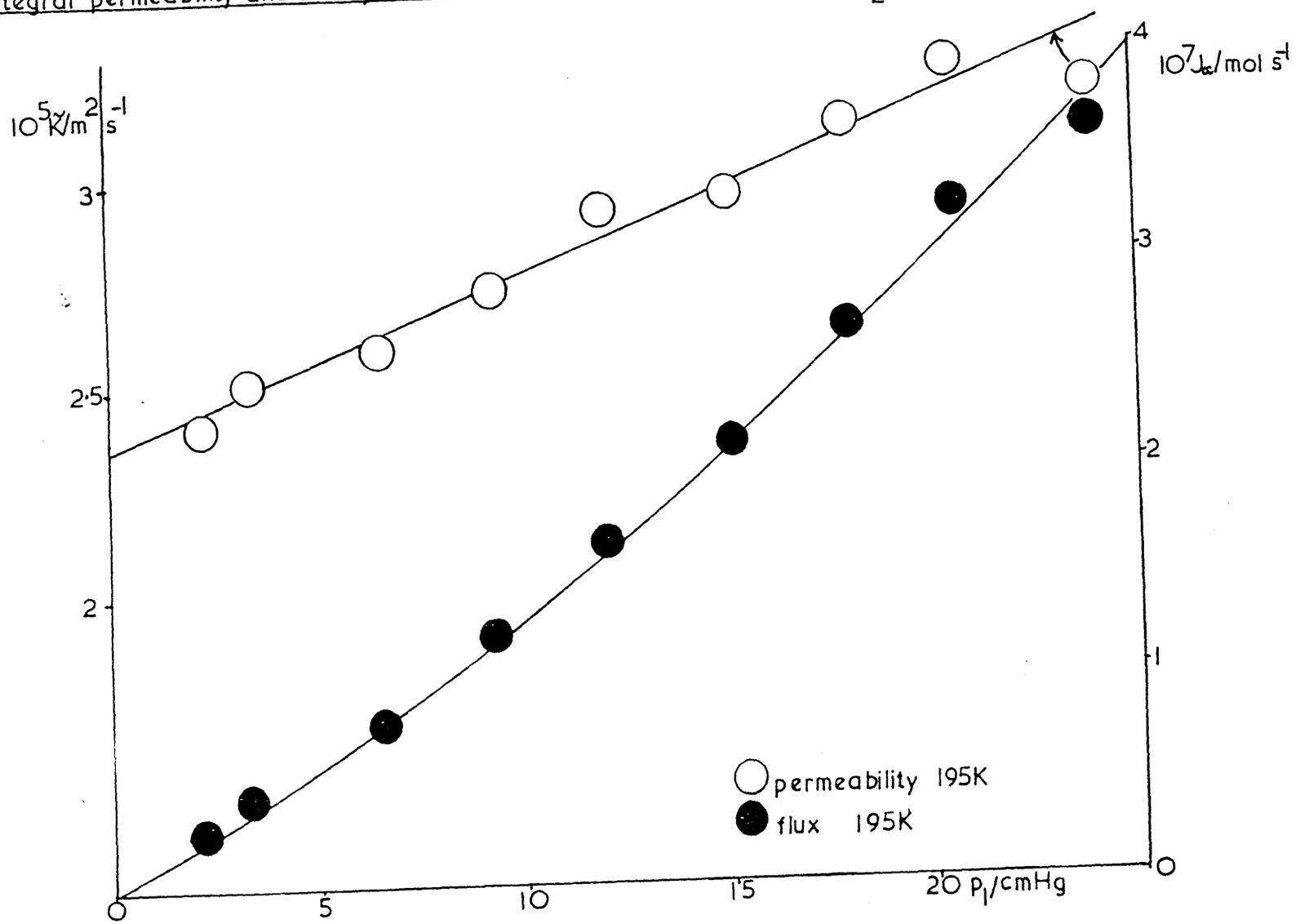
(fig 4·27) Integral permeability and steady state flux versus ingoing pressure : He flow through Zeolite membrane 2



(fig 4·2·8) Integral permeability and steady state flux versus ingoing pressure: N_2 flow through Zeolite membrane 2

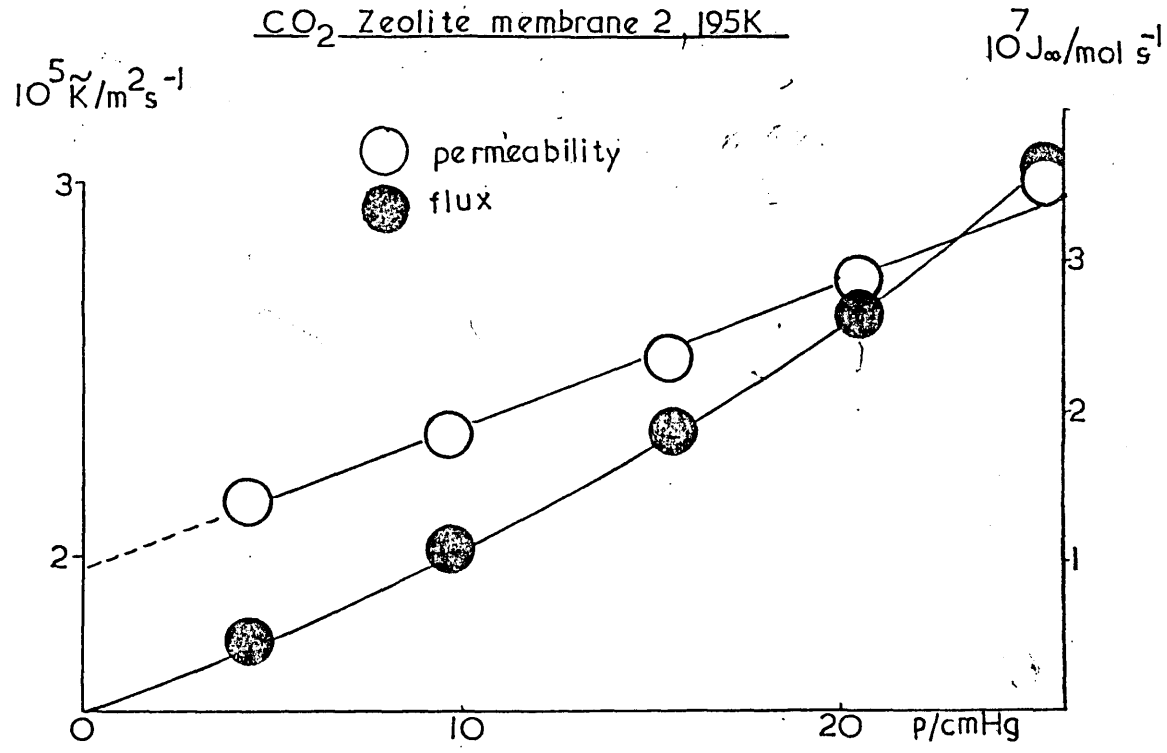


(Fig 4·2·9) Integral permeability and steady state flux versus ingoing pressure; H_2S flow through Zeolite membrane 2

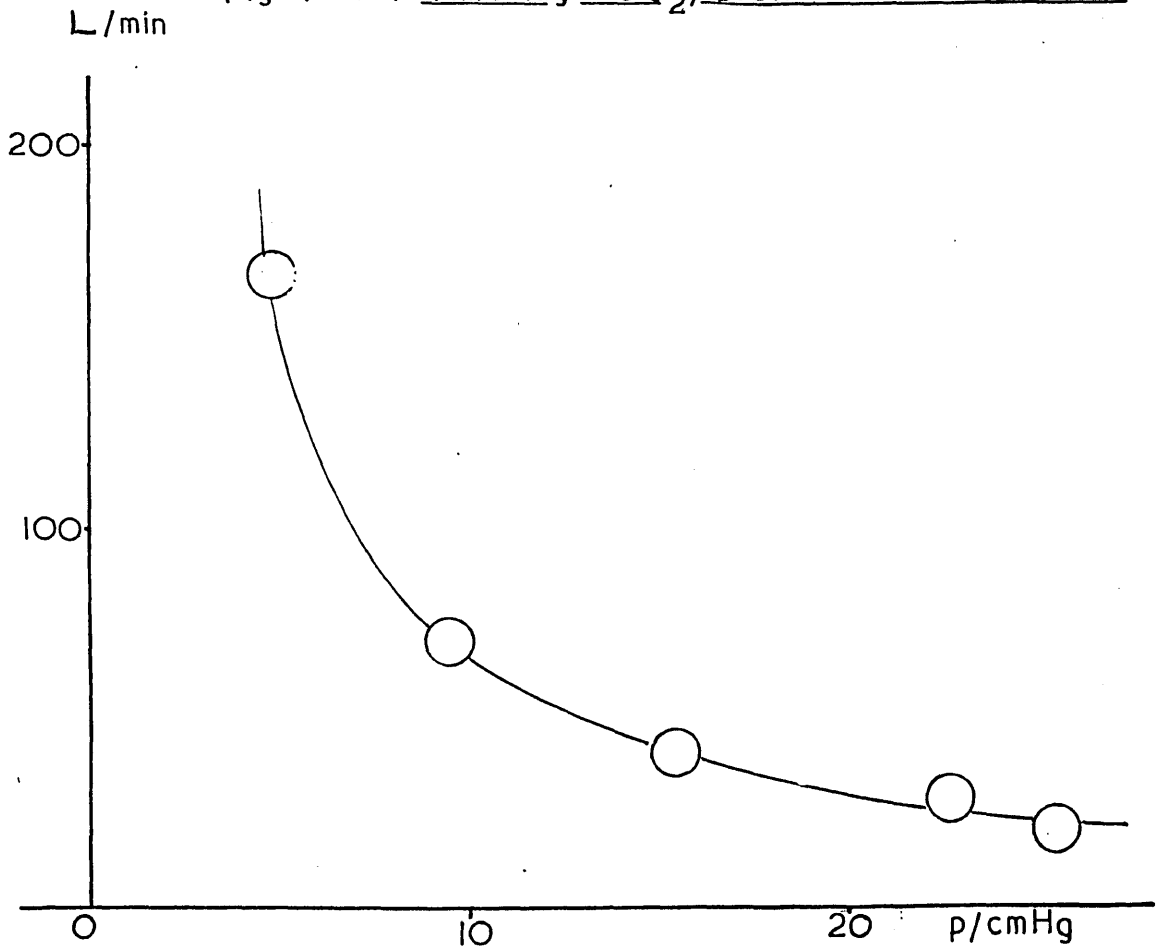


(fig 4·2·9a) Integral permeability and steady state flux

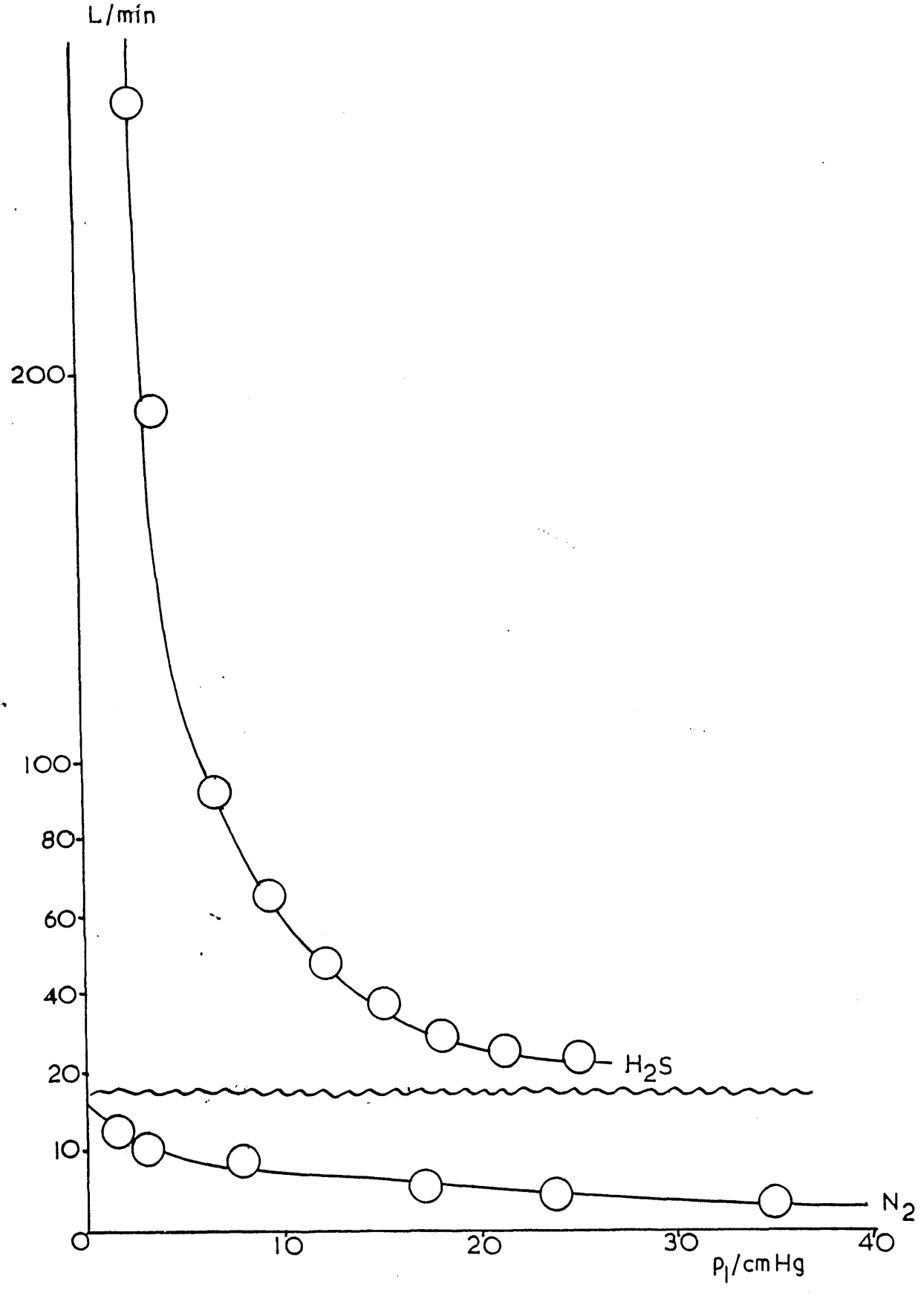
CO_2 Zeolite membrane 2, 195K



(fig 4·2·9b) Time lags CO_2/Zeolite membrane 2/195K



(fig 4·2·10) Time lag versus ingoing pressure: N_2 and H_2S flow through Zeolite membrane 2



4.2.4 Single gas flow results for CMS membrane

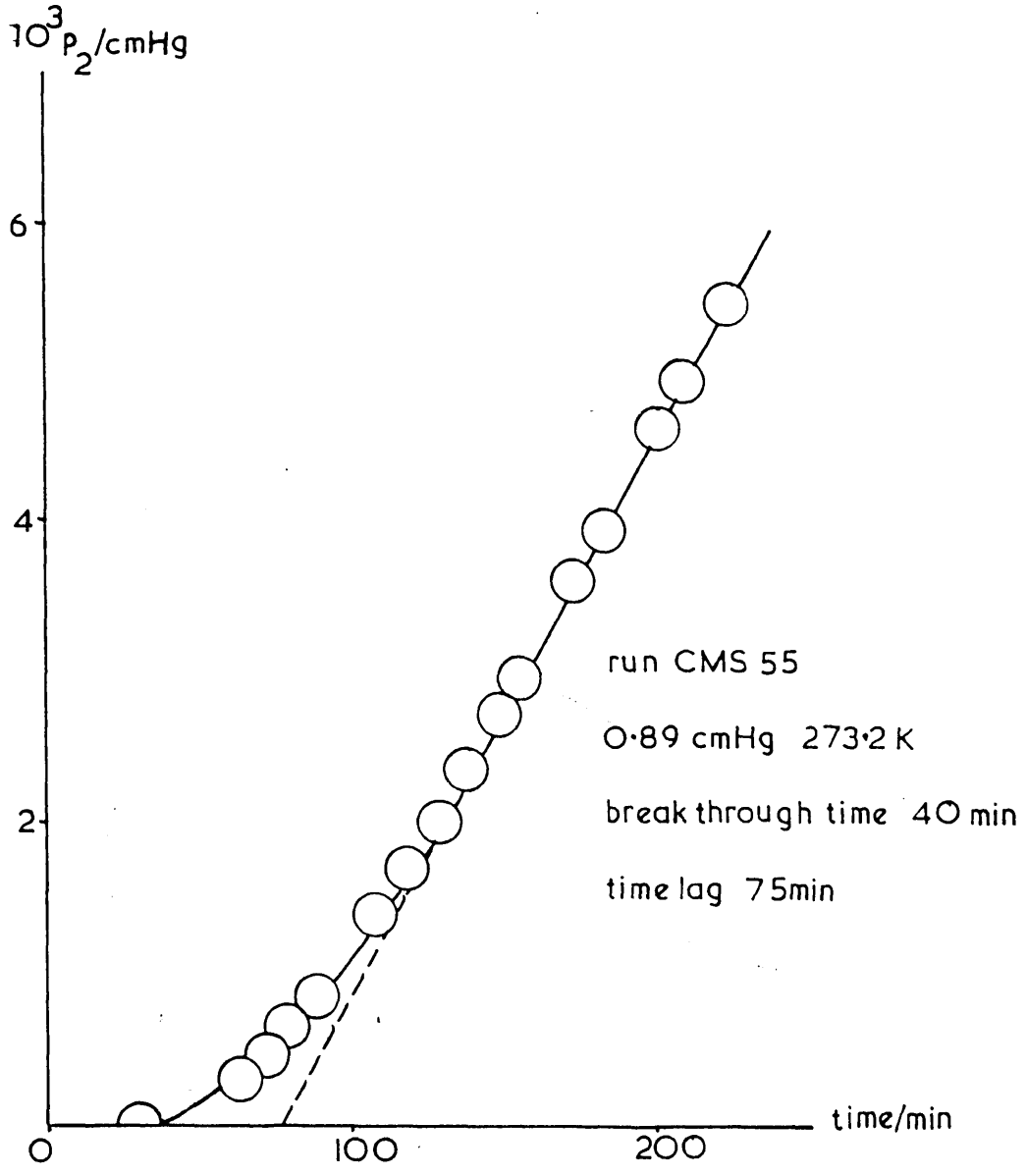
The carbon molecular sieve membrane was constructed in order to have comparable dimensions to zeolite membrane 1. Initially He flow was investigated, followed by N_2, CO_2 and H_2S in that order, finally the membrane was "re-calibrated" with He. The only gas to exhibit measurable time lags when passed through the membrane was CO_2, and a sample outgoing pressure versus time graph is included (fig. 4.2.11).

Fig. 4.2.12 and 4.2.13 show the integral permeability and steady state flux of He through the CMS membrane, at 195K and 273.2K, before and after exposure to other gases. The graphs are similar in form with the permeability increasing linearly with ingoing pressure (indicating the presence of Poiseuille flow) however the final measurements (fig. 4.2.13) show a greater permeability and flux than the initial ones (fig. 4.2.12) at the same ingoing pressure. This is due to membrane restructuring during H_2S flow experiments. N_2 and H_2S showed no time lag when passed through the CMS plug, in comparison with the considerable time lags which were obtained for N_2 and H_2S flow through NaX, (fig. 4.2.10). Fig. 4.2.14 and 4.2.15 show the steady state flux and integral permeability of the CMS membrane to these two gases, it is noticable that for N_2 the integral permeability is not linearly related to ingoing pressure, but exhibits a shallow minimum at 4 cmHg.

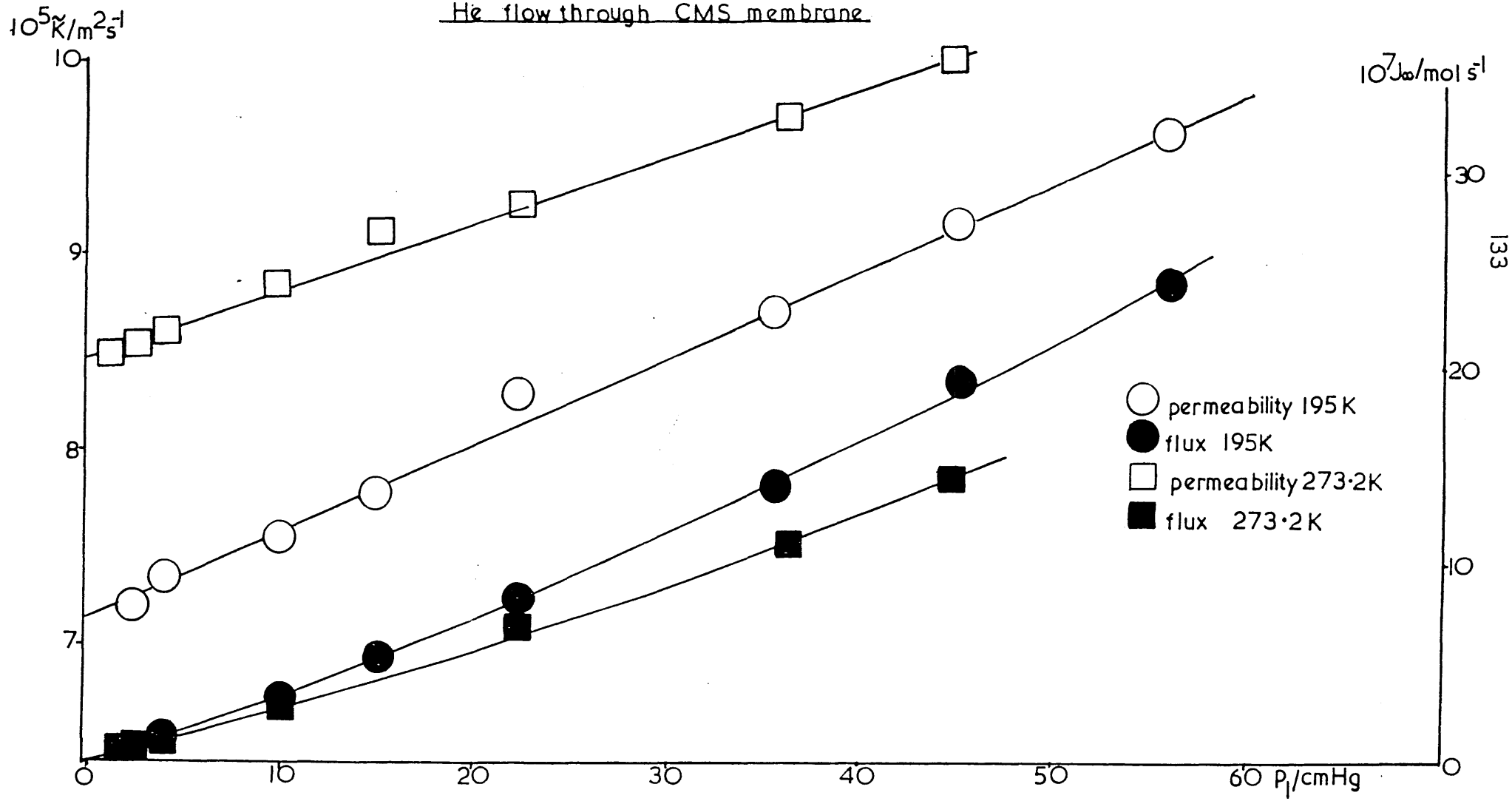
CO_2 was the only gas used which was adsorbed in (cf. section 4.1. 4) sufficient quantity by the carbon molecular sieve to produce a

(fig 4·2·11) Sample outgoing pressure versus time graphs

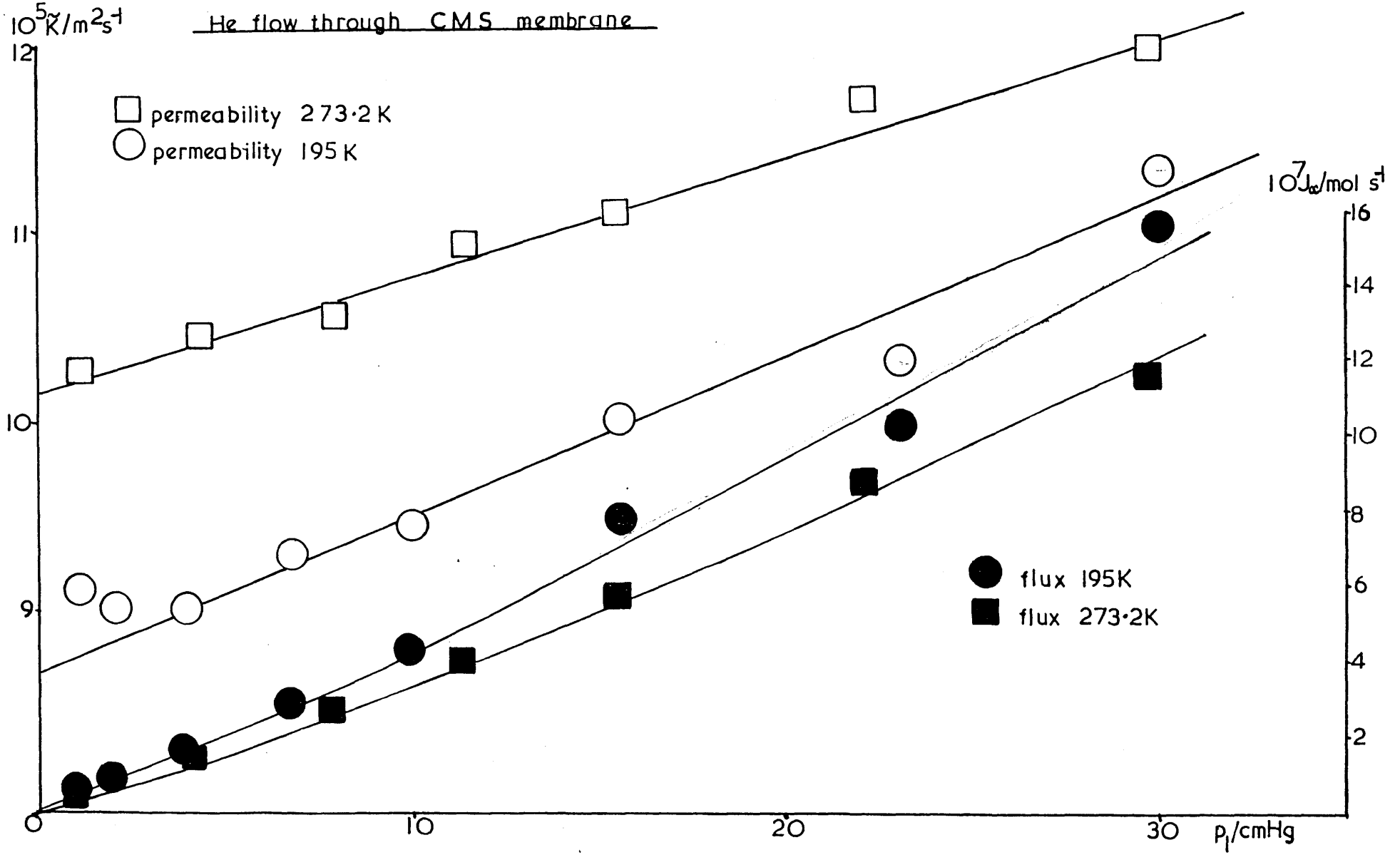
CO_2 flow through Carbon Molecular Sieve membrane



(fig 4·2·12) Integral permeability and steady state flux versus ingoing pressure
He flow through CMS membrane

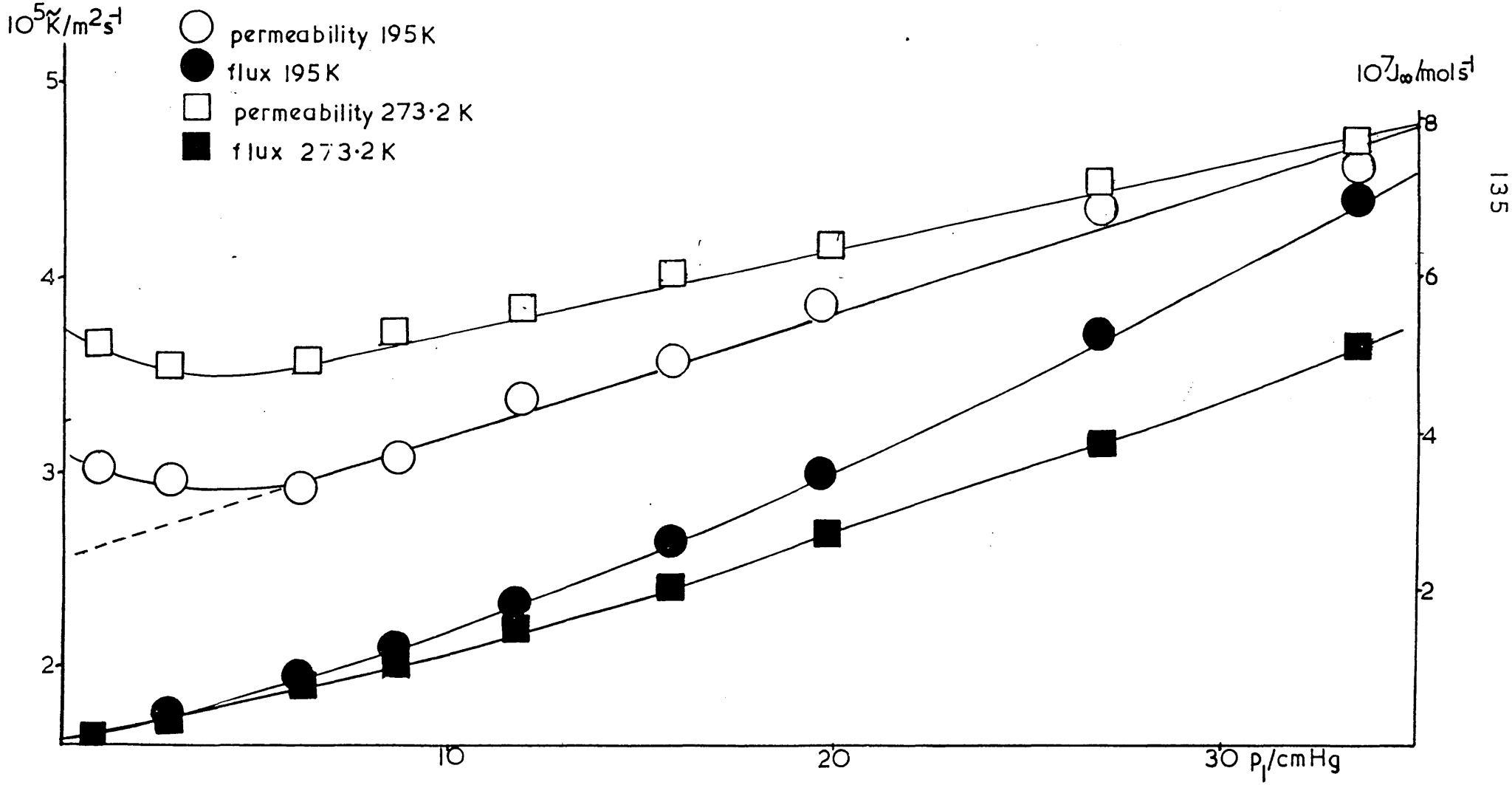


(fig 4·2·13) Integral permeability and steady state flux versus ingoing pressure



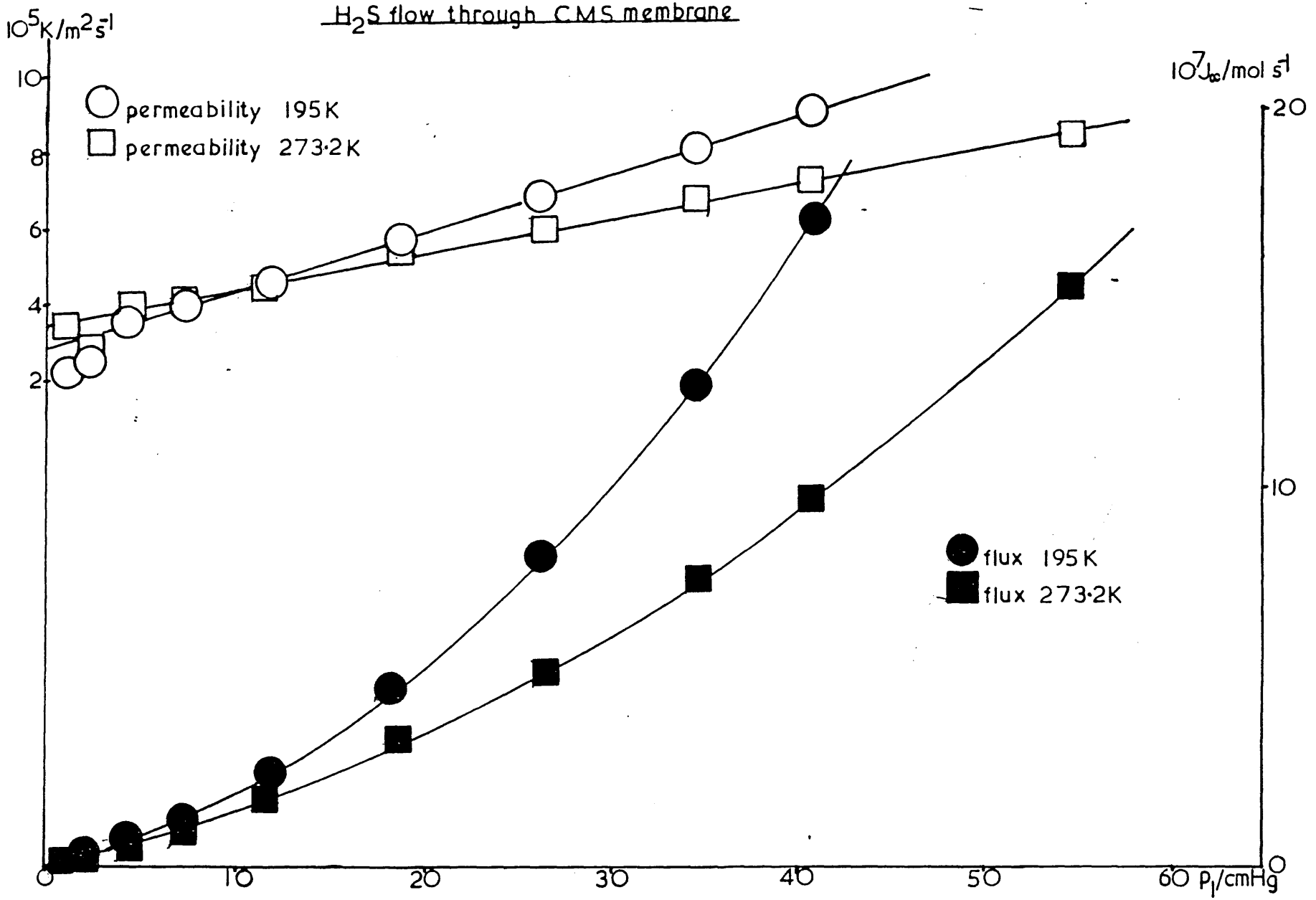
(Fig 4.2.14) Integral permeability and steady state flux versus ingoing pressure

N_2 flow through CMS membrane



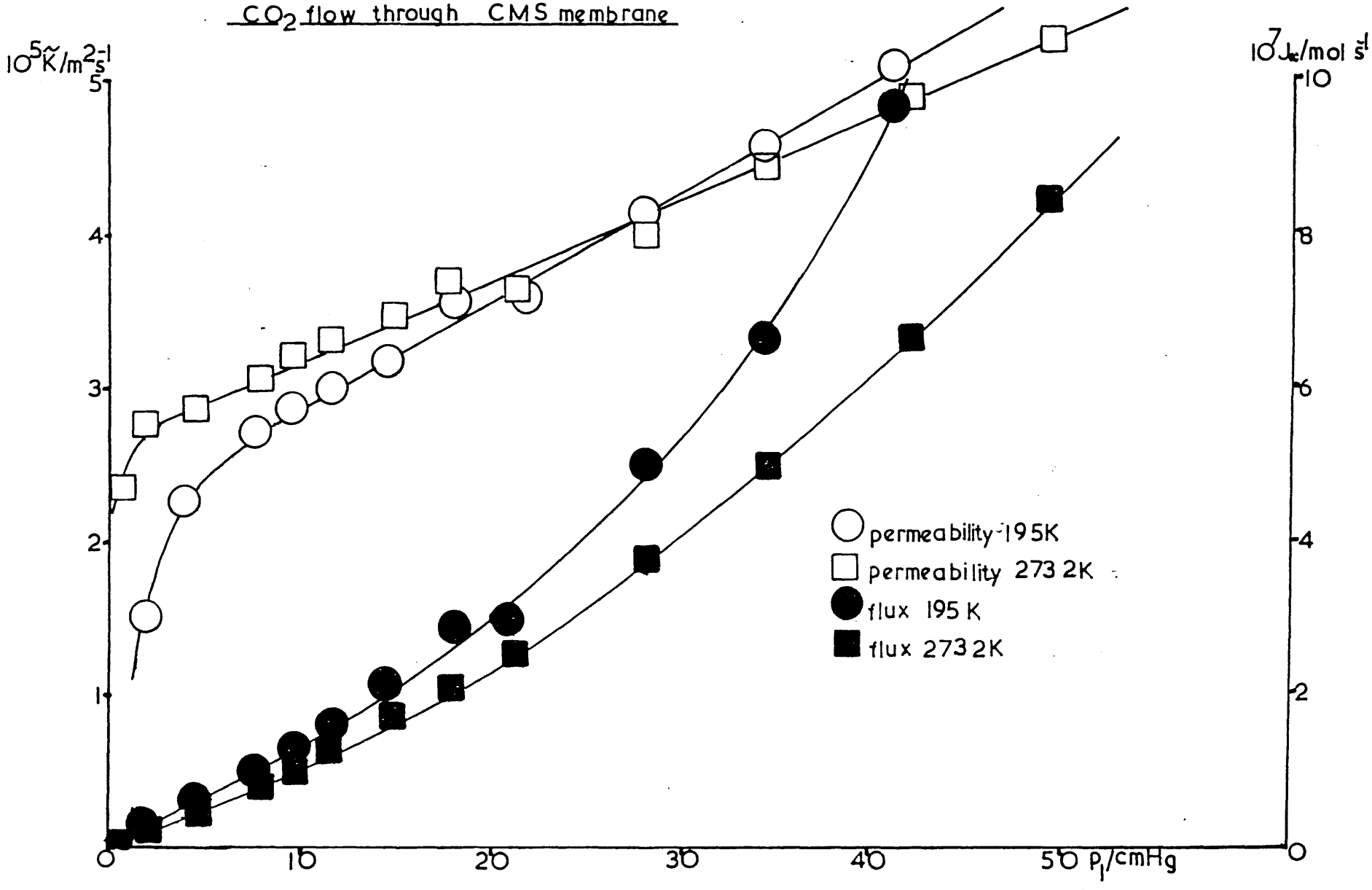
(fig 4·2·15) Integral permeability and steady state flux versus ingoing pressure

H_2S flow through CMS membrane

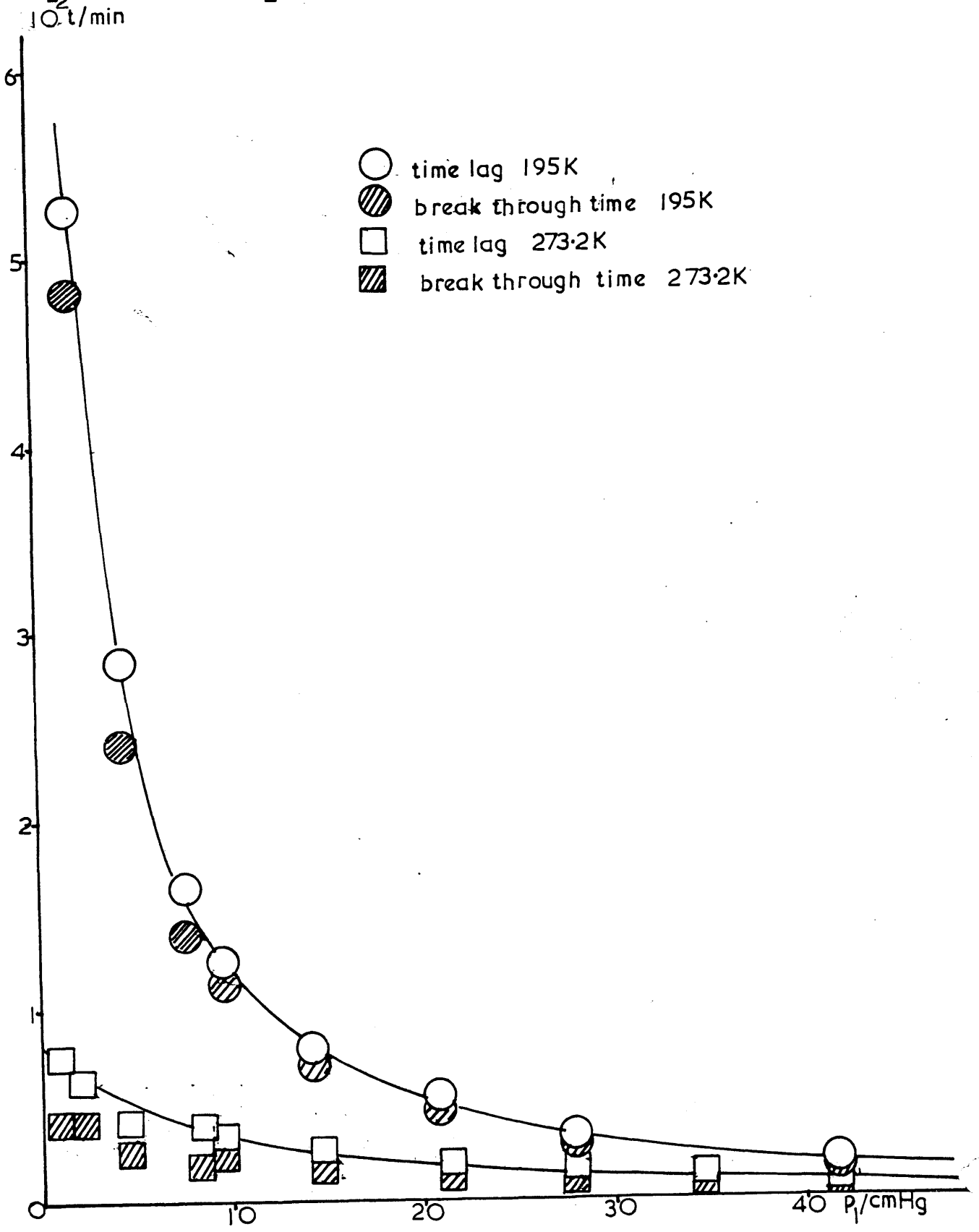


(fig 4·2·16) Integral permeability and steady state flux versus ingoing pressure

CO_2 flow through CMS membrane



(fig 4·2·17) Time lag and break through time versus ingoing pressure CO_2 flow through CMS membrane



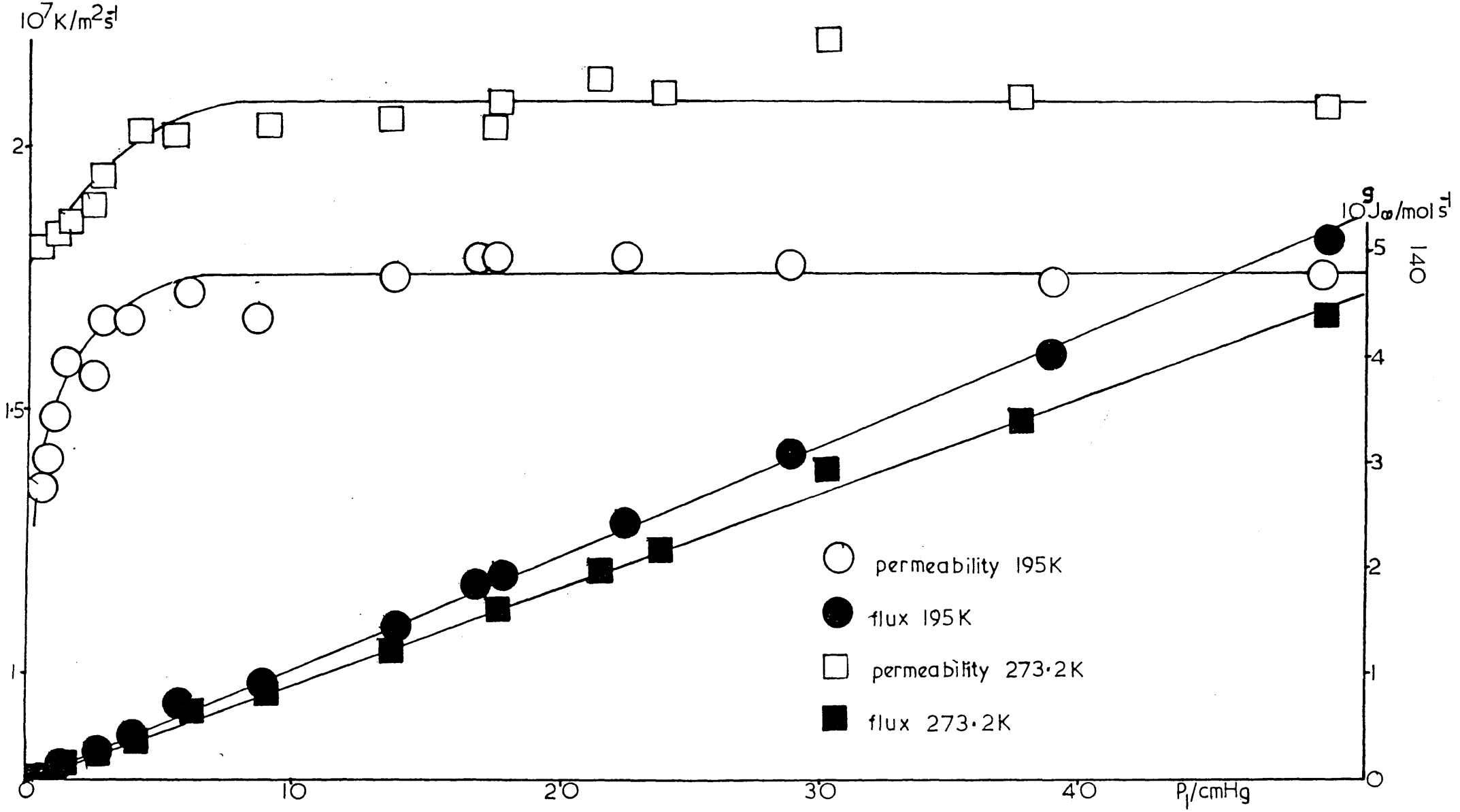
time lag. The time lags obtained were of the same order of magnitude as those obtained for CO_2 on NaX but the outgoing pressure versus time graphs for the CMS membrane were less rectangular in form (cf. fig. 4.2.2, fig. 4.2.11). Fig. 4.2.16 shows the integral permeability and steady state flux for this system. The most vivid feature is the sharp deviation from linearity of the permeability graph at pressures below 5 cmHg.

4.2.5 Single gas flow results for Carbolac

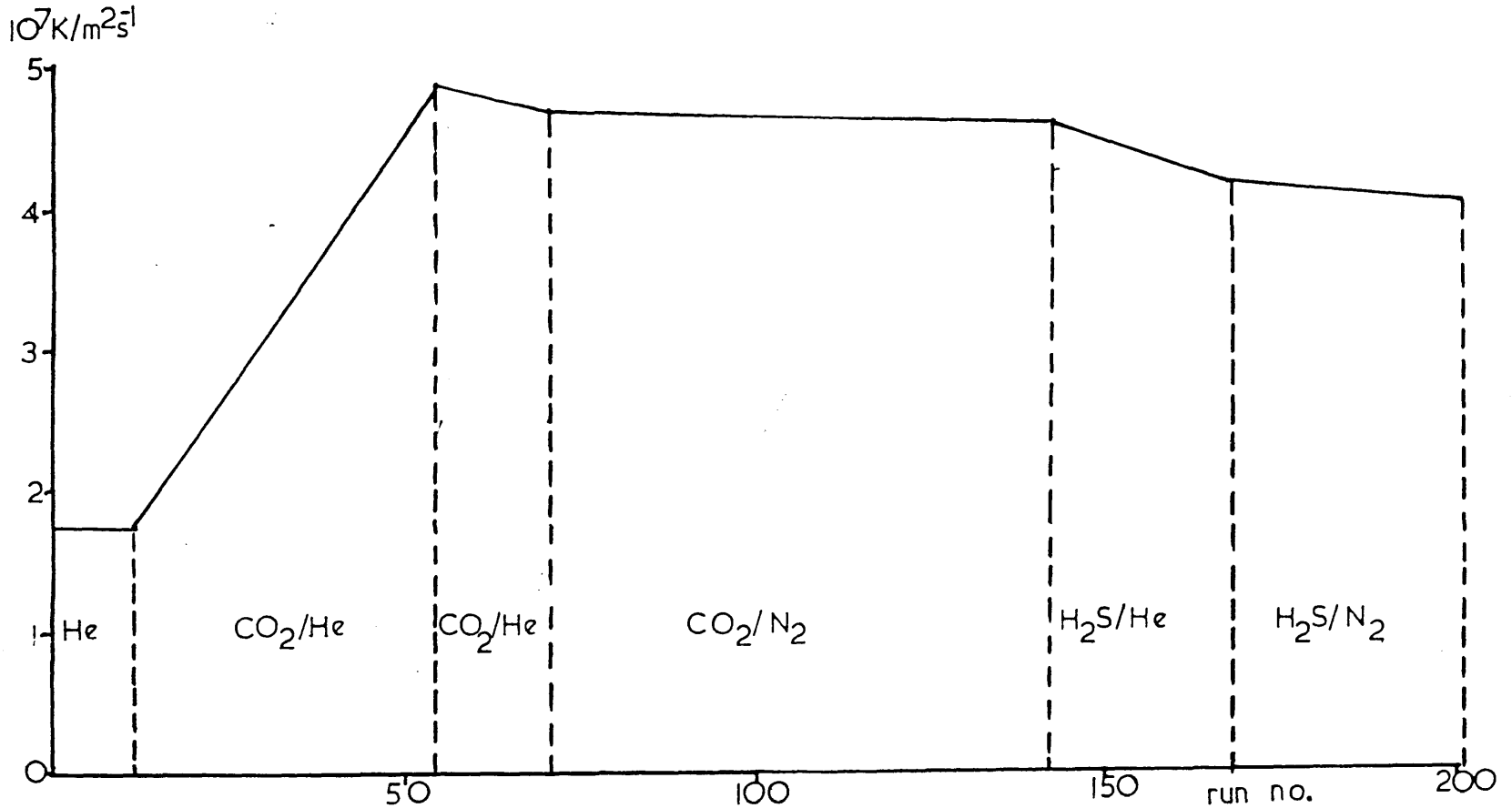
In a previous study (Ash, Barrer and Lowson 1973) the Carbolac membrane currently in use was found to undergo irreversable swelling after strong sorption of condensable gases, causing alteration in its flow characteristics. For this reason the membrane was initially calibrated using He and periodic checks were made on the He or N_2 permeability between series of experiments with CO_2 and H_2S. The initial He permeability and flux are shown in fig. 4.2.18 and the initial N_2 permeability and flux in fig. 4.2.21. These two graphs are similar in form, both showing a drop in permeability at low pressures, however the He permeability shows greater temperature dependence than the N_2 permeability for which the graphs obtained at 195K and 273.2K are virtually coincident. The flux in each case appears to be linearly dependent upon pressure.

Fig. 4.2.19 and 4.2.22 show the variation of the He and N_2 permeability at 195K throughout the course of the investigation. It can be seen that the initial exposure to CO_2 caused a change in the membrane which increased the permeability to approximately three times its initial value. The ingoing pressure of CO_2 was

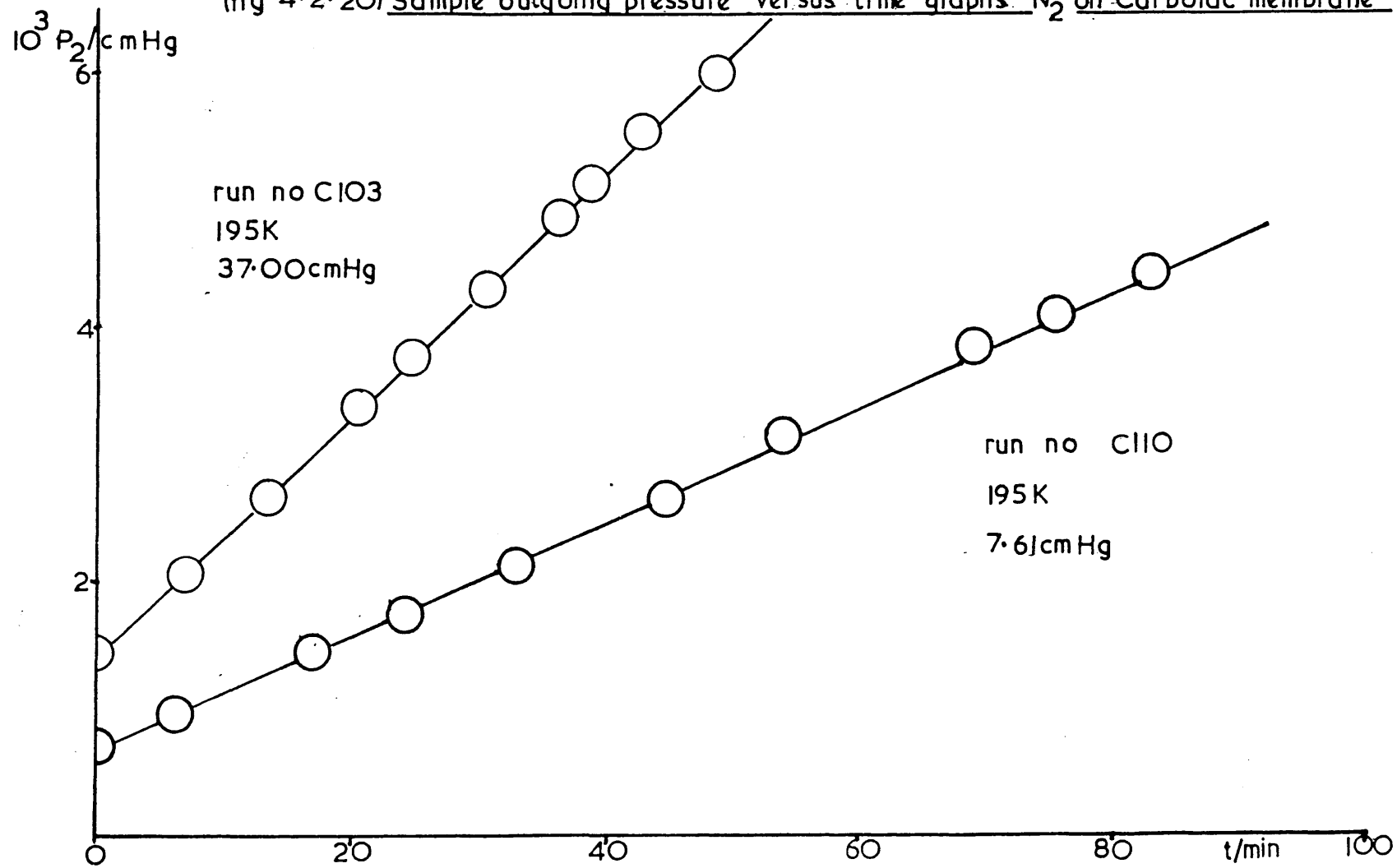
(fig 4·2·18) Integral permeability and steady state flux versus ingoing pressure; He flow through Carbolac membrane



(fig 4·2·19) Variation of He permeability at 195K with run number Carbolac membrane

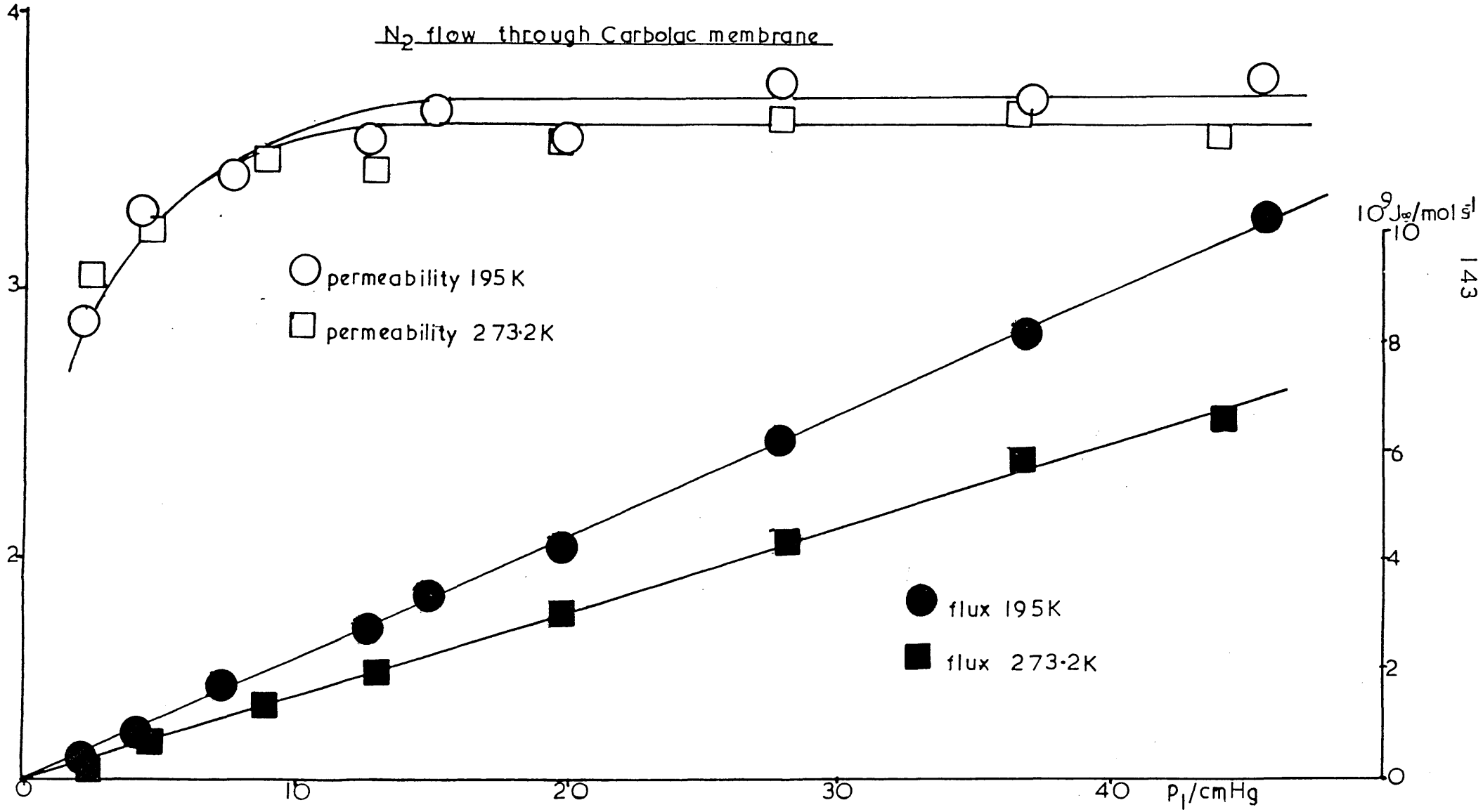


(fig 4·2·20) Sample outgoing pressure versus time graphs N_2 on Carbolac membrane

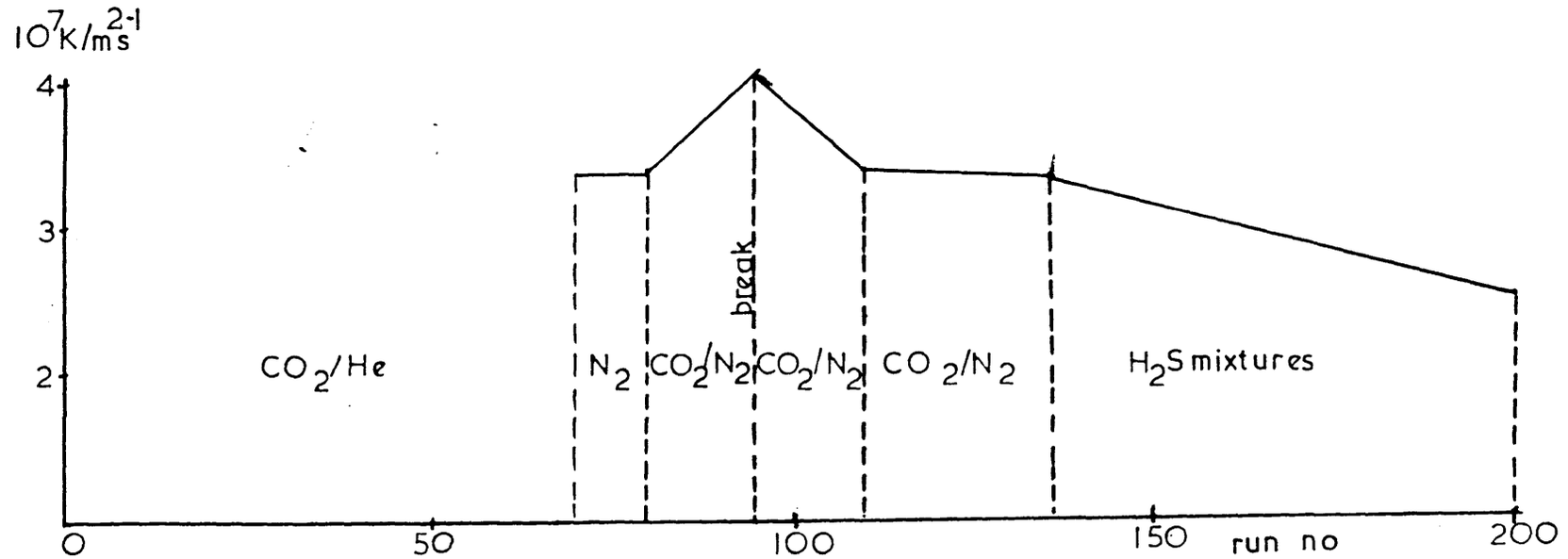


(fig 4·2·21) Integral permeability and steady state flux versus ingoing pressure

N_2 flow through Carbolac membrane



(fig 4·2·22) Variation of N_2 permeability with run number at 195K Carbolac membrane

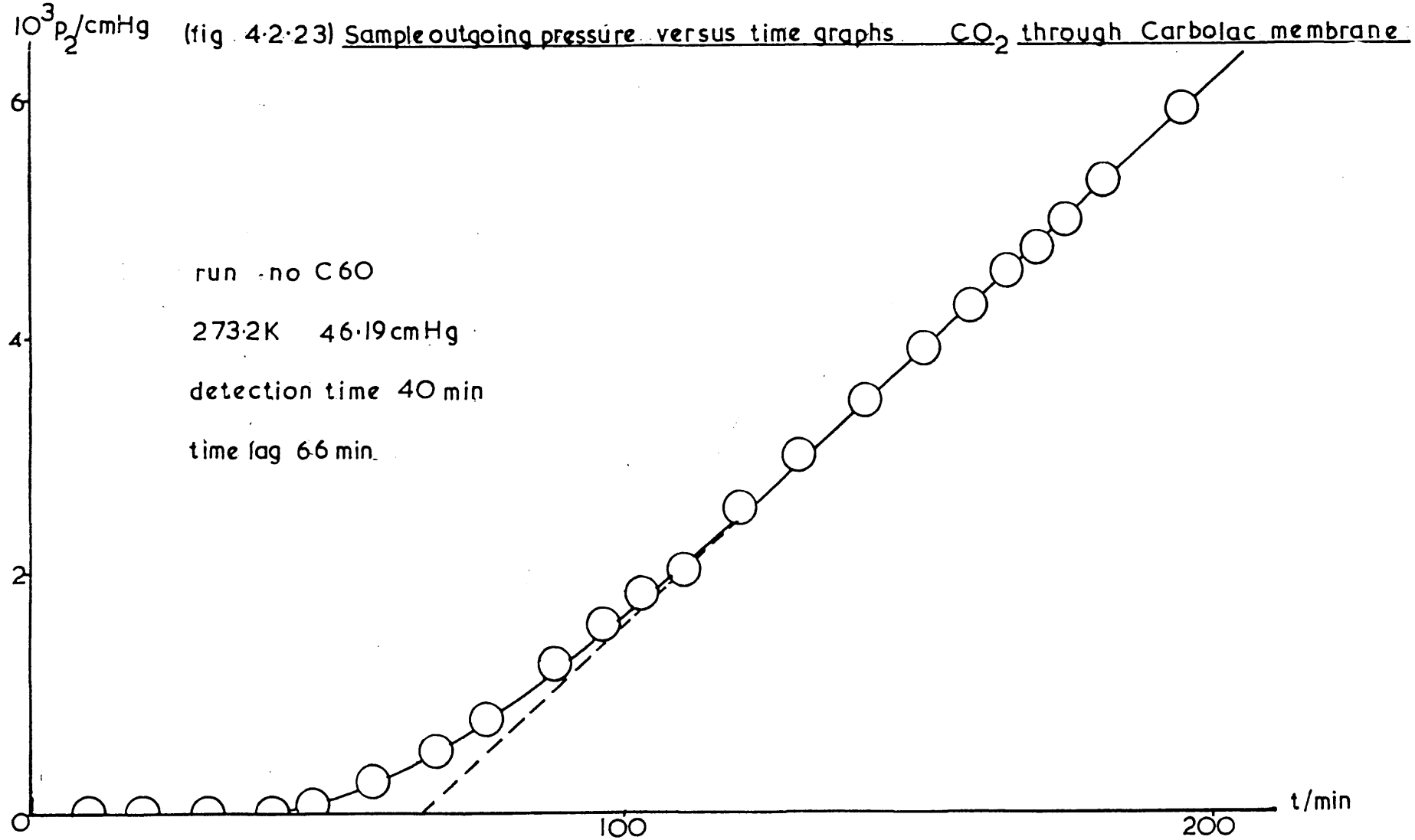


not subsequently raised above this initial level and the flow characteristics remained approximately constant throughout. From fig. 4.2.22 it can be seen that the membrane underwent a change after run 97 due to a break in the apparatus letting in air at atmospheric pressure, but subsequently the permeability returned to its initial level. The effect of the exposure of Carbolac to H_2S is only evident in a slight lowering of both the He and the N_2 permeability through the membrane during the series of experiments. Using extreme care it was possible to maintain constant flow characteristics of the membrane, throughout the course of a series of experiments and only in this way could the blockage of He and N_2 be examined. The linearity of the flux graphs and independence of the permeability from the ingoing pressure indicate the absence of Poiseuille flow and the possible applicability of Knudsens relationship to the Carbolac system.

$$\tilde{K} \sqrt{M/T} = \text{constant}$$

Structural changes in the membrane unfortunately caused variation of $\tilde{K} \sqrt{M/T}$ with time, however agreement between results at 195K and 273.2K is good as can be seen from table 4.2.2.

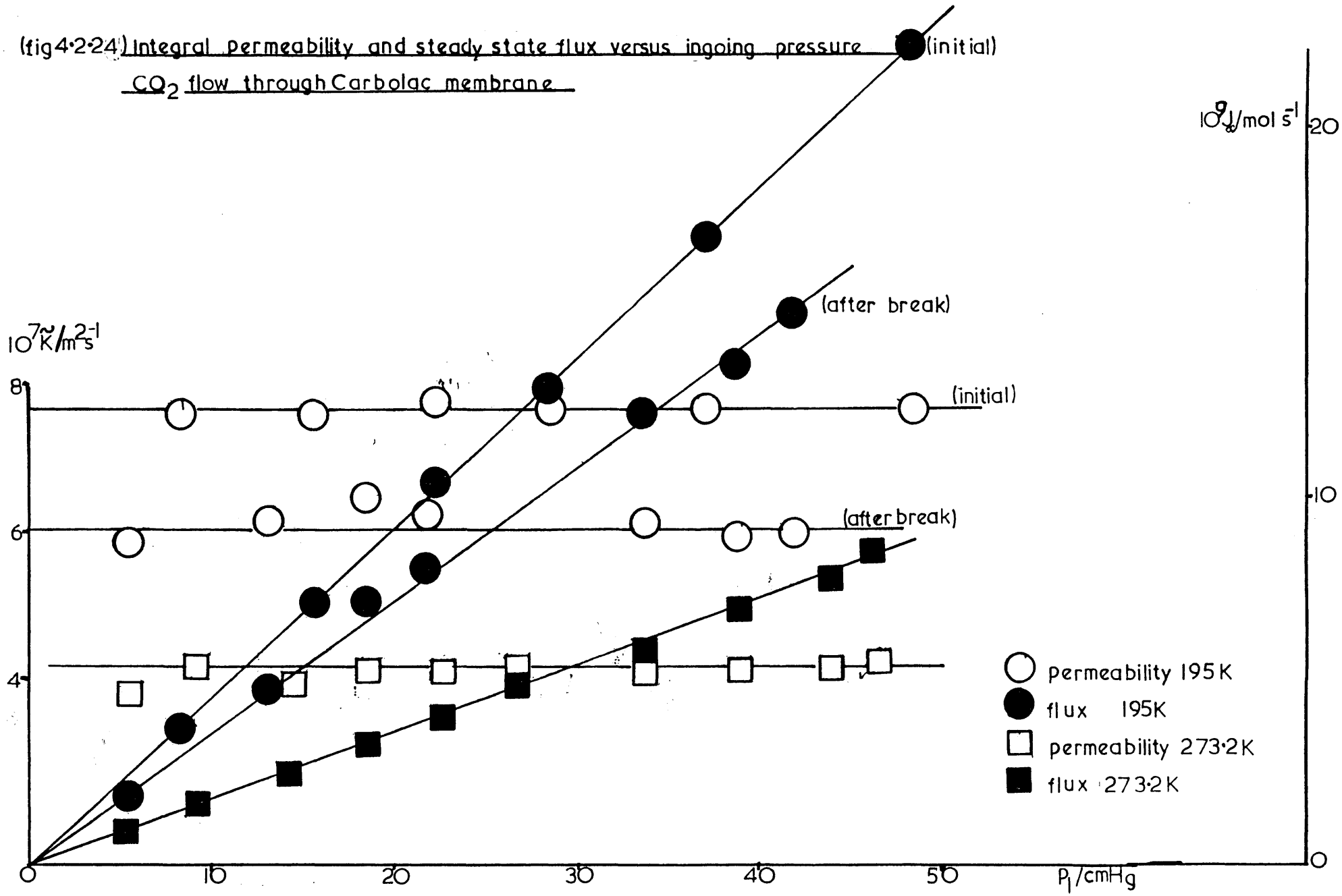
He is assumed non sorbed and N_2 is adsorbed little by Carbolac. As a result the steady state flow was quickly achieved for these two gases. Two sample steady state outgoing pressure versus time graphs are shown in fig. 4.2.20. In contrast to this CO_2 and H_2S, which are both copiously adsorbed, exhibited large timelags, which increased rapidly when the ingoing pressure was lowered. (fig. 4.2.25



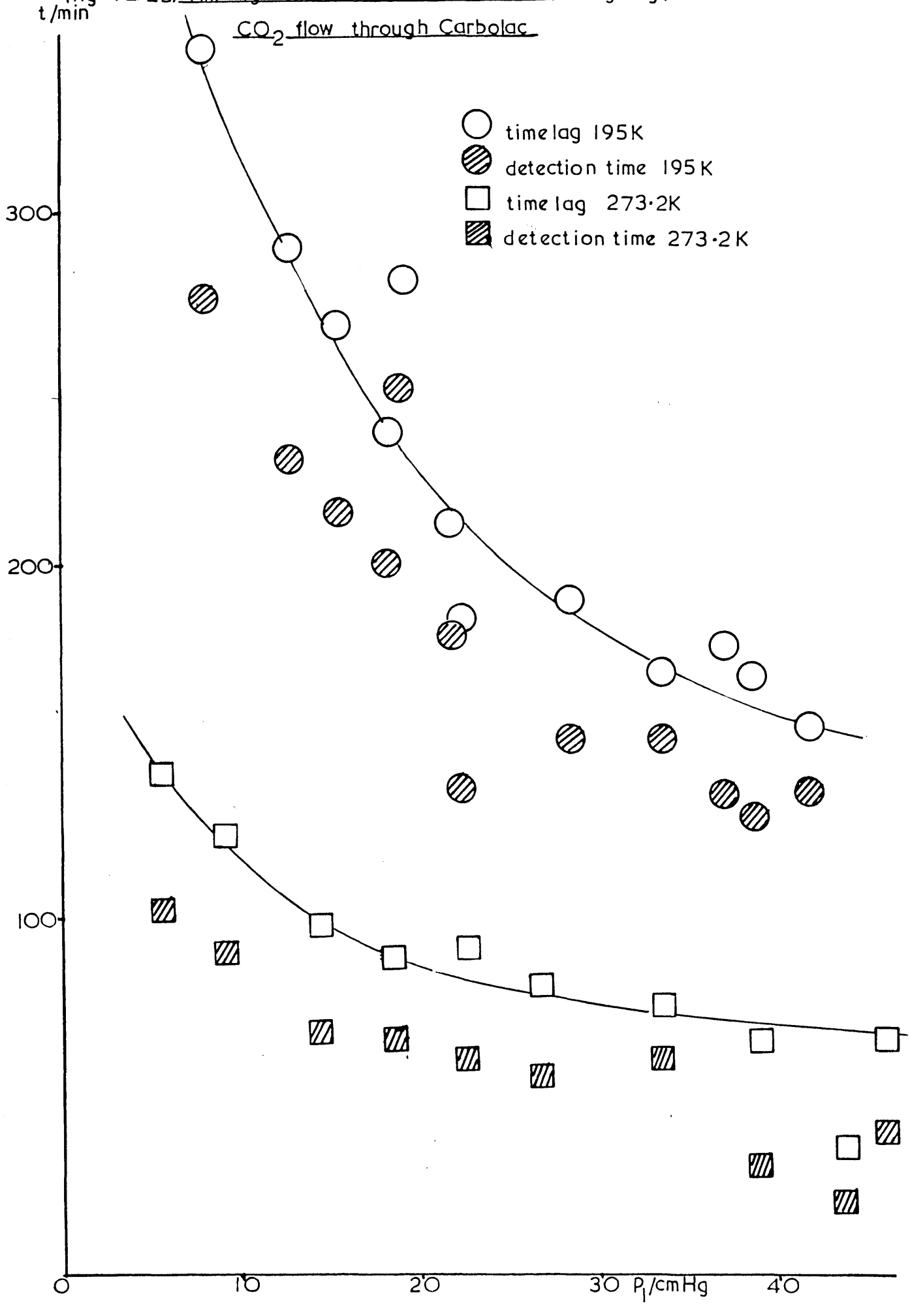
(fig 4·2·23) Sample outgoing pressure versus time graphs CO_2 through Carbolac membrane

(fig 4·2·24) Integral permeability and steady state flux versus ingoing pressure

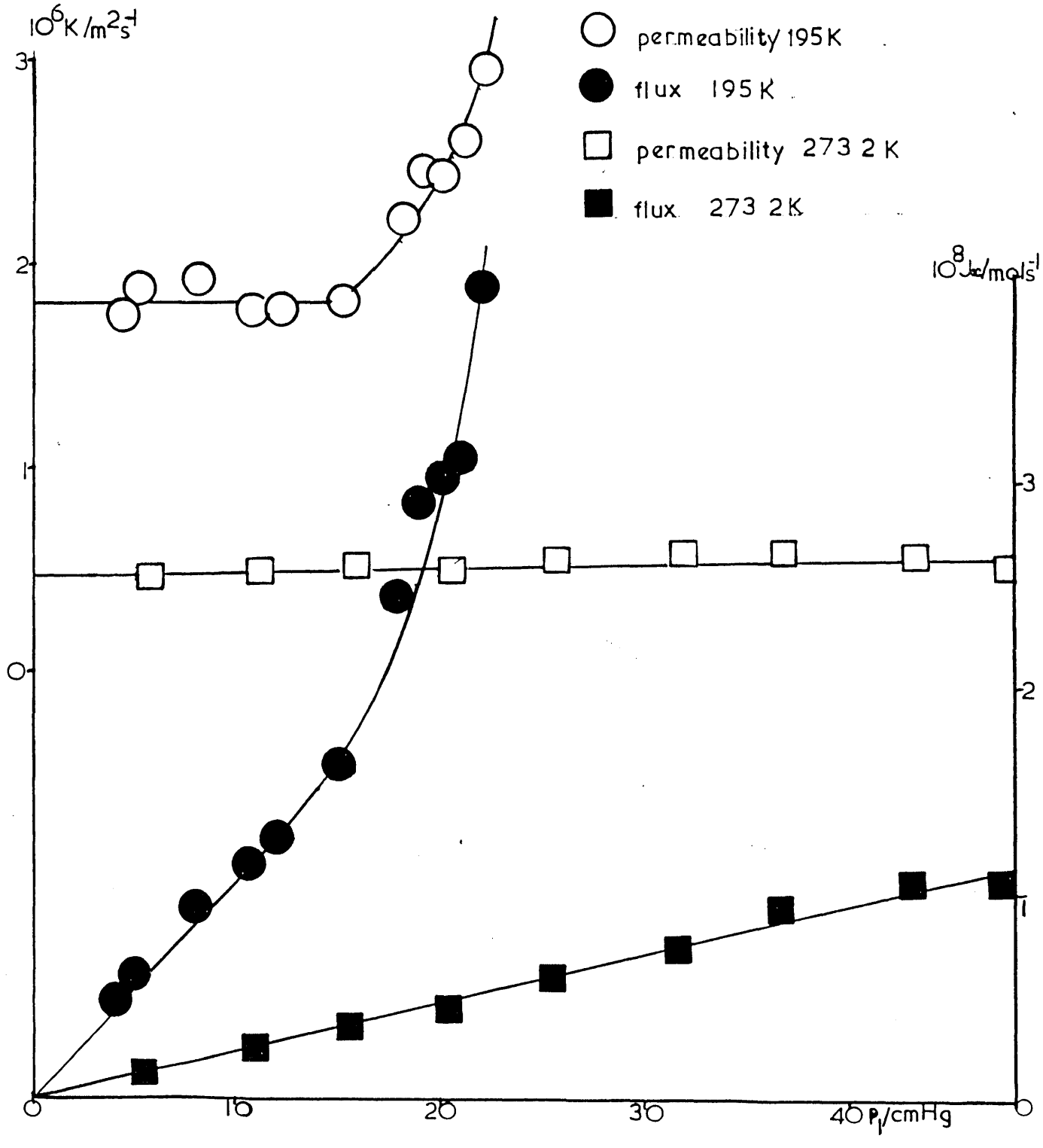
CO_2 flow through Carbolac membrane

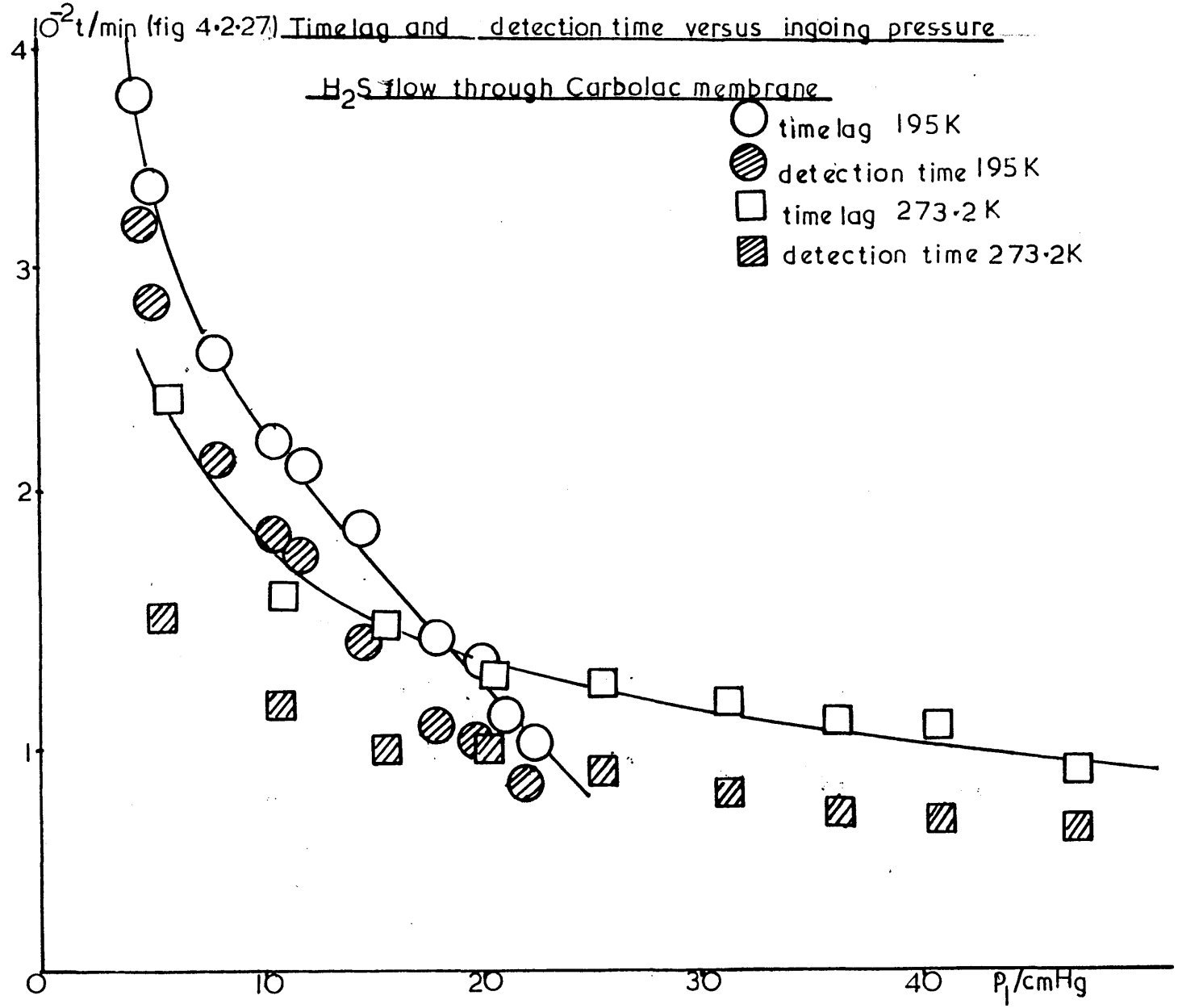


(fig 4·2·25) Timelag and detection time versus ingoing pressure CO_2 flow through Carbolac



(fig 4-2-26) Integral permeability and steady state flux versus ingoing pressure ; H_2S flow through Carbolac membrane




10^{-2}t/min (fig 4·2·27) Timelag and detection time versus ingoing pressure
H_2S flow through Carbolac membrane
time lag 195K
detection time 195K
time lag 273·2K
detection time 273·2K
4
3
2
1
0
10
20
30
40
P_1/cmHg

and fig. 4.2.27). A sample outgoing pressure versus time graph is shown in fig. 4.2.23 and it may be seen that gas may be detected on the outgoing side of the membrane long before steady state flow is achieved. A long curved section of the pressure versus time graph precedes the linear portion, and for this reason the phenomena may not be regarded as a true 'break through' of gas therefore gas"detection times" have been listed instead of breakthrough times as for the molecular sieve membranes.

The steady state integral permeability and flux obtained for CO_2 and H_2S flow through the Carbolac membrane are shown in fig. 4.2.24 and fig. 4.2.26. The permeability of CO_2 is independent of pressure and the flux linear, however a break in the apparatus altered the flow characteristics of the membrane midway through the series of experiments. The result of this change is not evident at 273.2K, but at 195K it was necessary to show two separate sets of results, for the CO_2 permeability and flux, initially and after the break (fig. 4.2.25).

The H_2S permeability at 273.2K shows very slight linear dependence on ingoing pressure, (fig. 4.2.26), however at 195K the permeability shows an initial constant value follwed by a sharp increase above an ingoing pressure of 15cmHg. This is reflected in the flux versus ingoing pressure graph, which has an initial linear section followed by a curve convex to the pressure axis.

Table 4.2.2

$\tilde{K}\sqrt{M/T}$ values for He flow on this Carbolac membrane

Source	T/K	$10^7 \tilde{K}\sqrt{M/T}/m^2 s^{-1}(gmol^{-1}K^{-1})^{\frac{1}{2}}$
This study (initial reading)	273.2	.248
" " (after CO_2 runs)	"	.750
(after H_2S runs)	"	.575
This study (initial reading)	195	.243
" " (after CO_2 runs)	"	.702
" " (after H_2S runs)	"	.577
R.T. Lowson (1968)(initial reading)	273.2	.183
" (subsequent reading)	"	.153
R.T. Lowson (1968)	233.2	.172

4.2.6 Single gas flow runs through Graphon membrane

The Graphon membrane used in this study had previously been investigated by R. T. Lowson (1968), A.D. Hamilton (1980), P. Ferdani (1982) and A.P. Sharpe (1983). The flow characteristics had changed very little over this period of time, however the membrane was 'calibrated' using He in order to check that no irreversible changes had occurred. The integral permeability and steady state flux of He through the Graphon membrane are plotted against pressure in fig. 4.2.28. The flux graphs were linear passing through the origin and the permeability independent of pressure; this indicated the absence of any Poiseuille flow and the possible applicability of the Knudsen relationship $\tilde{K}\sqrt{M/T}$ constant.

(Fig 4·2·28) Integral permeability and steady state flux versus ingoing pressure: He flow through Graphon membrane

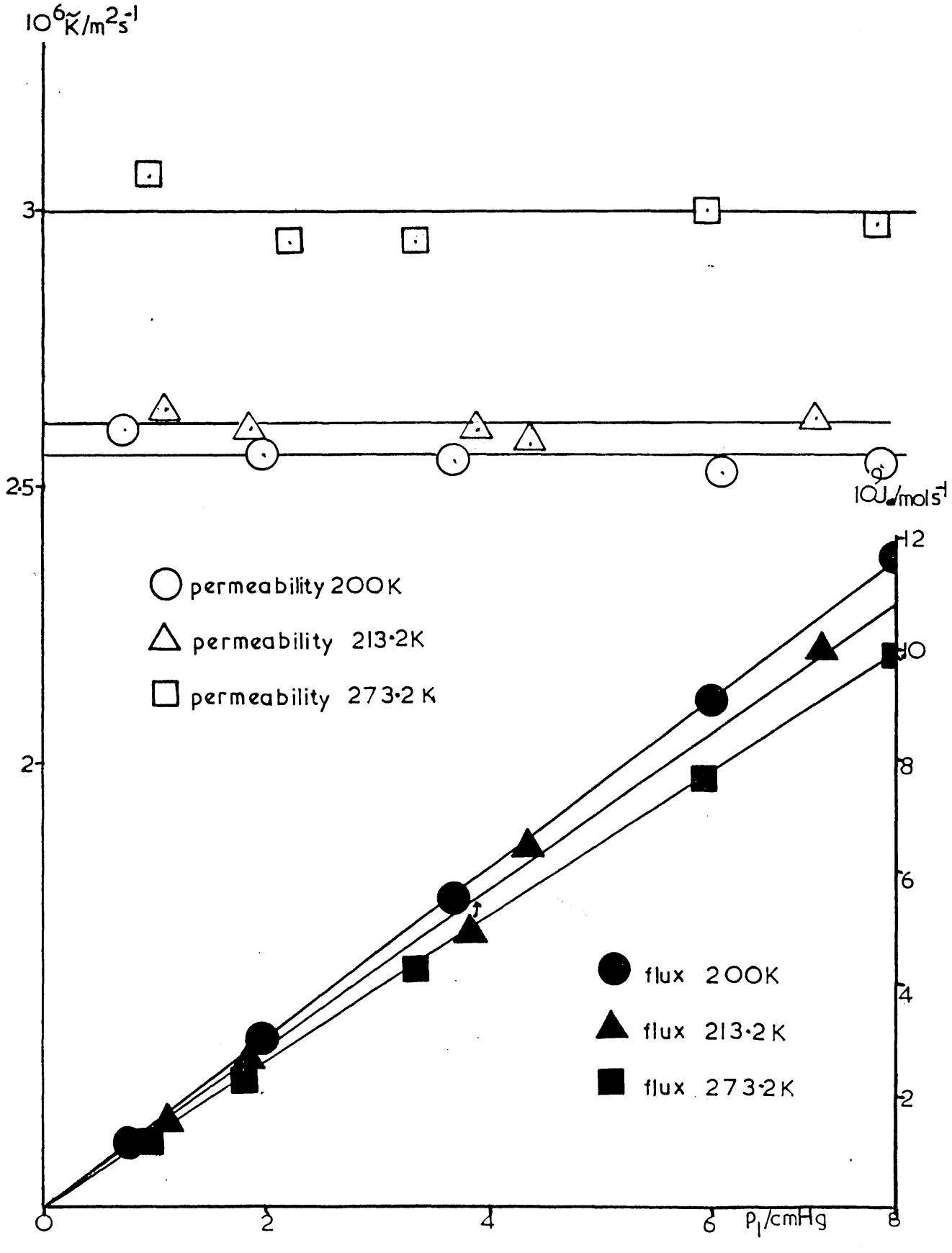


Table 4.2.3

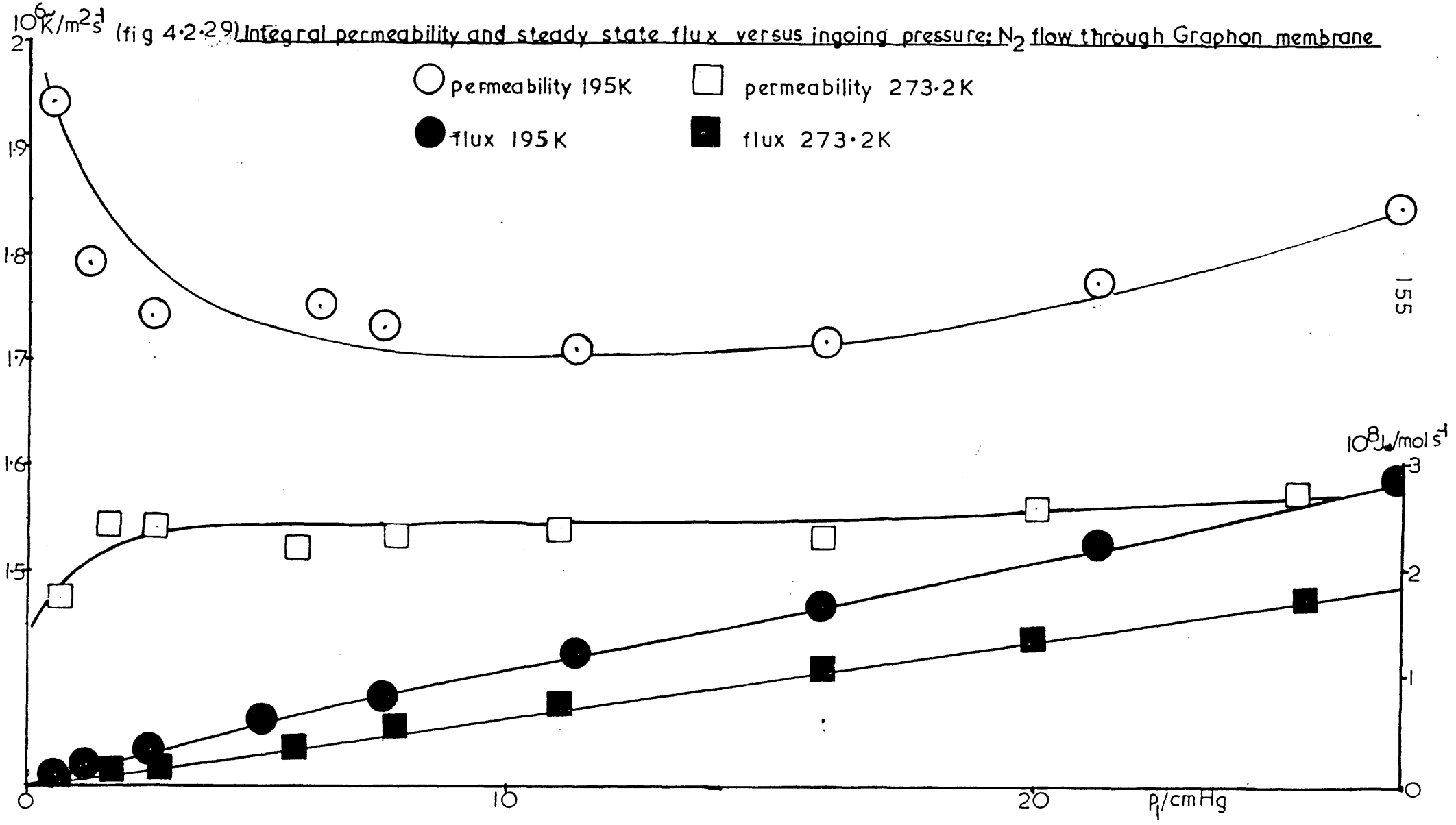
Values of $\tilde{K}\sqrt{M/T}$ for He flow through this Graphon membrane

Source	T/K	$10^6\ \tilde{K}\sqrt{M/T}/m^2s^{-1}\ g^{\frac{1}{2}}mol^{-\frac{1}{2}}K^{-\frac{1}{2}}$
This study	200	.360
"	213.2	.356
"	273.2	.359
A. P. Sharpe (1983)	195	.355
"	273.2	.349
P. Ferdani (1982)	195	.354
"	273.2	.357
A. D. Hamilton (1980)	213.2	.356
"	233.2	.356
"	273.2	.357
R. T. Lowson (1968)	198.2	.303
"	273.2	.305

Table 4.2.3 shows the variation of $\tilde{K}\sqrt{M/T}$ for He flow through this membrane since 1968, it can be seen that there has been negligible change in $\tilde{K}\sqrt{M/T}$ since 1980 and less than 15% change since 1968.

Nitrogen flow was investigated at 195K and 273.2K and the resulting integral permeability and steady state flux as functions of ingoing pressure are shown in fig. 4.2.29.

All gases flowing through the Graphon membrane attained steady state of flow in a very short time so that no time lags were observed, even for the more highly adsorbed gases. (CO_2, H_2S, C_3H_8, SF_6)

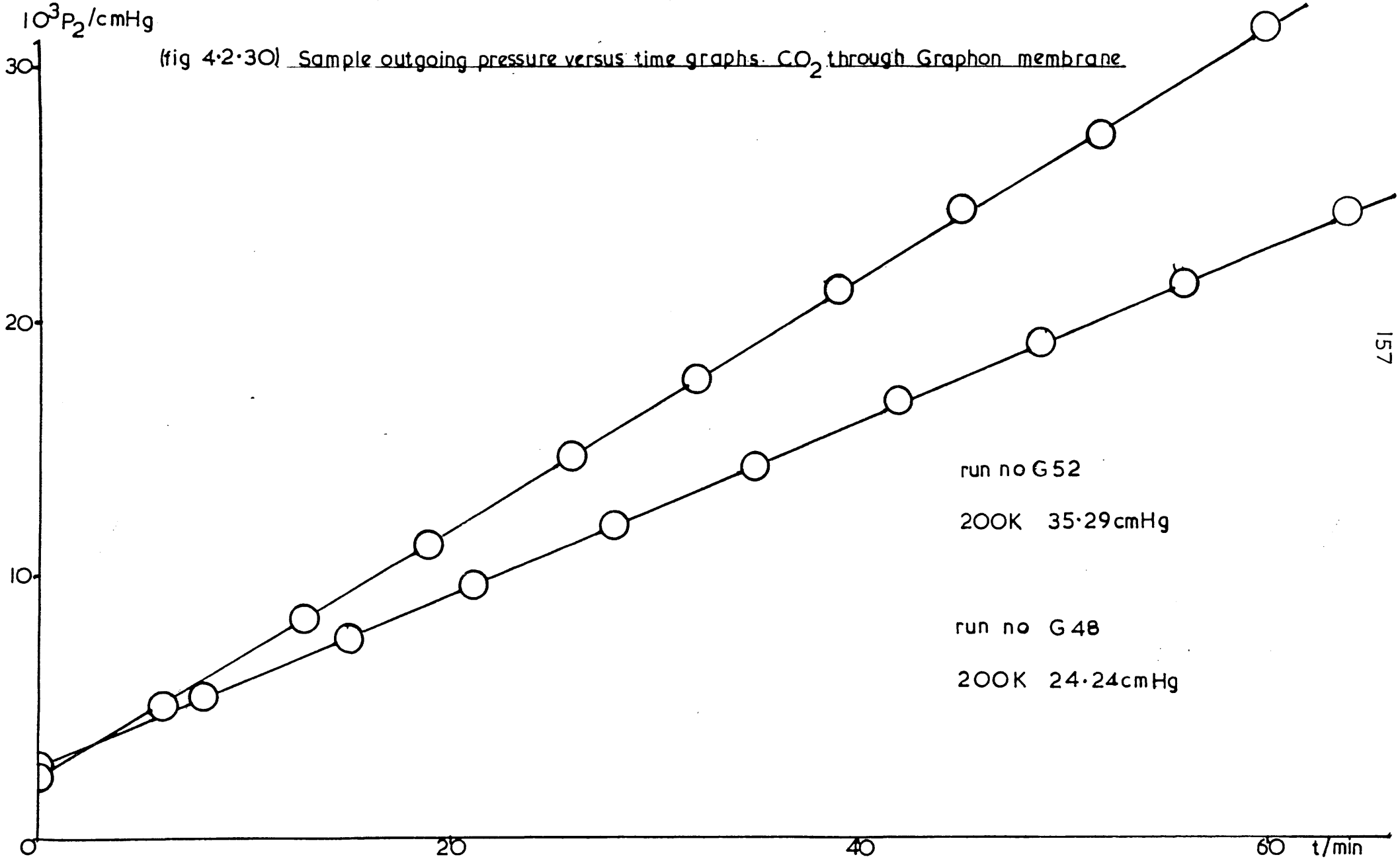


(fig 4·2·29) Integral permeability and steady state flux versus ingoing pressure: N_2 flow through Graphon membrane

Sample outgoing pressure versus time graphs for CO_2 are shown in fig. 4.2.30. CO_2 flow through the membrane had previously been studied by A. P. Sharpe and P. Ferdani at 195K, 213.2K and 273.2K using a cardice/ethanol cryostat system. These results are also shown in fig. 4.2.31. However the more accurate temperature control provided by the leaky-dewar system revealed the previous temperature control to have been insufficient and the results of Ferdani and Sharpe were re-analysed and found to be at 200K, 218.2K and 273.2K. Experiments were performed by the author over a wide range of temperatures from 184K to 273.2K, this proved the efficiency of the cryostat and enabled previous results to be corrected for temperature. The results obtained are shown in fig. 4.2.31 and fig. 4.2.32. The integral permeability versus pressure graph rises steeply at low pressures and at 184K appears to pass through a maximum value. The resulting flux curves are sigmoid in shape.

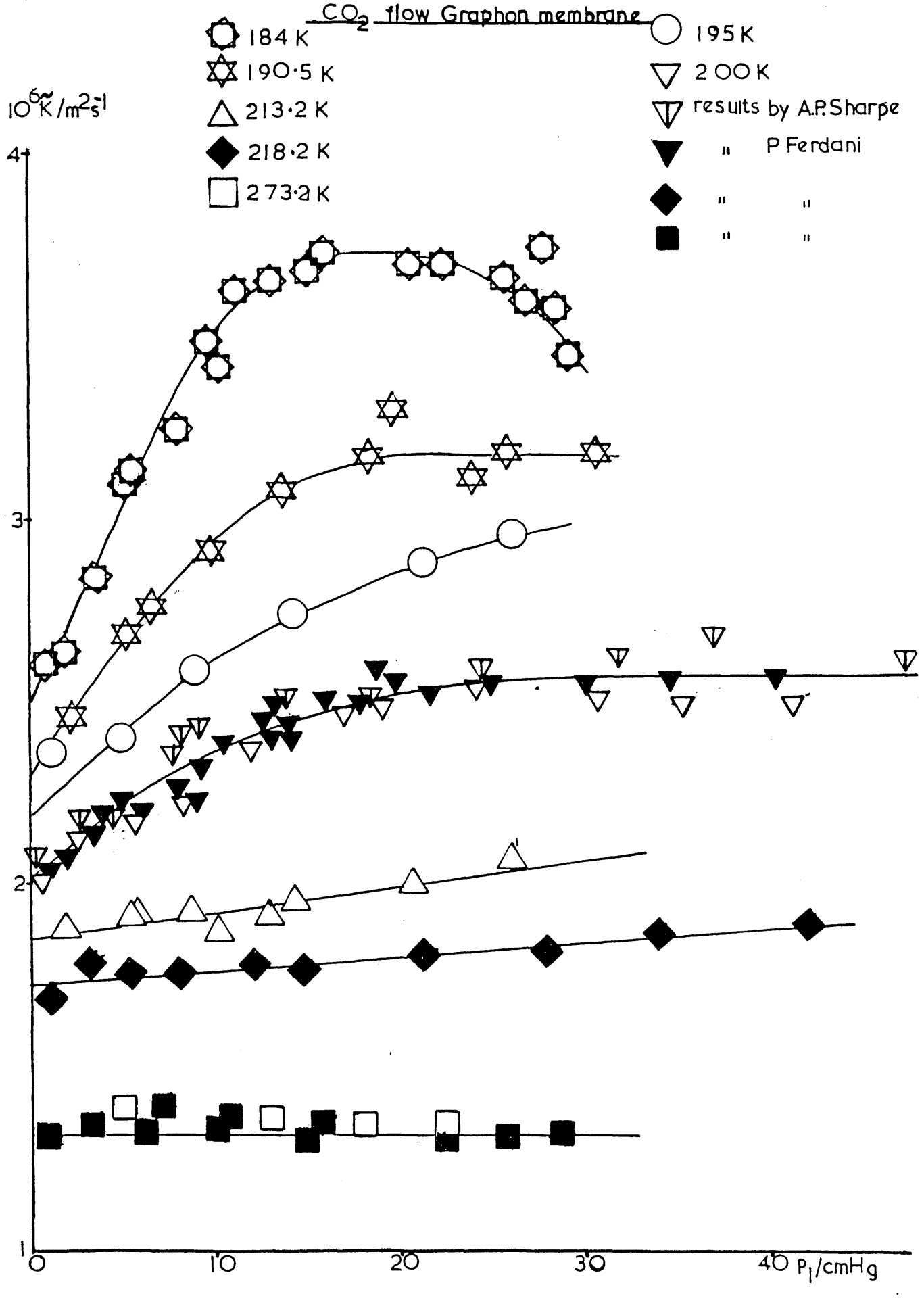
The integral permeability and steady state flux of H_2S are shown as functions of p_1 in fig. 4.2.33 and 4.2.34. They follow the same general trends as those for CO_2, however the flow rate of H_2S is approximately three times greater at any temperature and pressure.

In order to check the blockage behaviour (section 4.3.3) and the 'extra flow' capacity of the Graphon membrane had not changed, the flow of C_3H_8 was examined and compared to that obtained by A.D. Hamilton (1980). The graphs of the integral permeability (fig. 4.2.35) and the flux (fig. 4.2.36) show that no change had



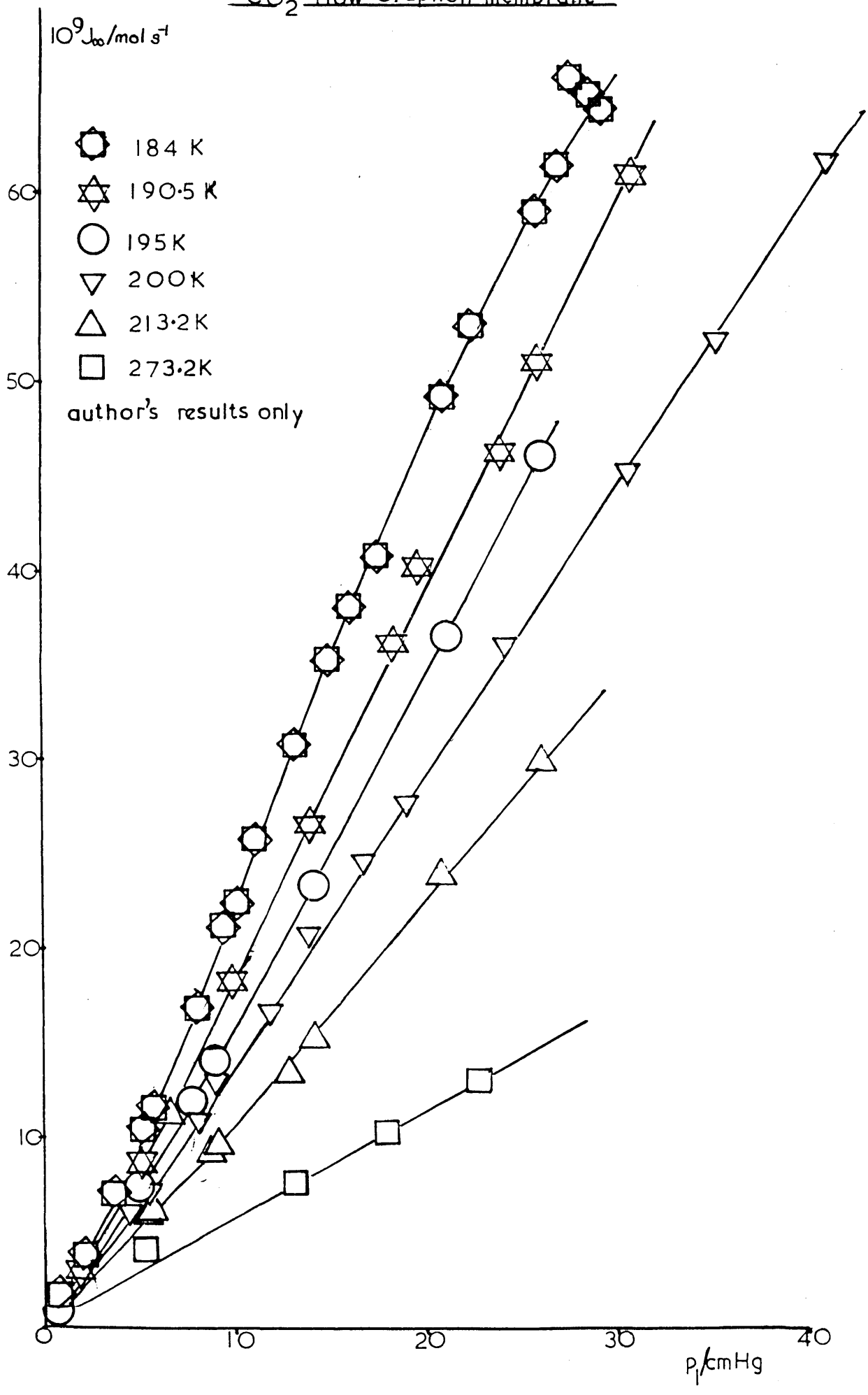
(fig 4·2·30) Sample outgoing pressure versus time graphs. CO_2 through Graphon membrane

(fig 4·2·31) Integral permeability versus ingoing pressure

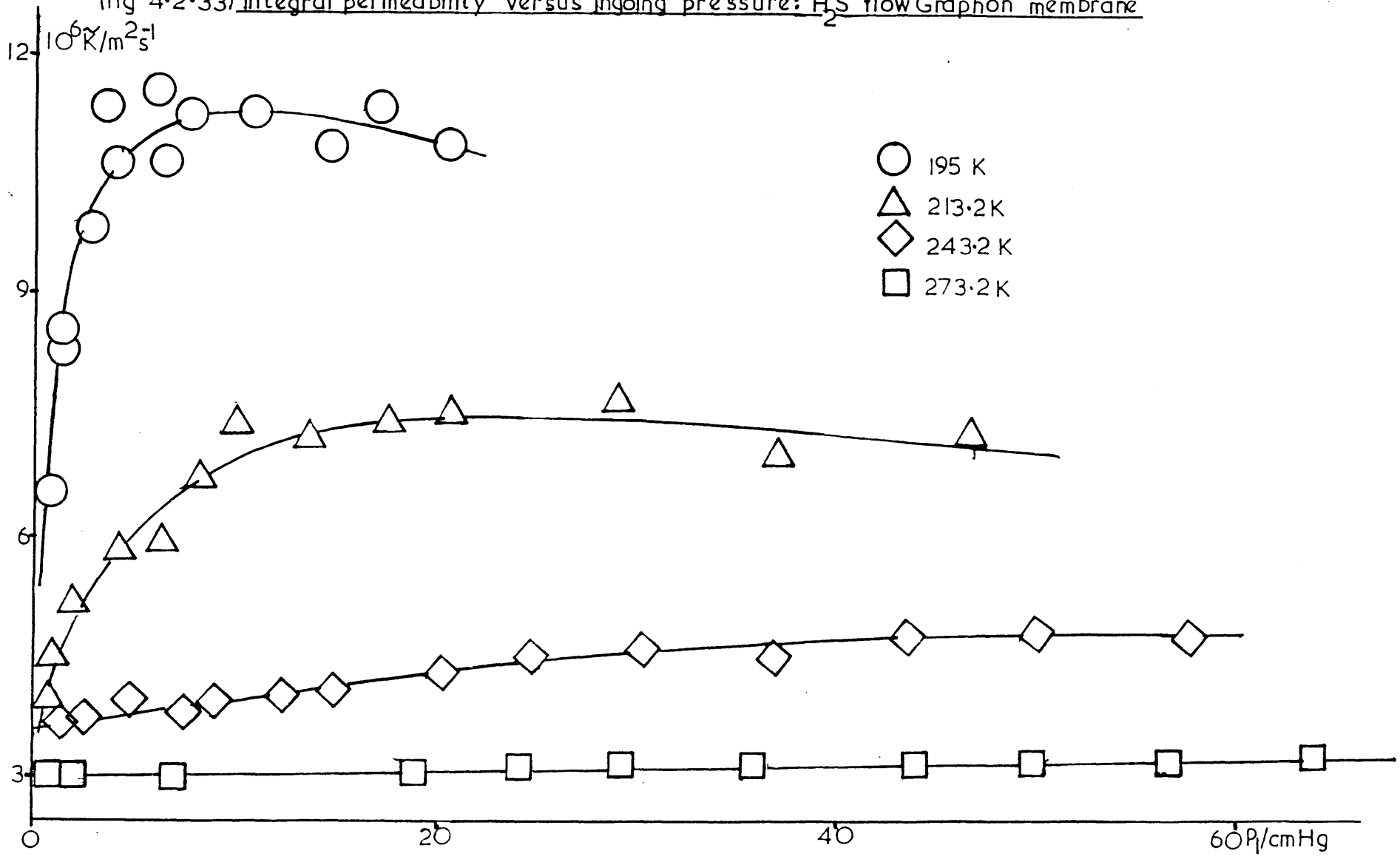


(fig 4·2·32) Steady state flux versus ingoing pressure

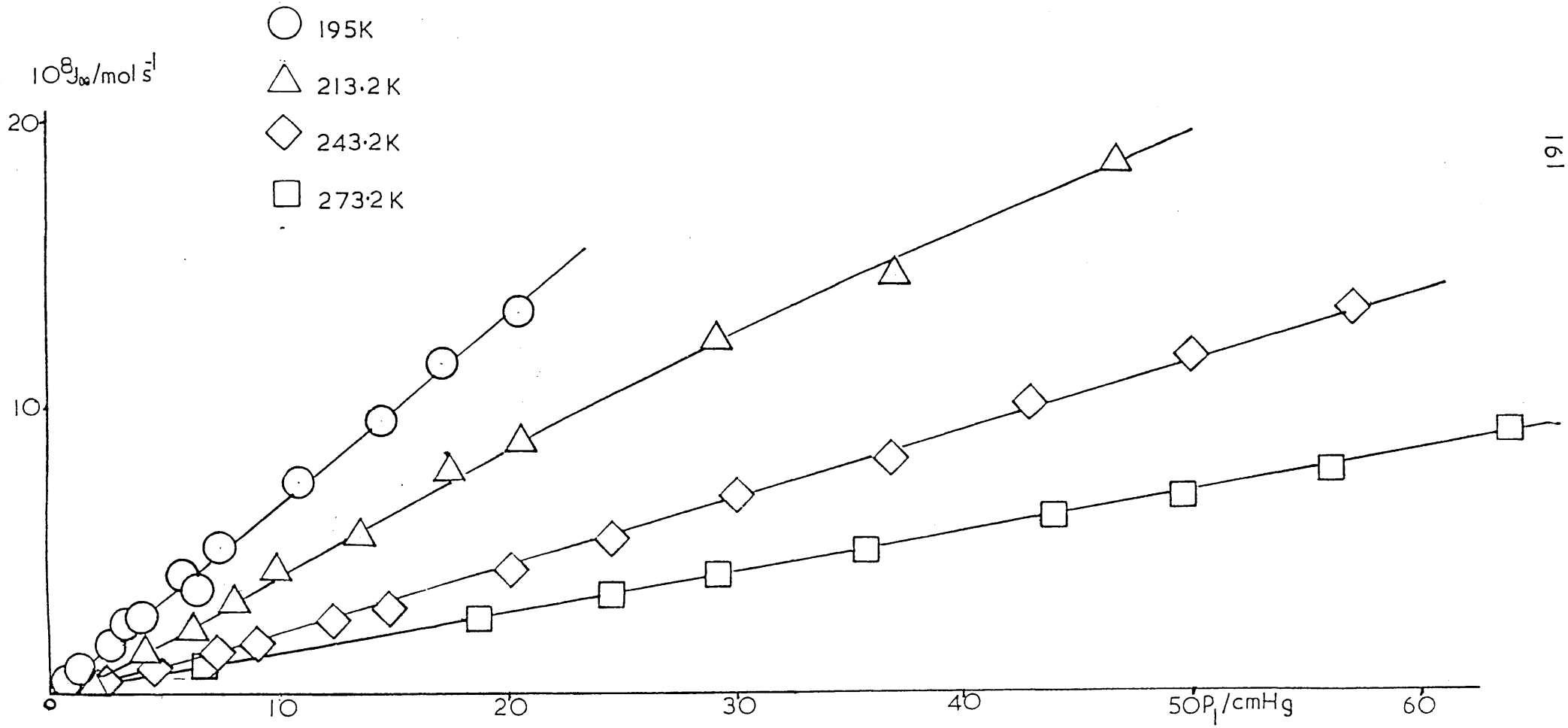
CO_2 flow Graphon membrane



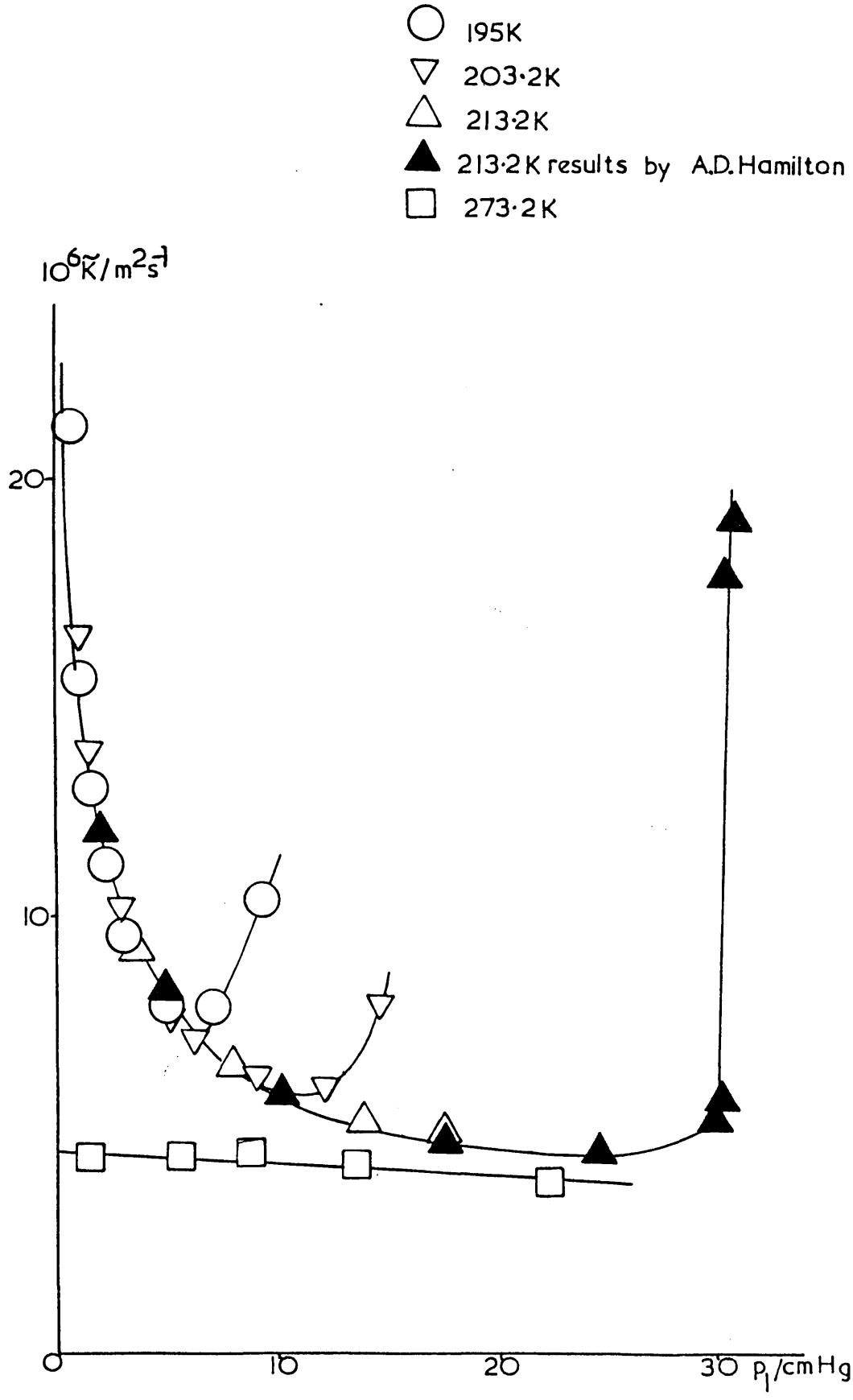
(fig 4·2·33) Integral permeability versus ingoing pressure: H_2S flow Graphon membrane



(fig 4·2·34) Steady state flux versus ingoing pressure: H_2S flow through Graphon membrane

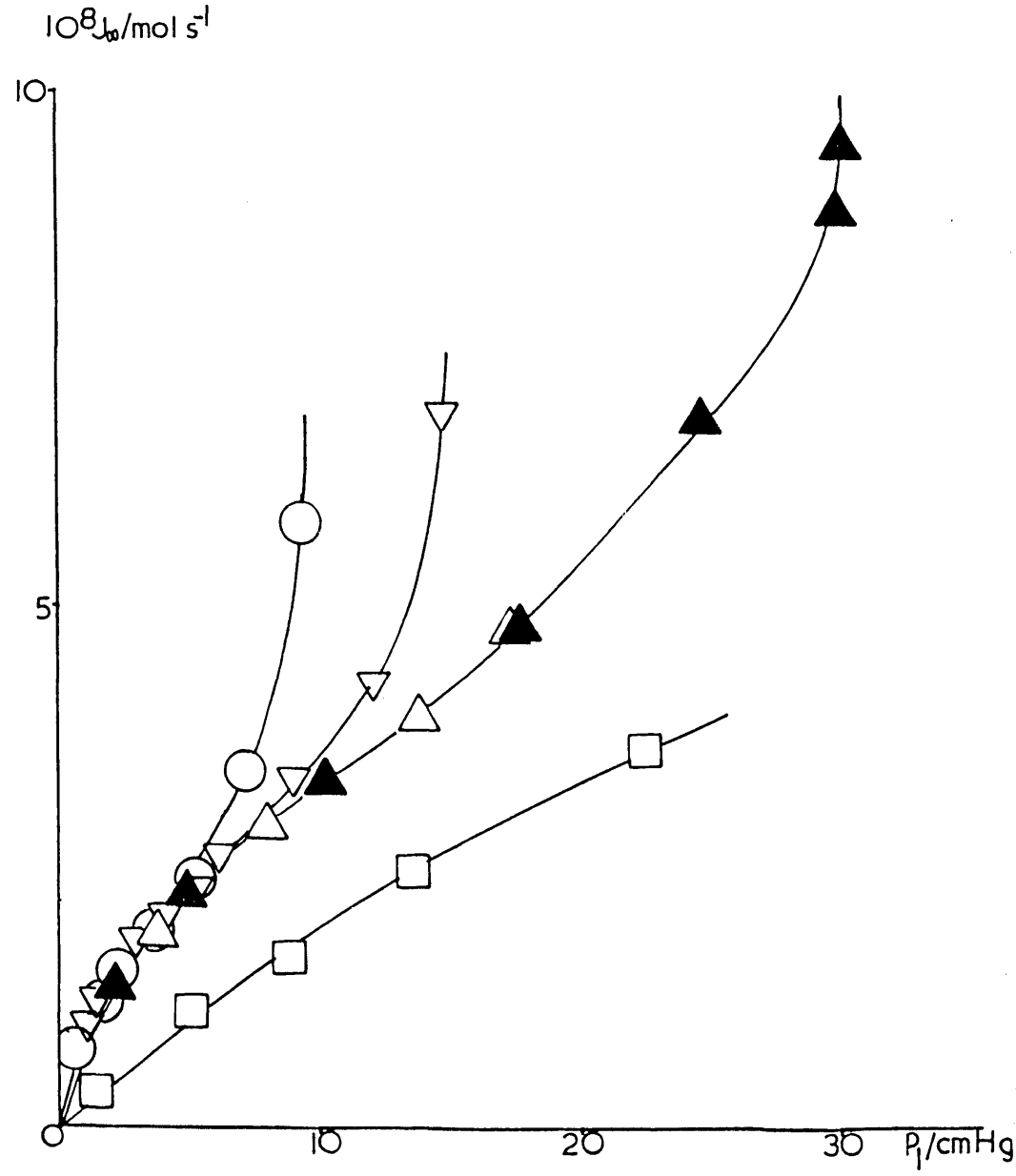


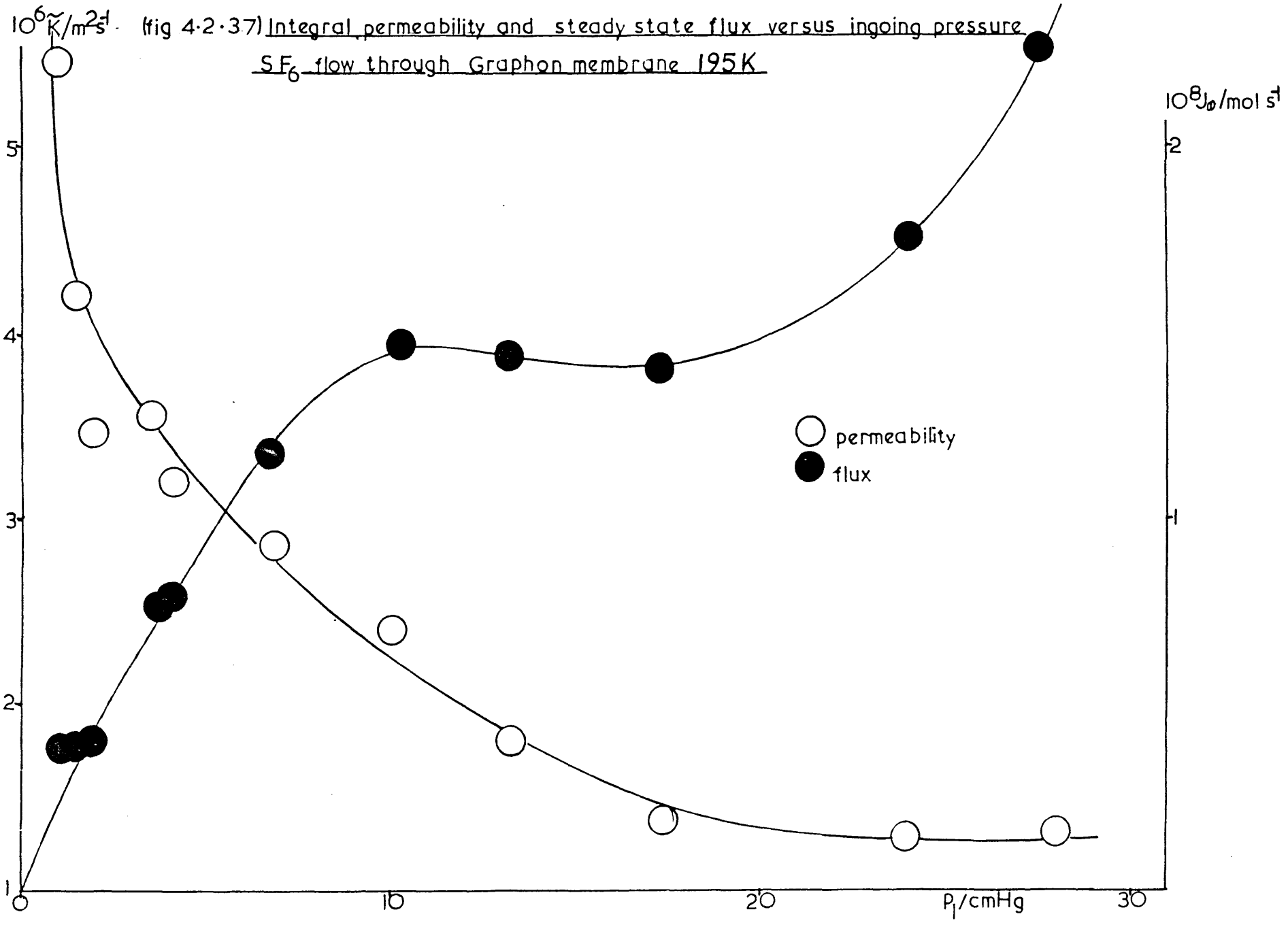
(fig 4·2·35) Integral permeability versus ingoing pressure
C_3H_8 flow through Graphon membrane



(fig 4·2·36) Steady state flux versus ingoing pressure C_3H_8 flow through Graphon membrane.

○ 195 K
▽ 203·2 K
△ 213·2 K
▲ 213·2K results by A.D.Hamilton
□ 273·2K

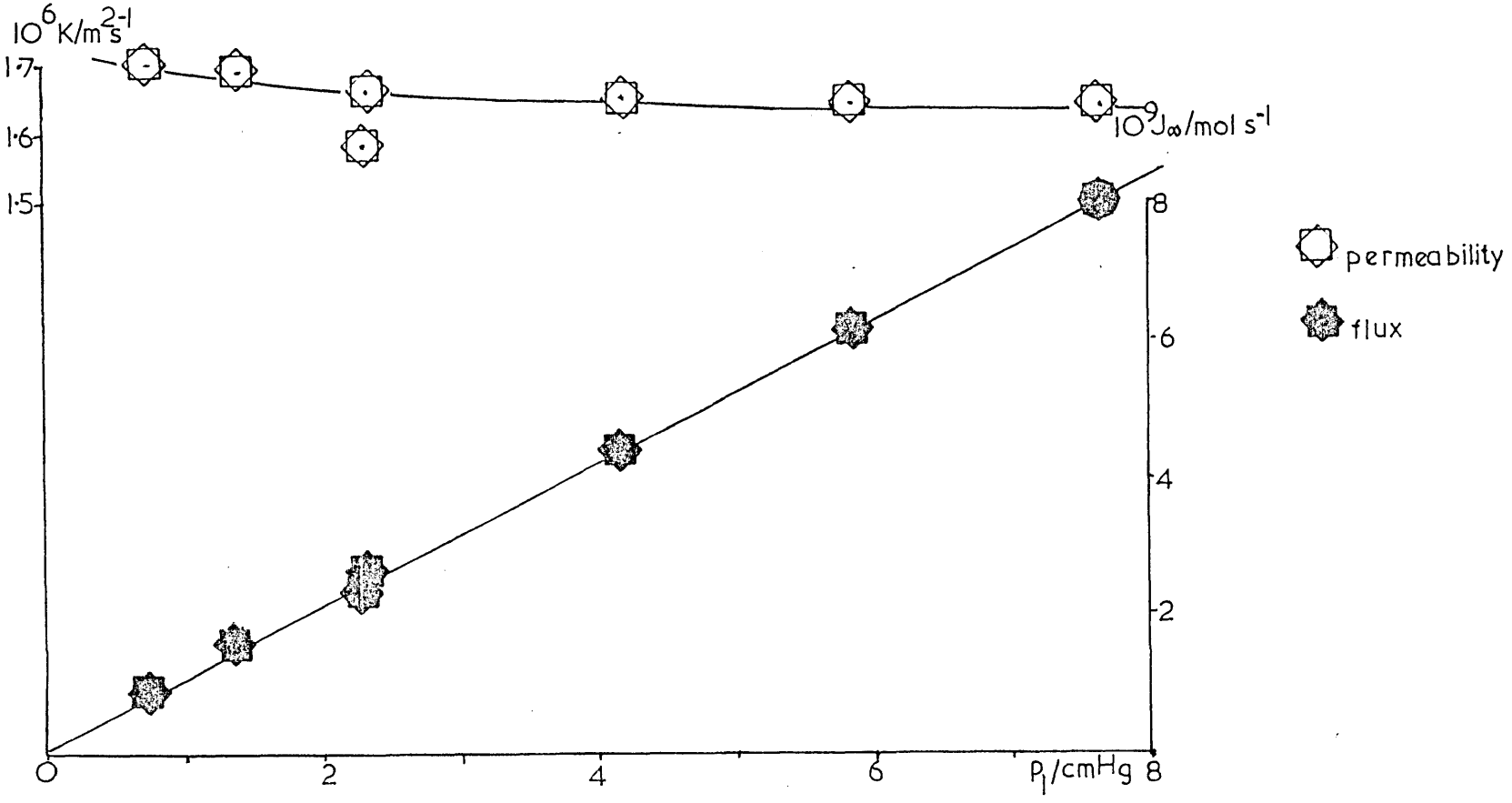




(fig 4·2·37) Integral permeability and steady state flux versus ingoing pressure SF_6 flow through Graphon membrane 195K

(fig 4·2·38) Integral permeability and steady state flux versus ingoing pressure

Ar flow through Graphon membrane 184K



occurred and results obtained at 195K, 203.2K, 213.2K and 273.2K are shown with those obtained at 213.2K by Hamilton. The permeability graphs show a minima,in contrast to the maxima observed for CO_2 and H_2S flow and the flux graph is curved concave to the pressure axis at low pressures and (except at 273.2K) convex at higher pressures.

The flow of SF_6 was also investigated at 195K, as it gives an adsorption isotherm similar in shape to that of CO_2. However the resulting permeability and flux fig. 4.2.37 showed a pressure dependence more similar to that of propane than CO_2 with permeability decreasing with increasing pressure and a pronounced point of inflection (or even possibly a maximum and minimum) in the flux curve.

Fig. 4.2.38 shows the integral permeability and flux of Ar at 184K which was measured in order to obtain a permeability value for pure Ar flow, for use in the analysis of results from Ar/CO_2 mixture flow through Graphon at the same temperature.

4.3 Binary Mixture Flow Results

4.3.1 Introduction

Binary mixture flow could be studied only on the membranes which included a side port at the ingoing face to ensure good circulation of the ingoing gas mixture (cf. section 3.1.5). The systems studied are listed in table 4.3.1.

Table 4.3.1

Binary mixtures studied

Membrane	Sorbable Component	Less sorbable component
Carbolac	CO_2	He
"	"	N_2
"	H_2S	He
"	"	N_2
Graphon	CO_2	He
"	"	(N_2 results by Miss C. Bott)
"	"	Ar
"	H_2S	He
"	"	N_2
"	SF_6	He
"	C_3H_8	He

In each case the permeability of the less sorbable component was measured as described in chapter 3.5.5 and compared to the permeability of the pure gas. In this way the blocking effect of adsorbed layers of the sorbable component could be investigated. It was found in this study and by Dr. A. D. Hamilton (1980) that the blockage results for each system studied over a range of temperatures fell upon a common curve if the relative permeability ($\tilde{K}_R$) was plotted against p_1/p_o.

where p_1 = ingoing pressure of sorbable component

p_o = saturated vapour pressure of sorbable component.

The results have therefore been presented in this way.

4.3.2 Binary mixture flow through Carbolac membrane

Fig. 4.3.1 and fig. 4.3.2 show the blockage curves obtained on the Carbolac membrane. The CO_2 blockage curves show an initial drop, followed by a slow decrease in the relative He or N_2 permeability, with increasing pressure of CO_2.

Unfortunately the saturated vapour pressure of CO_2 at 195K exceeded the upper limit of the manometer range so experiments near to $p_1/p_o = 1$ were impossible and it is not known whether a complete blockage of He or N_2 flow would be obtained at that point. Extensive time lags approaching 400 min. precluded a completely comprehensive study of Carbolac/CO_2 systems, however the general similarity in shape of the CO_2/He and CO_2/N_2 curves and the greater blockage of N_2 than He is evident from fig. 4.3.1.

By comparison the H_2S/He and H_2S/N_2 blockage curves (fig. 4.3.2) appear to be coincidental and follow a smooth curve achieving complete blockage at $p_1/p_o = 1$. By comparing the CO_2/He and H_2S/He blockage curves it may also be seen that for similar values of p_1/p_o adsorbed H_2S restricts He flow through the membrane to a greater extent than CO_2.

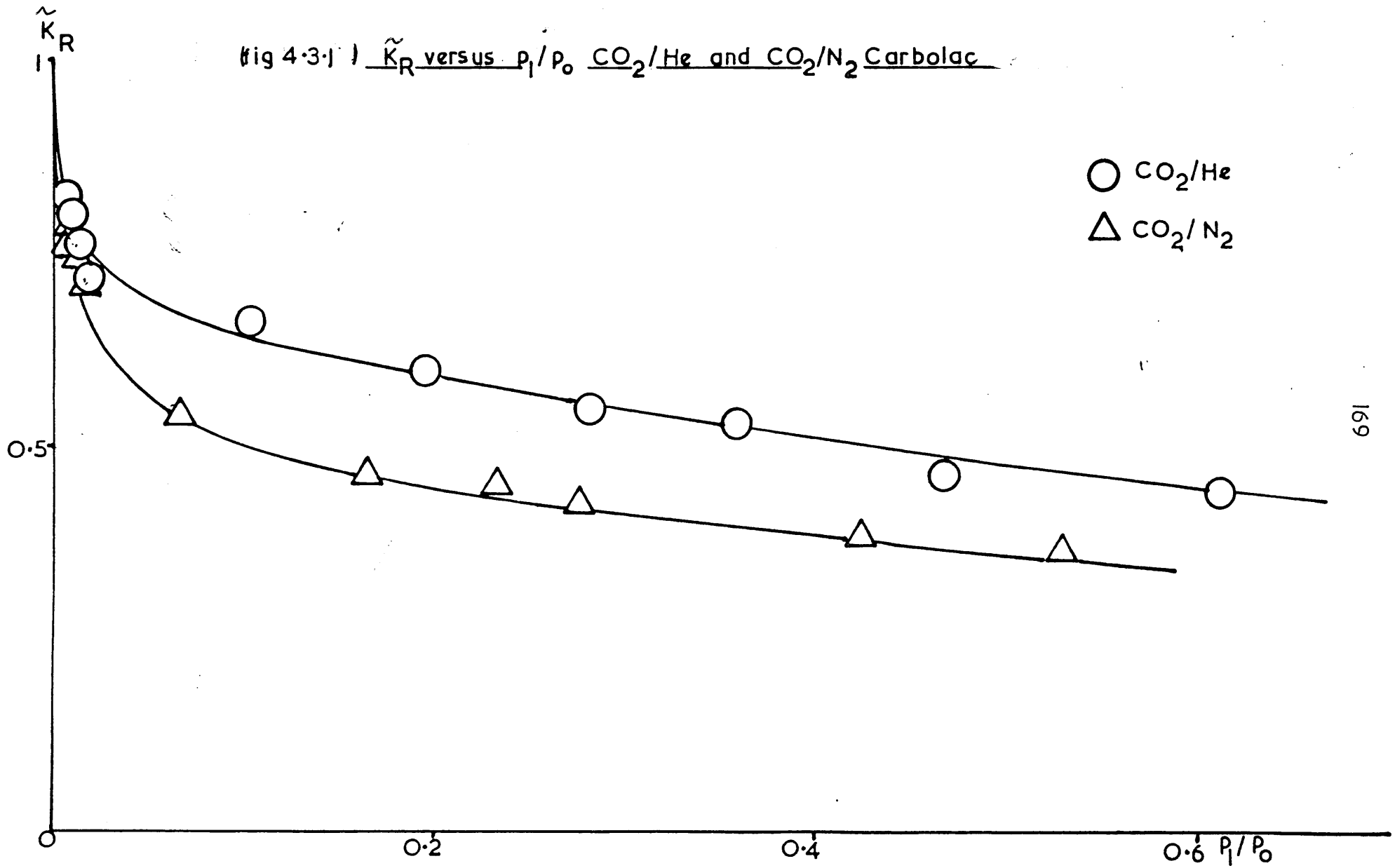
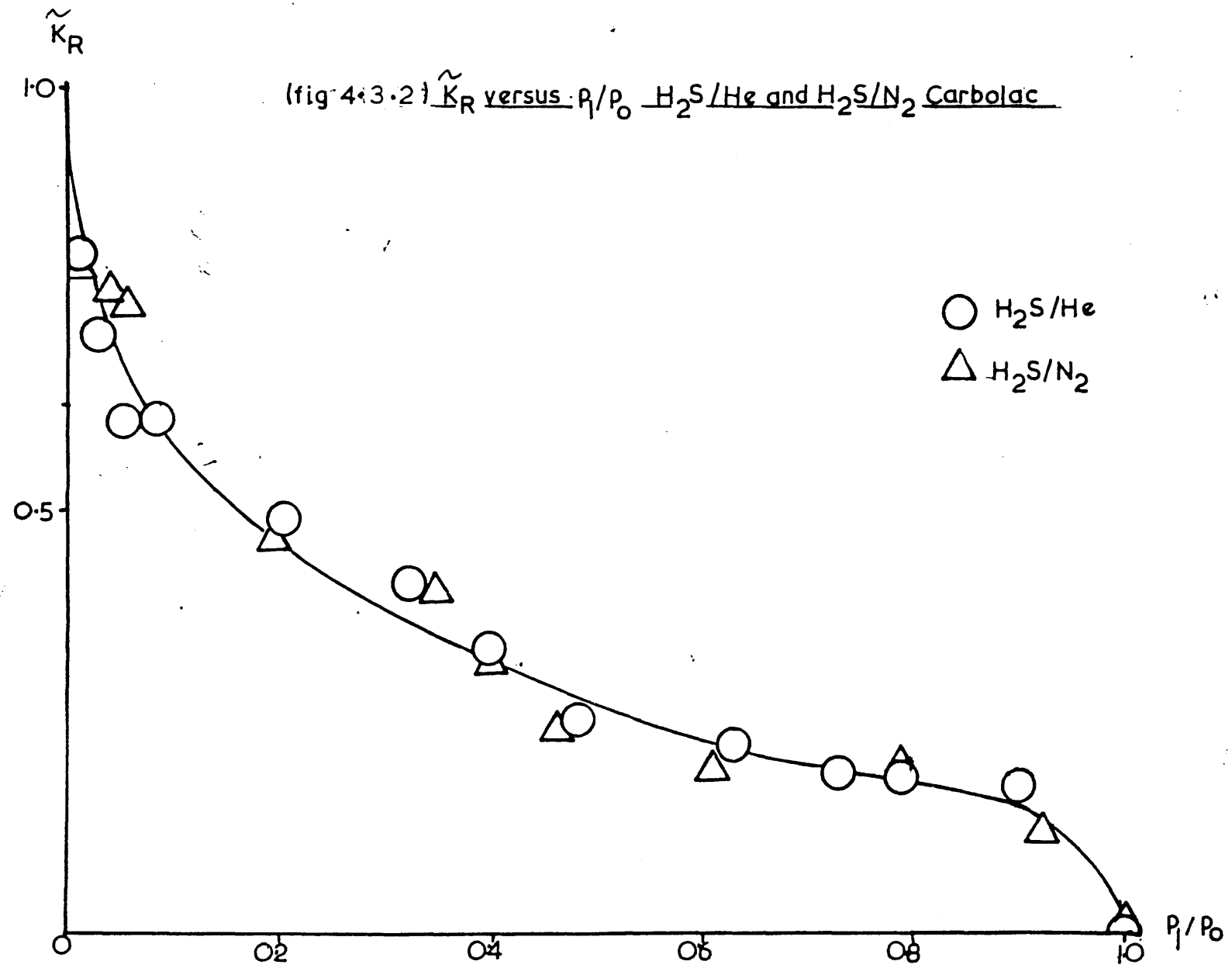


Fig 4·3·1) $\tilde{K}_R$ versus P_1/P_o CO_2/He and CO_2/N_2 Carbolac



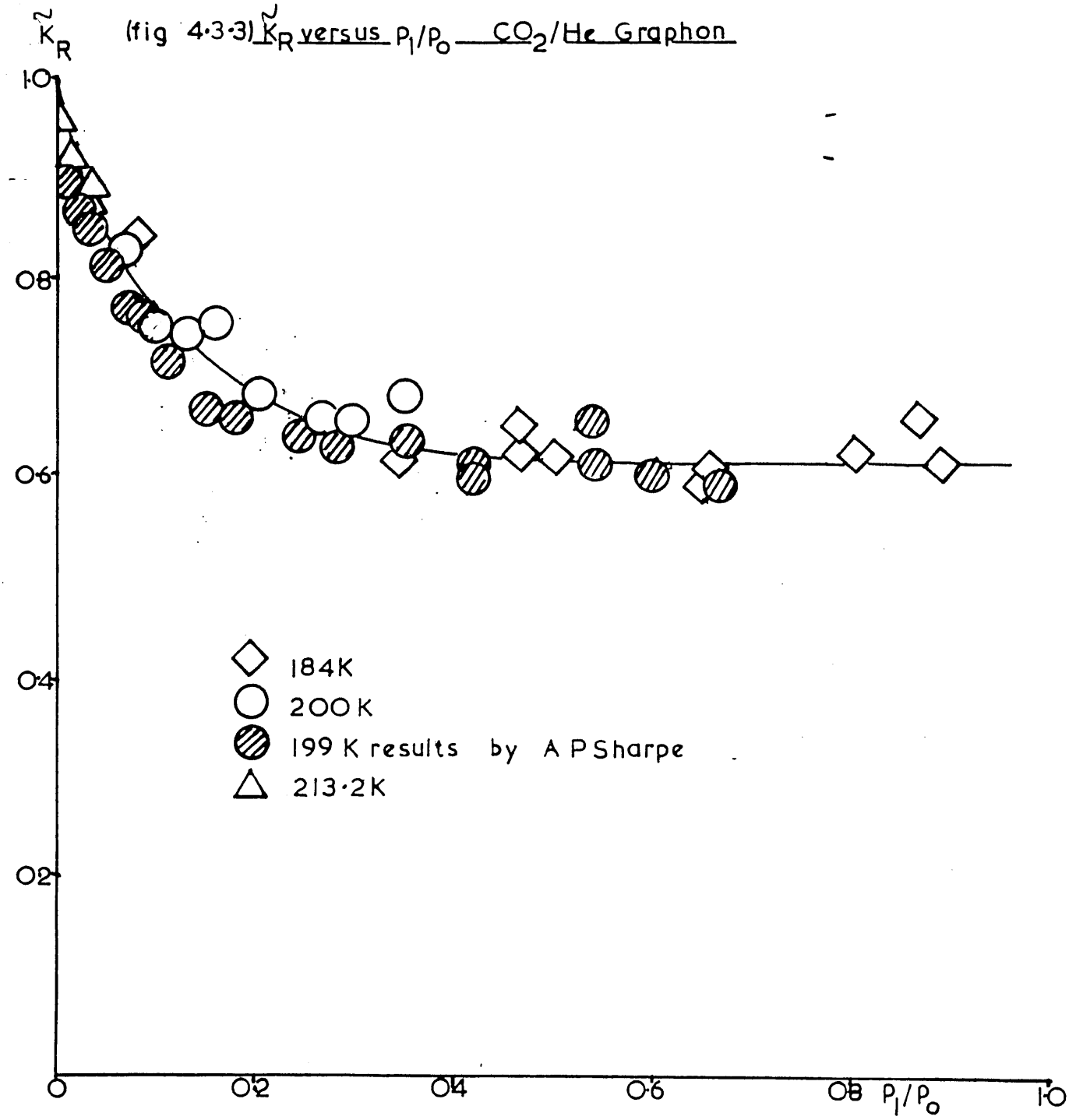
(fig 4·3·2) $\tilde{K}_R$ versus P_1/P_0 H_2S/He and H_2S/N_2 Carbolac

4.3.3 Binary mixture flow through Graphon membrane

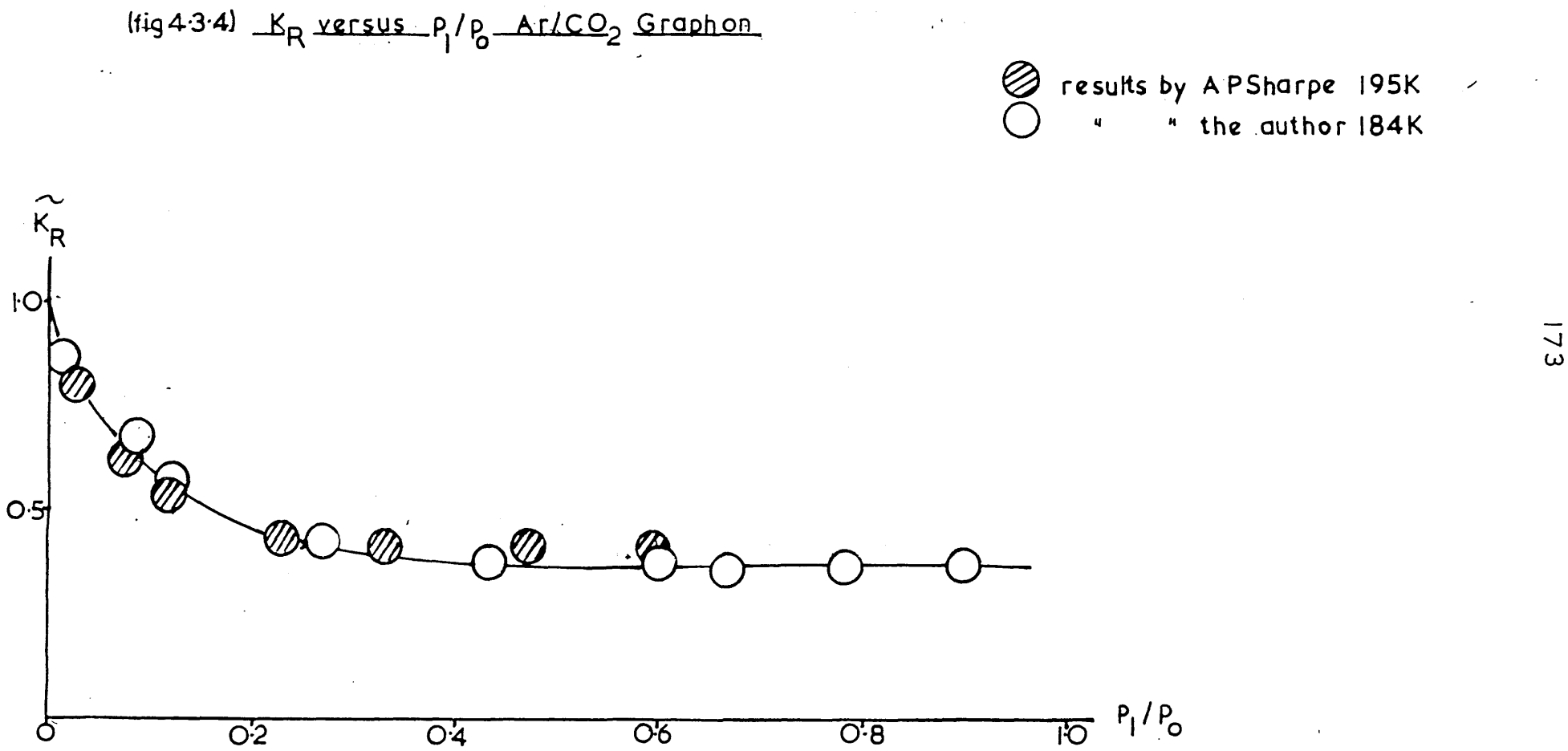
CO_2/He and CO_2/Ar flow had previously been investigated by A.P. Sharpe and his results are compared with those of the author in fig. 4.3.3 and fig. 4.3.4. For these systems and the others subsequently studied on the Graphon membrane the blockage curve showed an initial drop followed by a flat portion. This characteristic curve was similar in form but not identical to the blockage curve obtained by Dr. A. D. Hamilton for blockage of He by hydrocarbons on Graphon. Although $p_1/p_0 = 0.9$ was reached there was no evidence of complete blockage of He or Ar flow by CO_2. This was also the case for H_2S/He and H_2S/N_2 blockage curves which are shown in fig. 4.3.5 and fig. 4.3.6 and are similar in shape and magnitude to those for CO_2.

Following the similarity between the CO_2/He and Hamilton's hydrocarbons/He blockage curves, some pure gas C_3H_8 runs and some C_3H_8/He mixture runs were carried out by the author in order to determine whether the slight difference between the blockage curves was a fundamental characteristic of the membrane or whether it was due to a structural change following CO_2 adsorption, as occurs in Carbolac membranes. The C_3H_8/He mixture points were determined at 195K, 203.2K and 213.2K and were well within the error limit of Hamilton's Hydrocarbon blockage curve (Hamilton's C_3H_8/He points are shown in fig. 4.3.7 with those determined by the author). It was concluded that the slight difference in blockage curves was a property of the membrane.

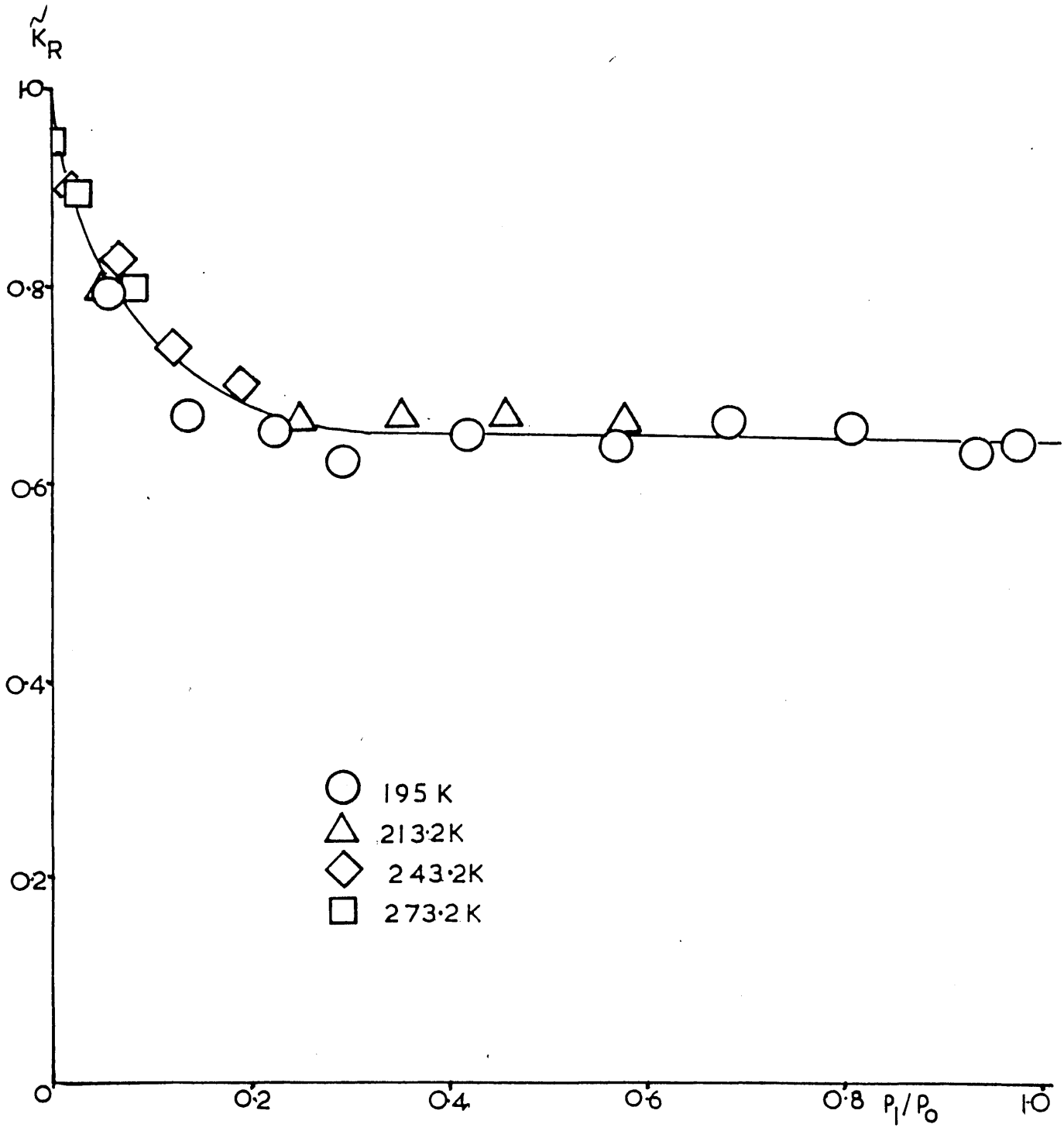
(fig 4·3·3) $\tilde{K}_R$ versus P_1/P_o — CO_2/He Graphon



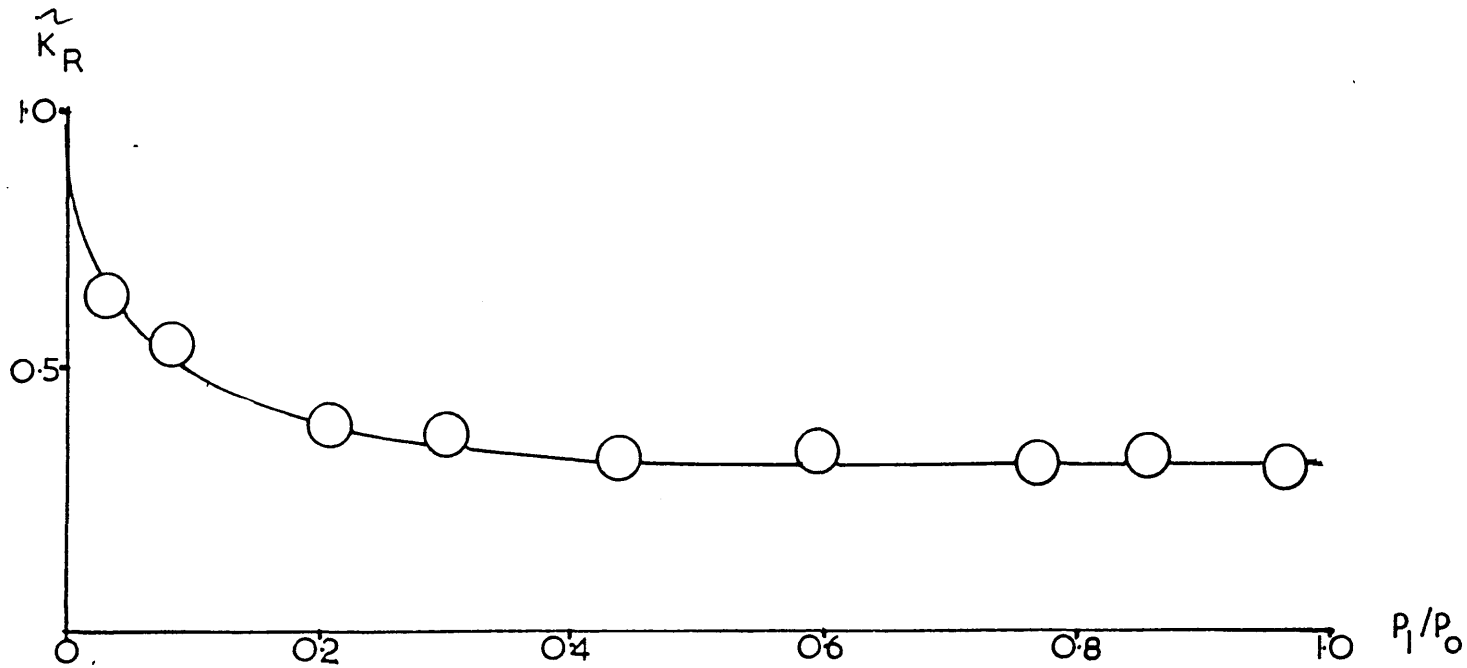
(fig 4·3·4) K_R versus P_1/P_o Ar/CO_2 Graphon



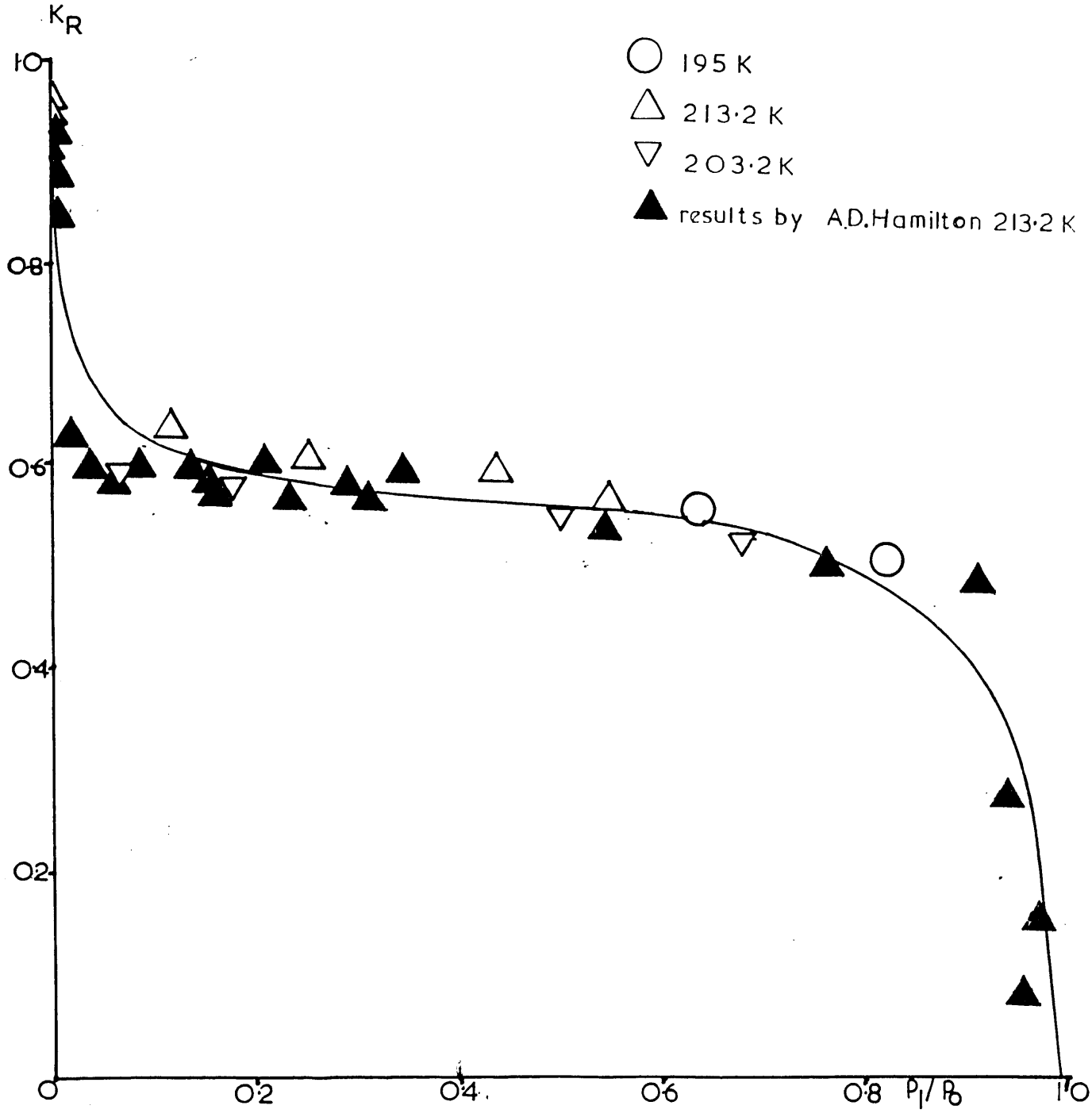
(fig 4·3·5) $\tilde{K}_R$ versus P_1/P_o H_2S/He Graphon



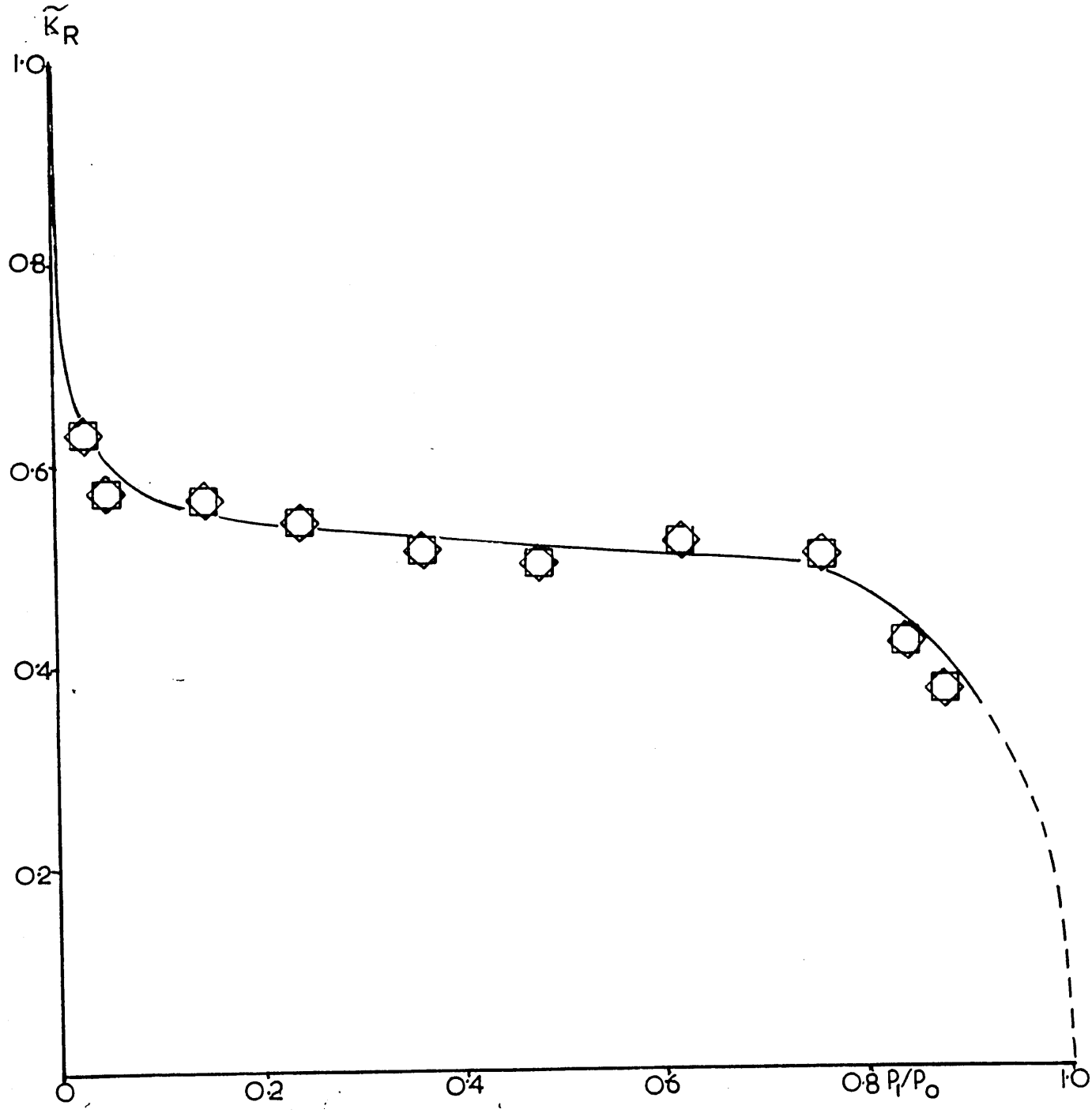
(fig 4·3·6) $\tilde{K}_R$ versus P_1/P_o H_2S/N_2 Graphon 195K



(fig 4·3·7) $\tilde{K}_R$ versus P_1/P_o C_3H_8/He Graphon



(fig 4·3·8) $\tilde{K}_R$ versus p_1/p_o SF_6/He Graphon 184K



The SF_6/He system was studied because SF_6 produces a type III/ type V isotherm when adsorbed on Graphon, very similar to that of CO_2.

The single gas flow experiments using SF_6 produced integral permeability and steady state flux graphs more similar in shape to that of C_3H_8 than CO_2 and this likeness was also evident in the blockage curve. (fig. 4.3.8). After an initial drop the relative permeability maintained a value of 0.52 closer to that of propane (0.55) than CO_2 (0.62), until p_1/p_o = .84 at which point $\tilde{K}_R$ dropped again, suggesting that at p_1/p_o = 1 complete He blockage might be obtained as with C_3H_8.

4.3.4 Error analysis

The main sources of random error in gas flow experiments resulted from uncertainty in the membrane dimensions, in the volume calibrations, the temperature measurement, and the ingoing and outgoing pressure measurement.

Membrane Dimensions:	Cross-sectional area, Ac,	$\pm$ 1.5%
	length , ℓ,	$\pm$ 1.0%
	weight ,	$\pm$ 0.1%
Volume Calibrations:	by water ,	$\pm$ 0.1%
	by He ,	$\pm$ 1.0%
Temperature :	Cryostat bath, $\pm$ 1K,	$\pm$ 0.5%
	Room temperature, $\pm$ 2.5K,	$\pm$ 1.0%
Ingoing pressure:	manometer $\pm 10^{-5}$m,	$\pm$ 1.0%
Outgoing pressure:	McLeod gauge,	$\pm$ 1.0%

The error in reading the outgoing pressure was minimised by the use of specially cleaned mercury in the McLeod gauges. The ingoing pressure was maintained at a constant value by use of large ingoing buffer volumes and where necessary the Toepler pump and was read to $\pm$ 0.002 cm using a cathometer. In mixture experiments there was some doubt concerning constant composition of the ingoing gas mixture, however calculations by Hamilton proved that the change in composition could be considered negligible except in cases near to the saturated vapour pressure of the sorbable component, in which slight temperature changes could alter the ingoing pressure, so extreme care was taken.

The measurement of integral permeability and flux involved the calculation of the gradient of the p_2 versus t graph. The error in the gradient will include the aforementioned errors in room and membrane temperatures, volume calibrations and ingoing

and outgoing pressures. The overall error in the gradient was calculated for every experiment by the least squares method using the micro computer and the experiment continued until it was less than 0.5%.

The calculated maximum errors in permeability and flux are listed in table 4.3.2, and it was found that most of the experimental results lay well within these limits.

Table 4.3.2

Estimated maximum errors

Quantity	Error
Integral Permeability, $\tilde{K}$	$\pm$ 4.0%
Steady state molar flux J	$\pm$ 1.3%

Chapter 5 Discussion

5.1 Discussion of adsorption isotherms

5.1.1 Isotherms on molecular sieve materials

5.1.2 Carbolac isotherms

5.1.3 Graphon isotherms

5.1.4 Isosteric heats of adsorption

5.2 Discussion of flow results on molecular sieve membranes NaX1, NaX2 and CMS

5.2.1 Introduction

5.2.2 Low pressure behaviour of the integral permeability

5.2.3 Knudsen and Poiseuille permeabilities

5.2.4 $\tilde{K}\sqrt{M}$ versus $1/\bar{\lambda}$ plots

5.2.5 Break-through time procedure

5.2.6 Theoretical determination of time lags

5.3 Discussion of flow results on Carbolac and Graphon membranes

5.3.1 Introduction

5.3.2 Helium flow

5.3.3 Flow of sorbable gases : $\tilde{K}$ and J_∞

5.3.4 Flow of sorbable gases: $\tilde{K}_s/\tilde{K}_g$ and $\tilde{K}_s/A$

5.3.5 Diffusion coefficients

5.4 Binary mixture flow

5.4.1 Relationship between ν, $\tilde{K}$ and $\tilde{K}_{R(He)}$

5.4.3 The shape of the blockage curve

5.4.4 Blockage behaviour of different sorbable gases

5.4.5 Blockage of gases other than He

5.5 Application of results to gas separation

5.5.1 Introduction

5.5.2 Continuous flow separation of gas mixtures

5.5.3 Transient state separations

5.5.4 Separation of H_2S from gas mixtures

CHAPTER 5

DISCUSSION

5.1 Discussion Of Adsorption Isotherms

5.1.1 Isotherms on molecular sieve materials

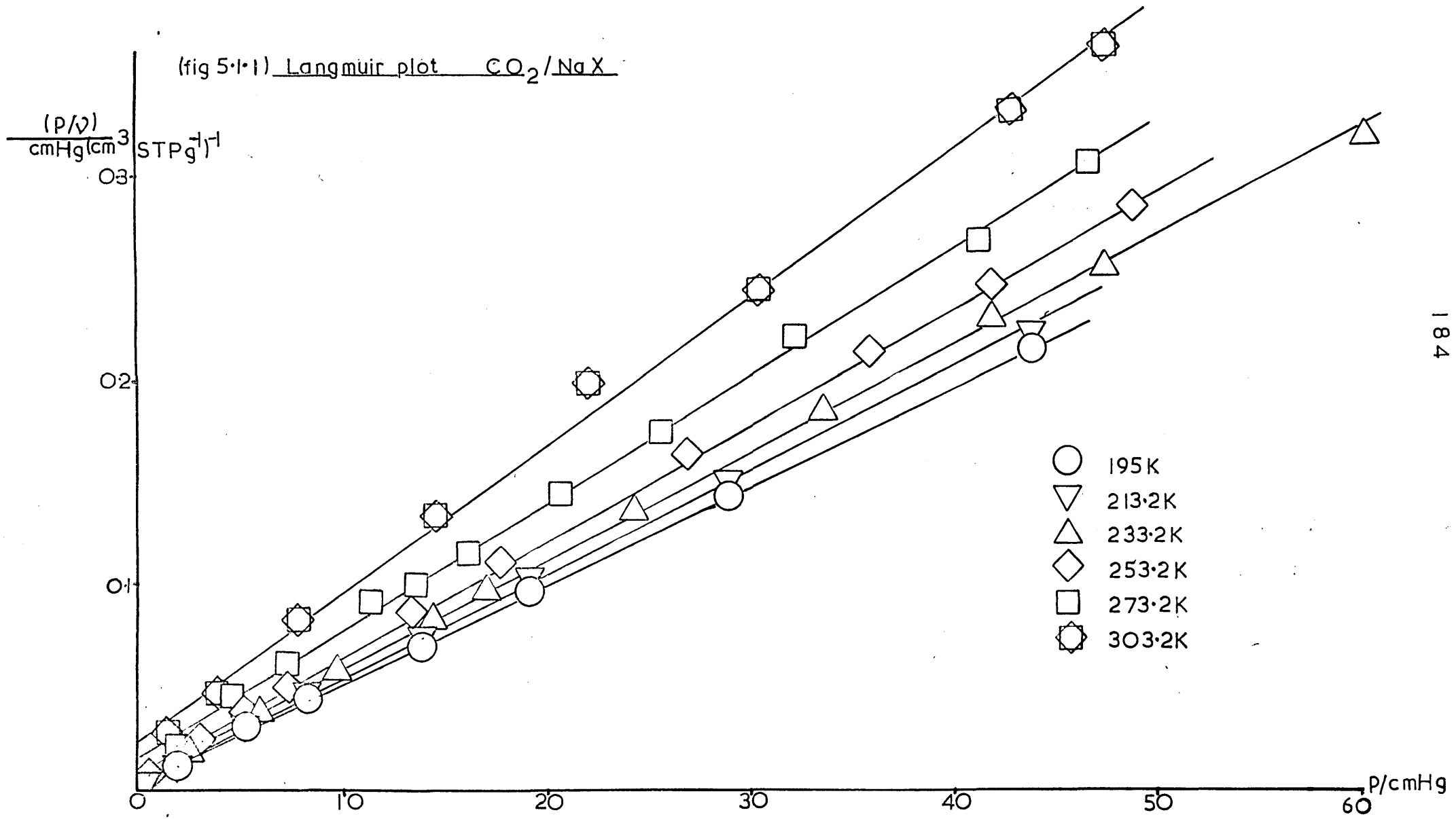
The isotherms obtained for CO_2 and H_2S adsorption on NaX and CO_2 adsorption on the carbon molecular sieve (fig. 4.1.1, 4.1.2, 4.1.4 and 4.1.5) were rectangular in form exhibiting a steep initial rise followed by an almost constant plateau.

Isotherms of this shape are characteristic of type 1 in the BET classification and are commonly obtained from adsorbents with pore diameters in the molecular range e.g. zeolites (Barrer and Sutherland 1956) and activated carbons (Koresh 1981). The classical interpretation of type I isotherms utilises the Langmuir model, (section 2.7) although this was originally formulated (Langmuir 1916) for adsorption upon a free surface. The type 1 isotherms obtained in this study were successfully fitted to the Langmuir equation

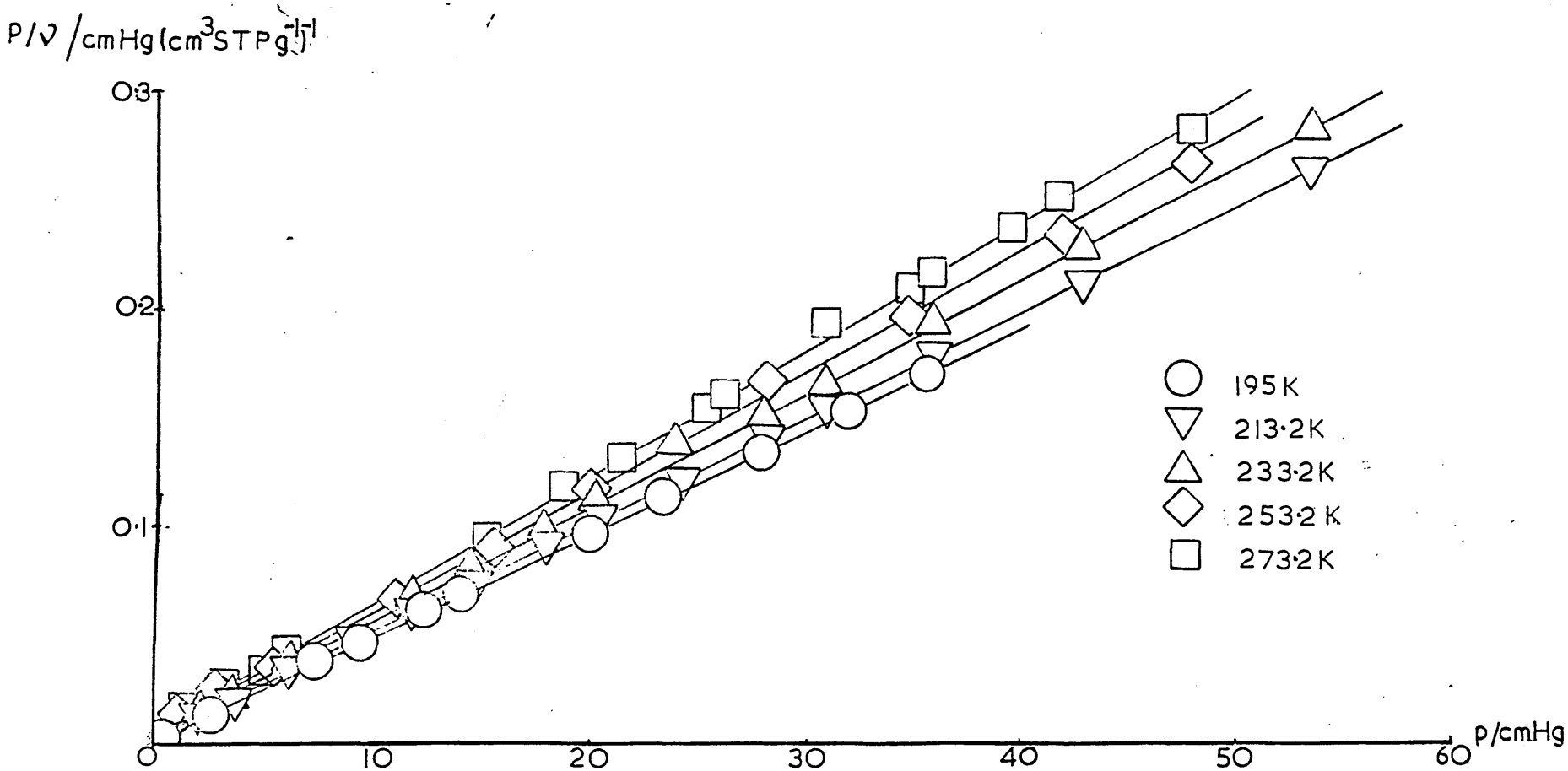
$$\frac{\nu}{\nu_m} = \frac{bp}{1 + bp} \quad \text{or} \quad \frac{p}{\nu} = \frac{1}{b\nu_m} + \frac{p}{\nu_m}$$

and the resulting linear relationship between p/ν and p is shown in fig. 5.1.1 to fig. 5.1.4. These graphs show a high degree of linearity over the whole extent of the isotherm indicating a good fit to the Langmuir equation. However it has been pointed out that conformity to the form of the Langmuir equation does not necessarily

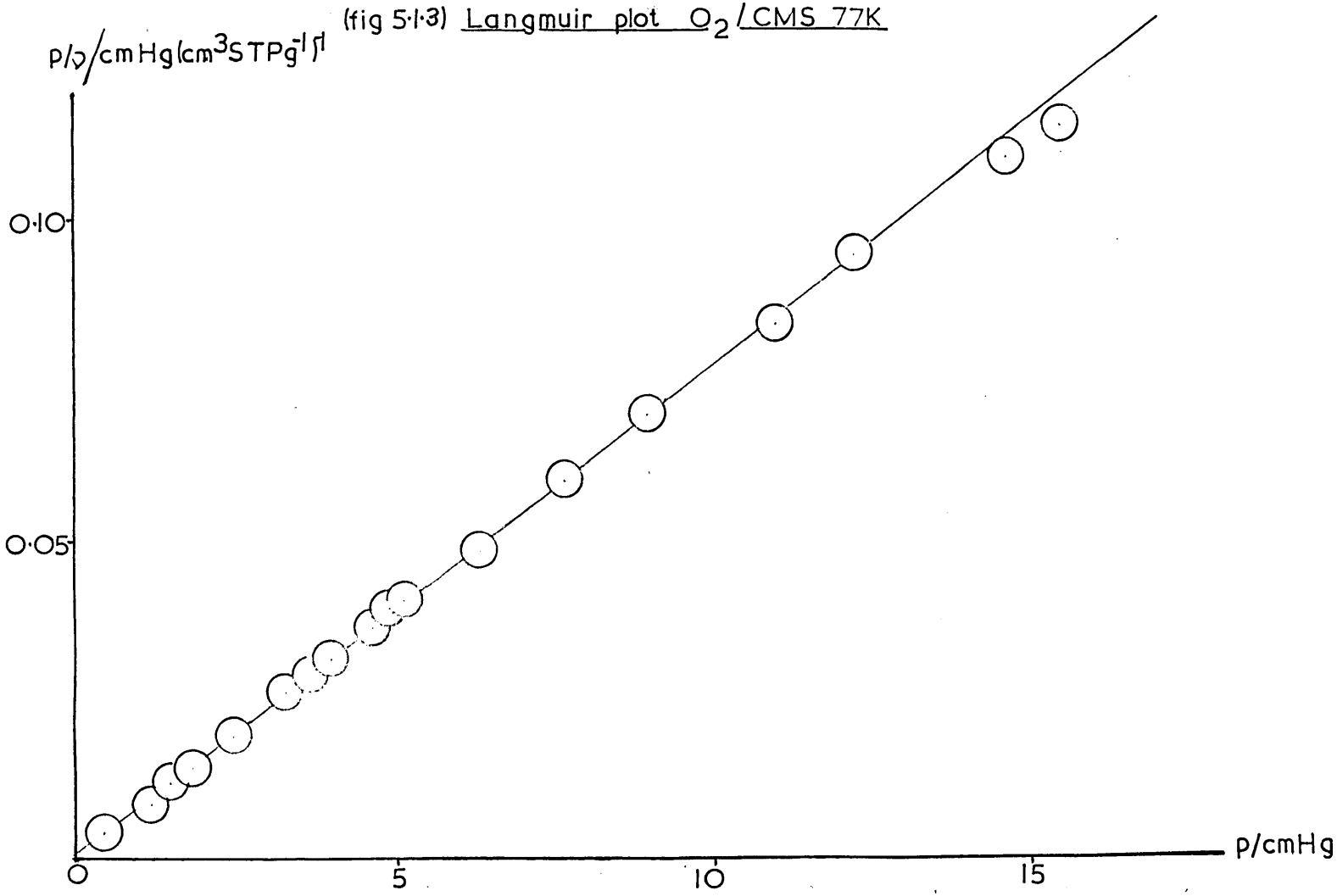
(fig 5·1·1) Langmuir plot CO_2 / Na X



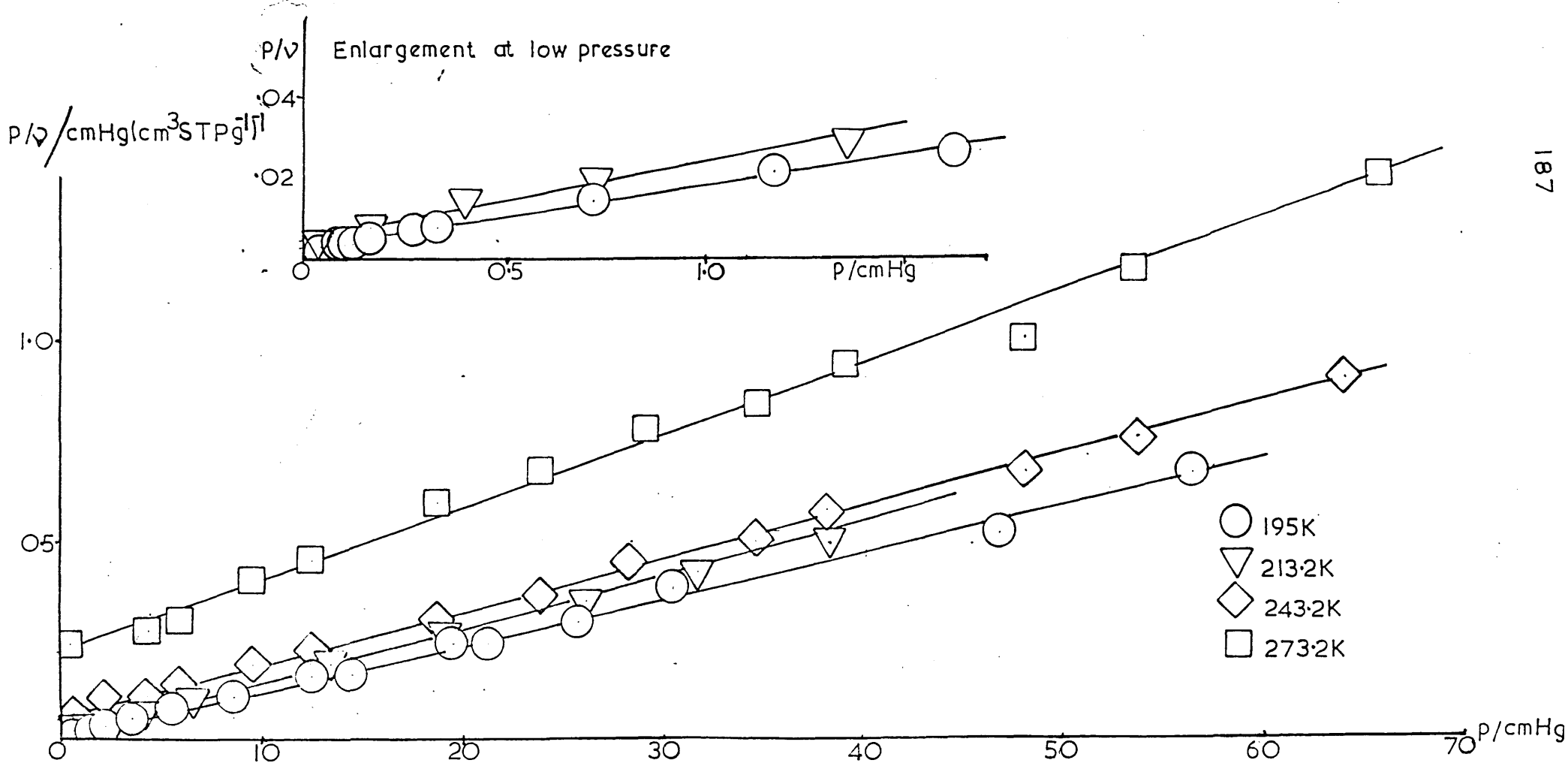
(fig 5·1·2) Langmuir plots H_2S/NaX



(fig 5·1·3) Langmuir plot O_2 / CMS 77K



(fig 5·1·4) Langmuir plot CO_2/CMS



constitute conformity to the ideal localised monolayer model upon which it is based (Young and Crowell 1962).

The values of b and ν_m obtained are tabulated in Table 5.1.1. If the isotherm is plotted in the form ν versus p then the product $b\nu_m$ is equal to the initial slope of the isotherm which decreases with increasing temperatures (as the isotherm becomes less rectangular in shape). For CO_2 adsorption on CMS b varies from 0.081 $cmHg^{-1}$ at 273.2K to 6.024 $cmHg^{-1}$ at 195K and the highest b value(7.60 $cmHg^{-1}$) is obtained for O_2 adsorption on CMS at 77K, the isotherm for which is extremely rectangular (fig. 4.1.4). Fowler (1935) derived the Langmuir equation statistically and obtained an explicit expression for b.

$$b = \frac{h^3}{(2\pi m)^{3/2} (kT)^{5/2}} \quad \frac{f_{a(T)}}{f_g(T)} \quad e^{q_{ST}/kT}$$

where h = Plancks constant, m = molecular mass, $f_a(T)$ and $f_g(T)$ are the internal partition functions for a molecule in the adsorbed and gaseous state respectively and q_{ST} is the isosteric heat of adsorption. A constant value of b might therefore result from mutual cancellation of variations in q_{ST} and $f_a(T)$. For the systems studied q_{ST} has been calculated as a function of coverage using the Clausius-Clapeyron equation and is plotted in fig. 5.1.16 and fig. 5.1.17.

The ν_m values obtained from Langmuir plots decreased with increasing temperature, and showed good agreement with the values

obtained from the plateau section of the isotherms. It is interesting to note that the ν_m values for CO_2 and H_2S adsorption on NaX agree with each other to within 6% at each temperature. This corresponds to the theory of the Langmuir model which assumes that the molecules of gas are adsorbed upon defined adsorption sites, each of which can accommodate only one adsorbed molecule, the energy of which is independent of neighbouring molecules.

Equivalent surface area values may be calculated from the saturation capacities for any gas.

These depend upon the area assigned to an adsorbed molecule and in table 5.1.2.a) and b) several alternatives are listed.

Table 5.1.2a

Equivalent Surface areas of NaX

Calculated from isotherms at 195K BET ν_m values

Gas	Area/Å^2	Source	Equivalent surface area/m^2g^{-1}
CO_2	16.3	liquid density	934
CO_2	20.6	Kodera Onishi (1960)	1180
CO_2	22.2	Lemcoff and Sing (1977)	1272
H_2S	15.5	liquid density	884

Table 5.1.2b

Equivalent Surface areas of CMS

Calculated from ν_m values from BET plots of CO_2 at 195K and O_2 at 77.4K isotherms

Gas	Area/Å^2	Source	Equivalent surface area/m^2g^{-1}
O_2	14.1	liquid density	493
CO_2	16.3	liquid density	386
CO_2	20.6	Kodera and Onishi (1960)	488
CO_2	22.2	Lemcoff and Sing (1977)	526

The surface areas obtained for NaX may be compared to a value of 702 m^2g^{-1} obtained from the N_2 saturation capacity measured by Sutherland (1956) using a value of 16.2 Å^2 for an adsorbed N_2 molecule. This is considerably lower than any of the values obtained in this study. No carbon molecular sieve surface area from the literature was available for comparison with measured values. It is debatable whether the saturation capacity of a molecular sieve should be used to calculate an equivalent surface area value or a void volume (using the volume of an adsorbed molecule). Gregg and Sing (1982) suggest that the adsorbate is condensed in the pores, in a form having a density close to that of the bulk liquid, this being the case then void volumes would certainly be more meaningful, these are shown in table 5.1.2c.

Table 5.1.1

Comparison of b an ν_m values from Langmuir plots

Adsorbent	Gas	Temp/K	b/cmHg^{-1}	ν_m/cm^{3}STPg^{-1}
NaX	CO_2	195	1.6	213
		213.2	1.7	198
		233.2	0.30	192
		253.2	0.74	179
		273.2	0.41	161
		303.2	0.32	138
NaX	H_2S	195	4.7	212
		213.2	1.6	207
		233.2	1.3	192
		253.2	1.1	182
		273.2	0.96	172
CMS	CO_2	195	6.0	83
		213.2	2.8	71
		243.2	0.28	71
		273.2	0.081	56
CMS	O_2	77	7.6	132

Table 5.1.2c Void Volumes (VV)

Sorbent	gas	T/K	ν_m/cm^3STPg^{-1}	$10^{29}V_m/m^3$	$10^4VV/m^3kg^{-1}$
NaX	CO_2	195	213	7.75	4.46
NaX	H_2S	195	212	6.22	3.53
CMS	O_2	77	132	4.85	1.69
CMS	CO_2	195	83	7.75	1.72

5.1.2 Carbolac Isotherms

Table 5.1.3 shows a review of surface area values for Carbolac obtained in previous studies upon powder pellet and plug samples. An average of 980 m^2g^{-1} was obtained from these literature values. This average excluded values obtained by Ash Barrer and Pope (1963) on a Carbolac plug as it was suspected that the Carbolac powder might have been partially covered by soldering flux during the plug's construction.

Isotherms for CO_2 on Carbolac have been measured by Ash, Barrer and Sharma (1976) and are shown in fig. 5.1.6. These and the H_2S isotherms for Carbolac (fig. 4.1.7) are of type II in the BET classification being curved concave to the pressure axis throughout their entire range.

The most widely used method for interpretation of type II isotherms is that of Brunauer, Emmett and Teller (1938) which extended the kinetic model postulated by Langmuir to cover multilayer

adsorption. The BET equation is as follows (section 2.7).

$$\frac{\nu}{\nu_m} = \frac{c(p/p_0)}{(1-p/p_0)(1+(c-1)p/p_0)}$$

where p_0 is the saturation vapour pressure of the adsorbate and

c, a parameter given by $c = \frac{a_1 v_2}{a_2 v_1} e^{(q-q_L)/RT}$

where a_1 and a_2 are the condensation coefficients for the first and second layer of adsorbed molecules, v_1 and v_2 are the frequency of oscillation of those molecules in a direction normal to the surface, q is the isosteric heat of adsorption and q_L the molar heat of condensation.

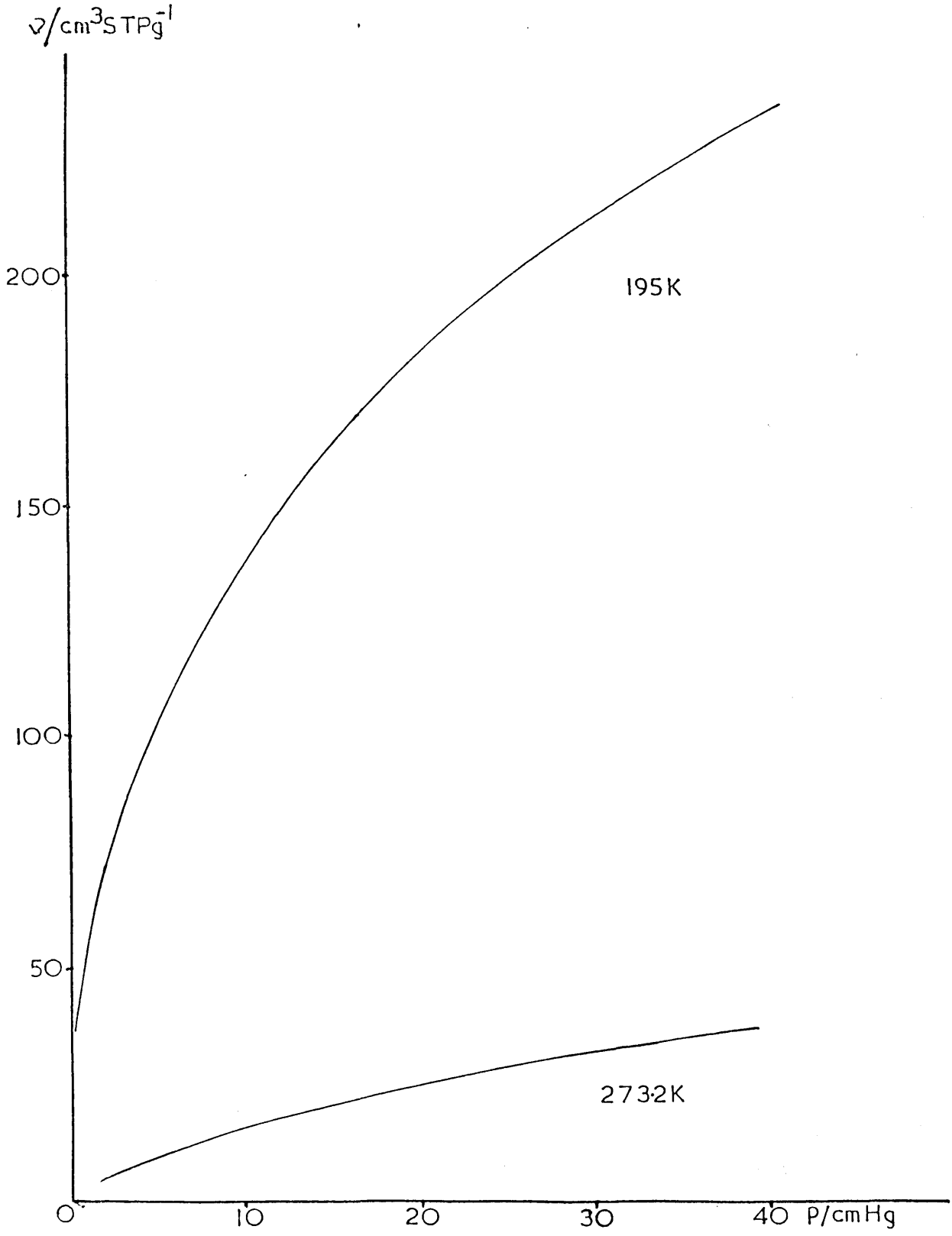
The experimental results obtained were fitted to the BET equation by plotting $\frac{p/p_0}{\nu(1-p/p_0)}$ against p/p_0

This was done for the isotherms at temperatures at which p/p_0 values fell between 0.05 to 0.30 over which range the BET equation is usually valid.

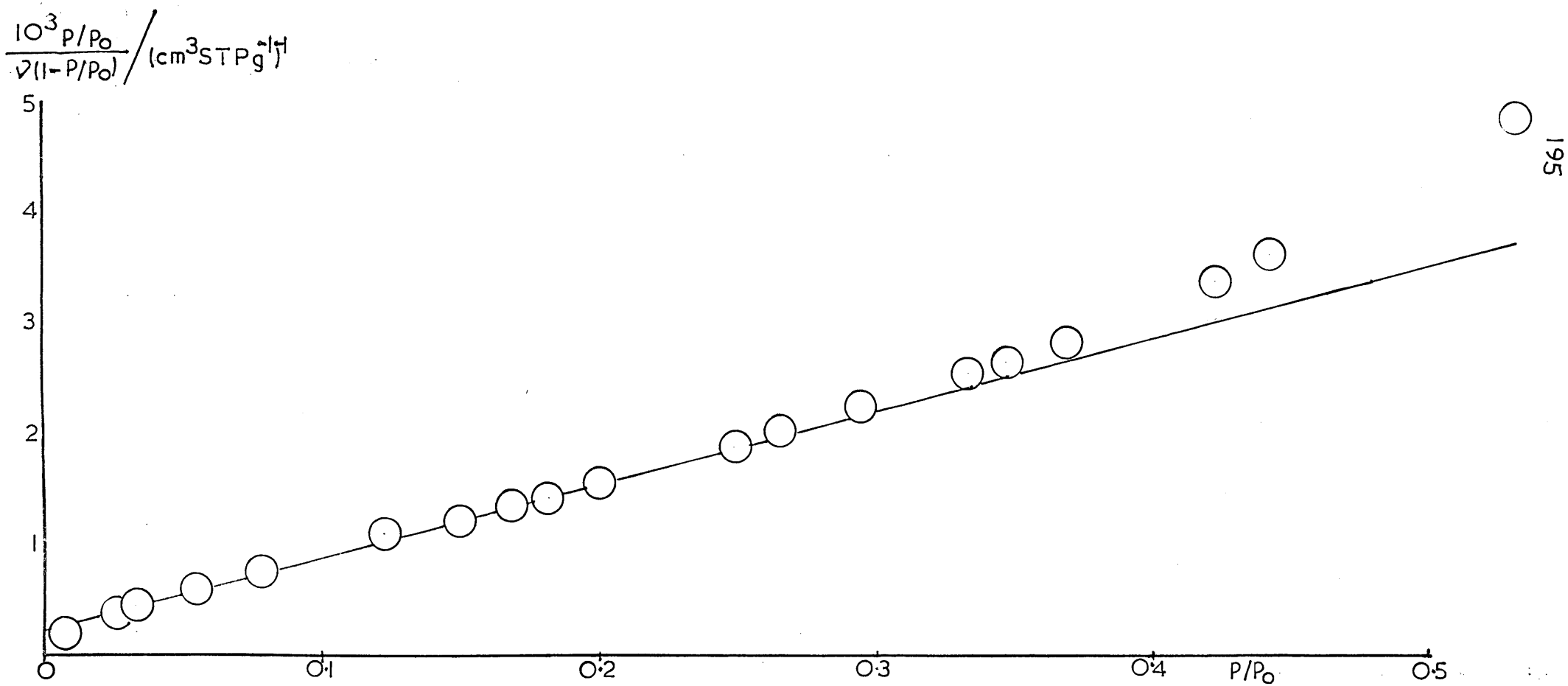
The resulting graphs fig. 5.1.8 and fig. 5.1.9 are linear below $p/p_0 = 0.30$ and from the slopes and the intercepts with the y axis values for c, ν_m and hence surface areas could be obtained, these are shown in table 5.1.4.

(fig 5·1·6) Adsorption isotherms P. Sharma

CO_2/Carbolac powder



(fig 5·1·7) BET plot P Sharma's results CO_2/Carbolac/195K



(fig 5·1·8) BET plot H_2S / Carbolac

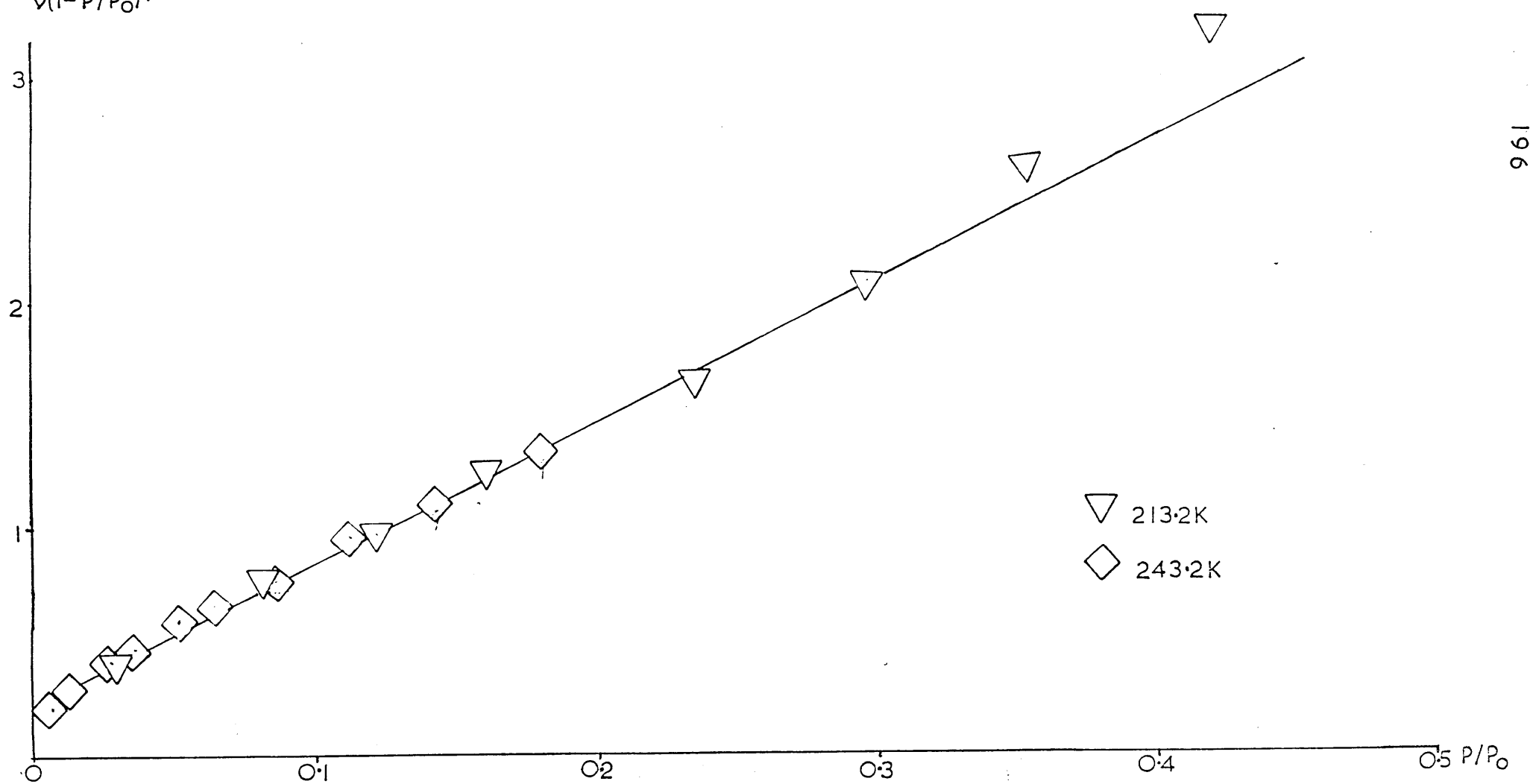


Table 5.1.3

Surface area of Carbolac obtained from BET plots

SAMPLE TYPE	TEMPERATURE /K	GAS	MOLECULAR AREA $Å^2$	Surface Area $/m^2g^{-1}$	Reference
POWDER	90.1	Ar	14.4	1060	Barrer & Strachan
PLUG	90.1	Ar	14.4	987	"
"	90.1	Ar	14.4	933	"
"	90.1	Ar	14.4	901	"
"	90.1	Ar	14.4	890	"
"	90.1	Ar	14.4	795	"
"	90.1	Ar	14.4	839	"
POWDER	77.4	N_2	16.2	1020	Ash Barrer Pope
POWDER	90.1	Ar	14.4	970	"
POWDER	273.2	SO_2	18.2	720	"
PLUG	77.4	N_2	16.2	370	"
"	77.4	Ar	13.8	380	"
"	90.1	Ar	14.4	370	"
"	190.1	CO_2	15.3	370	"
"	273.2	SO_2	18.2	360	"
POWDER	77.4	N_2	16.2	940	Clint 1966
POWDER	77.4	N_2	16.2	960	Ash Barrer Lowson
POWDER	77.4	N_2	16.2	1006	Ash Barrer Sharma
PELLETS	77.4	N_2	16.2	993	"
"	90.2	Ar	14.4	956	"
"	273.2	nC_4H_{10}	47.0	1019	"
PLUG	77.4	N_2	16.2	972	"
"	273.2	nC_4H_{20}	47.0	949	"
POWDER	195	CO_2	22.2	890	This study
POWDER	195	CO_2	24.4	980	using Sharma's isotherms
POWDER	195	H_2S	15.5	660	This study

Table 5.1.4 Carbolac surface areas (this study)

System	10^4 slope / $cm^{-3}g$	10^4 intercept / $cm^{-3}g$	c	ν_m / cm^3g^{-1}	a_m / $\AA^2$	Surface area / m^2g^{-1}
CO_2/195K	66.0	2.1	32	149	22.2	890
					24.4	980
H_2S/213.2K	62.6	2.2	29	154	15.5	660
and 243.2K					23.6	980

The value of 890 m^2g^{-1} for the surface area of Carbolac obtained, when Lemcoff and Sing's area for an adsorbed CO_2 molecule is used (a_m = 22.2 $\AA^2$) (cf table 5.1.2a), is low in comparison to the quoted literature values.

Similarly the value of 660 m^2g^{-1}, which occurs when the surface area is calculated using the liquid density of H_2S (a_m = 15.5 $\AA^2$), is also low. This discrepancy may arise from the uncertainty in the area occupied by more complicated adsorbed molecules. Evidence for this lies in the low Carbolac powder surface area obtained by Ash, Barrer and Pope (1963) when SO_2 was used as an adsorbate (720 m^2g^{-1}), and that obtained by Sharma (1976) when he calculated the surface area from his C_3H_8 isotherms (696 m^2g^{-1}, 648 m^2g^{-1}) using the area for an adsorbed C_3H_8 molecule calculated from the liquid density (a_m = 32 $\AA^2$). This differs from that suggested by Wynne-Jones (1958) (a_m = 47 $\AA^2$) which gives the surface area values quoted in Table 5.1.3. An area of 24.4 $\AA^2$ for an adsorbed CO_2 molecule which corresponds to the maximum on the

differential heat of adsorption versus coverage curve (Beebe et al 1958) produces a surface area of 980 m^2g^{-1} from Sharma's CO_2 isotherms, corresponding to the average literature value. If this value of the surface area is assumed, an area of 23.6 $Å^2$ for an adsorbed H_2S molecule results from the H_2S isotherms. This value cannot be confirmed due to the lack of published data concerning H_2S adsorption.

From the c value of the isotherm, an estimate of the isosteric heat of adsorption may be obtained as $a_1v_2/a_1v_2 \simeq 1$

giving $$c = e^{(q-q_L)/RT}$$

hence $$q - q_L = RT\&nc$$

This leads to q values of 25.8 $kJmol^{-1}$ and 26.7 $KJmol^{-1}$ at 213K and 243K respectively for H_2S and 17.0 $kJmol^{-1}$ for CO_2 at 195K which may be compared to the isosteric heat versus coverage curve (section 5.1.4). The values of q_L used were 11.4 $kJmol^{-1}$ and 19.92 $kJmol^{-1}$ for CO_2 and H_2S respectively.

5.1.3 Graphon Isotherms

Table 5.1.5 shows the surface area of Graphon determined from the N_2 isotherm at 77K in all previous studies. The area of 80.0 m^2g^{-1} suggested by Hamilton has been used in this work, as it was determined in this laboratory from the same bulk sample of Graphon powder as that used in this investigation.

Most of the Graphon isotherms measured in this study (fig. 4.1.8 to fig. 4.1.11) were of type III/type V in the BET classification being initially convex to the pressure axis with a possible point

of inflection at higher pressures. This shape is characteristic of weak gas-solid interactions and the number of well documented cases in which it occurs is relatively few.

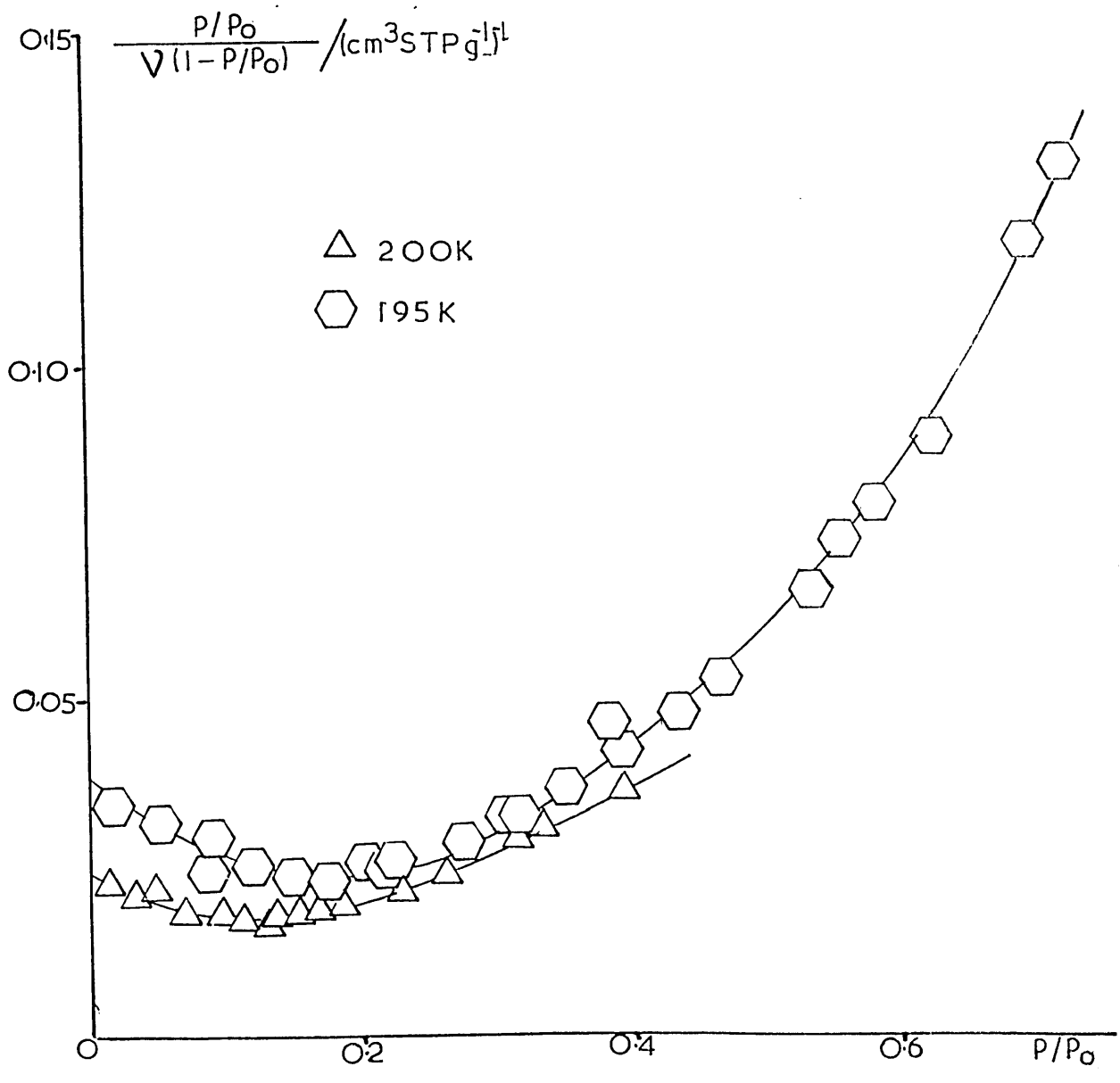
Gregg and Sing conclude that the BET procedure for evaluation of monolayer capacity is not applicable to type III or type V isotherms due to the probable building up of multilayers while the monolayer is incomplete. This is also evident from fig. 5.1.9 and 5.1.11 which show that the BET plots for CO_2 and H_2S adsorption on Graphon are not linear and exhibit a minimum at all temperatures investigated. The relative pressure at which the minimum occurred was examined and found to be linearly related to temperature for both gases (fig. 5.1.10, fig. 5.1.11), it was also found to be similar but not identical to the relative pressure at which a point of inflection occurred in the isotherm. These pressures are listed in table 5.1.6.

Table 5.1.5

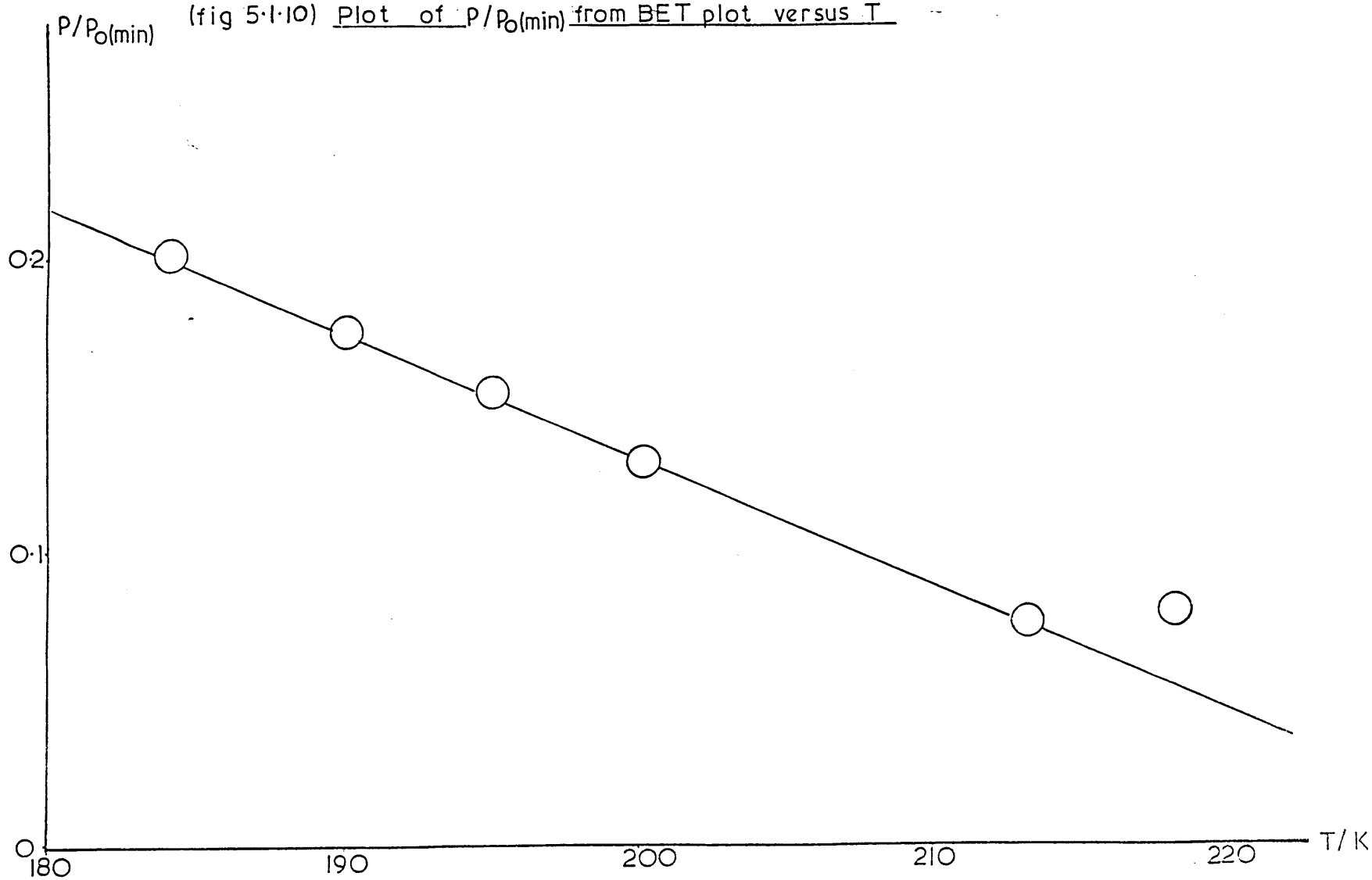
Graphon, BET surface area from low temperature N_2 isotherms

REFERENCE	Surface area m^2g^{-1}
Polley, Schaeffer, Smith	84.1
Chirnside, Pope	89.4
Ross, Good	84.1
Beebe, Briscoe, Smith, Wendell	85.0
Joyner, Emett	80.3
Murray	86.2
Pope	89.0
Cabot Technical Data Sheet	89.7
Hamilton	80.0
Riley	75.7

(fig 5·1·9) BET plot CO_2 /Graphon



(fig 5·1·10) Plot of $P/P_{o(min)}$ from BET plot versus T



(fig 5·1·11) BET plots and correlation of p/p_o at the minimum with T

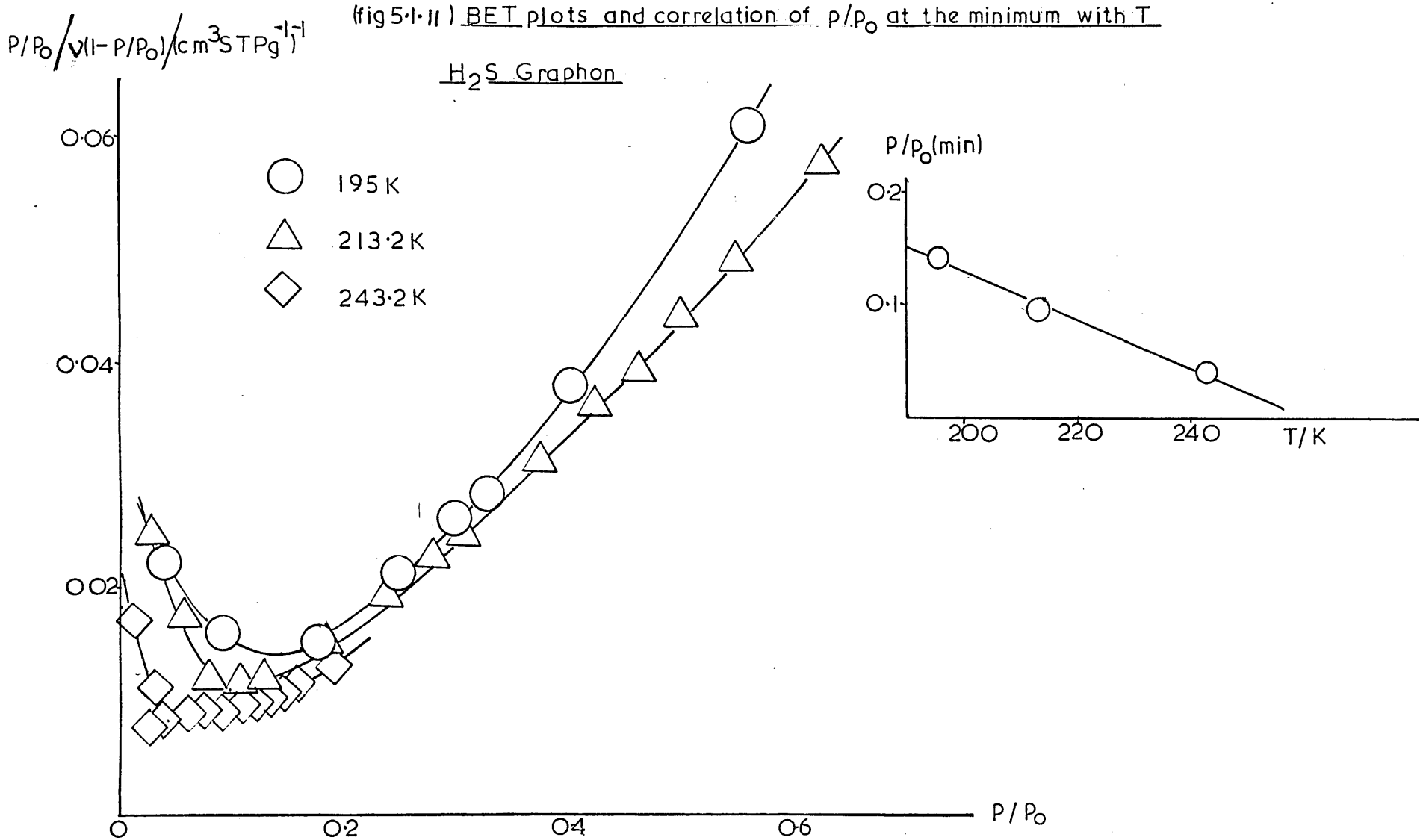


Table 5.1.6

Correlation between the pressure at the minimum of the BET plot and that at the point of inflection of the isotherm

CO_2/Graphon

T/K	p(min)/cmHg	p(inflection)/cmHg
184	6.0	4.8 ± 0.6
190	8.7	7.0 ± 1.0
195	11.8	10.6 ± 1.0
200	15.0	11.5 ± 1.0
213.2	21.9	22.0 ± 2.0

H_2S/Graphon

T/K	p(min)/cmHg	p(inflection)/cmHg
195	3.5	2.5 ± 0.2
213.2	8.0	5.5 ± 1.0
243.2	10.5	12.0 ± 2.0

In the absence of a classical approach towards the analysis of type III/type V isotherms the method of Beebe et al (1964) (as discussed in section 2.7) was used. This utilized an equation for localised monomolecular adsorption

$$p/p_o = \frac{\theta}{K_1(1 - \theta)} e^{-K_m\theta}$$

where K_1 = the adsorbate adsorbent equilibrium constant and $K_m = w/kT$ where w is the interaction energy of a pair of neighbouring molecules. This may be written in the form

$$\ell n \left(\frac{\theta}{1-\theta}\right) - \ell n\left(\frac{p}{p_o}\right) = \ell n K_1 + K_m\theta$$

which should give a straight line when $\ell n \left(\frac{\theta}{1-\theta}\right) - \ell n \left(\frac{p}{p_o}\right)$ is plotted against θ, for this to be done a value of the surface area and of the area occupied by an adsorbed molecule must be assumed. In this case Hamilton's value of 80.0 m^2g^{-1} for the surface area of Graphon was used, and three different molecular areas were tested, each giving a different monolayer capacity and hence differing θ values.

The molecular areas used are tabulated in table 5.1.7.

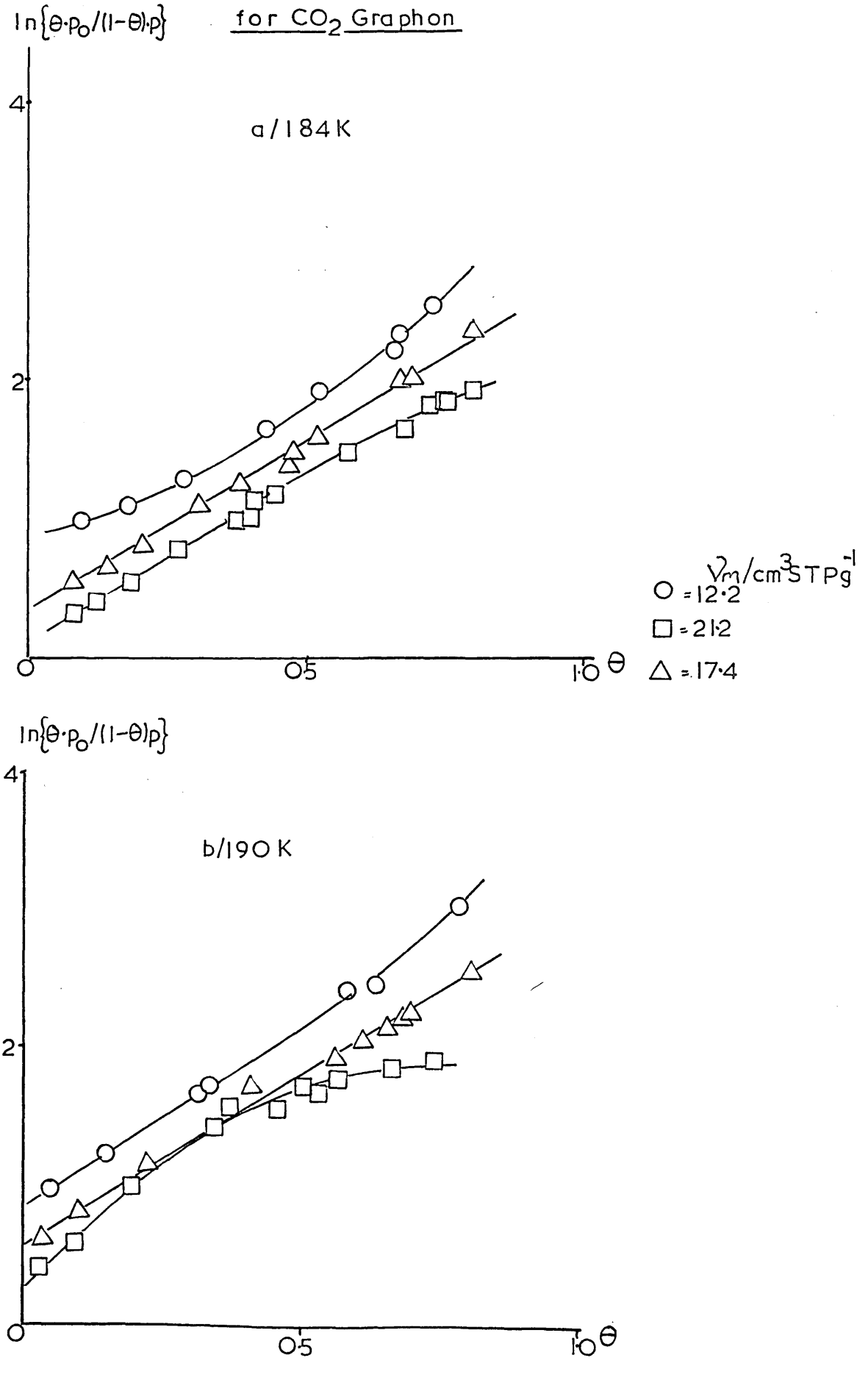
Table 5.1.7

CO_2 Molecular areas and associated monolayer capacities from Graphon (surface area 80.0 m^2g^{-1}

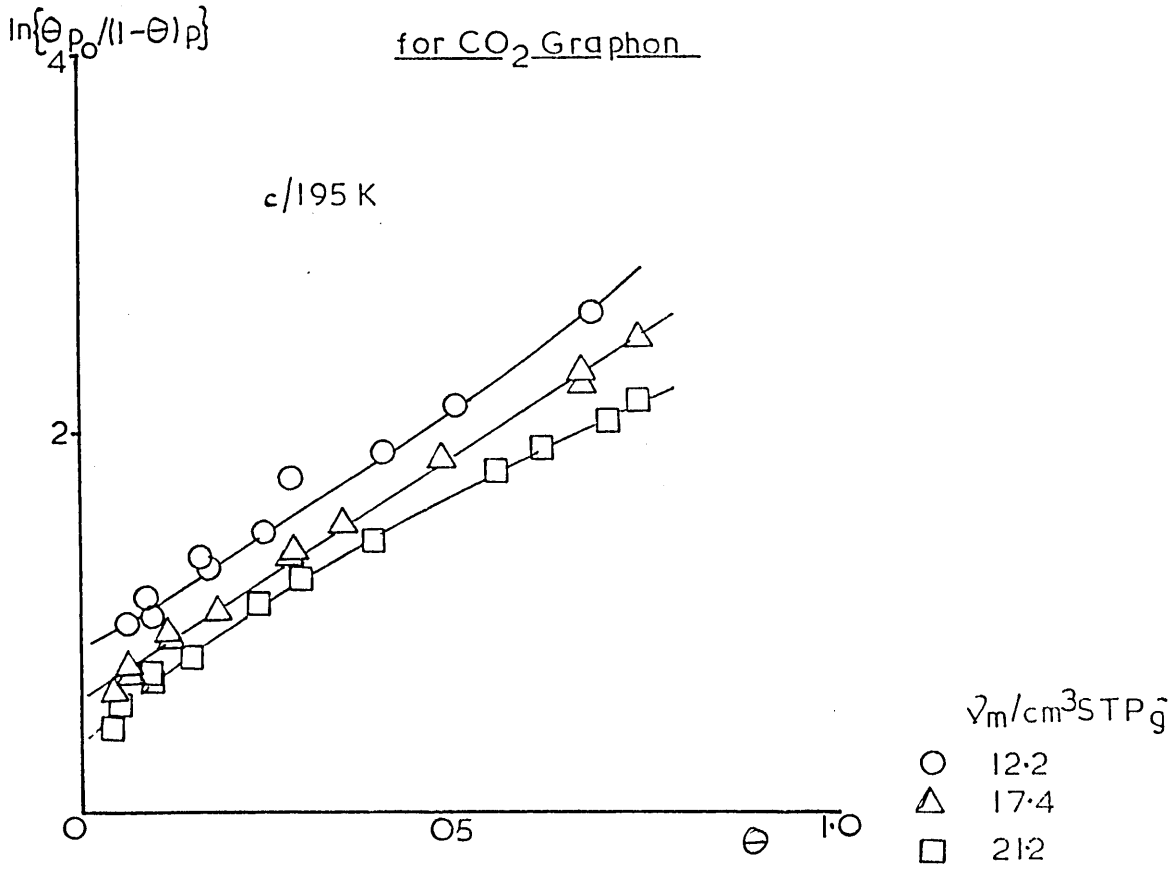
$a_m/\text{Å}^2$	v_m/cm^3STPg^{-1}	Source
14.1	21.2	Spencer Amberg and Beebe (1958)
17.1	17.4	"
24.4	12.2	Beebe et al (1964)

The resulting graphs at 184K, 190K, 195K and 200K are shown in fig. 5.1.12 and Fig. 5.1.13. It can be seen that the best straight line is obtained when a molecular area of 17.1 Å^2 is used. This value is that computed by Spencer et al (1958) for hexagonaly packed molecules, it is less than the molecular area obtained for CO_2 adsorbed on Carbolac (24.4 Å^2) and greater than the value obtained by Beebe et al (1964) (14.1 Å^2) for CO_2 adsorption on Stirling MT (surface area 7.65 m^2g^{-1}). This suggests that the surface area occupied by an adsorbed CO_2 molecule increases with increasing surface area of the adsorbent, possibly due to increasing inhomogeneity of the surface. Beebe et al (1964) concluded that the fit of results to the localised monolayer equation and the low molecular area obtained suggested the adsorption of CO_2 molecules in "extended form" and the possible arrangement of oxygen atoms over the carbon hexagons in the basal plane of graphite, which favours localisation. Baker (1966) however discusses this treatement of adsorption isotherms concluding that "obtaining fair agreement of the theoretical result with the

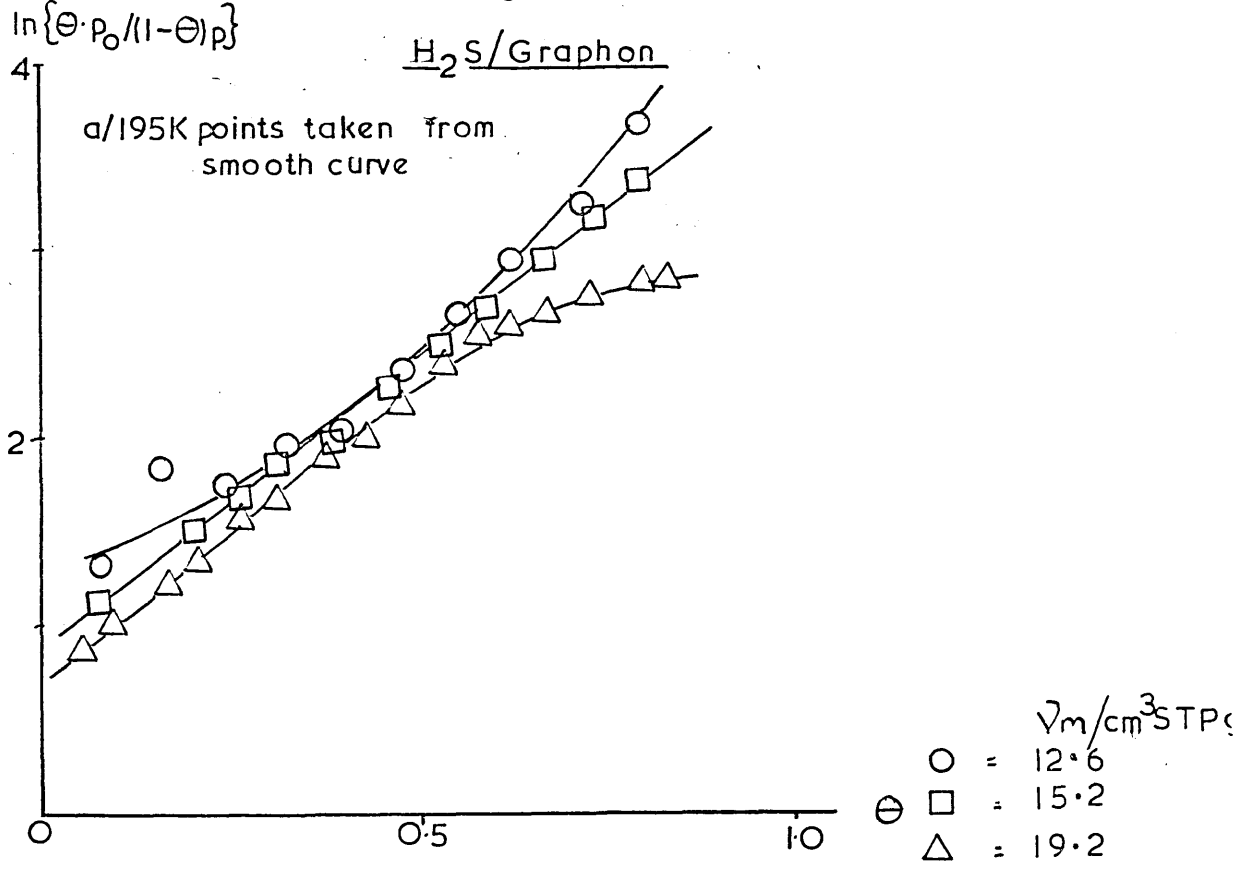
(fig 5·1·12) $\ln\{\theta p_0/(1-\theta)p\}$ versus θ for CO_2 Graphon

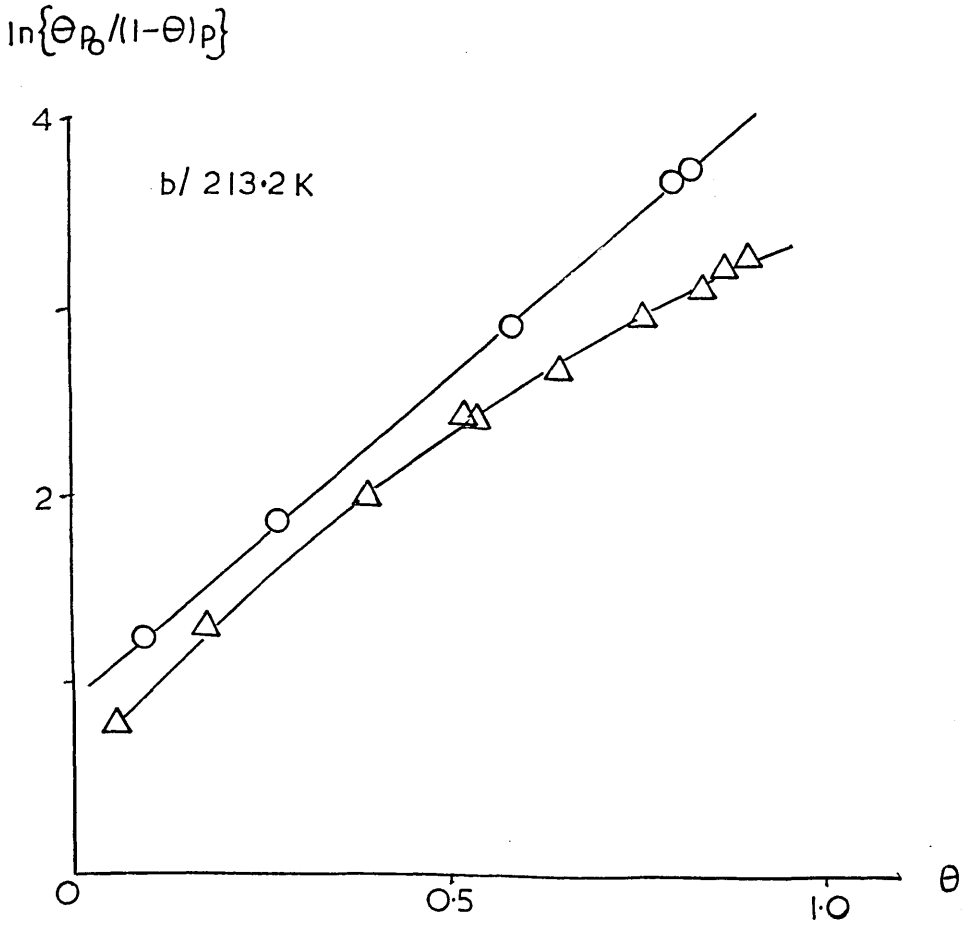


(fig 5·1·13) $\ln\{\theta \cdot p_o/(1-\theta)p\}$ versus θ for CO_2 Graphon



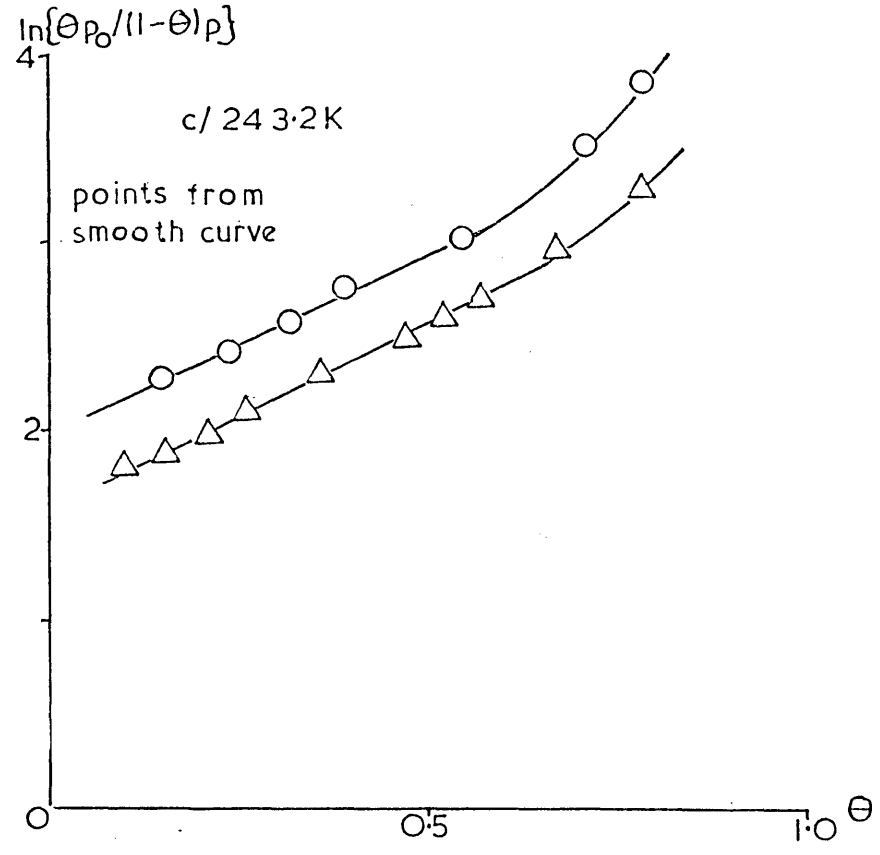
(fig 5·1·14) $\ln\{\theta p_o/(1-\theta)p\}$ versus θ





(fig 5·1·15) $\ln\{\theta p_o/(1-\theta)p\}$ versus θ

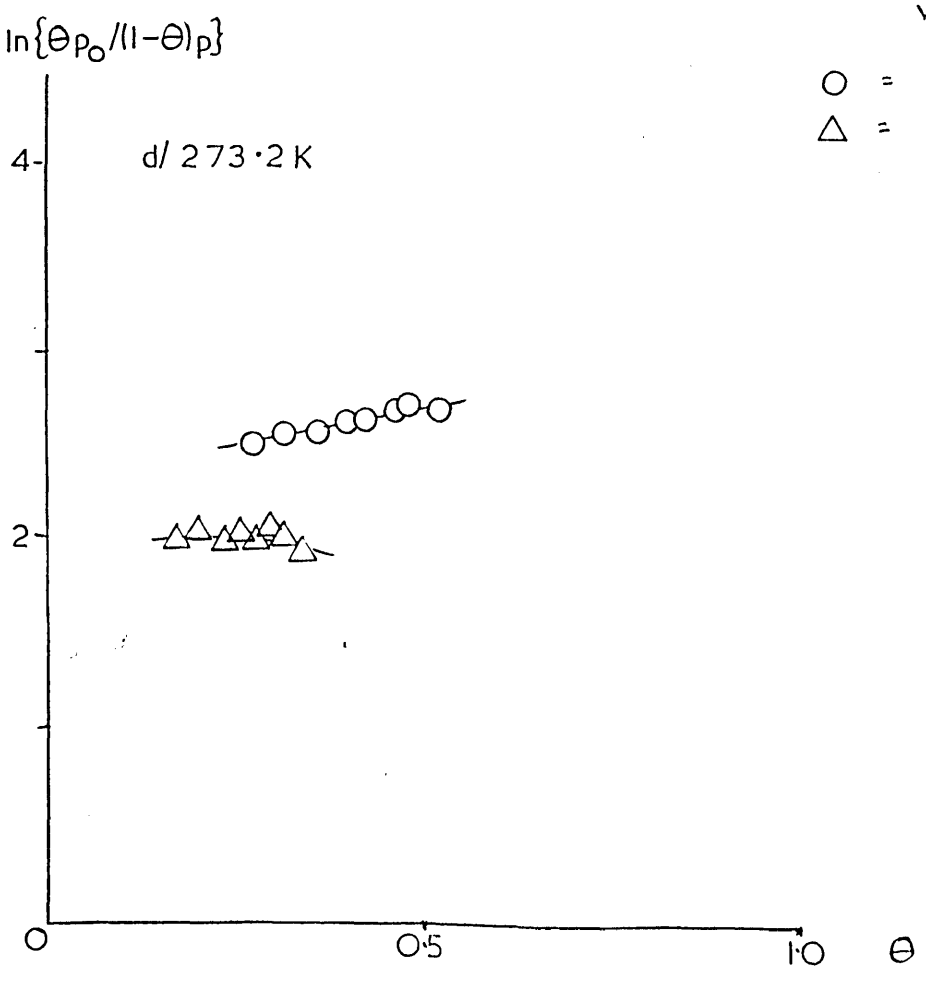
H_2S Graphon



$v_M/cm^3 g^{-1}$

○ = 12·3

△ = 19·2



experimental result is not conclusive evidence as to the reality of the model used, since an entirely different model may also give similar results".

Fig. 5.1.14 and fig. 5.1.15 show the graphs obtained when Beebe's localised monolayer equation was applied to the H_2S isotherms (fig. 4.1.11). For this system no conclusive results were obtained, the molecular areas used are listed in table 5.1.7.

Table 5.1.7b

Molecular areas of H_2S on Graphon and the associated monolayer capacities

$a_m/\text{Å}^2$	v_m/cm^3STPg^{-1}	Source
23.6	12.6	this study for H_2S on Carbolac
19.6	15.2	arbitrary
15.5	19.2	Harris and Emmett 1949

At 195K the best straight line occurs when a molecular area of 19.6 Å^2 is used, at 213.2K the best straight line corresponds to 23.6 Å^2, and at 243.2K and 273.2K no straight line can be obtained for any molecular area. In the absence of convincing conformity of the H_2S/Graphon isotherms to the localised monolayer model, they were fitted to an equation for polymolecular non-localised adsorption, (Beebe et al, 1964) also with no success. This model was used by Beebe et al for analysis of SF_6 isotherms on Stirling MT, however neither the SF_6/Graphon isotherm or the H_2S/Graphon isotherms determined in this study fitted the equation used.

$$\frac{z}{1-z} + \ell n \frac{z}{1-z} - \ell n \frac{p/p_o}{1-p/p_o} = \ell n K_1 + K_2 z$$

where $z = \theta(1 - p/p_o)$, $K_2 = 2a_2/b_2kT$ and a_2 and b_2 are constants from the Van der Waals equation of state for a monolayer.

This suggests that real systems are more complicated than allowed for by any of the models used.

5.1.4 Isosteric heats of adsorption

The isosteric heats of adsorption q_{ST} were calculated for each set of isotherms by plotting (fig. 5.1.22) ℓnp versus $1/T$ for various values of coverage (θ) and measuring the gradient.

Using the Clausius-Clapeyron type equation (section 2.7)

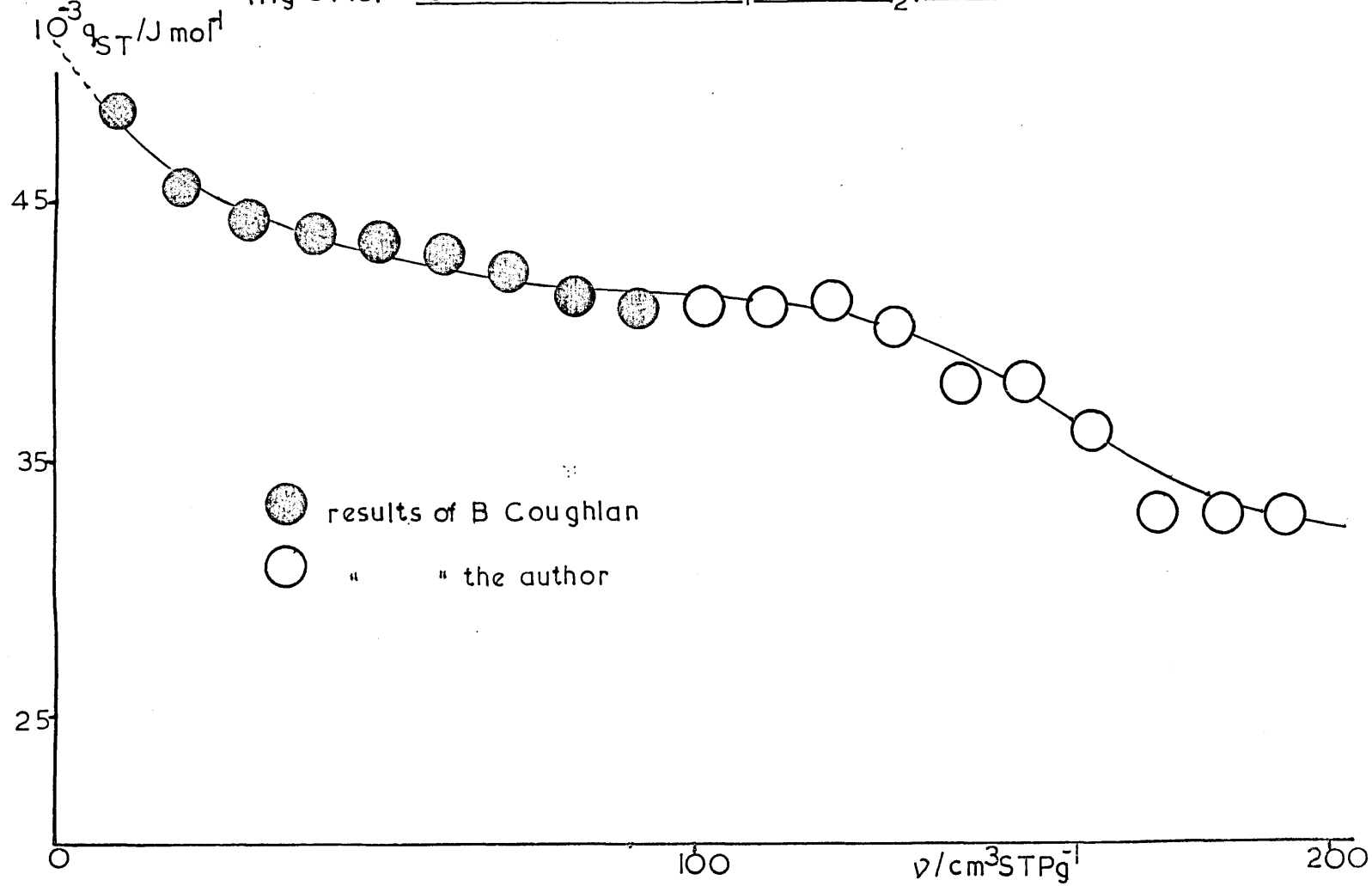
$$\left(\frac{\partial \ell np}{\partial T}\right)_\theta = \frac{q_{ST}}{RT^2}$$

graphs of q_{ST} versus coverage were obtained. This method was not possible where the isotherms were very rectangular, (e.g for NaX) and the two-temperature version of the equation was used.

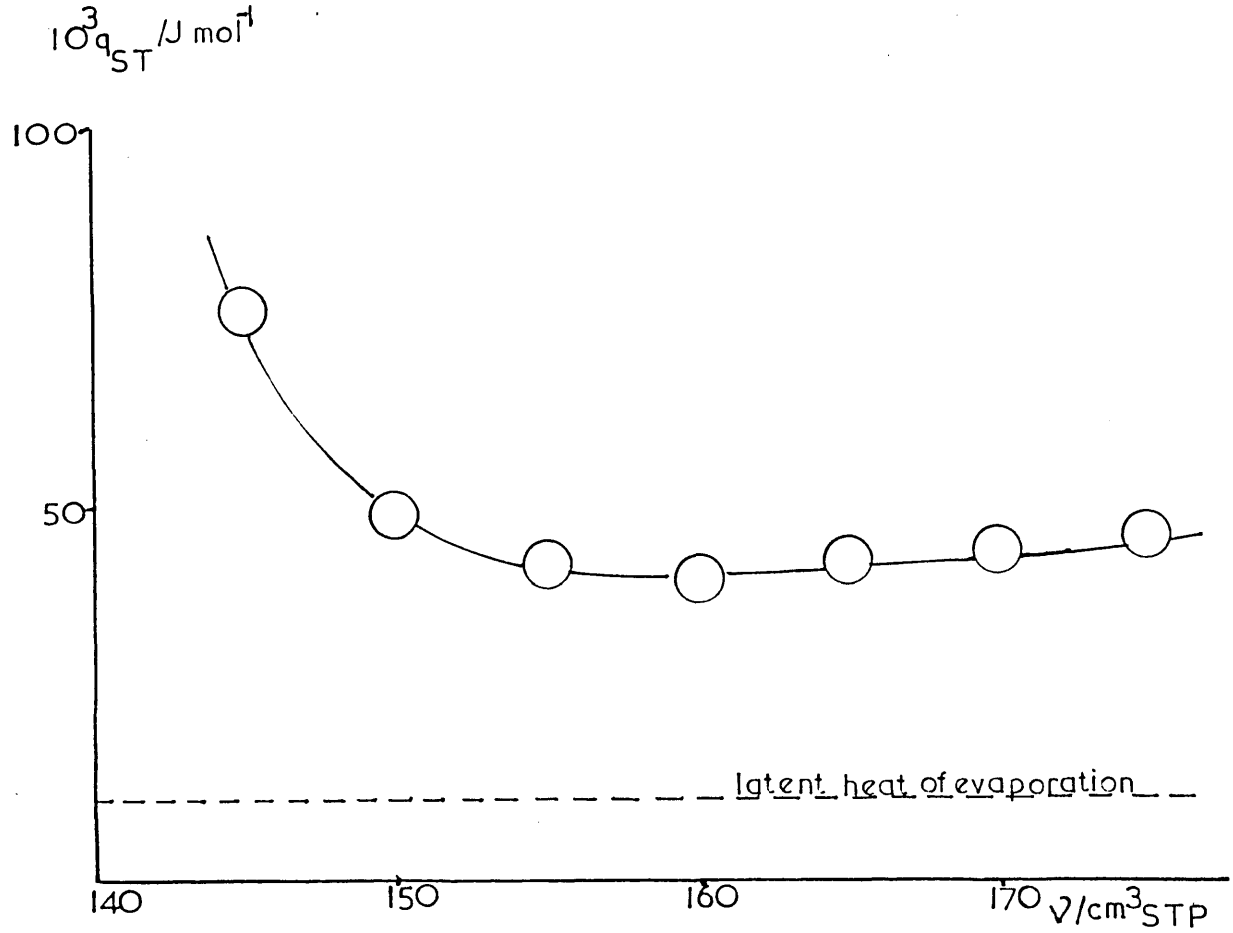
$$q_{ST} = \frac{(-)RT_1T_2}{T_1-T_2} (\ell np_2 - \ell np_1)_\theta$$

where p_1 and p_2 are the pressures at which coverage θ is obtained for isotherms at temperatures T_1 and T_2. The isosteric heat for CO_2 adsorption on NaX agrees well with the values obtained by Coughlan (1964) as shown in fig. 5.1.16.

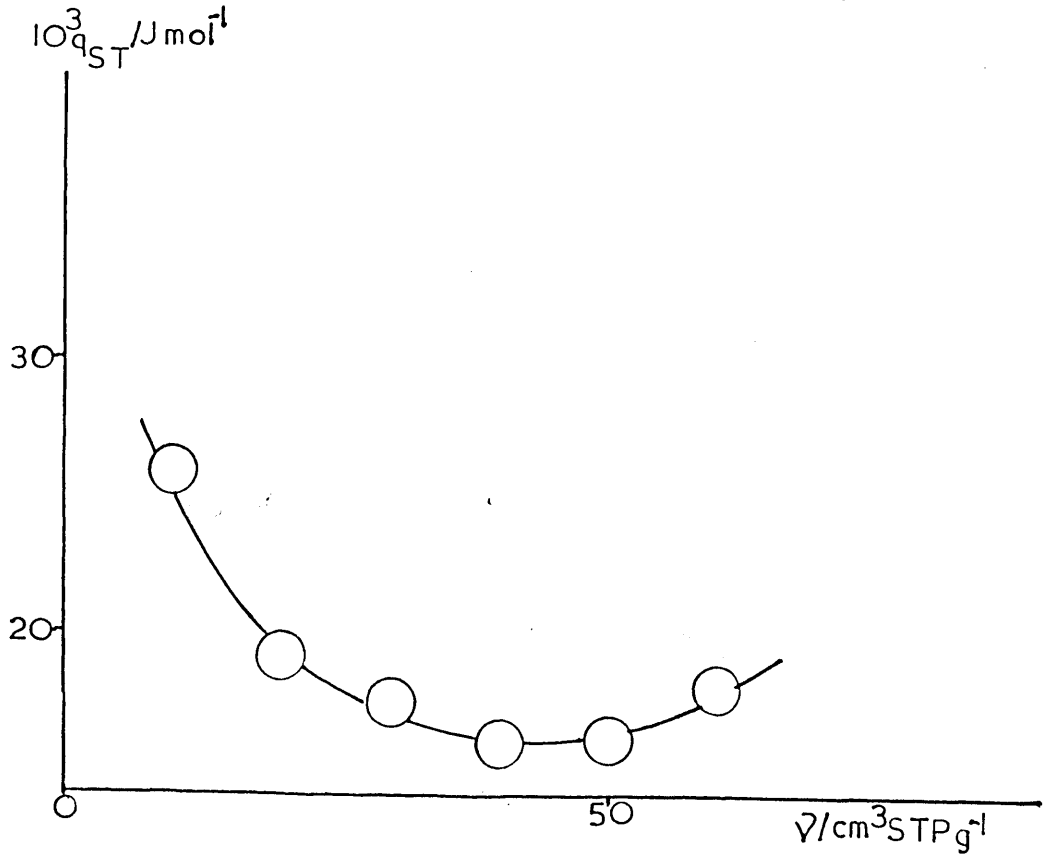
(fig 5·1·16) Isosteric heat of adsorption CO_2 /NaX

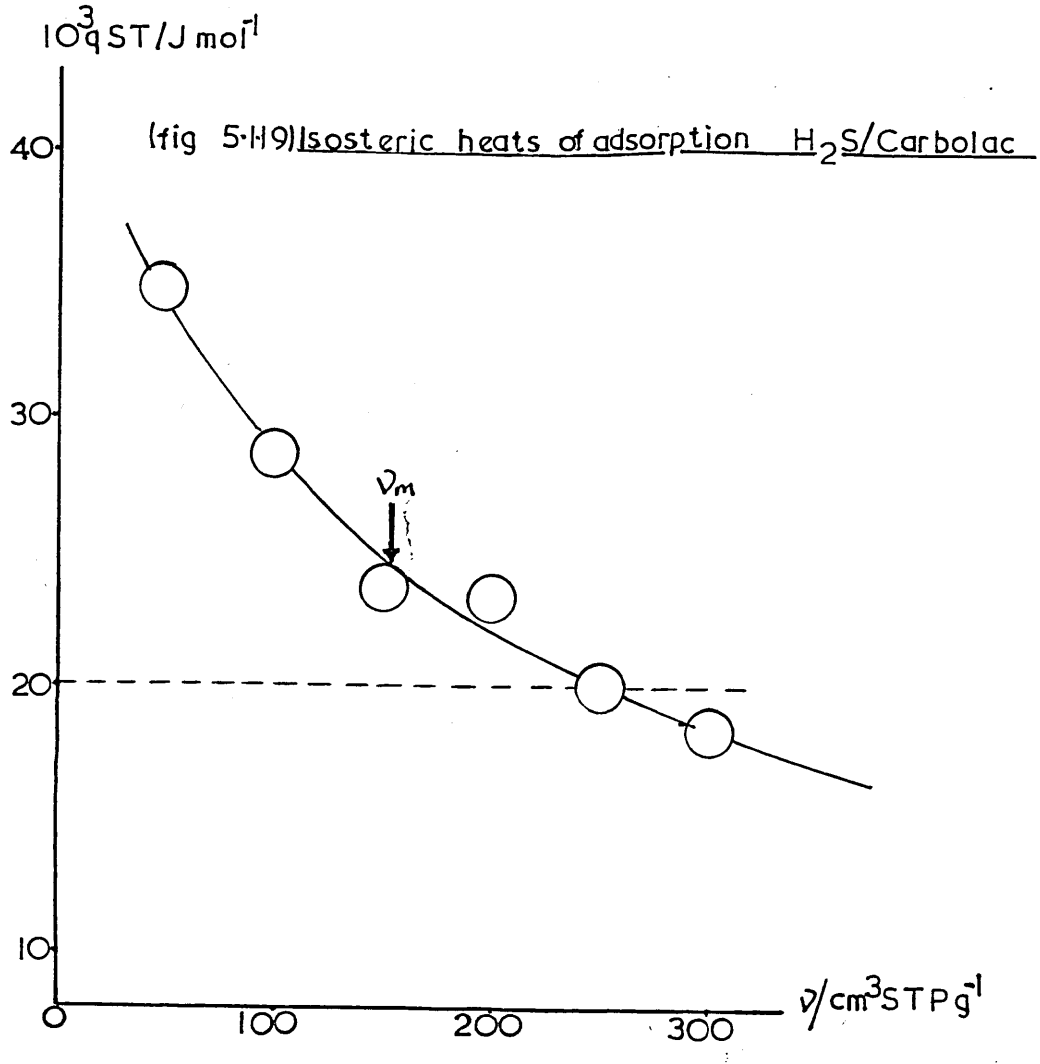


(fig 5·1·17) Isosteric heats of adsorption H_2S/NaX

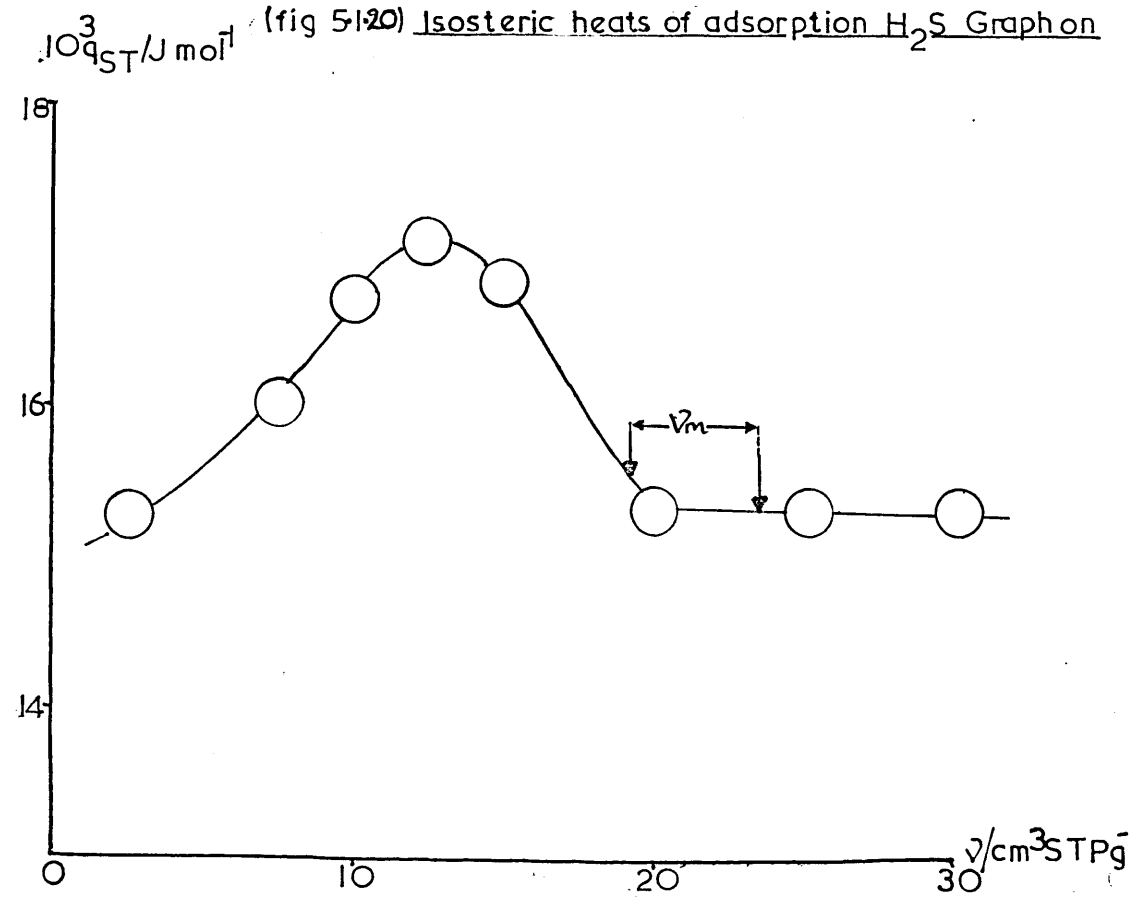


(fig 5·1·18) Isosteric heats of adsorption CO_2/CMS



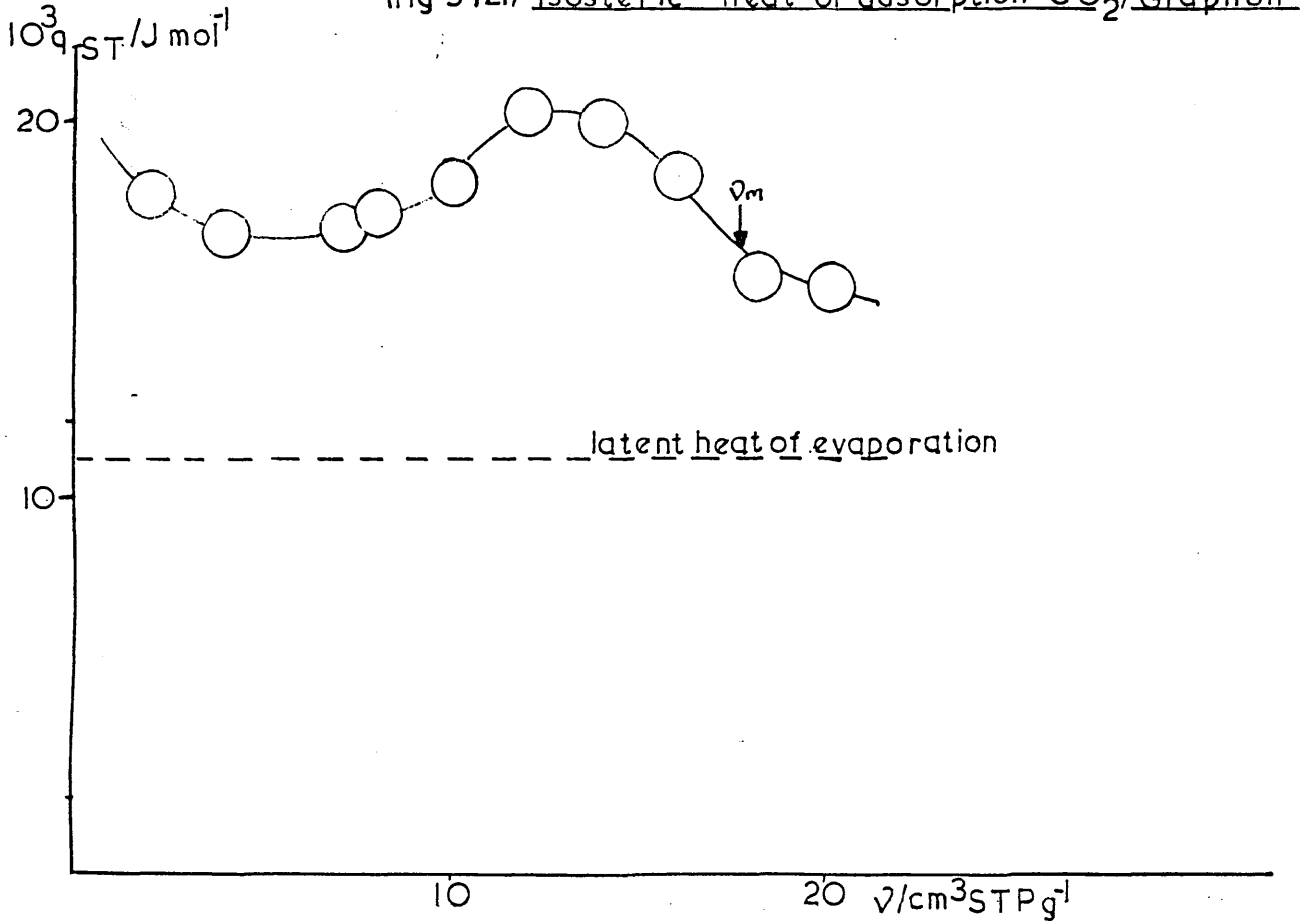


(fig 5·119) Isosteric heats of adsorption H_2S/Carbolac

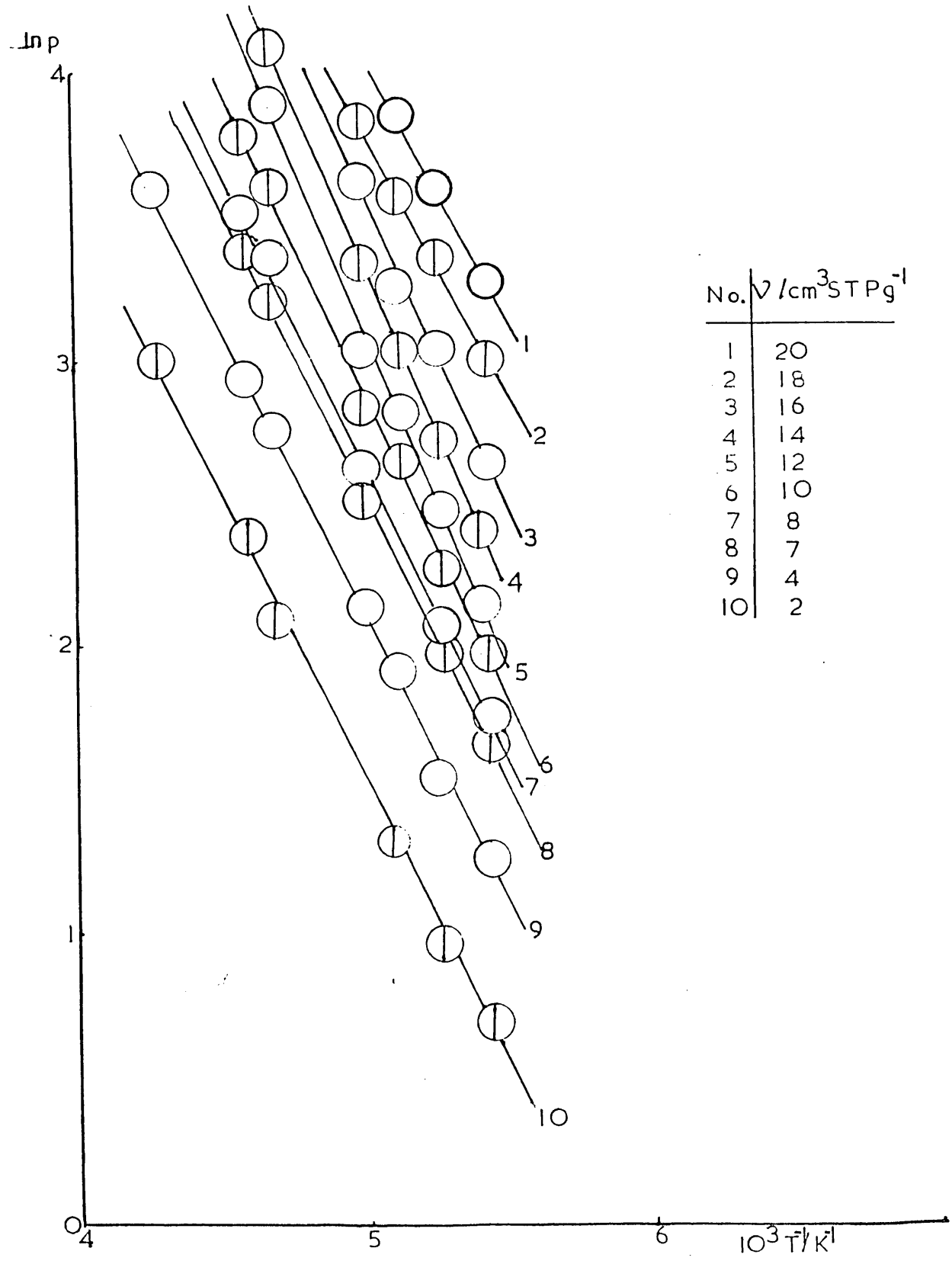


(fig 5·120) Isosteric heats of adsorption H_2S Graphon

(fig 5·1·21) Isosteric heat of adsorption CO_2/Graphon



(fig 5-1-22) ln(p) versus 1/T plots: CO_2 /Graph on



No.	V /cm^3 STP g^{-1}
1	20
2	18
3	16
4	14
5	12
6	10
7	8
8	7
9	4
10	2

This curve, and that for CO_2 on the carbon molecular sieve fig. 5.1.18 (which shows a minimum) are both well above the latent heat for CO_2 (11.4 $kJmol^{-1}$). Fig. 5.1.17 shows the isosteric heat of adsorption for H_2S on NaX; this also exhibits a minimum and is above the latent heat of H_2S (19.9 $kJmol^{-1}$). The Langmuir model assumes a constant isosteric heat of adsorption below monolayer capacity and examination of fig. 5.1.16, fig. 5.1.17 and fig. 5.1.18 shows that in this case the assumption is not valid. Fig. 5.1.19 shows the isosteric heat of adsorption of H_2S on Carbolac, it follows the same trends as that for CO_2 on Carbolac (Sharma 1970), decreasing with increasing coverage towards the latent heat of evaporation of H_2S (shown as ------). The monolayer capacity is marked $\nu_m\downarrow$(154 cm^3STPg) and it is interesting to note that the value of q_{ST} (24.3 $kJmol^{-1}$) at $\nu_m = 1$ is only slightly below the values obtained from the "c" value of the BET equation (q = 25.9 $kJmol^{-1}$ @ 213.2K, q = 26.7 $kJmol^{-1}$ @ 243.2 $kJmol^{-1}$). This was not the case for the q value obtained from the BET plot of Sharma's CO_2 results which was substantially below his curve of q_{ST} versus θ.

The graphs showing the isosteric heat of adsorption for H_2S and CO_2 on Graphon (fig. 5.1.19, fig. 5.1.20) both show a maximum below monolayer coverage. The maxima correspond to 'humps' in the isotherms and are therefore caused by the lateral interactions between adsorbed molecules. The form of these graphs is characteristic of a carbon surface made homogeneous by graphitisation and has been observed by Hamilton (1980) and Beebe et al (1953). While the

isosteric heat of adsorption for CO_2 decreases towards the latent heat of vapourization of CO_2, the isosteric heat for H_2S adsorption is below the latent heat of vapourization of H_2S for all values of coverage. This behaviour has been observed for water adsorption on a block copolymer (Jellinek et. al. 1979) and for Benzene adsorption on silica, the surface of which has been covered with $Si(Me)_3$ groups (Kiselev 1961). Both these systems give type III isotherms, Jellinek explains the low heat of adsorption by the existence of very few 'non energetic adsorption sites'.

5.2 Discussion Of Flow Results On Molecular Sieve Membranes NaX1, NaX2 and CMS

5.2.1 Introduction

Fig. 4.2.1, fig. 4.2.2, fig. 4.2.3 and fig. 4.2.11, show examples of outgoing pressure versus time graphs for gas flow through the zeolite and carbon molecular sieve membranes. By comparison with the appropriate adsorption isotherms it can be seen that the overall time-lag and break-through-time for a gas increase with its adsorbability upon the membrane and decrease with increasing p_1. It is also evident that the more rectangular isotherms (e.g. CO_2 adsorption on NaX at 195K fig. 4.1.1) lead to a sharper 'break-through' after which the steady state is quickly obtained (that is, the time-lag equals the breakthrough-time; e.g. fig. 4.2.2); while the less rectangular isotherms (e.g. CO_2 adsorption on NaX at 273.2K) lead to a more gentle 'break-through' and an ensuing curved section of the p_2 versus t graph before the steady state is reached (e.g. fig. 4.2.3).

The steady state integral permeability showed a linear relationship with pressure, at moderate pressures for all systems studied (fig. 4.2.4 to fig. 4.2.16) in accordance with the Carman-Arnell equation (section 2.3 equation (19)).

$$\tilde{K} = \frac{\varepsilon^3 \bar{p}}{kA^2\eta} + \frac{4\delta\varepsilon^2}{3k'A}\sqrt{\frac{8RT}{\pi M}}$$

$\bar{p}$ = mean pressure i.e. $p_1/2$, η = viscosity of the gas, A = surface area/m^2 (m^{-3} porous medium), ε = porosity of the medium, k = Kozeny constant and δ and k' are coefficients about which there has been much discussion (Carman 1950). This equation has two terms, one representing Kundsen flow and the other Poiseuille flow, and it may be written as

$$\tilde{K} = \tilde{K}_p \bar{p} + \delta\tilde{K}_K \quad \text{(Section 2.3 equation 19a)}$$

where $\tilde{K}_p$ and $\tilde{K}_K$ are termed the Poiseuille and Knudsen permeabilities respectively and δ is a constant. At pressures where this equation was obeyed the corresponding flux versus pressure graphs were curved convex to the pressure axis for all gases as expected for increasing $\tilde{K}$.

5.2.2 Low pressure behaviour of the Integral Permeability

At low pressures a wide variety of behaviour was observed in the pressure dependence of the integral permeability which is summarised in table 5.2.1.

Table 5.2.1

Low pressure behaviour of $\tilde{K}$ versus p_1

Membrane	gas	T/K	$\tilde{K}$ vs p_1 form at low p_1
NaX1	He	195	flattening
NaX1	He	273.2	linear
NaX1	CO_2	195	linear
NaX1	CO_2	273.2	linear
NaX2	He	195	flattening
NaX2	He	273.2	linear
NaX2	N_2	195	linear
NaX2	N_2	273.2	linear
NaX2	H_2S	195	linear
NaX2	CO_2	195	linear
CMS	He	195	linear
CMS	He	273.2	minimum
CMS	N_2	195	minimum
CMS	N_2	273.2	minimum
CMS	H_2S	195	linear
CMS	H_2S	273.2	linear
CMS	CO_2	195	decrease
CMS	CO_2	273.2	decrease

From table 5.2.1 it can be seen that for the NaX membranes the integral permeability versus pressure graphs were linear throughout the whole range studied with the exception of Helium flow at 195K, which showed a flattening of the curve at low pressures. The carbon molecular sieve membrane produced a wide variety of behaviour in the low pressure region of the $\tilde{K}$ versus p_1 curve, including minima for gases with relatively long mean free paths (He at 273.2K and N_2), linearity (He at 195K, and H_2S) and sharp downward curvature (CO_2). These types of behaviour have all been observed previously, however they have not all been detected on a single membrane, as in this study (CMS).

Knudsen (1909) predicted a minimum permeability at low pressures for gas flow through a capillary, and verified this with experiments using H_2, O_2 and CO_2. This behaviour was also reported by Gaede (1913) for gas flow through rectangular slits. Pollard and Present(1948) attributed the minimum to the lessening of molecule/molecule collisions along the direction of flow as λ increased, but predicted that it would not occur in porous media. Subsequently graphs which flattened or passed through a minimum were observed by Grove and Ford (1958), Barrer and Grove (1951), Ash and Grove (1960) and Ash, Barrer and Coughan (1972), for gas flow through different porous media contrary to Pollard and Present's predictions. Weber (1950) developed a 3 term equation for $\tilde{K}$ which took into account these low pressure deviations from linearity (however for simplicity only the 2 term equation has been used in this study). In this and previous investigations permeability minima were usually observed only for gases with long path lengths (e.g. He) and it has been

suggested (Ash, Barrer and Coughlan) that a flattening would be observed for all gases, if low enough pressures were used.

This seems unlikely in cases (e.g. the CO_2/CMS system) in which a downward trend in the permeability is evident at low pressures. This type of behaviour has also been observed for gas flow through porous pyrex disks (Hirsch 1961) and through Sitka spruce (Petty 1970).

Barrer and Nicholson (1965) predicted a decrease in permeability at low pressures, similar to that observed by Hirsch and Petty, when they calculated the permeability of pairs of long capillaries with unequal radii. This work was extended to include cases in which extra flow occurred by Nicholson and Petropoulos (1968).

5.2.3 Knudsen and Poiseuille permeabilities

The Poiseuille permeability $\tilde{K}_p$, given by the slope of the linear portion of the graph of $\tilde{K}$ against p, should be inversely proportional to the viscosity of the gas if the Carman-Arnell equation is obeyed. Viscosity values have been taken from Weast (1970) and are listed in table 5.2.4. The permeability constant $\tilde{K}_1 = \tilde{K}_p \eta$ should then be independent of the gas and a property only of the membrane.

Table 5.2.3 shows K_p' and K_1' for the zeolite and carbon molecular sieve membranes (where $\tilde{K}_p' = \tilde{K}_p/2$ and $\tilde{K}_1' = \tilde{K}_p' \eta = \tilde{K}_1/2$ because the permeability has been plotted against p_1 and under the boundary conditions used $\bar{p} \simeq p_1/2$ as $p_1 >> p_2$). Barrer and Grove (1950) and Ash and Grove (1960) have reported values of $\tilde{K}_1$ which are sensibly constant at 298.2K for gas flow through a porous ceramic

Table 5.2.3a

Poiseuille Permeability constants $\tilde{K}_1'$

Gas	T/K	$\eta/10^{-6}$ poise	$10^7\tilde{K}_p'/m^3skg^{-1}$	$10^{15}\tilde{K}_1'/m^2$
	NaX Membrane 1			
He	273.2	187	3.70	6.91
He	195	153	3.75	5.74
CO_2	273.2	139	3.98	5.53
CO_2	195	97.2	7.13	6.92
	Results of Mr. R. Ash NaX Membrane 1			
He	90	80.5	8.18	6.58
N_2	90	41	10.39	4.26
N_2	195	126	4.73	5.95
	NaX Membrane 2			
He	273.2	187	1.28	2.38
He	195	153	1.75	2.67
N_2	273.2	165	1.80	2.97
N_2	195	126	2.48	3.12
CO_2	195	97.2	2.85	2.77
H_2S	195	60.0	3.08	1.85
	CMS Membrane			
He	273.2	187	2.55	4.77
He	195	153	3.32	5.08
N_2	273.2	165	3.26	5.38
N_2	195	126	4.73	5.95
CO_2	273.2	139	4.01	5.58
CO_2	195	97.2	5.29	5.14
H_2S	273.2	116	6.99	8.16
H_2S	195	60.0	11.52	6.91
He	273.2	187	4.65	8.76
He	195	153	6.30	9.64

and a bed of analcite crystals. In both cases the value obtained for He flow was raised and Barrer and Grove also reported a raised value for the flow of NH_3 which was strongly sorbed. The analysis of data obtained in this study has been made more complicated by physical changes in the membranes used, caused by the flow of H_2S. Zeolite membrane 1 shows $\tilde{K}_1'$ values between $5.53 \times 10^{-15} m^2$ and $6.92 \times 10^{-15} m^2$, the highest of which are obtained for He at 273.2K (as in previous studies) and for CO_2 at 195K. These values are similar to those obtained by Mr. R. Ash (also quoted in table 5.2.3) using the same membrane.

Zeolite membrane 2 did not produce a raised value of $\tilde{K}_1'$ for He; however the value for N_2 at 195K is higher than expected. This could be due to 'extra flow' caused by a limited amount of inter-crystalline transport, as the isotherm at this temperature is curved, producing a concentration gradient in the adsorbed phase. The value of $\tilde{K}_1'$ for H_2S may not be compared with that for the other gases studied, because of a change in the membrane structure.

The CMS membrane produced almost constant values of $\tilde{K}_1'$ until H_2S flow altered its structure, when $\tilde{K}_1'$ increased. Following this, the lower $\tilde{K}_1'$ value obtained at 195K for H_2S may shed doubt upon the viscosity value used; however no alternative value could be found in the literature.

The Knudsen permeabilities $\tilde{K}_K'$ and $\tilde{K}_K$ are the values of $\tilde{K}$ at $p_1 = 0$, $\tilde{K}_K'$ being the value obtained by extrapolating the linear portion of the $\tilde{K}$ versus p_1 graph and $\tilde{K}_K$ the value which takes

Table 5.2.3b

Knudsen Permeabilities $\tilde{K}_K$ and $\tilde{K}'_K$

Gas	T/K	$10^5\tilde{K}_K/m^2s^{-1}$	$10^5\tilde{K}'_K/m^2s^{-1}$	$10^7\tilde{K}_2/m^2s^{-1}$ $(kgmol^{-1}K^{-1})^{\frac{1}{2}}$	$10^7\tilde{K}'_2/m^2s^{-1}$ $(kgmol^{-1}K^{-1})^{\frac{1}{2}}$
	NaX Membrane 1				
He	273.2	13.57	13.26	5.19	5.06
He	195	-	11.24	-	5.09
CO_2	273.2	-	4.70	-	5.98
CO_2	195	-	3.31	-	4.96
	Results of Mr. R. Ash. NaX Membrane 1				
He	90	-	7.16	-	4.78
N_2	90	-	2.89	-	5.10
N_2	195	-	4.53	-	5.42
	NaX Membrane 2				
He	273.2	7.31	7.11	2.80	2.72
He	195	-	6.14	-	2.78
N_2	273.2	-	2.88	-	2.92
N_2	195	-	2.56	-	3.07
CO_2	195	-	1.96	-	2.94
H_2S	195	-	2.36	-	3.11
	CMS Membrane				
He	273.2	-	8.47	-	3.23
He	195	-	7.14	-	3.23
N_2	273.2	3.74	3.29	3.79	3.32
N_2	195	3.03	2.56	3.64	3.07
CO_2	273.2	-	2.63	-	3.35
CO_2	195	-	2.15	-	3.23
H_2S	273.2	-	3.50	-	3.89
H_2S	195	-	2.85	-	3.76
He	273.2	-	10.16	-	3.88
He	195	-	8.67	-	3.92

into account low pressure deviation from linearity.

The permeability constants $\tilde{K}_2 = \tilde{K}_K \sqrt{M/T}$ and $\tilde{K}'_2 = \tilde{K}'_K \sqrt{M/T}$ are also shown in table 5.2.3. For NaX membrane 1, $\tilde{K}'_2$ is reasonably constant except for a slightly raised value for CO_2 flow at 273.2K. The $\tilde{K}'_2$ values obtained by Mr. R. Ash (also shown in table 5.2.3) are in fair agreement with the author's results. $\tilde{K}'_2$ results for NaX membrane 2 show an increase of approximately 10% over the whole range of gases. As noticed in previous studies, the $\tilde{K}'_2$ values were higher for more sorbable gases, indicating the presence of a possible 'extra-flow' component in the membrane.

The CMS membrane gave the most constant value of $\tilde{K}'_2$ for all gases used. This increased to a higher value after H_2S flow had been investigated due to changes in the membrane. Accurate $\tilde{K}_2$ values were only obtained for N_2 flow, for which they were greater than $\tilde{K}'_2$.

5.2.4 $\tilde{K}\sqrt{M/T}$ versus $1/\bar{\lambda}$ plots

The correlation between different gases flowing through the same membrane was investigated in greater detail using a universal plot. Observations of low pressure deviations in permeability by Huggill (1952) caused Berman and Lund (1958) to devise such a plot, to examine such phenomena.

The Carman-Arnell equation was used in the form

$$\tilde{K}\sqrt{\frac{M}{T}} = \frac{\varepsilon^3}{kA^2}\, 2\sqrt{R}\, \sqrt{\frac{\pi}{8}} \cdot \frac{1}{\bar{\lambda}} + \frac{4}{3}\,\frac{\delta}{k'}\,\frac{\varepsilon^2}{A}\,\sqrt{\frac{8R}{\pi}}$$

5.2.4

Table of Viscosities and $\bar{\lambda}_1$ values

Viscosity /10^{-6} poise

Gas	90K	195K	273.2K
He	80.5	153	187
N_2	41	126	165
CO_2	-	97.2	139
H_2S	-	60.0	116

$10^6\bar{\lambda}_1$/m

Gas	90K	195K	273.2K
He	3.28	9.17	13.2
N_2	0.631	2.85	4.42
CO_2	-	1.75	2.97
H_2S	-	1.23	2.83

(where $\bar{\lambda}$ = mean free path length) and $\tilde{K}\sqrt{\frac{M}{T}}$ plotted against $\frac{1}{\lambda}$ for noble gas flow through porous media, capillary and orifice. Barrer and Nicholson (1965) also used this approach successfully in their investigation of slip flow in single capillaries.

$\bar{\lambda}$ is inversely proportional to viscosity (η) and in this study the value of $\bar{\lambda}$ at $\bar{p}$ = 1cmHg ($\bar{\lambda}_1$) (from which the $\bar{\lambda}$ values at other pressures could be calculated using the relationship $p\lambda$ = constant for a fixed temperature) was evaluated and listed in table 5.2.4.

The Chapman-Enskog formula was used:

$\eta = 0.499\ \rho\bar{c}\bar{\lambda}$ where density (ρ) = $\frac{p_1}{2}\frac{M}{RT}$

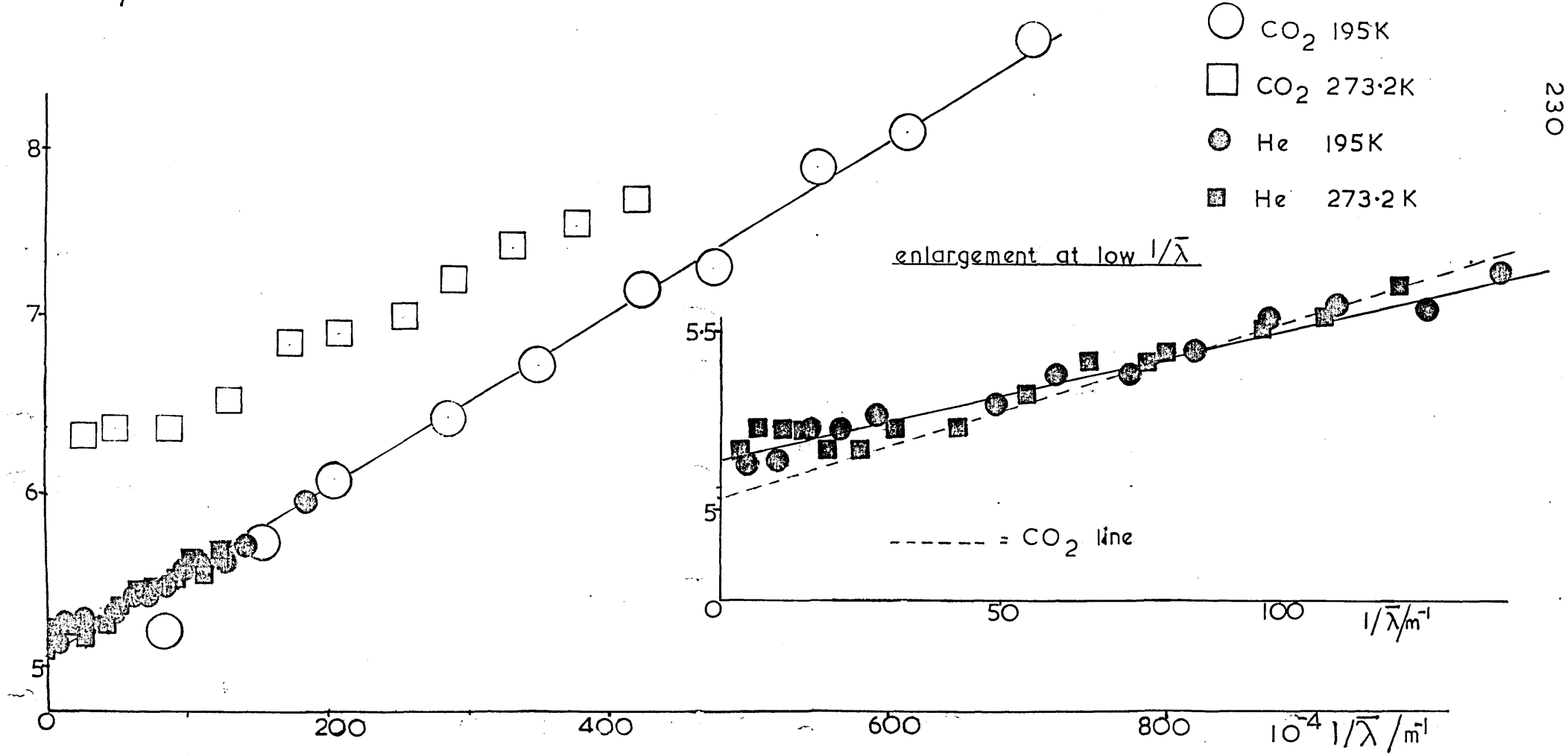
and mean speed $(\bar{c}) = \sqrt{\frac{8RT}{\pi M}}$

Fig. 5.2.1 to 5.2.4b show the $\tilde{K}\sqrt{\frac{M}{T}}$ versus $1/\bar{\lambda}$ graphs obtained in this study.

For NaX membrane 1 the CO_2 results at 195K and He results (Fig. 5.2.1) fell on the same line, although enlargement of the low $1/\bar{\lambda}$ portion showed up a slight divergence of the He results at 195K. The CO_2 graph at 273.2K gave a different straight line with a lower gradient and higher intercept, which was also reflected in table 5.2.2 and table 5.2.3.

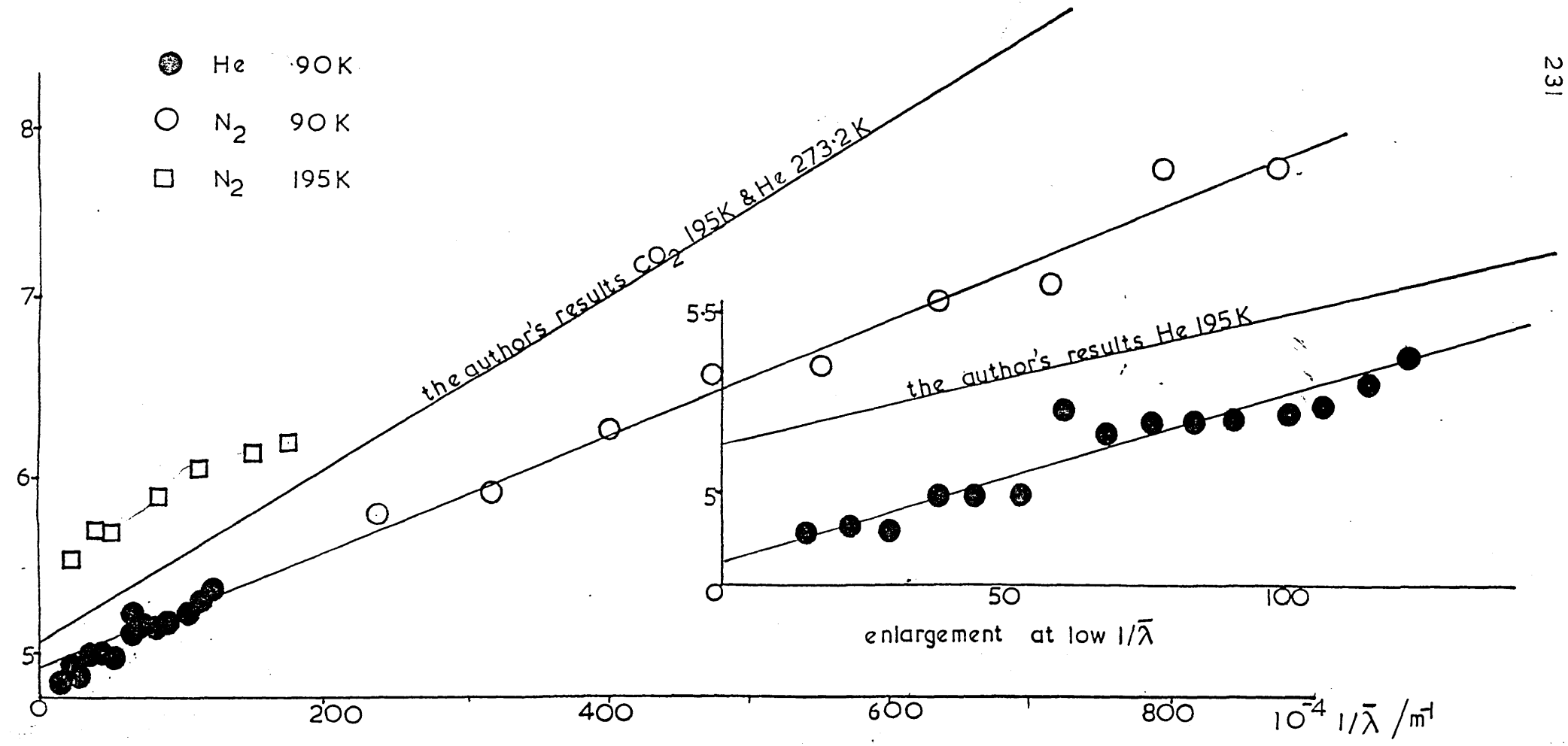
In Fig. 5.2.2 the results obtained by Mr. R. Ash are compared with those of the author. Although N_2 and He at 90K exhibit fairly consistent behaviour within themselves, they differ from N_2 results at 195K and from those obtained by the author for He and CO_2. For transport through NaX membrane 2 (Fig. 5.2.3a) there is little internal

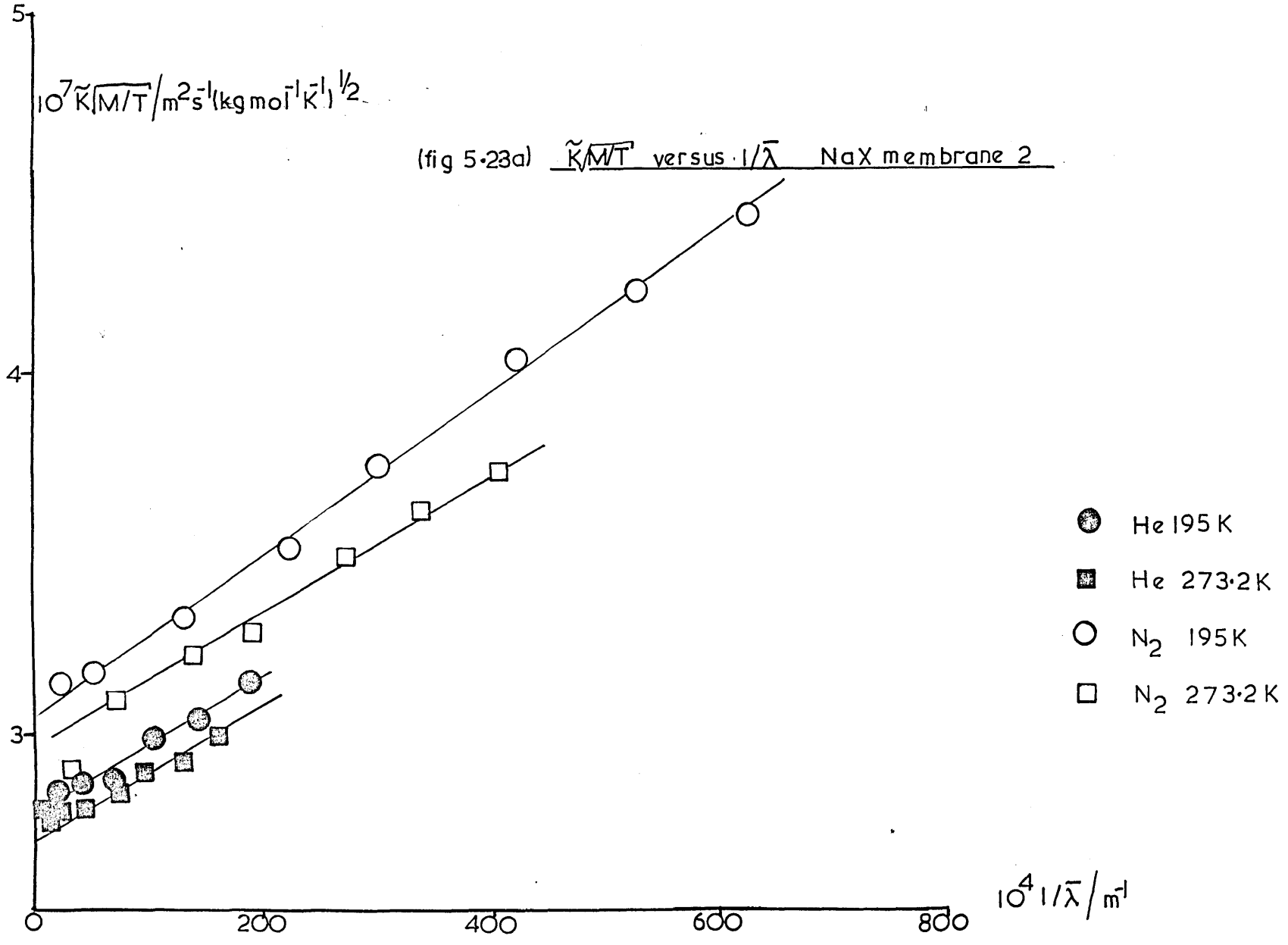
(fig 5·2· 1) $\tilde{K}\sqrt{M/T}$ versus $1/\bar{\lambda}$ NaX membrane 1



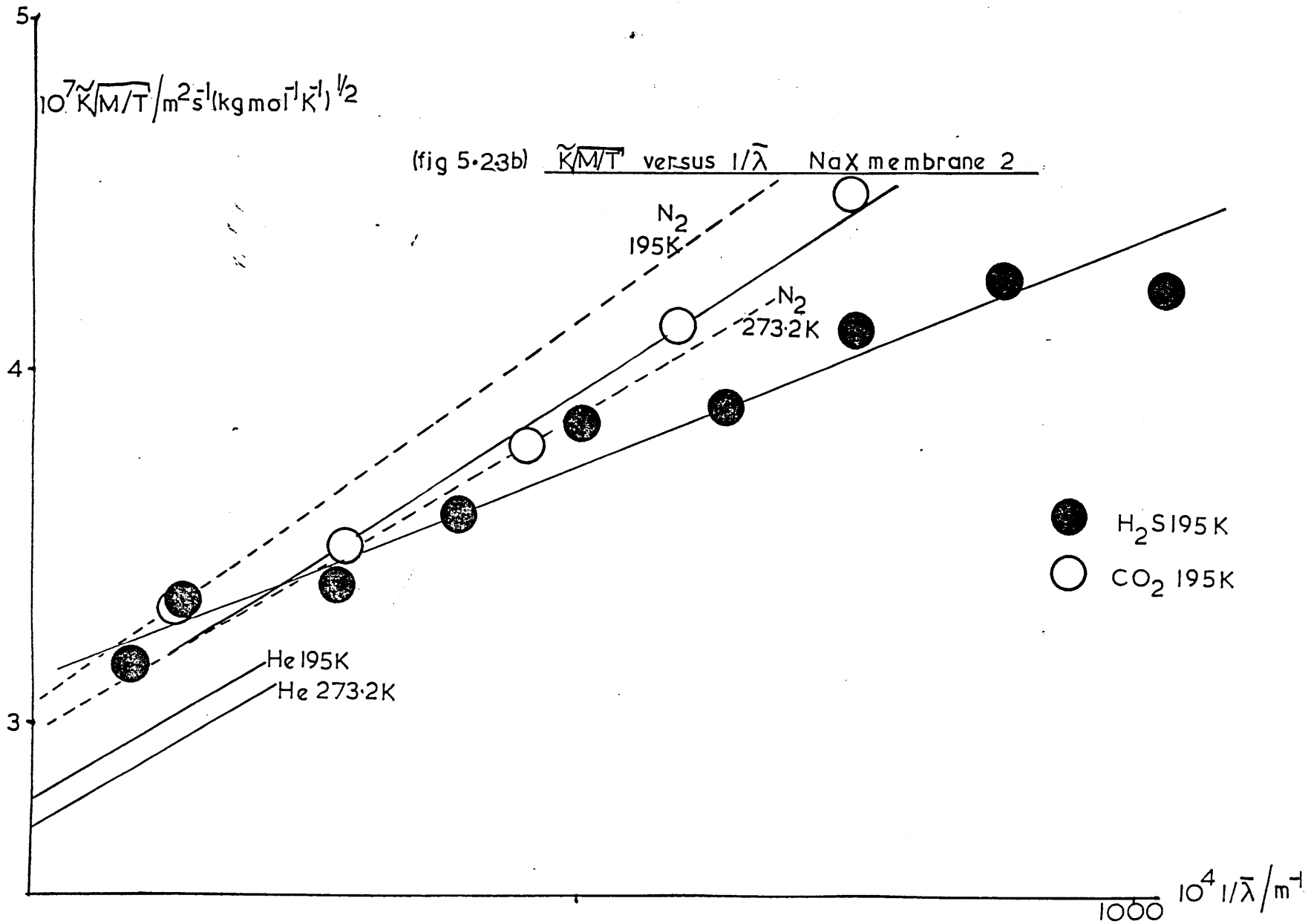
(fig 5·2·2) $\tilde{K}\sqrt{M/T}$ versus $1/\bar{\lambda}$ Na X membrane I

results of Mr R Ash compared with those of the author

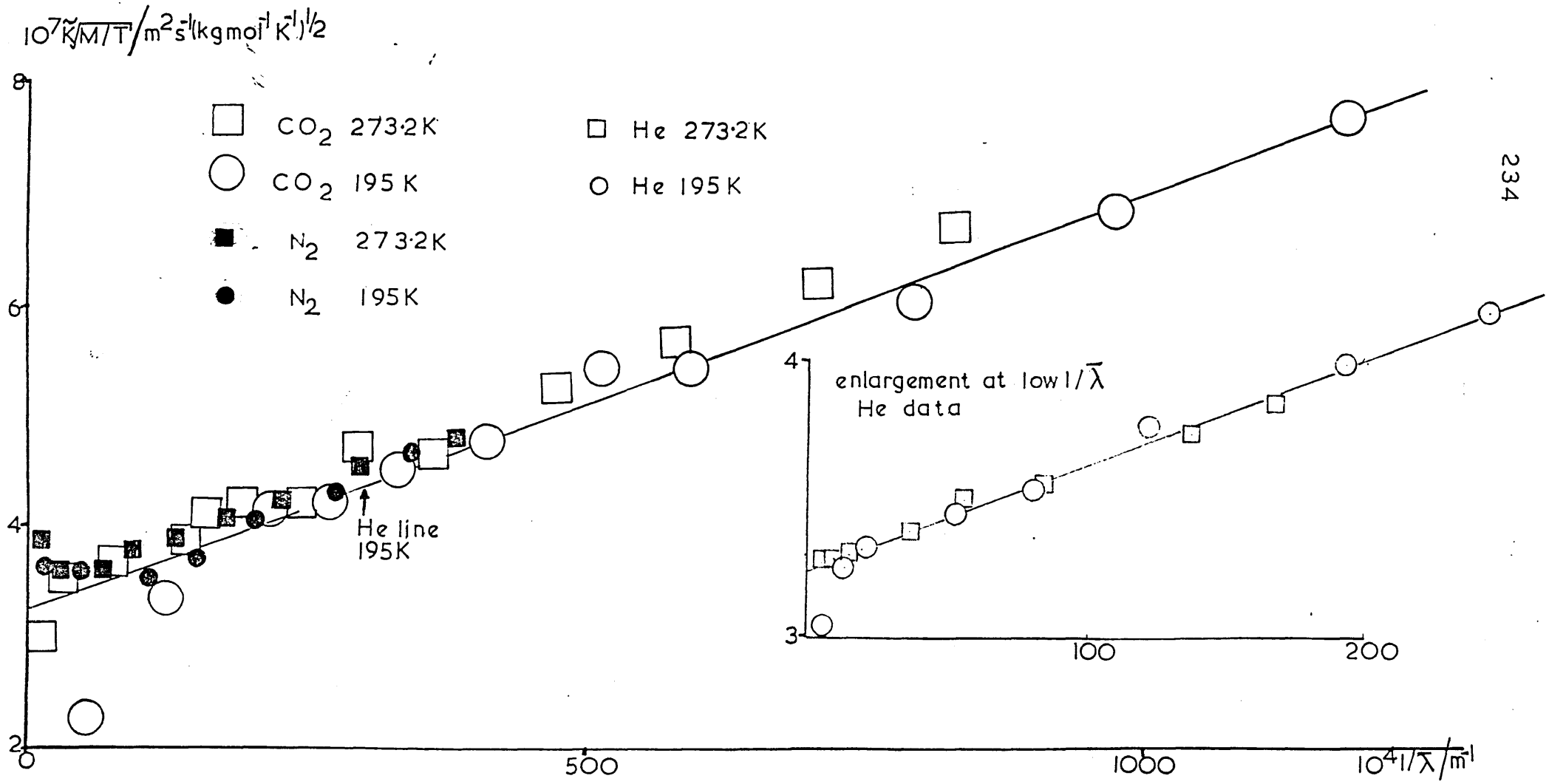


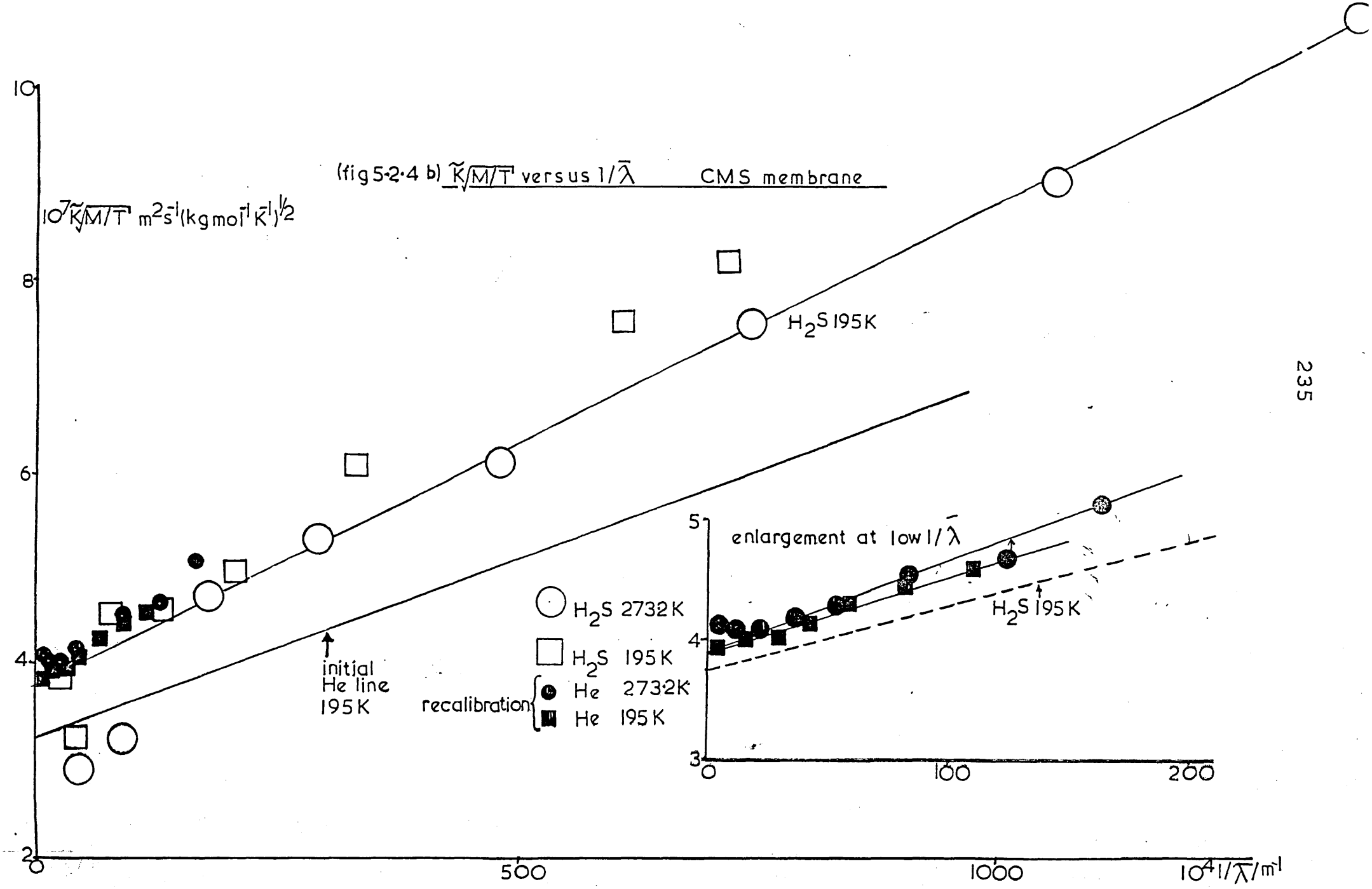


(fig 5·23a) $\tilde{K}\sqrt{M/T}$ versus $1/\bar{\lambda}$ NaX membrane 2


5
4
3
$10^7 \tilde{K}\sqrt{M/T} / m^2 s^{-1} (kg\,mol^{-1} K^{-1})^{1/2}$
(fig 5·23b) $\tilde{K}\sqrt{M/T}$ versus $1/\tilde{\lambda}$ NaX membrane 2
N_2 195K
N_2 273·2K
He 195K
He 273·2K
H_2S 195K
CO_2 195K
1000
$10^4\, 1/\tilde{\lambda} / m^{-1}$

(fig 5·2·4 a) $\tilde{K}\sqrt{M/T}$ versus $1/\bar{\lambda}$ CMS membrane




(fig 5-2-4 b) $\tilde{K}\sqrt{M/T}$ versus $1/\bar{\lambda}$ CMS membrane
$10^7 \tilde{K}\sqrt{M/T}$ $m^2 s^{-1} (kg\,mol^{-1} K^{-1})^{1/2}$
10
8
6
4
2
0
500
1000
$10^4 1/\bar{\lambda}/m^{-1}$
H_2S 195K
H_2S 273.2K
H_2S 195K
He 273.2K
He 195K
recalibration
initial He line 195K
enlargement at low $1/\bar{\lambda}$
5
4
3
0
100
200
H_2S 195K

correlation. While N_2 and He give straight lines of similar gradient, the N_2 plot falls above that for He. For both gases the plots for 195K are above the corresponding graphs for 273.2K.

The $\tilde{K}\sqrt{M/T}$ versus $1/\bar{\lambda}$ plots for CO_2 and H_2S results at 195K on NaX membrane 2 Fig. 5.2.3b do not coincide with any of the N_2 or He results and cannot be compared with them, as a change in the membrane structure may have occurred on exposure to H_2S.

The CMS results for CO_2, He and N_2 (Fig. 5.2.4a) fall on a common line with very little deviation similar to that obtained by Berman and Lund. Fig. 5.2.4b show the results obtained after exposure of the membrane to H_2S. These experimental points show slightly more scatter but fall on a definite line of greater gradient and intercept than that in Fig. 5.2.4a. This shows that a definite change in the membrane structure had occurred, as is evident from table 5.2.2 and table 5.2.3.

5.2.5 Break through time procedure

In 1954 an equation relating the break through time to the amount of gas adsorbed was derived by Professor R.M. Barrer for cases where the steady state and time-lag diffusion coefficients were equal. In 1963 he commented that a further limitation arose where the isotherms were not sufficiently rectangular.

The relationship is as follows: (derived in Section 2.5.1)

$$2J_{\infty} \times BTT = \ell Ac'_s . Ac$$

where J_{∞} = flux /mol s^{-1}

BTT = breakthrough time /s

ℓ = length of membrane /m

Table 5.2.5 BREAKTHROUGH TIME PROCEDURE

a. CO_2 flow NaX membrane 1

195K, Ag = $934 m^2 g^{-1}$, $A_m = 16.3 Å^2$ 273.2K, Ag = $705 m^2 g^{-1}$, $A_m = 16.3 Å^2$

$\frac{Ac\ell}{2}\ Ac'_S = 1.20 \times 10^{-3}$mol $\frac{Ac\ell}{2}\ Ac'_S = 9.00 \times 10^{-3}$mol

p/cmHg	$J_\infty 10^3$ x BTT/mol	p/cmHg	$10^4 J_\infty$ x BTT/mol
2.99	1.15	1.58	2.64
5.41	1.19	2.90	3.70
7.36	1.29	5.17	4.50
10.02	1.30	7.61	5.29
12.26	1.30	10.19	6.10
14.75	1.22	12.30	6.29
16.66	1.33	14.96	6.94
19.27	1.35	17.17	6.94
21.47	1.33	19.51	7.32
24.70	1.36	22.34	6.94
		24.89	7.03

b. CO_2 flow NaX membrane 2

195K Ag = $934 m^2 g^{-1}$, $A_m = 16.3 Å^2$

$\frac{Ac\ell}{2}\ Ac'_S = 5.40 \times 10^{-4}$mol

p/cmHg	$10^4 J_\infty$ x BTT/mol
4.38	4.30
9.75	4.47
15.47	4.42
20.28	4.42
25.55	4.32

5.2.5 BREAKTHROUGH TIME PROCEDURE continued

c. N_2/NaX membrane 2

195K Ag = $304 m^2 g^{-1}$, $A_m = 16.2 Å^2$	
$\frac{Acl}{2} Ac'_s = 1.77 \times 10^{-4}$ mol	
p/cmHg	$10^4 J_\infty$ xBTT/mol
1.54	$.13_7$
3.03	$.23_4$
7.81	$.51_6$
17.10	$.83_4$
23.84	1.03
30.14	1.06
35.76	1.10

d. H_2S flow NaX membrane 2

195K Ag = $884 m^2 g^{-1}$, $A_m = 15.5 Å^2$	
$\frac{Acl}{2} Ac'_s = 5.40 \times 10^{-4}$ mol	
p/cmHg	$10^4 J_\infty$ x BTT/mol
2.24	4.12
3.31	4.60
6.60	4.31
9.32	4.68
12.00	4.63
15.19	4.70
18.05	4.63
21.28	4.89
24.98	4.98

Table 5.2.5 BREAKTHROUGH TIME PROCEDURE Continued

e. CO_2 flow CMS membrane

195K Ag = $386 m^2 g^{-1}$ A_m = 16.3Å^2 273.2KA = $245 m^2 g^{-1}$ A_m = 16.3Å^2

$\frac{Acl}{2}$ Ac's = 13.4×10^{-4}mol $\frac{Acl}{2}$ Ac's = 8.52×10^{-4}mol

p/cmHg	$10^4 J_\infty$.BTT/mol	p/cmHg	$10^4 J_\infty$. x BTT/mol
1.87	3.74	0.89	0.168
4.30	6.19	1.99	0.432
7.52	7.90	4.48	0.630
9.51	8.35	8.36	0.875
11.61	8.57	9.50	1.43
14.45	9.95	14.70	1.70
20.85	9.83	21.17	1.81
27.94	8.79	28.03	1.80
41.61	9.27	34.37	2.40
		41.93	1.59
		49.29	1.52

A = specific surface area / $m^2(m^{-3}$porous medium)

c' = surface conc^n/mol m^{-2}

However, as yet the equation has not been applied to any experimental data. J_∞.BTT was evaluated for all the results obtained upon molecular sieve membranes in this study and the results are listed in table 5.2.5a) to table 5.2.5e). For each system the surface area per gram of sorbent (A_g), area permolecule (A_m) and Ac.ℓ.Ac$'_s$/2 are also quoted, as calculated from the saturation capacity of the sorbent.

For CO_2/NaX systems J_∞.BTT is approximately constant only at 195K, at 273.2K and also for N_2/NaX, and H_2S/NaX the limitation of insufficient rectangularity probably applies and J_∞.BTT increases with increasing p_1. Only for CO_2/NaX at 195K was J_∞.BTT close to AcℓAc$'_s$/2 in value. (J_∞.BTT exceeding AcℓAc$'_s$/2 by approximately 8% at the higher pressures). For all the other systems studied AcℓAc$'_s$/2 exceeded J_∞.BTT, the worst agreement being at 273.2K where less rectangular isotherms were obtained. J_∞.BTT increased with p_1 and was considerably less than AcℓAc$'_s$/2 for CO_2/CMS despite this system giving a very rectangular isotherm at 195K. The discrepancies observed may be accounted for by loss of sorptive capacity resulting from compaction of the sorbent, packing inhomogeneities giving rise to the possible differences between the steady state and transient state diffusion coefficients.

5.2.6 Theoretical determination of time lags

An expression for the time-lag of a gas flowing through a molecular sieve membrane has been developed by Mr. R. Ash for systems obeying the Langmuir equation. The time-lag has been expressed in terms of the Langmuir constants b and ν_m the ingoing pressure p_1,

the Knudsen permeability $\tilde{K}'_K$ and the Poiseuille permeability $\tilde{K}'_p$ using the following equation.

$$L = \frac{\varepsilon \ell^2 \{1/6 + 5\theta/12 + 4\theta^2/15\}}{\tilde{K}'_K (1+\theta)^3}$$

$$+ \frac{\ell^2 b c_m RT}{\tilde{K}'_K y^5 (1+\theta)^3} \times \{[(y^3(y+2)/2) - y^2(1+y)\ell n\,(1+y)]$$

$$+ \theta[(y^2(2y+3)(y-2)/2) + y(y+1)(3-y)\ell n(1+y)]$$

$$+ \theta^2[y(\frac{y^3}{2} - \frac{4y^2}{3} - y+2) + 2(y^2-1)\ell n(1+y)]\}$$

where $y = bp_1$, $\theta = \tilde{K}_p' p_1 / \tilde{K}'_K$ and $bc_m/molN^{-1}m^{-1}$

is calculated from $b/cm\,Hg^{-1}$ and $\nu_m/cm^3STP_g^{-1}$

using $c_m = \frac{76}{101325} \quad \frac{\nu_m}{22414} \times \frac{w}{\ell \times Ac}$

w = membrane outgassed weight g

ℓ = membrane length /m

Ac = membrane cross sectional area $/m^2$

ε = membrane outgassed porosity m^2m^{-3} (porous medium).

The derivation for this equation is shown in Section 2.5.2.

Time-lags as a function of p_1 at a given temperature were calculated for the following systems CO_2/Na X 1, CO_2/NaX2, H_2S/NaX2 and CO_2/CMS. In these cases the fit of the adsorption isotherm to the Langmuir equation was good (cf Section 5.1) and, as the condition of sufficient rectangularity (necessary for the breakthrough-time procedure) did not

apply to this equation, time lags were calculated both at 195K and 273.2K where experimental data permitted. The first term in the equation was found to be negligible in all cases.

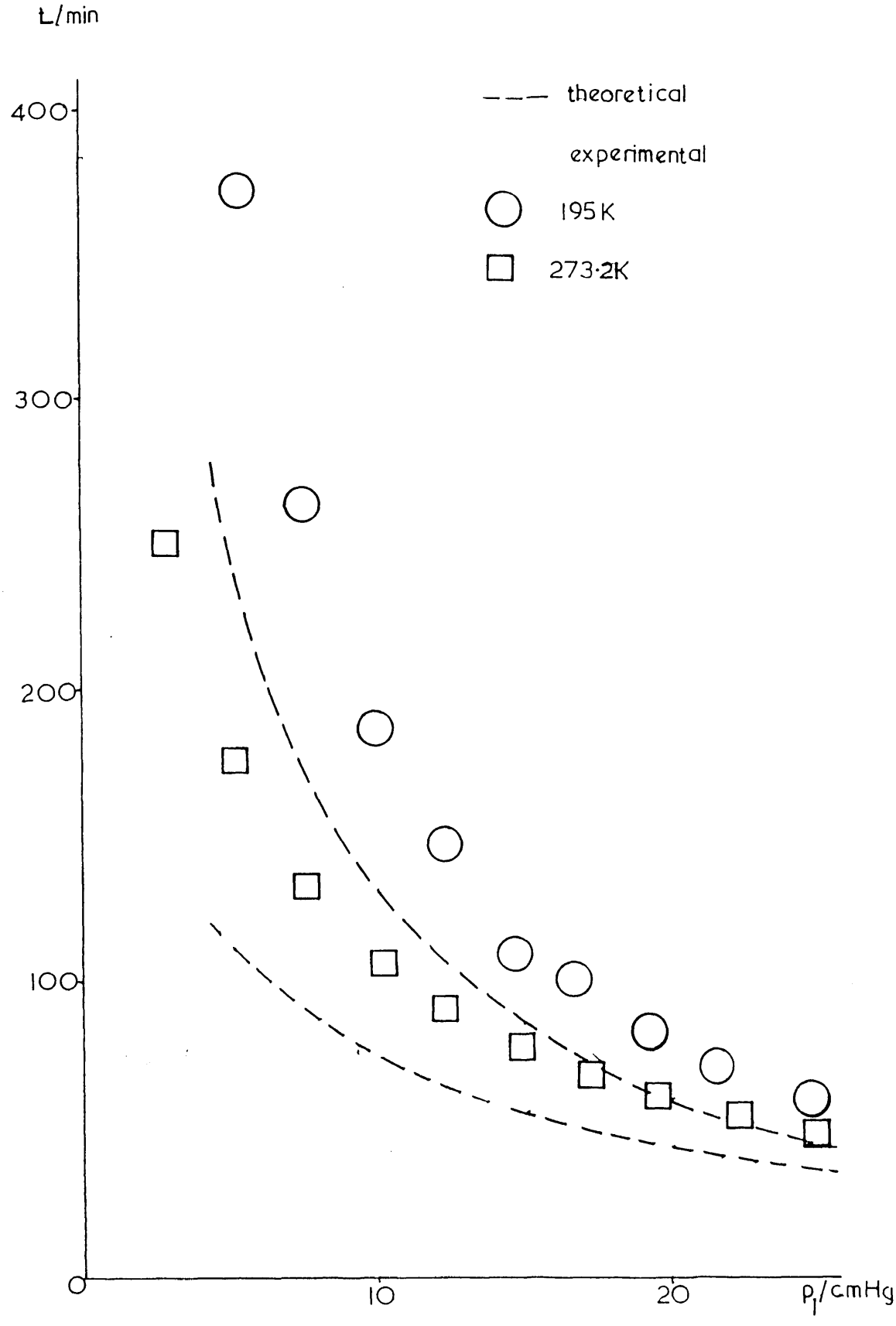
Fig. 5.2.5 to Fig. 5.2.7 show the agreement between the calculated and experimental values of L. It may be seen that for membrane NaX.2 (Fig. 5.2.6) and the CMS membrane (Fig. 5.2.7) the agreement of theoretical and experimental values is good especially at higher ingoing pressures. Only for NaX1 is there a discrepancy, the calculated curve falling below the experimental one (Fig. 5.2.5), strangely, it is for this system at 195K that the break through time procedure gives values of $J_{\infty}.BTT$ which are closest to $Ac\ell Ac'_s/2$.

The NaX membrane 1 was both the oldest and the least compact membrane studied (porosity 0.72 cm^3cm^{-3}). It was therefore possible that the low calculated value of L was due to a difference between the steady state and transient state diffusion coefficients produced by packing inhomogeneities. (A low calculated value of L could not be accounted for by loss of sorpitive capacity on compaction). Experimental error in the determination of the membrane dimensions and weight may also be possible causes.

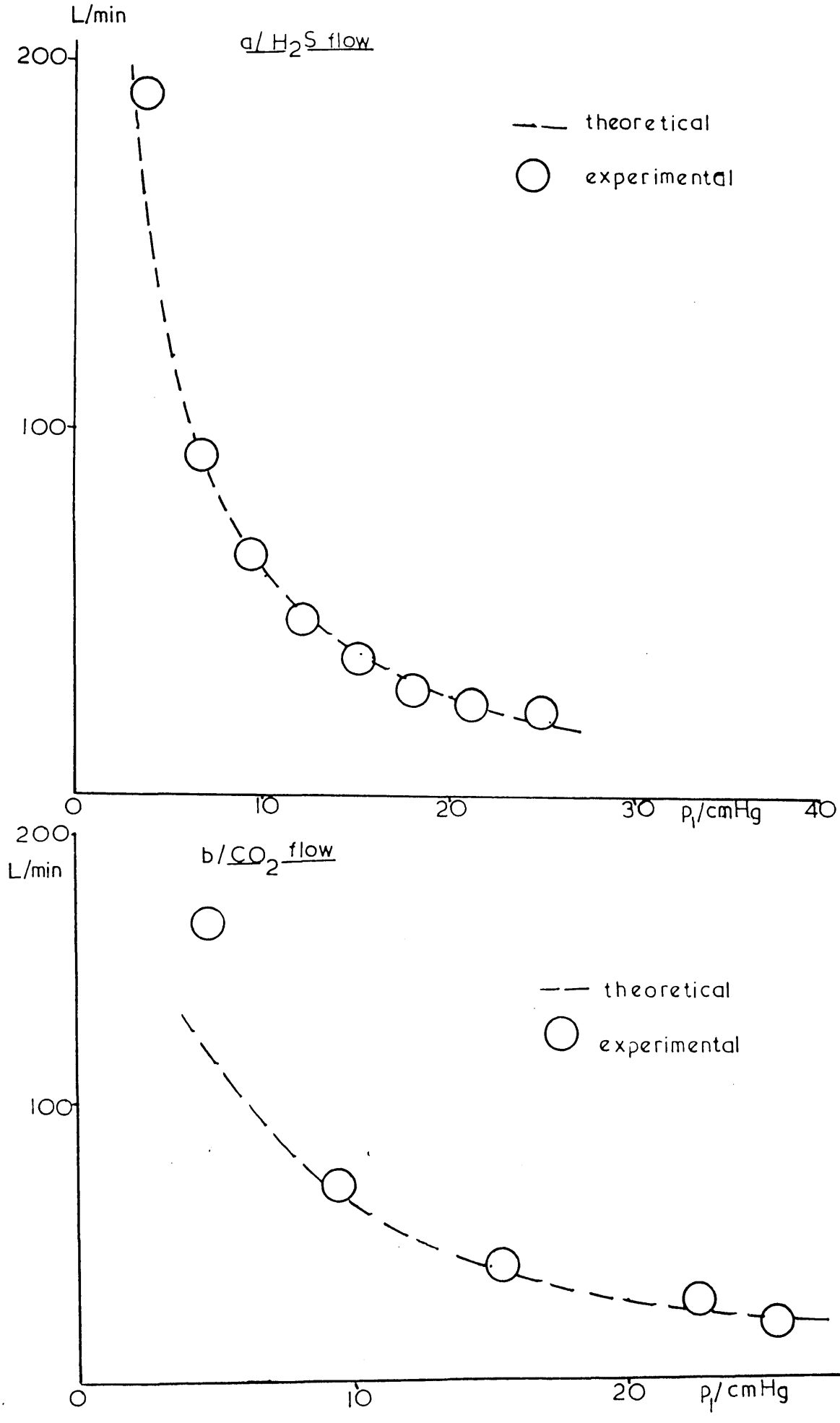
Whilst the use of this equation may lack the simplicity of the breakthrough-time procedure, it has now been shown to produce results which show excellent agreement with experimentally obtained time lags, for three different systems and at two temperatures. It therefore seems to be a more widely applicable relationship than the breakthrough time procedure and as such warrants further investigation.

(fig 5·2·5) Theoretical and experimental time lags

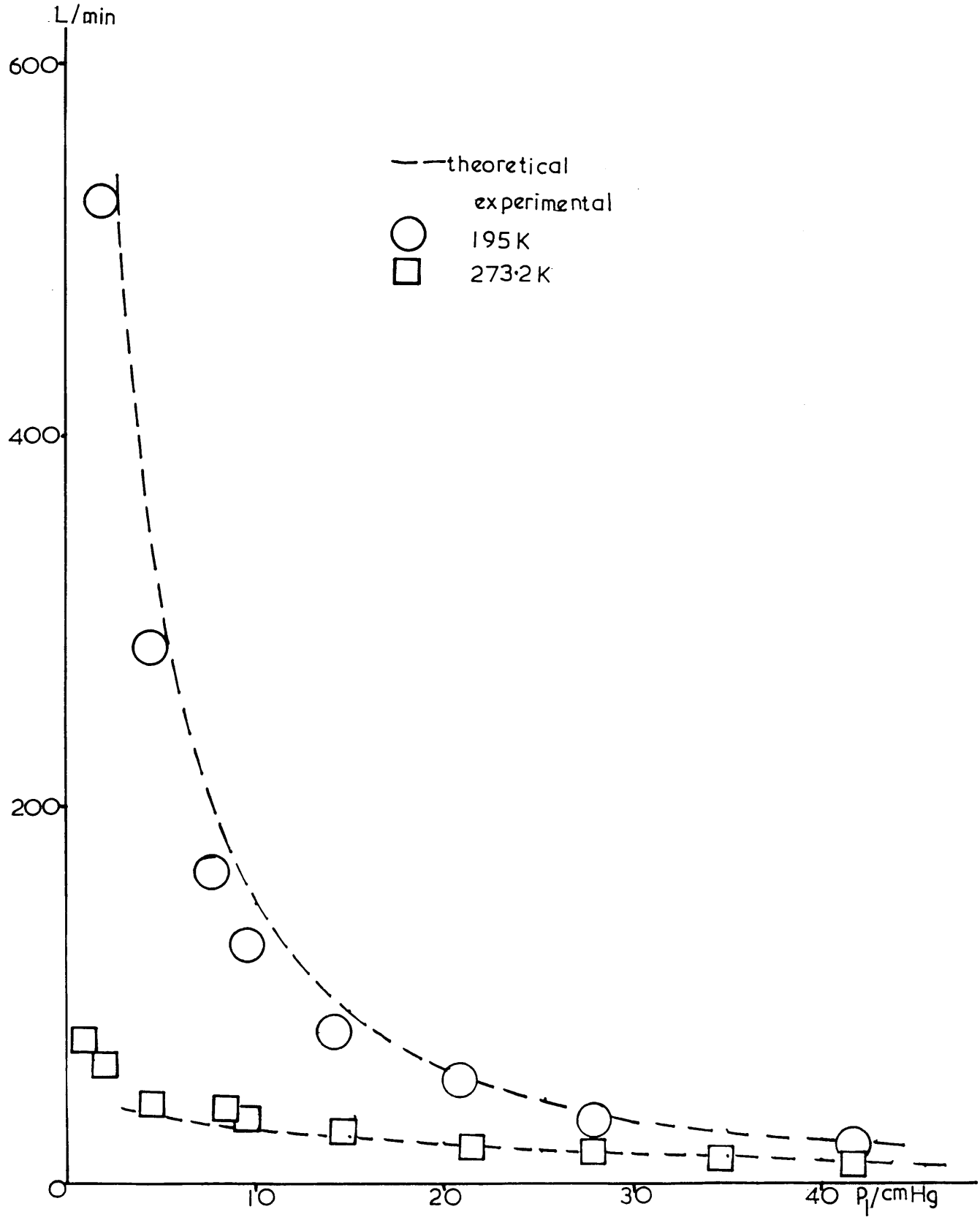
CO_2 flow through Zeolite membrane1



(fig 5·2·6) Theoretical and experimental time-lags : Zeolite membrane 2 at 195K



(fig 5·2·7) Theoretical and experimental time-lags
CO_2 flow through CMS membrane



5.3 Discussion of flow results on Carbolac and Graphon membranes

5.3.1 Introduction

Fig. 4.2.23 and Fig. 4.2.30 show examples of outgoing pressure versus time graphs for CO_2 flow through the Carbolac and Graphon membranes. For Carbolac, time-lags were measured for H_2S and CO_2; however no measurable time lags for any gas at any temperature studied were observed on the Graphon membrane. This is probably due to the greater surface area and hence sorptive capacity of Carbolac (approximately 10 x that of Graphon) as the dimensions of the two membranes are very similar. The outgoing pressure versus time graphs for Carbolac, show a gentle curve prior to the steady state and a sharp break-through, analogous to that observed for some of the molecular sieve membranes, does not occur.

The pressure dependence of the integral permeabilities for gas flow through the Carbolac and Graphon membranes showed considerable variation of form (Fig. 4.2.18 to Fig. 4.2.38).

In most of the graphs, no linear increase in permeability was evident with increasing pressure contrary to the behaviour observed previously for the CMS and NaX membranes. Therefore it was concluded that Poiseuille flow did not play a significant role in the transport of gases through these membranes. In these systems, the total permeability may be split into two components: $\tilde{\ }$ (cf Section 2.6) a purely gas phase component, $\tilde{K}_g$ and a component $\tilde{K}_s$ due to the extra flow generated by the adsorbed film of gas,

where $\tilde{K} = \tilde{K}_g + \tilde{K}_s$ (cf Section 2.6 eq^{n}48).

The $\tilde{K}_s$ component is absent from the flow through molecular sieve membranes, despite high adsorption, because the gases are adsorbed into cavities in the crystal structure and inter crystalline transport does not readily occur, as proved by Ash Barrer and Coughlan (1972). For these reasons the methods of analysis used in this section differ from those used in Section 5.2.

5.3.2 Helium flow

In the absence of Poiseuille flow, He may be used as a calibrating gas, as it is assumed to be non-sorbed and therefore obeys the relationship

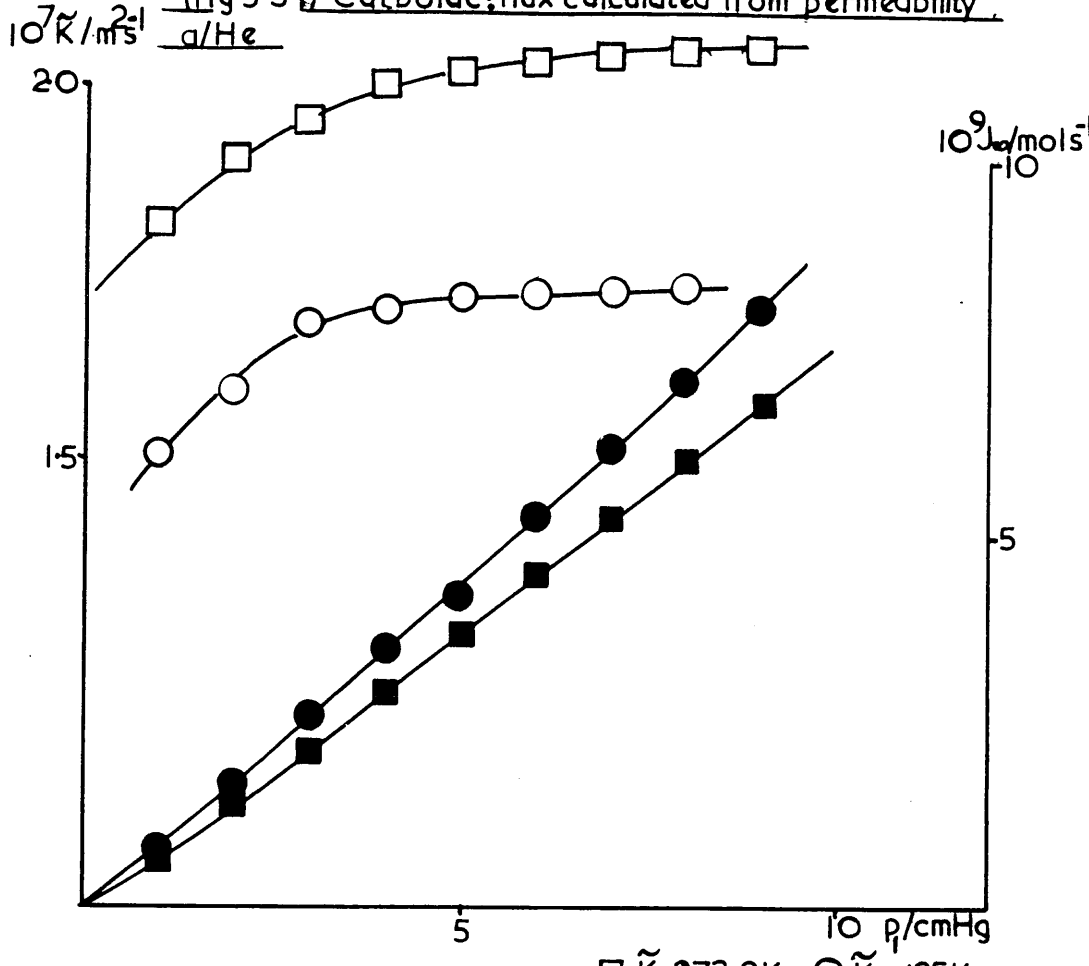
$\tilde{K}(M/T)^{\frac{1}{2}}$ = constant for any given membrane. (cf Section 2.6)

The He permeability for Graphon (fig. 4.2.28) is independent of pressure and table 5.3.1 shows that $\tilde{K}\sqrt{\frac{M}{T}}$ is constant for all temperatures and agrees well with the values obtained in previous studies (table 4.2.3)

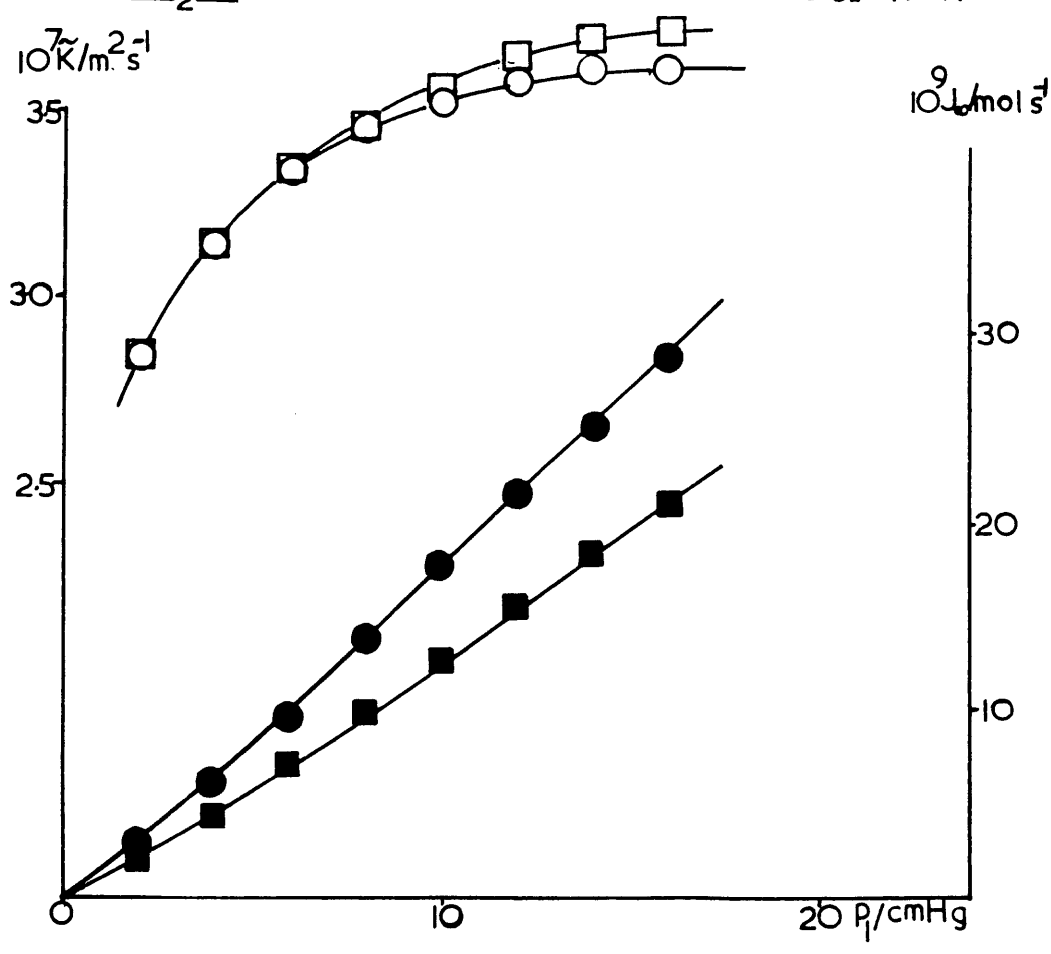
For He flow through Carbolac a decrease in permeability is observed below 5 cm Hg. This divergence is also noticeable in the flux plot, which shows curvature when back calculated from the permeability results at low pressure (Fig. 5.3.1(a)). Similar behaviour was observed for N_2 (which is only slightly adsorbed) for which low pressure plots of $\tilde{K}$ and back-calculated J_∞ are shown in Fig. 5.3.1(b). Deviation of N_2 and He permeabilities through a Carbolac membrane have previously been observed by Rizvi (1982) who obtained a rise in permeability below 2 cmHg ingoing pressure for He, H_2, N_2, CH_4 and noble gases.

(fig 5·3·1) Carbolac: flux calculated from permeability.

a/He



b/N_2



Hwang and Kammermeyer (1966) observed a variation in $\tilde{K}\sqrt{\frac{M}{T}}$ with temperature for He and N_2 flow through porous glass. In this study $\tilde{K}\sqrt{\frac{M}{T}}$ for He flow at 195K and 273.2K are in good agreement (table 5.3.1) if the 'plateau' value of $\tilde{K}$ is taken, however at lower pressures the two values diverge, as illustrated in the graph of $\tilde{K}\sqrt{\frac{M}{T}}$ versus $1/\overline{\lambda}$ for this system (Fig. 5.3.2).

Ash Barrer and Lowson (1970) have studied the use of He as a calibrating gas and concluded that it is justified for micro porous high area carbon membranes at temperatures where there is no evidence of surface transport of He (above 77K). These results appear to conflict with those of Hwang and Kammermeyer, however Nicholson and Petropoulos (1973) (1975) and (1980) have developed a theory using a narrow slit as a pore model, which allows for both types of behaviour.

This model predicts a minimum in a plot of $\tilde{K}\sqrt{\frac{M}{T}}$ versus T for weakly adsorbed gases, the size of which decreases with increasing pore size. In this study He has been assumed non-sorbed and used as a calibrating gas. However the Carbolac membrane needed careful calibration, as its structure and hence permeability changed with time (Fig. 4.2.19 and Fig. 4.2.22). This ageing of Carbolac membranes has also been observed by Ash Barrer and Pope (1963a) and Ash Barrer and Sharma (1976) and has been attributed to irreversible swelling of the membrane, following high adsorption.

This particular membrane has previously shown ageing when exposed to NH_3 by Ash Barrer and Lowson (1973). If the gas phase permeability $\tilde{K}_g$ is independent of pressure, a steady state gas phase diffusion coefficient D_g may be calculated $\tilde{K}_g = \varepsilon D_g$. (derived in Section 2.6 equation (55) to (60)). A gas phase diffusion coefficient D_g^{cyl} may be calculated for a reference medium consisting of parallel cylindrical capillaries (of radius $r = 2\varepsilon/A$) using the equation

$$D_g^{cyl} = \frac{4}{3} r \sqrt{\frac{2RT}{\pi M}}$$

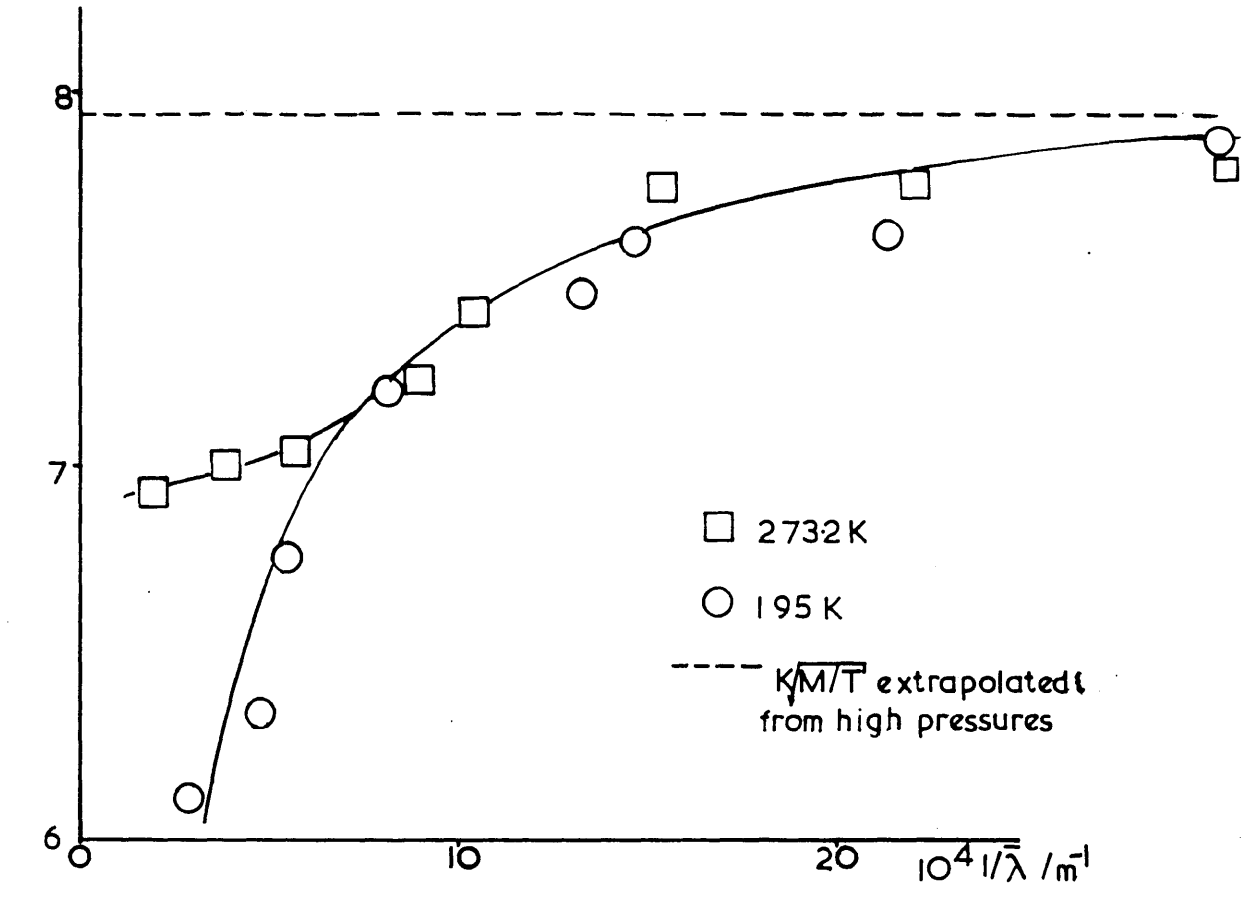
A gas phase structure factor κ_g, initially defined by Barrer and Gabor (1959) may then be calculated.

$$\kappa_g = D_g/D_g^{cyl}$$

D_g, D_g^{cyl} and κ_g are listed in table 5.3.2 and it may be seen that the structure factors are less than unity for both Graphon and Carbolac, indicating that constrictions in the pores are important to the gas flow. Previous examples of this type of system are the Graphon and two Carbolac membranes studied by Ash et al(1973)which showed structure factors of 0.47, 0.26 and 0.25 respectively using Ag Graphon = $79 m^2 g^{-1}$ and Ag Carbolac = $940 m^2 g^{-1}$. The value of $\kappa_g = 0.60$ for this Graphon membrane is not in good agreement with that obtained by Hamilton (0.18). This is due to the discrepancy in values of Ag for Graphon used.

(Hamilton $89.7 m^2 g^{-1}$, this study $80.0 m^2 g^{-1}$)

(fig 5·3·2) $\tilde{K}\sqrt{M/T}$ versus $1/\bar{\lambda}$ He flow:Carbolac



(fig 5·3·7) $\tilde{K}_s/\tilde{K}_g$ N_2 flow : Carbolac

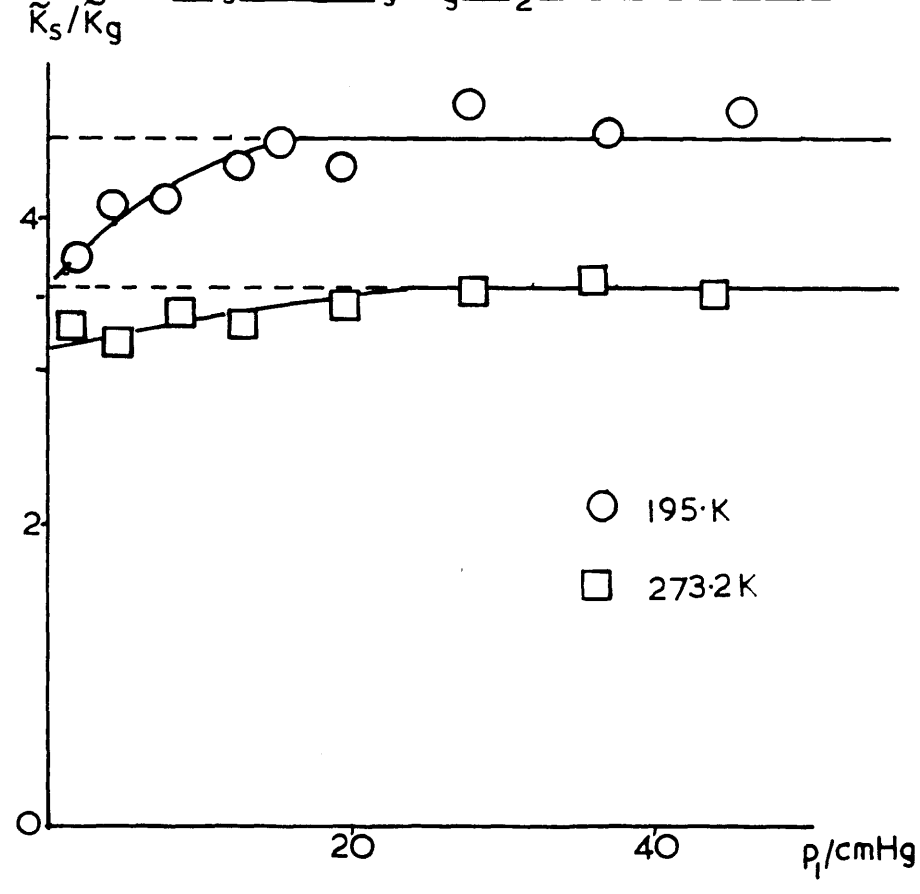


Table 5.3.1

$\tilde{K}\sqrt{\frac{M}{T}}$ for Helium flow

T/K	$10^7\tilde{K}/m^2s^{-1}$	$10^{10}\tilde{K}\sqrt{\frac{M}{T}}/m^2s^{-1}(kgmolK^{-1})^{\frac{1}{2}}$
Carbolac membrane		
195	1.7_7	7.93
273.2	2.0_8	7.96
Graphon membrane		
184	$24._1$	112
200	25_5	114
213.2	$26._1$	113
273.2	29_8	114

Table 5.3.2

D_g, D_g^{cyl} and κ_g for Helium flow

T/K	$10^7D_g/m^2s^{-1}$	$10^7D_g^{cyl}/m^2s^{-1}$	κ_g
Carbolac membrane			
195	3.31	7.30	$.45_3$
273.2	3.94	8.65	$.45_5$
Graphon membrane			
184	48.8	81.5	$.59_9$
200	51.6	84.9	$.60_2$
213.2	52.8	87.7	$.60_2$
273.2	60.3	99.3	$.60_7$

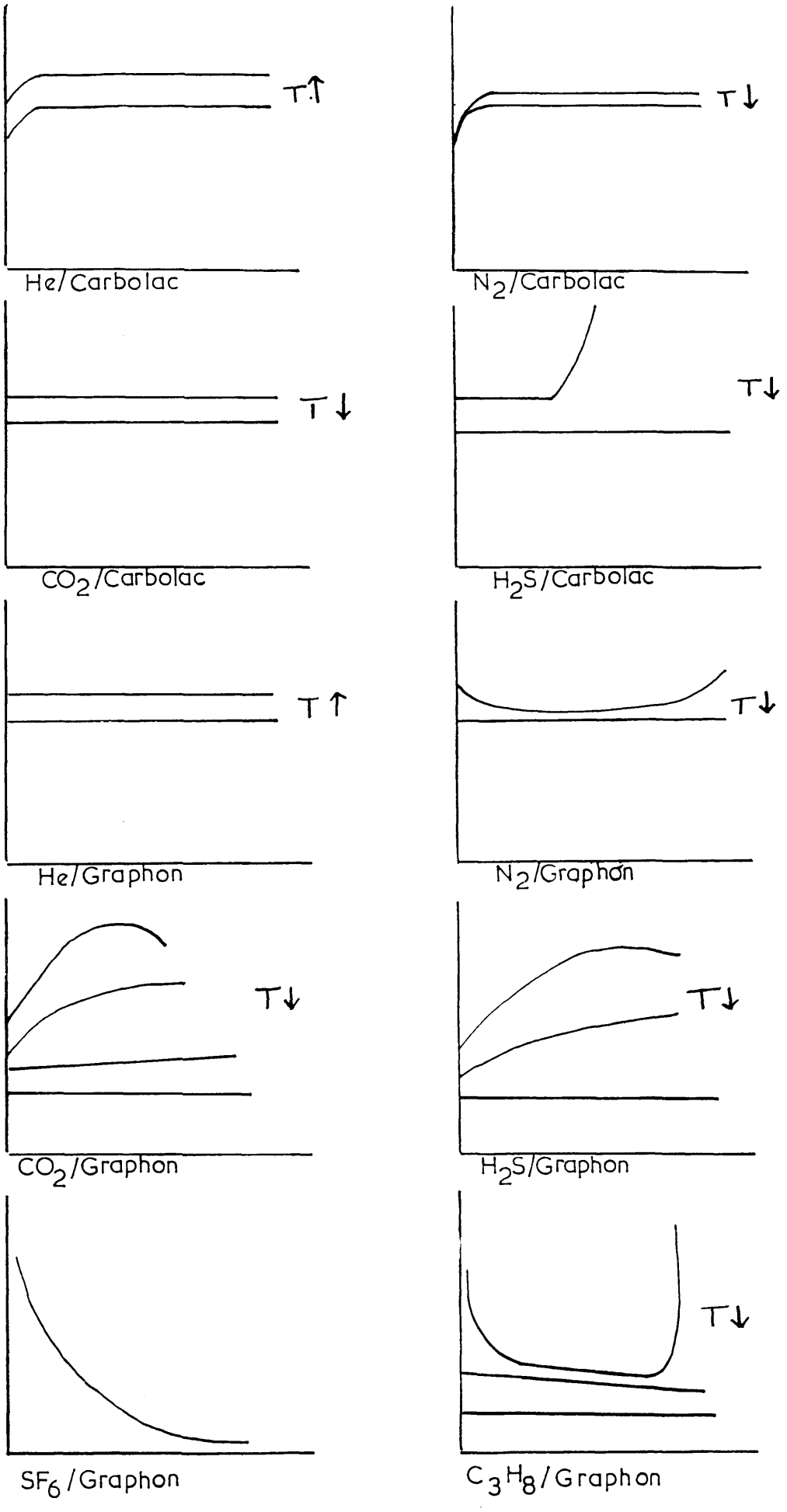
5.3.3 Flow of sorbable gases: $\tilde{K}$ and J_∞

A wide variety of behaviour has been observed in $\tilde{K}$ versus p_1 graphs for Carbolac and Graphon, it is summarized in Fig. 5.3.3. In all cases the variation in $\tilde{K}$ versus p_1 was reflected in the flux curve. A constant value of $\tilde{K}$ gives a linear graph of J_∞ versus p_1, increasing $\tilde{K}$ gives a flux curve convex to the pressure axis and decreasing $\tilde{K}$ gives a flux curve concave to the pressure axis.

The unexpected decrease in $\tilde{K}$ at low pressures for He and N_2 has been discussed (Section 5.3.2). It is also unusual to observe a constant value of $\tilde{K}$ with increasing p_1 for CO_2 flow on Carbolac outside the Henry Law adsorption range due to the presence of an 'extra' flow of CO_2. Carman and Raal (1951) and Pope (1969), both observed $\tilde{K}$ versus p_1 decreasing for CO_2 flow through Carbolac as in Fig. 5.3.4(a). The H_2S permeability for the same membrane is approximately constant below p_1 = 15 cm Hg, however above this a rapid increase is observed at 195K but not at 273.2K. The monolayer capacity for H_2S adsorption on Carbolac at 195K is achieved at 17cm Hg of H_2S, so this behaviour may be due to multilayers near to $p_1/p_0 = 1$. The effect of surface tension lowers the vapour pressure of the adsorbed gas and the driving force is not the measured gas pressure but a much larger capillary pressure difference. Carman (1951) observed a rapid increase in $\tilde{K}$ near to $p_1/p_0 = 1$ for CF_2Cl_2 flow through Carbolac (Fig. 5.3.4(b)) as did Hamilton (1980) for hydrocarbon flow on Graphon, (Fig. 5.3.4(c)) both of which were attributed to multilayer formation.

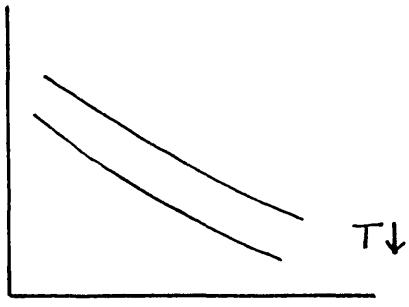
The Graphon membrane exhibits examples of permeability both increasing and decreasing with pressure for different gases, and in

(fig 5·3·3) Schematic diagram of $\tilde{K}$ versus p_T behaviour

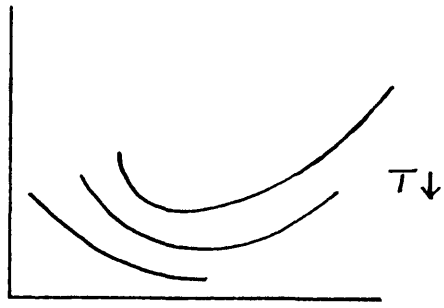


↓ = direction of increasing temperature

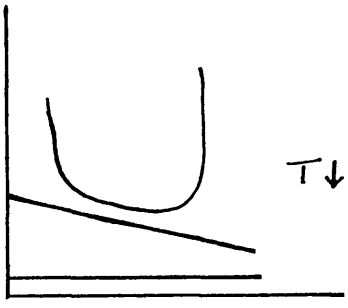
(fig 5·3·4) Schematic diagram of $\tilde{K}$ versus p_t behaviour



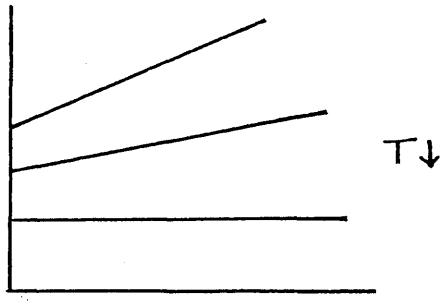
a/ CO_2/Carbolac



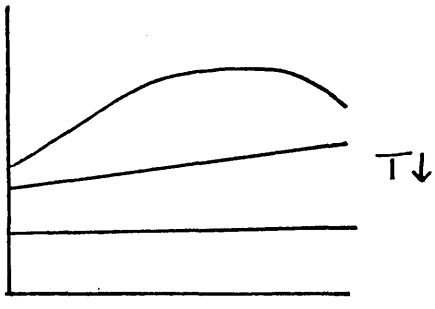
b/ CF_2Cl_2/Carbolac



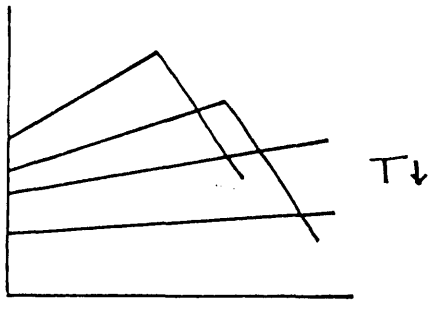
c/ hydrocarbons/ Graphon



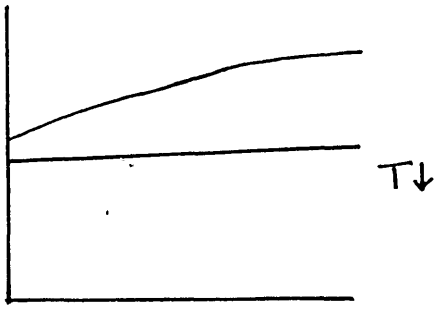
d/ C_6H_6/alumina-silica catalyst



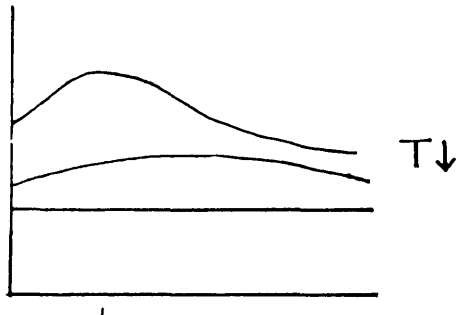
e/ C_3H_8/ Sterling S



f/ NH_3/ Carbolac



g/ CO_2/ Sterling S



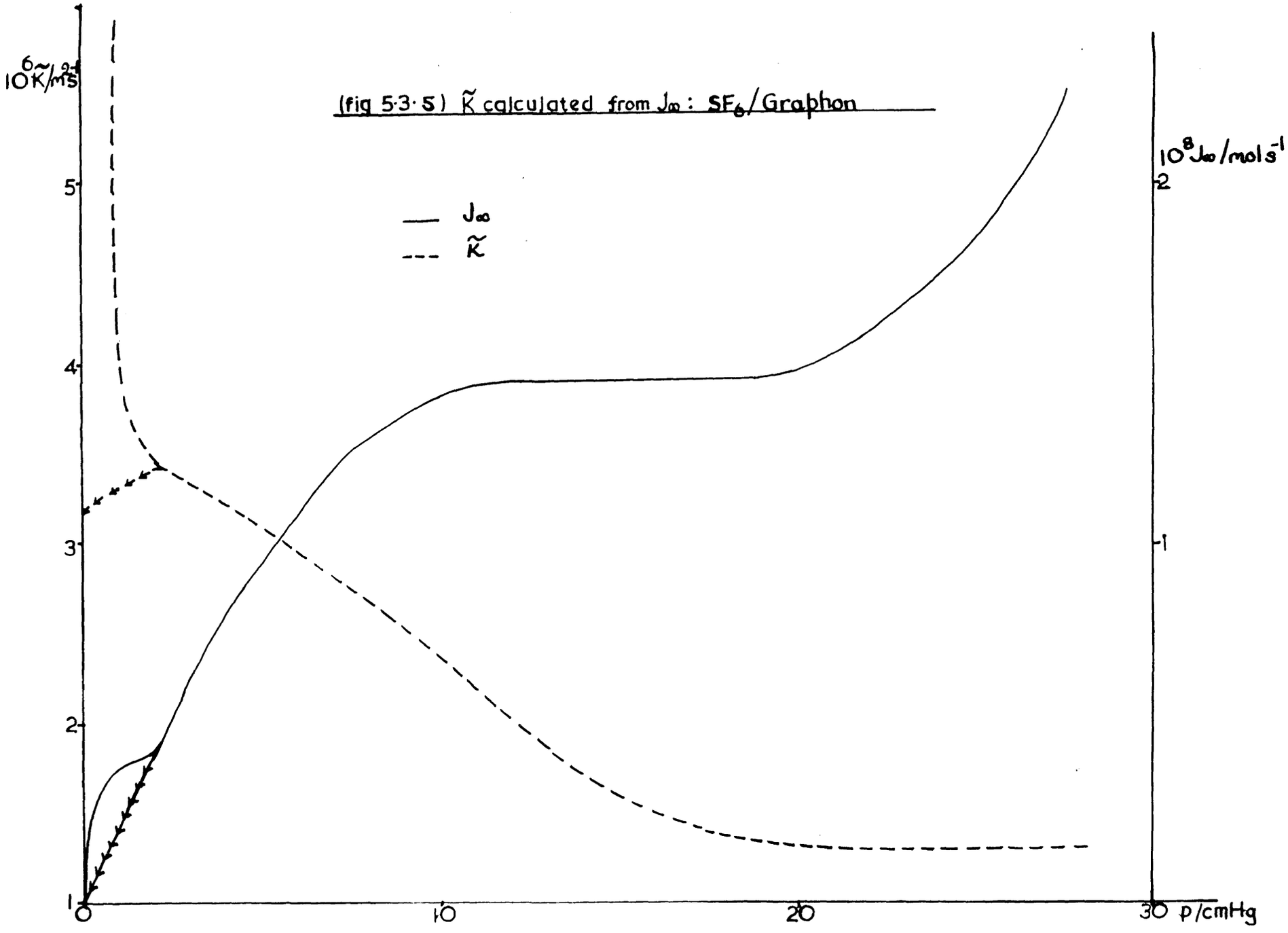
h/ Xe/Sterling S

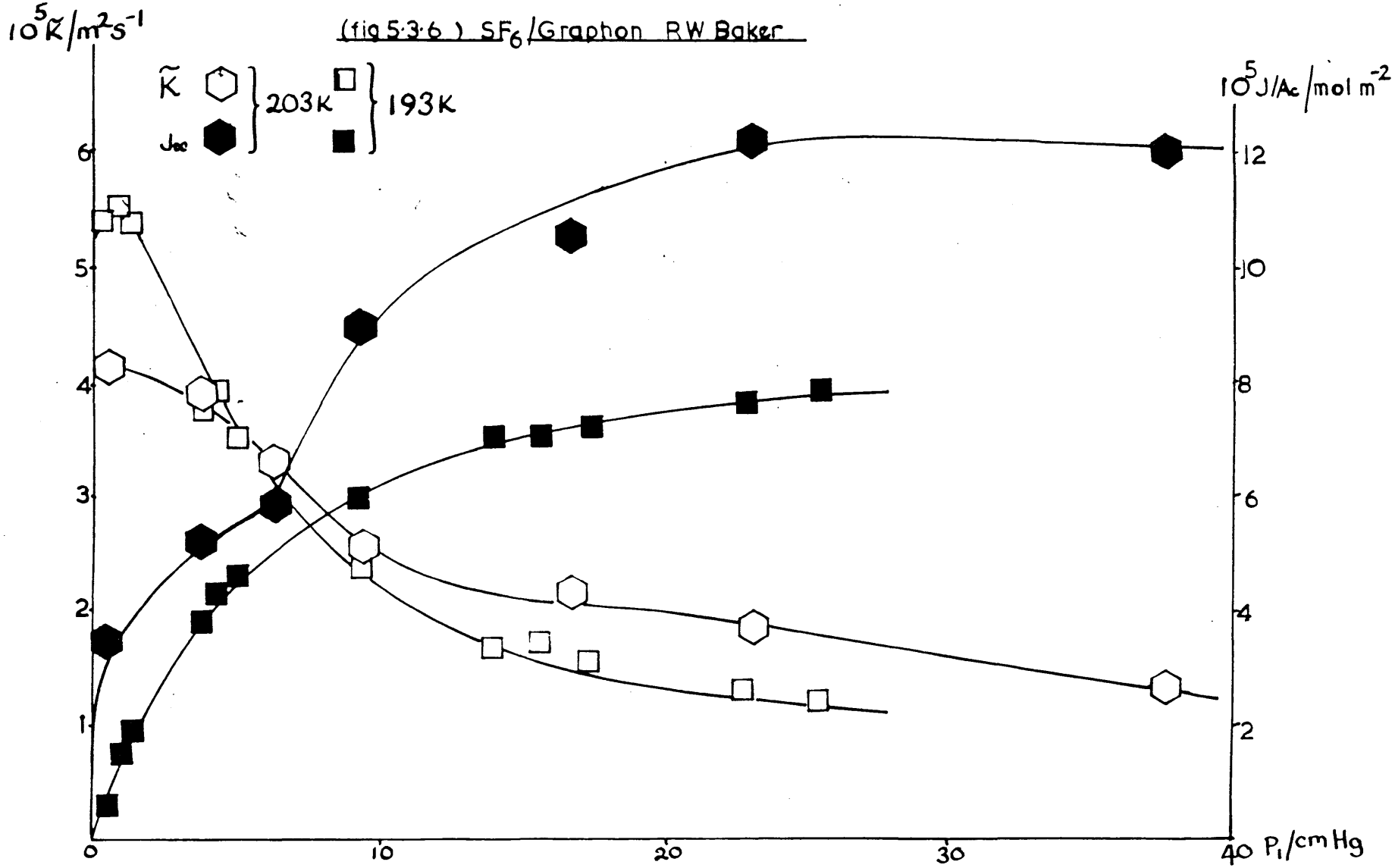
some cases maxima or minima are observed. In all cases the most dramatic behaviour of $\underset{\sim}{K}$ occurs at the lowest temperature, indicating that the variation is due to 'extra' flow. H_2S and CO_2 both give $\underset{\sim}{K}$ versus $p_{1_{\sim}}$ graphs which increase and even show a maximum at 195K. Increasing K has also been observed by Ash Barrer and Logan for Benzene and other hydrocarbons flowing through an alumina-silica cracking catalyst (Fig. 5.3.4d). Whiting (1981) who studied gas flow through a Sterling S membrane also observed an increase in permeability for ethane and an increase followed by a maximum for propane (Fig. 5.3.4e).

The only other published results showing a maximum $\underset{\sim}{K}$ are those of Ash Barrer and Lowson (1973) for Ammonia on Carbolac (Fig. 5.3.4(f)).

SF_6 flow through Graphon produces permeability values which decrease with increasing pressure, and a corresponding flux plot (Fig. 4.2.37) which shows a point of inflection. The SF_6 permeability has been back calculated from the smooth flux curve and is shown in Fig. 5.3.5. Fig. 5.3.6 shows some SF_6/Graphon results obtained by Ash Barrer and Baker (1967); the flux has been calculated from the permeability values given and is similar in form to that observed in this study.

The permeability of C_3H_8, like that of SF_6, decreases with increasing pressure. However it shows a minimum at lower temperatures and a shallower minimum was also observed in the Nitrogen permeability at 195K. Decreasing permeability with increasing pressure, sometimes showing a minimum, was also observed by Hamilton (1980) and by Ash et al (1973) for hydrocarbon flow through Graphon, by Ash, Baker and Barrer (1967) for Ar flow through Graphon and by Carman and Raal (1951) for CF_2Cl_2 on Carbolac. It was suggested by Nicholson and Sing (1979)


(fig 5·3·5) $\tilde{K}$ calculated from J_∞ : SF_6/Graphon
$10^6 \tilde{K}$/ms^{-1}
$10^8 J_\infty$/mols^{-1}
J_∞
$\tilde{K}$
1
2
3
4
5
1
2
0
10
20
30
p/cmHg


(fig 5·3·6) SF_6/Graphon RW Baker
$10^5\tilde{K}/m^2s^{-1}$
$\tilde{K}$
J_{∞}
203K
193K
$10^5 J/A_c/mol\ m^{-2}$
0
10
20
30
40
$P_1/cm\ Hg$

that the initial decrease in $\tilde{K}$ was due to blockage of some of the pores by adsorbed molecules. However Hamilton's results and those obtained in this study indicate that blockage effects exist when there is no pressure dependence of $\tilde{K}$ (e.g. CO_2/He blockage on Carbolac).

Other examples of Carbon membranes which exhibit a wide variety of behaviour in the pressure dependence of $\tilde{K}$ are the Sterling S membrane used by D.E.G. Whiting ($\tilde{K}$ increasing for hydrocarbon flow and $\tilde{K}$ decreasing for Xe flow) and a similar Sterling S membrane used by the author (1983) ($\tilde{K}$ increasing for CO_2 and $\tilde{K}$ decreasing for Xe Fig. 5.3.4 (g) and (h)).

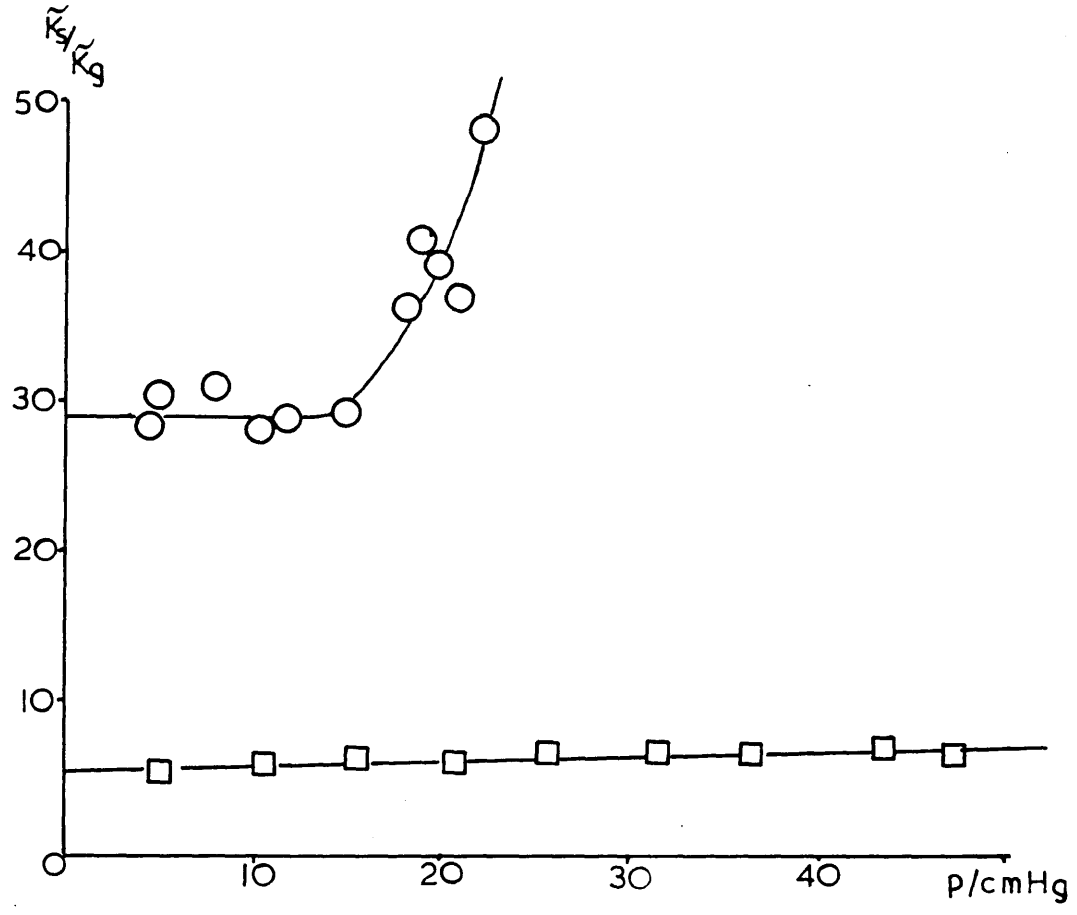
5.3.4 Flow of Sorbable gases: $\tilde{K}_s/K_g$ and $\tilde{K}_s/A$

Assuming non-sorbed Knudsen flow for Helium the gaseous component of a sorbed gas may be calculated from the measured helium permeability as shown in Section 2.6

$$\tilde{K}_{He}\sqrt{\frac{M_{He}}{T_1}} = \tilde{K}_g\sqrt{\frac{M}{T_2}}$$

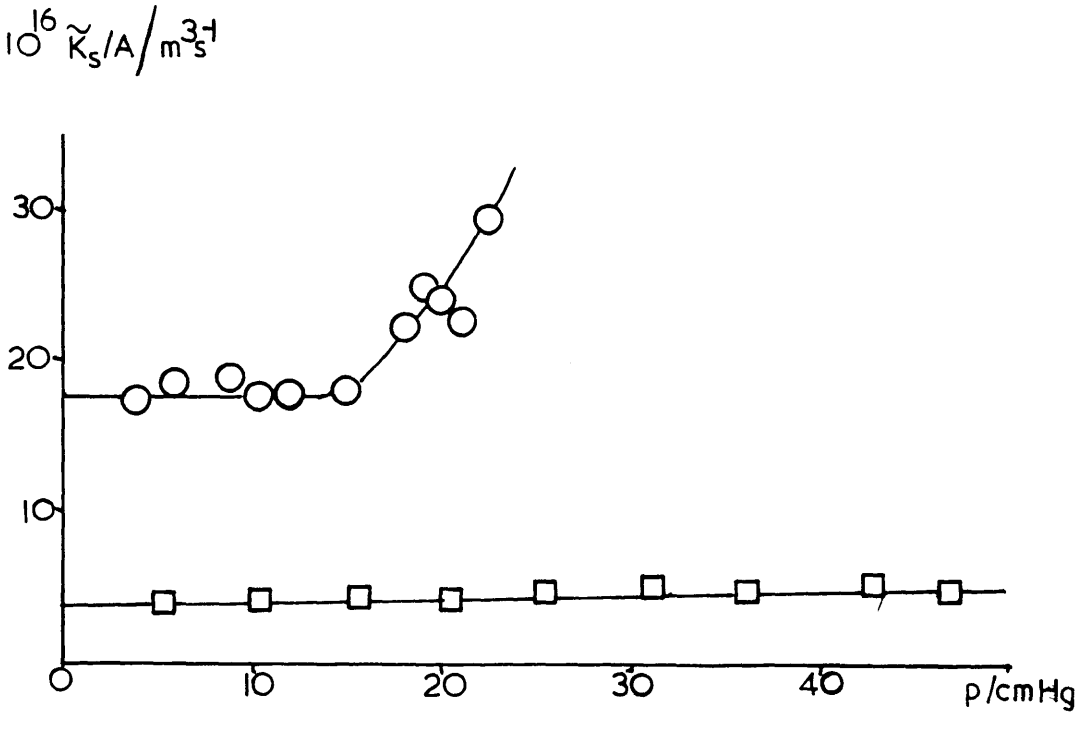
where M_{He} and M are relative molar masses and T_1 and T_2 respective temperatures $\tilde{K}_s$ then follows from the relationship: $\tilde{K}_s = \tilde{K}-\tilde{K}_g$. The ratios $\tilde{K}_s/\tilde{K}_g$ have been calculated and in table 5.3.3 they are listed for a fixed value of p_1. Fig. 5.3.7 (p251) and Fig. 5.3.8 show $\tilde{K}_s/\tilde{K}_g$ for N_2 and H_2S as a function of pressure on Carbolac. It can be seen that for both gases the shape of the $\tilde{K}$ versus p_1 curve is influenced only by the $\tilde{K}_s$ component which is much greater for the more sorbable gases. Fig. 5.3.10 and Fig. 5.3.11 show $\tilde{K}_s/\tilde{K}_g$ as a function of pressure for N_2, SF_6, CO_2 and H_2S on Graphon. Again the most

(fig 5·3·8) $\tilde{K}_s/\tilde{K}_g$ H_2S flow Carbolac

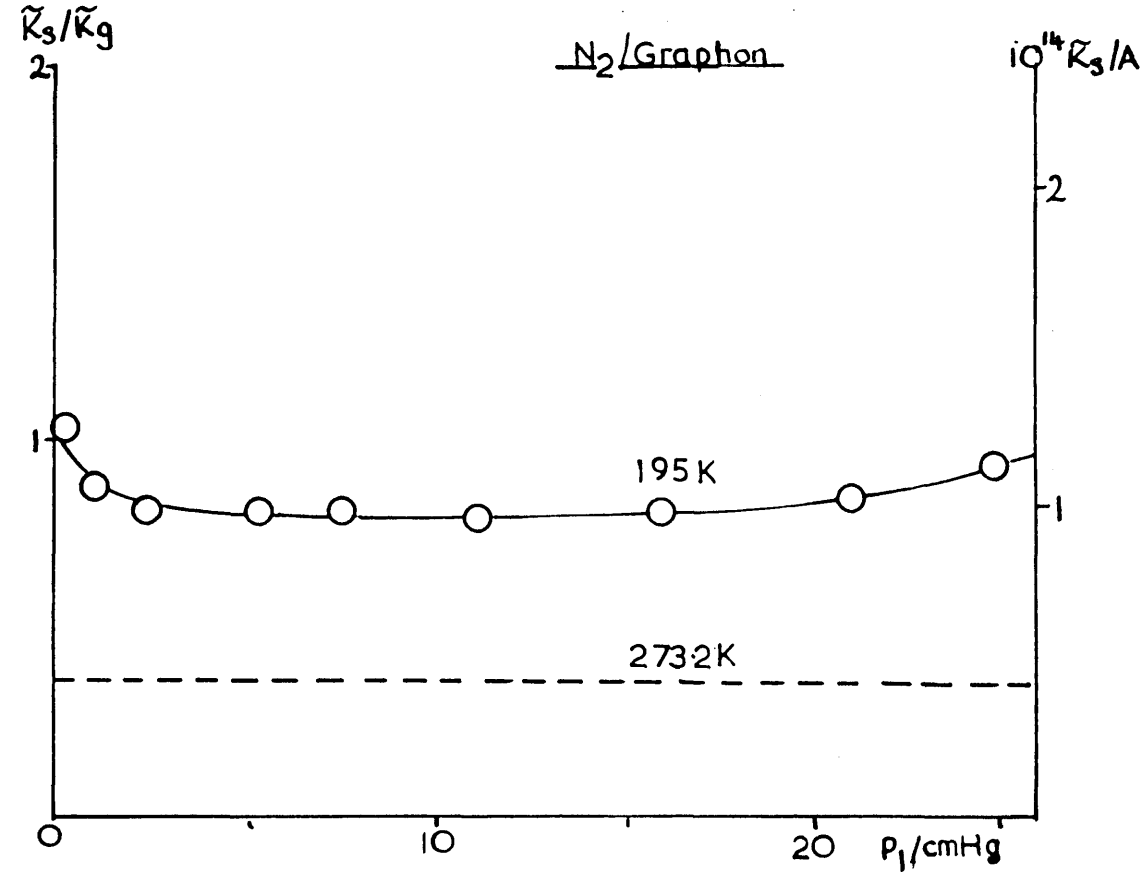


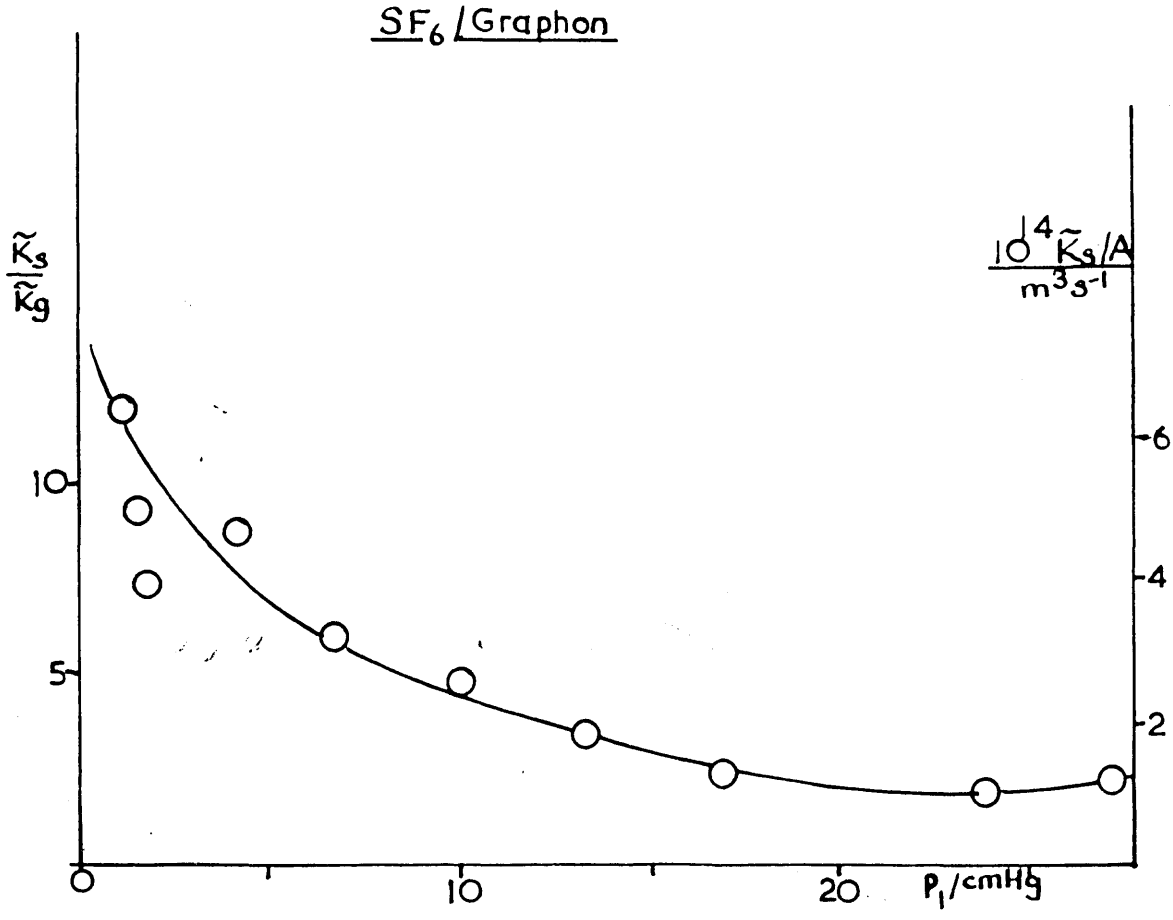
○ = 195 K □ = 273·2 K

(fig 5·3·9) $\tilde{K}_s/A$ H_2S flow Carbolac

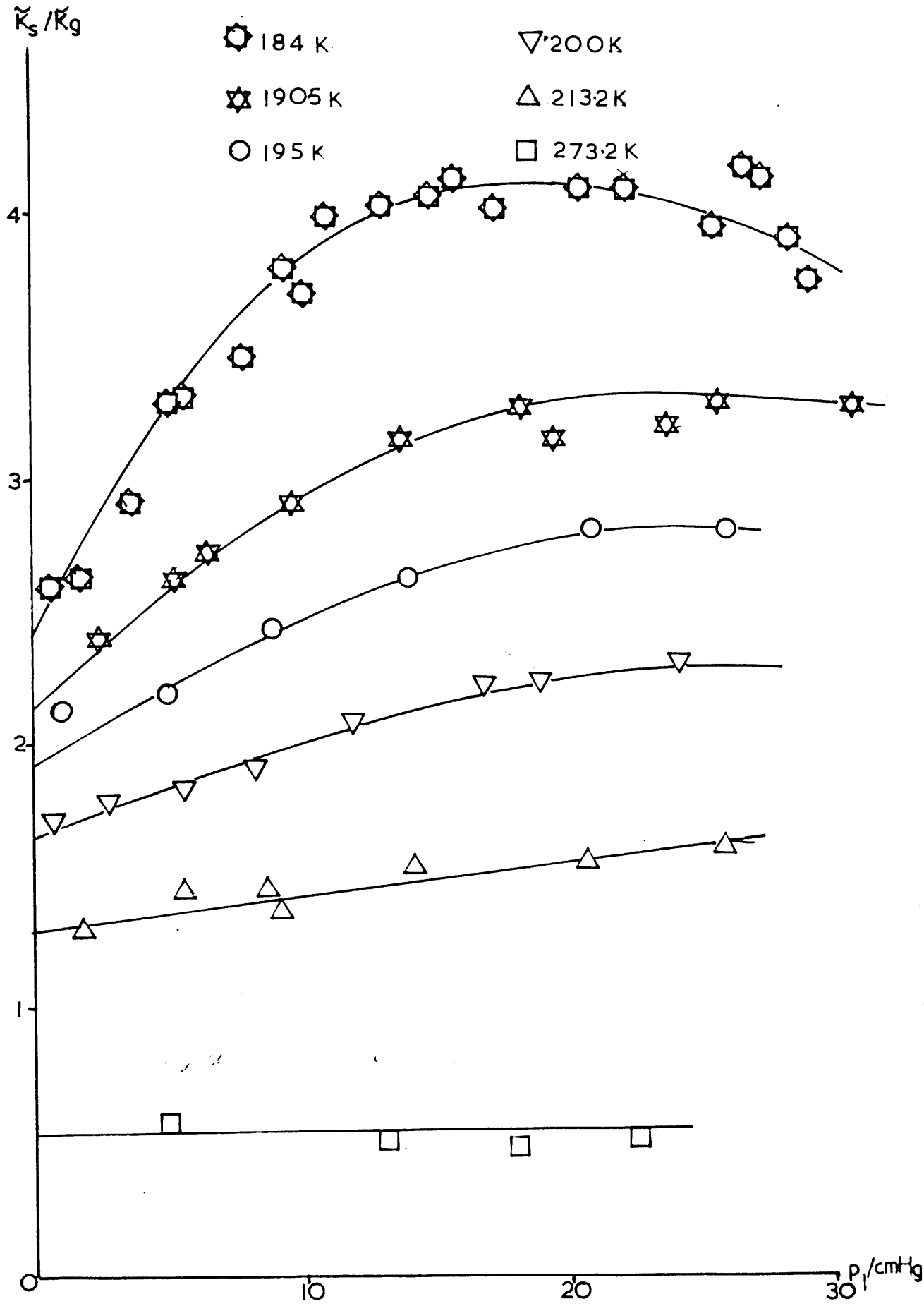


(fig 5·3·10) $\tilde{K}_s/\tilde{K}_g$ and $\tilde{K}_s/A$

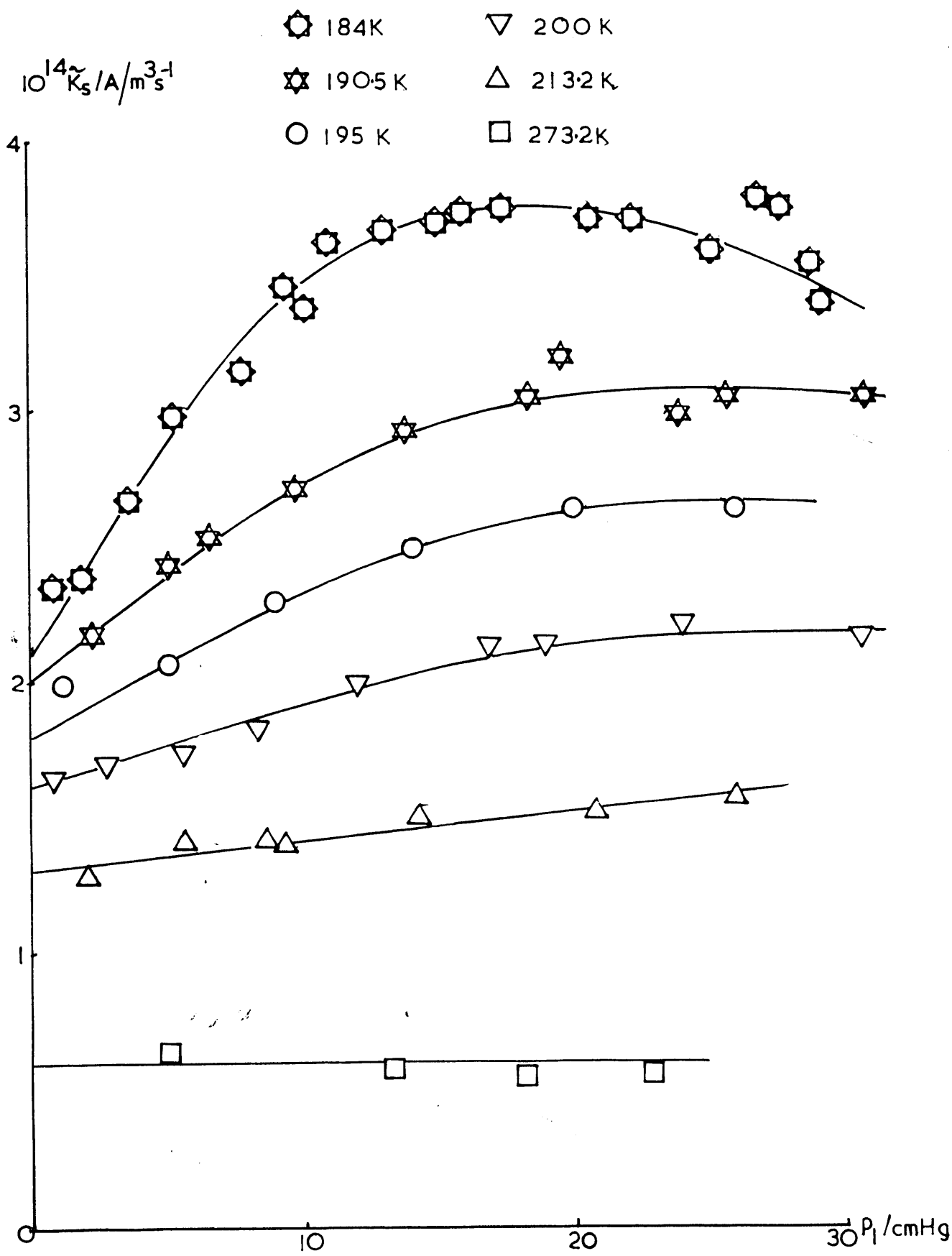




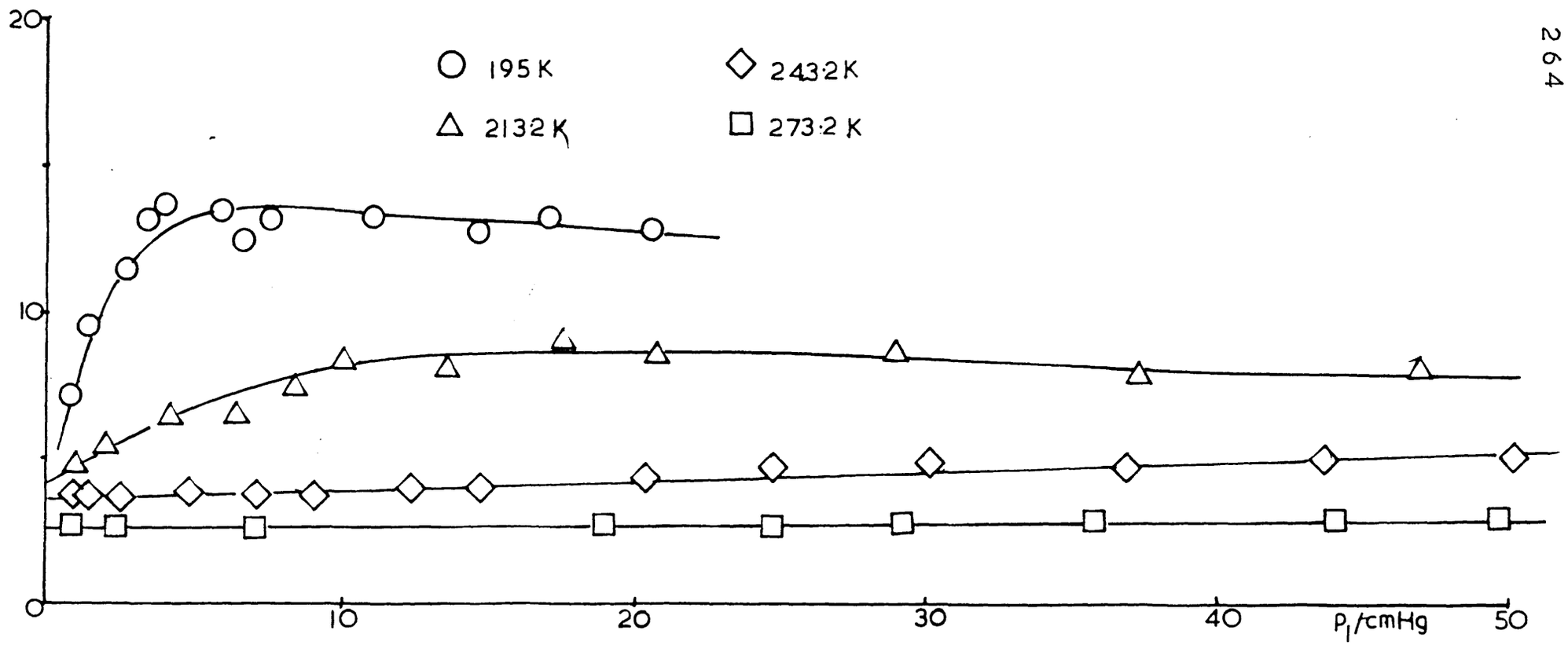
(fig 5·3·11) $\tilde{K}_s/\tilde{K}_g$: CO_2/Graphon



(fig 5·3·12) $\tilde{K}_s/A$: CO_2/Graphon



(fig 5·3·13) $\tilde{K}_s/A$ versus p_1 ; H_2S Graph on

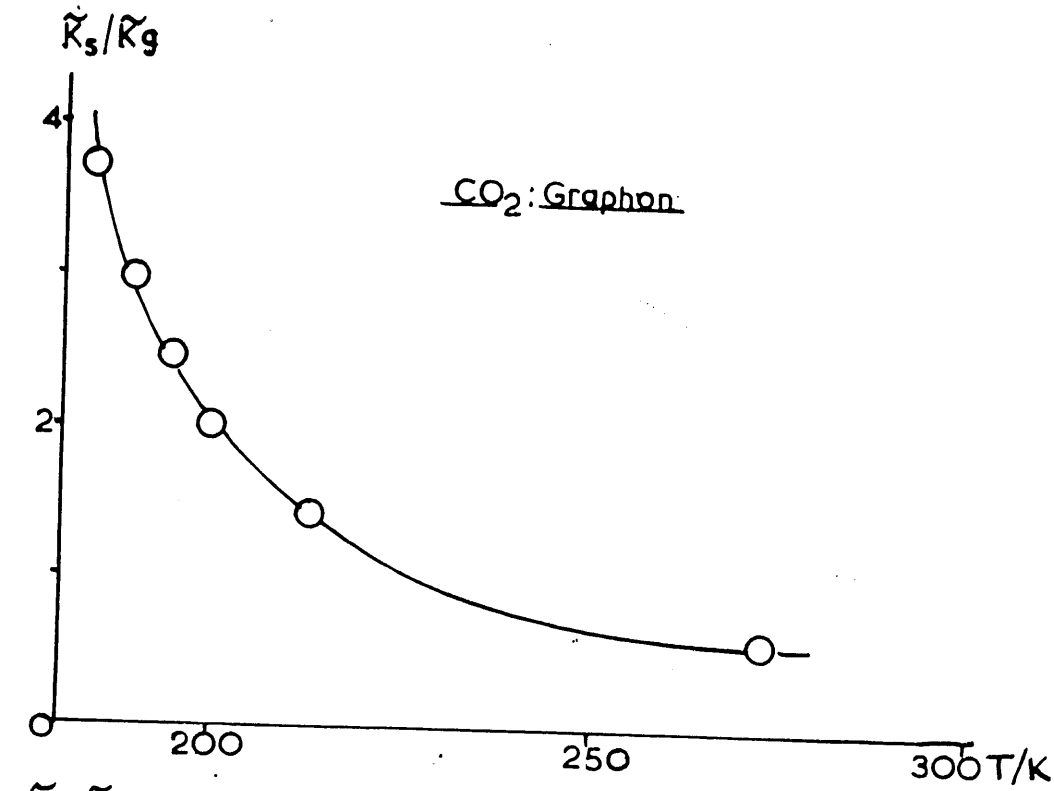


sorbable gases exhibit a greater $\tilde{K}_s$ component; however $\tilde{K}_s/\tilde{K}_g$ for Graphon is smaller in each case than for the corresponding value on the Carbolac membrane.

This is probably due to the smaller surface area and hence extra flow on Graphon. Fig. 5.3.14 shows the variation of $\tilde{K}_s/\tilde{K}_g$ with temperature for CO_2 and H_2S flow on Graphon. Hamilton (1980) obtained similar graphs for the temperature dependence of $\tilde{K}_s/\tilde{K}_g$ for hydrocarbons on Graphon.

The quantity $\tilde{K}_s/A$ (where A is the surface area in m^2 per m^3 porous medium) has been considered a measure of the effectiveness of the carbon in promoting extra flow (Ash Baker and Barrer 1967). This has therefore been evaluated and is listed in table 5.3.3 and plotted against pressure in Fig. 5.3.9, Fig. 5.3.10, Fig. 5.3.12 and Fig. 5.3.13 for some of the systems studied. The $\tilde{K}_s/A$ values obtained for Carbolac fall almost two orders of magnitude below those for Graphon, indicating that the surface is inhomogeneous with blind pores and micro pores as already indicated by crystallographic studies (Briscoe and Warren 1942). This degree of roughness in the surface made the Carbolac less effective in promoting extra flow than Graphon which has a smooth homogeneous surface (Heckman and Harling 1966, Beebe, Millard, Cynarski 1953) upon which molecules may move easily. The mechanism by which extra flow occurs may be visualised in two ways, either as a random walk diffusive process (Aylmore and Barrer 1966) or in hydrodynamic terms. (Gilliland 1958). The random walk model is based upon the idea of molecules moving from one adsorption site to another, and it results in the definition of diffusion coefficients. The hydrodynamic model is more applicable beyond monolayer coverage

(fig 5·3·14) $\tilde{K}_s/\tilde{K}_g$ versus T



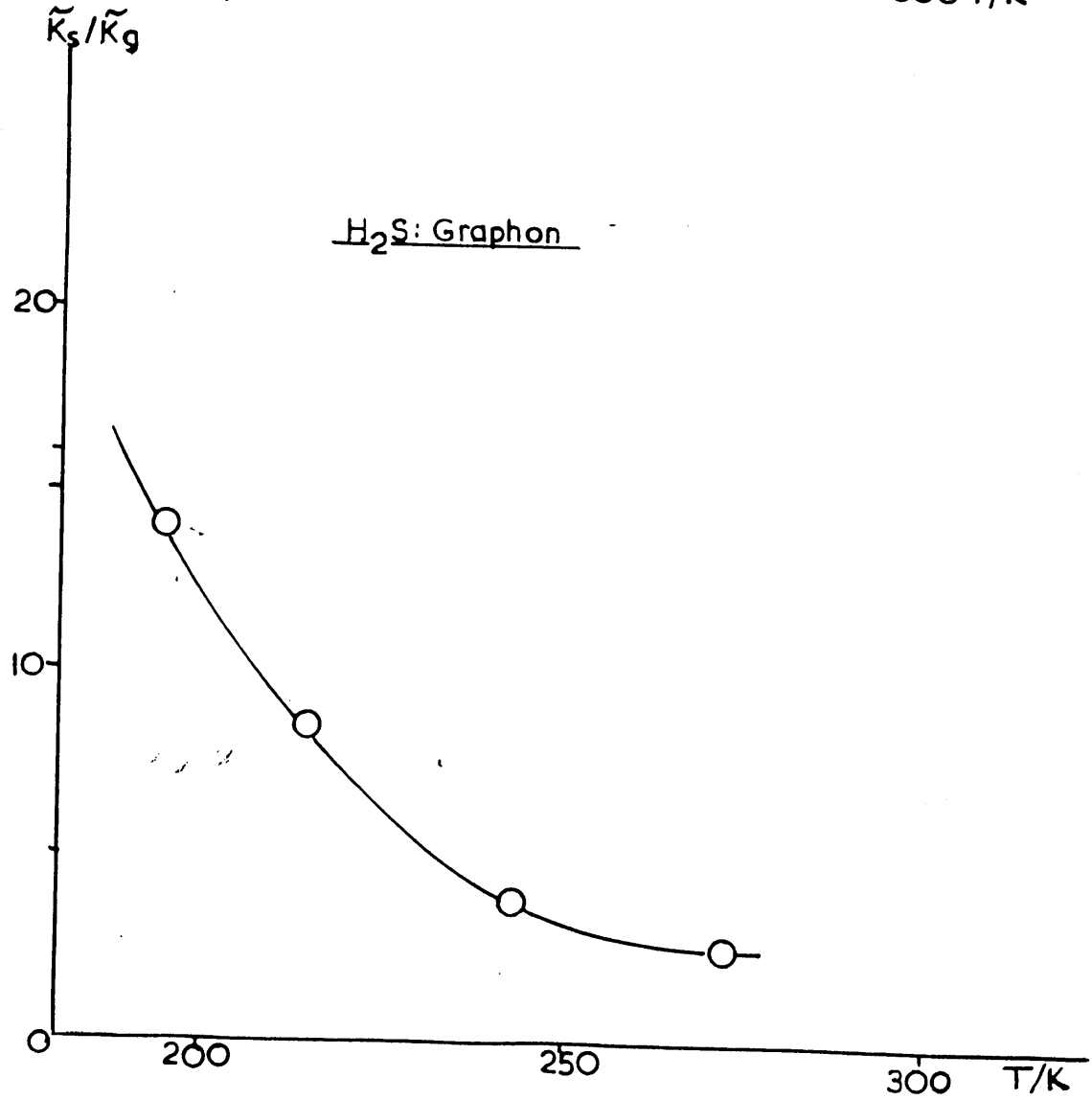


Table 5.3.3

$\tilde{K}_s/\tilde{K}_g$ and $\tilde{K}_s/A$

Carbolac (Where $\tilde{K}$ vs p_1 is constant)

Gas	T/K	$10^7\tilde{K}/m^2s^{-1}$	$10^8\tilde{K}_g/m^2s^{-1}$	$10^7\tilde{K}_s/m^2s$	$\tilde{K}_s/\tilde{K}_g$	$10^{16}\tilde{K}_s/A/m^3s^{-1}$
N_2	195	1.75	6.61	2.99	4.52	3.03
	273.2	2.08	7.86	2.79	3.55	2.82
CO_2	195	7.73	5.28	7.20	13.65	7.29
	273.2	4.18	6.27	3.55	5.67	3.59
H_2S	195	18	6.00	17.40	29.00	7.61
	273.2	4.70	7.13	3.99	5.59	5.66

Graphon (at p_1 = 10 cmHg)

N_2	195	17.1	95.8	7.52	0.785	94.3
	273.2	15.4	113	4.10	0.36	51.4
CO_2	184	34.2	74.2	26.8	3.60	336
	190.5	29.0	75.5	21.4	2.84	268
	195	26.0	76.4	18.4	2.40	231
	200	23.0	77.4	15.26	1.97	191
	213.2	18.6	79.9	10.61	1.33	133
	273.2	13.7	90.6	4.65	0.51	58.3
H_2S	195	112.1	86.9	103	11.9	1290
	213.2	74.2	90.9	65.1	7.16	816
	243.2	40.0	97.0	30.3	3.12	380
	273.2	30.6	102.8	20.3	1.98	254
SF_6	195	24.1	41.7	19.9	4.78	249
Ar	184	16.4	77.9	8.61	1.11	108

and has thereforenot been used in this study. It relates the flow of adsorbed molecules to the shear stress between them and the surface.

5.3.5 Diffusion coefficients

The first comprehensive study of diffusion coefficients relative to both temperature and coverage was that of Carman and Raal (1951) in which they derived diffusion coefficients for the flow of SO_2 and CF_2Cl_2 through Carbolac and Linde Silica membranes. In their work and in later studies the variation of the differential diffusion coefficient with coverage was very distinctive, an initial increase being observed followed by a maximum at approximately $\frac{\nu}{\nu_m} = 1$. After this a minimum occurred followed by a relatively constant value in the region of multilayer formation. As $p_1/p_0 = 1$ was approached the diffusion coefficient once more increased and poor reproducibility was obtained as capillary condensation started. In this study the integral diffusion coefficient $\tilde{D}$ and the differential diffusion coefficient D were obtained using the following equations (Section 2.6)

$$\tilde{D}(c^\circ) = \frac{\ell}{Ac} \frac{J_\infty}{c^\circ} \qquad (50)$$

where c° = total ingoing concentration

$$c^\circ = c_g + c_s$$

$$= c_g' + Ac_s' \qquad (54)$$

$$D(c^\circ) = \frac{\ell}{Ac} \left(\frac{\partial J}{\partial c^\circ}\right)$$

$\tilde{D}$ is an average value over a large concentration difference in the membrane and D relates to an infinitessimally small concentration difference. The two are related by the equation as shown in Section 2.6.

$$\tilde{D}(c^\circ) = \frac{1}{c^\circ} \int_0^{c^\circ} D(c^\circ)dc \quad \text{for the boundary conditions used} \qquad (51)$$

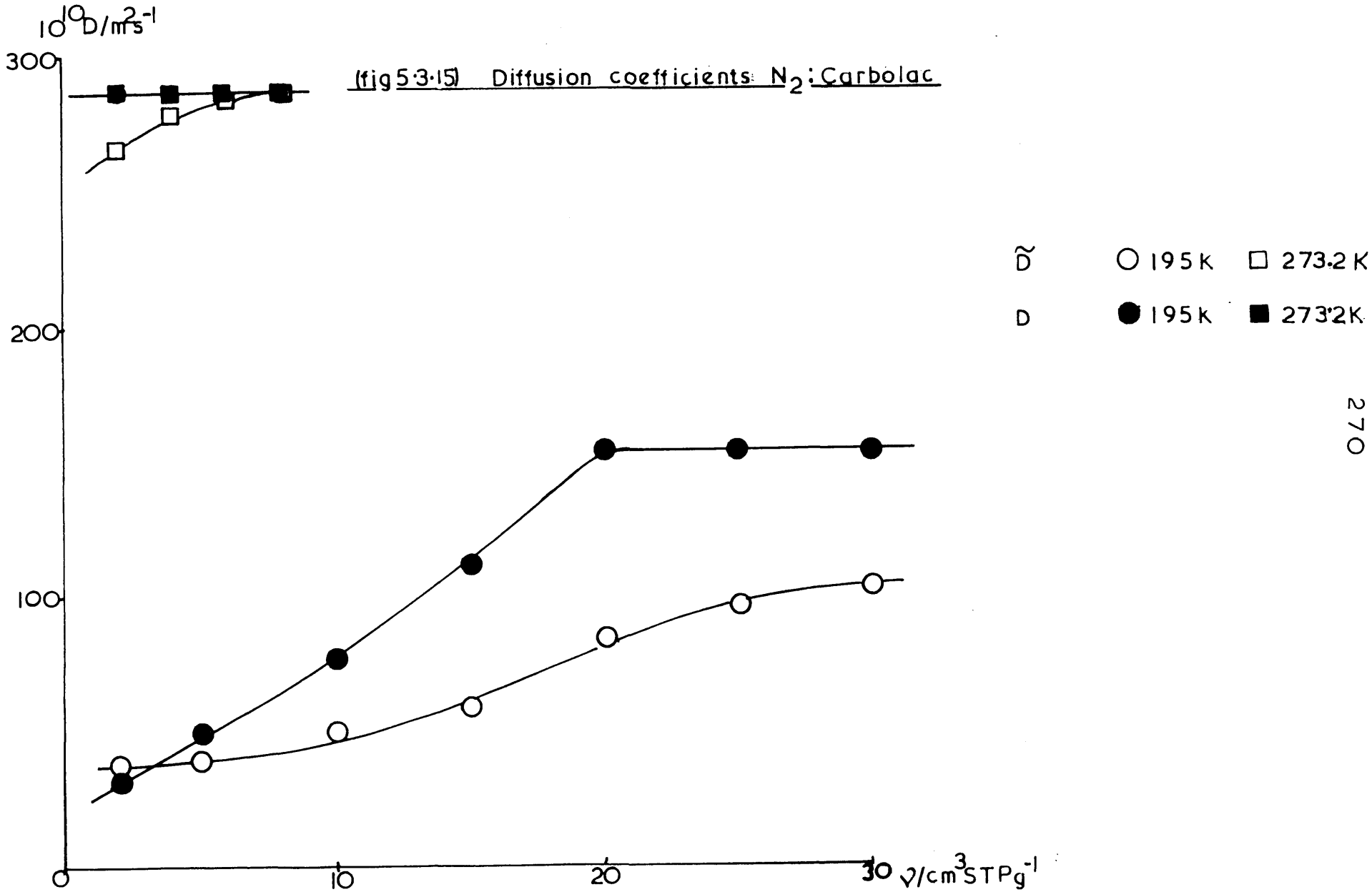
In this study $\tilde{D}$ and D were calculated from the steady state flux and from the gradient of J_∞ plotted against $c^\circ/molm^{-3}$ of which Fig. 53.21a is typical. Other methods of evaluation, utilizing the slope of the isotherm and differential permeabilities, were disregarded as they involved two graphical differentiations and were therefore in principle less accurate. Surface and gas phase diffusion coefficients may be evaluated, however table 5.3.3 shows that gas phase flow is small for the systems studied here and that the extra flow approximates to the total flow. Therefore only total diffusion coefficients have been evaluated.

Fig. 5.3.15 to fig. 5.3.17 show $\tilde{D}$ and D for transport through the Carbolac membrane. These increase with increasing coverage for all gases, and in the case of CO_2 and H_2S they carry on increasing beyond monolayer coverage in contrast to the observations of Carman and Raal. Graphs of similar form were obtained by Ash Barrer and Pope (1963) for CO_2 and N_2 flow through Carbolac at 190K and by Ash Barrer and Lowson (1973) for N_2 flow through Carbolac at 233.15K.

In Fig. 5.3.15 and fig. 5.3.17 it can be seen that where the curve for $\tilde{D}$ passes through a maximum or a minimum it is crossed by that for D. This could have been predicted from the relationship

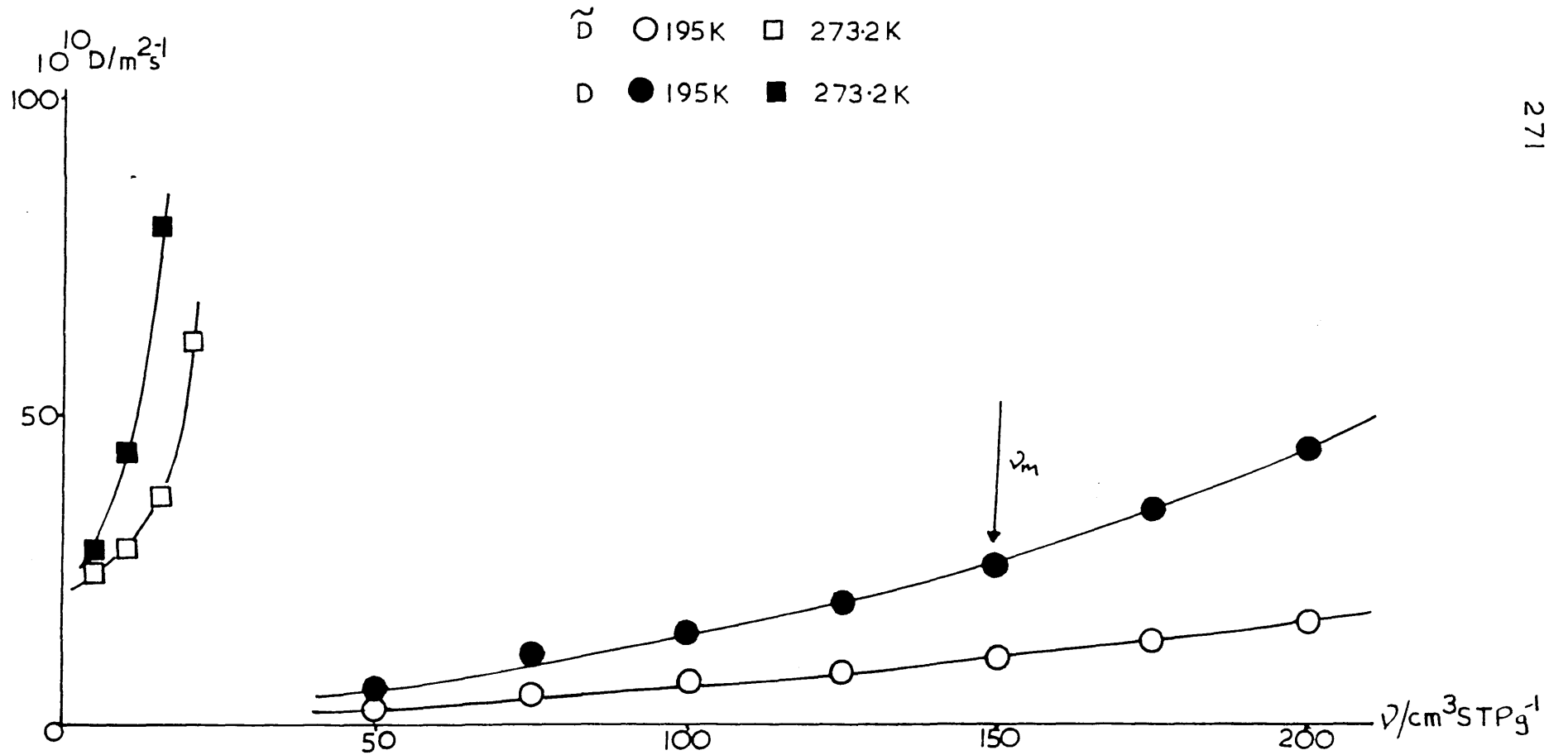
$$D(c^\circ) = \tilde{D}(c^\circ) + c^\circ \left[\frac{\partial \tilde{D}}{\partial c^\circ} (c^\circ) \right] \qquad (52)$$

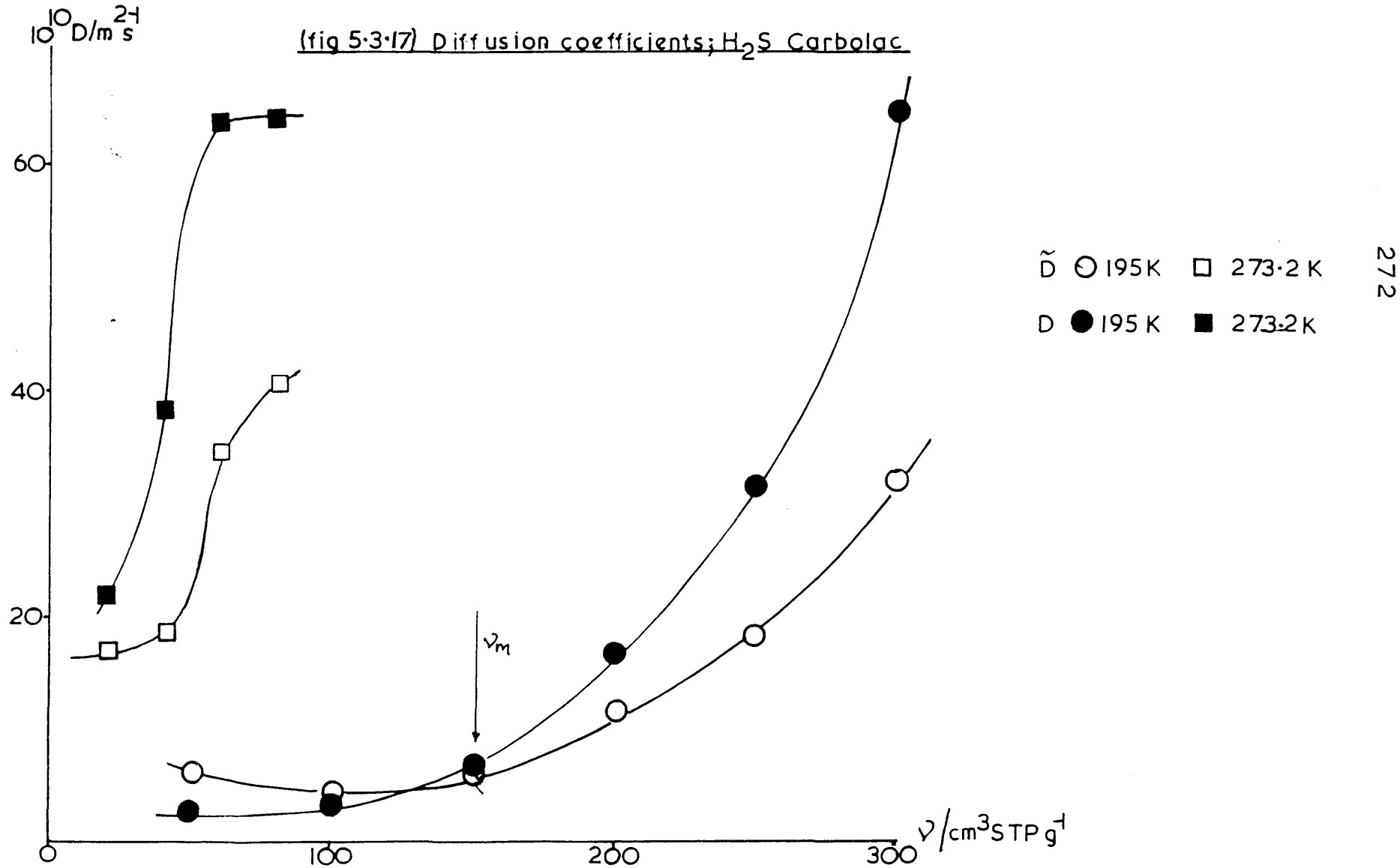
and is also evident for the Graphon membrane diffusion coefficients. (fig. 5.3.18, fig. 5.3.21 and fig. 5.3.22)



(fig 5·3·15) Diffusion coefficients: N_2 : Carbolac

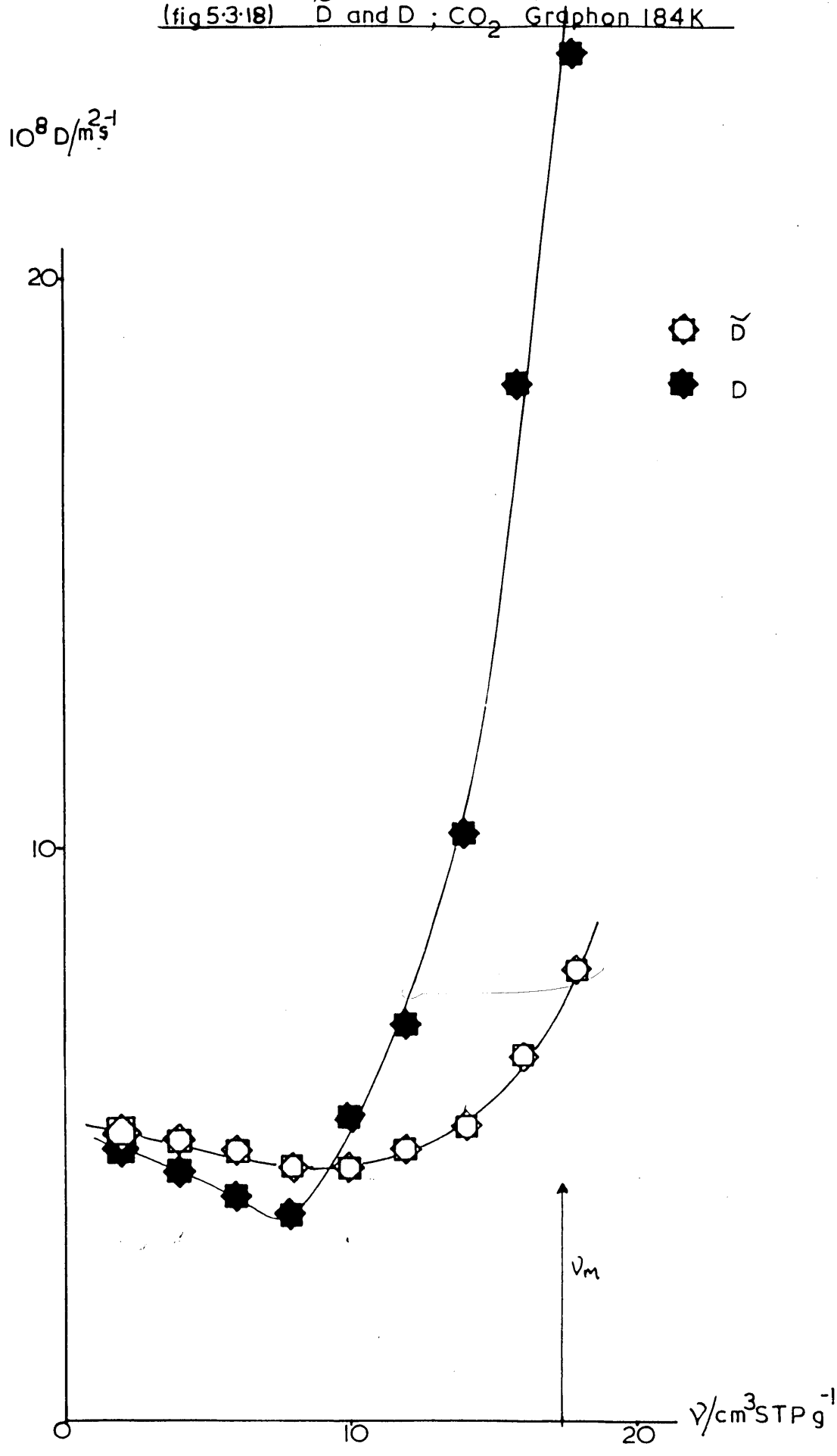
(fig 5·3·16) Diffusion coefficients CO_2: Carbolac



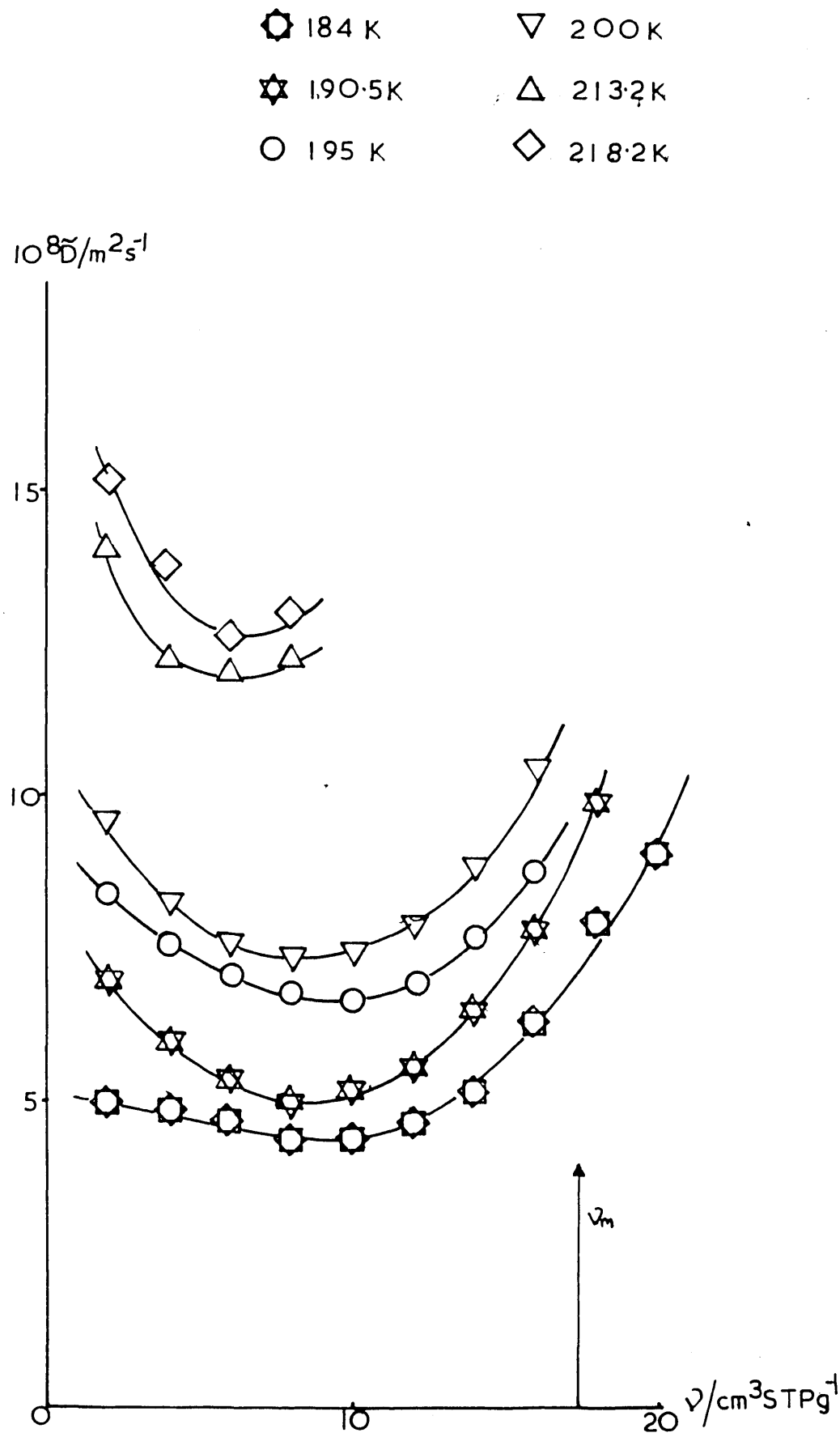


(fig 5·3·17) Diffusion coefficients; H_2S Carbolac

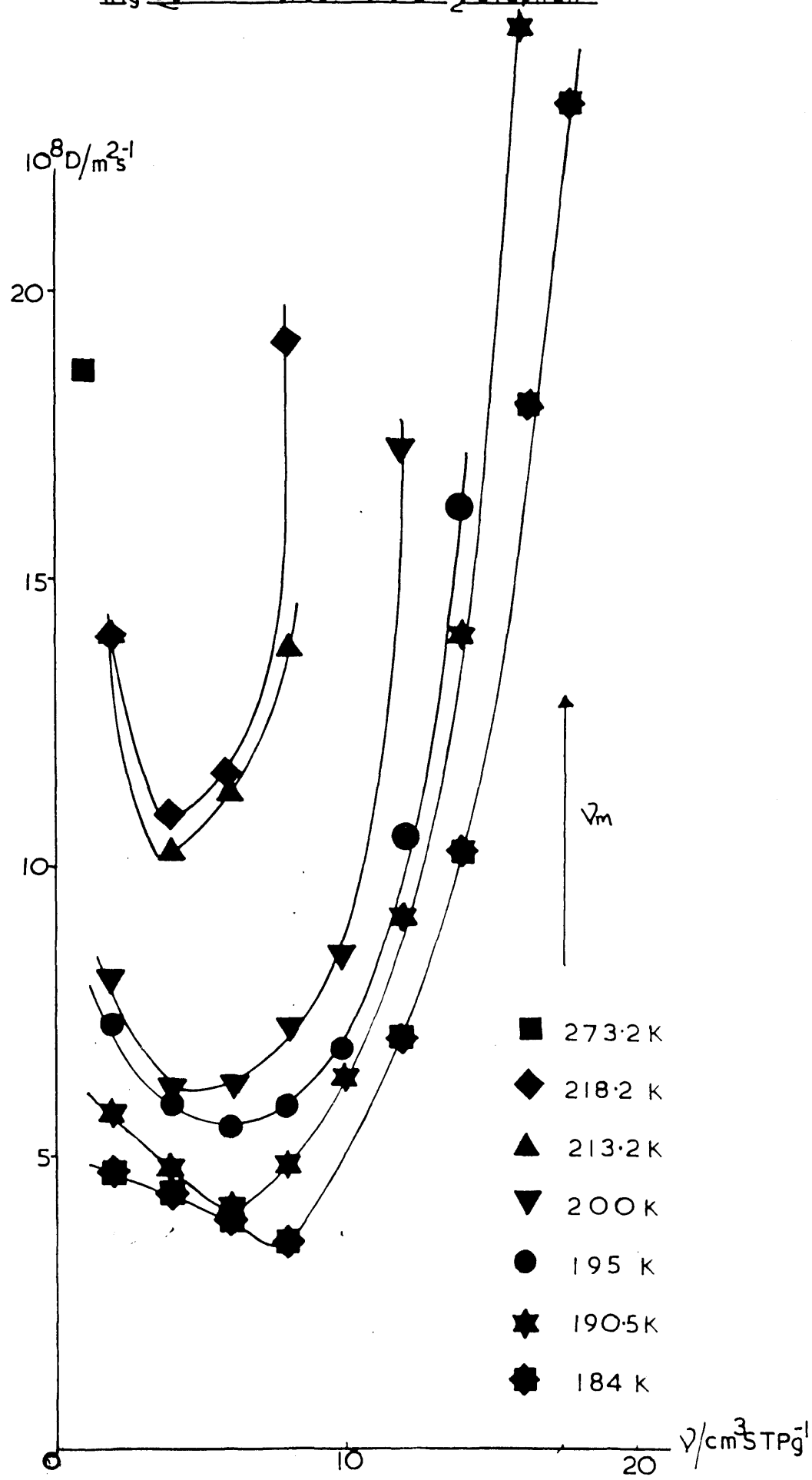
(fig 5·3·18) $\tilde{D}$ and D ; CO_2 Graphon 184 K



(Fig 5·3·19) $\tilde{D}$ versus v : CO_2 Graphon

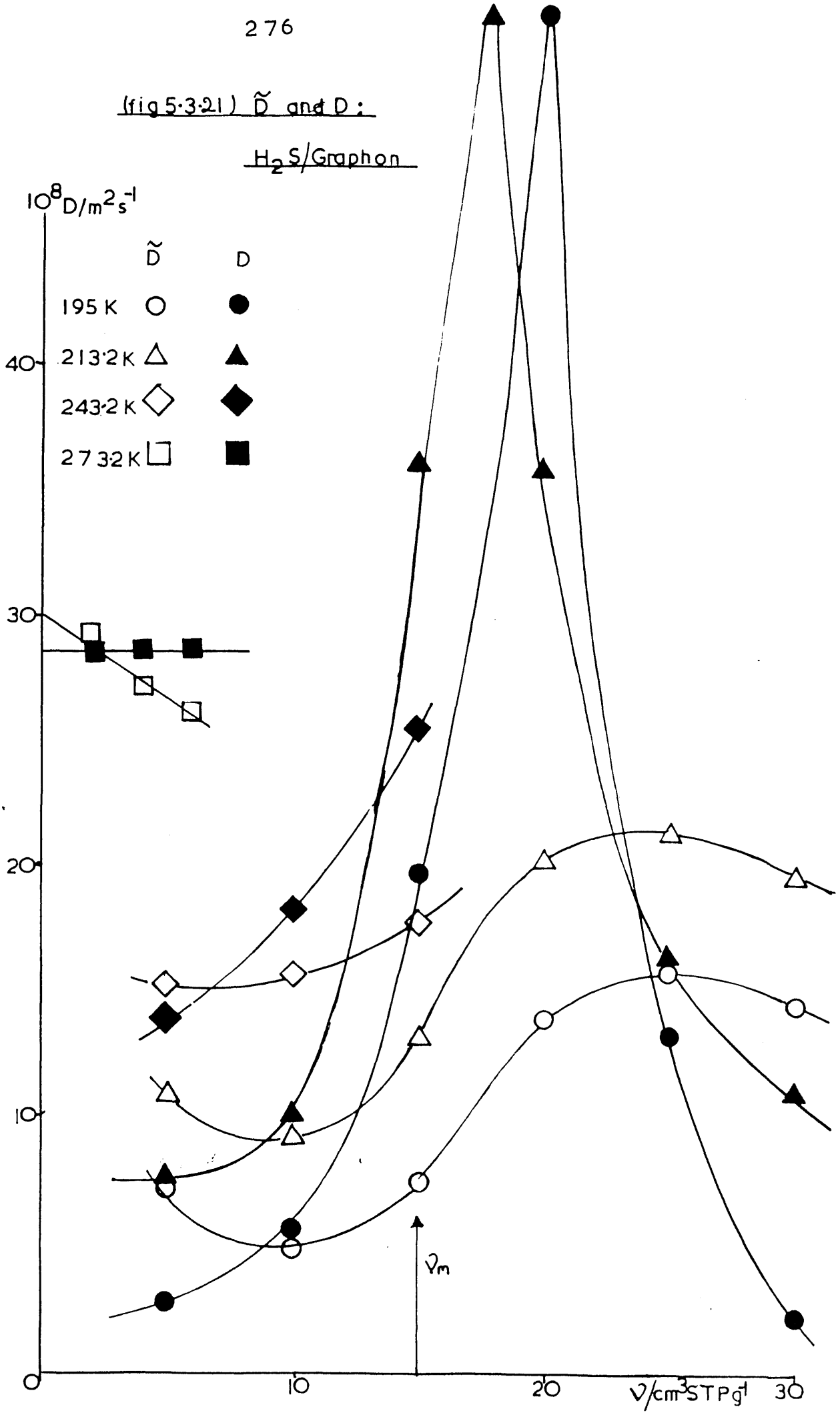


(fig 5.3.2d) D versus ν : CO_2/Graphon

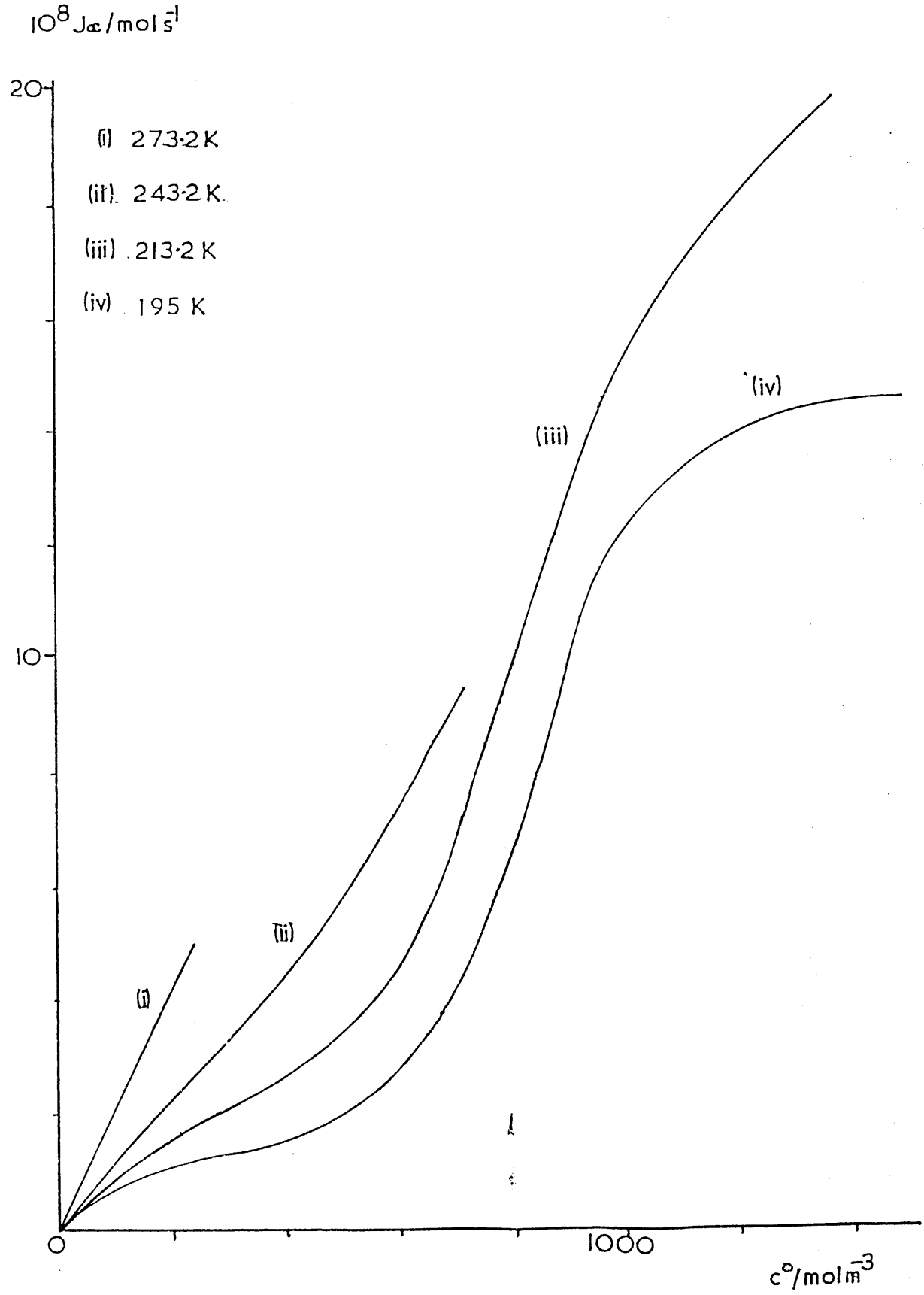


(fig 5·3·21) $\tilde{D}$ and D :

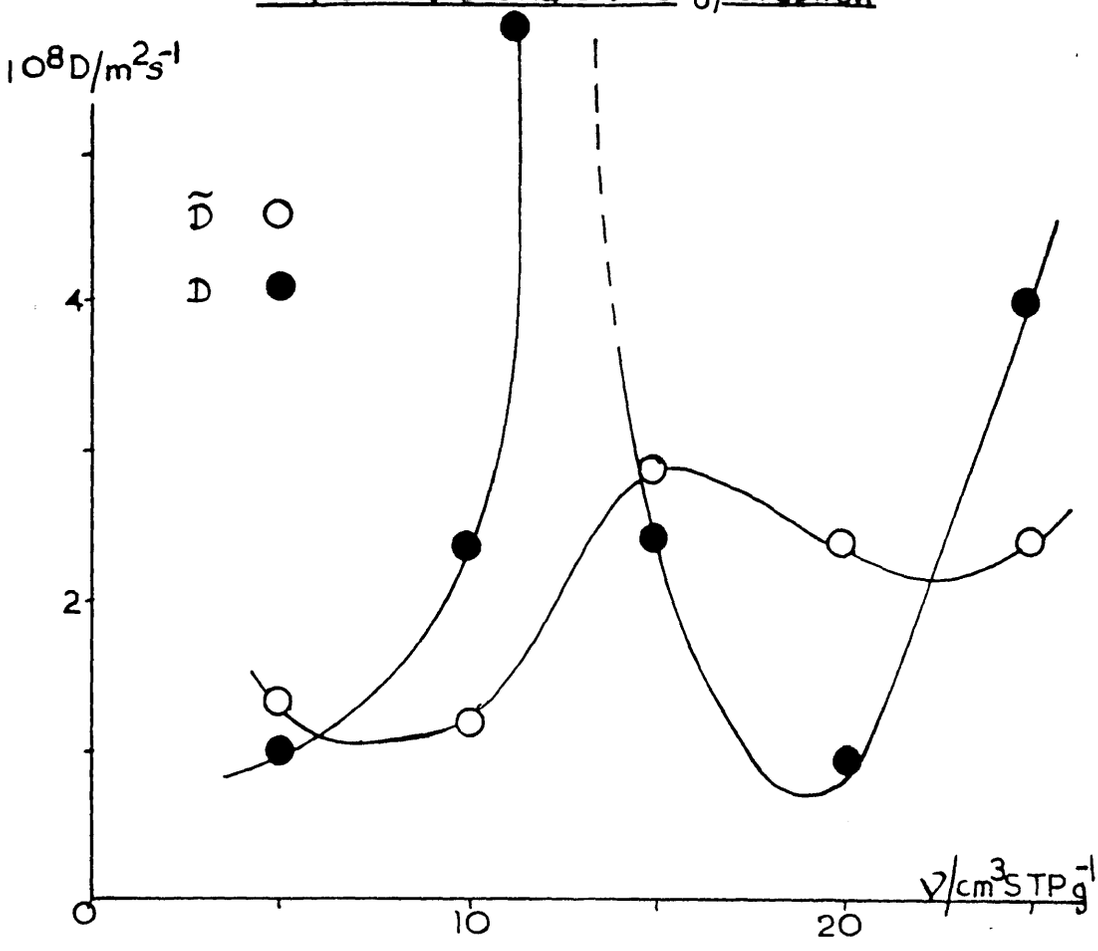
H_2S/Graphon



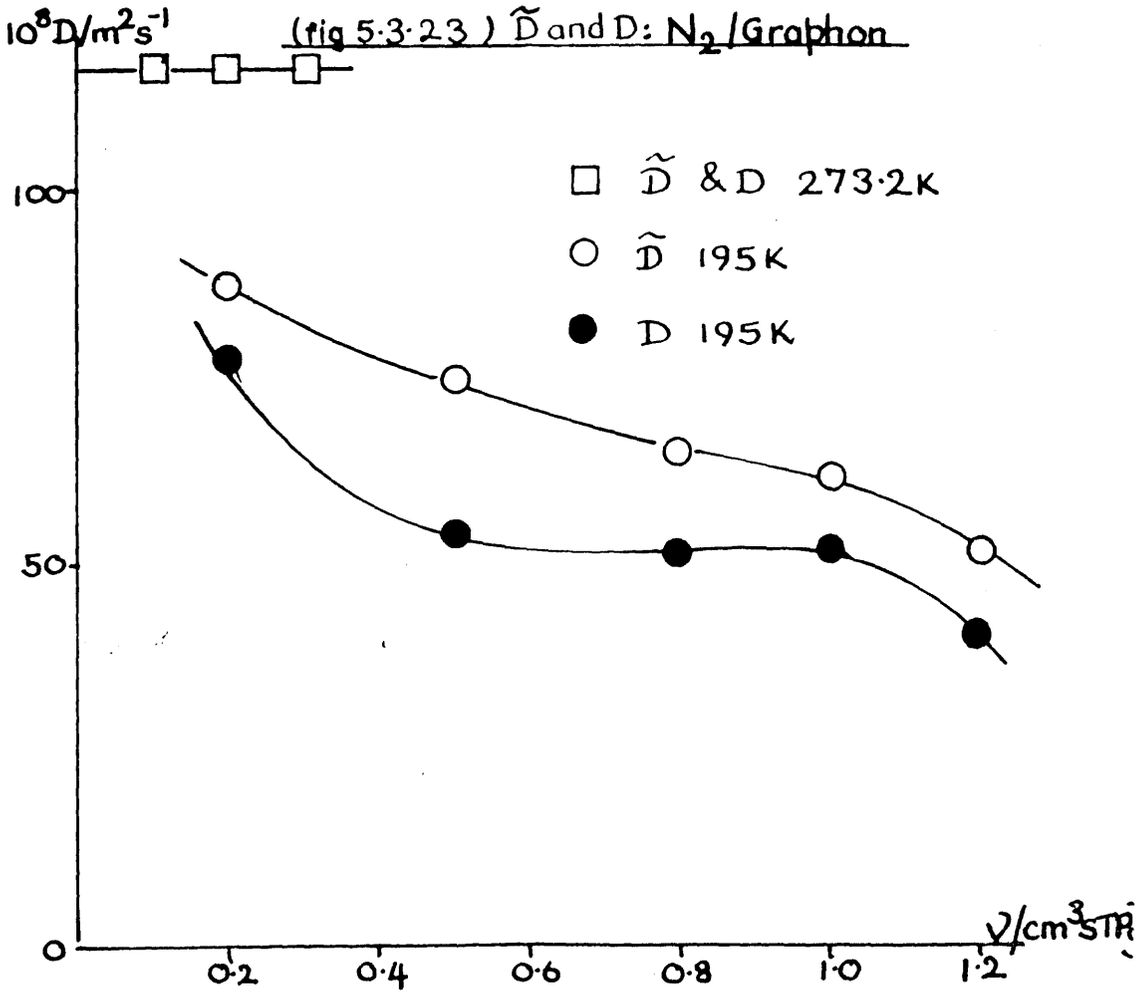
(fig 5·3·21a) J_∞ versus c_1 / H_2S / Graphon



(fig 5·3·22) $\widetilde{D}$ and D : SF_6/Graphon



(fig 5·3·23) $\widetilde{D}$ and D: N_2/Graphon



The integral and differential diffusion coefficients as a function of coverage for gas flow through Graphon are shown in fig. 5.3.18 to fig. 5.3.23. For all systems studied the form of the graphs obtained is similar to that described by Carman and Raal and $\tilde{D}$ and D are similar in magnitude to the $\tilde{D}$ and D values for hydrocarbon flow through Graphon which were evaluated by Hamilton (1980) It can be seen that $\tilde{D}$ and D for H_2S flow through Graphon are twice the value of those for CO_2 flow at the same coverage possibly due to increased adsorption of H_2S. Also that the diffusion coefficients for Graphon are two orders of magnitude larger than those for Carbolac, due to efficiency of extra flow generation, as discussed in Section 5.3.4. Fig. 5.3.22 shows $\tilde{D}$ and D for SF_6 flow through Graphon at 195K with increasing coverage. The integral diffusion coefficient passes through a minimum, followed by a maximum and then another minimum and the differential diffusion coefficient crosses the curve in each of the three places where $\frac{\partial \tilde{D}}{\partial c^\circ} = 0$. Very similar curves were obtained by Ash Baker and Barrer (1967) for SF_6 flow through another Graphon membrane. For this system the maximum and minimum at $\frac{\nu}{\nu_m} = 1$ and the increase in D near to $P_1/P_0 = 1$ as described by Carman and Raal are clearly visible (fig. 5.3.22). Fig. 5.3.23 shows $\tilde{D}$ and D for N_2 flow through Graphon at 195K, at low coverage. Both curves decrease gently with increasing coverage as the monolayer capacity is at a much higher value of ν.

The C_3H_8/Graphon system was not analysed in detail in this study as a full analysis has already been given by Hamilton.

It may be seen from fig. 5.3.18 to fig. 5.3.21 that the diffusion coefficients obtained are dependent upon temperature. This dependence can be described by an Arrhenius type of relationship.

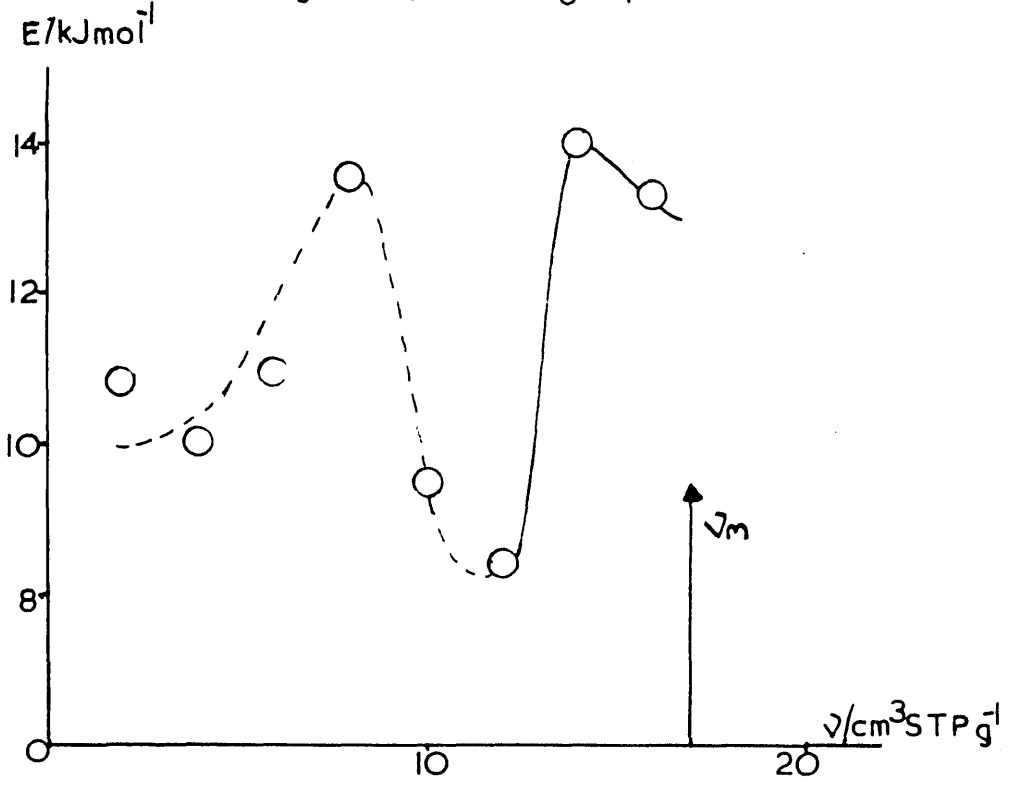
$$D = D_0 \exp(-E/RT)$$

where $E(Jmol^{-1})$ is the activation energy of diffusion at constant coverage. In previous studies (Carman & Raal (1951) and Hamilton (1980)) the activation energy was found to remain constant with increasing coverage until monolayer capacity was obtained, at which point a sharp decrease to another constant value was observed. However an initial decrease in E was observed by Barrer and Strachan(1955) for Ar, Kr and N_2 flow through Carbolac which they explained in terms of a heterogeneous surface, the most energetic sites of which were filled first, requiring the largest energy for diffusion.

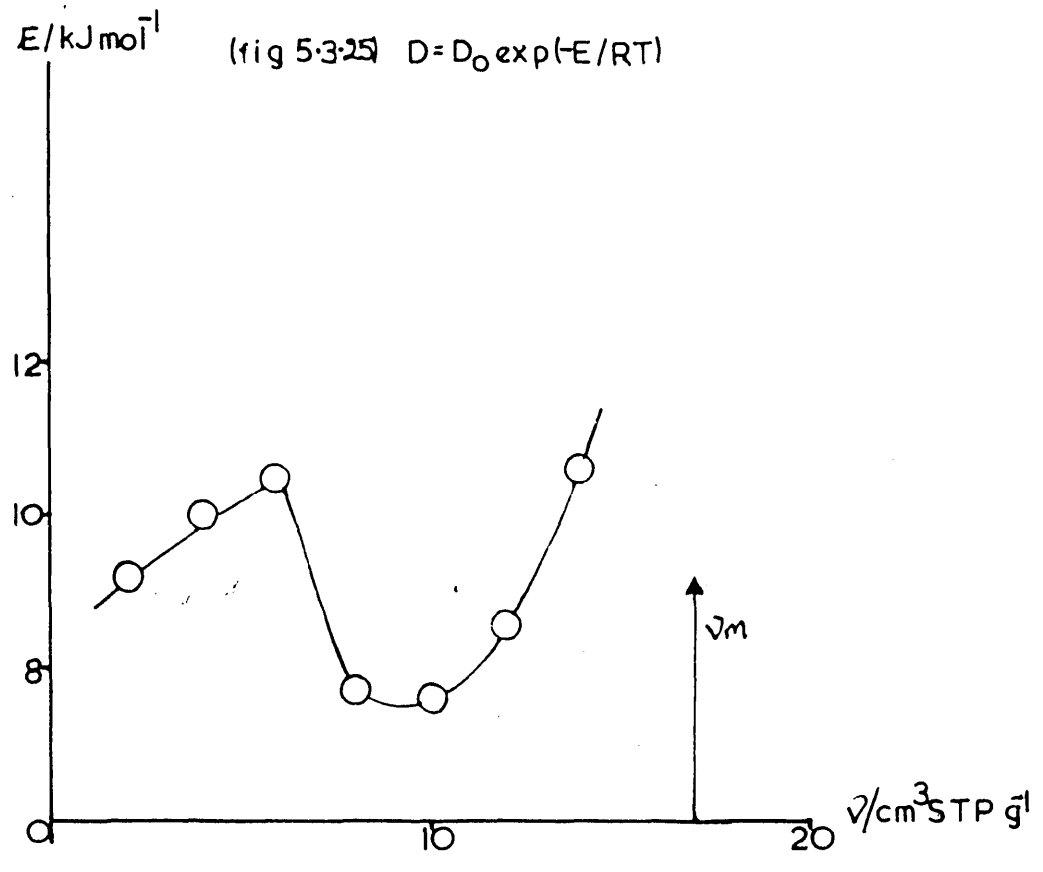
Ross and Good (1956) in a study of n-Butane flow through Graphon however observed an initial increase in E followed by a maximum at monolayer coverage. They attributed this to attractions between adsorbed molecules which become greater as coverage increased, inhibiting diffusion. The activation energies obtained in this study were calculated from graphs of $\ln D$ versus $^1/_T$ (e.g. fig. 5.3.27) and are shown in fig. 5.3.24 to 5.3.26. The results for CO_2 flow upon Graphon are rather scattered, however for both CO_2 and H_2S a maximum value of E is evident at or near ν_m, followed by a sharp decrease in the case of H_2S. These observations coincide with those of Ross and Good, supporting the interpretation of their results in terms of the importance of molecular interactions. In the CO_2/Graphon and H_2S/Graphon systems this phenomenum has already manifested itself in that both systems gave type III adsorption isotherms.

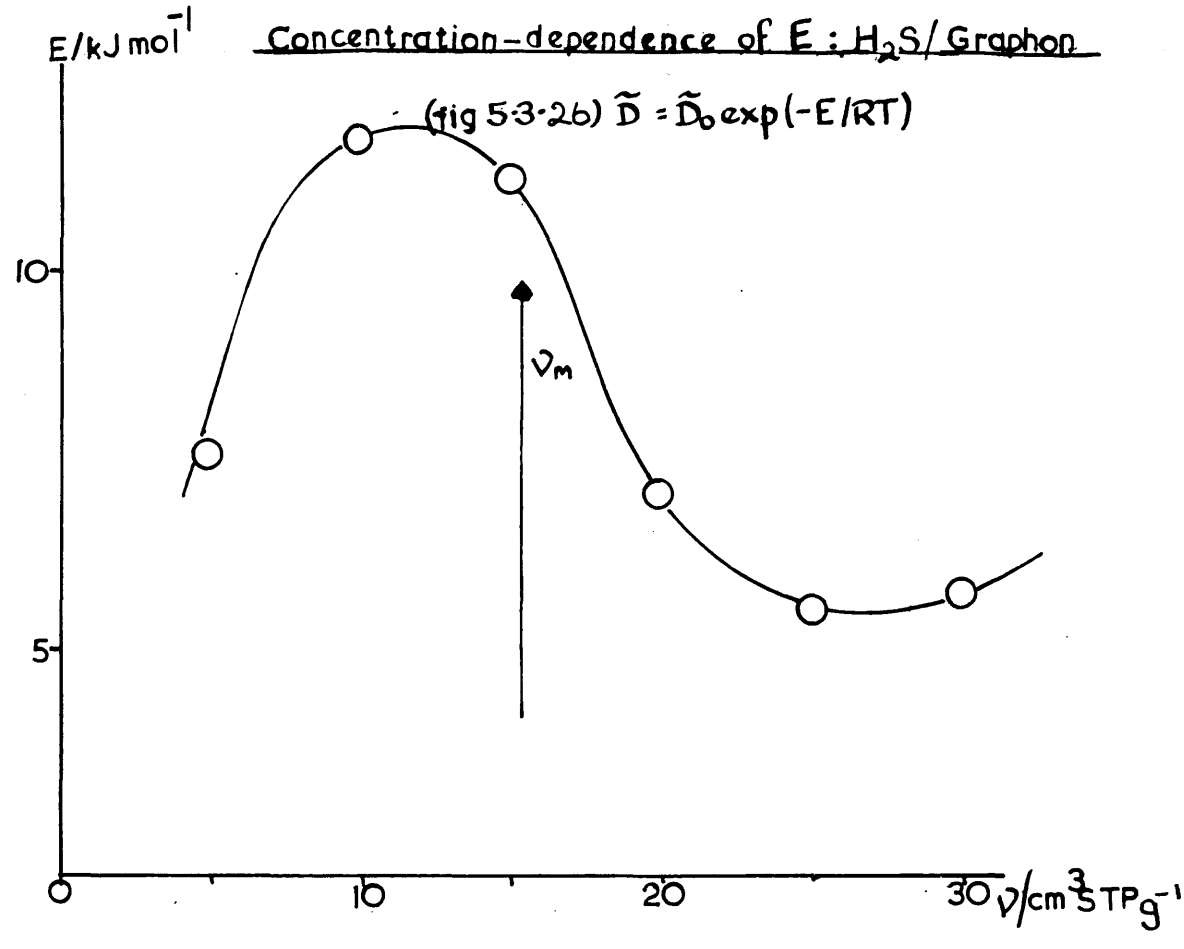
Concentration-dependence of E : CO_2 /Graphon

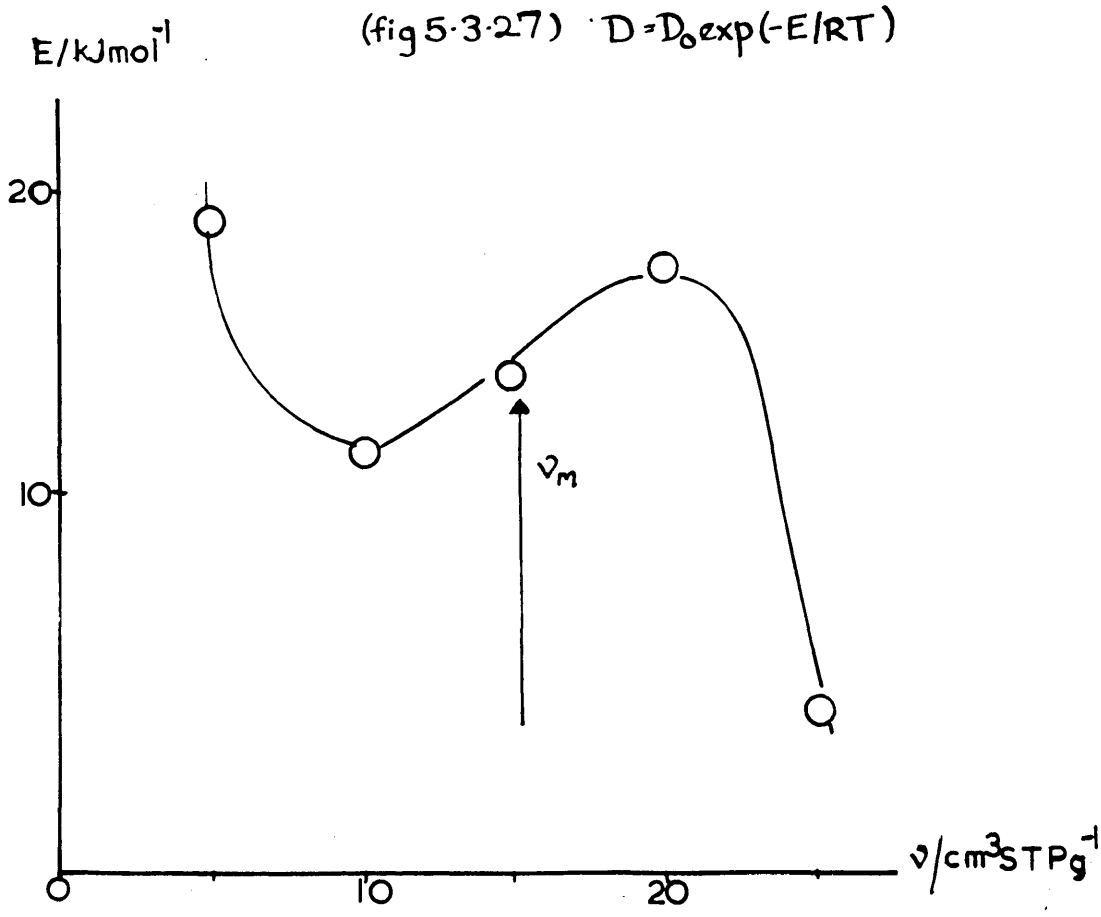
(fig 5·3·24) $\tilde{D} = \tilde{D}_0 \exp(-E/RT)$



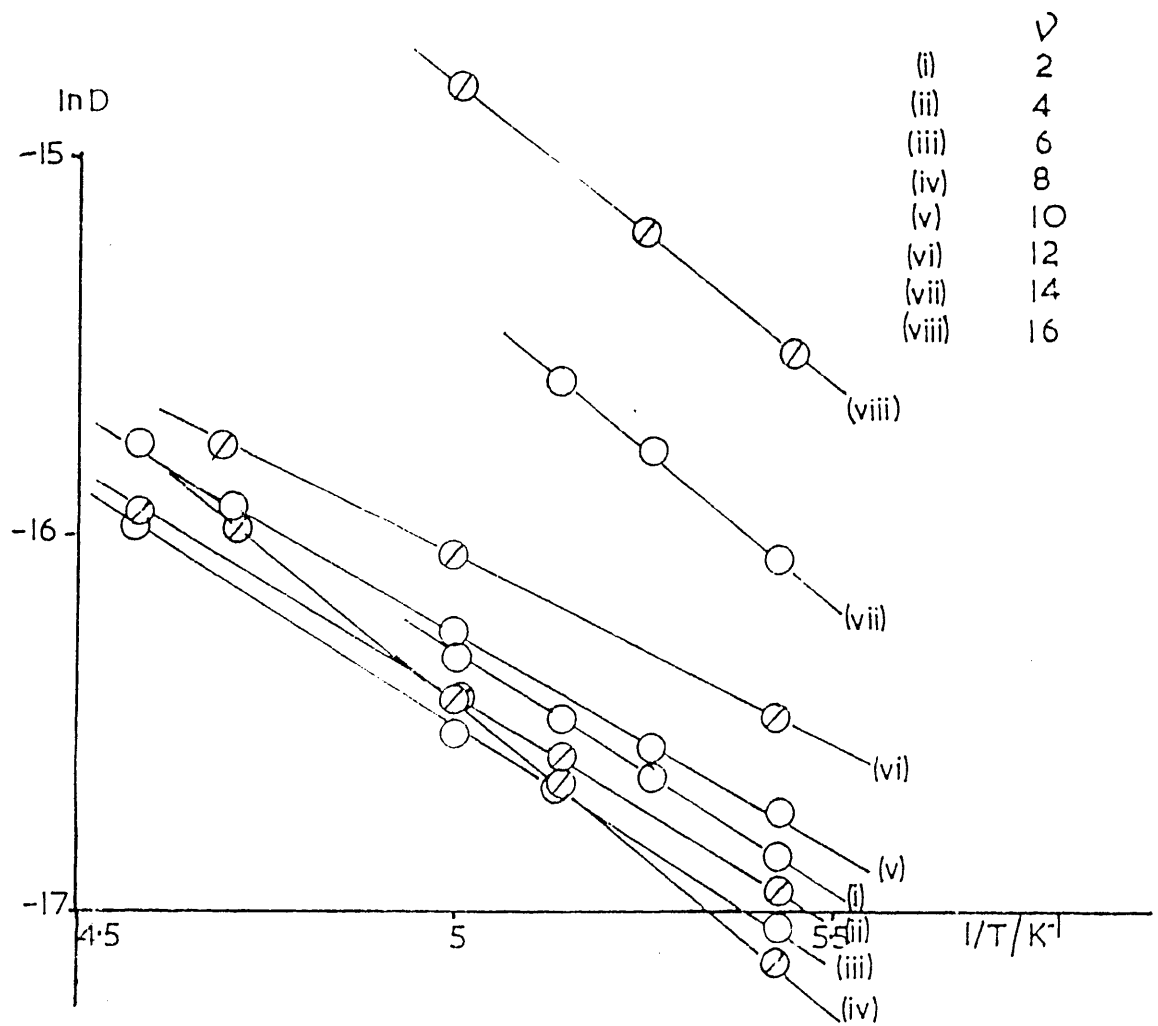
(fig 5·3·25) $D = D_0 \exp(-E/RT)$




E/kJ mol⁻¹
Concentration-dependence of E : H₂S/Graphon
(fig 5·3·26) D̃ = D̃₀ exp(-E/RT)
10
5
νm
0
10
20
30
ν/cm³STPg⁻¹


E/kJmol⁻¹
(fig 5·3·27) D = D₀ exp(-E/RT)
20
10
νm
0
10
20
ν/cm³STPg⁻¹

(fig 5·3·28) LnD versus 1/T /CO_2/Graphon



5.4 Binary mixture flow

5.4.1 Introduction

The flow of binary gas mixtures through the Graphon and Carbolac membranes was investigated. The holders of both these membranes had been constructed as shown in fig. 3.2, in order to allow circulation of the ingoing gas mixture. Steady state flow of the sorbable component was first achieved and then the second ('indicator') gas was introduced to the ingoing side and its permeability measured. In this way the blocking effect of the adsorbed film could be quantified.

If the transport of a mixture of gases occurs entirely by gas phase flow in the Knudsen regime, then the components of the mixture flow independently of each other. Kammermeyer (1958) assumed that extra flow and gas phase flow were also independent of each other for dilute adsorbed films, and following this Aylmore and Barrer (1966) showed that when Henry Law adsorption occurred two gases exhibiting extra flow would each be transported independently. Outside the Henry's Law range, stronger adsorption can cause the pores to become partially blocked by the adsorbed molecules which results in a reduction of gas phase flow. Thus extra flow and gas phase flow are no longer independent of each other. Ash Barrer and Pope (1963b) (Ash Barrer and Lowson 1973 and Ash Barrer and Sharma 1976) have shown that the presence of an adsorbed layer of molecules inhibits or, in some cases, totally blocks the flow of a non sorbed gas. A substantial extra flow of the sorbable component still occurs however in the adsorbed layer, making the membrane effectively semi-permeable.

Hamilton (1980) plotted the relative permeability against P_1/P_0.

This produced a "universal" curve for the blockage of He (flowing through the Graphon membrane used in this study) by two hydrocarbons at various temperatures.

The same method for presentation of data has also been adopted in this investigation (Section 4.4).

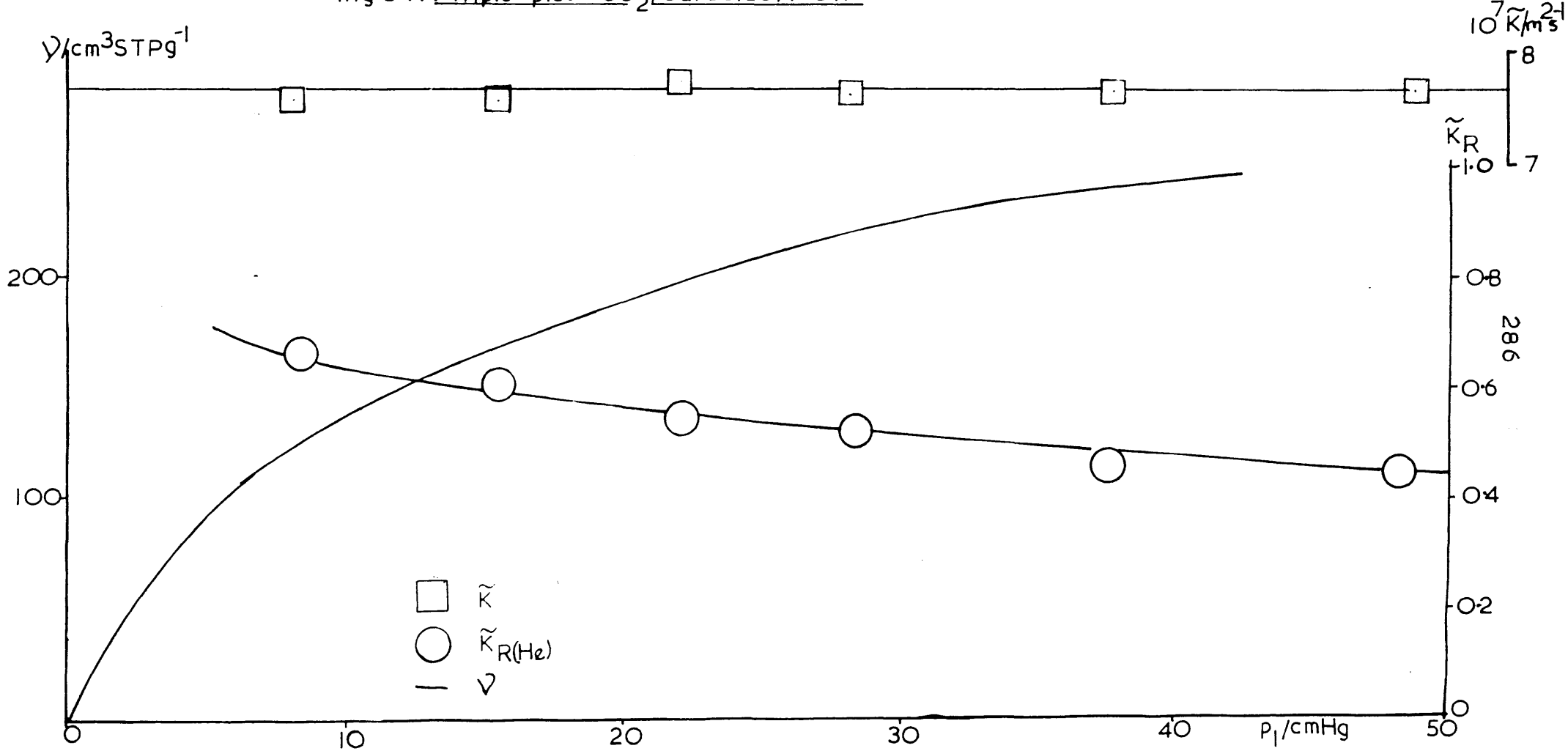
Helium has been used as a non-sorbed indicator gas, and the blockage of nitrogen and argon (weakly-sorbed indicator gases) has also been investigated.

The determination of relative permeabilities for gas flow through the Carbolac membrane was particularly difficult, due to the instability of the membrane. It was therefore necessary to check the pure He and pure N_2 permeabilities at frequent intervals.

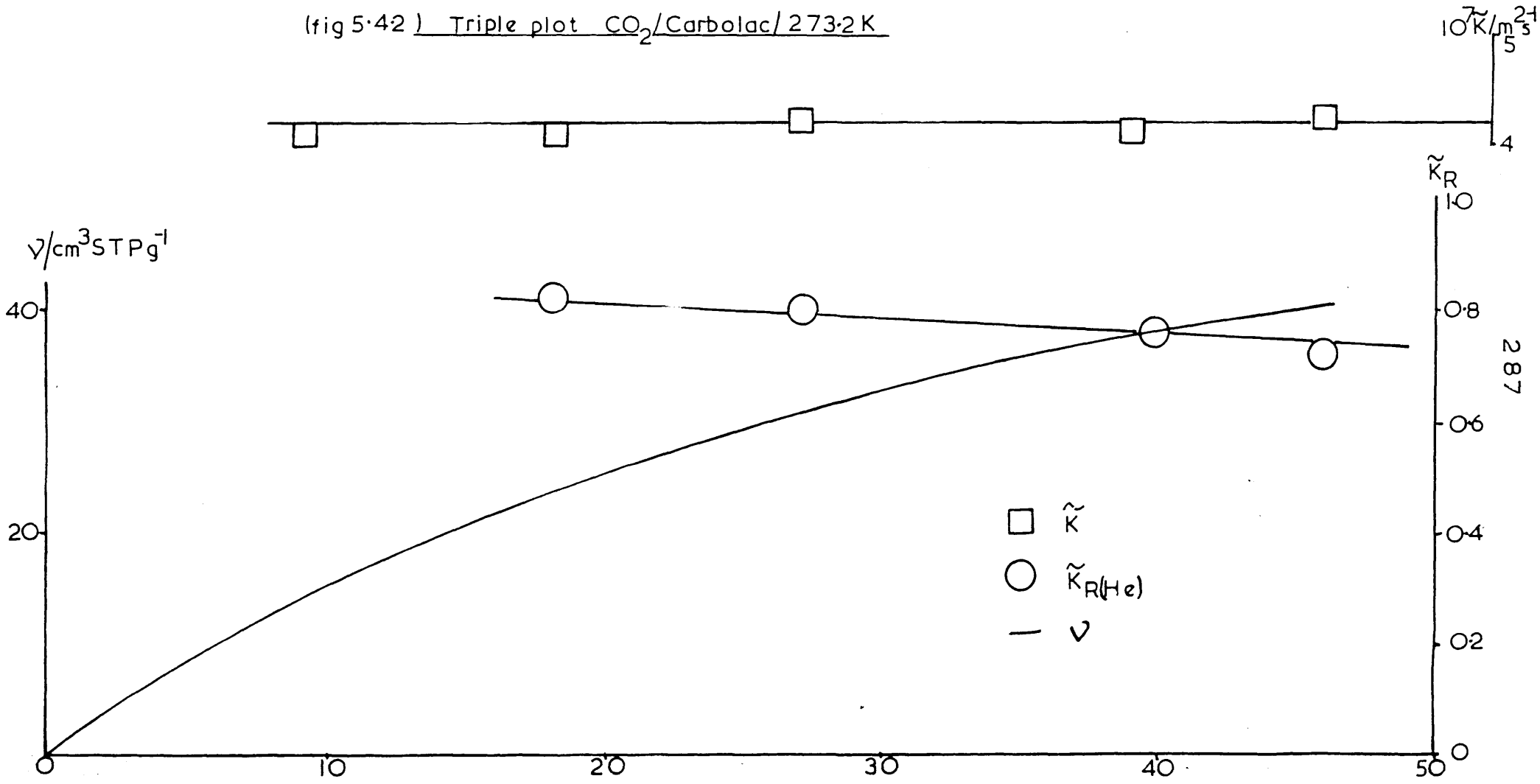
5.4.2 Relationship between ν, $\tilde{K}$ and $\tilde{K}_R$(He)

In order to show a possible relationship between the amount of gas adsorbed, the permeability of the sorbable gas and the degree of blockage, triple plots have been constructed (fig. 5.4.1 to fig. 5.4.9). These show $\tilde{K}$ and ν for the sorbable gas, and $\tilde{K}_{RHe}$(mix). If $\tilde{K}_R$ equals unity, there is no blockage effect, however if K_R equals zero the helium flow has been totally prevented by layers of the sorbable gas inside the pores. Throughout the study it was assumed that the flow of the sorbable component was not inhibited by the presence of the indicator gas. It has since been shown by measurement of the blocked N_2 permeability followed by the total flux for the CO_2/N_2/Graphon system, that N_2 does inhibit the flow of CO_2 to a limited extent. (Cf. Bott 1986).

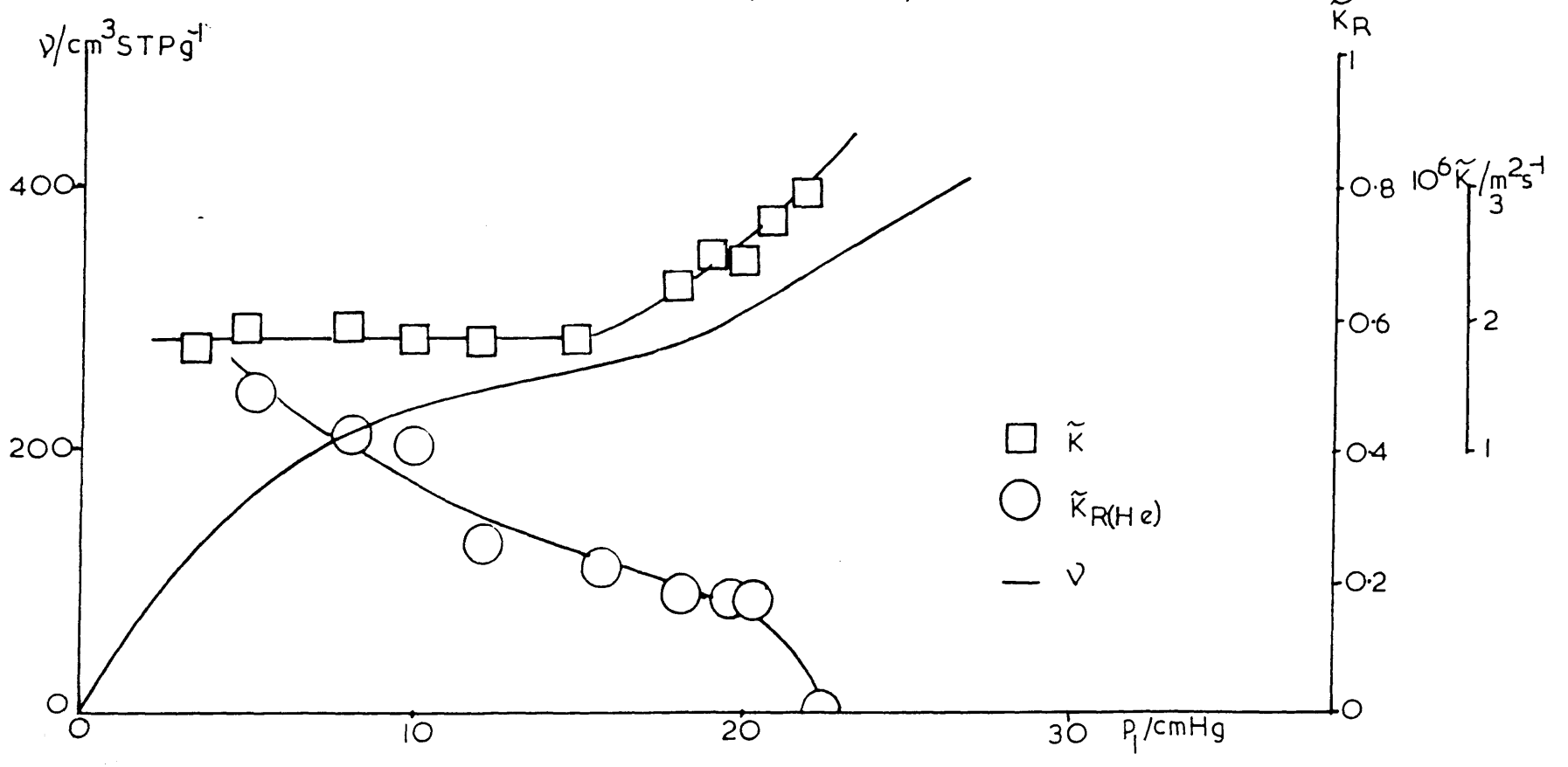
(fig 5·4·1) Triple plot CO_2/Carbolac/195 K



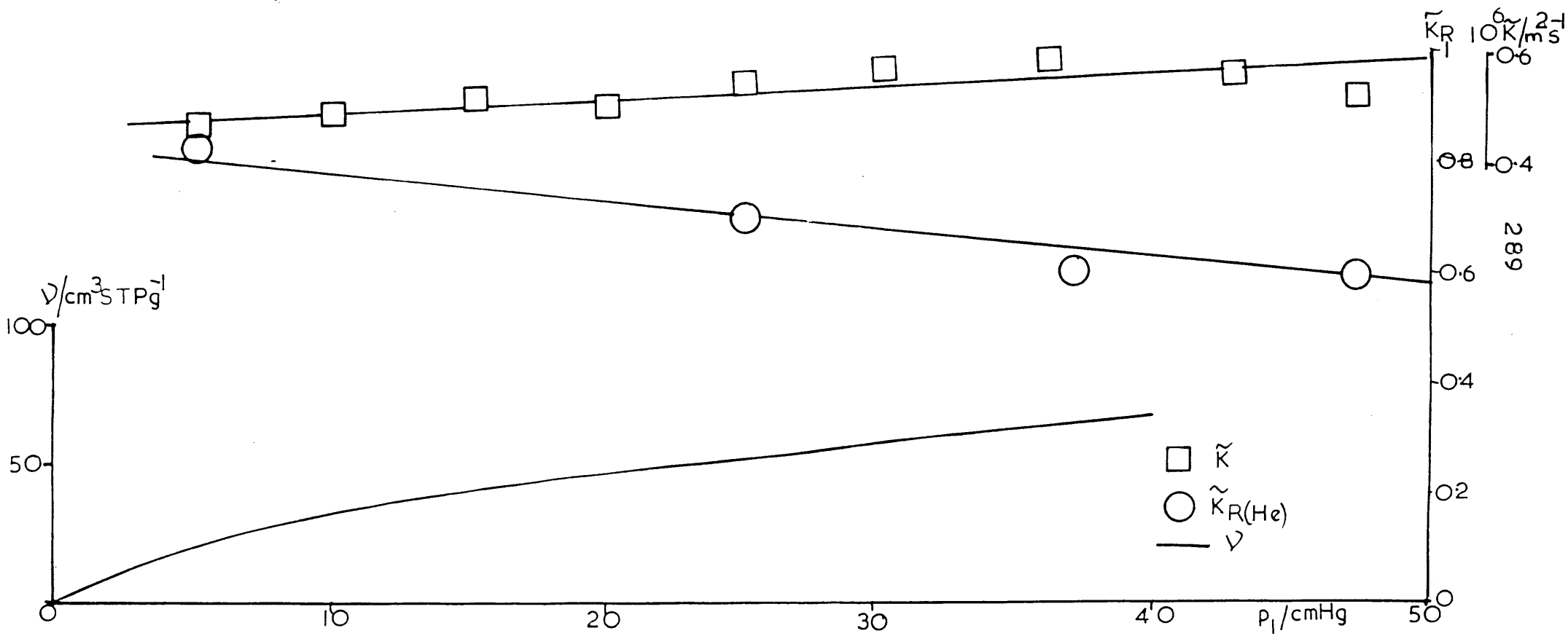
(fig 5·42) Triple plot CO_2/Carbolac/273·2 K



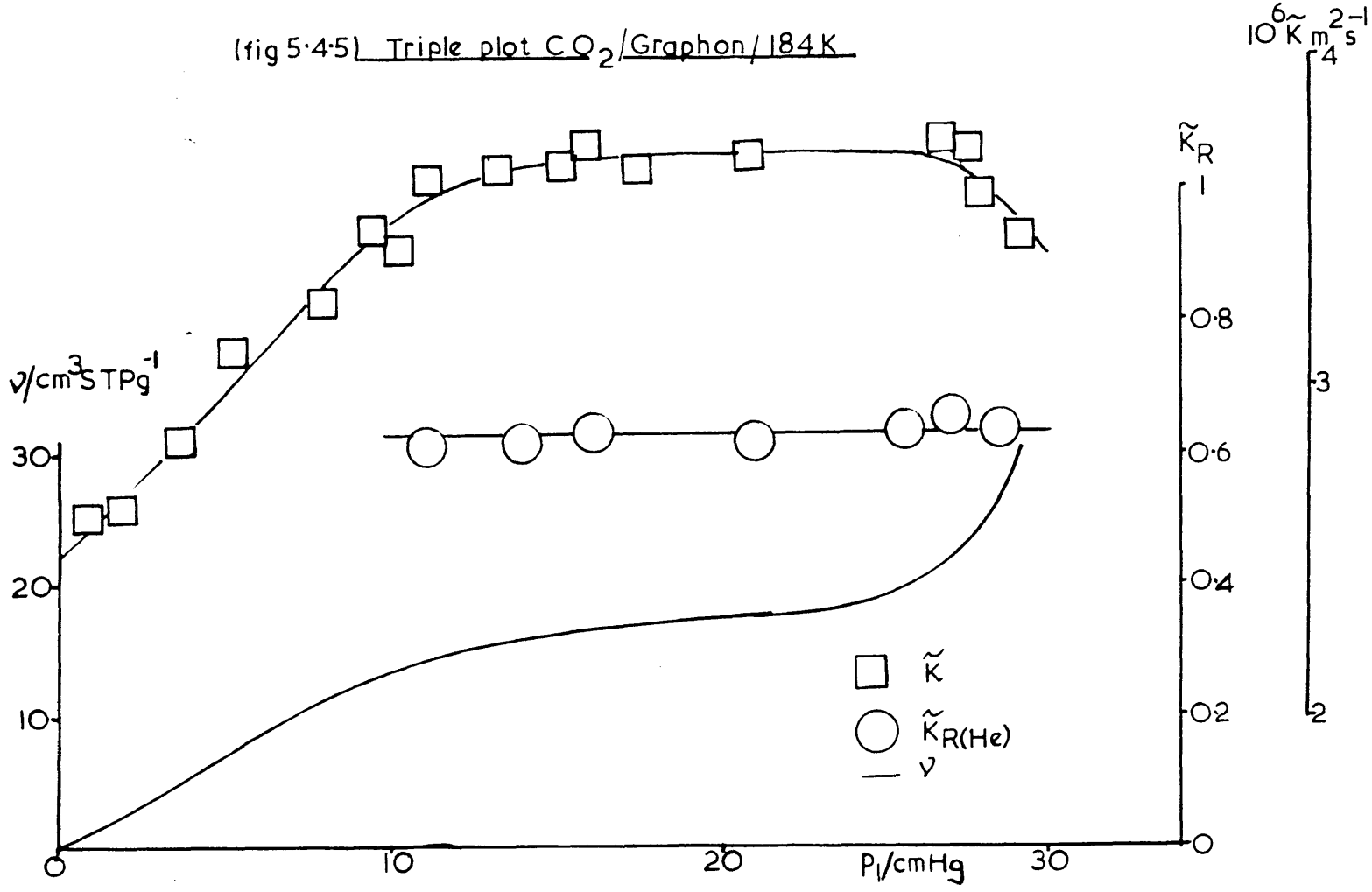
(fig 5·4·3) Triple plot H_2S/Carbolac/195 K



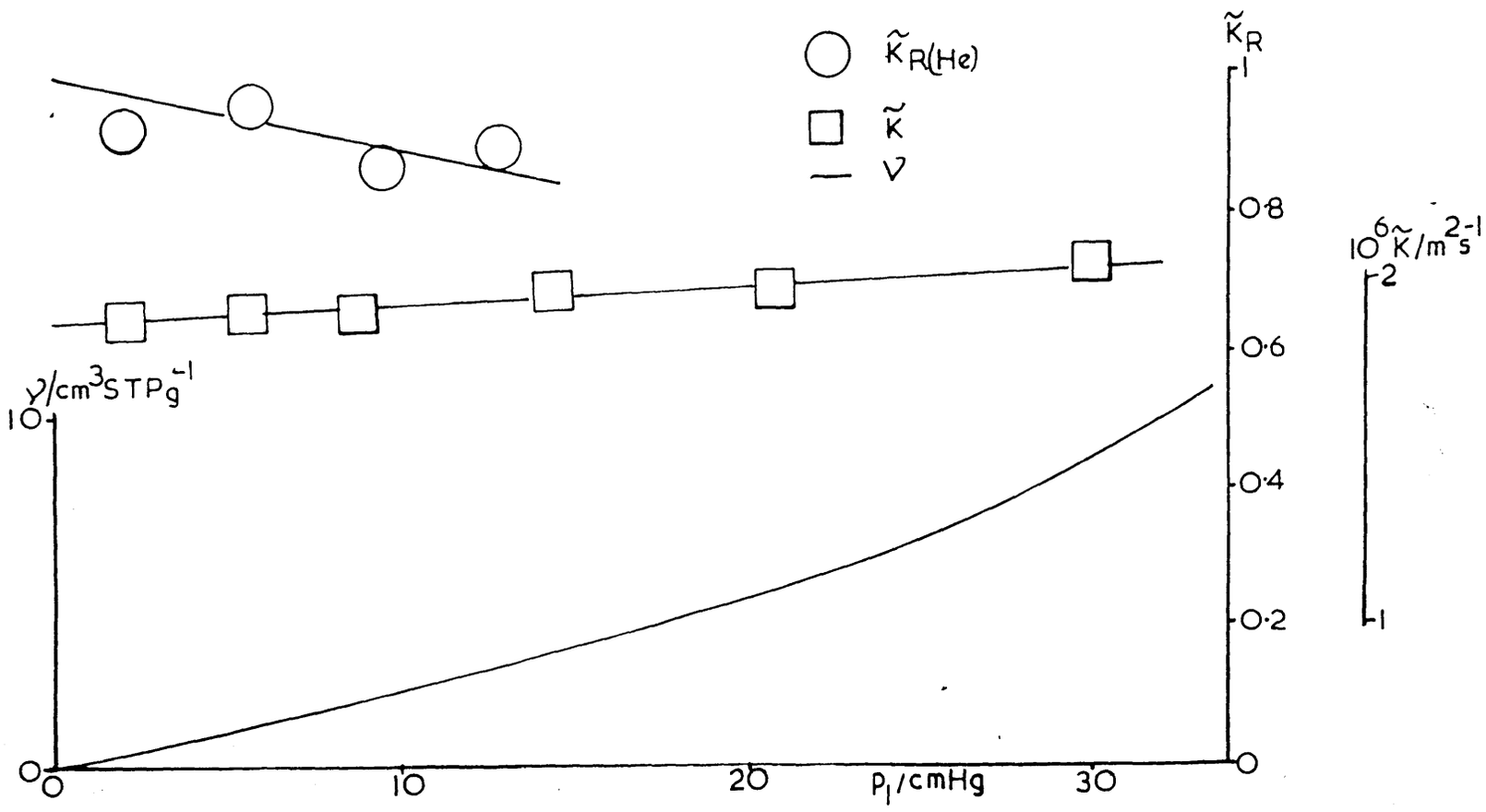
(fig 5·4·4) Triple plot H_2S/Carbolac/273·2 K



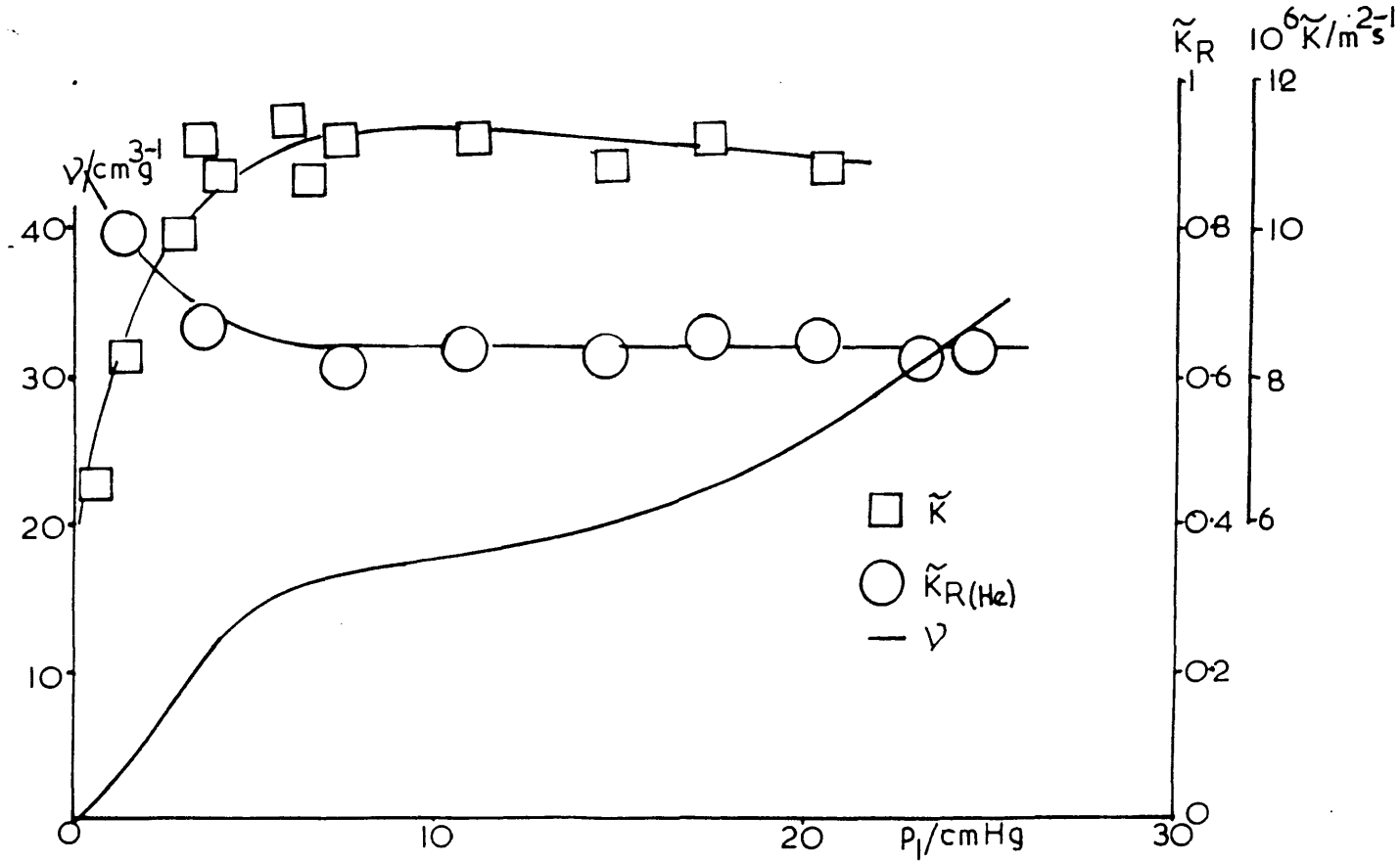
(fig 5·4·5) Triple plot CO_2/Graphon/184K



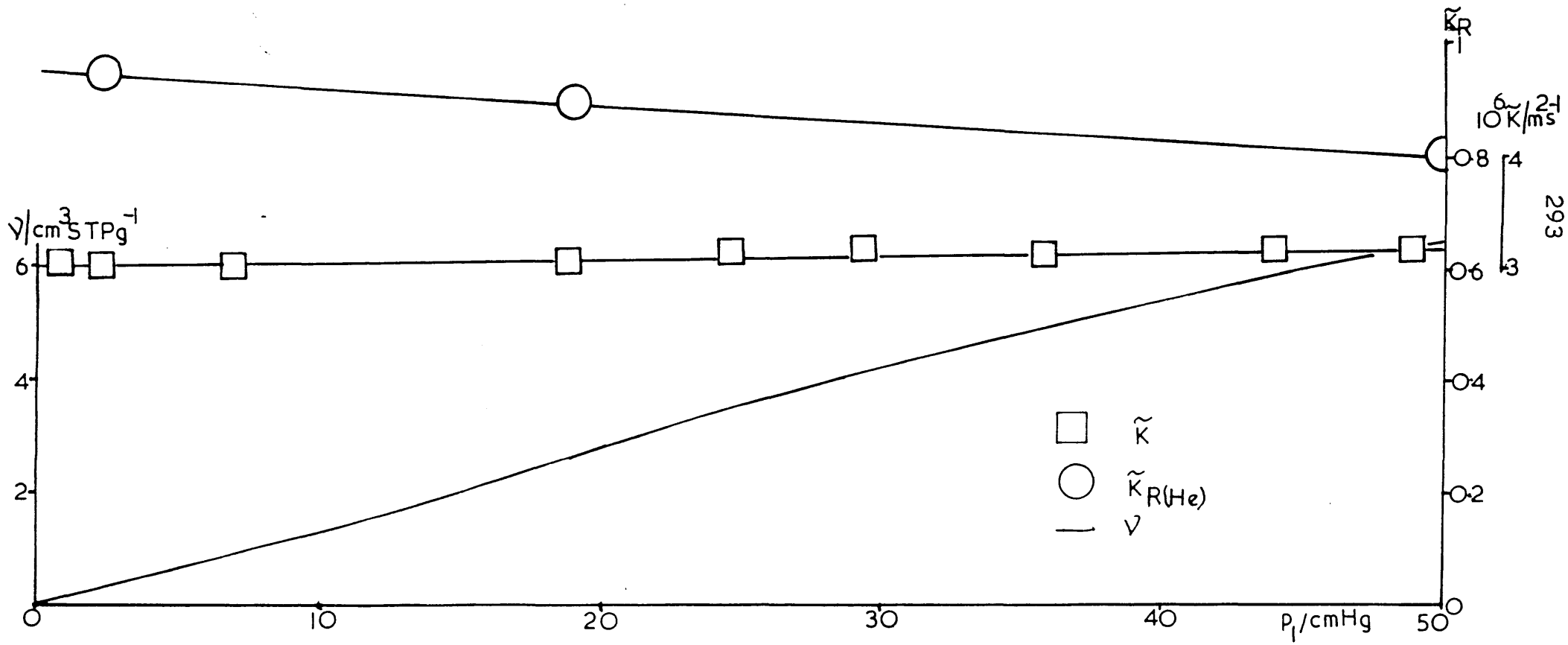
(fig 5·4·6) Triple plot CO_2/Graphon/ 213·2K



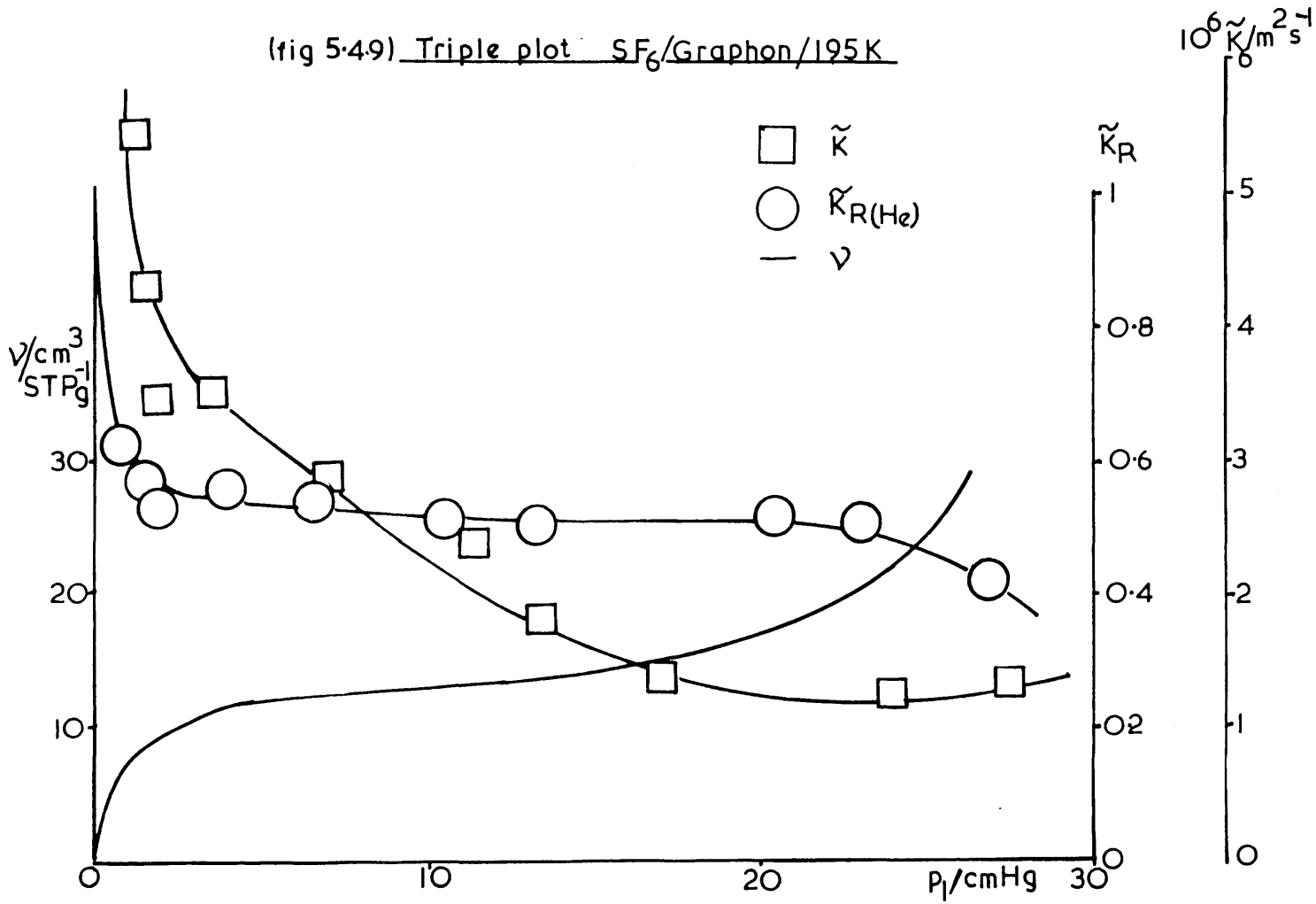
(fig 5·4·7) Triple plot H_2S /Graphon/195 K



(fig 5·4·8) Triple plot H_2S/Graphon/273·2 K



(fig 5·4·9) Triple plot SF_6/Graphon/195K



It may be seen from the triple diagrams for 273.2K (fig. 5.4.2, fig. 5.4.4 and fig. 5.4.8) that at this temperature adsorption isotherms are only slightly curved. This indicates proximity to the Henry Law range and the corresponding single gas permeabilities vary little with ingoing pressure as expected in this range. However for all binary mixtures studied, some blockage of the indicator gas was observed, that is, $\tilde{K}_R$ is always less than unity. The work of Aylmore and Barrer (1966) and of Ash Barrer and Lowson (on N_2/H_2/Carbolac at 273K and 233K) (1973) has shown that a mixture of two Henry Law range, weakly adsorbed gases will exhibit no blockage effects. Blockage effects were, however observed for all systems studied in this investigation, this could be due to the curvature of the isotherms obtained for H_2S on Graphon and Carbolac and for CO_2 on Carbolac,but the isotherm for CO_2 at 273K on Graphon is linear. Blockage of He flow by a gas which was adsorbed in the Henry Law range has also been observed by Hamilton 1980 for the $i\text{-}C_4H_{10}$/He/Graphon system at 452.3K.

From Hamilton's results and, those obtained in this study, it is evident, that blockage effects manifest themselves even when adsorption is slight. This indicates the presence of constrictions in the pores and key adsorption sites which are instrumental in governing the rate of gas phase flow. This has previously been suggested (Section 5.3.2) by the low values of κ_g (the structure factor) for both membranes.

At lower temperatures (fig. 5.4.1, fig. 5.4.3, fig. 5.4.5, fig. 5.4.6, fig. 5.4.7, and fig. 5.4.9) it can be seen that increasing adsorption produces a higher value of $\tilde{K}$ and a greater degree of blockage. Fig. 5.4.1 (CO_2/195K/Carbolac) shows that the single gas

permeability may be independent of pressure, when a type II isotherm is obtained, and that $\tilde{K}_R$ still decreases with increasing pressure. The blockage curves obtained for Carbolac, exhibit a decrease in $\tilde{K}_R$ with increasing pressure over the whole range studied. For CO_2 limitations in the apparatus made $p_1/p_0 = 1$ unobtainable, however for H_2S (fig. 5.4.3) complete blockage was obtained at $p_1/p_0 = 1$ and the blockage curve produced showed a point of inflection. This occurred at a pressure similar to that at which the isotherm exhibited a point of inflection and the single gas permeability started to increase from a constant value (p_1 = 15-18 cmHg 195K) and it may be due to the onset of capillary condensation. Complete blockage of the less sorbable component has previously been obtained by Ash, Barrer and Pope (1963) for H_2/SO_2/Carbolac, by Ash Barrer and Lowson (1973) for He/NH_3/Carbolac and by Hamilton (1980) for He/hydrocarbon/Graphon. However this must be interpreted with caution, as the design of the membrane holder makes blockage of the inlet tube by condensate of the sorbable component possible if a large excess of liquid is present at the saturated vapour pressure. In this region regulation of the ingoing pressure was also extremely difficult as large variations in the saturation pressure result from small temperature fluctuations. The blockage curves obtained for Graphon at lower temperatures (fig. 5.4.5, fig. 5.4.7 and fig. 5.4.9) show an extensive plateau section ($\tilde{K}_R$ = constant) while ν increases with ingoing pressure. This has also been observed on this Graphon membrane by Hamilton (1980), and may be attributed to the filling of blind pores which do not influence the steady state flow rate. It is interesting to note that where as all previous investigations have indicated that complete blockage may be obtained at $p_1/p_0 = 1$ for any weakly adsorbed gas mixed with a strongly adsorbed component,

this is not the case for H_2S/Graphon or CO_2/Graphon systems (fig. 5.4.8 and fig. 5.4.7). In both cases the blockage curve maintains the plateau value until $p_1/p_o = 1$, the reasons for which are not clear. It is possible that the pores of the Graphon membrane are more regular (i.e. straighter and with a more uniform cross section) than those of the Carbolac membrane as indicated by the higher κ_g value, and hence close to $p_1/p_o = 1$ the degree of capillary condensation assumes greater importance to blockage of larger pores than does adsorption at key sites. CO_2 sublimes at lower temperatures therefore capillary condensation and hence total blockage to the gaseous component would not occur.

The triple diagram for SF_6 (fig. 5.4.9) shows that for this system a downward trend is evident near $p_1/p_o = 1$, indicating that total blockage might be achieved, for this system. However limitations of the apparatus again prevented $p_1/p_o = 1$ from being obtained.

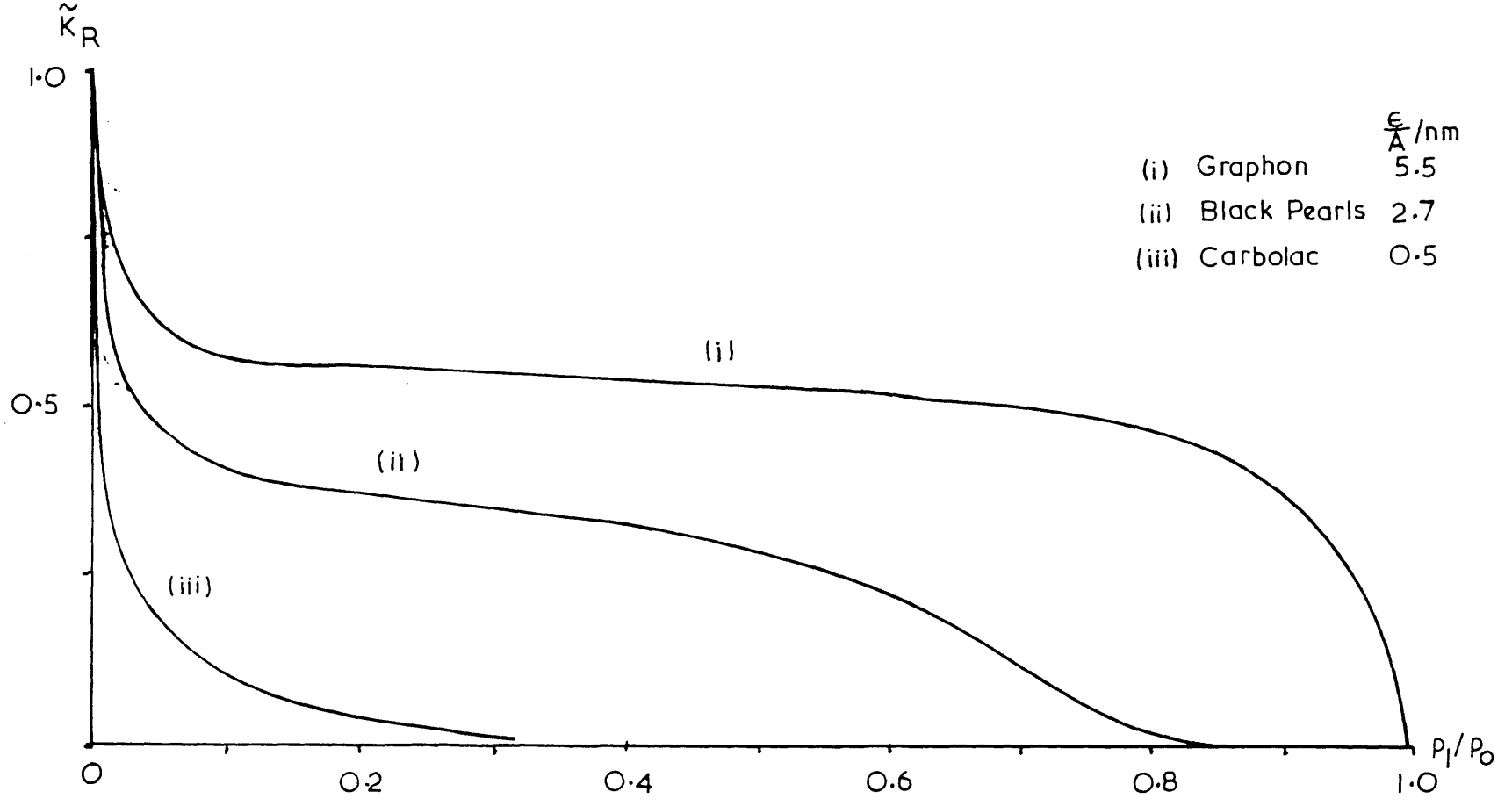
5.4.3 The shape of the blockage curve

With the exception of previous work from this laboratory (references mentioned Section 5.4.2) little investigation has been made into extra flow through micro porous media as a method of gas separation. Exceptions to this include some investigations of porous glass membranes (Kammermeyer and Wyrick 1958, Kameyama et al 1979 and Shindo et al 1985). Work has also been carried out by Bell (1971) who investigated the He/C_3H_8/Graphon system and by Lee and O'Connell (1986) who extended their statistical mechanical model for adsorption and flow of pure gases through microporous solids to include the counter flow of binary mixtures, below monolayer coverage. The study of binary mixtures in this

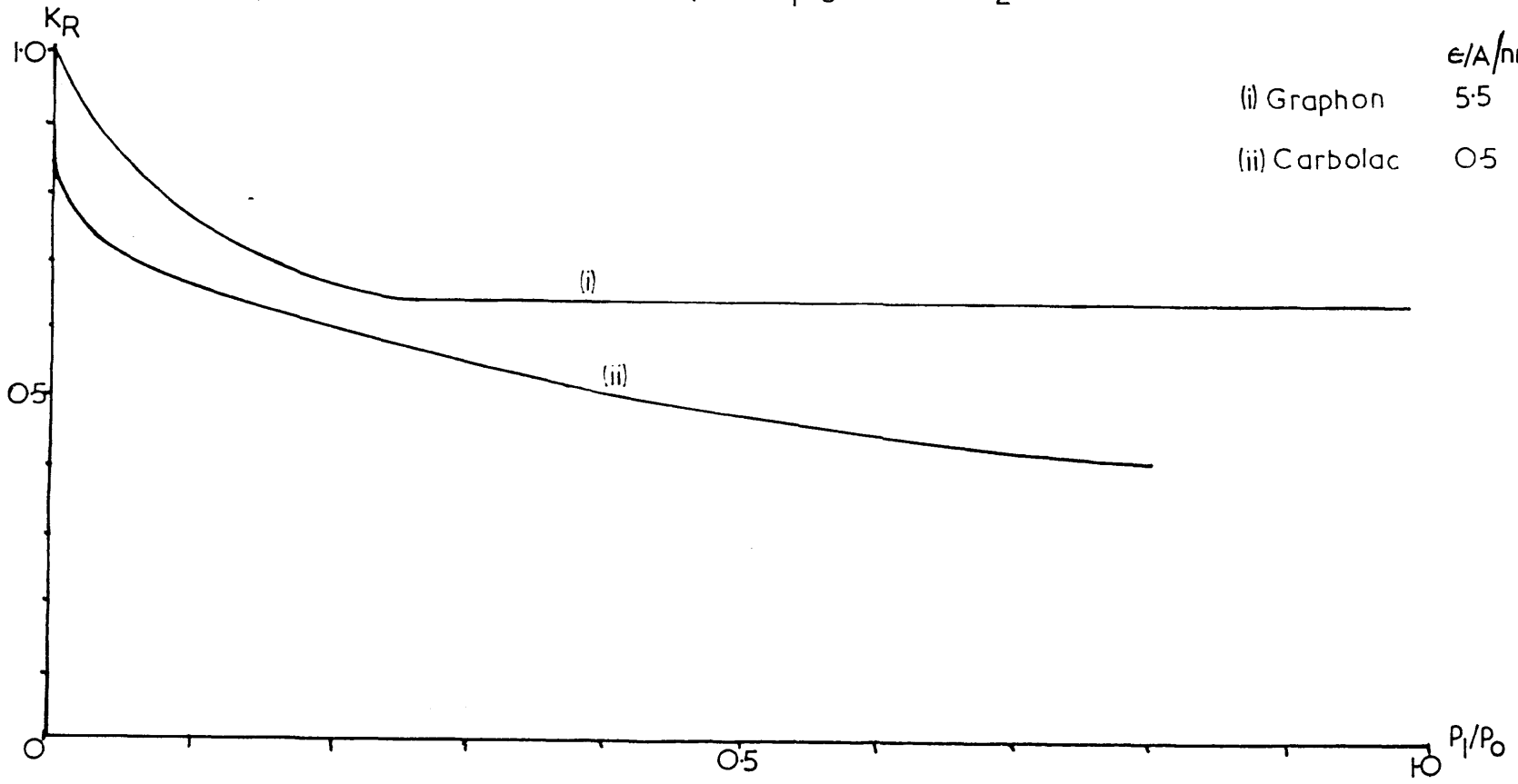
laboratory initially centred upon Carbolac membranes, Ash Barrer and Pope (1963), Aylmore and Barrer (1966) Ash Barrer and Lowson (1973) and Ash Barrer and Sharma (1976), however it has been extended in this study and that of Hamilton (1980) to include work on Graphon and Black Pearls membranes (surface area 220 m^2g^{-1}). It can be seen from fig. 5.4.10 (taken from A.D. Hamilton Ph.D. Thesis 1980) that for He/hydrocarbon mixtures variation in the shape of the blockage curve exists between the three different membranes. The results for Graphon and Black Pearls are those of Hamilton, while the Carbolac data is that of Ash Barrer and Sharma (1976), measured using the pressure decay technique. The form of the curve appears to vary with the hydraulic radii of the pores (ε/A); this is given in fig. 5.4.1 and as ε is approximately constant it varies inversely with A (the specific surface area). As expected the Carbolac membrane, which possesses the smallest hydraulic radius, becomes totally blocked at a lower pressure than the other two membranes, while the Black Pearls and Graphon membranes respectively exhibit decreasing degrees of blockage at the same pressure. Fig. 5.4.10a and fig. 5.4.10b show that the blockage curves for He/CO_2 and He/H_2S on the Carbolac and Graphon membranes used in this study, exhibit the same trends as those observed for He/hydrocarbon blockage. Despite this correlation for three gas mixtures the relationship between the blockage curve and ε/A must be interpreted with caution as Hamilton notes that "It would be expected that if blockage was characteristic of a given ε/A, different curves would result from different sized hydrocarbons, which is not the case."

Fig. 5.4.11 shows the variation of $\tilde{K}_R$ with p_1/p_0 for various mixtures flowing through two Carbolac plugs with different ε/A values.

(fig 5·4·10) Variation of $\tilde{K}_R$ with p_1/p_0 for He/Hydrocarbon mixtures

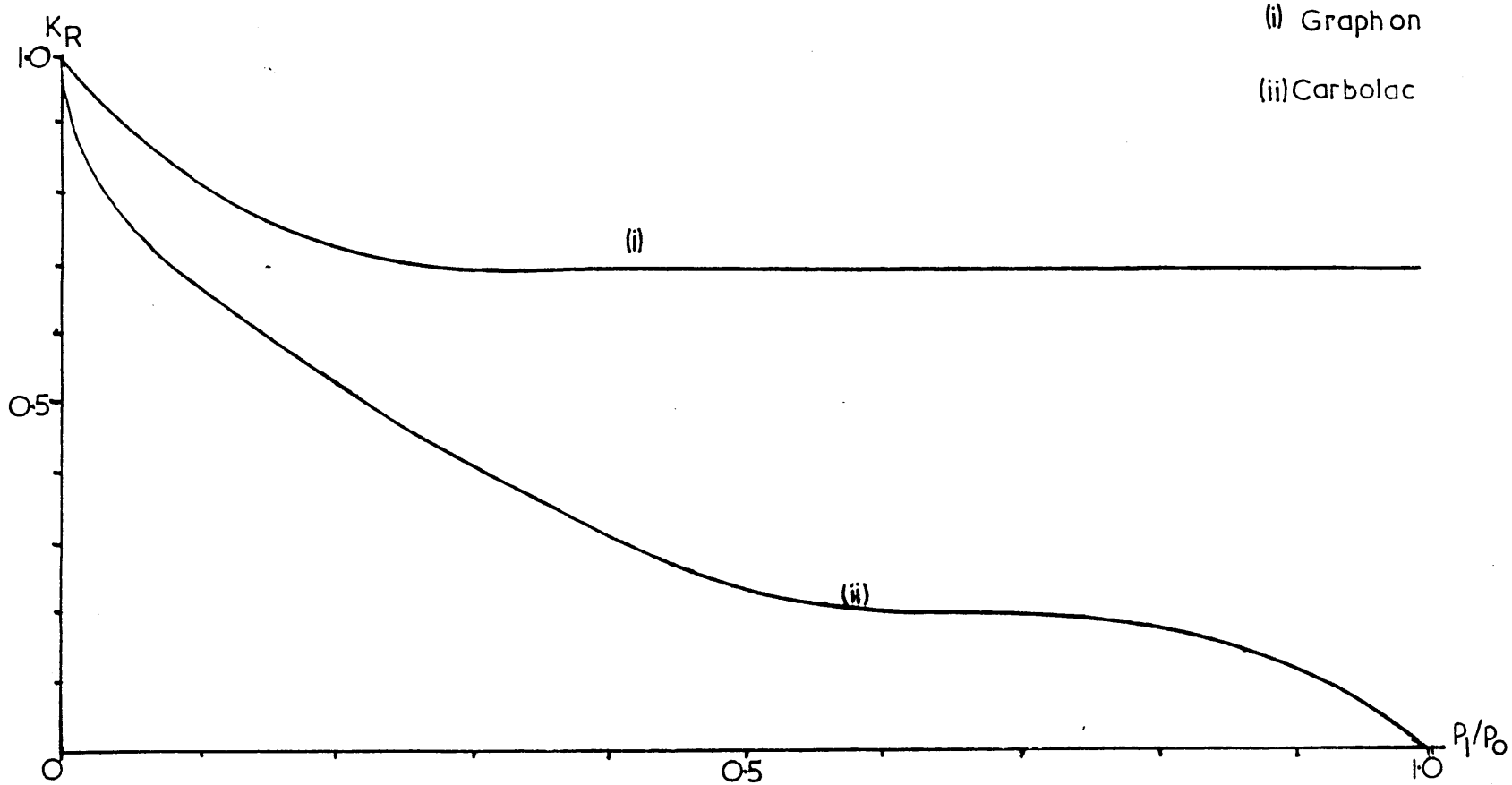


(fig 5·4·10a) Variation in $\tilde{K}_R$ with P_1/P_0 for He/CO_2 mixtures

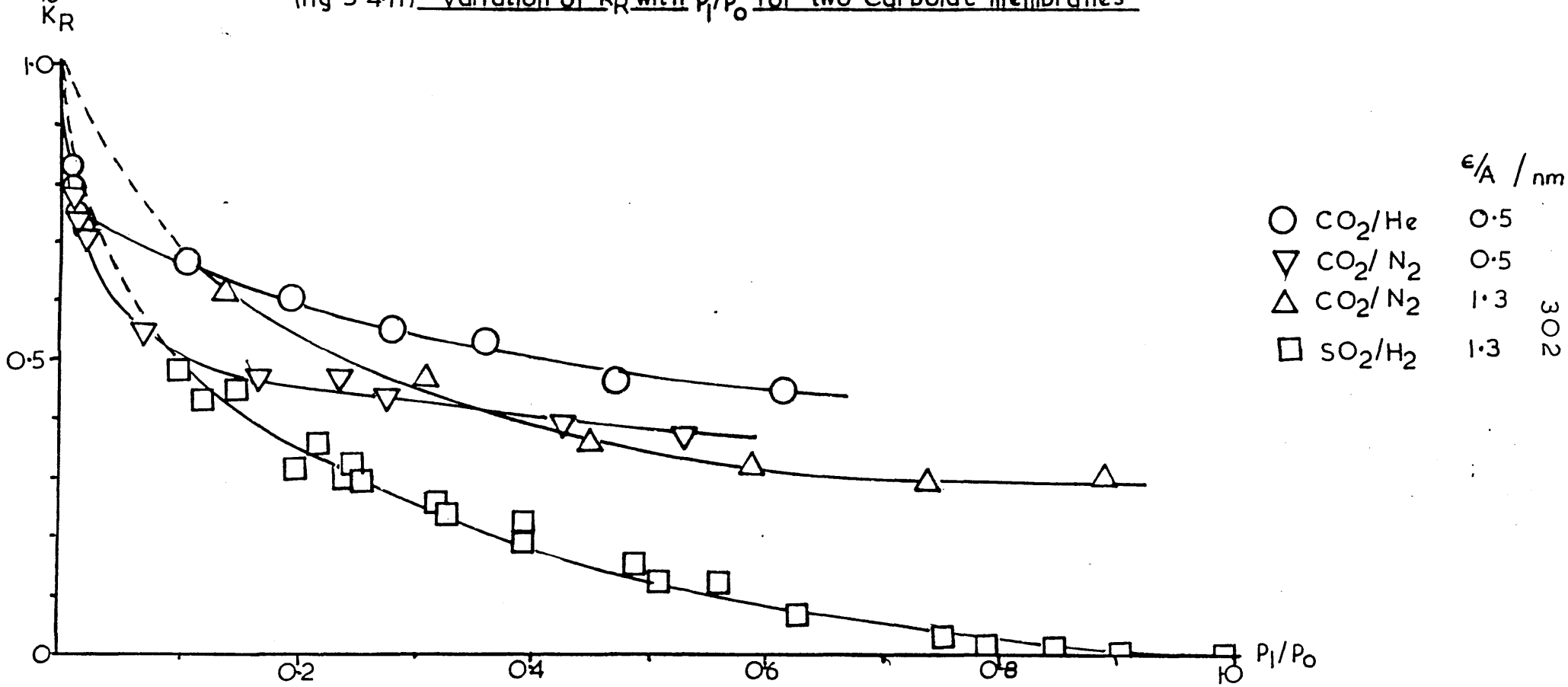


(fig 5·4·10b) Variation of K_R with P_1/P_0 for H_2S/He mixtures

	ε/A/nm
(i) Graphon	5·5
(ii) Carbolac	0·5



(fig 5·4·11) Variation of $\tilde{K}_R$ with P_l/P_o for two Carbolac membranes



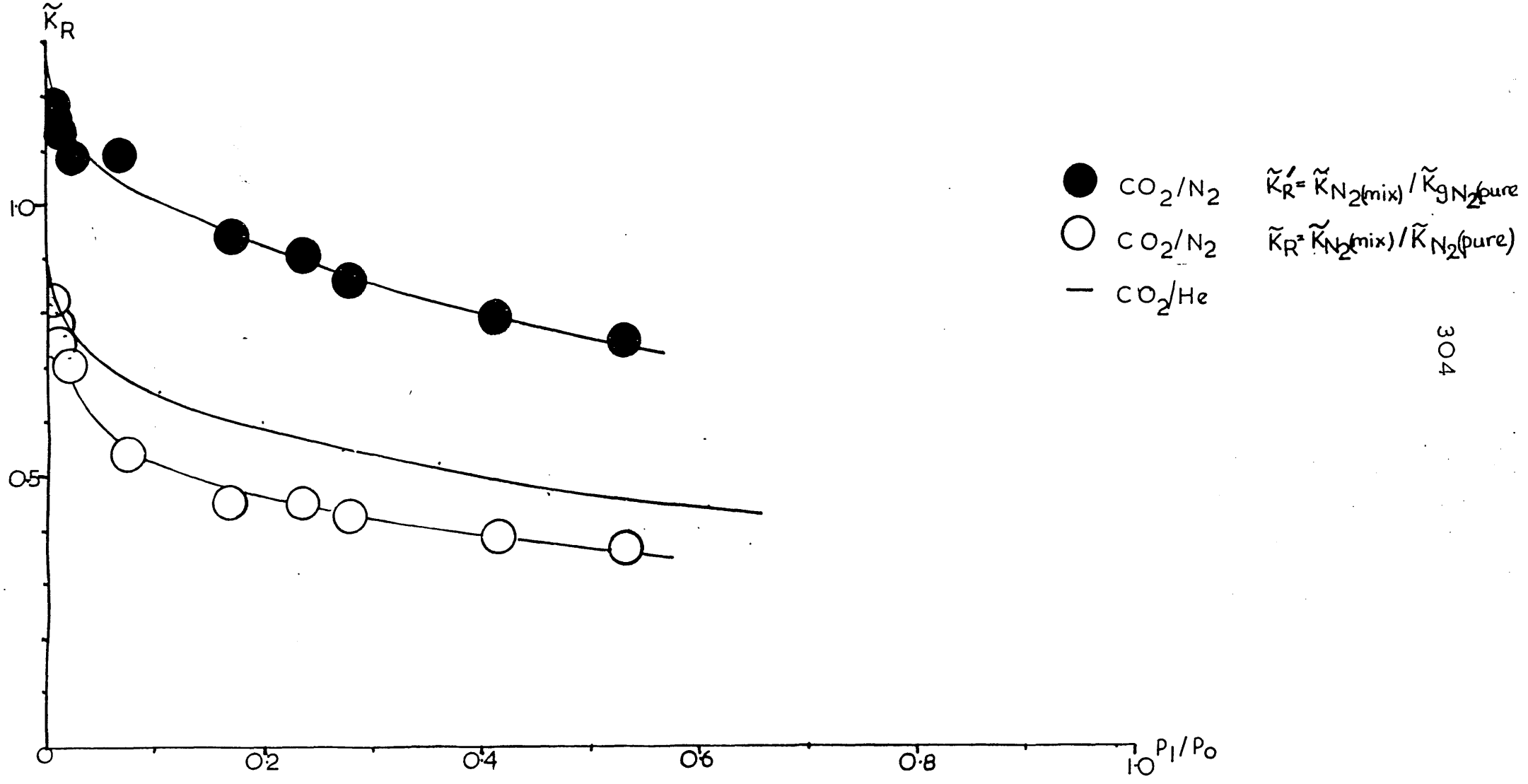
(The Carbolac membrane used by Pope (1961) possessed a very low specific surface area(A) compared to other membranes). In this case no correlation between ε/A and the form of the blockage curve is evident, although the CO_2/N_2 results obtained in this study are close to those recalculated from Popes CO_2/N_2 work.

5.4.4 Blockage behaviour of different sorbable gases

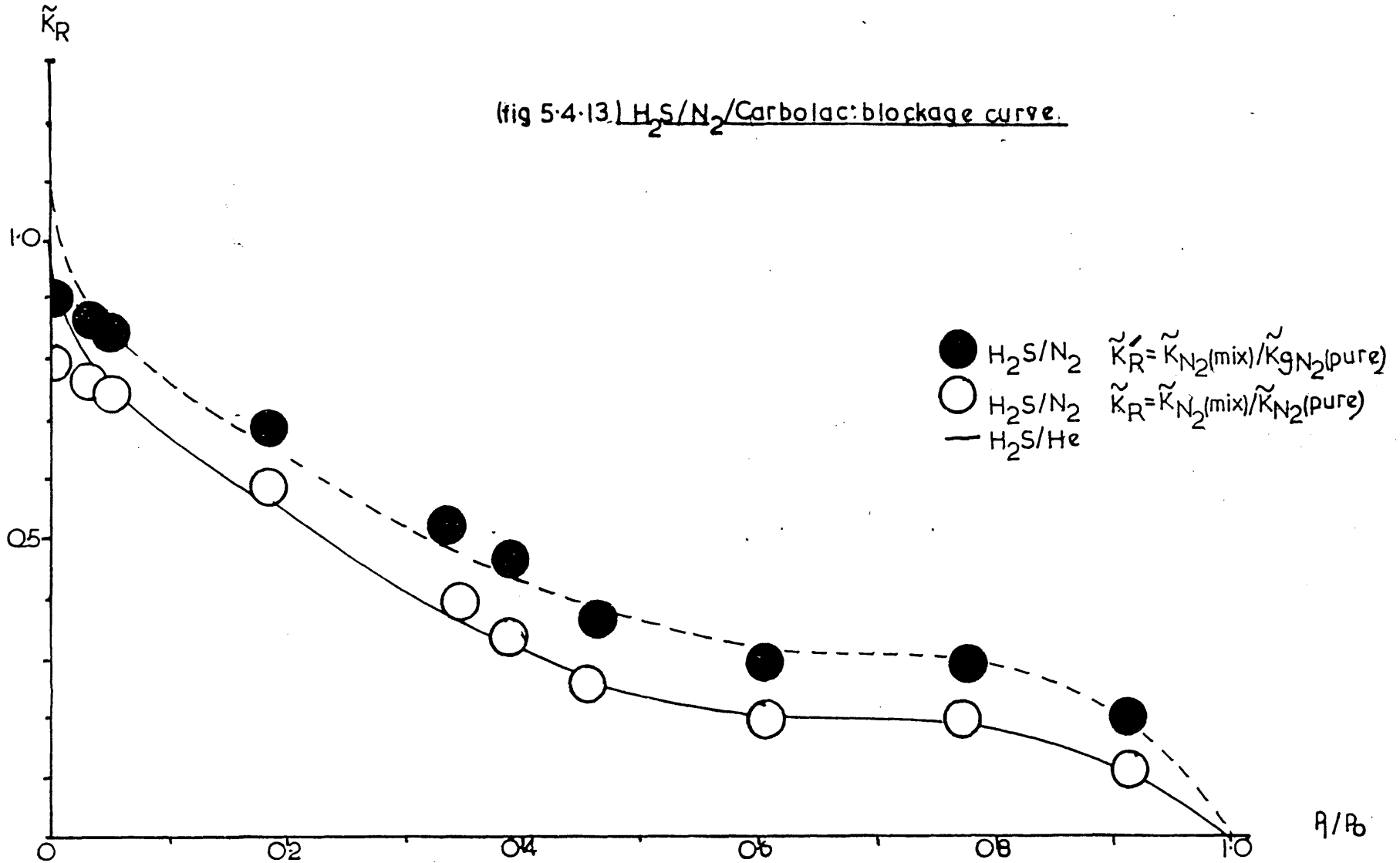
By reference to fig. 5.4.11 and fig. 5.4.13 it can be seen that for the Carbolac membrane a greater degree of He blockage is obtained by use of H_2S than by CO_2. Fig. 5.4.15 however shows that the H_2S/He and CO_2/He blockage curves for the Graphon membrane lie very close together, with the H_2S/He results slightly above those for CO_2 at $p_1/p_o > 0.4$. This seems to indicate that for the Graphon membrane the degree of blockage is due more to the membrane structure than to the sorbable component, whilst blockage of the Carbolac membrane depends to a greater degree upon the sorbable component used, as shown for two Carbolac plugs in fig. 5.4.11.

Fig. 5.4.14 shows the "universal" blockage curve obtained by Hamilton for He/hydrocarbon/Graphon, the He/C_3H_8 results obtained in this study lie on the curve, while the CO_2/He results are slightly above. He blockage by H_2S and SF_6 for the same membrane are also shown in fig. 5.4.15. All the blockage curves obtained thus far for this Graphon membrane, while not identical, are similar in both form and magnitude to each other, with $\tilde{K}_R$ at a fixed p_1/p_o decreasing as the molecular size of the sorbable gas increases. This could be an indication of a more regular pore structure (cf Section 5.4.2) which does not show increased blockage after the initial key sites have been filled. Hamilton attributed the plateau section of the blockage curve

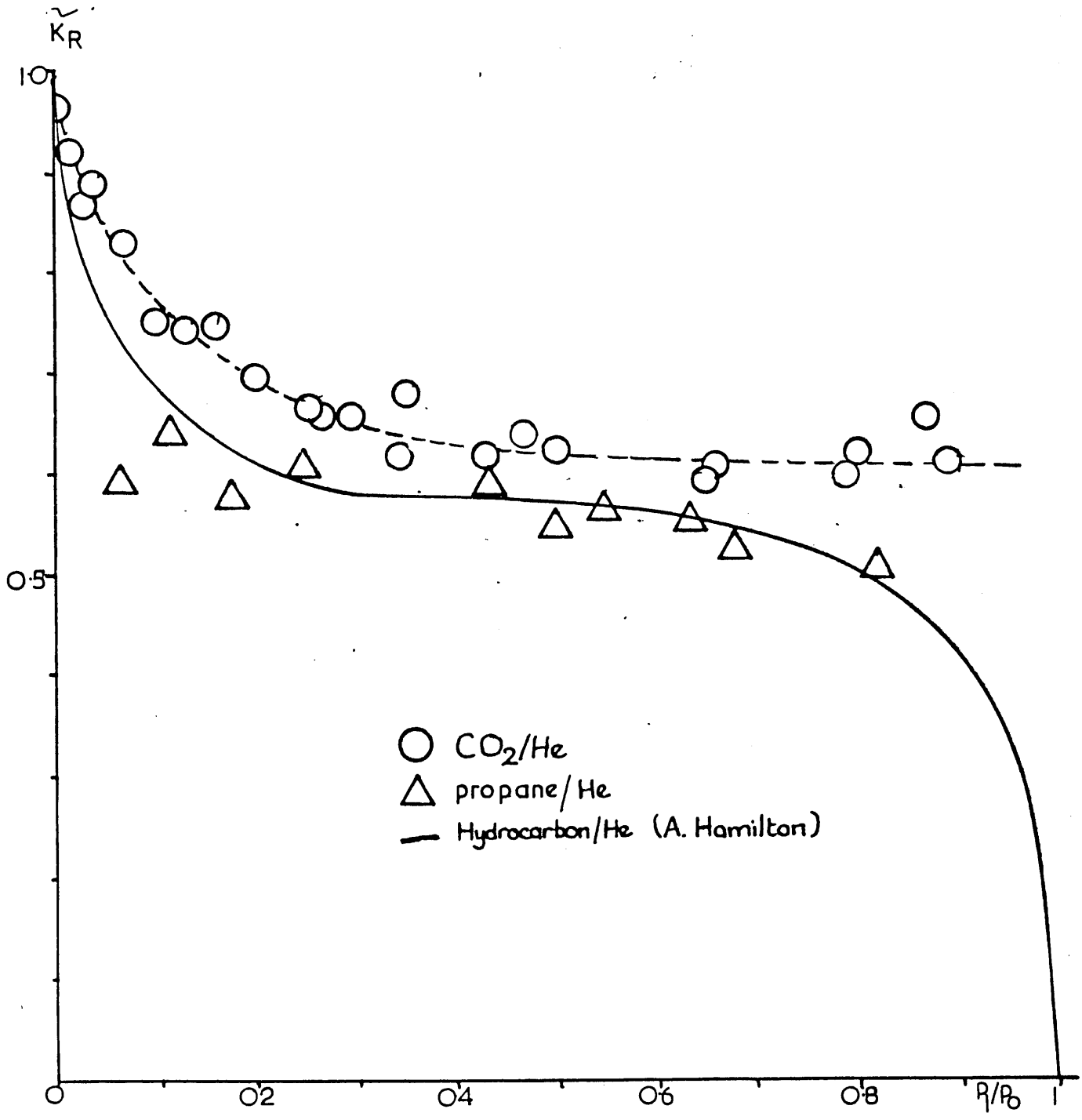
(fig 5·4·12) CO_2/N_2 / Carbolac : blockage curve



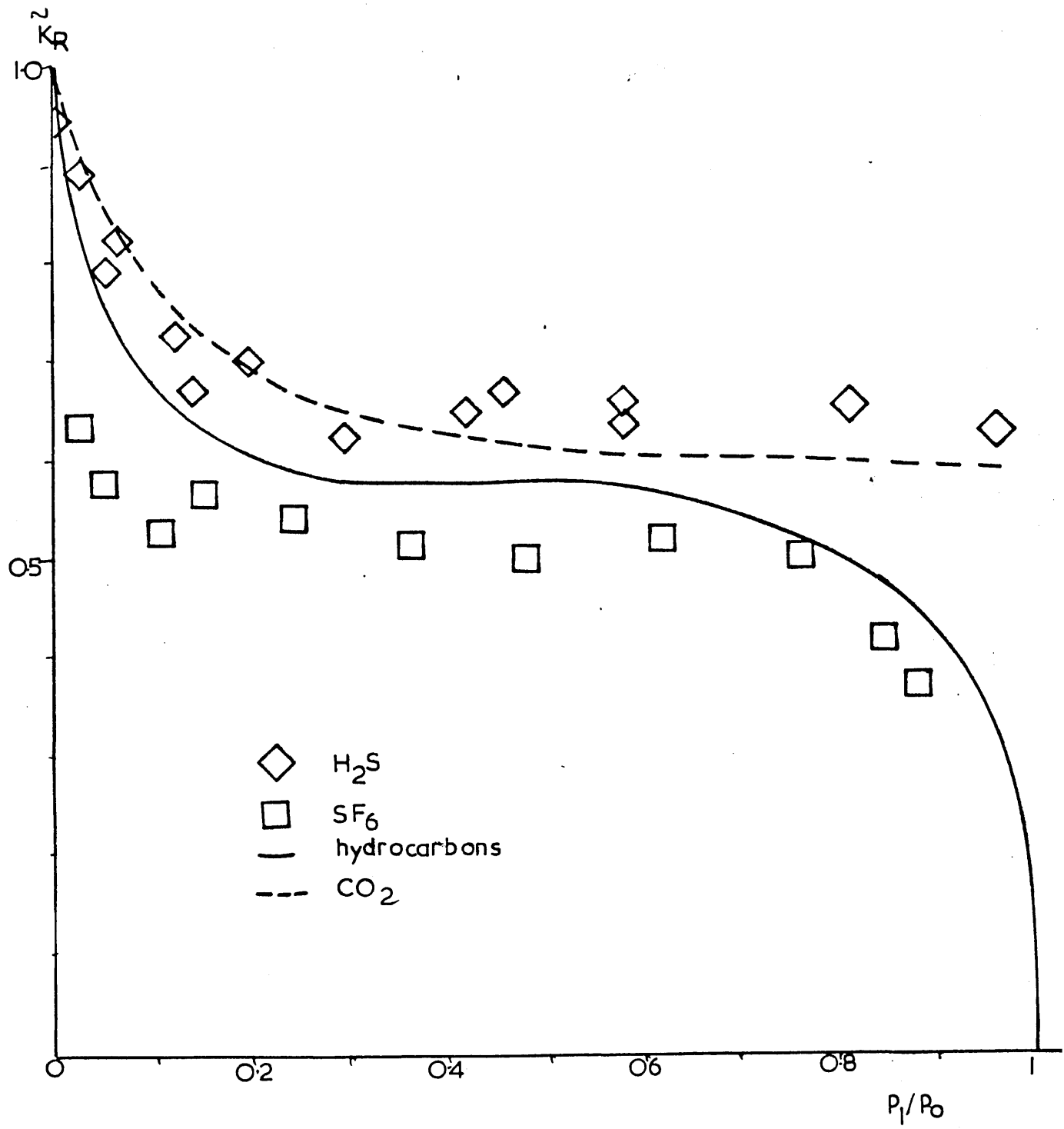
(fig 5·4·13) H_2S/N_2/Carbolac: blockage curve.



(fig 5·4·14) Blockage of He by CO_2 or hydrocarbons / Graphon



(fig 5·4·15) He blockage / Graphon membrane



obtained on the Graphon membrane to the filling of blind pores which do not contribute to steady state flow. The results obtained in this study however seem to indicate a regular pore structure which once blocked at one point along its length will show no further decrease in gas flow rate corresponding to adsorption at other points. The theory of a regular pore structure for Graphon membranes is also supported by crystallographic results mentioned in Section 3.1.4 (Hess et al 1968) which suggest a regular partical structure, and the structure factor κ_g ($\sim$.60 for Graphon) which is closer to unity than that obtained for Carbolac (0.45).

5.4.5 Blockage of gases other than He

N_2 and Ar have been used as indicator gases in addition to He in this study. The results obtained may be presented in the form

$$\tilde{K}_R = \tilde{K}_{N_2(mix)} / \tilde{K}_{N_2(pure)}$$

or in the form

$$\tilde{K}'_R = \tilde{K}_{N_2(mix)} / \tilde{K}_{gN_2(pure)}$$

where $\tilde{K}_{gN_2(pure)} = \tilde{K}_{He} \sqrt{\frac{M_{He}}{MN_2}}$ for He results at the same temperature as N_2 flow.

When the permeability is split into gas phase and extra components it may be shown that a "universal curve" for the blockage of gas phase flow is expected thus:

$$\tilde{K}_x = \tilde{K}_{sx} + \tilde{K}_{gx}$$

and $\tilde{K}_R = \tilde{K}_{x(mix)}/\tilde{K}_{x(pure)}$

therefore

$$\tilde{K}'_R = \frac{\tilde{K}_{sx(mix)}}{\tilde{K}_{gx}} + \frac{\tilde{K}_{gx(mix)}}{\tilde{K}_{gx}}$$

where

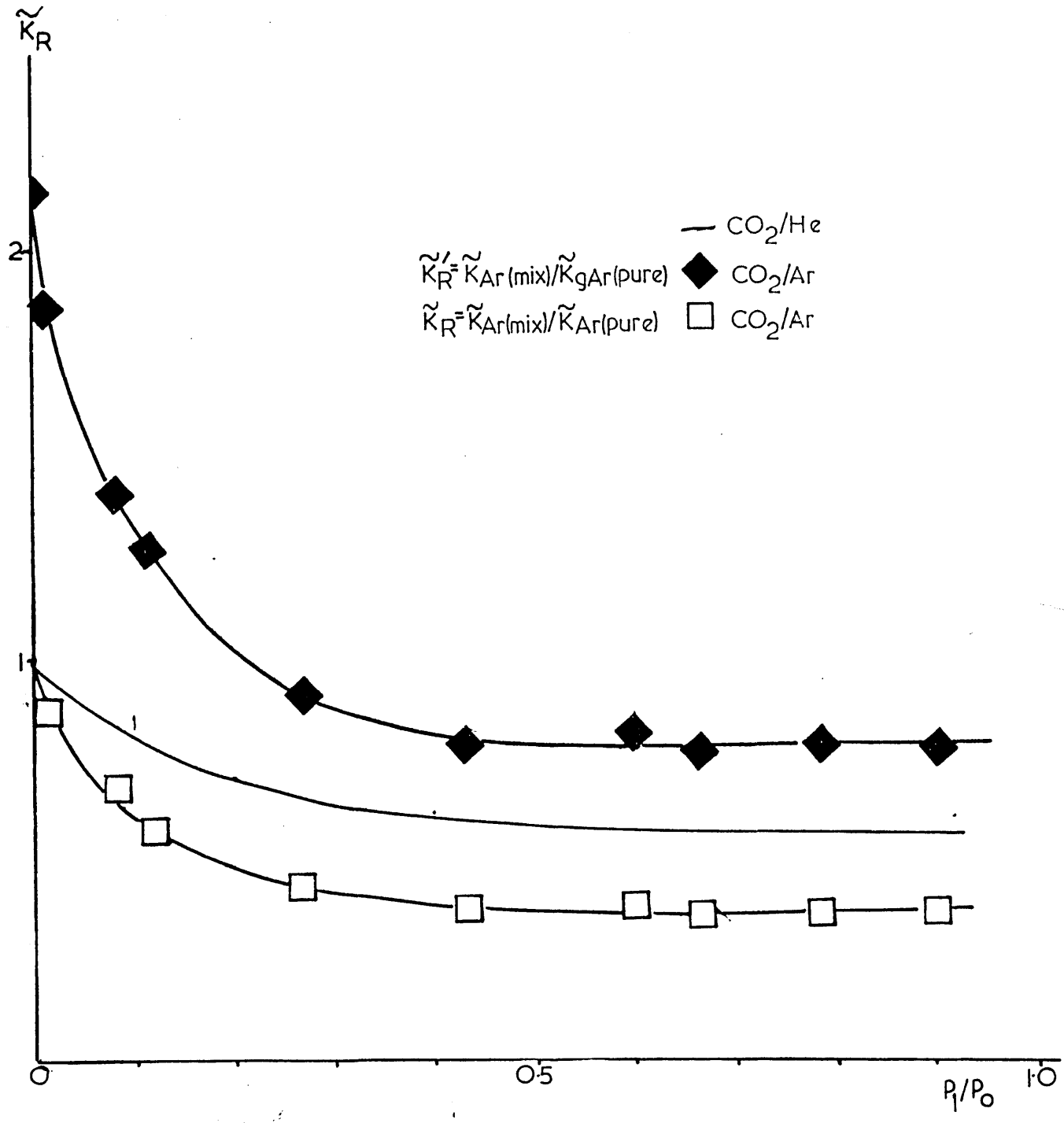
$$\frac{\tilde{K}_{gx(mix)}}{\tilde{K}_{gx}} = \frac{\tilde{K}_{He(mix)}\sqrt{\frac{MHe}{Mx}}}{\tilde{K}_{He}\sqrt{\frac{MHe}{Mx}}}$$

therefore $\tilde{K}'_R$ for gas x is equal to $\tilde{K}_R$ for He, if $\tilde{K}_{sx(mix)}/\tilde{K}_{gx}$ is negligible.

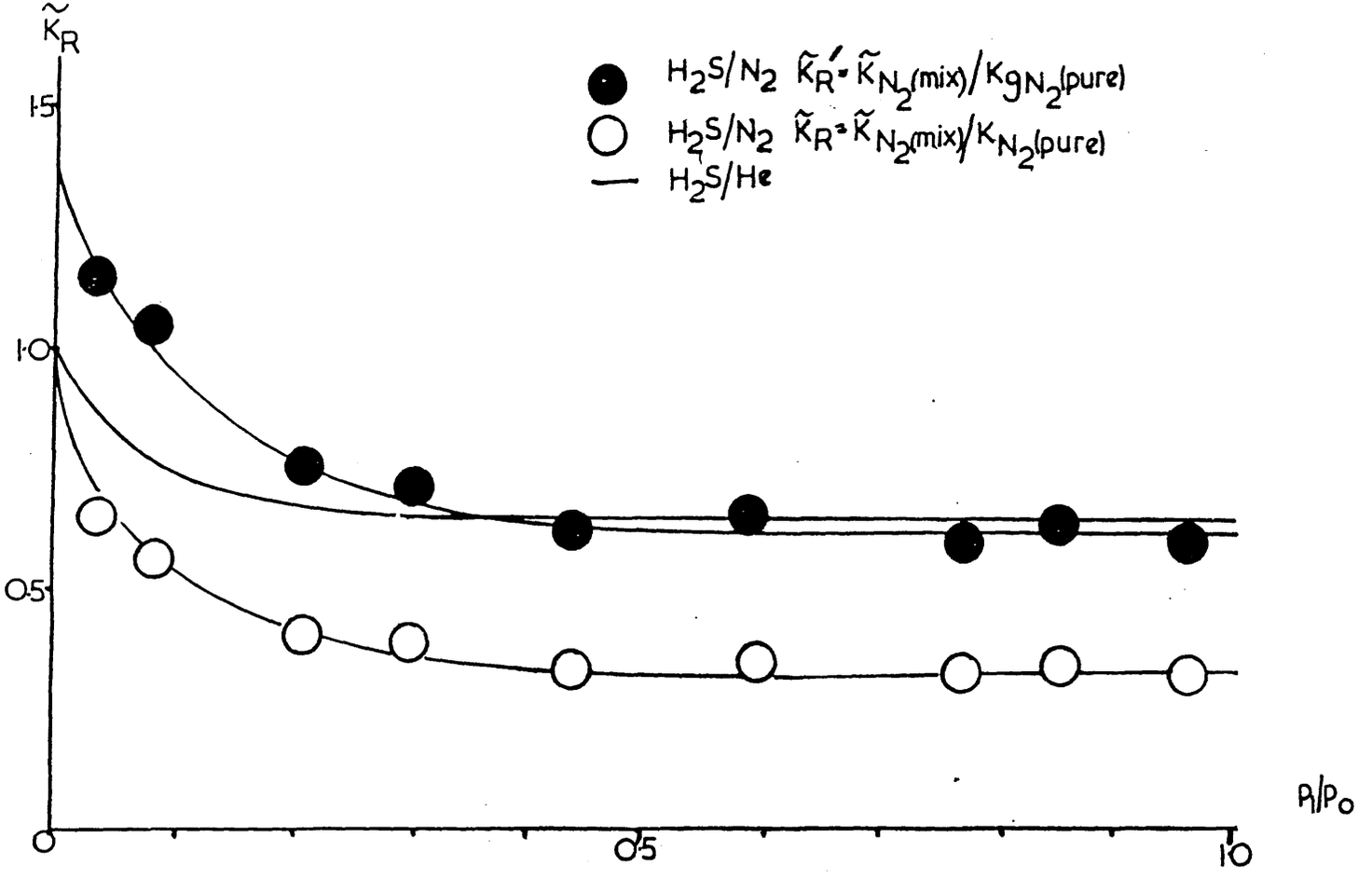
Fig. 5.4.12 and fig. 5.4.13 show the N_2/Carbolac blockage results presented in both ways. When blocked by CO_2 the curve for $\tilde{K}_{RN_2}$ falls below that for $\tilde{K}_{RHe}$ (also shown) indicating that some blockage of the N_2 extra flow has occurred in addition to gas phase blockage. The curve for $\tilde{K}'_{RN_2}$ however lies above $\tilde{K}_{RHe}$ showing that not all the extra flow has been prevented.

The H_2S/N_2/Carbolac system is represented in fig. 5.4.13. $\tilde{K}_{RN_2}$ and $\tilde{K}_{RHe}$ are equal indicating that H_2S adsorption has apparently not affected the extra flow of N_2, and $\tilde{K}'_{RN_2}$ again lies above the curve. More detailed analysis of these results will not be attempted due to the difficulties in obtaining correct values for $\tilde{K}_{N_{2(mix)}}$, $\tilde{K}_{N_{2(pure)}}$ and $\tilde{K}_{He}$ at any point in time, for such an unstable membrane. Fig. 5.4.16 to fig. 5.4.18 show blockage curves for Ar/CO_2, N_2/H_2S and N_2/CO_2 upon

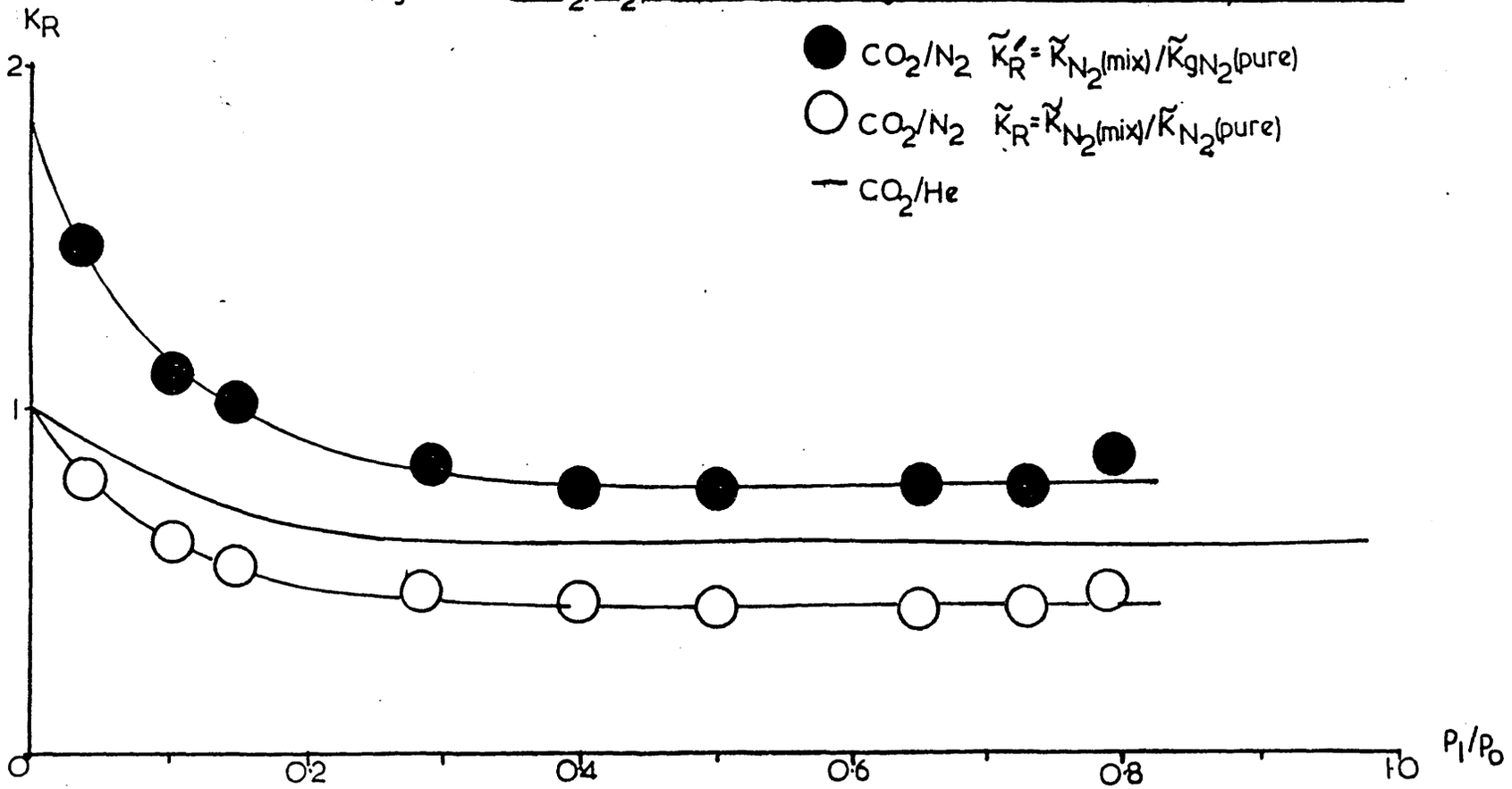
(fig 5·4·16) CO_2/Ar/Graphon; blockage curve



(fig 5·4·17) H_2S/N_2 /Graphon : blockage curve



(fig 5·4·18.) CO_2/N_2 /Graphon: blockage curve determined by- C.F Bott



the Graphon membrane (the N_2/CO_2 results were obtained by Miss C.F. Bott). In all cases the $\tilde{K}_R$ blockage curve for the weakly sorbed gas lies below that for He, indicating some degree of blockage of the extra as well as gas phase flow. For CO_2/N_2 and CO_2/Ar, $\tilde{K}'_R$ lies above $\tilde{K}_{RHe}$ indicating that not all the extra flux has been prevented, however for H_2S/N_2 $\tilde{K}'_{RN_2}$ is equal to $\tilde{K}_{RHe}$ at $p_1/p_o > .35$ this shows that all the extra flow of N_2 has been prevented and only semi-blocked gas phase flow remains.

These results indicate that H_2S shows greater competitive adsorption than CO_2 under similar conditions and cautious predictions may be made regarding the blockage effect of adsorbed H_2S upon CO_2 flow. In this case total prevention of CO_2 extra flow would be unlikely as CO_2 is more strongly adsorbed than N_2. However partial CO_2 blockage could result from competitive adsorption of such a binary mixture.

Mixed adsorption isotherms and flow experiments upon Graphon using H_2S/CO_2 mixtures would provide much information about the separation of two strongly sorbed gases which has as yet not been investigated.

5.5. Application of results to gas separation

5.5.1 Introduction

The technology of gas separation is a field to which extensive effort has been devoted for many years, and with the advent of polymeric hollow fibre membranes interest in devising commercial gas separation techniques is increasing rather than diminishing. The physical methods of separating gas mixtures fall into three broad categories.

(i) Cryogenic methods (distillation)

(ii) Selective adsorption

(iii) Membrane permeation

The steady state results obtained in this study may be applied to gas separations, forming the basis of continuous flow membrane methods (Section 5.5.2), while the adsorption isotherms and transient state results might be used as the basis of a separation process by selective adsorption, for example pressure swing adsorption (PSA) (Section 5.5.3).

5.5.2 Continuous flow separation of gas mixtures

Despite interest in gas permeation since 1831, (when Mitchell first observed that different gases permeated through rubber membranes at unequal rates), and much work by Graham (1863 and 1866) it was not until the early 1930's (when separation of isotopes became a necessity) that a serious attempt was made to appraise the potential of gas permeation as a large-scale separation technique.

The enrichment (in the form of its hexafluoride UF_6) of natural uranium in the lighter isotope ^{235}U, developed by the US Atomic Energy Commission, is still the most important application of microporous membranes. This separation proceeds by means of Knudsen flow in which the permeability of any component is inversely proportional to the square root of its molar mass. The degree of separation obtained by a single stage is therefore small for $^{235}UF_6/^{236}UF_6$ and a series of permeation units is necessary.

Another application of this method is to the purification of hydrogen using palladium or palladium alloy foils. One such process has been developed commercially by Union Carbide (McBride and McKinley

1965). The membrane is operated at approximately 400°C and separation proceeds by atomic diffusion allowing complete separation of H_2 in a single stage. This and similar commercial processes have been reviewed by Hwang and Kammermeyer (1975).

The efficiency of a membrane may be quantified by the definition of a separation factor $\eta_{A:B}$ in terms of the mole fractions of the component gases A and B in (i) the permeate stream, y and in (ii) the feed stream, x

$$\eta_{A:B} = \frac{y_A}{y_B} \cdot \frac{x_B}{x_A}$$

For systems in which an extra flow component is present, large separation factors are often obtained indicating an efficient separation of the gas mixture.

Huckins and Kammermeyer (1953) investigated the flow of H_2/CO, H_2/O_2 and H_2/N_2 through Vycor porous glass, for which separation factors of 2.3, 2.45 and 2.3 have been calculated (A. Rizvi 1982) for small values of the fraction permeated ("cut" → 0). Rizvi also calculated a separation factor of ∿ 1.2 at "cut" → 0 for propane, in the propane/CO_2/ porous glass system studied by Kammermeyer and Weyrick (1958) at 298K and ingoing pressure 2.3 atmospheres. As CO_2 and C_3H_8 have similar molar masses, this separation must be due to the existence of an extra flow component. The large extra flow component and blockage effect present when gases are flowed through carbon membranes, has led to very large separation factors in some cases. The work of Ash Barrer and Pope (1963) using Carbolac gave rise to separation factors of 8-1000 for SO_2 in H_2/SO_2 mixtures between 273.2 and 242K, and complete

H_2 blockage occurred at lower temperatures. Separation factors in the range 5.5 to 24.6 were obtained for CO_2 from CO_2/N_2 at 190K where the difference in sorbabilities and hence the magnitude of the extra flow was less. The smallest separation factors were obtained for pairs of gases with similar sorbabilities (Ar/N_2: η = 1.2 to 1.7). This was also found to be the case by Ash Barrer and Lowson (1973) who reported low values of η for N_2/H_2 mixtures, but high values for NH_3 in NH_3/He, NH_3/He and NH_3/N_2 mixtures at 233K again using a Carbolac membrane.

Fig. 5.5.1 to fig. 5.5.5 show the steady state separation factors obtained in this study; they have been calculated using the equation

$$\eta_{A:B} = \frac{y_A}{y_B} \cdot \frac{x_B}{x_A} = \left(\frac{c'_{gA}}{c'_{gB}}\right)_{x=\ell} \circ \left(\frac{c'_{gB}}{c'_{gA}}\right)_{x=0} \quad \text{for an ideal gas}$$

therefore

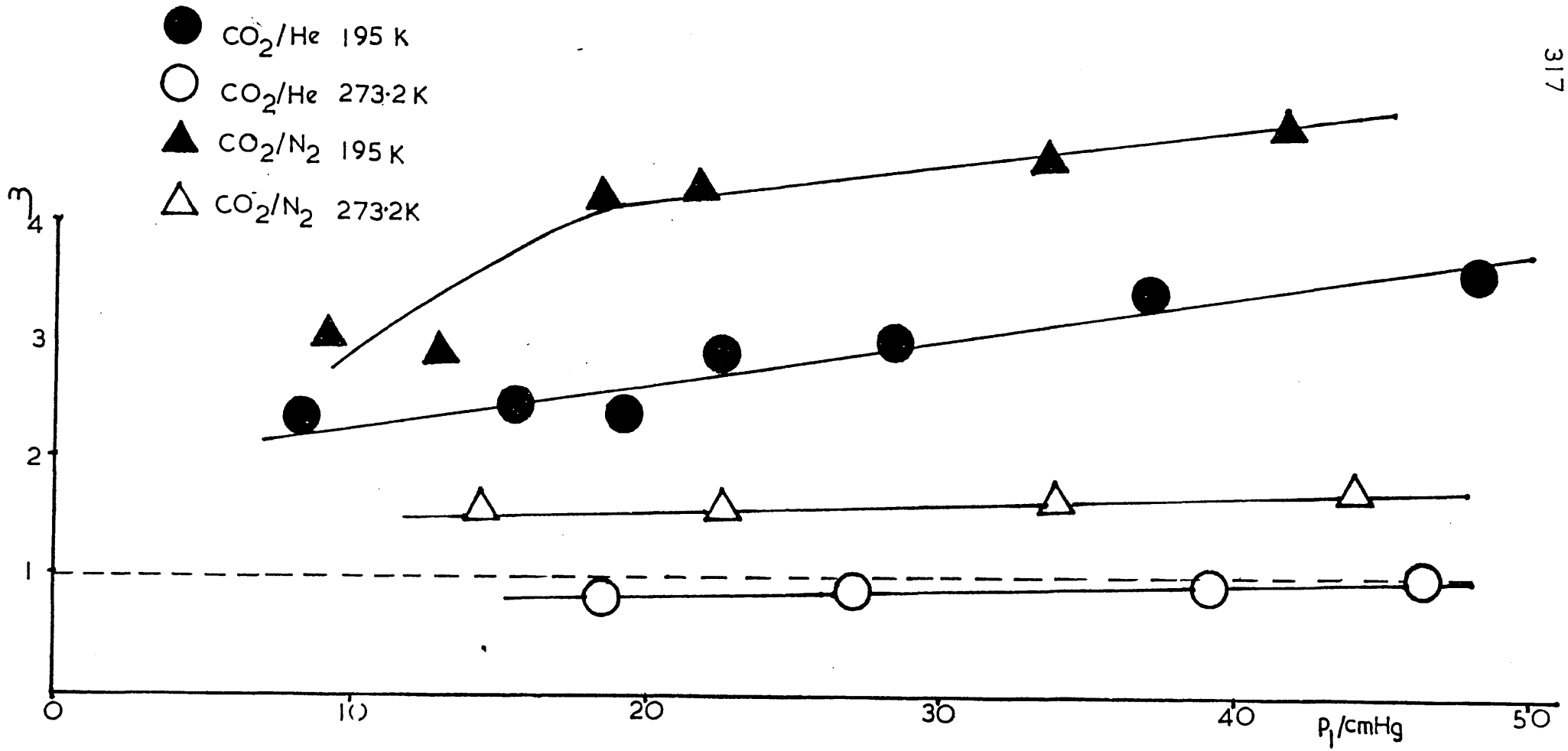
$$\eta_{A:B} = \frac{J_{\infty A}}{(c'_{gA})\ x=0} \circ \frac{(c'_{gB})\ x=0}{J_{\infty B}}$$

and assuming ideality $c'_g = p/RT$ this gives

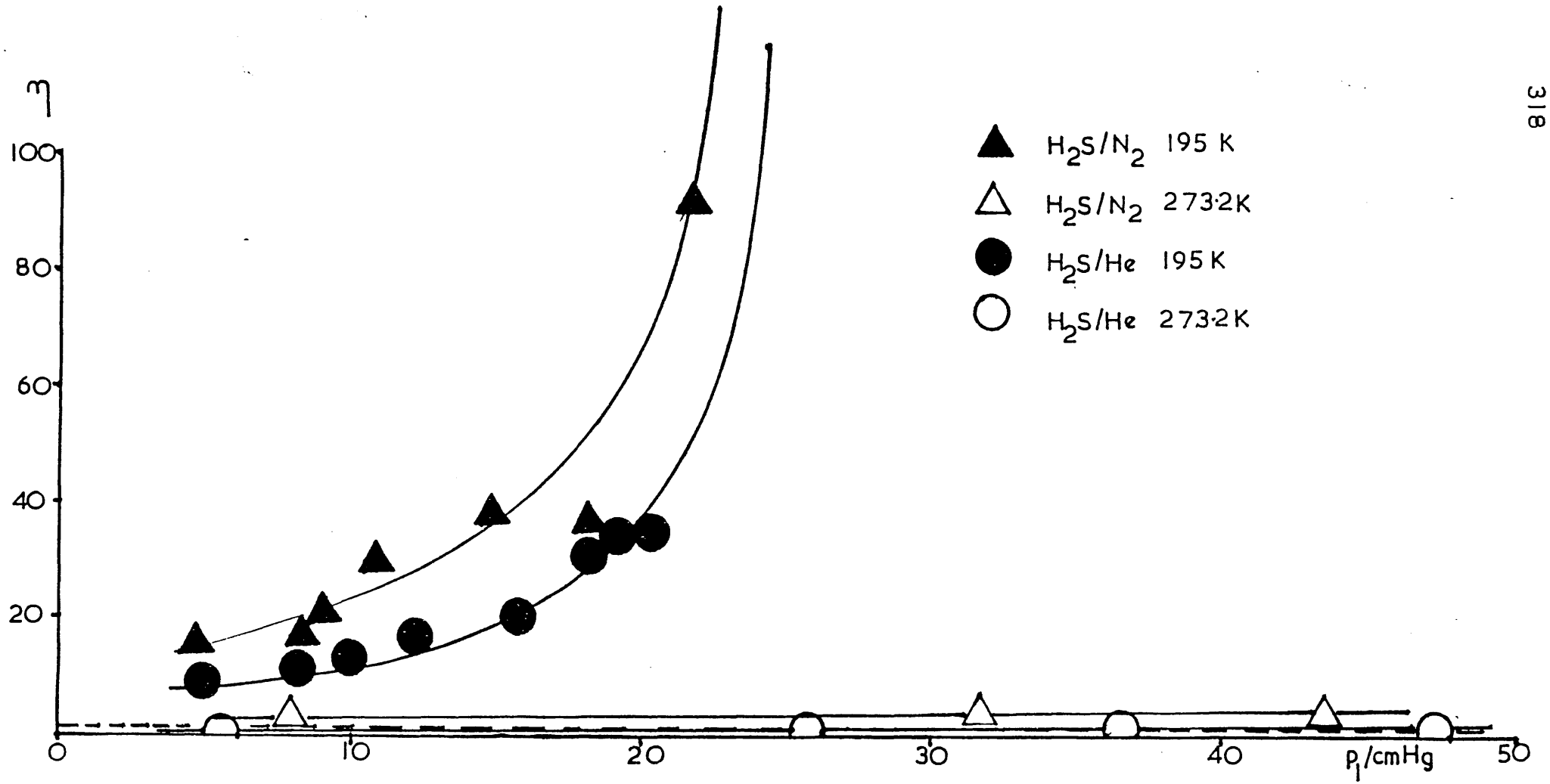
$$\eta_{A:B} = \frac{\tilde{K}_A}{\tilde{K}_B} \quad \text{or} \quad \eta_{A:B} = \frac{\tilde{K}_A}{\tilde{K}_{B(mix)}} \quad \text{for blocked permeabilities for}$$

a binary mixture of gases A and B where c'_{gx} = the gas phase concentration of component x. The position of no separation (i.e. η = 1) has been marked on each diagram by a dotted line. It can be seen that for each system the separation factors for the more sorbable components increase with decreasing temperature. Fig. 5.5.1 shows that at 273.2K, helium is preferentially transported through the Carbolac membrane from

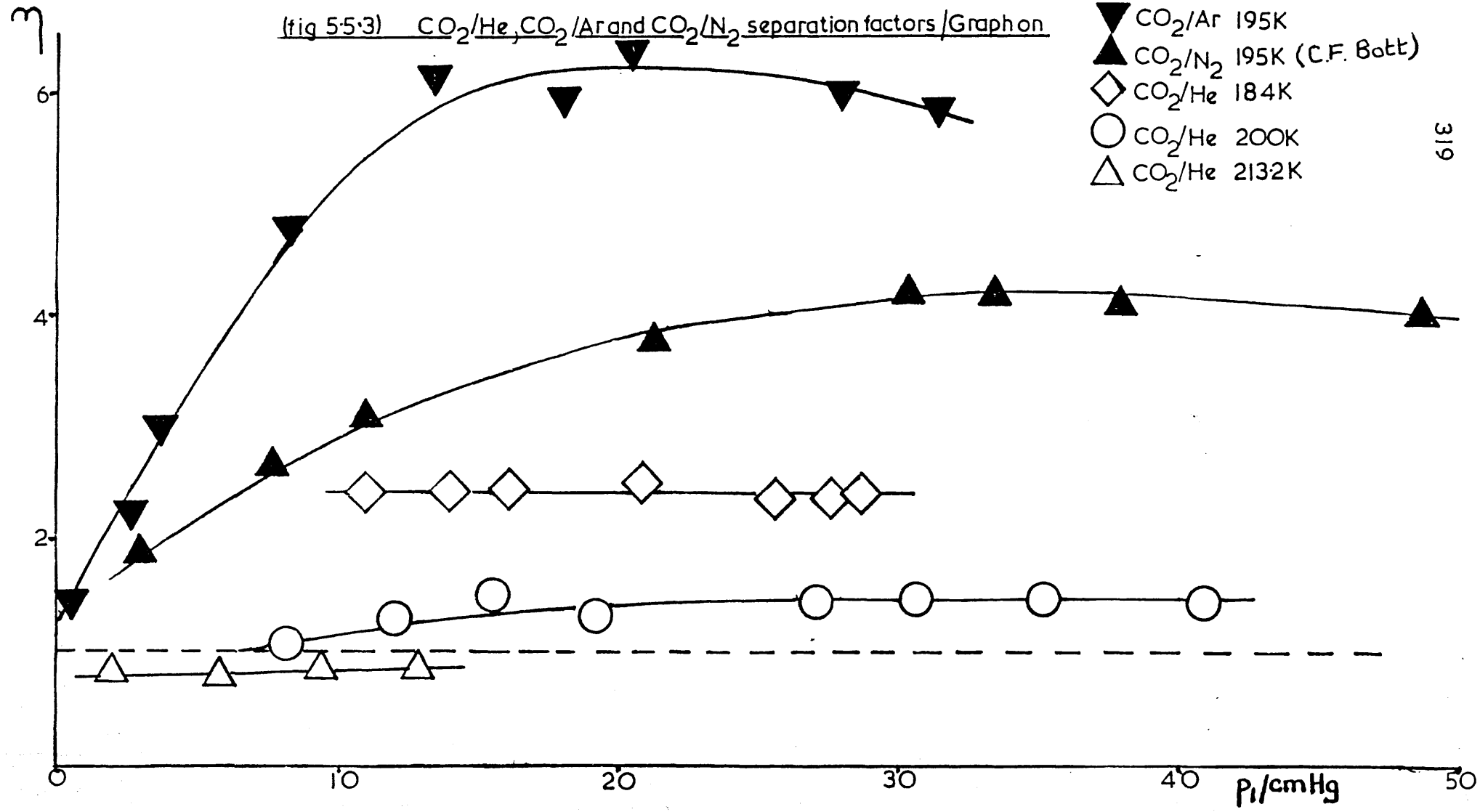
(fig 5·5·1) CO_2/He and CO_2/N_2 separation factors /Carbolac



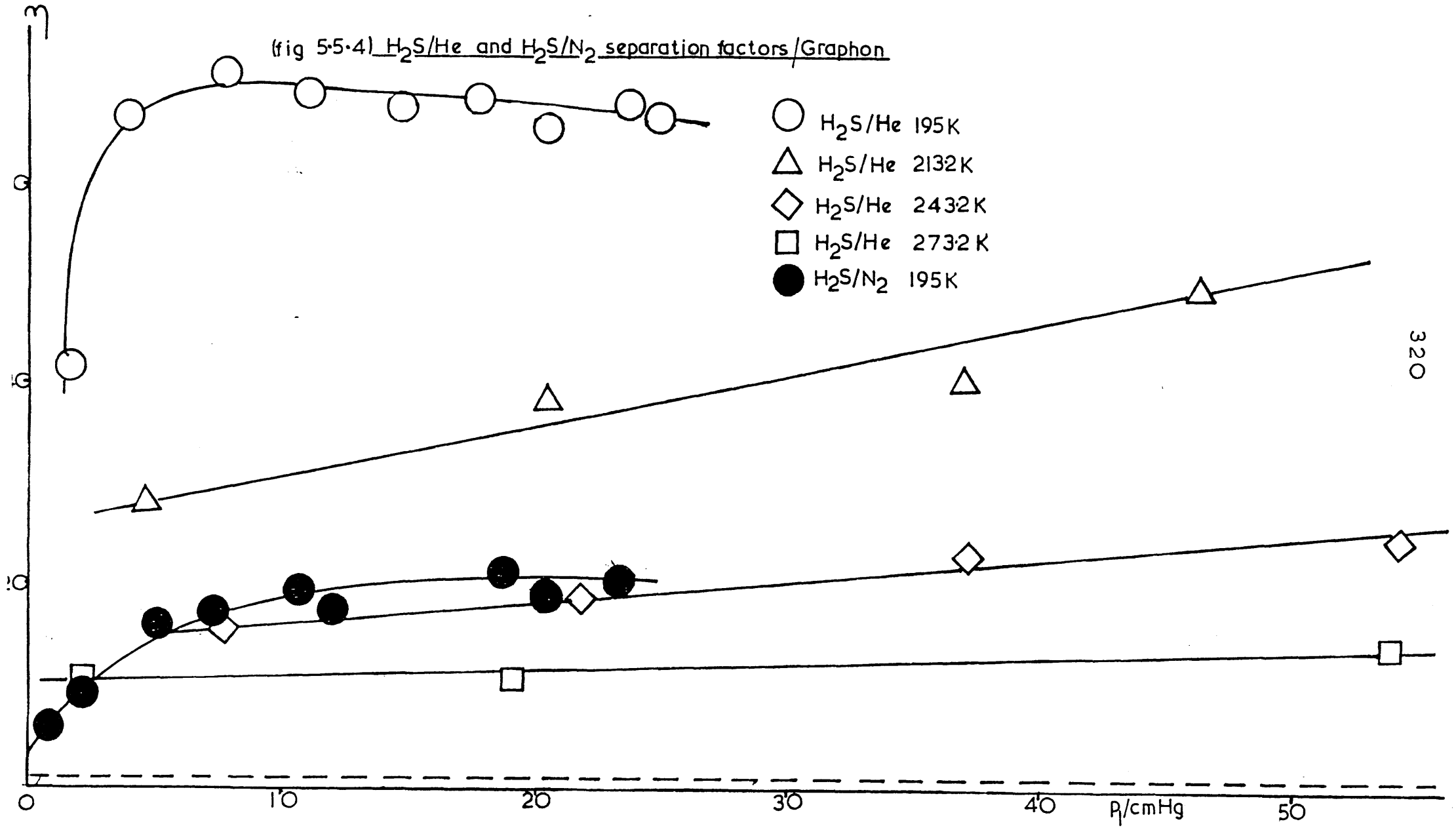
(fig 5·5·2) H_2S/He and H_2S/N_2 separation factors/ Carbolac



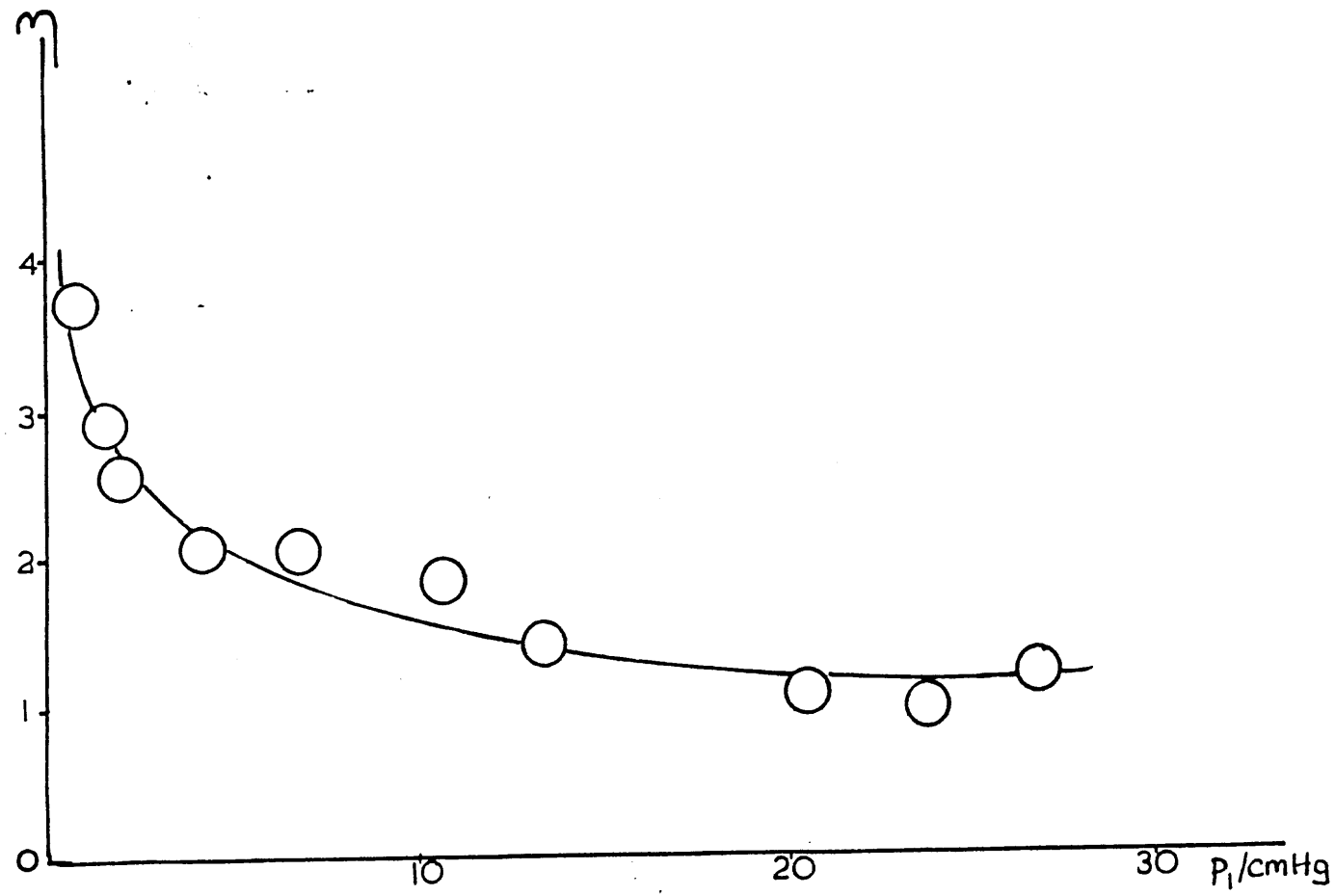
(fig 5·5·3) CO_2/He, CO_2/Ar and CO_2/N_2 separation factors / Graph on



(fig 5·5·4) H_2S/He and H_2S/N_2 separation factors/Graphon



(fig 5·5·5) SF_6/He separation factors Graph on 195K



a He/CO_2 mixture, however at 195K, n for CO_2 rises to approximately 3 for He/CO_2 mixtures and 4 for N_2/CO_2 mixtures. H_2S is similarly transported through the Caroblac membrane giving rise to separation factors which rise dramatically to values exceeding 100 at ingoing pressure 20 cm Hg of H_2S and increase until total blockage of the less sorbable component is obtained (cf fig. 4.3.2).

In both these cases, and for CO_2 flow through Graphon (fig. 5.5.3), greater separation is obtained for mixtures of a strongly sorbed gas and a weakly sorbed gas e.g. CO_2/N_2 than for a strongly sorbed gas and a non sorbed gas e.g. CO_2/He due to the blockage of the weaker extra flow component and the separative effect of Knudsen flow (on a $\sqrt{M}$ basis). This shows that the separation factor is not merely dependent upon the difference in sorbability of the gas mixtures if two sorbable gases are being separated.

The separation factors obtained for CO_2/He, CO_2/Ar and CO_2/N_2 (the latter measured by C.F. Bott) through the Graphon membrane are shown in fig. 5.5.3 and lie in the range 0.8 to 6.0. Fig. 5.5.4 shows the separation factors for H_2S from H_2S/He and H_2S/N_2 mixtures through Graphon which both greatly exceed $\eta_{CO_2:He}$ and $\eta_{CO_2:N_2}$. At 273K a value of approximately 10 is obtained for the separation of H_2S from He using the Graphon membrane, this rises to $\sim$60 at 195K. The H_2S/N_2 separation factors obtained for this membrane are low in comparison to $\eta_{H_2S:He}$; this must be solely due to the separative effect of Knudsen flow, as fig. 5.4.17 indicates that in this case complete blockage of the N_2 extra flow occurred. Finally fig. 5.5.5 shows the separation factors for SF_6 in the SF_6/He/Graphon system. Despite

the large separation factors obtained when porous carbon membranes are used, no commercial processes have yet been developed in which they are employed. This is probably due to the difficulties involved in the fabrication of flexible sheets, or tubes from carbon powders. This difficulty is not present when membranes are fabricated from polymeric material, and it is probably for this reason that the study of polymer membranes has exceeded that of porous membranes for continuous gas separation in recent years. In general the magnitudes of permeabilities of gases through non-porous polymers are up to three orders of magnitude smaller than those through porous media, as the gas molecule must first dissolve in the polymer and then diffuse through it both of which are slow processes in comparison with gaseous diffusion. For this reason, composite membranes consisting of a porous layer and a thin non-porous coating 50-250 nm thick have been made, (Henis and Tripodi 1981). The fabrication of these membranes in the form of hollow fibres is also possible, increasing the surface area/volume ratio and hence the permeability. Much work in this field has been done by SA. Stern who has also reviewed the subject (1972).

5.5.3 Transient state separations

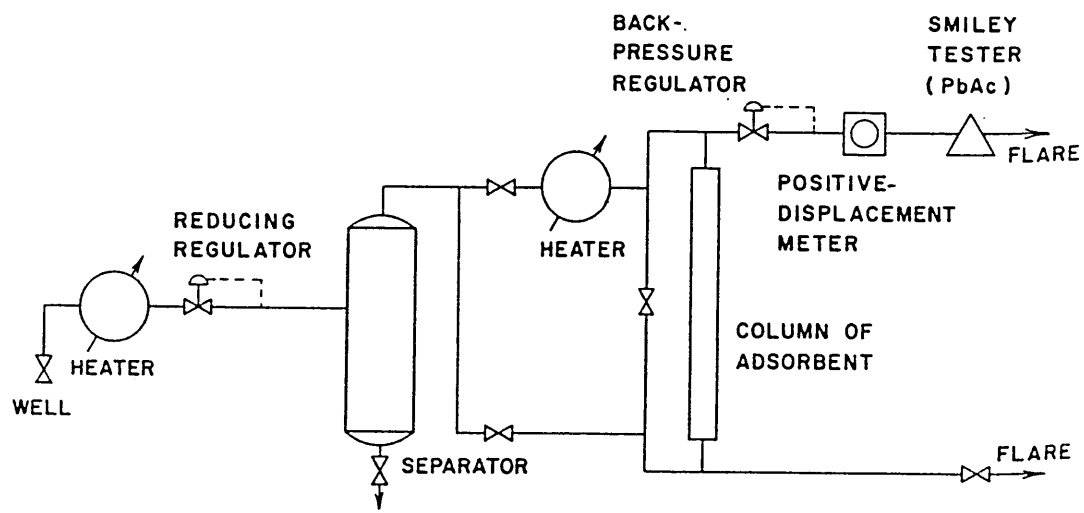
The transient state of flow occurs mainly as a result of adsorption within the membrane, and it was therefore not observed upon membranes with a low sorptive capacity e.g. the Graphon membrane. Transient state gas separation processes will therefore usually be governed by selective adsorption of one component in a mixture and will utilize methods such as the pressure swing adsorption technique. This type of process involves the passage of the gas mixture through a column of the adsorbent, removing all the sorbable components until

the column has reached saturation capacity. The adsorbent must then be regenerated, either by reduction of pressure, application of heat or flushing with another gas, or a combination of the three. This kind of process has been commercialized and is widely used both on a large and small scale. Zeolites, obtainable from the Linde Silica Co. are supplied in the form of small cylindrical pellets and are used for the removal of water vapour and other gases, both in the laboratory and in industrial applications. The use of zeolites for the removal of acid gases (H_2S and CO_2) from natural gas has also been much studied. One such on-site investigation has been made by Fails and Harris (1960) at the Magnolia Petroleum Co's Clayton Ranch, using the apparatus shown in fig. 5.5.6a). The experimental column used was 3" in diameter and 6' long and contained a combination of a zeolite and commercial dessicant "Mobil beads". The tests revealed that of the zeolites studied zeolite 5-A possessed the greatest ability for the selective adsorption of H_2S, in a CO_2 rich environment. A commercially operational column was built and tested and found to be both chemically satisfactory and under certain circumstances economical.

Similar investigations into the separation of H_2S from H_2S/H_2 mixtures (Whitley and Hamrin 1980) and H_2S from H_2S/Hydrocarbon mixtures (Yearout 1971) have also resulted in the development of PSA processes using zeolites 4A and 13X.

Carbon molecular sieve materials are increasingly being used for the separation of gas mixtures by selective adsorption. A carbon molecular sieve similar to the one used in this study is commercially used by Bergbau-Forschung Gmbtt to recover H_2 from coke oven gas, or "steam reforming gas" from other gases and also in the recovery of He.

(fig 5·5·6) Apparatus used to investigate the use of Zeolites as selective adsorbents for H_2S



A four column PSA process has been developed details of which are given in fig. 5.5.7a. The feed gas flows through the adsorbent from the bottom to the top of one vessel. At the same time one of the other vessels is purged while the other two vessels equalize the pressure and repressurize or depressurize.

The four process steps are

(i) adsorption of the sorbable impurities

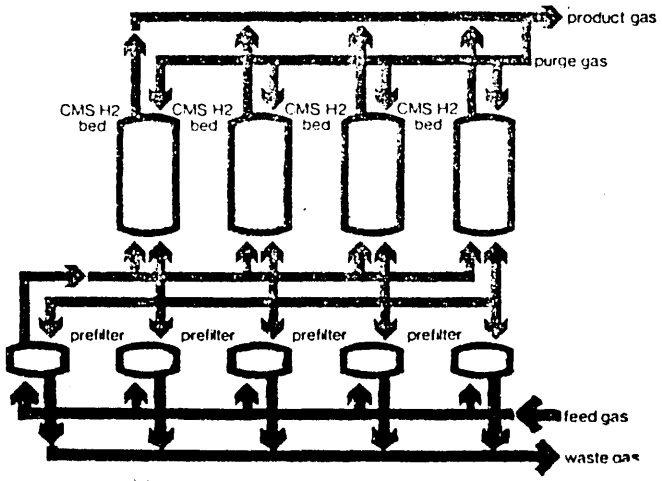
(ii) pressure reduction in two steps, initially, pressure equalization followed by depressurization

(iii) repressurization also in two steps.

Figure 5.5.7b shows the sequence of process steps and the pressure versus time graph for each vessel. This method provides a continuous separation process and its manufacturers also claim that it has the advantages of quick shut-down and start up characteristics, low investment and maintenance costs and a high degree of flexibility. A similar two column process is used commercially for the separation of O_2/N_2 mixtures using the carbon molecular sieve examined in this study. (Juntgen et al 1981).

Other pressure (or temperature) swing adsorption processes may use charcoal, or activated carbons as the adsorbate (Kreul et al 1971) or may even use adsorption followed by catalytic reactions such as oxidation (Batzler et al 1972). The initial research for gas separation by selective adsorption involves the measurement of adsorption isotherms and break through times. Hence, by reference to the results in chapter 4 the suitability of the adsorbents studied for utilization in a PSA type process may be examined. The results are summarized in table 5.5.1.

(fig 5·5·7a) Diagram of four column PSA system developed by Bergbau-Forschung GmbH



(fig 5·5·7b) Sequence of process steps in a PSA four column system

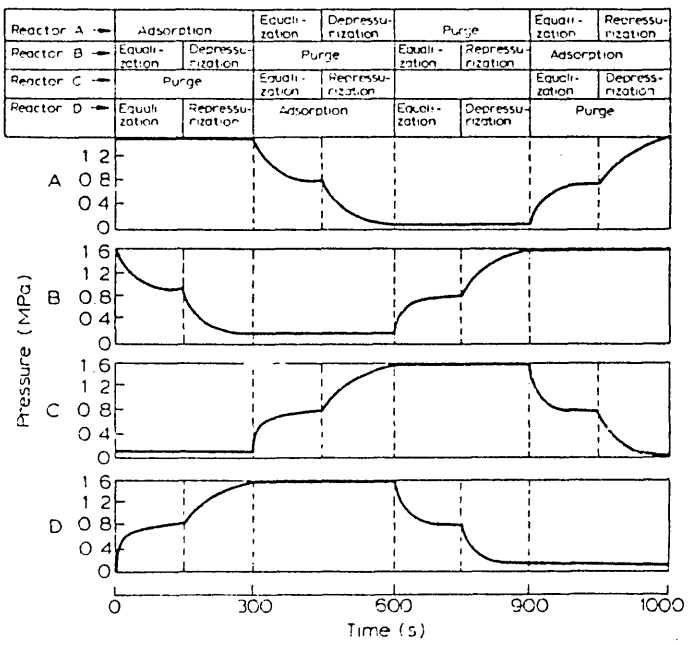


Table 5.5.1

Summary of adsorption and detection time results

Adsorbent	H_2S	CO_2	N_2	He
NaX	strong adsorption BTT: long	strong adsorption BTT: long	weak adsorption t_1: short	non-sorbed t_1: none observed
CMS	little adsorption t_1: none observed	strong adsorption BTT: long	little adsorption t_1: none observed	non-sorbed t_1: none observed
Carbolac	strong adsorption t_1: long	strong adsorption t_1: long	weak adsorption t_1: none observed	non-sorbed t_1: none observed

Table 5.5.1 shows that using NaX N_2 and He should be separable from each other or from the more strongly adsorbed gases H_2S or CO_2. There is little difference between the adsorption of H_2S and CO_2, H_2S being slightly more strongly adsorbed (by 10% to 20%) indicating that this mixture could not be easily separated using a NaX column for this reason and also due to the catalytic effect of NaX upon H_2S.

Only CO_2 is strongly adsorbed by the CMS, suggesting that CO_2/He, CO_2/N_2 or CO_2/H_2S separations would be possible using this material. It must be admitted that in this study only single gas measurements have been made, and that when gas mixtures are passed through adsorbent columns, competitive adsorption may lessen the separative ability of the column However in the examples previously quoted (Fails and Harris 1960 and Juntgen et al 1981) competitive adsorption has not been found to be a problem if the gas mixture is pre-dried.

When steady state flow is achieved through either molecular sieve membrane, the mixture will flow with a bulk viscosity and not with those of the component gases so no separation will occur.

The Carbolac membrane appears to have the ability to separate N_2 or He from H_2S or CO_2 in the transient state; however in the steady state (particularly at lower temperatures) the more sorbable component is transported preferentially. The steady state separation factors for the Carbolac membrane have already been calculated from the binary mixture experiments (Section 5.5.2). Since this system does not exhibit a Poiseuille flow component the transport of the sorbable component can reasonably be assumed independent of a weakly-sorbable gas (at least to a first approximation). This being the case it is possible to calculate not only the steady state separation factor but also transient state separation factors, assuming that both gases are admitted to the membrane coincidentally. The equation

$$\eta_{A:B} = \left(\frac{c_g{}^A}{c_g{}^B}\right)_{x=1} \Big/ \left(\frac{c_g{}^A}{c_g{}^B}\right)_{x=0} \qquad \text{for an ideal gas}$$

is used as in Section 5.5.2,

where at time t $\quad (c_g{}^A)_\ell\ (t) = \dfrac{Q_A(t)}{V}$

and $\quad (c_g{}^B)_\ell\ (t) = \dfrac{Q_B(t)}{V}$

with $Q_x(t)$, the number of moles of gas x on the outgoing side and V, the outgoing volume

$$Q_x(t) = \frac{p_{2x}(t) \times V}{RT_R}$$

where p_{2x} is the outgoing pressure of gas x

hence
$$\eta_{A:B} = \frac{Q_A(t)}{Q_B(t)} \Bigg/ \left(\frac{p_A}{p_B}\right)_o$$

This may be expressed in terms of p_{2x}.

$$\eta_{A:B} = \left(\frac{p_{2A}(t)}{p_{2B}(t)}\right) \Bigg/ \left(\frac{p_A}{p_B}\right)_o$$

It is this equation which has been used to calculate transient state values of η for the Carbolac membrane. η may also be expressed in terms of the flux (J_{∞_x}) of a component and its time lag (L_x), leading to the form

$$\eta_{A:B} = \frac{J_{\infty_A}(t - L_A)}{J_{\infty_B}(t - L_B)} \Bigg/ \left(\frac{p_A}{p_B}\right)_o$$

$$= \frac{\tilde{K}_A}{\tilde{K}_B} \frac{(t - L_A)}{(t - L_B)}$$

When gas has been flowing for long periods of time such that $t \gg L_A, L_B$ the above equation should become

$$\eta_{A:B} = \frac{\tilde{K}_A}{\tilde{K}_B} \quad \text{(the steady state value).}$$

The transient state separation factors η for mixtures of CO_2 or H_2S with N_2 or He, flowing through the Carbolac membrane are shown in fig. 5.5.8 to fig. 5.5.15 by the continuous lines. From these diagrams it can be seen that even after 1000 min η is still increasing and the steady state separation factor has not been attained, despite the fact that in most cases steady state flow has been in process for more than 800 minutes. The separation factor for the sorbable component is close to zero until the detection time, occurs, showing that only the less-

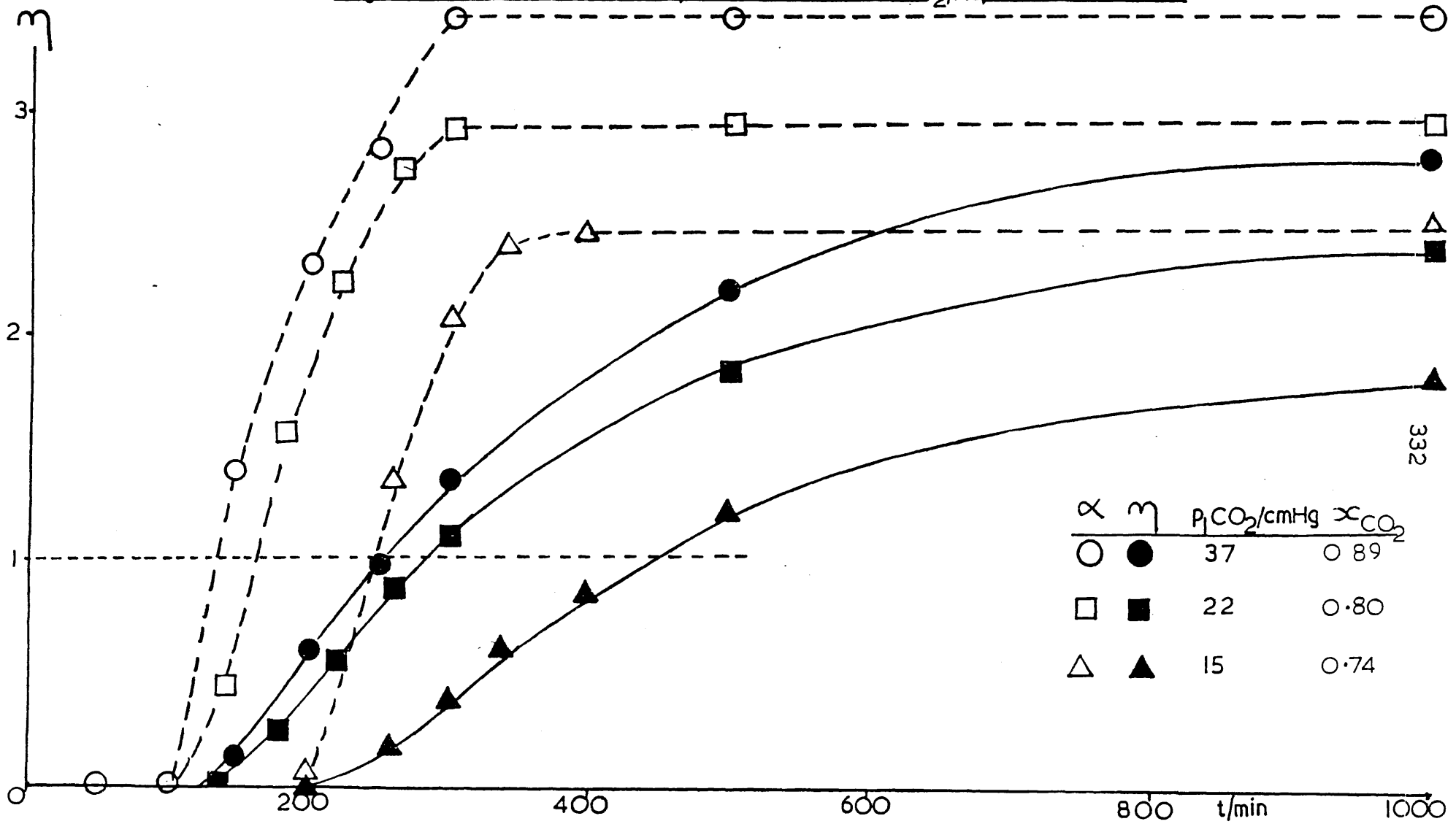
sorbable component is present at the outgoing side and complete separation has been obtained, by selective adsorption. This is also shown by the high separation factor for the less sorbable gas as shown for example in fig. 5.5.8a for the He/CO_2/Carbolac system. After the detection time the pressure of the sorbable component increases, but no indication of the attainment of steady state flow is apparent from the graphs of η versus t. Separation factors calculated in this way would be useful in a static system, where the permeate gas was collected until a certain composition was obtained, however most PSA type processes involve the flow of the permeate gas away from the column and in this case the separation factor η has little meaning. For this reason α (a second separation factor) has also been calculated where

$$\alpha = \left[\frac{\frac{dp_{2A(t)}}{dt}}{\frac{dp_{2B(t)}}{dt}}\right] \Big/ \left[\frac{p_A}{p_B}\right]_o$$

$$= \left[\frac{J_{A(1,t)}}{J_{B(1,t)}}\right] \Big/ \left[\frac{p_A}{p_B}\right]_o = \left[\frac{\frac{dQ_{A(t)}}{dt}}{\frac{dQ_{B(t)}}{dt}}\right] \Big/ \left[\frac{p_A}{p_B}\right]_o$$

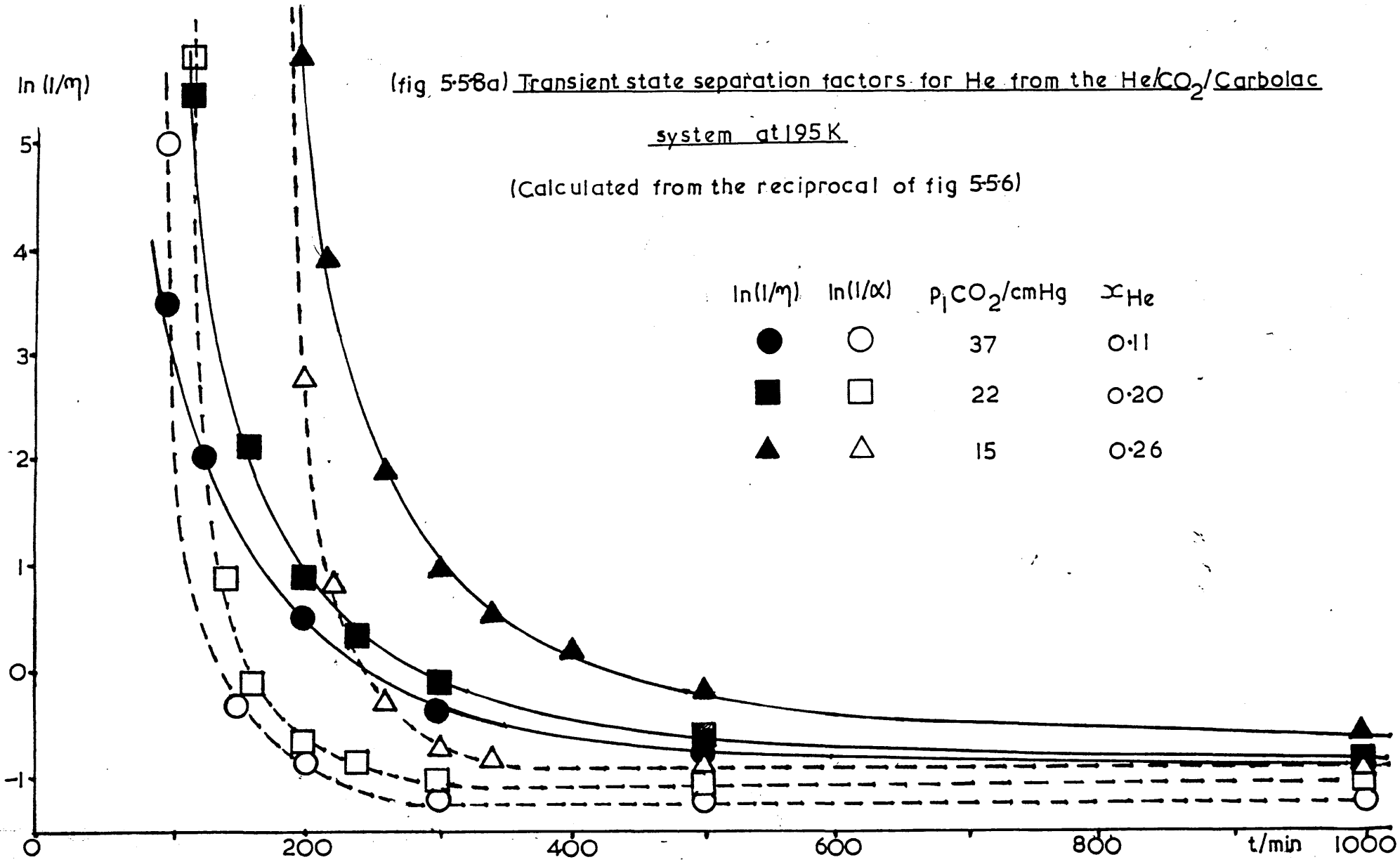
α shows the degree of separation obtained in the gas mixture leaving the membrane at time (t), and therefore conforms to the definition of a separation factor given in Section 5.5.2. Like η, α has a value of 0 before the break through time of the sorbable component, it then increases abruptly, and should attain the steady state value of η at the moment steady state flow begins. Graphs of α versus t might be

(fig 5.5.8) Transient state separation factors CO_2/He/Carbolac 195 K

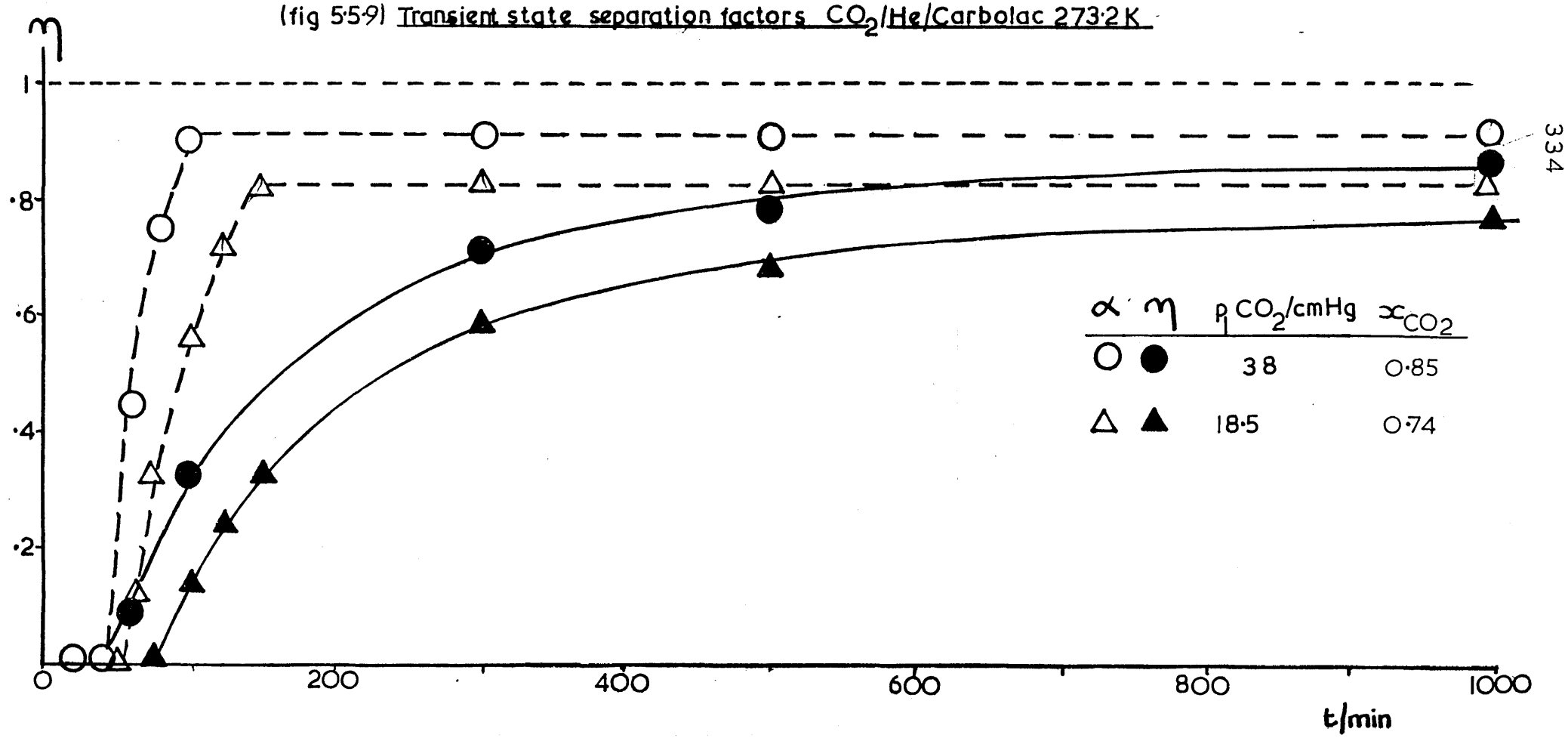


(fig 5·56a) Transient state separation factors for He from the He/CO_2/Carbolac system at 195 K

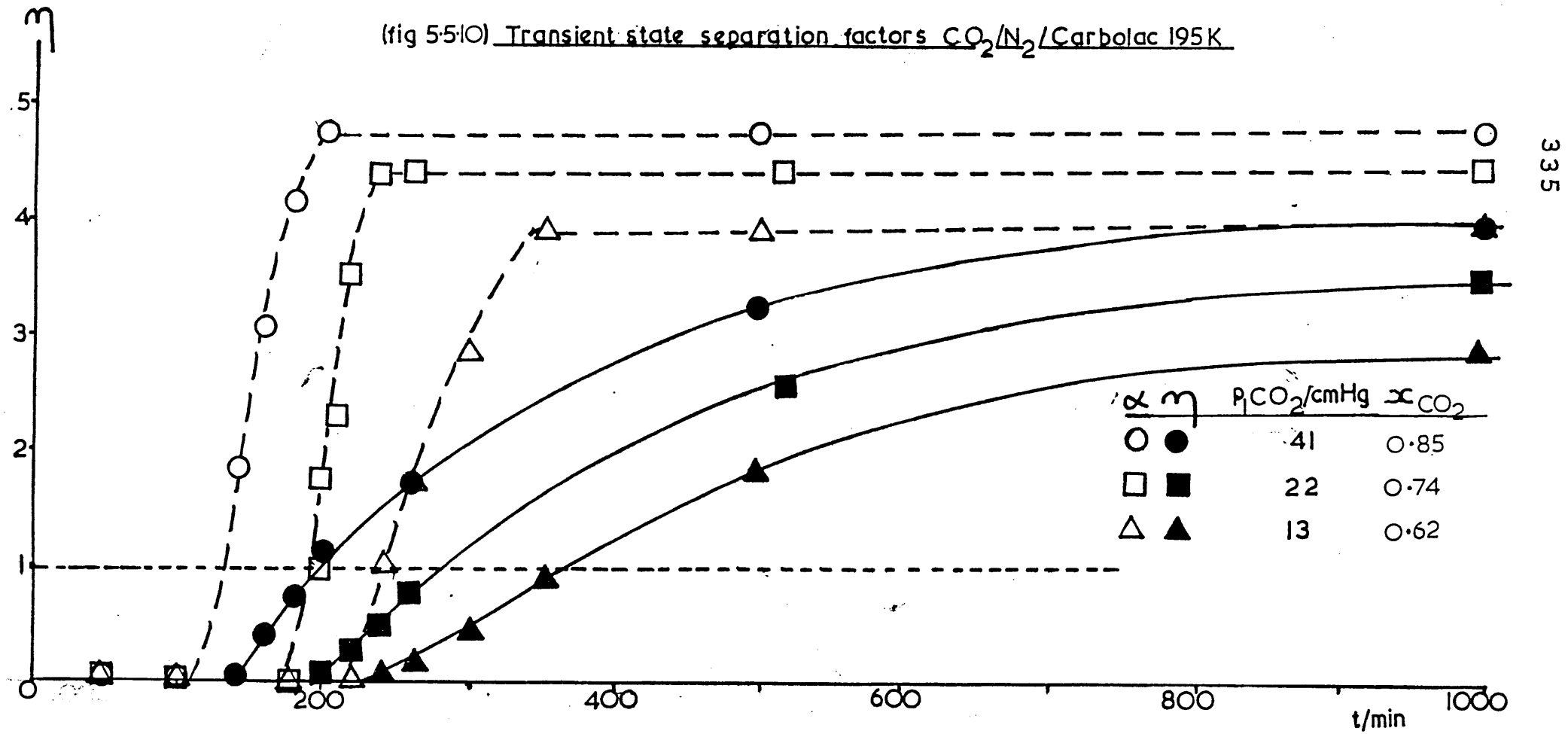
(Calculated from the reciprocal of fig 5·56)



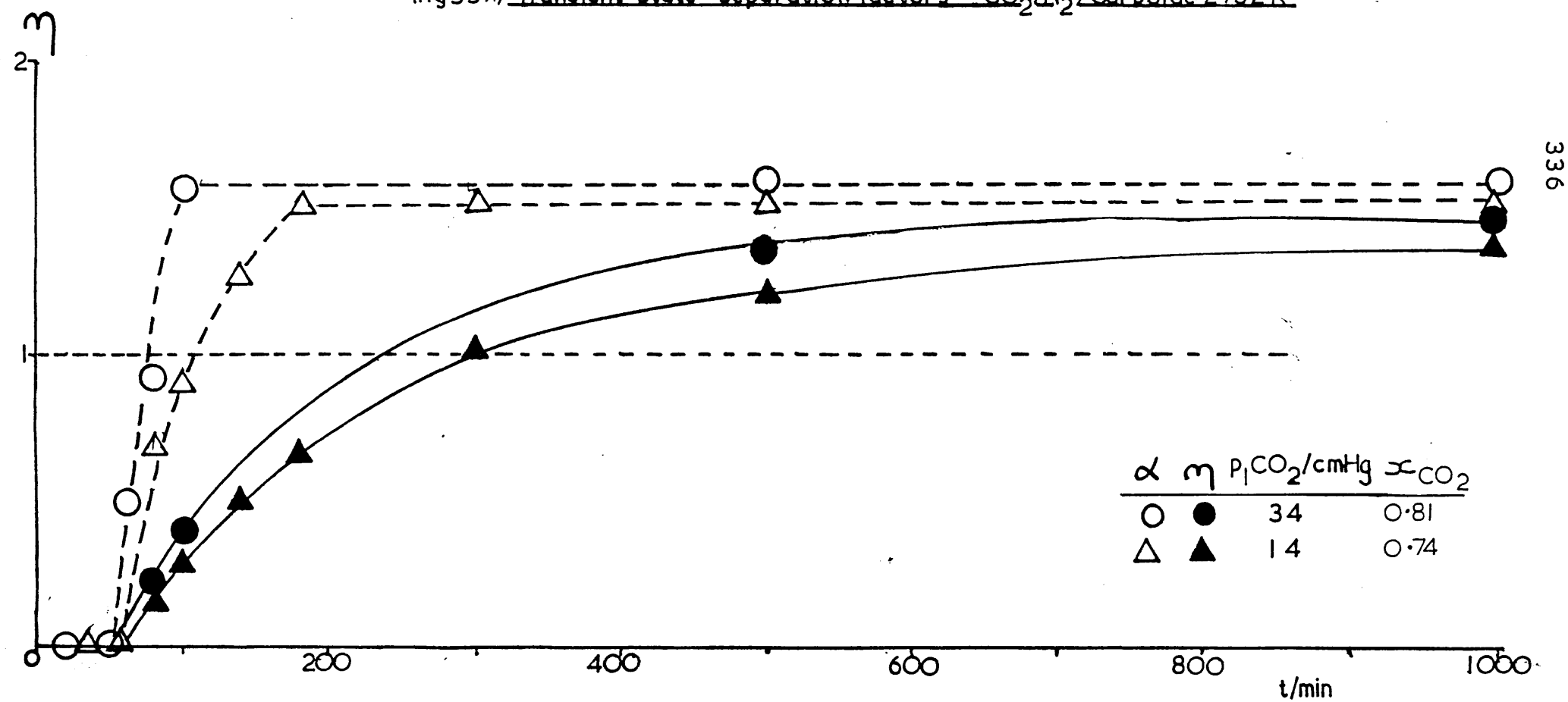
(fig 5·5·9) Transient state separation factors CO_2/He/Carbolac 273·2 K



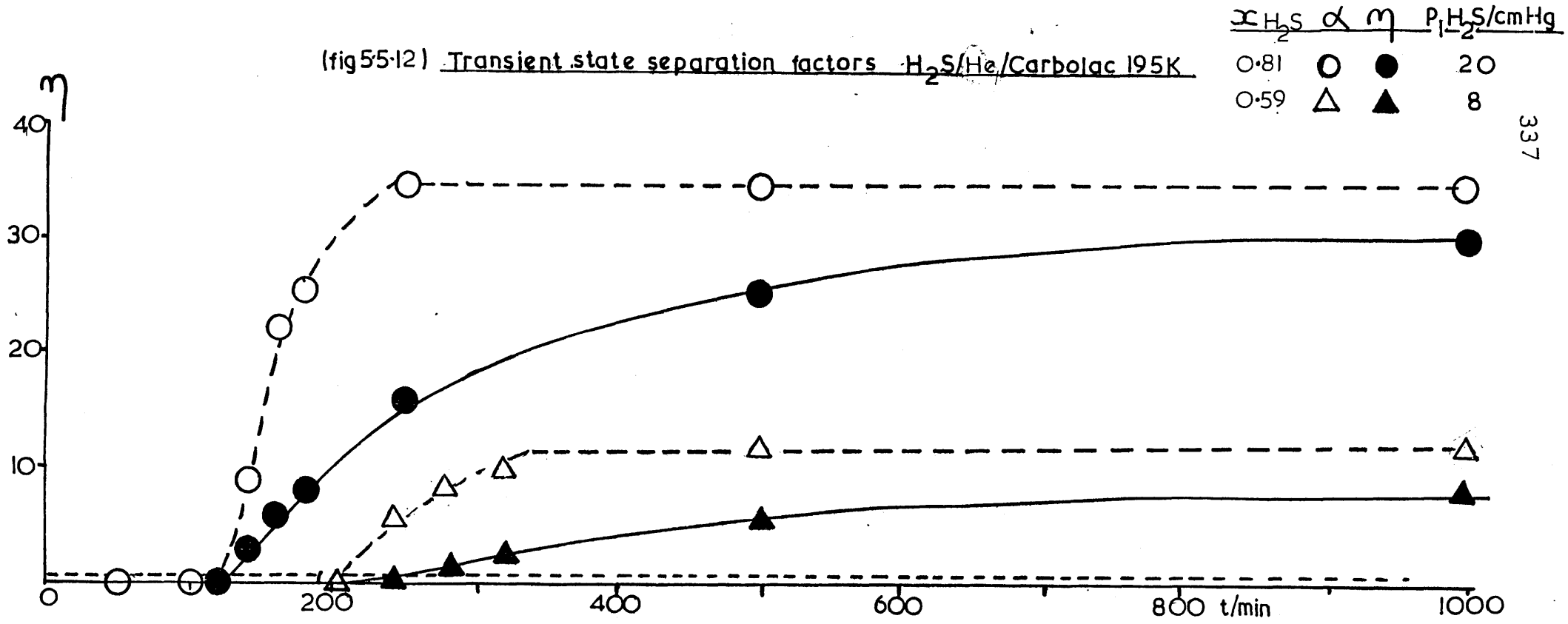
(fig 5·5·10) Transient state separation factors CO_2/N_2/Carbolac 195K



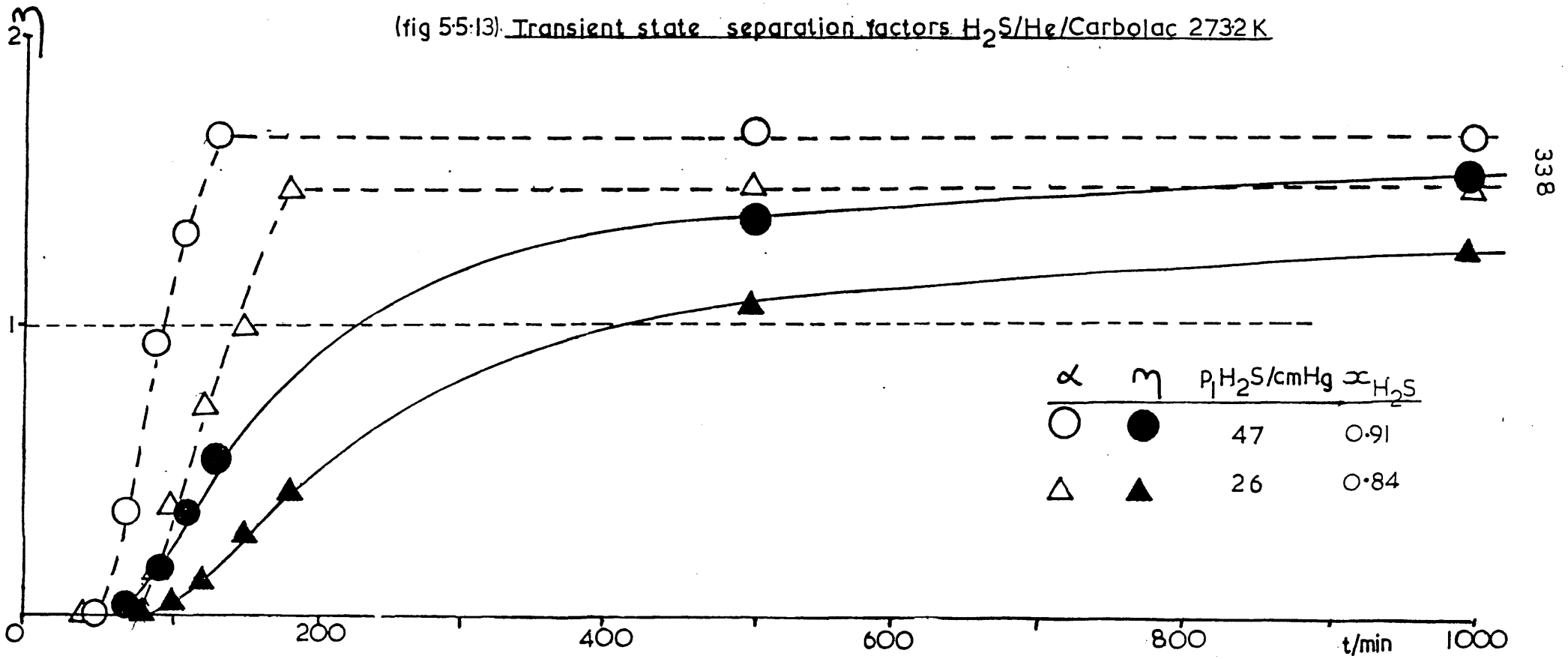
(fig 5·511) Transient state separation factors CO_2/N_2 /Carbolac 273·2 K



(fig 5·5·12) Transient state separation factors H_2S/He/Carbolac 195K

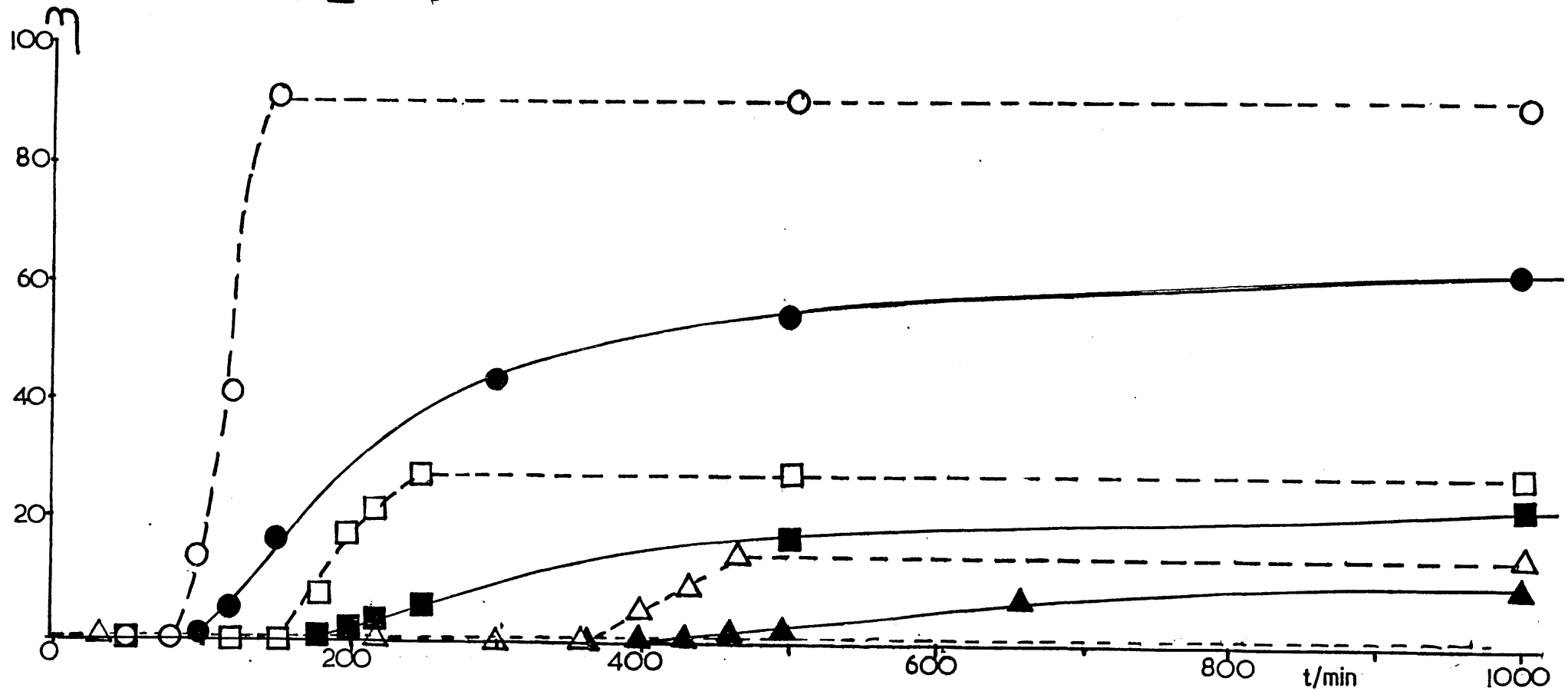


(fig 5·5·13) Transient state separation factors H_2S/He/Carbolac 273·2 K

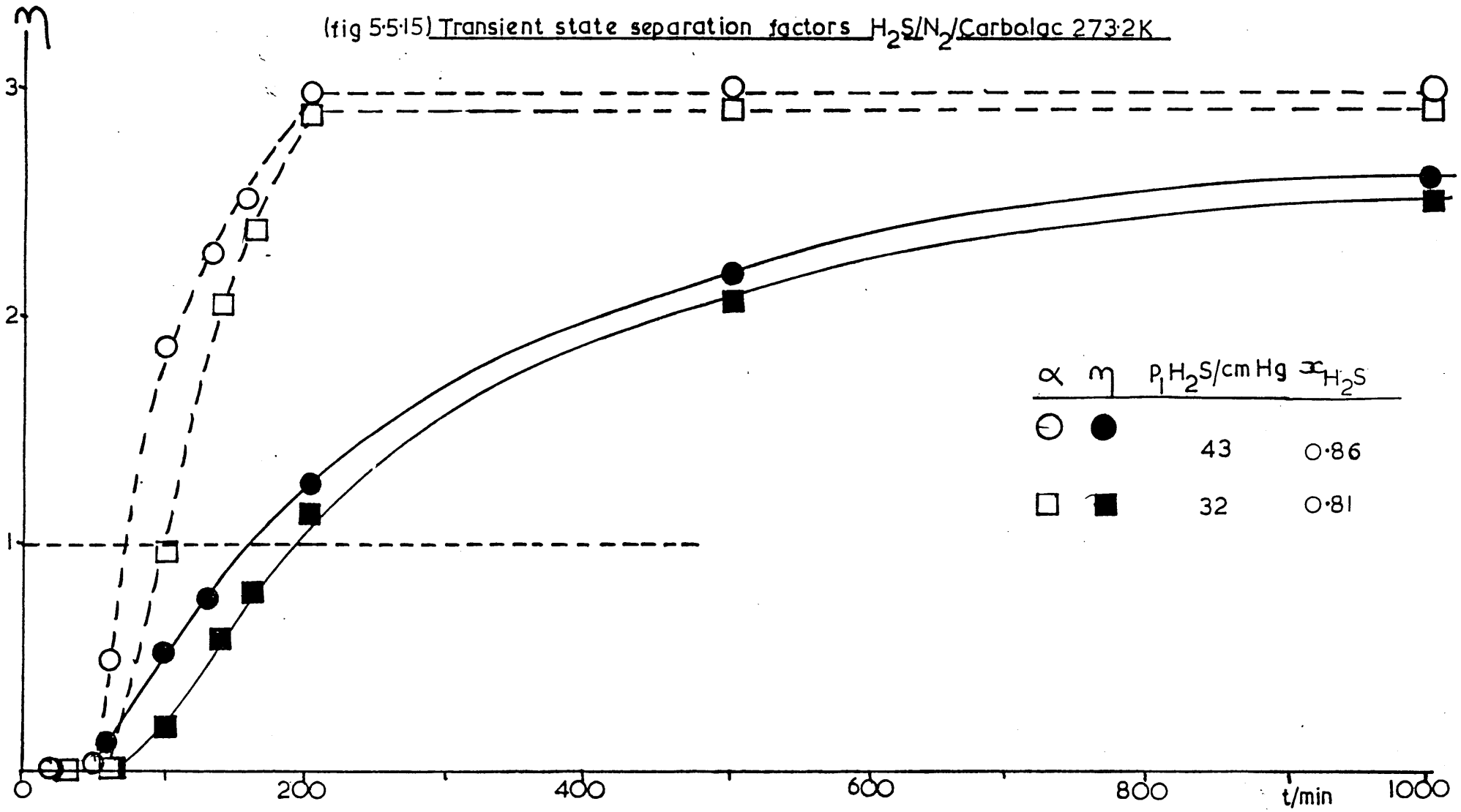


(fig 5·5·14) Transient state separation factors H_2S/N_2/Carbolac 195K

α	ϖ	P_1 H_2S/cmHg	x_{H_2S}
○	●	21	0·76
□	■	11	0·57
△	▲	5	0·37



(fig 5·5·15) Transient state separation factors H_2S/N_2/Carbolac 273·2K



useful in the determination of cycle times for a PSA process, the permeate stream of which must not drop below a given composition. In fig. 5.5.6 to fig. 5.5.13 α versus t is shown for each gas mixture, at different ingoing compositions by a dotted line. In all cases it can be seen from reference to fig. 5.5.1 and fig. 5.5.2 that the steady state separation factors are indeed attained, when steady state flow begins.

5.5.4 Separation of H_2S from gas mixtures

Large quantities of H_2S are produced as a by-product in the purification of natural gas, petroleum and in coal-coking operations. The removal and recovery of H_2S is important for both economic and environmental reasons. Sulphur produced from the H_2S recovered from "sour" natural gas is currently the largest source of "non-Frasch" elemental sulphur. Hydrogen sulphide is usually removed from the sour gas by absorption in an alkaline solution (alkanolamines are widely used). The adsorbed H_2S must then be removed from the solution by heating and stripping with another gas, and the resulting gas stream usually contains H_2S and some CO_2. The concentrated H_2S stream may then be converted to sulphur using a modified Claus process, however the Claus process itself produces a waste gas which must be scrubbed of H_2S and SO_2 before release into the atmosphere. Much work has therefore been done in order to discover scrubbing processes for the removal of H_2S present in high or low concentrations. One of these is the process of the Institut Francais du Petrole's process using a solvent catalyst system to remove and oxidise the H_2S (IFP 1971). More commonly used in Britain is the Stretford process, which is currently employed by British Gas to remove H_2S from Substitute Natural Gas. The

Stretford process uses an alkaline solution generally containing a vanadium catalyst so that the H_2S is both adsorbed and also oxidised to form sulphur.

The methods by which H_2S may be removed from gas streams may be divided into four categories.

(i) Chemical reaction absorption.

This category includes processes using monoethanolamine diethanolamine, and diglycolamine, also hot carbonate processes such as the Benfield process (Benson 1974) which uses solutions of hot potassium carbonate, and the iron sponge processes which use a solution of quinone to convert H_2S to sulphur.

(ii) Physical absorption

These methods of H_2S removal include the Fluor solvent process which uses a refrigerated solvent consisting of anhydrous propylene carbonate, and other methods which use the dimethyl ether of polyethylene glycol or methanol as solvents.

(iii) Adsorption

This category includes the use of zeolites and other molecular sieves as discussed in Section 5.5.3.

(iv) Selective permeation

Investigation into polymer membranes has produced the possibility of a continuous method of separating H_2S from other gases. Coady and Cooley have patented a process using cellulose acetate membranes for H_2S and CO_2 separation from hydrocarbons, and work into the permeability of vinylidine chloride to H_2S has been done by Heilman et al (1956).

The work done in the current study has increased the amount of data available concerning H_2S adsorption and flow through microporous media (about which there is little published information). In particular the comparison of data for CO_2 and H_2S has made possible tentative suggestions for methods of separating CO_2/H_2S mixtures which are difficult to separate by conventional means. Transient state flow experiments and adsorption isotherms indicate that CO_2/H_2S mixtures could not be efficiently separated by selective adsorption using NaX or Carbolac, but that a separation process of the PSA type which uses the carbon molecular sieve material as an adsorbent might be useful, especially for the separation of mixtures containing more H_2S and other non-sorbed gases than CO_2.

The flow experiments using the Carbolac and Graphon membranes constitute the first work with H_2S and H_2S mixtures on membranes of this type. The separative ability of these membranes upon a mixture of two strongly adsorbed gases has yet to be tested, however binary mixture results using a weakly adsorbed gas such as Ar and N_2 in admixture with a strongly adsorbed gas have produced high steady state separation factors (Section 5.5.2) due to the blockage of the extra flow of the less sorbable component. On the basis that CO_2, although highly sorbable upon both Graphon and Carbolac, is only half as well adsorbed as H_2S (the volume of H_2S adsorbed is approximately twice that of CO_2 at a given temperature and pressure) and the extra flow of H_2S is more than double that of CO_2 through both membranes, it is possible that adsorbed layers of H_2S might block CO_2 flow. This would constitute the basis of a continuous separation process for H_2S/CO_2 mixtures. In this study the investigation of H_2S/CO_2 mixtures flowing

through Graphon and Carbolac membranes was not possible due to lack of time and of analytical facilities and it is recommended that these systems receive attention in the near future.

CHAPTER 6

SUMMARY OF RESULTS AND RECOMMENDATIONS FOR FURTHER WORK

(A) Adsorption and flow of H_2S, CO_2, N_2 and He have been investigated at different temperatures on four membrane materials.

(B) Adsorption isotherms have been analysed by means of the Langmuir model for type 1 isotherms, the BET model for type II isotherms and the analysis of Beebe et al (1964) for type III isotherms to give the monolayer capacity for each system.

(C) Gas flow through the NaX and CMS membranes was found to contain a Poiseuille flow component and was analysed in terms of the Carman-Arnell equation (Carman and Arnell 1948). $\tilde{K}_1'$ and $\tilde{K}_2'$ were calculated and were both found to be approximately constant for each membrane except where structural changes occurred.

(D) The correlation between different gases flowing through each molecular sieve membrane was analysed by means of the "universal plot" of Berman and Lund (1958). This produced a universal curve for the CMS but not the NaX membranes.

(E) The break-through time procedure of Barrer (1954) was tested and found to give $J_\infty x\ BTT = \frac{Acl}{2} \times Ac'_s$ for CO_2 flow through NaX membrane I at 195K but not for any other systems, possibly due to packing inhomogeneities or to loss of sorptive capacity on compaction.

(F) An expression giving the time lag in terms of the Langmuir coefficients and the Poiseuille and Knudsen permeabilities (Ash 1986) was used and found to give values of L which were in good agreement with experimental results for H_2S and CO_2 flow through NaX membrane 2 and CO_2 flow through the CMS membrane.

(G) The flow of sorbable gases through the Carbolac and Graphon membranes was analysed in terms of the extra flow component $\tilde{K}_s$ and the ability of each membrane to promote extra flow as indicated by $\tilde{K}_s/A$ was discussed. Graphon gave the higher $\tilde{K}_s/A$ values; this was attributed to its homogeneous surface.

(H) Integral and differential diffusion coefficients were calculated for Carbolac and Graphon systems. These showed a marked concentration dependence and exhibited maxima in the region of monolayer coverage. They were also described by an Arrhenius type relationship resulting in the determination of an activation energy for diffusion.

(I) Blockage of He by layers of an adsorbed gas were presented in the form of blockage curves as given by Hamilton (1980). For both Graphon and Carbolac an initial sharp decrease in $\tilde{K}_R$ was obtained indicating blockage of pores at key sites. $\tilde{K}_R$ then continued to decrease with increasing p_1/p_o for the Carbolac membrane, however the Graphon membrane exhibited a "plateau" value of $\tilde{K}_R$ which was maintained up to $p_1/p_o = 1$ for CO_2 and H_2S. This was interpreted in terms of a uniform pore structure with pores of approximately constant dimmensions.

(J) The blockage of weakly sorbed gases Ar and N_2 by CO_2 and H_2S has been investigated and in all cases some blockage of the extra flow of the more weakly sorbed component was observed.

(K) Steady state separation factors were evaluated for the sorbable component of each binary mixture studied. They ranged between 0.6 and 70 for the Graphon membrane and 0.8 to ∞ (complete blockage of the less sorbable component) for the Carbolac membrane.

(L) Transient state separation factors were calculated for binary mixtures flowing through the Carbolac membrane. These showed complete 'hold up' of the sorbable component (separation factor for He $\rightarrow\infty$) before the detection time and then increased towards the steady state separation factor which favoured the sorbable component.

Recommendations for further work.

1. It is felt that both the Break-through time procedure and the time lag equation merit application to further systems, as both methods have been found to predict experimental results in certain cases.

2. The carbon molecular sieve has shown interesting adsorption characteristics due to its narrow pore size distribution and further investigation of both adsorption and flow possibly using O_2 and CO is suggested.

3. The results obtained from binary mixture experiments using one strongly adsorbed and one weakly adsorbed gas have indicated partial blockage of the extra flow of the more weakly adsorbed component. Experiments using two strongly adsorbed gases are suggested in order to see if this trend continues.

4. The measurement of the total flux as well as the flux of one component in binary mixture experiments would enable the effect of the 'indicator' gas upon the 'blocking gas' to be quantified.

5. Flow experiments above atmospheric pressure would

(a) indicate the suitability of this type of membrane to industrial applications.

(b) eliminate the need for low temperature experiments (as an equivalent degree of adsorption could be obtained at room temperature)

(c) make possible the investigation of blockage effects at higher pressures.

APPENDICES

APPENDIX A. ISOTHERMS i) Zeolite isotherms

1. Zeolite NaX / CO_2
2. Zeolite NaX / H_2S

ii) Carbon Molecular Sieve Isotherms

3. Carbon Molecular Sieve / Oxygen
4. Carbon Molecular Sieve / CO_2
5. Carbon Molecular Sieve / N_2

iii) Carbolac Isotherms

6. Carbolac / N_2
7. Carbolac / H_2S

iv) Graphon Isotherms

8. Graphon / N_2
9. Graphon /CO_2
10. Graphon / H_2S
11. Graphon / SF_6

Appendix 1 Adsorption isotherms

1. CO_2/NaX

P/cmHg	v/cm^3STPg^{-1}
195 K	
0.456	11.1
1.901	85.2
4.408	135.1
8.436	192.1
19.323	198.4
28.906	201.3
44.000	205.4
14.062	199.0
5.391	189.7
2.055	186.5
213.2K	
0.456	85.0
1.901	86.9
4.408	135.0
8.436	179.3
19.323	188.9
28.906	193.4
44.000	197.7
14.062	189.3
5.391	179.7
2.055	170.2
233.2K	
0.152	93.6
0.532	120.5
2.660	151.2
6.004	161.3
14.516	173.5
33.744	183.9
47.652	187.2
60.268	188.7
41.876	182.6
24.320	178.6
17.176	176.2
9.880	168.9
1.064	133.8
253.2K	
0.760	108.5
3.116	134.6
5.396	144.1
27.056	165.8
35.872	169.4
49.021	173.1
42.028	171.4
17.860	162.0
13.528	155.0
7.524	151.9
2.204	126.9
0.456	96.8

1. CO_2/NaX continued

P/cmHg	$v/cm^3 STP g^{-1}$	P/cmHg	$v/cm^3 STP g^{-1}$
273.2K		303.2K	
0.076	18.1	0.076	18.9
0.684	54.4	0.380	33.9
7.144	115.3	1.444	51.9
11.552	124.6	43.168	129.8
16.340	141.8	55.708	134.2
32.300	146.9	47.652	130.7
46.816	152.7	30.476	124.4
41.268	153.6	22.192	118.3
25.612	146.5	14.592	109.7
20.748	142.8	7.904	94.4
13.600	135.7	3.800	81.7
4.636	114.7		
2.128	99.9		

2. H_2S/NaX

P/cmHg	v/cm^3STPg^{-1}
195K	
1.748	193.6
2.508	198.4
7.296	203.0
9.272	203.5
12.236	205.8
19.912	207.4
20.368	210.3
23.332	208.2
32.072	211.1
32.604	211.6
35.720	211.5
27.968	210.6
14.136	208.3
0.532	192.6
213.2K	
2.052	185.2
6.156	192.6
11.856	196.0
18.088	197.9
28.196	199.8
42.940	202.6
53.352	203.0
43.168	202.1
36.024	201.3
30.932	200.6
28.880	201.2
24.320	200.3
20.596	199.9
14.744	197.7
9.044	194.5
3.724	188.4
0.684	175.1
233.2K	
2.052	166.7
6.156	175.3
11.856	180.7
18.088	183.8
28.196	185.3
42.940	188.8
53.352	189.4
43.168	188.4
36.024	187.3
30.932	187.0
28.980	186.3
24.320	185.7
20.596	185.3
14.744	184.1
9.044	181.6
3.724	176.5
0.684	166.8

2. H_2S/NaX continued

P/cmHg	v/cm^3STPg^{-1}
253.2K	
1.444	151.4
3.040	157.9
15.580	173.3
29.296	176.4
35.036	179.5
47.956	182.0
42.180	180.2
20.216	174.8
11.172	171.1
5,680	161.1

P/cmHg	v/cm^3STPg^{-1}
273.2K	
1.444	134.4
3.040	143.1
4.940	146.9
6.156	148.3
10.260	152.8
15.580	159.7
19.076	161.2
21.660	162.1
26.296	164.6
31.768	164.5
35.036	167.3
36.024	167.3
39.748	167.8
47.956	169.7
42.180	168.7
25.536	164.2
20.216	164.2
15.352	160.2
11.172	156.9
5.168	149.8

3. O_2/CMS 77K

P/cmHg	$\nu/cm^3 STPg^{-1}$	P/cmHg	$\nu/cm^3 STPg^{-1}$
0	2.791	15.622	138.512
0	4.686	15.826	146.640
0	10.073	15.833	153.775
0	16.814	15.835	161.911
0	18.014	6.277	129.864
0	25.716	4.681	128.781
0	31.983	3.708	128.020
0	33.835	2.441	126.677
0	39.624	1.853	125.570
0	48.797	1.240	124.532
0	51.687	0.964	123.675
0	61.505		
0	68.114		
0	75.789		
0	87.969		
0	94.130		
0	98.032		
0	106.487		
0.449	116.950		
1.467	121.533		
3.285	126.615		
3.974	127.340		
4.910	126.457		
5.144	128.486		
7.678	130.057		
8.945	129.295		
11.088	133.248		
12.256	131.414		
14.675	133.773		
15.500	135.000		

4. CO_2/CMS

P/cmHg	v/cm^3STPg^{-1}
195K	
0.836	39.0
3.496	58.8
7.752	68.1
19.684	76.7
41.040	80.8
61.080	83.5
53.428	83.1
45.524	83.9
30.020	83.7
213.2K	
0.836	31.2
3.496	53.9
7.752	67.6
19.684	79.9
41.040	85.3
61.180	88.1
53.428	88.3
45.524	88.9
30.020	86.6

P/cmHg	v/cm^3STPg^{-1}
243.2K	
0.532	8.1
2.508	21.6
6.080	44.0
12.462	54.5
23.790	65.4
34.350	69.0
48.032	72.2
65.588	73.0
75.848	76.2
53.580	71.4
39.140	69.1
18.622	59.9
4.481	39.3
273.2K	
0.532	2.2
2.508	7.9
6.080	19.9
12.462	27.7
23.790	35.5
34.350	40.7
48.032	45.6
65.588	46.4
75.848	49.9
53.580	45.5
39.140	41.5
18.622	31.4

4. CO_2/CMS (Volumetric determination)

P/cmHg	v/cm^3STPg^{-1}
195K	
0	1.150
0	2.714
0	4.410
0	6.042
0	8.070
0	9.191
0	11.705
0	14.918
0.039	18.801
0.085	21.157
0.085	23.482
0.100	28.825
0.118	37.800
0.165	35.669
0.274	42.573
0.330	45.528
0.721	52.041
1.177	56.611
1.630	60.401
2.289	64.057
3.649	70.239
3.803	68.990
5.633	72.344
8.599	75.385
12.432	77.870
14.414	78.938
19.441	80.734
21.089	87.269
33.449	87.992
46.760	89.629
56.333	90.570
25.685	88.100

P/cmHg	v/cm^3STPg^{-1}
213.2K	
0.031	12.444
0.173	22.776
0.402	30.344
0.733	38.003
1.355	46.294
1.433	54.178
4.198	60.658
6.572	65.333
13.337	70.404
25.954	74.967
31.488	76.294
38.206	77.565
19.065	73.632

4. CO_2/CMS powder 195K (Volumetric determination)

P/cmHg	$v/cm^3 STP g^{-1}$	P/cmHg	$v/cm^3 STP g^{-1}$
0.274	42.573	49.195	92.480
2.254	66.955	40.460	90.837
12.084	80.753	33.279	89.165
17.997	83.501	26.410	87.625
21.363	84.904	20.970	86.197
25.760	86.241	7.523	79.727
41.862	88.791	4.275	75.806
50.705	92.502		
62.884	94.587		

5. N_2 on CMS (i) powder (ii) pellets

(i) 195K

P/cmHg	v/cm^3STPg^{-1}	P/cmHg	v/cm^3STPg^{-1}
0.327	1.620	26.092	27.618
1.882	6.323	45.200	34.075
4.021	11.641	37.837	32.373
5.118	14.493	30.305	30.992
12.210	20.512	20.785	27.961
17.445	23.382	14.050	20.269
26.364	26.365	8.335	19.269

(ii) 77K		273.2K	
5.632	0.535	1.514	0.262
11.200	0.873	5.650	0.842
14.206	0.924	8.185	1.644
18.271	1.012	12.690	2.319
22.876	1.170	17.485	3.073
27.923	1.269	27.255	4.193
34.270	1.757	42.508	5.745
42.055	2.345	33.809	5.068
		19.536	2.751
		9.295	0.745

6. N_2/Carbolac (Volumetric determination)

P/cmHg	v/cm^3STPg^{-1}	P/cmHg	v/cm^3STPg^{-1}
195K		273.2K	
2.571	3.605	0.985	0.501
3.575	4.001	6.211	1.035
5.828	6.967	8.397	1.185
7.823	8.119	11.830	1.734
10.452	10.640	16.707	2.572
10.723	10.731	23.038	3.738
13.742	13.413	28.507	4.197
14.533	13.839	38.680	6.248
18.488	16.480	50.552	8.738
19.678	17.051	25.097	4.266
25.932	20.538	18.342	2.963
27.781	21.249	13.020	2.200
29.235	22.086	9.299	1.330
36.555	25.200	6.921	0.766
46.267	30.185		
28.263	21.423		
20.833	18.010		
16.191	15.255		
15.944	16.177		
12.367	10.579		
11.844	12.003		
9.445	7.932		
8.898	9.589		
1.500	2.200		

7. H_2S/Carbolac

P/cmHg	v/cm^3STPg^{-1}
195K	
2.356	135.5
6.384	197.0
12.768	243.0
18.772	283.3
28.348	409.0
23.788	385.0
9.652	220.9
213.2K	
2.356	75.8
6.384	113.2
12.768	154.2
18.772	187.2
28.348	211.6
40.508	253.9
49.932	283.9
33.592	224.7
23.788	203.8
9.652	141.1

P/cmHg	v/cm^3STPg^{-1}
243.2K	
2.128	34.5
8.284	69.8
15.048	92.8
25.384	127.3
42.028	150.2
53.200	164.2
33.288	131.4
18.848	105.1
10.792	80.5
3.800	47.6
273.2K	
2.128	13.1
8.284	28.7
15.048	42.7
25.384	56.6
42.028	78.4
53.200	87.1
33.288	66.2
18.848	43.6
10.792	30.5
3.800	19.2

8. N_2/Graphon

P/cmHg	v/cm^3STPg^{-1}	P/cmHg	v/cm^3STPg^{-1}
195K		278.2K	
2.050	0.011	2.009	0.00
3.972	0.191	4.248	0.039
6.875	0.162	7.102	0.022
9.242	0.284	9.558	0.046
12.296	0.448	12.943	0.100
12.680	0.422	13.417	0.086
16.749	0.670	17.996	0.165
16.945	0.634	24.865	0.244
21.962	0.883	33.099	0.387
23.069	0.883	44.540	0.476
29.164	1.280	34.459	0.394
32.856	1.544	18.759	0.179
33.050	1.570	14.028	0.120
38.939	1.800		
25.542	1.089		
21.353	0.879		
19.100	0.779		
15.410	0.603		
14.350	0.554		
10.966	0.362		
5.645	0.216		
2.040	0.048		

9. CO_2/Graphon pellets Volumetric determination

P/cmHg	v/cm^3STPg^{-1}	P/cmHg	v/cm^3STPg^{-1}
184K			
1.180	1.153	5.798	8.139
2.252	2.237	4.386	5.330
3.188	3.412	3.358	2.530
4.792	6.397	190K	
4.882	7.205	1.002	0.602
6.437	8.901	2.739	1.864
8.088	11.675	4.458	3.855
12.403	15.127	4.710	3.647
13.217	15.627	7.596	7.770
14.301	15.899	10.312	10.507
17.745	17.087	11.408	11.800
21.064	18.187	15.513	13.967
23.615	19.079	19.761	15.424
24.184	19.505	23.468	16.600
24.328	19.746	28.092	17.644
25.965	20.398	34.716	19.247
28.251	20.978	37.189	20.259
28.509	26.385	41.108	21.275
29.360	30.507	35.758	19.311
31.499	36.649	31.423	18.933
27.928	21.798	29.152	17.792
21.380	18.709	26.781	17.512
18.608	17.700	21.903	16.214
15.282	16.638	19.202	15.521
14.037	16.241	17.633	15.159
11.195	13.921	15.977	14.800
10.955	12.916	13.929	13.558
9.530	13.675	11.147	11.893
8.453	11.823	10.888	11.325

9. CO_2/Graphon pellets (Volumetric determination) continued

P/cmHg	v/cm^3STPg^{-1}	P/cmHg	v/cm^3STPg^{-1}
190K continued		28.915	16.610
8.835	9.693	29.739	16.683
6.408	7.250	31.645	17.128
6.100	5.776	34.059	17.423
4.488	4.126	35.559	18.088
195K		38.430	18.389
0.597	0.286	42.203	19.043
0.812	0.286	43.018	19.321
1.801	0.745	47.730	19.91
2.458	1.133	51.694	20.880
2.700	1.195	57.487	22.415
3.824	2.012	60.386	23.004
4.355	2.124	45.399	20.147
4.870	2.583	29.948	17.134
5.786	3.105	27.331	16.574
6.387	3.912	23.683	15.349
7.695	4.962	19.833	13.736
8.191	5.554	16.779	13.114
8.930	6.130	14.186	11.796
9.948	6.775	13.154	10.412
11.656	9.361	9.188	9.197
11.840	8.363	5.282	3.563
12.482	9.206		
15.276	11.611		
15.371	11.854		
18.164	12.961		
22.138	14.438		
22.653	14.867		
23.379	15.290		
24.734	15.679		

9. CO_2/Graphon pellets (Volumetric determination)

P/cmHg	$v/cm^3 STPg^{-1}$	P/cmHg	$v/cm^3 STPg^{-1}$
200K		213.2K	
0.821	0.208	1.273	0.288
1.838	0.722	4.030	0.870
4.114	1.851	9.132	2.170
8.412	4.399	10.079	2.314
15.594	9.868	17.206	4.334
18.326	10.478	18.139	4.551
18.763	11.159	25.604	6.844
22.129	12.658	26.893	7.345
30.795	14.963	35.029	9.483
37.680	15.931	39.302	10.417
37.806	15.978	39.335	10.536
46.217	18.098	48.824	12.226
39.227	16.634	55.406	13.488
32.680	15.276	59.900	13.912
31.441	14.754	51.623	12.827
26.630	13.885	46.253	12.160
21.887	12.052	42.070	11.067
21.866	12.396	34.056	9.413
20.119	11.306	30.677	8.609
15.835	9.073	26.295	7.100
13.697	7.820	22.282	6.230
11.857	6.504	15.056	3.974
10.485	5.847	5.748	1.299
6.219	2.643	5.028	1.251

9. CO_2/Graphon pellets (Volumetric determination) continued

P/cmHg	$\nu cm^3 STOg^{-1}$
218.2K	
1.696	0.306
2.483	0.454
4.805	0.849
8.855	1.609
11.691	2.293
13.974	2.739
18.212	3.767
20.117	4.255
21.751	4.609
24.500	5.498
25.341	6.192
30.147	7.025
30.209	6.919
36.736	8.727
51.447	11.312
42.973	10.087
39.366	8.585
33.709	7.851
28.280	6.108
23.114	5.307
18.859	4.071
17.726	3.551
14.055	6.825
5.407	1.062

9. CO_2/Graphon pellets (Volumetric determination) continued

P/cmHg	v/cm^3STPg^{-1}	P/cmHg	v/cm^3STPg^{-1}
273.2K			
1.542	0.051	48.728	1.218
1.618	0.039	37.592	0.982
4.457	0.113	29.125	0.751
7.105	0.157	24.765	0.741
9.437	0.303	21.655	0.552
14.239	0.253	18.730	0.491
18.927	0.438	16.188	0.473
23.208	0.713	13.715	0.358
26.136	0.612	10.164	0.269
31.261	0.929	8.963	0.215
33.255	0.966	0.785	0.182
33.584	0.804		

CO_2/Graphon powder (Volumetric determination 195K)

P/cmHg	ν/cm^3STPg^{-1}	P/cmHg	ν/cm^3STPg^{-1}
1.622	0.821	28.725	15.494
3.312	1.965	28.747	15.755
3.689	2.891	35.406	17.154
5.941	3.261	35.653	16.698
8.210	5.905	40.343	18.287
8.433	6.227	43.510	18.562
9.869	7.640	52.145	19.530
10.325	6.582	42.960	17.882
13.221	10.285	39.585	17.980
15.132	11.297	35.653	16.698
15.293	11.482	27.699	14.909
15.831	11.310	26.328	15.199
18.234	12.796	16.604	12.525
18.686	12.818	10.976	8.035
21.508	14.502	7.232	5.547
22.724	14.380	2.950	2.772
23.381	14.239		

10. H_2S/Graphon

P/cmHg	$\nu/cm^3 STP g^{-1}$	P/cmHg	$\nu/cm^3 STP g^{-1}$
195K		7.676	10.0
0.988	1.8	6.384	7.4
1.800	4.5	2.432	1.2
4.560	14.0	243.2K	
8.436	17.1	3.800	0.7
10.336	17.4	9.988	3.3
14.440	20.4	11.324	4.7
19.608	25.6	13.528	3.7
22.116	28.5	22.572	9.4
24.320	35.0	32.148	12.9
18.848	23.6	39.748	15.3
7.676	16.0	46.968	16.0
6.384	15.5	56.468	17.3
3.510	11.0	42.560	15.4
2.432	6.4	36.100	13.9
213.2K		27.132	11.1
0.988	0.0	16.720	6.9
4.560	3.4	7.600	3.6
8.436	10.3	273.2K	
10.336	12.4	1.660	0.4
14.440	14.9	3.268	0.6
19.608	16.5	9.880	1.0
22.116	16.9	13.528	1.2
24.320	17.9	22.572	3.4
33.516	20.0	32.148	4.5
36.708	21.6	39.748	5.3
39.748	22.5	46.968	6.1
49.780	28.5	56.468	6.5
43.700	24.6	42.560	5.8
29.560	18.7	36.100	5.0
18.848	16.1	27.132	4.0
		16.720	2.7
		7.600	2.1

11. SF_6/Graphon 195K

P/cmHg	$\nu/cm^3 STOg^{-1}$
0.678	6.61
1.457	9.99
3.379	11.23
5.316	11.68
9.124	12.49
11.221	12.93
23.761	20.80
25.710	24.11
26.786	26.62
25.349	25.67
24.608	24.14
22.904	21.61
20.643	17.73
16.26	14.779

Determined by Mr. R. Bhusate

P/cmHg	$\nu/cm^3 STPg^{-1}$
0.455	2.583
4.032	11.258
23.376	19.102
24.670	21.483
23.309	19.924
20.992	17.555
20.250	17.026
16.393	15.028
13.852	14.151
10.030	12.790
5.142	11.584
2.717	10.569
1.420	9.698
0.990	9.060

Determined by the author

APPENDIX B FLOW DATA

i) Zeolite NaX

1) Zeolite Membrane 1/He
2) Zeolite Membrane 1/CO_2
3) Zeolite Membrane 2/He
4) Zeolite Membrane 2/N_2
5) Zeolite Membrane 2/H_2S
6) Zeolite Membrane 2/CO_2

ii) Carbon Molecular Sieve

7) Carbon Molecular Sieve/He
8) Carbon Molecular Sieve/N_2
9) Coabon Molecular Sieve/CO_2
10) Carbon Molecular Sieve/H_2S

iii) Carbolac

11) Carbolac/He
12) Coabolac/N_2
13) Carbolac/CO_2
14) Carbolac/H_2S
15) Carbolac/CO_2/He
16) Carbolac/CO_2/N_2
17) Carbolac/H_2S/He
18) Carbolac/H_2S/N_2

iv) Graphon

19) Graphon/He

20) Graphon/N_2

21) Graphon/CO_2

22) Graphon/H_2S

23) Graphon/CO_2/He

24) Graphon/H_2S/He

25) Graphon/H_2S/N_2

26) Graphon/Ar

27) Graphon/CO_2/Ar

28) Graphon/SF_6

29) Graphon/SF_6/He

30) Graphon/Propane

31) Graphon/Propane/He

Appendix B

1. Zeolite membrane 1 Helium Flow

TEMPERATURE/K	Run Number	PRESSURE/cmHg	PERMEABILITY $10^4 K/m^2 s^{-1}$	FLUX $10^7 J/mols^{-i}$
195K	Z14	0.87	1.13	0.27
	Z13	1.73	1.13	0.54
	Z12	2.77	1.15	0.88
	Z11	3.88	1.15	1.28
	Z10	5.02	1.16	1.61
	Z9	9.10	1.17	2.92
	Z8	11.09	1.19	3.62
	Z7	13.37	1.19	4.37
	Z6	15.60	1.20	5.16
	Z5	17.97	1.22	6.02
	Z4	20.30	1.23	6.88
	Z3	23.20	1.23	7.60
	Z2	25.55	1.25	8.78
	Z1	28.80	1.28	10.12
273.2K	Z30	0.88	1.35	0.23
	Z29	1.71	1.36	0.46
	Z28	2.78	1.36	0.74
	Z27	3.85	1.36	1.03
	Z26	5.05	1.35	1.34
	Z25	6.49	1.35	1.72
	Z24	8.31	1.37	2.23
	Z23	11.23	1.37	3.03
	Z22	14.34	1.39	3.93
	Z21	17.41	1.41	4.84
	Z20	20.22	1.41	5.62
	Z19	21.15	1.42	5.91
	Z18	24.09	1.44	6.82
	Z17	24.30	1.45	6.91
	Z16	27.27	1.46	7.79
	Z15	32.26	1.47	9.30

2. Zeolite Membrane 1 Carbon Dioxide Flow

T/K	Run No.	p_1/cmHg	BTT/min	TL/min	PERMEABILITY $10^5 K/m^2 s^{-1}$	FLUX $10^7 J/mol s^{-1}$
195	Z50	2.99	660	678	3.45	0.29
	Z48	5.41	360	371	3.78	0.55
	Z46	7.36	255	263	4.03	0.84
	Z44	10.02	185	185	4.25	1.17
	Z42	12.26	146	146	4.46	1.48
	Z40	14.75	108.5	108.5	4.74	1.88
	Z38	16.66	100	100	4.82	2.21
	Z36	19.27	83	83	5.20	2.71
	Z34	21.47	71.5	71.5	5.33	3.10
	Z32	24.70	59.5	59.5	5.69	3.80
273.2						
	Z51	1.58	314	356	4.73	0.14
	Z49	2.90	220	250	5.02	0.28
	Z47	5.17	150	175	4.95	0.50
	Z45	7.61	116	132	5.11	0.76
	Z43	10.19	95	106	5.35	1.07
	Z41	12.30	80	90	5.40	1.31
	Z39	14.96	76	76	5.48	1.55
	Z37	17.17	60.5	67.5	5.65	1.91
	Z35	19.51	54	60	5.77	2.26
	Z33	22.34	45	53	5.88	2.57
	Z31	24.89	40	46	6.00	2.93

3. Zeolite Membrane 2 Helium Flow

TEMPERATURE/K	Run Number	PRESSURE/cmHg	PERMEABILITY $10^4 K/m^2 s^{-1}$	FLUX $10^7 J/mol s^{-1}$
195	NZ 54	34.65	6.97	11.2
	NZ 55	26.30	6.74	8.26
	NZ 58	19.50	6.62	5.70
	NZ 59	12.88	6.36	3.85
	NZ 62	7.54	6.37	2.27
	NZ 63	4.00	6.30	1.19
	NZ 66	1.54	6.15	0.44
	NZ 67	0.71	6.16	0.20
273.2	NZ 52	43.40	7.85	11.5
	NZ 53	34.82	7.68	9.04
	NZ 56	26.05	7.60	6.63
	NZ 57	19.60	7.42	4.92
	NZ 60	12.82	7.34	3.26
	NZ 61	7.27	7.32	1.79
	NZ 64	3.96	7.24	.98
	NZ 65	1.54	7.28	.37

4. Zeolite Membrane 2 Nitrogen Flow

TEMPERATURE/K	Run no.	p_1/cmHg	TL/min	PERMEABILITY $10^5 K/m^2 s^{-1}$	FLUX $10^7 J/mol s^{-1}$
195	NZ69	35.76	3	3.71	6.26
	NZ70	30.14	3.5	3.55	5.02
	NZ73	23.84	4.5	3.38	3.79
	NZ74	17.10	5.5	3.13	2.52
	NZ77	12.55	-	3.09	1.83
	NZ78	7.81	8.5	2.80	1.01
	NZ81	3.03	10	2.66	0.39
	NZ82	1.54	12	2.61	0.19
273.2	NZ68	35.90	0	3.71	4.45
	NZ71	29.97	0	3.62	3.64
	NZ72	24.00	0	3.46	2.79
	NZ75	16.92	0	3.27	1.86
	NZ76	12.65	0	3.19	1.37
	NZ79	7.14	0	3.06	0.74
	NZ80	3.03	0	2.87	0.29

5. Zeolite Membrane 2 Hydrogen Sulphide Flow

TEMPERATURE/K	Run no.	p_1/cmHg	TL/min	PERMEABILITY 10^5K/m^{2}s^{-1}	FLUX 10^7 J/mols^{-1}
195	NZ91	2.24	270	2.41	0.254
	NZ90	3.31	190	2.55	0.403
	NZ89	6.60	92	2.58	0.782
	NZ88	9.32	65	2.73	1.20
	NZ87	12.00	47	2.93	1.64
	NZ86	15.19	37	2.96	2.12
	NZ85	18.05	29	3.12	2.66
	NZ84	21.28	25	3.24	3.26
	NZ83	24.98	23	3.20	3.61

6. Zeolite Membrane 2 Carbon Dioxide Flow

TEMPERATURE/K	Run no.	p_1/cmHg	TL/min	PERMEABILITY 10^5K/m^{2}s^{-1}	FLUX 10^7 J/mols^{-1}
195	NZ96	4.38	163	2.14	0.44
	NZ95	9.75	69	2.34	1.08
	NZ94	15.47	40	2.53	1.84
	NZ93	20.28	28	2.75	2.63
	NZ92	25.55	20	3.00	3.60

7. Carbon Molecular Sieve Membrane Helium Flow

TEMPERATURE/K	Run Number	PRESSURE/cmHg	PERMEABILITY $10^5 K/m^2 s^{-1}$	FLUX $10^7 J/mol s^{-1}$
195	CMS 17	1.36	6.71	0.23
	CMS 14	2.53	7.17	0.83
	CMS 13	4.03	7.34	1.35
	CMS 10	9.91	7.55	3.09
	CMS 9	14.95	7.77	5.30
	CMS 6	22.43	8.29	8.30
	CMS 5	35.40	8.69	14.11
	CMS 2	45.16	9.16	18.80
	CMS 1	55.97	9.62	24.50
273.2	CMS 16	1.32	8.50	.36
	CMS 15	2.51	8.52	.63
	CMS 12	4.07	8.60	1.14
	CMS 11	9.91	8.83	2.84
	CMS 8	15.11	9.11	4.56
	CMS 7	22.39	9.25	6.73
	CMS 4	36.57	9.71	11.40
	CMS 3	44.50	10.00	14.54
195	CMS 96	1.19	9.10	0.49
	CMS 86	1.95	9.00	0.82
	CMS 85	3.91	9.01	1.60
	CMS 84	6.64	9.28	2.83
	CMS 93	9.96	9.43	4.27
	CMS 92	15.56	10.00	7.08
	CMS 90	23.00	10.31	10.31
	CMS 87	30.04	11.32	15.51
273.2	CMS 95	1.20	10.26	.40
	CMS 94	4.18	10.45	1.42
	CMS 83	7.77	10.51	2.67
	CMS 82	11.33	10.95	4.04
	CMS 91	15.40	11.21	5.59
	CMS 89	22.12	11.66	8.38
	CMS 88	29.66	11.98	11.61

8. Carbon Molecular Sieve Membrane Nitrogen Flow

TEMPERATURE/K	Run Number	PRESSURE/cmHg	PERMEABILITY 10^{5} K/m^{2}s^{-1}	FLUX 10^{7} J/mols^{-i}
195	CMS 35	0.92	3.00	0.12
	CMS 32	2.76	2.96	0.37
	CMS 31	6.10	2.92	0.81
	CMS 28	8.63	3.06	1.20
	CMS 27	11.72	3.37	1.80
	CMS 24	15.70	3.57	2.56
	CMS 23	19.67	3.86	3.46
	CMS 20	26.47	4.35	5.42
	CMS 19	33.52	4.56	6.98
273.2	CMS 34	0.91	3.82	0.11
	CMS 33	2.73	3.53	0.31
	CMS 30	6.32	3.57	0.72
	CMS 29	8.52	3.71	1.03
	CMS 26	11.88	3.84	1.48
	CMS 25	15.70	4.02	2.05
	CMS 22	19.79	4.16	2.68
	CMS 21	26.36	4.48	3.84
	CMS 18	33.52	5.43	5.94

9. Carbon Molecular Sieve Membrane Carbon Dioxide Flow

T/K	Run No.	p_1/cmHg	BTT/min	TL/min	PERMEABILITY 10^5 K/m^{2}s^{-1}	FLUX 10^7 J/mols^{-1}
195	CMS54	1.87	480	525	1.50	0.13
	CMS52	4.30	240	284	2.22	0.43
	CMS61	7.52	140	164	2.75	0.94
	CMS48	9.51	115	124	2.80	1.21
	CMS47	9.66	-	-	3.02	1.32
	CMS59	11.61	91	98	2.98	1.57
	CMS46	14.45	70	79	3.17	2.10
	CMS57	17.99	-	-	3.58	2.93
	CMS43	20.85	47.5	51.5	3.58	3.45
	CMS42	27.94	29	32	4.00	5.05
	CMS39	34.31	-	-	4.55	7.11
	CMS38	41.61	16	18.5	5.10	9.66
273.2	CMS55	0.89	40	75	2.34	0.07
	CMS53	1.99	40	62	2.75	0.18
	CMS50	4.48	25	39.5	2.87	0.42
	CMS56	8.36	18	39	3.04	0.81
	CMS49	9.50	24	33	3.21	0.99
	CMS60	11.49	-	-	3.31	1.24
	CMS45	14.70	17	25	3.49	1.67
	CMS58	17.70	-	-	3.70	2.06
	CMS44	21.17	12	18.5	3.64	2.51
	CMS41	28.03	8	14	4.11	3.75
	CMS40	34.37	8	11.5	4.45	4.99
	CMS37	41.93	4	7	4.87	6.64
	CMS36	49.29	3	6	5.25	8.42

10. Carbon Molecular Sieve Membrane Hydrogen Sulphide Flow

TEMPERATURE/K	Run Number	PRESSURE/cmHg	PERMEABILITY 10^{-5} K/m^{2}s^{-1}	FLUX 10^{7} J/mols^{-1}
195	CMS80	1.05	2.20	0.11
	CMS79	2.22	2.41	0.24
	CMS76	4.22	3.56	0.73
	CMS75	7.16	4.00	1.27
	CMS72	11.81	4.61	2.47
	CMS71	18.37	5.70	4.75
	CMS68	26.30	6.85	8.14
	CMS67	34.20	8.15	12.73
273.2	CMS81	1.05	3.45	0.12
	CMS78	2.24	2.90	0.20
	CMS77	4.21	4.05	0.57
	CMS74	7.22	4.10	0.96
	CMS73	11.52	4.45	1.66
	CMS70	18.65	5.46	3.31
	CMS69	26.20	6.03	5.10
	CMS66	34.47	6.81	7.63
	CMS65	40.68	7.32	9.68

11. Carbolac Membrane Helium Flow

TEMPERATURE/K	Run Number	PRESSURE/cmHg	PERMEABILITY 10^{7} K/m^{2}s^{-1}	FLUX 10^{9} J/mols^{-1}
195	C19	0.51	1.35	0.041
	C27	0.36	1.40	0.072
	C18	1.00	1.49	0.087
	C26	1.49	1.59	0.144
	C15	2.44	1.56	0.23
	C23	2.70	1.68	0.28
	C14	3.93	1.67	0.39
	C11	6.10	1.74	0.64
	C10	8.63	1.67	0.88
	C 7	13.98	1.75	1.42
	C22	17.08	1.80	1.83
	C 6	17.88	1.79	1.92
	C 4	22.63	1.79	2.43
	C32	29.04	1.77	3.08
	C31	38.90	1.73	4.08
195	C54	4.93	4.88	1.44
	C55	12.54	4.92	3.64
	C70	5.28	4.70	1.47
	C71	12.28	4.90	3.59
	C142	8.50	4.60	2.33
	C143	18,92	4.75	5.38
	C146	29.25	4.94	8.64
	C149	3.72	4.54	1.01
	C167	7.93	4.05	1.94
	C168	4.95	4.15	1.22
	C200	7.86	4.03	1.89

11. Carbolac Membrane Helium Flow (cont.)

TEMPERATURE/K	Run Number	PRESSURE/cmHg	PERMEABILITY $10^{7}K/m^{2}s^{-1}$	FLUX $10^{9}J/mols^{-1}$
273.2	C20	0.49	1.81	0.018
	C17	1.01	1.83	0.078
	C25	1.51	1.84	0.12
	C16	2.40	1.89	0.19
	C24	2.76	1.94	0.23
	C13	4.10	2.03	0.36
	C12	5.88	2.02	0.72
	C 9	9.00	2.04	0.78
	C 8	13.82	2.05	1.21
	C21	17.60	2.03	1.53
	C 5	17.82	2.08	1.59
	C 7	21.67	2.13	1.97
	C 3	24.04	2.10	2.16
	C 2	30.41	2.21	2.94
	C30	37.88	2.09	3.38
	C29	49.61	2.07	4.39
273.2	C56	7.47	6.20	1.97
	C57	5.31	6.00	1.36
	C68	10.27	5.96	2.62
	C69	5.44	5.76	1.34
	C144	18.66	5.75	4.59
	C145	29.28	5.87	7.35
	C147	10.15	5.82	2.62
	C148	3.69	5.82	0.88
	C175	7.34	5.90	1.85
	C176	4.70	5.56	1.12
	C201	7.98	4.75	1.61

12. Carbolac Membrane Nitrogen Flow

TEMPERATURE/K	Run Number	PRESSURE/cmHg	PERMEABILITY 10^{7} K/m^{2}s^{-1}	FLUX 10^{9} J/mols^{-i}
195	C83	8.59	3.46	1.77
	C82	12.25	3.42	2.50
	C75	22.33	3.57	4.68
	C79	22.61	3.47	4.71
	C74	27.21	3.27	5.34
	C78	28.47	3.39	5.78
195	C95	22.31	4.05	5.40
	C94	29.14	3.90	6.83
	C89	36.40	3.89	8.50
	C88	41.68	3.80	9.44
	C86	49.51	3.84	12.00
195	C112	2.05	2.86	0.34
	C111	4.02	3.27	0.77
	C110	7.61	3.40	1.60
	C109	12.66	3.54	2.67
	C98	14.90	3.64	3.24
	C108	19.86	3.53	4.19
	C107	27.82	3.75	6.34
	C103	37.03	3.68	8.15
	C102	45.66	3.78	10.32
195	C136	9.60	3.36	1.94
	C137	3.44	3.06	0.63
	C199A	7.78	2.52	1.18
	C199B	13.00	2.60	2.60

12. Carbolac Membrane Nitrogen (cont.)

TEMPERATURE/K	Run Number	PRESSURE/cmHg	PERMEABILITY 10^{7} K/m^{2}s^{-1}	FLUX 10^{9} J/mols^{-i}
273.2	C84	8.34	2.94	1.05
	C81	12.66	3.00	1.63
	C77	15.38	3.02	1.99
	C76	20.71	3.00	2.64
	C80	21.83	3.13	2.92
	C73	29.28	3.18	3.98
	C72	34.35	3.19	4.68
273.2	C97	15.51	4.13	
	C96	21.47	4.00	3.66
	C92	29.34	4.11	5.16
	C92	34.65	4.23	6.27
	C91	40.20	3.92	6.74
	C90	47.92	3.86	7.91
	C87	46.22	3.81	7.54
273.2	C114	1.41	3.04	0.18
	C113	4.58	3.20	0.63
	C106	8.77	3.46	1.29
	C105	12.94	3.42	1.89
	C104	19.60	3.53	2.96
	C101	27.88	3.61	4.30
	C100	36.27	3.65	5.68
	C99	43.96	3.57	6.52
273.2	C138	10.06	2.65	1.15
	C139	18.00	2.82	2.16
	C140	7.11	2.73	0.83
	C141	2.68	2.47	0.28
	C184	7.96	2.50	0.84

13. Carbolac Membrane Carbon Dioxide Flow

T/K	Run No.	p_1/cmHg	D T /min	TL/min	PERMEABILITY 10^7 k/m^{2}s^{-1}	FLUX 10^9 J/mols^{-1}
195	C39	19.19	250	280	5.16	5.92
	C37	38.60	125	156	5.80	13.41
195	C62	8.20	275	346	7.60	3.74
	C66	15.58	215	260	7.59	7.07
	C58	22.25	136	184	7.78	10.40
	C43	28.47	150	194	7.66	12.91
	C64	37.03	135	177	7.66	16.90
	C52	48.29	110	188	7.68	22.20
195	C134	5.39	390	426	5.81	1.83
	C131	12.97	230	272	6.18	4.82
	C127	18.39	200	238	6.50	7.20
	C125	21.73	180	212	6.27	8.19
	C121	33.56	150	169	6.14	12.33
	C117	41.84	136	154	6.00	15.00
273.2	C47	9.14	90	123	4.18	1.63
	C50	18.54	65	88	4.13	3.28
	C41	26.98	55	80	4.17	4.89
	C45	38.94	40	65	4.15	6.91
	C60	46.19	40	66	4.25	8.49
273.2	C133	5.60	104	140	3.81	0.90
	C129	14.44	68	98	3.86	2.38
	C123	22.65	60	92	4.10	3.96
	C119	33.70	60	75	4.04	5.75
	C115	43.90	20	35	4.13	7.74

14. Carbolac Membrane Hydrogen Sulphide Flow

T/K	Run No.	p_1/cmHg	D T/min	TL/min	PERMEABILITY $10^6 k/m^2 s^{-1}$	FLUX $10^9 J/mol s^{-1}$
195	C171	5.03	284	338	1.88	5.61
	C169	8.09	210	260	1.92	9.25
	C162	12.08	170	208	1.78	12.25
	C158	18.17	110	120	2.24	24.30
	C152	19.09	110	124	2.51	28.80
	C173	20.15	105	140	2.41	30.01
	C150	22.54	84	95	2.95	39.44
195	C195	4.53	320	380	1.75	4.29
	C191	10.51	175	220	1.78	11.42
	C189	14.99	140	180	1.81	16.04
	C186	21.18	100	114	2.78	28.81
273.2	C165	5.51	160	239	0.460	1.08
	C164	15.71	100	155	0.527	3.47
	C160	25.63	90	128	0.545	5.95
	C156	36.30	70	110	0.593	9.18
	C154	47.26	64	89	0.526	10.77
273.2	C185	10.65	120	148	0.495	2.33
	C183	20.40	104	133	0.495	4.28
	C181	31.63	80	120	0.571	7.20
	C179	43.35	68	108	0.570	10.60

15. Carbolac membrane CO_2/He Mixtures

Temp/K	Run No.	PRESSURE CO_2 cmHg	P_1/Po	PERMEABILITY He $10^7 \tilde{K}^{He}_{mix}$ $m^2 s^{-1}$	$\tilde{K}_R$
273.2	C51	18.54	.008	5.04	.826
	C42	26.98	.011	4.89	.802
	C46	39.13	.015	4.65	.762
	C61	46.35	.019	4.38	.718
195	C63	8.20	.104	3.30	.663
	C67	15.53	.196	2.93	.600
	C40	19.19	.243	2.20	.451
	C59	22.16	.281	2.68	.549
	C44	28.47	.359	2.55	.523
	C65	37.05	.468	2.25	.461
	C53	48.26	.611	2.16	.442

16. Carbolac Membrane CO_2/N_2 Mixtures

Temp/K	Run No.	PRESSURE CO_2 cmHg	P_1/Po	PERMEABILITY N_2 $10^7 \tilde{K}^{He}_{(mix)} m^2 s^{-1}$	$\tilde{K}_R$
273.2	C130	14.44	.006	2.54	.753
	C124	22.65	.009	2.59	.785
	C120	33.70	.014	2.49	.743
	C116	43.90	.018	2.42	.713
195	C135	9.04	.068	1.89	.542
	C132	12.97	.164	1.60	.463
	C128	18.35	.232	1.55	.453
	C126	21.73	.275	1.46	.424
	C122	33.56	.424	1.35	.386
	C118	41.84	.529	1.25	.365

17. Carbolac Membrane H_2S/He Mixtures

T/K	Run No.	Pressure H_2S /cmHg	p_1/p_o	Permeability He $10^7 \tilde{K}_{He(mix)}$ /$m^2 s^{-1}$	$\tilde{K}_R$
273.2	C166	5.51	.007	4.38	.802
	C161	25.63	.003	3.78	.700
	C157	36.30	.047	3.23	.598
	C155	47.26	.061	3.26	.604
195	C172	5.03	.200	1.99	.482
	C170	8.09	.320	1.68	.410
	C177	10.03	.410	1.37	.401
	C163	12.08	.480	1.05	.257
	C178	15.73	.630	.910	.222
	C159	18.17	.724	.742	.181
	C153	19.09	.790	.738	.180
	C174	20.15	.900	.707	.172
	C151	22.54	1.0	0	0

18. Carbolac Membrane H_2S/N_2 Mixtures

T/K	Run No.	Pressure H_2S /cmHg	p_1/p_o	Permeability N_2 $10^7 \tilde{K}_{N_2(mix)}$ /$m^2 s^{-1}$	$\tilde{K}_R$
273.2	C198	7.87	.006	1.95	.781
	C182	31.77	.041	1.88	.752
	C180	43.47	.056	1.85	.741
195	C196	4.50	.195	1.15	.469
	C193	8.25	.350	1.00	.401
	C197	8.90	.390	0.810	.324
	C192	10.72	.465	0.601	.240
	C190	14.81	.609	0.475	.190
	C194	18.07	.788	0.501	.200
	C187	21.180	.920	0.304	.121
	C188	22.54	1.0	0	0

19. Graphon Membrane Helium Flow

TEMPERATURE/K	Run Number	PRESSURE/cmHg	PERMEABILITY $10^{6}K/m^{2}s^{-1}$	FLUX $10^{9}J/mols^{-1}$
184	G93	3.41	2.41	5.19
200	G39	0.73	2.60	1.12
	G38	1.98	2.55	2.96
	G37	3.67	2.54	5.48
	G36	6.09	2.52	9.01
	G35	7.94	2.53	11.77
213	G19	1.09	2.64	1.59
	G22	1.84	2.60	2.60
	G21	3.89	2.60	4.88
	G20	4.35	2.57	6.19
	G18	6.95	2.62	10.05
273	G27	0.95	3.06	1.24
	G23	1.77	2.94	2.23
	G24	3.34	2.94	4.23
	G25	5.96	3.00	7.67
	G26	8.29	2.97	10.61

20. Graphon Membrane Nitrogen Flow

TEMPERATURE/K	Run Number	PRESSURE/cmHg	PERMEABILITY $10^6 K/m^2 s^{-1}$	FLUX $10^8 J/mol s^{-i}$
195	G190	0.55	1.94	0.06
	G189	1.08	1.79	0.12
	G184	2.33	1.74	0.25
	G183	5.38	1.75	0.57
	G181	7.65	1.73	0.80
	G180	11.26	1.71	1.16
	G179	16.04	1.72	1.66
	G174	21.17	1.77	2.25
	G175	25.77	1.84	2.87
273.2	C191	0.59	1.47	0.037
	C188	1.57	1.54	0.11
	C186	2.47	1.54	0.16
	C185	4.98	1.52	0.33
	C187	8.94	1.53	0.52
	C182	11.06	1.54	0.73
	C178	16.08	1.53	1.08
	C177	20.04	1.56	1.35
	C176	25.38	1.57	1.70

21. Graphon Membrane Carbon Dioxide Flow

TEMPERATURE/K	Run Number	PRESSURE/cmHg	PERMEABILITY $10^6 K/m^2 s^{-1}$	FLUX $10^9 J/mol s^{-1}$
184	G62	0.87	2.60	1.45
	G63	1.85	2.63	3.19
	G94	2.33	2.46	3.55
	G64	3.71	2.85	6.75
	G73	5.23	3.11	10.40
	G65	5.75	3.13	11.52
	G66	7.99	3.24	16.58
	G78	9.45	3.48	20.99
	G67	10.20	3.42	22.26
	G74	11.10	3.62	25.71
	G68	13.20	3.65	30.75
	G76	15.12	3.67	35.33
	G96	16.06	3.72	38.36
	G69	17.47	3.64	40.78
	G79	20.80	3.09	49.10
	G70	22.45	3.69	52.87
	G81	25.80	3.60	58.91
	G71	26.90	3.75	61.32
	G84	27.70	3.73	65.90
	G86	28.74	3.56	65.14
	G72	29.26	3.44	64.32
190	G100	5.13	2.68	8.68
	G105	6.59	2.76	11.24
	G95	9.36	2.90	18.21
	G98	13.89	3.08	26.51
	G112	18.38	3.17	36.15
	G108	19.62	3.30	40.36
	G88	23.90	3.12	46.18
	G110	25.84	3.18	50.93
	G111	30.91	3.18	60.82

21. Graphon Membrane Carbon Dioxide Flow

TEMPERATURE/K	Run Number	PRESSURE/cmHg	PERMEABILITY 10^{6} K/m^{2}s^{-1}	FLUX 10^{9} J/mols^{-1}
195	G106	1.19	2.36	1.69
	G101	5.07	2.40	7.31
	G109	9.00	2.58	14.01
	G105	14.16	2.73	28.22
	G91	21.10	2.87	36.56
	G90	21.33	3.05	39.18
	G113	25.95	2.86	46.02
200	G60	0.77	2.09	0.94
	G59	2.78	2.13	3.45
	G58	5.63	2.17	7.16
	G44	8.28	2.23	10.83
	G40	11.97	2.37	16.66
	G42	15.58	2.79	20.86
	G61	16.91	2.47	24.60
	G46	18.91	2.48	27.62
	G48	24.24	2.54	36.09
	G50	30.72	2.50	45.12
	G52	35.29	2.52	52.23
	G56	41.09	2.49	60.15
213.2	G15	1.89	1.81	1.88
	G102	5.54	1.92	5.89
	G11	5.75	1.93	6.10
	G103	8.70	1.92	9.26
	G13	9.30	1.86	9.57
	G104	14.26	1.99	15.30
	G114	20.81	2.00	23.72
	G115	25.96	2.05	29.85
273.2	C116	5.02	1.40	3.05
	C9	13.17	1.36	7.70
	C10	18.14	1.34	10.39
	C117	22.65	1.35	13.72

22. Graphon Membrane Hydrogen Sulphide Flow

TEMPERATURE/K	Run Number	PRESSURE/cmHg	PERMEABILITY $10^6 K/m^2 s^{-1}$	FLUX $10^8 J/mol s^{-1}$
195	C209	0.80	6.50	0.31
	C206	1.42	8.34	0.71
	C207	1.44	8.47	0.72
	C203	2.89	9.85	1.63
	C204	3.45	11.26	2.33
	C210	4.01	10.64	2.55
	C192	4.31	13.20	3.43
	C212	5.90	11.50	4.04
	C213	6.56	10.62	3.57
	C200	7.46	11.21	5.00
	C198	10.94	11.21	7.36
	C196	14.61	10.82	9.40
	C201	17.12	11.30	11.50
	C194	20.50	10.85	13.23
213	C215	1.05	4.50	0.27
	C216	2.09	5.14	0.51
	C218	4.24	5.78	1.35
	C214	6.31	5.91	2.03
	C220	8.28	6.69	3.03
	C219	9.90	7.42	4.03
	C221	13.53	7.21	5.31
	C225	17.54	7.90	7.69
	C222	20.67	7.56	8.69
	C224	28.95	7.66	12.20
	C228	37.19	6.95	14.21
	C226	46.75	7.21	18.45

22. Graphon Membrane Hydrogen Sulphide Flow

TEMPERATURE/K	Run Number	PRESSURE/cmHg	PERMEABILITY $10^6 K/m^2 s^{-1}$	FLUX $10^7 J/mol s^{-i}$
243.2	G262	0.81	3.98	0.15
	G243	1.40	3.70	0.25
	G239	2.47	3.71	0.45
	G244	4.80	3.92	0.92
	G241	7.50	3.83	1.39
	G240	9.09	3.95	1.74
	G232	12.31	4.05	2.41
	G230	14.74	4.10	2.91
	G234	20.21	4.31	4.20
	G232	24.65	4.52	5.37
	G233	30.11	4.64	6.73
	G230	36.77	4.56	8.10
	G245	43.51	4.75	9.98
	G246	50.08	4.81	11.70
	G247	57.35	4.78	13.31
273.2	G262	0.81	3.04	0.11
	G260	2.17	3.05	0.28
	G258	6.96	3.03	0.91
	G256	18.87	3.06	2.49
	G255	24.61	3.12	3.30
	G238	29.28	3.17	3.99
	G254	35.72	3.13	4.82
	G253	44.00	3.20	6.09
	G252	49.68	3.18	6.79
	G251	56.12	3.22	7.73
	G249	63.80	3.30	9.04

23. Graphon Membrane CO_2/He Mixtures

Temp/K	Run No.	PRESSURE CO_2 /cmHg	R/Po	PERMEABILITY He $10^6/m^2 s^{-1}$	$\tilde{K}_R$
213.2	G16	5.75	.006	2.51	.966
	G12	1.88	.091	2.26	.926
	G14	9.295	.030	2.25	.866
	G34	12.755	.041	2.33	.892
200	G45	8.26	.071	2.13	.836
	G41	11.95	.103	1.90	.745
	G43	15.56	.134	1.89	.742
	G47	18.88	.162	1.93	.757
	G49	27.04	.208	1.74	.682
	G51	30.68	.268	1.72	.662
	G53	35.22	.303	1.75	.659
	G57	41.03	.352	1.79	.702
184	G75	11.05	.346	1.52	.620
	G99	13.81	.430	1.50	.615
	G97	16.03	.503	1.53	.623
	G92	20.88	.655	1.49	.608
	G82	25.64	.804	1.53	.624
	G85	27.56	.865	1.61	.657
	G87	28.59	.897	1.51	.616
	G89	23.91	.750	1.59	.648
	G80	20.75	.651	1.45	.592
	G77	15.06	.473	1.53	.625

24. Graphon Membrane H_2S/He Mixtures

Temp/K	Run No.	Pressure H_2S cmHg	P_1/Po	PERMEABILITY He 10^7 $\tilde{K}/m^2s^{-1}$	$\tilde{K}_R$
273.2	G261	2.17	.003	2.80	.943
	G257	18.87	.024	3.02	.896
	G250	63.60	.082	2.38	.801
243.2	G242	7.52	.025	2.50	.896
	G235	20.17	.068	2.31	.828
	G231	36.64	.122	2.04	.729
	G248	56.98	.193	1.95	.699
213.2	G218	4.20	.053	2.07	.796
	G223	20.24	.253	1.73	.664
	G228	36.91	.461	1.74	.669
	G229	46.42	.580	1.72	.661
195	G208	1.43	.057	2.03	.795
	G205	3.41	.136	1.70	.669
	G201	7.38	.295	1.58	.620
	G199	10.53	.421	1.65	.647
	G197	14.20	.570	1.62	.635
	G264	17.17	.684	1.67	.654
	G195	20.21	.808	1.67	.654
	G212	23.41	.936	1.60	.627
	G265	24.47	.979	1.63	.639

25. Graphon Membrane H_2S/N_2 Mixtures

Temp/K	Run No.	Pressure H_2S cmHg	P_1/Po	PERMEABILITY N_2 10^7 K/m^2s^{-1}	K_R
195	G276	0.88	.036	11.4	.644
	G275	2.04	.083	9.79	.551
	G270	5.01	.208	7.01	.395
	G274	7.20	.300	6.69	.377
	G273	10.47	.437	5.74	.323
	G268	11.79	.592	6.59	.342
	G271	18.41	.767	5.40	.340
	G272	20.40	.850	5.80	.327
	G269	23.12	.960	5.46	.307

26. Graphon Membrane Argon Flow

TEMPERATURE/K	Run Number	PRESSURE/cmHg	PERMEABILITY 10^6 K/m^{2}s^{-1}	FLUX 10^9 J/mols^{-1}
184	G128	0.75	1.70	0.82
	G127	1.40	1.69	1.52
	G119	2.31	1.58	2.34
	G126	2.38	1.66	2.53
	G123	4.16	1.65	4.36
	G120	5.84	1.64	6.11
	G122	7.64	1.64	8.01

27. Graphon Membrane Ar/CO_2 Mixtures

TEMPERATURE/K	Run No.	PRESSURE CO_2 /cmHg	P_1/P_o	PERMEABILITY Ar 10^7 K$^{Ar(mix)}_m$s^{-1}	K_R
184	G133	0.43	.014	14.14	.857
	G132	2.55	.085	11.10	.673
	G124	3.62	.118	9.57	.579
	G121	8.25	.269	6.84	.417
	G125	13.26	.432	5.99	.365
	G131	17.97	.599	6.16	.373
	G118	20.42	.681	5.79	.353
	G130	28.06	.783	5.92	.361
	G129	31.46	.900	5.92	.361

28. Graphon Membrane Sulphur Hexafluoride Flow

TEMPERATURE/K	Run Number	PRESSURE/cmHg	PERMEABILITY 10^6 K/m^{2}s^{-1}	FLUX 10^8 J/mols^{-i}
195	G294	1.18	5.45	0.39
	G296	1.47	4.30	0.38
	G285	1.92	3.46	0.40
	G297	3.57	3.56	0.76
	G283	4.08	3.00	0.79
	G272	6.76	2.87	1.17
	G281	10.14	2.41	1.47
	G291	13.3	1.80	1.44
	G289	17.00	1.37	1.40
	G287	24.00	1.23	1.75
	G279	27.51	1.32	2.26

29. Graphon Membrane SF_6/He Mixtures

TEMPERATURE/K	Run No.	PRESSURE SF_6 /cmHg	P/P_o	PERMEABILITY He 10^6 K/m^{2}s^{-1}	K_R
195	G298	0.79	.029	1.61	.631
	G295	1.44	.052	1.46	.572
	G286	1.93	.112	1.34	.525
	G284	4.07	.146	1.44	.565
	G278	6.76	.241	1.38	.541
	G282	10.14	.362	1.30	.510
	G292	13.23	.481	1.27	.497
	G293	20.46	.618	1.32	.518
	G290	23.60	.761	1.28	.502
	G288	26.87	.846	1.06	.416

30. Graphon Membrane Propane Flow

TEMPERATURE/K	Run Number	PRESSURE/cmHg	PERMEABILITY 10^6 K/m^{2}s^{-1}	FLUX 10^3 J/mols^{-i}
195	G160	0.61	21.20	0.77
	G163	1.13	15.41	1.04
	G156	1.57	12.84	1.21
	G157	2.20	11.27	1.50
	G164	3.14	9.52	1.80
	G159	3.50	9.33	1.96
	G158	5.08	7.91	2.42
	G154	7.20	7.86	3.41
	G152	9.29	10.31	5.78
203.2	G143	0.99	16.30	0.94
	G161	1.49	13.77	1.16
	G142	2.95	11.00	1.77
	G138	3.70	9.15	1.85
	G162	3.91	8.82	2.00
	G149	6.20	7.11	2.55
	G144	9.05	6.31	3.29
	G148	12.10	6.02	4.20
	G146	14.10	7.88	6.84
	G165	5.08	7.55	2.22
213.2	G138	3.70	9.15	1.85
	G136	8.04	6.47	2.87
	G140	13.98	5.18	3.98
	G134	17.58	4.99	4.84
273.2	G173	1.56	4.35	0.29
	G172	5.66	4.42	1.07
	G170	8.75	4.42	1.66
	G168	13.60	4.15	2.42
	G166	22.35	3.81	3.65

31. Graphon Membrane C_3H_8/He Mixtures

T/K	Run No.	Pressure C_3H_8 /cmHg	p_1/p_o	Permeability He $10^6 \tilde{K}_{He(mix)} / m^2 s^{-1}$	$\tilde{K}_R$
213.2	G139	3.65	.114	16.60	.638
	G137	8.02	.250	15.81	.608
	G141	13.92	.435	15.52	.596
	G135	17.55	.548	14.75	.565
203.2	G156	1.11	.062	14.77	.591
	G151	3.12	.175	14.73	.574
	G145	9.01	.501	13.93	.543
	G147	12.03	.678	13.20	.520
195	G154	7.13	.637	13.91	.555
	G153	9.22	.823	12.76	.507

References

1. Anderson, R.B., Emmett, P.H., J. Phys. Chem. 56, 753 (1952)

2. Ash, R.. Private communication 1986

3. Ash, R., Baker, R.W., Barrer, R.M., Proc. Roy. Soc. A, 299, 434 (1967)

4. Ash, R., Barrer, R.M., Clint, J.H., Dolphin, R.T., Murray, C.L., Phil. Trans. Roy. Soc. A, 275, 255 (1973)

5. Ash, R., Barrer, R.M., Coughlan, B.J., Colloid and Int. Sci., 38, 1, 61, (1972)

6. Ash, R., Barrer, R.M., Edge, A.V.J., Foley, T., J. Membrane Sci. 10, 183, (1982)

7. Ash, R., Barrer, R.M., Logan, A., Unpublished work.

8. Ash, R., Barrer, R.M., Lowson, R.T., Surface Sci. 21, 265, (1970)

9. Ash, R., Barrer, R.M., Lowson, R.T., J. Chem. Soc. Faraday Trans. I 69, 2166, (1973).

10. Ash, R., Barrer, R.M., Nicholson, D.,Z.Physik Chem 37,(5/6).257.(1963)

11. Ash, R., Barrer, R.M., Pope, C.G., Proc. Roy. Soc. A 271, 1, (1963)

12. Ash, R., Barrer, R.M., Pope, C.G., Proc. Roy. Soc. A 271, 19, (1963)

13. Ash, R., Barrer, R.M., Sharma, P., J. Membrane Sci. 1, 17 (1976)

14. Ash, R., Grove, D.M., Trans. Faraday Soc. 56, 9, 1357, (1960)

15. Aylmore, L.A.G., Barrer, R.M., Proc. Roy. Soc. A, 290, 477, (1966)

16. Baker, R.W., Ph.D. Thesis, University of London (1966)

17. Barrer, R.M., Disc Faraday Soc. 3, 61, (1948)

18. Barrer, R.M., Brit. J. Appl. Phys. S3, 41 (1954)

19. Barrer, R.M., Appl. Mat. Res. 2, 129, (1963)

20. Barrer, R.M., "Zeolites and Clay Minerals as Sorbents and Molecular sieves", London NY. Ac. Press (1978)

21. Barrer, R.M., "Surface and Volume flow in Porous Media" in "The Gas Solid Interface" ed. E.A. Flood (1979)

22. Barrer, R.M., Gabor, T., Proc. Roy. Soc. A 251, 353, (1959).

23. Barrer, R.M., Grove, D.M., Trans. Faraday Soc. 47, 826, (1951)

24. Barrer, R.M., Nicholson, D., Brit. J. Appl. Phys. 16 , 1377 (1965).

25. Barrer, R.M., Robins, A.B., Trans. Faraday Soc. A. 49, 807, (1953).

26. Barrer, R.M., Strachan, E., Proc. Roy. Soc. A. 231, 52, (1955)

27. Barrer, R.M., Sutherland, R.W., Proc. Roy. Soc. A. 237, 439 (1956)

28. Barton, S.S., Koresh, J., Sepn Sci and Tech 79, 1147, (1983)

29. Batzler, K., Herbert, W., Hoehne, R., Storp, K., US Patent 3637352 (1972).

30. Beebe, R.A., Briscoe, J., Smith, W.R., Wendell, C.B., J. Am. Chem. Soc. 69, 95, (1947).

31. Beebe, R. A., Kiselev, A.V., Kovaleva, N.V., Tyson, R.F.S., Holmes, J.M., Russ. J. Phys. Chem. 3o, 3, 372 (1964).

32. Beebe, R.A., Millard, B., Cynarski, J., J. Am. Chem. Soc. 75, 839 (1953).

33. Bell, W.K., Dissertation University of California (1971).

34. Benson, H.E., US Patent 3823222 (1974).

35. Berman, A.S., Lund, J.M., Proc. 2nd Int. Conf. on "Peaceful uses of Atomic Energy" 4, 359, (1958).

36. Bott, C.F., 3rd Year Project Report Chem. Dept., Imperial College (1986).

37. Breck, D.W., "Zeolite Molecular Sieves", Wiley (1974).

38. Briscoe, J., Warren, B.E., J. Appl. Phys. 13, 364, (1942).

39. Brunauer, S., Emmett, P.H., Teller, E., J. Am. Chem. Soc., 60, 309, (1938).

40. Butler, S., 3rd Year Project Report, Chem. Dept. Imperial College (1983).

41. Carman, P.C., Proc. Roy. Soc. A., 203, 55, (1950).

42. Carman, P.C., "Flow of Gases in porous media" Butterworth London (1956)

43. Carman, P.C., Arnell, J.C., Can. J. Res. A., 26, 128, (1948).

44. Carman, P.C., Roal, F.A., Proc. Roy. Soc. A, 209, 38, (1951).

45. Chirnside, G.C., Pope, C.G., J. Phys. Chem., 68, 2377, (1964).

46. Clint, J.H., PhD Thesis, University of London (1966).

47. Coady, A.B., Cooley, T.E., Canada. Patent 1080133.

48. Coughlan, B., Ph.D. Thesis, Univeristy of London (1964)

49. Craven, R.J.B., Ph.D. Thesis, University of London (1976)

50. Dacey, J.R., Thomas, D.G., Sepn. Sci. and Tech. 50, 740, (1954)

51. Derjaguin, B.F., Bakanov, S.P., Soviet Phys. Doklady, 2, 326, (1957).

52. Dwight, H.B., "Tables of Integrals and other Mathematical Data", Macmillan (1947).

53. Dwyer, J., Dyer, A., "Zeolites for Industry", Chem. and Ind., April (1984).

54. Fails, J.C., Harris, W.D., Oil and Gas J., 58, 28, 56 (1960)

55. Ferdani, P., 3rd Year Project Report Chem. Dept. Imperial College (1982).

56. Fick, A., Ann. Phys. 170, 59 (1855).

57. Flood, E. A., Thomlinson, R.H., Leger, E.A., Canad. J. Res. A., 30, 372, (1952).

58. Fowler, R.H., Proc. Cambridge Phil. Soc., 31, 260, (1935)

59. Fowler, R.H., Proc. Cambridge Phil. Soc., 32, 144 (1936).

60. Franklin, R.E., Trans. Farad. Soc., 45, 668, (1945).

61. Freeman, J., Stamires, F., J. Chem. Phys., 35, 799, (1961).

62. Frisch, H.L., J. Phys. Chem., 61, 93 (1957)

63. Gaede, W., Ann. Phys. (Lpz), 41, 289, (1913).

64. Gilliland, E.R., Baddour, R.F., Russell, R., J. Am. Inst. Chem. Engrs., 4, 90, (1958).

65. Godfrey L. Cabot Inc., Technical Data sheet.

66. Graham, T., Trans. Roy. Soc. Lond., 153, 385, (1863).

67. Graham, T., Phil. Trans. Mag. and J. of Sci. series 4, 32, 218, 401 (1866).

68. Gregg, S.J., Sing, K.S.W., "Adsorption, Surface Area and Porosity", Edn. 2, Ac. Press (1982).

69. Hamilton, A.D., Ph.D. thesis, University of London (1980).

70. Harris, B.L., Emmett, P.H., J. Phys. Chem. 53, 811, (1949).

71. Heckman, F.A., Harling, D.F., Rubber Chem. Tech., 39, 1, (1966).

72. Heilman, W., Tammela, V., Meyer, J.A. Stannet, V., Szwarc, M., Ind. Eng. Chem., 48, 821, (1956).

73. Henis, J.M.S., Tripodi, M.R., J. Membrane Sci., 8, 233, (1981).

74. Hess, W. M., Ban, L.L., Eckert, F.J., Chirico, V., Rubber Chem. Tech., 41, 356, (1968).

75. Hirsch, H.L., J. Appl. Phys., 32, 6, 977, (1961).

76. Hollinshead, K., 3rd Year Project Report Chem. Dept., Imperial College, (1985).

77. Huckins, H.E., Kammermeyer, K., Chem. Eng. Prog., 49, 6, 294, (1953).

78. Huggill, J. A. W., Proc. Roy. Soc. A, 212, 123, (1952).

79. Hwang, S.T., Kammermeyer, K., Can. J. Chem. Eng., 44, 82, (1966).

80. Hwang, S.T., Kammermeyer, K., "Membranes in separations" in "Techniques of Physical Chemistry VII" ed. Weissberger Wiley Interscience (1975).

81. Institute Francais du Petrole, May, 89. (1971).

82. Jellineck, H.H.G., Iwaki, T., J. Colloid and Int. Sci., 69, 17, (1979).

83. Joyner, L.G., Emmett, P.H., J. Am. Chem. Soc., 70, 2353, (1948).

84. Juntgen, H., Knoblauch, H., Harder,K., Fuel 60, 817, (1981).

85. Kameyama, T., Dokiya, M., Fikuda, K., Kotera, Y., Sepn. Sci. and Tech., 14, 10, 953, (1979).

86. Kammermeyer, K., Ind. Chem. Eng., 50, 697, (1958).

87. Kammermeyer, K., Weyrick, D.D., Ind. Chem. Eng., 50, 1309, (1958).

88. Kiselev XV, Quart. Rev., Chem Soc. XI, 116, (1961).

89. Knudsen, M., Ann. Phys. (Lpz), 28, 75 (1909).

90. Kodera, K., Onishi, Y., Bull. Chem. Soc., Japan, 33, 338, (1960).

91. Kotlhoff, I.M., Belcher, R., "Volumetric Analysis", Interscience NY, (1957).

92. Koresh, J., J. Colloid and Int. Sci., 88, 2, (1982).

93. Koresh, J.E., Soffer, A., J. Chem. Soc. Faraday Trans. 1, 76, 2457, (1980).

94. Koresh, J.E., Soffer, A., Sepn. Sci. amd Tech., 18, 723, (1983).

95. Kruel, M., Juentgen, H., Drwatwa,H., U.S. Patent 3578390, (1971).

96. Langmuir, I., J. Am. Chem. Soc., 38, 2219, (1916).

97. Langmuir, I., J. Am. Chem. Cos., 40, 1368, (1918).

98. Lee C.S., O'Connell, J.P., A. I. Chem. Eng. J., 32, 1, 96, (1986).

99. Lee, C.S., O'Connell, J.P., A. I. Chem. Eng. J., 32, 1, 107, (1986).

100. Lemcoff, N.O., Sing, K.S.W., J. Colloid and Int. Sci., 61, 227, (1977).

101. Lowson, R.T., Ph.D. Thesis, University of London (1968)

102. McBride, R.B., McKinley, D.L., Chem. Eng. Prog., 61, 381, (1965).

103. Millikan, R., Phys. Rev., 21, 224, (1923).

104. Mitchell, J.H., J. Roy. Inst., 2, 101, 307, (1831).

105. Murray, C.L., Ph.D. Thesis, University of London, (1976).

106. Nicholson, D., Petropoulos, J.H., J. Phys. D., 1, 1379, (1968).

107. Nicholson, D.,Petropoulos,J.H., J. Phys. D., 4, 181, (1971).

108. Nicholson, D., Petropoulos, J.H., J. Colloid and Int. Sci., 45, 459, (1973).

109. Nicholson, D., Petropoulos, J.H., J. Phys. D., 6, 1737, (1973).

110. Nicholson, D., Petropoulous, J.H., J. Phys. D., 8, 1430, (1975).

111. Nicholson, D., Petropoulos, J.H., Ber. Bunsen-Gesellshlaft, 79, 796, (1975).

112. Nicholson, D., Petropoulos, J. H.,J . Colloid and Int. Sci. 83, 2, 240, (1980).

113. Nicholson, D., Petropoulos, J.H., J. Chem. Soc. Faraday Trans. 1, 80, 1069, (1984).

114. Nicholson, D., Sing, K.S.W., Colloid Sci., 3, Spc. period, Rep. Chem. Soc. (1979).

115. Petty, J.A., Proc. Roy. Soc.London B, 175, 149, (1970).

116. Pollard,W.G., Present, R.D., Phys. Rev., 73, 762, (1948).

117. Polley, M.H., Schaeffer, W.D., Smith, W.R.S., J. Phys. Chem., 57, 469, (1953).

118. Pope, C.G., Ph.D. Thesis, University of London, (1961).

119. Riley, C.W., Private Communication (1983).

120. Rizvi, A.A., Ph.D. Thesis, University of London, (1981).

121. Roberts, A., J. Am. Chem. Soc., 53, 1810, (1931).

122. Ross, J.W., Good, R.J., J. Phys. Chem., 60, 1167, (1956).

123. Shamma, P., Ph.D. Thesis, University of London, (1970).

124. Sharpe, A.P., 3rd Year Project Report, Chem. Dept.,, Imperial College, (1983).

125. Shindo, Y., Yoshitome, H., Hakuta, T., Inoue, H., J. Chem. Eng., Japan, 18, 6, (1985).

126. Smith, W.R.S., Private Communication, (C.G. Pope Thesis, 1961).

127. Spencer, W.R., Amberg, C.H., Beebe, R.A., J. Phys. Chem., 62, 719, (1958).

128. Stern, S.A., "Gas permeation processes" in "Industrial processing with Membranes", ed. Lacey, R.E., Loeb, S., Wiley Interscience, (1972).

129. Sutherland, R.W., Ph.D. Thesis, University of London, (1956).

130. Weast, R.C. (ed.), Handbook of Chemistry and Physics, 51st Edn., (1970).

131. Weber, S., Kgl., Danske, Videnskab, Selskab, Mat. Fys. Medd., 28, (1954).

132. Whiting, D.R.G., Ph.D. Thesis, University of London, (1981).

133. Whitley, M.D., Hamrin, C.E., Am. Chem. Soc. Symp. Series 135, 14, 261, (1980)

134. Yearout, J.D., US Patent 3594983, (1971).

135. Young, D.M., Crowell, A.D., "Physical Adsorption of Gases", Butterworths, London, (1962).